Bangor University

DOCTOR OF PHILOSOPHY

The characterisation of thin insulating films on metal electrodes immersed in aqueous electrolytes using the AC Admittance Technique.

Macdonald, Andrew G.

Award date:
1991

Awarding institution:
Bangor University

"The characterisation of thin insulating films on metal electrodes immersed in aqueous electrolytes using the AC Admittance Technique"

by

Andrew G Macdonald, Bsc.

A Thesis submitted for the degree of Doctor of Philosophy

University of Wales,
March 1991

Summary

The full potential of Langmuir Blodgett (LB) Technology will only be realised in the development of sensors, such as coated metal electrodes, if the problems related to film stability in an aqueous environment can be overcome. To this end, the ac admittance technique has been applied to characterise LB films of Barium Stearate and Poly-Butyl-Methacrylate, deposited onto platinum, copper and aluminium electrodes immersed in a range of electrolytes. Cyclic voltammetry was used as a complementary characterisation technique for the coatings on platinum.

Equations were derived to relate the measured cell admittance to the equivalent circuit parameters. Approximations to these equations, valid for limited frequency ranges, enable parameter estimates to be made from the double log plots of capacitance and loss against frequency. The admittance data was analysed in terms of an equivalent circuit model adapted from the work of Macdonald (1952, 1971, 1973, 1974, 1976, 1985). This treatment enables the electrical measurements to be related to the electrical double layer, electrolyte and deposited film and represents the first attempt to characterise LB films in this way. The equivalent circuit model was rigorously applied to the characterisation of i) PCB electrodes spin coated with PVC and ii) sputtered copper electrodes coated with Barium Stearate using the LB Technique.

Several processes are found to contribute to the molarity, electrolyte and time dependent changes in coating admittance. For example, ionic uptake leads to an increase in coating admittance which can introduce a marked frequency dependent dispersion. For less stable coatings, film reorientation and desorption and changes in the oxide of the metal electrode can also affect the measured admittance. LB films of PBMA deposited onto platinum were sufficiently stable for immobilising electroactive species. Valinomycin incorporated in an LB film of PBMA and deposited onto platinum exhibited a reversible [K^+] dependent conductance.

Acknowledgements

First of all, I would like to thank Dr D M Taylor, who formulated the project and supervised the work. As well as the support given by him during my three years research at UCNW, Bangor, I would like to thank him for his continued encouragement over the last three and a half years during which I have been writing up the Thesis. My thanks are due to the SERC for funding the three years research at UCNW, Bangor.

Initial instruction in using the Langmuir Trough was given to me by Dr M Wilkinson to whom I am grateful. I would also like to thank Professor Lewis for useful discussions during the early stages of the work and to Drs H Morgan, O D'Oliviera and Van Der Sluijs for their help and encouragement during the latter period of the research.

Special thanks are due to many of the Technical Staff at SEES. In particular, Mr D Poirot for his advice on interfacing and programming, Mr J Tame for advice and assistance in preparing some of the substrates and to Mr Rees for performing several electron microscopy scans and for photographic work. I would also like to thank all the staff in the mechanical workshop who fabricated many essential pieces of apparatus for use during the experimental work.

Finally, I would like to thank my colleagues at the Northern Regional Medical Physics Department, NGH, in particular Dr P J Lowe, for their encouragement, assistance and patience, during my time here.

Dedication

To my parents.

Contents

Appendix A

1.0 Introduction

The science and technology of semiconductor fabrication has been the subject of considerable research and development during the past four decades. As a result, highly complex integrated circuits can now be manufactured at low cost. Such devices form an essential part of many of the appliances which play a role in our daily lives (Sibbald, 1983). If technological developments are to advance at the same rate as they have done so over the past three decades, it is probable that a comparable increase in circuit complexity will be required. However, the size of VLSI electronic components are now such that only a small reduction in size is necessary before they reach molecular dimensions. Indeed, following current trends, device geometries will be in the nanometer range by 2020. Such device sizes can not be realised in silicon and alternative fabrication techniques will be required. There is much speculation about using molecules instead of silicon to fabricate circuit elements viz "molecular electronics " (Roberts, 1990).

Molecular electronics may be defined as "the systematic exploitation of molecular materials in the field of electronics". Devices of commercial importance have already been produced which fit this definition. These include liquid crystal displays, piezoelectric polymers and chemical sensors (Roberts, 1985). An example of long term applied research in this area is the development of micro-structured electrodes. These electrodes use both spatial and chemical design to produce a selective response, an example of which is the ion gate (Chidsey and Murray, 1986). As for the future, "molecular transistors" have already been suggested (Carter 1982, 1987). A high priority in the advancement of molecular electronics will be the development of robust electroactive materials for use in micro structures (Chidsey and Murray, 1986).

In addition to the interest in using molecular electronics to fabricate electronic components, there is an increasing drive to couple existing integrated circuit technology and electroactive materials to develop novel sensors. These sensors offer distinct advantages over conventional sensors including small size, robustness and the potential for low cost, mass fabrication (Sibbald, 1983).

The most widely used device in this application is the insulated gate, field effect transistor (IGFET) which has been modified by substituting an electrochemically active material for the gate metal (Esashi and Matsuo, 1978). Such devices offer considerable potential for applications in the industrial, environmental, consumer and health care sectors. The latter is probably the largest current user of such technology. At present, clinical diagnosis, assisted by chemical analysis is only undertaken for the critically ill. There are many other patients who could benefit from a similar resource but for whom it is not yet considered "cost effective". As for the future, personal health monitoring devices have been proposed (Marshmann, 1986). Such systems would provide a means of regular screening for the early detection of disease. However, applications such as this will only be practical if a method of low cost fabrication can be developed.

The key component in chemical sensors is the molecular recognition system. Indeed, all chemical sensors require a suitably immobilised, electroative material, such as an ion carrier. Using this approach, potassium ion sensors have been constructed by immobilising Valinomycin at a metal electrode, within a polymer matrix such as PVC (Cattral and Tribuzio, 1974). Sensors may employ more complex recognition systems including enzymes (Renneburg, 1986; Cass, 1984) and antibodies (Aizawa et al; 1980). Any major advancement in sensor technology is therefore dependent upon the development of new and improved electroactive materials. Enhanced stability and device life time may result from bonding the electroactive materials into polymer networks to reduce loss of analyte (Edbon et al, 1982). The use of more elaborate films (Rechnitz, 1981) including antibody/antigen reactions (Aizawa et al, 1980; Janata, 1975) has also been suggested. In addition, it may be feasible to use other organic materials which react highly specifically and reversibly, such as receptor proteins. However, such molecules must be correctly oriented at the electrode surface (Sibbald, 1983; Bone and Zaba, 1987). Few techniques offer this level of control.

Clearly, any coating technique which can use either synthetic electroactive molecules or immobilise molecules with the necessary orientation, offers immense potential for both long and short term developments in the important area of molecular electronics. Langmiur Blodgett films offer this degree of control and there is therefore considerable interest in applying LB technology in this field. In fact LB films have already been used to fabricate an ion gate (Fujihira et al, 1986) and an enzyme sensitised film (Morizumii et al, 1987). These recent developments reflect the fact that current LB film research efforts are focused on developing materials and devices in the field of molecular electronics. In the long term, LB films offer potential for use in areas such as superconductivity, molecular switching and memory storage. In the short term, they present the possibility of enhancing existing devices (Roberts, 1985).

Areas of applied research include the development of magnetic monolayers (Pomerantz, 1980), pyroelectric devices (Blinov et al, 1982; 1983), electro-optics (Pit and Walpita, 1966; 1977; 2relatingPeterson and Girling, 1985; Barnes and Sambles, 1986), photolithography (Barraud, 1983; Broers and Pomerantz, 1983) photocells (Roberts et al, 1981) and electroluminescent cells (Winter et al, 1984). In semiconductor applications the LB technique offers advantages over alternative thin film deposition methods. As the Langmiur Blodgett method is a low temperature deposition process, no damage occurs to the surface of the semiconductor during deposition. In contrast, techniques such as evaporation, sputtering or plasma deposition damage the surface layer which can adversely affect the device properties (Roberts, 1985).

LB films have also been employed in applications such as electrocatalysis (eg

Fujihara and Poosittisak, 1986) and, as mentioned earlier, in sensor development (eg Holcroft and Roberts, 1987; Morizumii et al, 1987). For device applications such as electrocatalytic electrodes ($ 3.5.4, 3.5.5) and sensors ($ 3.5.6, 3.5.7), the Langmiur-Blodgett technique offers distinct advantages over existing technologies. For example, the LB technique combines the flexibility of solvent casting and polymer electrodeposition for immobilizing electroactive species in a matrix of electroinactive species. At the same time it offers greater control over film dimensions than that provided by covalent attachment and adsorption. However, before the full potential of LB technology can be exploited in sensor development such as coated metal electrodes, the problems related to film stability ($ 3.5.5; $3.5.6; $3.6.2.3) in an aqueous environment must be overcome. Consequently, one of the important aims of the present work is to develop a method for characterising LB films in an aqueous environment to gain insight into the causes of film instability. Armed with this knowledge, it will then be possible to determine which LB films are stable enough to produce electroactive electrode coatings for sensor applications. "Provided that the crucial problem of stability can be overcome, the future for LB films appears to be very bright" (Roberts, 1985).

In order to investigate LB film stability, a suitable measurement technique is required. A wide range of experimental techniques have been employed to study the structural properties of LB films (Roberts, 1985). These include the use of ellipsometry, electron spin resonance, surface potential, polarised resonance Raman spectroscopy, infra-red dichroism and diffraction techniques using electron reflection (Mobius and Bucher, 1972) and transmission (Peterson et al, 1983), X-rays (Matsuda et al, 1977) and neutrons (Nicklow et al, 1981). However, the primary goal of such research has been to elucidate the basic properties of the films such as monolayer thicknesses, ordering and molecular orientation. Apart from data on film re-ordering, no details of film stability have resulted from these studies.

If LB films are to be used successfully in sensor applications, they will have to survive in hostile environments such as blood and sea water. However, little work has been done to characterise LB films in such environments. Even investigations of the electrical properties of LB films have been based on dry metal/LB film/metal (MIM) structures. As a result of this research, dielectric behavior (Millany and Jonscher, 1980), electrical conduction, (Roberts, 1980) electrical breakdown (Agarwal, 1975b) and ionic transport mechanisms (Vincett and Roberts, 1979) have been elucidated. The admittance of dry MIM structures has also been measured from which loss mechanisms have been identified (Careem and Jonscher, 1977).

Whilst this work is of value for some semiconductor applications, such as the use of LB films to improve the breakdown strength of the native oxide (Peterson and Girling, 1985), it does not provide insight into film stability. Furthermore, the analysis of the admittance data has relied on empirical models (Careem and Jonscher, 1977). This means that the data can not be readily related to the physico-chemical properties of the LB film. Consequently there is an important gap in our current understanding of LB films both in terms of coating stability and characterisation in an aqueous environment. If LB films are to be successfully employed in sensor applications, these gaps must be filled.

The major goal of this research is therefore to develop a characterisation technique which will provide qualitative data on film properties in electrolytes. In order to achieve this goal, the ac admittance technique has been applied to LB films. The films were deposited onto a range of metal electrodes and immersed in various electrolytes. The data has been analysed in terms of an equivalent circuit model adapted from the work of Macdonald (1952, 1971, 1973, 1974, 1976, 1985). This treatment enables the electrical measurements to be related to the electrical double layer, electrolyte and deposited film. Furthermore, it represents the first attempt to characterise LB films in a range of electrolytes in this way.

The existing techniques for electrode coating are reviewed in Chapter 2. The strengths and weaknesses of methods of adsorption, covalent attachment, solvent casting, dipping, spin coating and electrodeposition are each considered and compared. The chapter concludes with a brief discussion of the possible advantages of using the Langmiur Blodgett technique. This method of electrode coating is detailed in Chapter 3. The current experimental practice and applications are first discussed before detailing the ways in which the LB technique could facilitate the fabrication of superior electrode coatings for sensor development.

The experimental methods employed to prepare the samples used in this work are discussed in chapter 4. The preparation of platinum wire, sputtered copper and evaporated aluminium on glass electrodes are considered followed by details of the thin film coating techniques. Once prepared, the samples were characterised using the AC Admittance Analysis technique. In chapter 5 both the theoretical and experimental aspects of the technique are examined. Preliminary results for PVC coated copper electrodes are presented and discussed. These results are shown to establish the AC Admittance Technique as a method for characterising thin films in an electrolyte environment. The AC admittance characterisation of the coated platinum wire electrodes was complemented by cyclic voltammetry (Chapter 6).

After establishing the usefulness of the AC admittance technique by characterising PVC coated copper electrodes, the characterisation of barium stearate and barium stearate/gramicidin LB multilayers was performed. The technique revealed that Barium Stearate coated onto platinum resulted in poor quality films. When deposited onto sputtered copper, the initial film quality was good, but soon deteriorated as the copper oxidised. Only barium stearate deposited onto aluminium produced high quality, stable coatings. In an attempt to fabricate a sensor, gramicidin was incorporated into the barium stearate film.

The poor quality and instability of the barium stearate LB films deposited onto platinum necessitated the use of alternative LB film forming materials. Consequently, poly-butyl-methacrylate (PBMA) was chosen. The results from the AC admittance characterisation of PBMA coated substrates are presented and discussed in chapter 8. The admittance results showed that the PBMA coatings onto platinum wire electrodes were of good quality and high stability. Therefore valinomycin was incorporated in the PBMA film to fabricate a potassium ion sensor. The AC admittance results prove that the PBMA/Valinomycin LB film functioned as a potassium sensitive coating.

The conclusions arising from this work are presented in chapter 9, including suggestions for further work. Finally, details of the mathematical basis of the AC admittance technique are presented in Appendix A.

2.0 Modified Electrodes

2.1 Introduction

The deliberate and controlled modification of metal electrodes is an important step in many technological applications. The electrode may be modified by liquid phase adsorption, spin or dip coating, electrodeposition or covalent attachment of specific molecules to the metal surface (Bard, 1983). Such coatings are obviously important as corrosion inhibitors (Hubrecht and Vereecken, 1985; McIntyre and Leidheiser, 1986) but increasingly it is recognized that electrodes modified in this way can be used as chemical (James, 1972; Martin and Freiser, 1980; Tamura et al, 1982; Buck, 1974, 1976) and biological sensors (Takatsu, 1987) and may have important electro-catalytic (Oyama and Anson, 1980; Halbert, 1985; Vining and Meyer, 1985) and photo- electrochemical properties ([illegible] Whitten, 1977).

Coated metal electrodes (CME's), are often fabricated using solvent casting techniques (James, 1972; Martin and Freiser, 1980; Cattrall and Freiser, 1971; Cattrall and Tribuzio, 1974) although adsorption has also been used (Rubinstein et al, 1987). Takatsu, (1987) developed a coated electrode enzyme sensor using techniques compatible with photolithography, whilst other electrocatalytic electrodes have been prepared by adsorption, (Collman et al 1980), and covalent bonding (Oyama and Anson, 1980). The common feature in all these applications is the use of an electrode coating to confer specific properties to a conductive substrate.

For these applications the ideal electrode coating technique should immobilize stably the species of interest at the electrode surface. If the coating contains electrochemically active sites, it is important that the sites remain accessible to reactant molecules (Oyama and Anson, 1980). Furthermore, the immobilisation technique should not impair the functionality of the site by altering either its geometrical conformation or chemical environment (Berezin, 1976; Pye and Chance, 1976).

The main techniques presently in use for preparing coated electrodes for various applications are considered below.

2.2 Electrode coating techniques

2.2.1 Adsorption

Adsorption was the earliest immobilisation technique employed for modifying electrode surfaces (Murray et al, 1987). Electrode materials such as platinum (Lane and Hubbard, 1973), carbon (Collman et al, 1980), gold (Rubinstein et al, 1987) and silver (Flanagan and Pantell, 1984) can be coated with organic molecules by placing the electrode in a solution containing the required species. Lane and Hubbard (1973) first investigated the technique by adsorbing quinone bearing olefins onto platinum.

Collman et al (1980), immobilized a dicobalt face-to-face porphyrin from dilute solution by adsorption onto a graphite disc electrode (fig 2.1). The electrodes were fabricated for the electrocatalytic 4-electron reduction of oxygen to water. Whilst not affecting the geometric conformation of the immobilized species, adsorption was insufficiently strong to prevent the catalyst from desorbing.

Cass et al (1984) developed a ferrocene mediated glucose enzyme electrode where adsorption was used to attach a ferrocene electron mediator, 1'-1- dimethyl ferrocene (0.1M in toluene) to graphite foil (fig 2.2a). The effects of loss of catalyst by desorption were reduced by employing a 10 hour electrochemical pretreatment of the electrode. This treatment, combined with the choice of a low solubility ferrocene derivative, resulted in

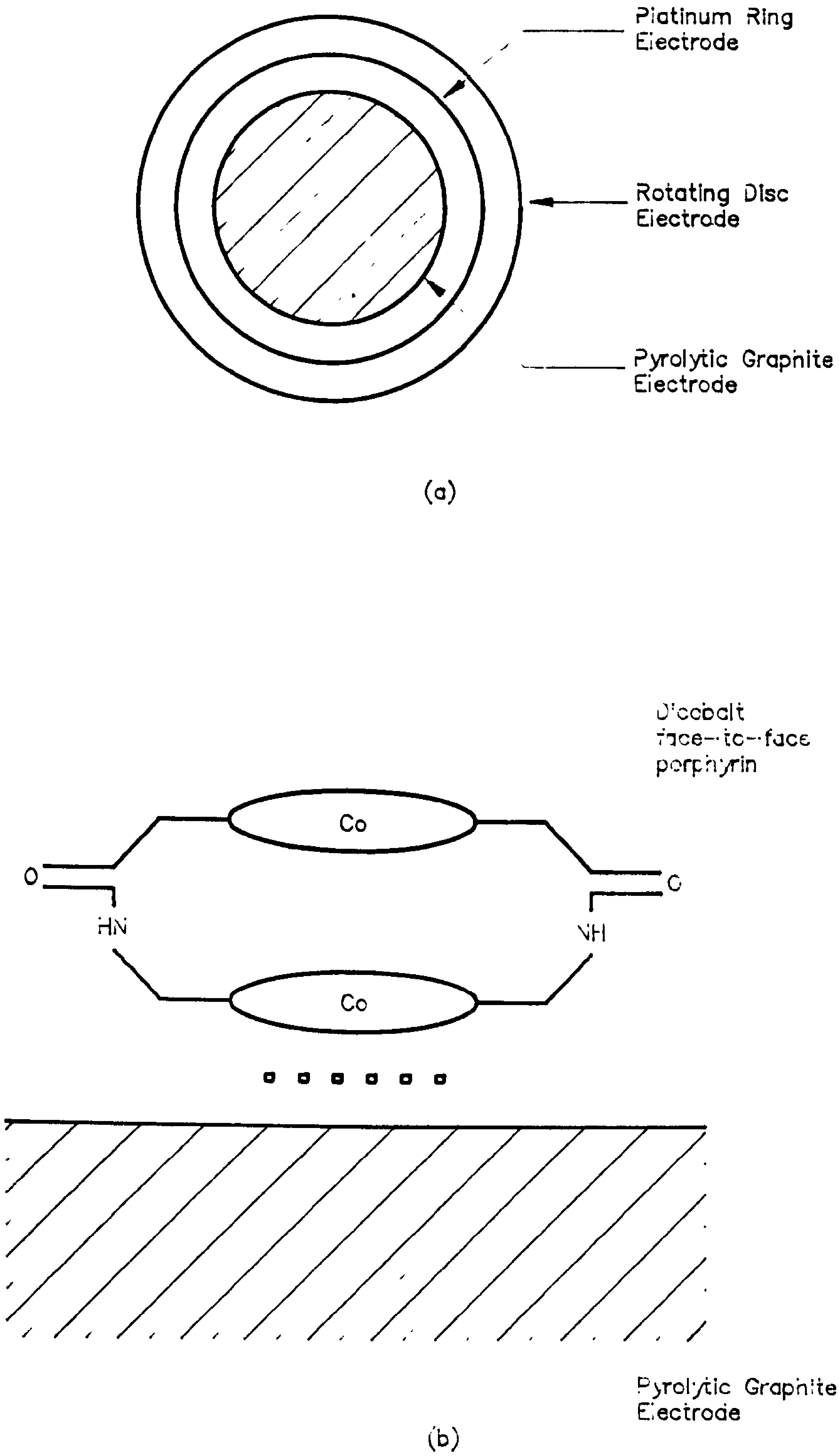

Fig 2.1 a) Simplified diagram showing the rotating disc electrode.
b) Dicobalt face-to-face porphyrin immobilised by adsorption at a pyrolytic graphite electrode (Collman, 1980).

$$\text{glucose} + GOD_{(ox)} \longrightarrow \text{gluconolactone} + GOD_{(red)}$$

$$GOD_{(red)} + 2Fecp_2R^+ \longrightarrow GOD_{(ox)} + 2Fecp_2R + 2H^+$$

$$2Fecp_2R \rightleftharpoons 2Fecp_2R^+ + 2e^-$$

(a)

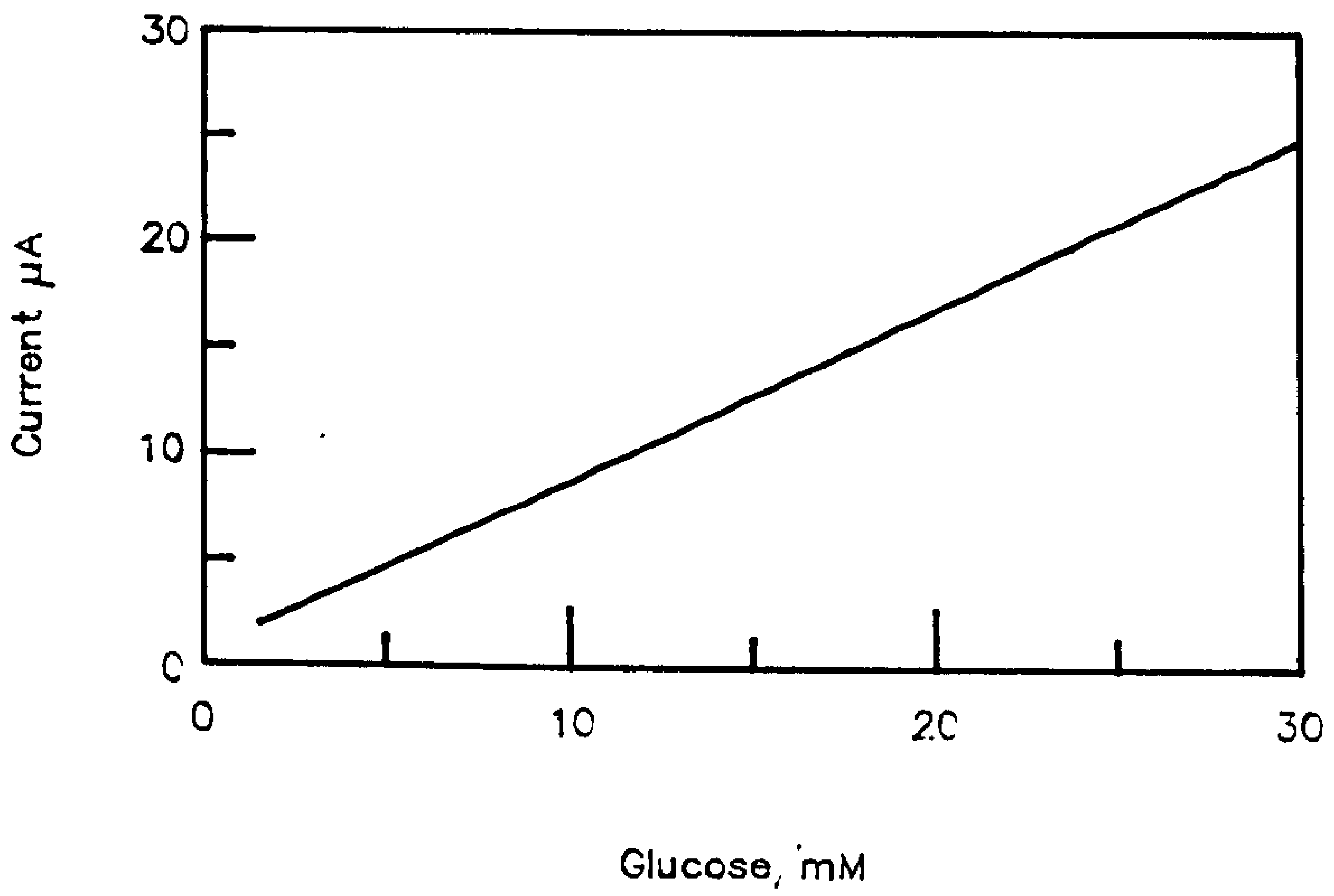

(b)

Fig 2.2 a) Reaction scheme for the Ferrocene–mediated enzyme electrode.

b) Calibration curve for the glucose enzyme electrode in air. Current measured at 160mV vs SCE, pH 7.0, 25°C (Cass, 1984).

a stable electrode response over a 50 hour period of use. The enzyme electrode permitted the rapid, reproducible analysis of glucose in solution and physiological samples (fig 2.2b).

Rubinstein et al (1987), produced high quality, ordered monolayers on gold by the adsorption of octadecyl mercaptan (OM) and octadecyl trichlorosilane (OTS) on the electrode surface. Their method involved sequential adsorption of the two compounds from the liquid phase. Contact angle and FTIR measurements indicate a high degree of molecular order and directionality. Electrochemical analysis also showed that the electrode could be rendered ion selective (Cu^{2+} ions) by the simultaneous adsorption of a thiol (TBEA) with OTS and OM (fig 2.3).

2.2.2 Covalent attachment

Recently, attempts have been made to improve the stability of immobilized species by covalent attachment of electroactive substances, such as o-hydroxy-benzene derivatives, to the electrode (Murray et al, 1987). A metal or carbon electrode can be oxidized to provide a surface consisting of hydroxyl groups. Such a surface can be silanized by reaction with an organosilane and then reacted with another molecule to produce a mechanically and chemically robust coating. A typical reaction scheme is shown in fig 2.4. Although monolayer coverage is expected, in practice the silanisation reaction frequently causes polymerisation of the electroactive species to take place and thicker layers, equivalent to several monolayers form (Bard, 1983).

Covalent attachment may be used to immobilize electro-active species in polymer matrices such as PVC and PVP, to induce specific electrochemical properties in an otherwise electro-inactive polymer coating. The mechanical and electro-chemical properties of the matrix then play a significant role in determining the behaviour of the immobilized species.

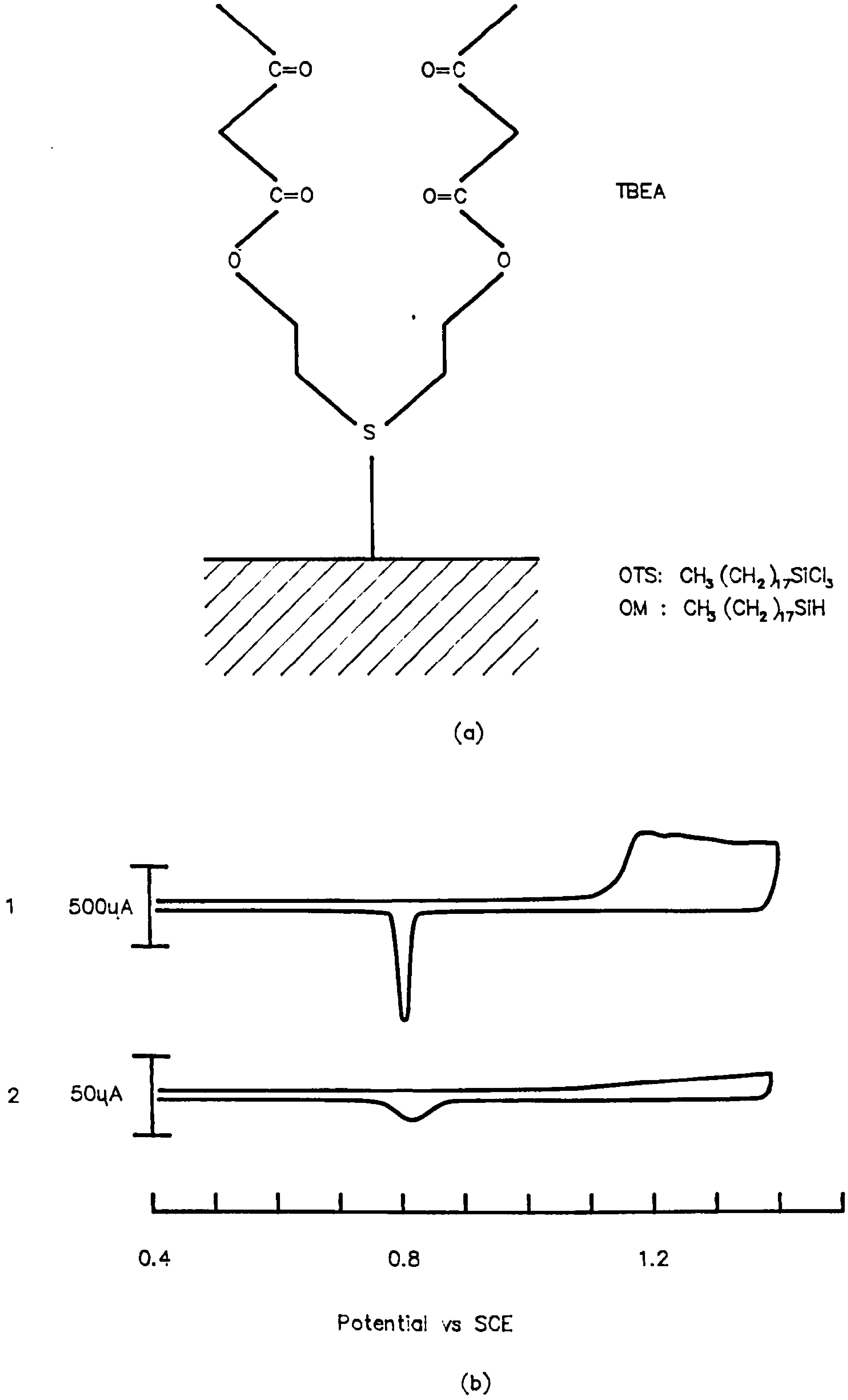

Fig 2.3 a) Cu^{2+} ion selective electrode coating produced by the adsorption of OTS, OM and TBEA on a gold film (only TBEA is shown).

b) Steady state cyclic voltammograms in 0.1 M H_2SO_4 for 1) uncoated Au and 2) Au/OTS+OM. Scan rate 0.05V/s, area 2.2cm^2). (Rubinstein, 1987).

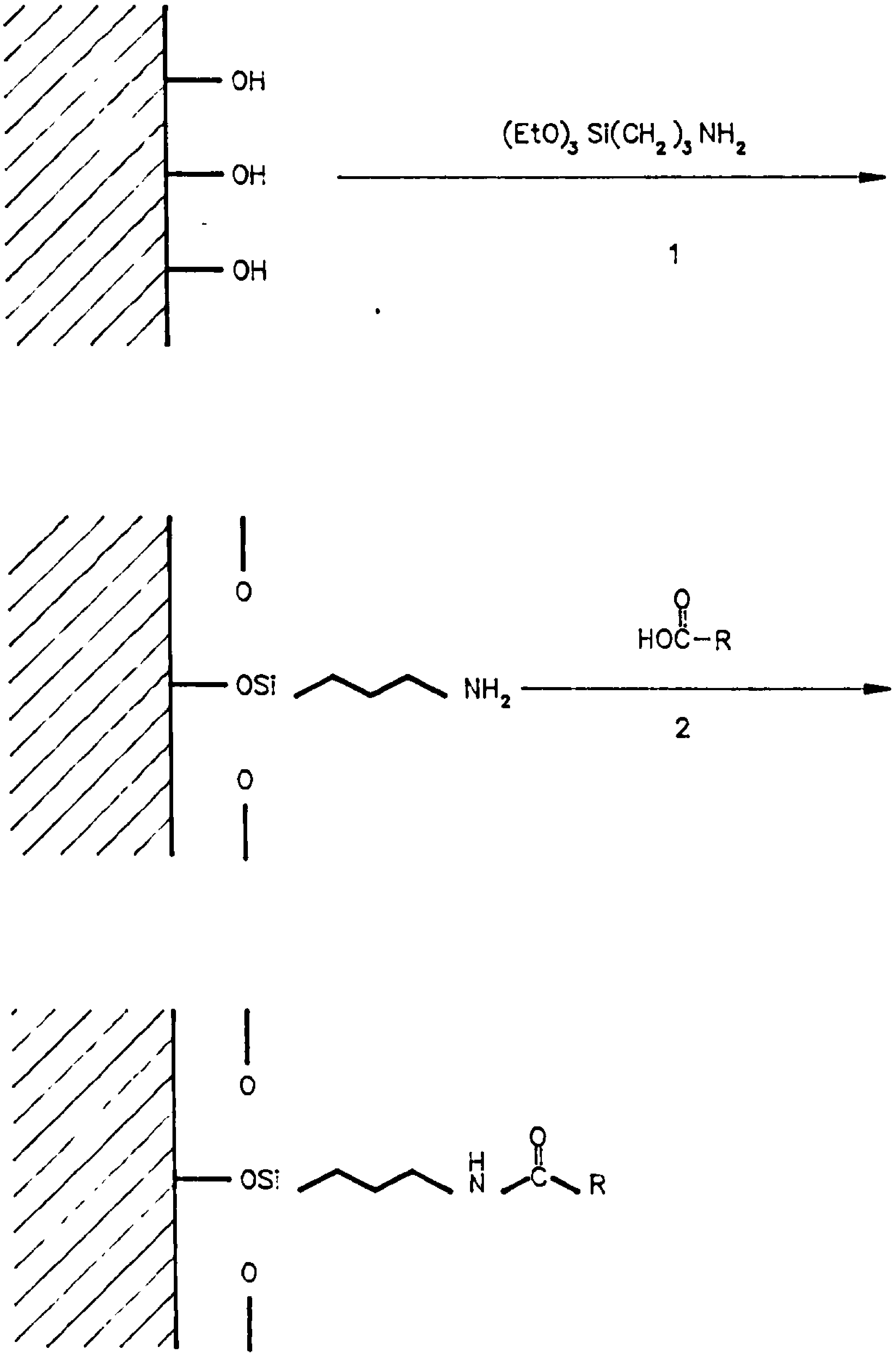

Fig 2.4 A general reaction scheme for the covalent attachment of an organic compound to an electrode surface to produce a chemically modified electrode (CME).

1) Oxidised carbon or metal electrode is treated with γ–aminopropyltriethoxysilane.

2) The silanised electrode is treated with the compound containing the desired group,R tobe attached (Bard, 1980).

For example, Oyama and Anson (1980) developed an electrocatalytic electrode for the oxidation of Fe^{2+} by covalently immobilising hexachloroiridate ions, $(IrCl_6)^{2-}$ in a protonated poly(-4-vinylpyridine) (PVP) coating (fig 2.5). Oyama and Anson showed that although the oxidation of Fe^{2+} at a pyrolytic graphite electrode is normally inhibited by PVP, the reaction can proceed when $(IrCl_6)^{2-}$ions are immobilized at the electrode. However, the catalytic activity of the immobilized species was less than for the corresponding reaction in solution. This suggests that the Fe^{2+} ions are unable to reach freely the $(IrCl_6)^{2-}$ sites in the PVP coating. The use of a more porous coating should therefore increase the effective electrocatalytic activity of the modified electrode.

Indeed, in the development of an enzyme immunosensor for the tumour antigen, α-fetoprotein (AFP), Aizawa et al (1980) used a solvent cast membrane of cellulose triacetate as the matrix for the covalent immobilisation of the antibody, anti-AFP (fig 2.6a). The choice of such a high porosity material resulted in a significant increase in site accessibility, as evidenced by its response time and sensitivity, compared with previous immobilisation techniques at a metal electrode (fig 2.6b).

2.2.3 Solvent cast, dipped and spin coated films

Several methods exist for coating electrodes in either passive or electro-active polymeric films from solution. They are the techniques of dipping (eg Cattrall and Tribuzio, 1974; Tamura et al, 1982), spin coating (eg McIntyre and Leidheiser, 1986) and the method of solvent casting (eg Trojanovicz et al, 1982), and for conventional membrane electrodes LeBlanc and Grubb (1976). In all these methods the polymer, dissolved in a suitable solvent, is applied to a solid support and the solvent allowed to evaporate, thus forming a robust polymeric film (Bard, 1983).

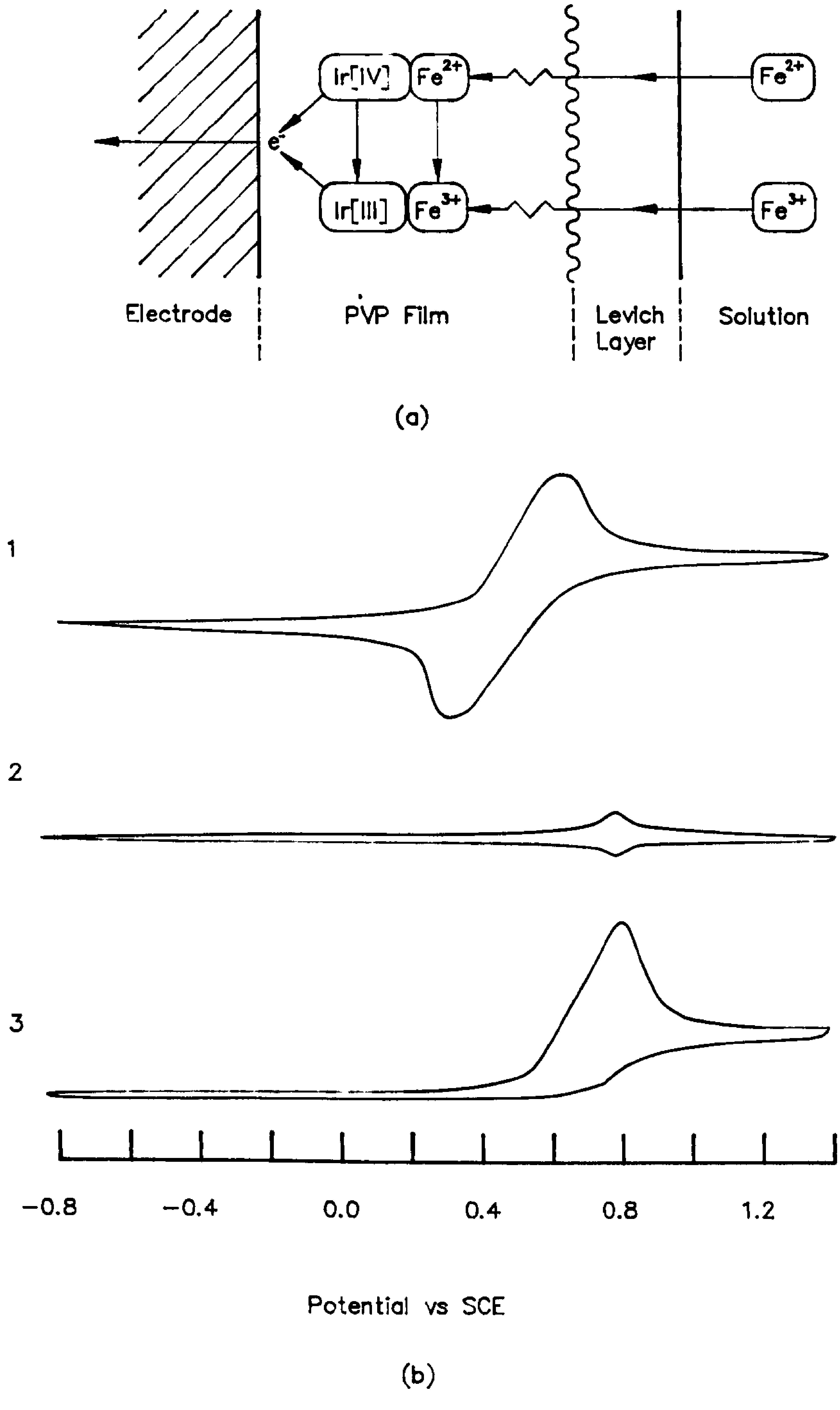

Fig 2.5 a) Schematic diagram showing the oxidation of Fe$^{2+/3+}$ catalysed by IrCl$_6^{2-}$ in a protonated PVP electrode coating.
b) Cyclic voltammograms for Fe$^{2+/3+}$ couple at a pyrolytic graphite electrode. 1) freshly cleaved electrode in 8mM FeSO$_4$+ 0.1M CF$_3$COONa + 0.1M CF$_3$COOH, 2) 5.10 mol/cm IrCl$_6^{2-}$ in PVP in the absence of Fe$^{2+/3+}$ 3) as 2) but with Fe$^{2+/3+}$ present.
Scan rate 100mV/s (Oyama, 1980).

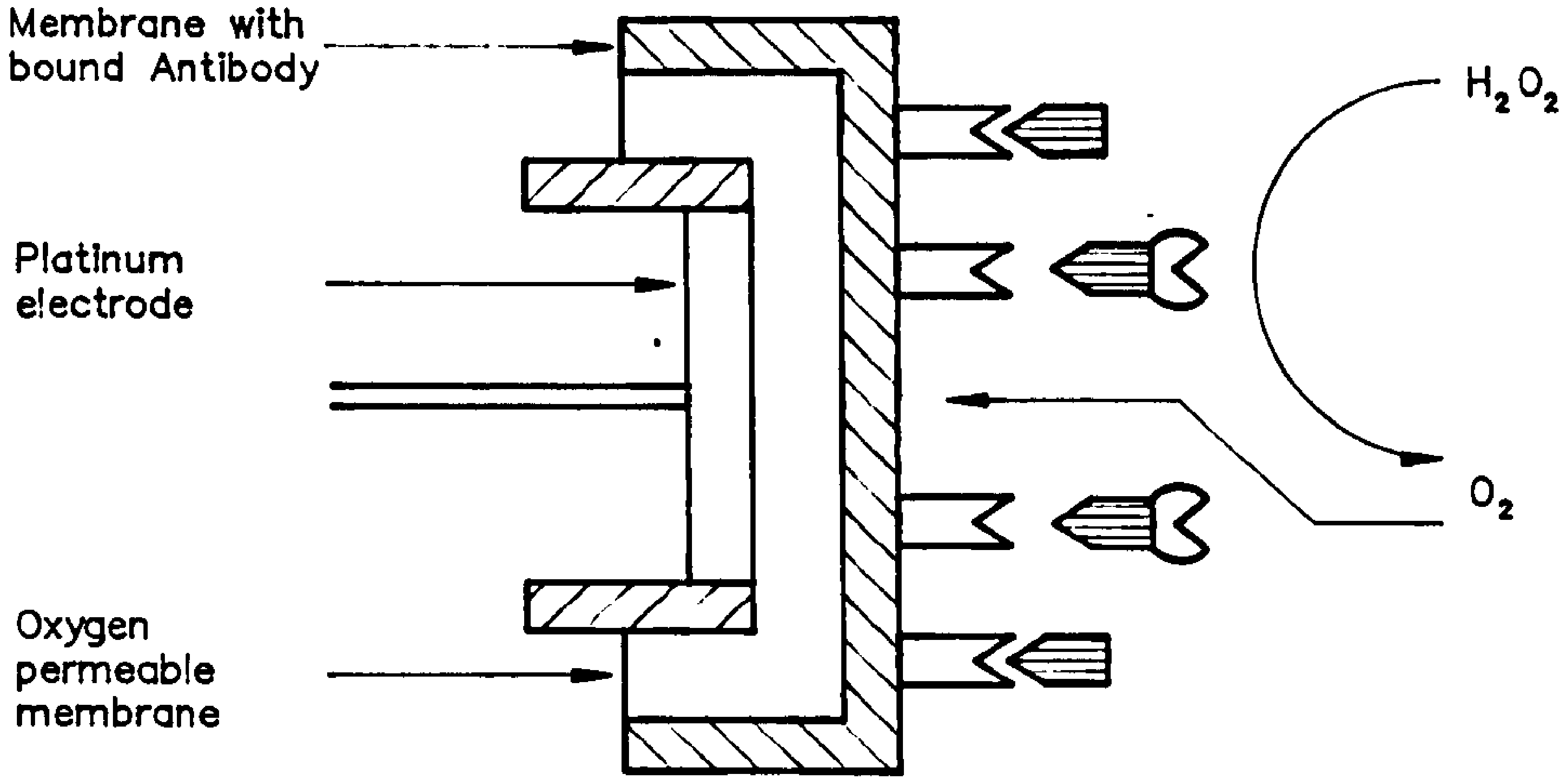

(a)

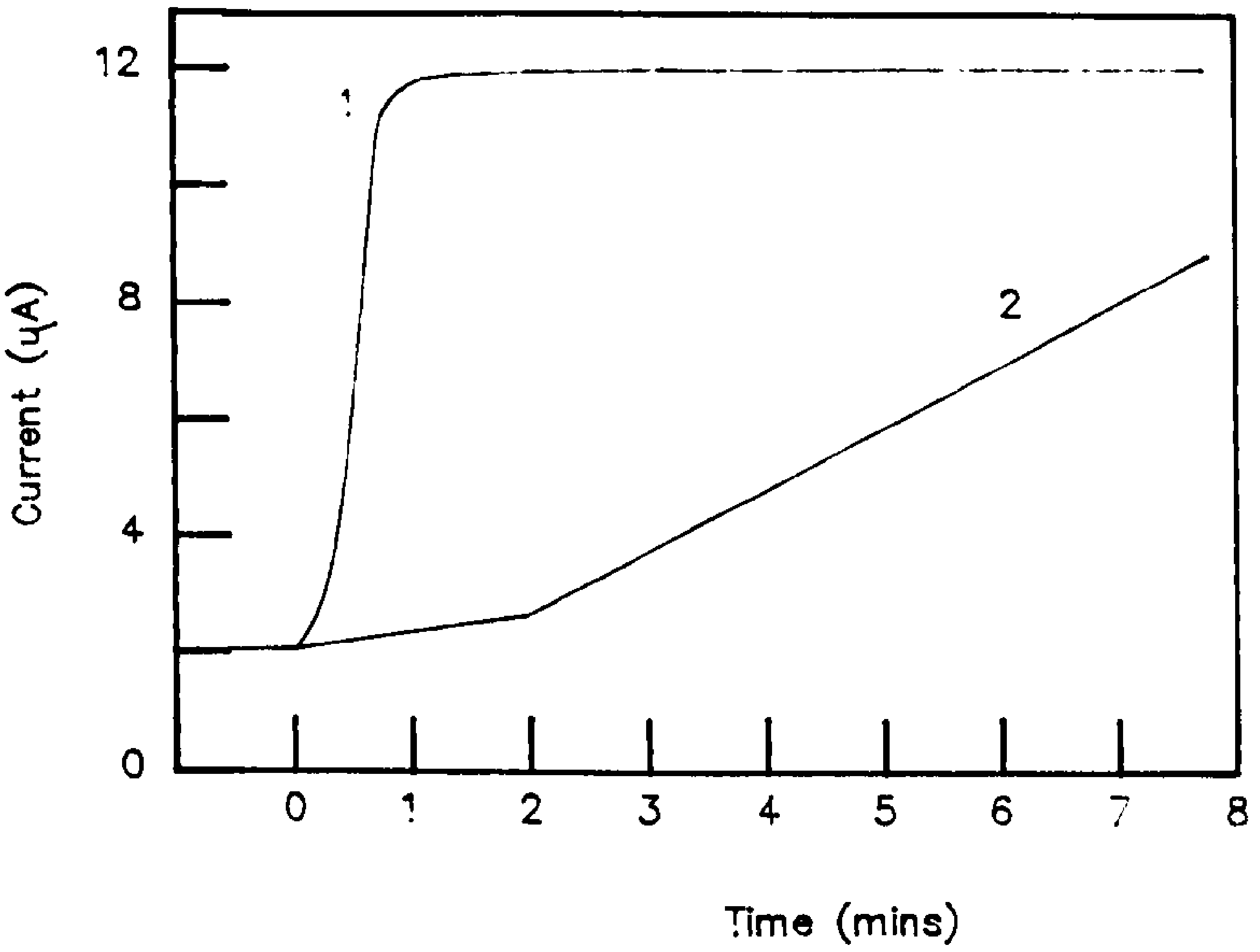

(b)

Fig 2.6 a) Schematic diagram of the Enzyme Immunoassay Sensor where ⊏< is the antibody, ◀ is the antigen and ◀ℨ is the catalase labelled antigen.

b) Typical response curve for the Enzyme Immunosensor.

1) Device with Cellulose Triacetate Membrane, 2) standard membrane. (Aizawa, 1980).

Electroactive films may be formed by coating the electrode in an electro-inactive polymer before incorporating electroactive species by ion exchange, (Vining and Meyer, 1985), or covalent attachment (Oyama and Anson, 1980).

For example, electro-inactive poly(4-vinylpyridene) (PVP) was applied to pyrolytic graphite electrodes by pipetting aliquots of a stock solution of the polymer in methanol over the surface of the electrode and allowing the solvent to evaporate. Scanning electron micrographs showed that the resulting coatings were uneven. However, it is stated that the PVP films had reproducible properties suggesting that there were no large topological differences across the films. The pure PVP coatings were stable indefinitely on electrodes stored in air and were stable for several days in 1M acid. The PVP coatings were rendered electrocatalytic either by the electrostatic immobilisation of Ru(III) edta, or by the covalent attachment of $(IrCl_6)^{2-}$ or $(IrCl_6)^{3-}$ by immersing the PVP coated electrode in a suitable solvent ($2.2.2). In the case of covalently bound $(IrCl_6)^{2-}$, the current-voltage characteristic stabilized after 20 minutes in 0.2M CF_3COOH, after which time the most accessible ions had been eluted. The total $(IrCl_6)^{2-}$ remaining in the film corresponded to 40% of the total charge on the protonated PVP coating.

The spin coating technique is used widely in the electronics industry for producing thin organic films of photoresist and therefore plays an important part in the photolithographic process. Spin coating has also been used in other areas, for example McIntyre and Leidheiser et al (1986), applied poly-butadiene to evaporated metal films on glass by this method in an investigation of corrosion inhibition. McIntyre and Leidheiser (1986) exposed a 9μm coating of polybutadiene on nickel to a 3% NaCl solution. The AC admittance of the coated metal electrode and the parallel DC resistance of the metal electrode alone were monitored. After three days, a significant increase in the DC resistance of the electrode was observed, indicating an interfacial corrosion reaction. This was confirmed by the observation that water was present at the coating/metal interface. Furthermore the adhesion of the film to the substrate was very poor after this period of exposure to the NaCl solution. Therefore, although spin-coating is a useful technique for applying smooth coatings to planar substrates, film adhesion and water penetration can limit device usefulness in an aqueous environment. In the case of ion selective membrane electrodes, LeBlanc and Grubb (1976) suggested that the long term decrease in electrode resistance which ultimately limited the life of the potassium ion sensitive electrode to 5 years, could be due to ionic pathways short circuiting the membrane.

An alternative to incorporating electroactive species into an already formed polymeric coating is to include the electroactive species in the casting solution eg valinomycin for a potassium ion selective membrane (Band 1976; Cattrall and Tribuzio, 1974). The CME developed by Cattrall and Tribuzio (1974) was capable of accurately measuring potassium ion concentrations in blood and sea water, provided that the electrode was calibrated before and after each measurement to permit correction for drifts in the electrode voltage response.

The potential drift of CME's, with respect to the external reference electrode during solution analysis is a well known, though poorly understood phenomenon. However, it is known that the oxidation state of the internal electrode is important (Arnold and Meyerhoff, 1984; Maj-Zurwaska and Hulanicki, 1982).

Maj-Zurwaska and Hulanicki (1982) have shown that preconditioning the internal platinum electrode can have a marked effect on the potential response of the CME. The potential of a nitrate selective PVC membrane was 170mV more positive after the internal electrode had been oxidized using sulphuric acid, compared to a similar CME for which the platinum had been reduced using hexacyanoferrate (fig 2.7). Furthermore, the potential response of the nitrate CME's with a pre-oxidized platinum electrode was less

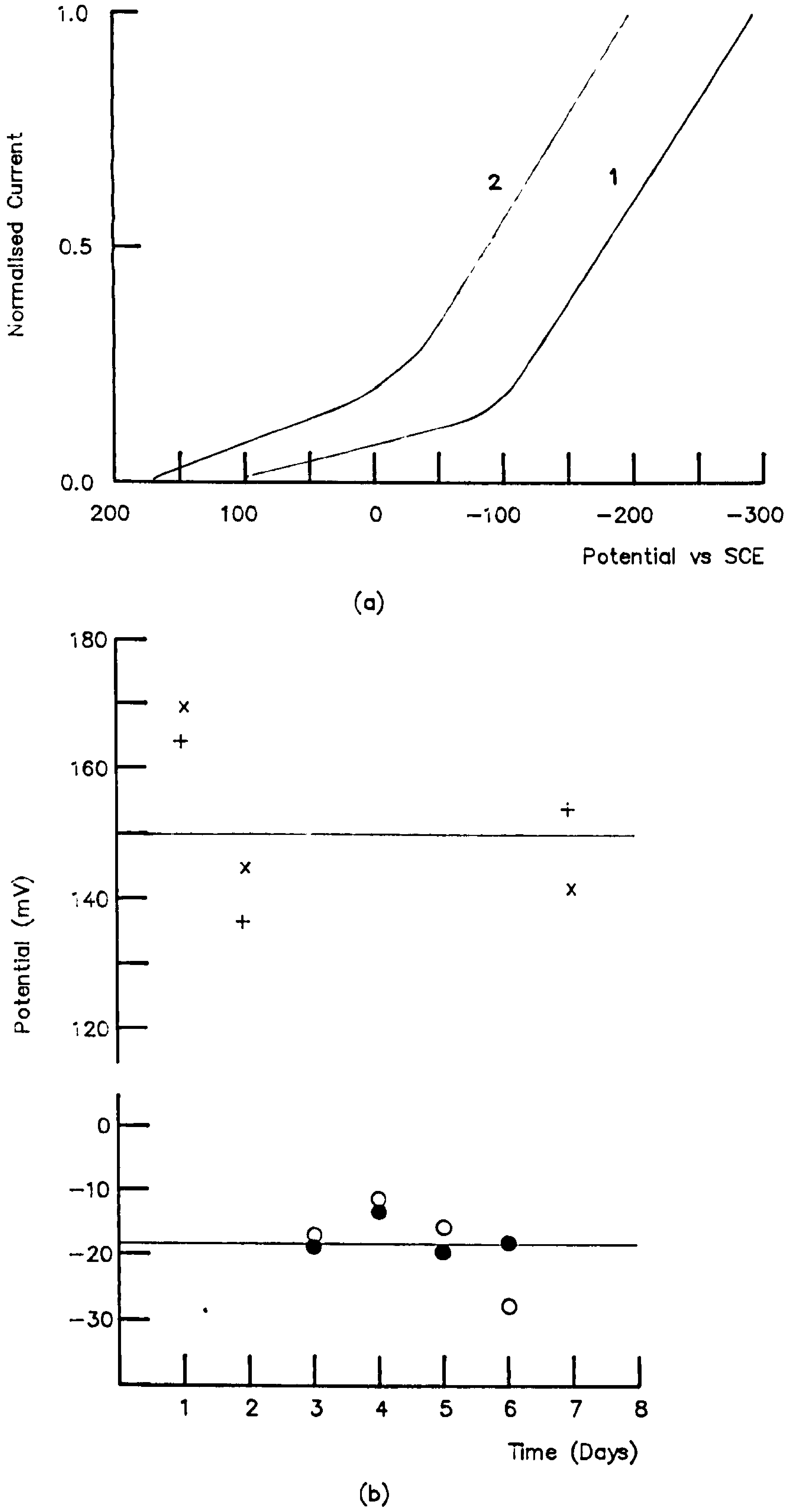

Fig 2.7 a) Polarisation curves for rotating platinum electrode in tris–bathophenanthroline, nickel nitrate solution in 2–nitro–p–cymene. 1) After pretreatment for 10hrs in 0.01 mol/l hexacyanoferrate (II). 2) after pretreatment for 10 mins in sulphuric acid. b) Potentials of nitrate sensitive electrodes in 10 mol/l potassium nitrate as a function of time. Electrodes with internal contact pretreated for 30 mins in 0.01 mol/l hexacyanoferrate (○ ●), and sulphuric acid (x +). (Maj–Zurwaska, 1982).

reproducible than for those with a reduced internal electrode, indicating that it is difficult to obtain reproducible oxidation of the platinum surface.

Arnold and Meyerhoff (1984) commented that these results suggest that if reducing or oxidizing agents penetrate the electrode coating, interaction at the electrode/coating interface will cause instability of the CME electrode potential. As PVC is permeable to oxygen, the PVC based CME's may respond to oxygen by this mechanism. The formation of an oxygen redox couple at the membrane/metal interface has even been postulated as the mechanism by which a reference potential is established, again indicating the importance of the internal electrode's oxidation state (Maj-Zurwaska and Hulanicki, 1982).

Therefore, a possible method for stabilising the CME potential may be to dope the ion-selective membrane with an organic redox species. Indeed, Stefanova et al (1983) have shown that the potential stability of PVC CME's can be enhanced by incorporating an organic redox couple, such as heme, in mixed Fe^{2+}/Fe^{3+} form, in the PVC matrix.

As well as incorporating electroactive species in the casting solution to confer ion selectivity to the membrane material or to stabilize the electrode potential, the composition of the casting solution can also be adjusted to optimize the dielectric permittivity and pH response of the membrane (LeBlanc and Grubb, 1976). The ability to adjust the dielectric permittivity is important because if the dielectric permittivity is too low, the membrane can prevent ion unpairing or electrical charge injection from taking place at the electrolyte/membrane interface. In this way, the host polymer matrix can prevent the electrolyte ions from accessing or interacting with the active sites (LeBlanc and Grubb, 1976).

When the electrode is to be used in laboratory analysis, it is often important for the electrode potential response to be stable over a wide range of pH. By adjusting the membrane potential, the effect of the pH dependent response of the internal electrode can be minimized.

2.2.4 Electrodeposition

Electrodeposition is a method for coating metal electrodes with a controlled thickness of polymer from a solution containing the monomer (Bard, 1983). Typical monomers are phenols, pyrroles and anilines. The former are electronic conductors under polymerisation conditions and can be used to produce films of thickness 10^2–10^4 Å, up to ten times thicker than for polyphenylene oxide films for which the polymerisation reaction is quickly quenched because the film is insulating (Glarum and Marshall, 1985).

Polymer films generally adhere to electrodes by chemisorption or because they are insoluble in the contacting solution (Murray et al, 1987). The precise experimental conditions used to form the film depend upon the monomer to be electrodeposited. For example polypyrrole tetrafluoroborate coated platinum electrodes can be prepared electrochemically from a solution of 0.05M pyrrole in 0.1M tetra-ethyl-ammonium-tetra-fluoroborate in acetonitrile (Diaz et al, 1981). The films were grown by the electro-oxidation of the monomer at constant potential in the absence of oxygen (fig 2.8). The total charge passed during electrodeposition was monitored to determine the film thickness.

Electrodeposited films, such as the polypyrroles, can be electrochemically driven between the oxidised (conducting) and neutral (insulating) form. The films are stable to this reaction and can be cycled repeatedly without evidence of decomposition, showing that they are electrochemically stable and therefore suitable for immobilizing electroactive

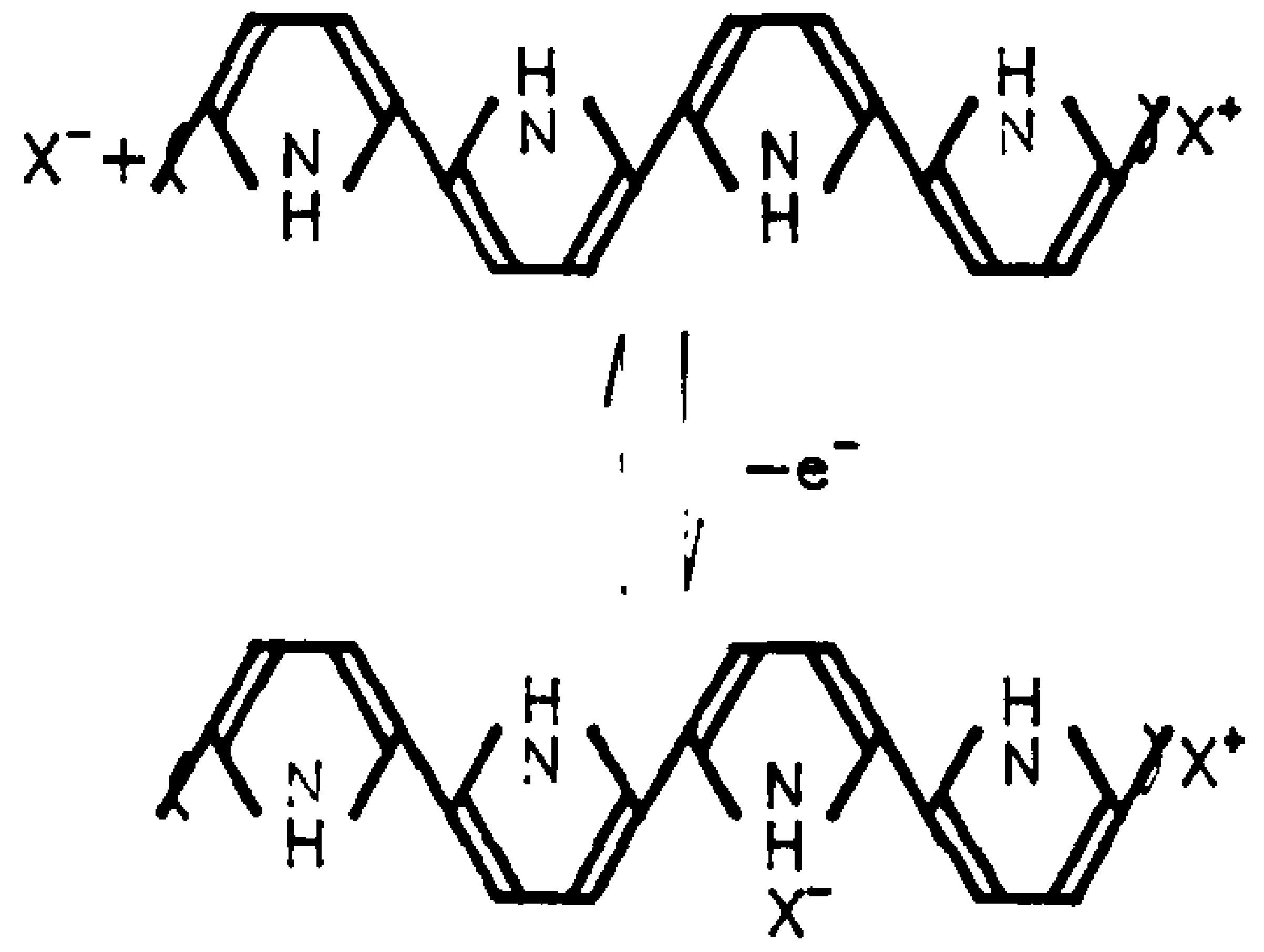

Fig 2.8 Diagram showing the structure of polypyrrole. Elemental analysis of the conducting films has shown that a tetraphyenylborate anion (X) is incorporated in the film for every four pyrrole units. The film is therefore cationic (2) rather than neutral (1). (Diaz, 1981).

species for the development of CME's. Indeed, polypyrrole has been used to immobilize glucose oxidase and phthalocyanines for sensor applications (Murray et al, 1987). However, in such applications the derivative of the polymer must be chosen carefully. This is because the stability of the electro-deposited polymer in air depends on the polymer derivative and its oxidation state. For example, whereas poly-N-methyl- pyrrole and thick, partially oxidized polypyrrole, are stable in air, thin films of polypyrrole are chemically altered by exposure to oxygen, thus rendering the latter unsuitable as an immobilizing matrix.

The density and integrity of the polymeric coating affect the ability of ions in solution to reach the intrinsic or dopant redox sites. For example, polypyrrole films are so densely packed that the redox reaction with ferrocene occurs only at the electrode surface /solution interface. Phenol oxide coated platinum shows no electrochemical reaction with Fe^{3+} ions, although it has a definite pH response. This shows that the film is porous to protons but not to the larger Fe^{3+} ions (Cheek et al, 1983). Indeed, electrodeposited films have been used to preconcentrate species at an electrode using the principle of membrane permeability (Murray et al 1987; Bard ,1983). Electroactive films can also be employed as electrocatalysts, for example polypyrrole has been used to enhance the oxidation rate of ascorbic acid.

2.3 Conclusions

2.3.1 Sample preparation

In terms of ease of preparation, adsorption is the simplest technique. Solvent casting and electrodeposition are also straight forward, whereas covalent binding requires at least two steps (Murray et al,1987). However, if a very thin coating is required, then covalent attachment would be the preferred technique, although control over film thickness is greatest for the electrodeposited films.

The electroactivity of the electrode coating is obviously an inherent property of the coating material. In the case of coatings formed by adsorption or covalent attachment, the bound molecules must exhibit both the desired electroactivity and binding properties, whereas electrodeposited and solvent cast polymers may be doped with the electroactive species. Of the two, solvent cast films are perhaps the most versatile, as the polymer film can be altered easily to optimize the properties of the coating to suit the required application ($2.2.3).

2.3.2 Properties

2.3.2.1 Uniformity of Coverage and Order within the Film

The uniformity of electrode coverage and the degree of molecular orientation can be high for both adsorbed and covalently bound electrode coatings. For example, evidence for ordering and high monolayer coverage for adsorbed films on gold electrodes, has been presented by Rubinstein et al (1987). However, uniformity of coverage depends on the species being immobilized. Indeed, Appleqvist (1985) and Flanagan and Pantell (1984) have shown that the adsorbed coating thickness can range from one to several monolayers.

For the techniques of electrodeposition and solvent casting, the active sites are randomly oriented with respect to one another, whilst being distributed homogeneously within the immobilizing layer. No preferred orientation can therefore be conferred using either of the polymer matrix based immobilization techniques.

2.3.2.2 Site Accessibility and Reactivity

As adsorbed or covalently bound coatings do not exceed more than a few monolayers, the active sites are readily accessible to substrate molecules (Bard, 1983). However, it is still necessary to optimize the orientation of the adsorbed or covalently bound species in order to maximize the reactivity of the surface sites.

For thicker films such as the solvent cast films, the porosity of the coating limits site access (Oyama and Anson, 1980). In addition, the polymer environment may reduce the activity of the bound molecules (Berezin, 1976; Pye and Chance, 1976). Thus, although the three dimensional structure of the thicker polymer films provides a greater number of active sites than the essentially two dimensional structure of the thinner films, the effective electroactivity of the coatings may not be significantly different (Fujihara and Poositisak, 1986(a,b)).

2.3.2.3 Mechanical/Chemical Stability

The chemical and mechanical stability is highest for the solvent cast and electrodeposited polymer films. Covalently bound films are chemically stable, but being only a few molecules thick, are more vulnerable to pin holes (Murray et al, 1987). Long term stability of adsorbed films is poor (Collman et al, 1980; Cass et al, 1984).

2.3.3 Problems/Future Developments

In the case of CME's, drift in the electrode potential with respect to a reference electrode can complicate analytical measurements. The use of a coating doped with redox species has been suggested as a means of stabilising the redox potential of the electrode ($ 2.2.3). Such a coating could be formed using electrodeposition, alternatively LB immobilisation of a redox film (Chapter 3) may be a possibility, although, to increase CME lifetime, the use of thicker membranes is suggested (LeBlanc and Grubb, 1976).

The drift in electrode potential with time is also a problem in ion selective field effect transistor (ISFET) development. Indeed, a better understanding of the factors affecting the stability of the voltage response of ISFET's is needed to improve their performance in the measurement of physiological samples such as blood. This requires an investigation of ISFET response to the individual species found in physiological samples and the effects of gate hydration on the initial response of the device (Sibbald et al, 1983; Arnold and Meyerhoff, 1984).

In terms of the limitations imposed by existing coating techniques in the fabrication of modified electrodes for specific applications, electro-catalytic electrodes could be improved by using a more stable thin film immobilisation technique than that offered by adsorption. Ideally, such a technique would orientate the catalytic sites to maximize their accessibility and reactivity with species in the electrolyte. Covalent immobilisation or the Langmuir Blodgett (LB) Technique could provide a suitable means of achieving this. Furthermore, the future development of enzyme sensors requires an immobilisation technique which can trap the enzyme at the electrode surface with the correct orientation to permit direct electron transfer from the enzyme to the electrode (Zaba and Bone; 1985). Immunosensors which use surface plasmon resonance to detect antibody-antigen binding could also benefit from a technique which can immobilize the antibody in an ordered layer.

In chapter 3, the feasibility of using the Langmuir Blodgett technique in the development of these electrode applications will be discussed.

3.0 Langmuir Blodgett Films (LB Films)

3.1 Introduction

Over the past two decades there has been a steady growth of interest in Langmuir Blodgett (LB) technology. Indeed, recently there have been three International Conferences devoted to the subject (Thin Solid Films numbers 68,99,131-133). For reviews of the field the reader is referred to Peterson and Girling, (1985); Roberts, (1985); Mobius and Bucher, (1972) and Agarwal (1975(a,b); Roberts, 1990).

The Langmuir Blodgett technique is a well established method for the controlled coating of solid substrates with ordered multilayer films. The technique involves spreading a monolayer of surfactant molecules at an air/water interface, compressing the monolayer and then transferring it to a solid substrate (Peterson and Girling, 1985).

Current interests can be summarised as research into the synthesis of new compounds for use as LB films, the characterisation of the floating monolayer and the transferred film and finally, device applications.

LB films have already shown potential in technologies such as optics (eg Peterson and Girling, 1985; Barnes and Sambles, 1986) and semiconductors (eg Fung and Larkins, 1985; Roberts et al, 1985), where the films are used in an environment protected from moisture and mechanical damage ($ 3.5).

LB films have also been employed in more demanding applications such as electrocatalysis (eg Fujihira and Poosittisak, 1986(a,b)), photoelectrochemistry (eg Fujihira et al, 1985a; Gaines et al, 1978), and sensor development (eg Holcroft and Roberts, 1987; Morizumii et al, 1987). Although many of these uses require the film to be stable in an aqueous environment, there is a shortage of information on the characterisation of LB films in such a medium. The main concern of the present work then, is the characterisation of LB films in an aqueous environment and consequently the LB deposition technique is the major electrode coating method employed.

3.2 Monolayer forming materials

Molecules suitable for LB film deposition are generally amphipathic ie they must possess a hydrophobic group which renders them insoluble in water and a hydrophilic group to facilitate orientation of the molecules at the air/water interface. Such materials are found within the discrete amphiphilic molecules such as the fatty acids, some polymeric molecules, for example the polydiacetylenes (eg Lieser et al, 1980; Sarkar and Lando, 1983; fig 3.1a) and aromatic macrocycles eg porphyrins and phthalocyanines (eg Roberts et al, 1985) (fig 3.1b). Molecules from these groups can be used as the foundation for designing and synthesising new or modified compounds with improved film forming properties and/or characteristics for special applications.

For example, Kakimoto et al, (1987) and Uekita et al (1987) have reported the synthesis of polyimide derivatives suitable for use as LB films (fig 3.2 a). The high mechanical and thermal stability of these compounds make them more suited for use in microelectronics than conventional materials such as long-chain fatty acids and polymerised, unsaturated fatty acids.

Fujihira et al,(1985a) have synthesised surfactant molecules with viologen, pyrene and ferrocene moieties to act as acceptor, spacer and donor elements in the development of an LB film photodiode ($ 3.5.2). A triad molecule incorporating all three functional units was also synthesised in order to overcome the difficulties encountered in aligning the moieties of three discrete elements.

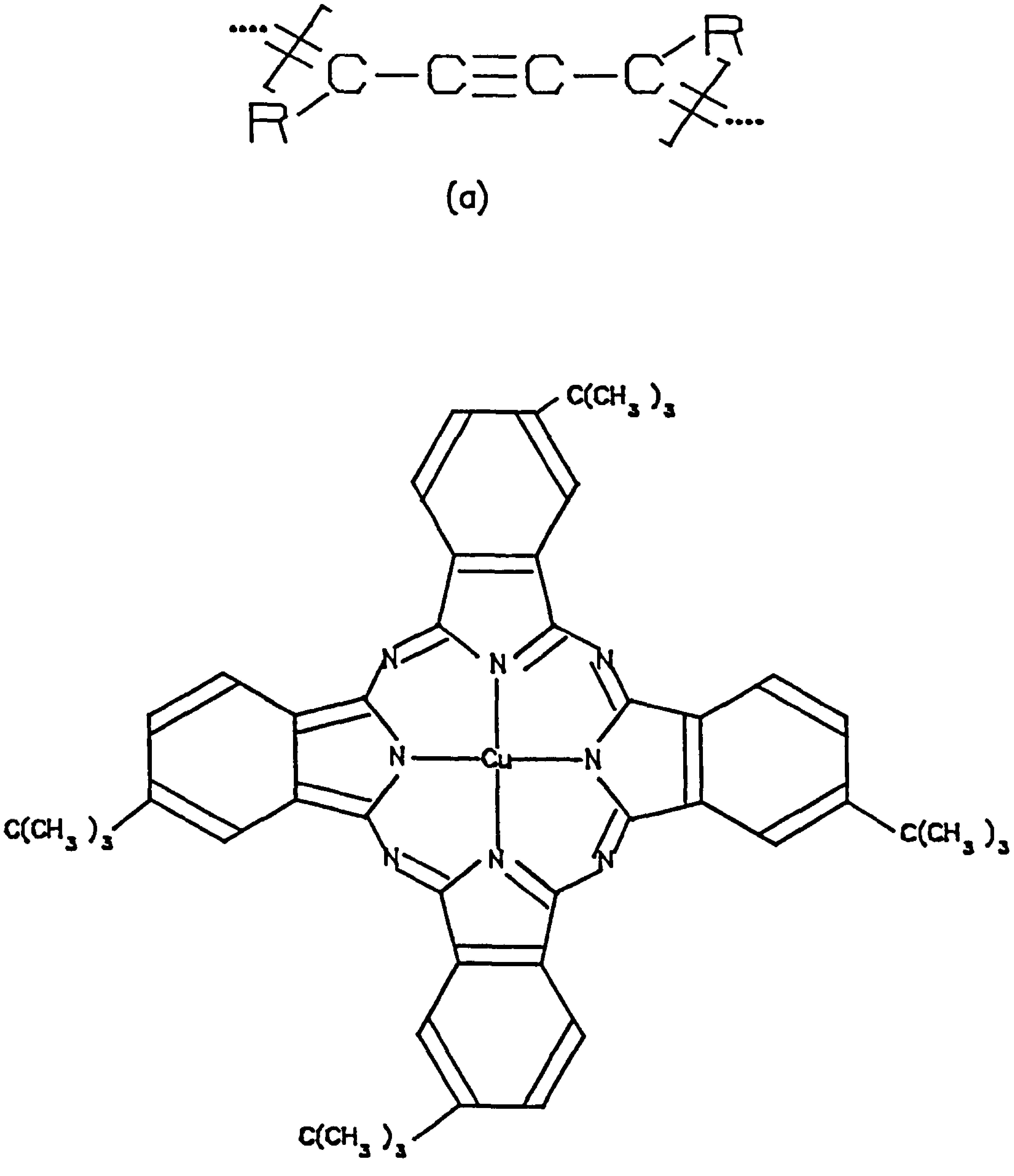

Fig 3.1 (a) The repeat unit for diacetylenes. (Lieser et al. 1980)

(b) The structure of tert-tert-butyl copper phthalocyanine (Roberts et al, 1985).

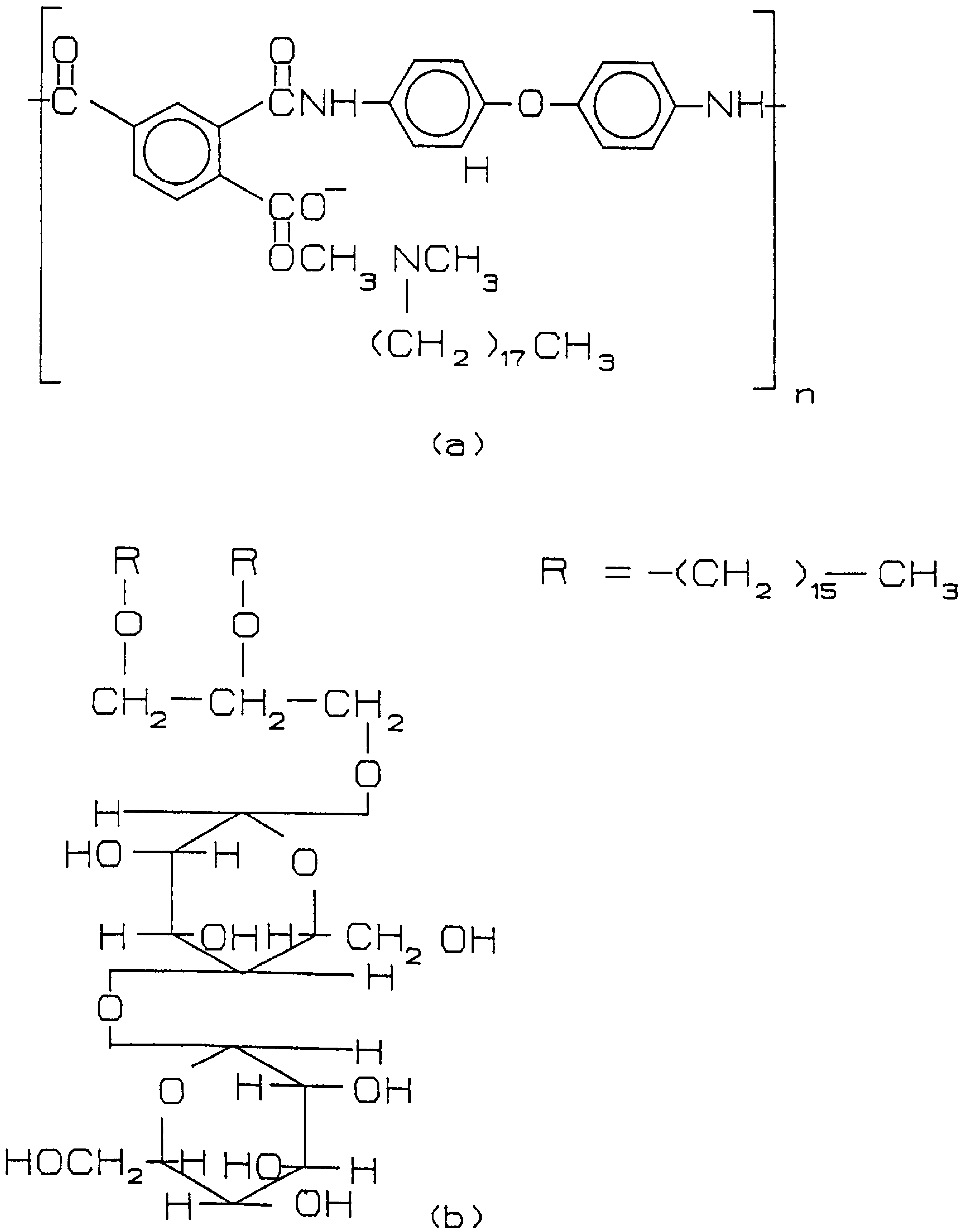

Fig 3.2

(a) The repeat unit of polyamide-amic acid - (Kakimoto et al, 1987)

(b) The chemical structure of β-2,3-dihexadecyloxyprolpylglucoside. (Heckmann et al, 1983).

In the development of hyperfiltration membranes, Heckmann et al, (1983) prepared surfactants by the addition of glucose, maltose or cellobiose residues (hydrophilic head group) to straight chain hydrocarbons (hydrophobic tail). Such compounds, eg the synthesised glucoside, β-2,3-di-hexa-decyl-oxy-propyl-glucoside, were modelled on natural lipoids to give improved throughput of liquid and reduced water retention compared with existing membranes (fig 3.2 b).

An alternative technique for obtaining monolayers with specific properties is to form a mixed monolayer of the surfactant and dopant material. For example, this procedure has been employed to create dye sensitised (eg Polymeropoulos et al, 1980; Fujihira et al, 1985b) and electrocatalytic LB films (eg Fujihira and Poositisak, 1986(a,b)) and also in enzyme sensor development (eg Morizumii et al, 1987).

3.3 Monolayer spreading and characterisation

A monolayer of surface active molecules is produced by spreading a solution of the compound, dissolved in a suitable solvent, on the surface of purified water. The monolayer is confined by a movable barrier and the surface pressure is monitored using a film balance. By adjusting the barrier position, the spread monolayer can be compressed or expanded while the resulting pressure changes are monitored to produce a pressure-area (π-A) isotherm (fig 3.3).

The π-A isotherm provides important information on molecular areas, molecular orientation and packing. In general, the molecular area, from the solid phase region of the π-A curve, is compared to the area predicted from space filling models to verify that the monolayer molecular area and orientation are as expected. For example, to optimize monolayer spreading conditions, Roberts et al (1985), compared the molecular areas calculated from π-A isotherms of phthalocyanine films with the areas predicted from the

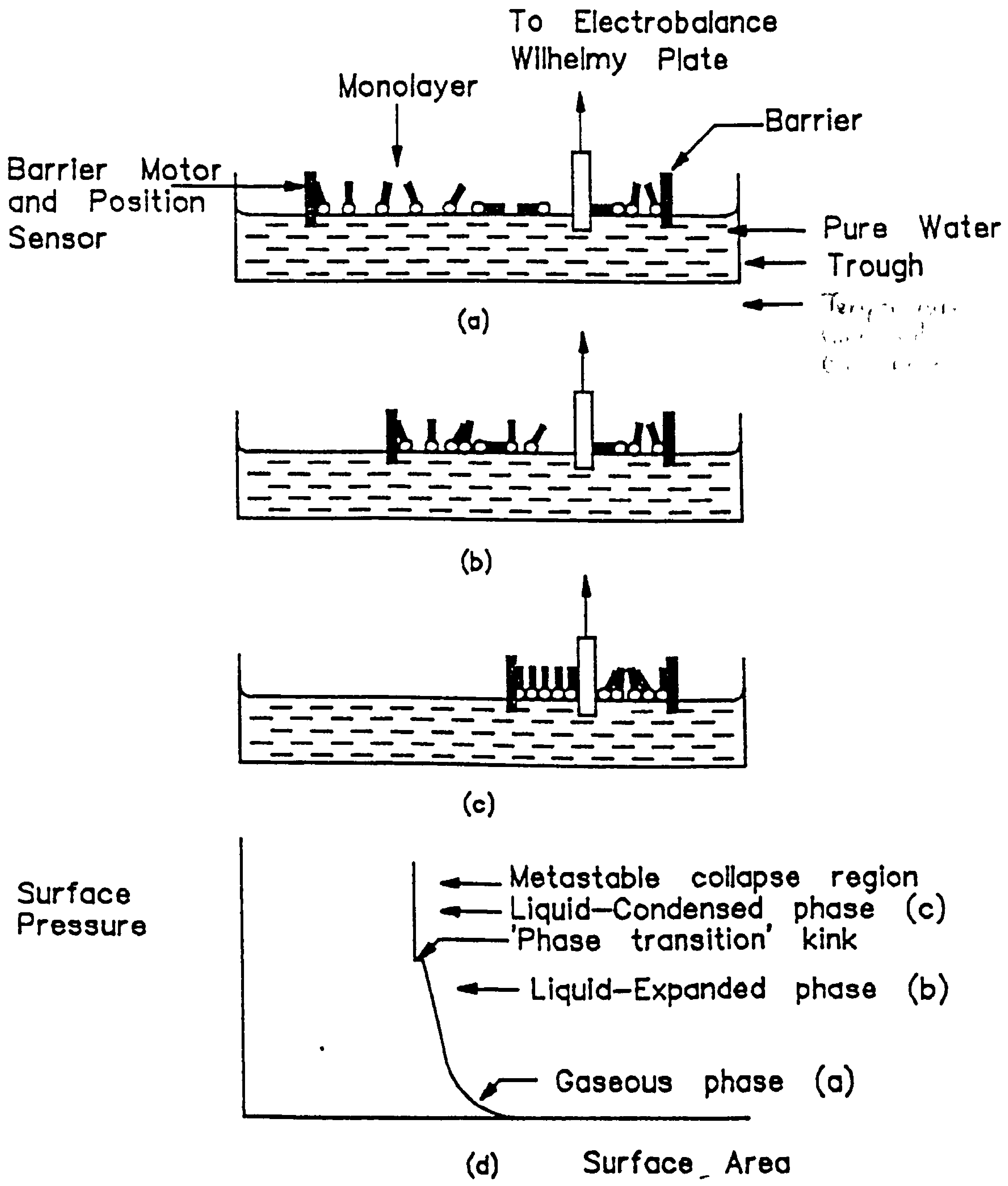

Fig 3.3 Essential features of an LB trough showing schematically, monolayer compression from (a) gas to (b) liquid–expanded to (c) condensed phase. (d) Pressure–Area Characteristic for a fatty–acid.

molecular structure. On this basis, the spreading solvent was chosen for which the resultant monolayer molecular area was closest to the theoretical value. For this to be so, meant that aggregation of the phthalocyanine molecules had been minimized to produce a high quality monolayer. In studies of polymeric LB films, π-A curves for polymerised monolayers of vinyl stearate have shown that the polymer produced directly in the monolayer packs more efficiently than solution or bulk solid state polymerised poly(vinyl stearate), spread at the air-water interface (Lando and Fort, 1977). This suggests that the integrity of the multilayer film is greatest when the film is polymerised as a monolayer and then transferred, rather than being transferred prior to polymerization. Hence, preformed or monolayer polymerized films will tend to produce higher quality built up films than can be obtained by polymerizing the transferred film (Hodge et al, 1987).

Finally, in film transfer experiments the π-A isotherm is used to determine the optimum surface pressure at which to carry out deposition. This is usually at a pressure just below the collapse region (Peterson and Girling, 1985). A useful adjunct to the π-A characteristic is the concurrent measurement of surface potential at the air/water interface. Although the exact interpretation of the results is difficult, surface potential measurement can be used to detect inhomogeneities, discriminate between monolayers of ionised and uncharged molecules and to monitor changes in the monolayer due to phase transitions or chemical reactions, including polymerisation (Mobius and Bucher, 1972; Lando and Fort, 1977).

More detailed information on monolayer structure can be obtained by measuring monolayer absorption and fluorescence (Peterson and Girling, 1985). For example, Losche et al, (1984) used fluorescence microscopy to investigate the influence of surface pressure and subphase conditions on the domain structure of phospholipid monolayers. Using this technique they were able to show that two distinct phases (0.20nm/chain and 0.24nm/chain) co-exist which appear to correspond to the gel and liquid crystal phases of lipid bilayers, although the actual crystal shapes were not definable in these terms (Peterson and Girling, 1985). The influence of temperature and electrical field effects on the domain size and organisation of phospholipid monolayers has also been studied using this technique. Furthermore, it has been shown that it may be possible to manipulate single domains using an external field (Heckl and Mowhald, 1987) which could assist in the production of high quality films.

Detailed structural information, such as molecular packing, can be obtained by X-ray diffraction, reflection and ellipsometry. For example, Kjaer et al, (1987) used X-ray diffraction to measure the d spacing for the phospholipid, di-myristoyl phosphatidic acid. A value of 0.416nm was obtained for the d spacing and bond orientational ordering was found to exceed 4nm at pressures close to the liquid/solid phase transition point. This suggests that molecular long range ordering does not occur at normal monolayer pressures. Ellipsometry has been used to obtain values for the refractive index and thickness of monolayer films. For example, Ducharme et al, (1987) have studied several phosphatidylcholines using this technique. They report values of 1.50 and 1.44 for the refractive index and 1.8nm and 1.44nm for the monolayer thickness of distearoyl phosphatidylcholine (DSPC) and dipalmitoyl phosphatidylcholine (DPPC) respectively. The results also indicate that the DSPC molecules are more upright than those of DPPC.

3.4 Film transfer and characterisation of "built up layers"

3.4.1 Film transfer

For device applications, Langmuir films must be transferred to a solid support. This is achieved by passing a suitable substrate through the film in a controlled manner. Typical substrate materials include quartz, silicon, germanium and glass. The latter is often coated by vapour deposition with a layer of aluminium, gold, silver or tin oxide. The speed at which the substrate is passed through the monolayer must not be too high or the transferring monolayer will not drain correctly, resulting in very patchy deposition. Veale et al (1985) has suggested that the maximum drainage speed is actually related to molecular mobility within the monolayer. Dipping speeds of up to 24mm/s and 18mm/s respectively have been used for fatty acids and w-tricosenoic acid on a pure water subphase although values of around 0.1mm/s are more typical. This speed is reduced markedly by the presence of small amounts of metal cations such as Fe^{3+} and Al^{3+} (Peterson and Girling, 1985). Consequently, a high degree of cleanliness is essential for the production of LB films.

For successful transfer, in addition to using the correct deposition speed, the angle between the deposition direction and the meniscus at the monolayer/substrate interface must be obtuse (fig 3.4). Consequently, a hydrophobic substrate will generally pick up a monolayer on immersion whereas a hydrophilic substrate will pick up its first monolayer on withdrawal. However, the actual type of film transfer is affected by subphase conditions including pH, salt concentration, impurities etc, as well as by the substrate (eg Hasmonay et al, 1980). The different types of layer deposition include X deposition (ie deposition on immersion only), Y deposition (ie deposition on dipping and withdrawal) and Z deposition (ie deposition on withdrawal only) (fig 3.4) (Mobius and Bucher, 1972).

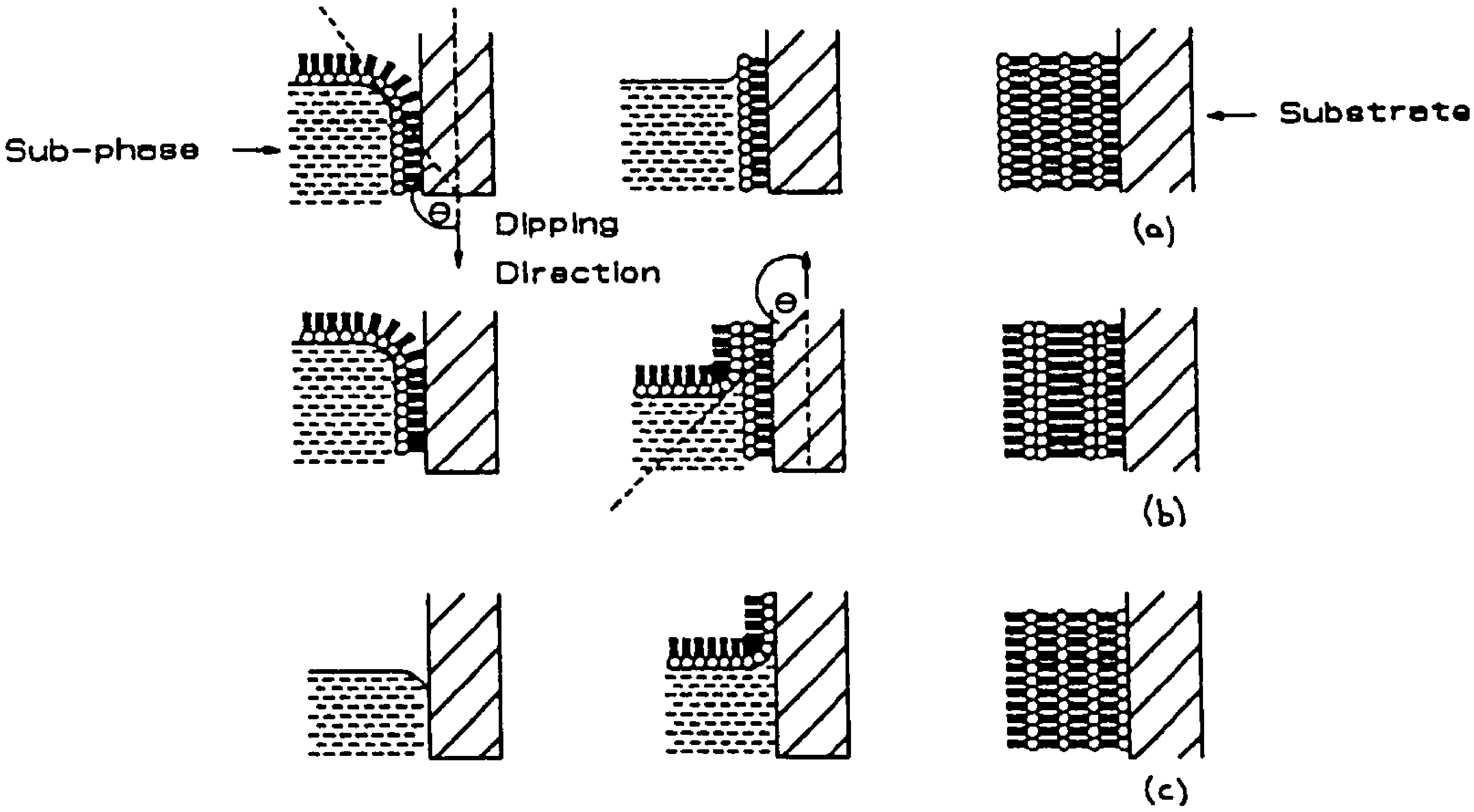

Fig 3.4 Schematic representation of the types of monolayer deposition and the resulting multilayer structure. The angle θ must be obtuse for deposition to occur. (a) X-deposition, (b) Y-deposition, (c) Z-deposition. The fatty acid molecules are represented by ▬o where o is the hydrophilic carboxyl group and ▬ is the hydrophobic, hydrocarbon chain. (Mobius, 1972).

In order to obtain a rough quantitative estimate for the area of film transferred during deposition, the deposition ratio, DR, is calculated (Hasmonay et al, 1980). DR is defined as the change in film area due to transfer, divided by the area of substrate passed through the monolayer. A deposition ratio of unity indicates good deposition although figures in the range 1.00±0.10 are usually acceptable. In practice it is not always possible to obtain an accurate value for DR because the true surface area and/or amount of film transferred can be difficult to measure precisely, particularly for small area substrates.

3.4.2 The structure and stability of multilayer LB films

The ideal for a "built up" LB film is a regularly ordered, stable, defect free, multilayer structure. For some device applications the ability to immobilize molecules reliably, in an ordered manner, is also an important criterion ($ 2). Although this ideal is not realised in practice, various film forming compounds approach it within certain constraints, such as a limited film area (eg for individual crystal domains).

A range of independent experiments have confirmed that the layer model, (fig 3.4) is valid for several classes of compound. For example, the thickness of fatty acid films measured using X-rays (Brundle et al, 79), surface plasmon resonance (Brown et al, 1983) and optical methods, has been found to increase linearly with the number of deposited monolayers as does the reciprocal capacitance (eg Roberts et al, 1978). In addition, shallow angle X-ray diffraction measurements have confirmed the alternating head-to-head, tail-to-tail arrangement of lipid molecules. However, LB films of the polymers and aromatic macrocycles do not demonstrate such a well defined layer structure (Peterson and Girling, 1985).

Another important criterion is the stability of the multilayer structure. Using X-ray diffraction, Langmuir (1938) discovered that several compounds reorder during or soon after deposition. For example, he found that X-type stearate films overturn to form a Y-type arrangement. More recently, Kopp et al, (1974) made a detailed study of the stability of barium stearate, cadmium arachidate and tripalmitin using electron microscopy and attenuated total reflection infrared spectroscopy. This work showed that the stability of the transferred layers depends on the monolayer and substrate material, the number of layers deposited and upon storage conditions. For example, although the first monolayer of barium stearate was shown to deposit homogeneously onto carbon and germanium, a 3 or 5 layer film on germanium developed marked inhomogeneities such as patches and islands. On carbon, a continuous process of transformations resulted in small aggregates and holes which eventually formed small flat islands. Furthermore, films of 2 and 4 layers, stored submerged in the subphase showed crystalline regions after 4 hours. Films of cadmium arachidate were found to rearrange more slowly than barium stearate films, with the resulting irregularities consisting of pores and small holes. This work also confirmed earlier microscopic and X-ray diffraction studies which indicated that the light scattering centres formed within a few weeks in multilayers of cadmium-arachidate/arachidic acid were holes or cracks running through the system (Mobius and Bucher, 1972).

The problems encountered with the production of high quality LB multilayers2~~light~~ using monomeric materials has led to great interest in polymerisable LB films as they have potential for producing more robust and stable films. However, the fabrication of high quality LB films using polymers has proved difficult. For example, Sarkar and Lando, (1983) carried out Infra Red Spectroscopy and Electron Diffraction experiments to investigate the effects of polymerisation on diacetylene multilayer films. Their results show that a phase transition, accompanied by a tilting of the side chains occurs. This implies that the correct orientation of co-immobilized species in a diacetylene film would be very difficult to achieve. In the case of the acid diacetylene, C_{10}-C_2-acid, cracks formed in multilayer films which were attributed to the large volume change on polymerisation. The volume change for the acid is approximately double that of the corresponding alcohol derivative. No cracks were observed in the case of the alcohol derivative film.

Lyall and Batchelder, (1985) employed Resonance Raman Spectroscopy to study the vibrational modes of the cadmium salt of the diacetylene, 10,12-pentacosadiynoic acid (PCDA), after polymerisation using ultra violet light. The low absorbtion coefficient for polarised light indicated that the polymer backbones were randomly oriented within different domains, whilst the large value of line width, compared to a single crystal of the polydiacetylene, showed that there were structural defects within the multilayer.

Such investigations yield important information on the film structure, including the effects of the polymerisation reaction and confirm that compounds, for which the volume change on polymerisation is low, should be used to minimize the defect level in the resultant multilayer film.

Information on LB film defects are also provided by the electrical characterisation of monolayers using a metal-monolayer-metal arrangement. Initially it was thought that the monolayer films were defect free and that conduction was due to electron tunnelling (eg Agarwal, 1975a). However, it is now believed that an extrinsic conduction mechanism is responsible for the current-voltage characteristic ($\log J \alpha V^{1/4}$). The presence of defects in the LB film, through which the upper metallisation diffuses, may explain this response (Peterson and Girling, 1985).

Optical techniques, which involve boosting the visible-light anisotropy of a film to the point where it can be observed using a polarizing microscope, have recently been used to investigate the large scale structure of transferred films. Results indicate that there are crystallite regions of uniform orientation, bounded by areas of finite width, with their own distinct orientation. The boundaries never cross, indicating that the crystalline structure is determined by the first layer (Peterson and Girling, 1985). It may well be that in the monolayer conductance experiments, the crystallite boundaries were the regions along which the metallisation diffused. It has also been found that the size of the crystallites is very dependent on the experimental conditions used to prepare the monolayer at the air/water interface. For example, electron diffraction and polarised light microscopy have shown that multilayers of 22-tricosenoic acid, deposited at speeds of up to 18mm/s, have better crystalline order than those deposited conventionally.

Film structure has been further assessed using transmission electron, X-ray and neutron diffraction. Transmission electron diffraction (TED) has been used to investigate electron interactions and has shown, for example, (Peterson, 1983) that there is a small amount of twinning in the orthorhombic packing of sub-cells in 21 layers of w-tricosenoic acid. Neutron diffraction has been employed to obtain data on lattice spacings, eg for fully deuterated cadmium arachidate on glass, a value of 2.56nm was measured (Highfield et al, 1983).

3.5 Applications

LB films have been used in a wide range of technologies including optics, semiconductors, microlithography, electrocatalysis, photochemistry and sensors; a brief account of which is presented below.

3.5.1 Optics

In optics, LB films have been used as passive waveguides (Peterson and Girling, 1985) where the technique provides closer control over dimensional and optical parameters than the existing method of evaporation. However, the optical attenuation of the LB films is such that they offer no significant advantage over the more robust evaporated films. The current emphasis is therefore on the production of higher quality films with lower attenuation (eg Carr et al, 1987). The use of LB films for active, non-linear signal processing (eg Swalen, 1987; Kajzar et al, 1987; Ledoux et al, 1987; Richardson et al, 1987) is also under investigation, where their hyperpolarizabilities are up to two orders of magnitude greater than the inorganic materials normally used (Peterson and Girling, 1985).

3.5.2 Semiconductors

Semiconductor applications of LB films include their use as gate insulators in silicon, indium phosphide and cadmium telluride devices and devices for gas sensing. A GaAs bistable switch and an electroluminescent MIS ZnSeS diode have also been reported (eg Fung and Larkins, 1985; Roberts, 1985).

As a method of improving the quality of the gate insulator, the LB film is thought to seal off any defects in the oxide layer (Peterson and Girling, 1985). Indeed, in the case of silicon oxide, a single monolayer has been observed to double the gate electrical breakdown strength. LB films have even been used to replace the oxide gate insulator. For example, Fung and Larkins (1985) used a 10 layer LB film of 16-8- poly(diacetylene) as the gate insulator for silicon insulated gate field effect transistors (IGFET's) (fig 3.5). The fabrication technique was compatible with conventional planar IC technology. The mechanical and chemical strength of the film was evidenced by an observation made during the IGFET fabrication process that the LB film was much more resistant to plasma ashing than the thicker photoresist. The drain current-voltage (I-V) characteristics were comparable to conventional IGFET's with thermal SiO_2 as the gate insulator although the curves were observed to drift upwards, before saturating after 15-20 minutes. The initial instability was attributed to cation drift or charge injection under the influence of the high gate field. It was suggested that the LB coating technique outlined in this work could

$$C_{16}H_{33}C-C\equiv C\equiv C_{8}H_{16}-COOH$$

(a)

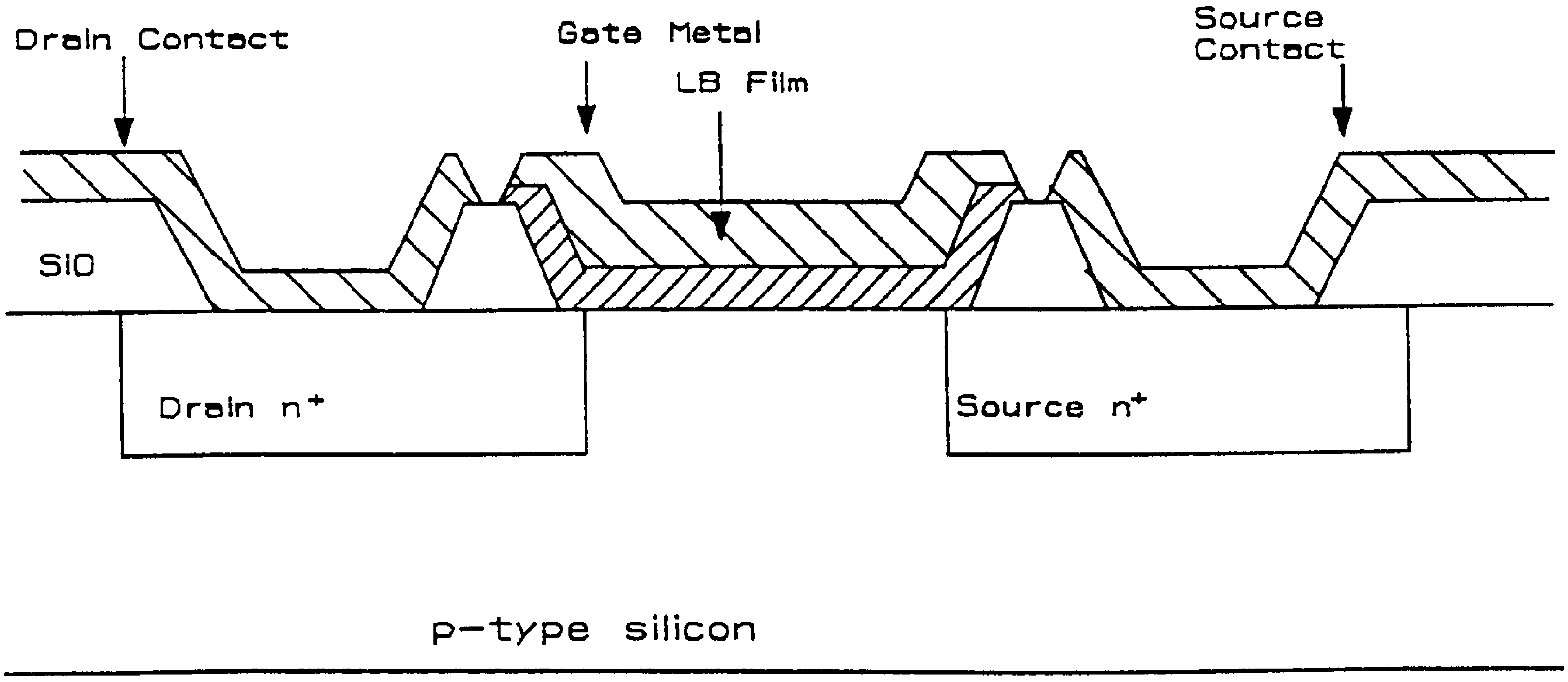

(b)

Fig 3.5

(a) 16-8 poly(diacetylene) used as the gate insulator

(b) A cross-sectional view of the IGFET with the LB film gate insulator

(Fung and Larkins, 1985)

be employed in the development of ISFET's. However, for practical devices, the active LB layer would have to be deposited on a passivating layer such as silicon nitride to eliminate the problems of cation drift (Janata, 1987).

3.5.3 High Resolution Microlithographical Photoresists

Another application that has received considerable attention is the development of high resolution microlithographical photoresists. The desire to produce higher levels of integration means that increased resolution is required. The dynamics of electron scattering mean that this necessitates the use of thinner resist coatings. Therefore, the ability to deposit ultra-thin electron sensitive materials using the LB technique offers significant advantages over existing spin coating techniques (Peterson and Girling, 1985). Promising materials include polymerisable amphiphiles (Boothroyd et al, 1985; Delaney et al, 1985) and 22-tricosenoic acid (Barraud et al, 1980; Peterson and Russel, 1985).

3.5.4 Electrocatalytic electrodes

In spite of efforts to synthesize species capable of performing H_2 and O_2 electrochemistry at inexpensive electrodes for the development of novel fuel cells, noble metals such as platinum still offer the highest and most stable catalytic activity.

In order to capitalize on the catalytic properties of platinum, Fujihira and Poosittisak, (1986) incorporated platinum as the counterion in a LB monolayer of EPADOV (ie N-ethyl-N'-[3-propylamido-N",n"di(n- octadecyl)]-4, 4'bipyridinium dibromide) (fig 3.6). A platinum loading of ca 2.6×10^{-10} mol cm^{-2} dip^{-1} was calculated from the area of the surface wave during the reduction of $PtCl_6^{2-}$ to metallic Pt, for dips ranging from one to eight. From the adsorbed hydrogen and oxygen wave/photocurrents, it was estimated that at least one third of the platinum was active. Furthermore, the high

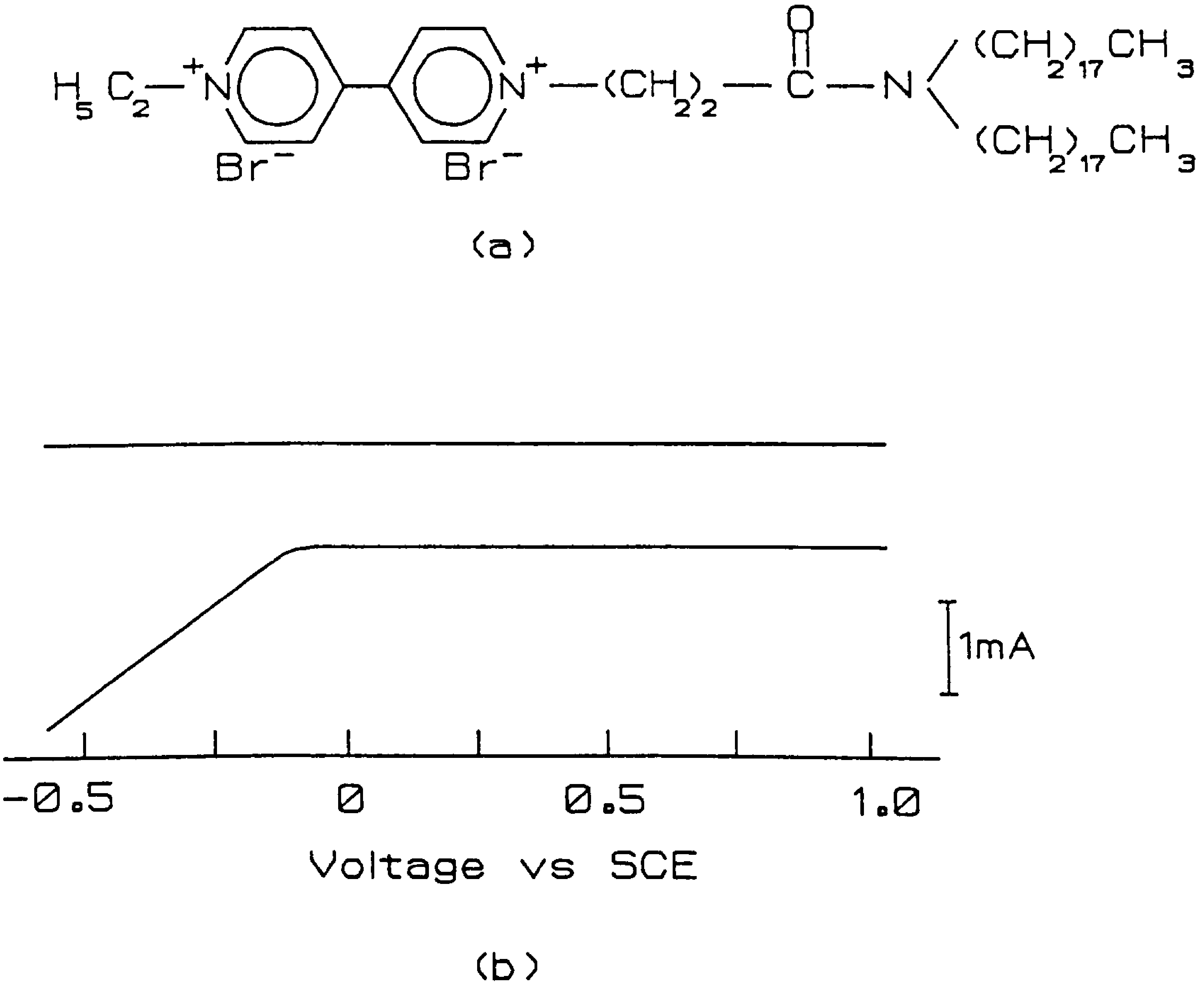

Fig 3.6

(a) EPADOV

(b) Current-potential curves for hydrogen evolution in 1M H_2SO_4. The upper trace is for an unmodified GC electrode. The lower trace is for the the GC electrode modified by an 8 dip coating of EPADOV film containing $PtCl_6^{2-}$. The paramters employed for the rotating disc voltammetry were a rotation velocity of 3600 rpm, a scan rate of $50mVs^{-1}$ with an electrode area of $0.064cm^2$. (Fujihara and Poosittisak, 1986) overpotential for hydrogen evolution on a glassy carbon electrode was reduced by 0.7 volts, whilst the current was doubled for oxygen reduction even by this low level of platinum loading. The results for the electrochemical reduction of oxygen to water also showed that the reaction was not limited by mass transfer of oxygen through the film. It was suggested that the platinum was immobilized on the electrode surface as adsorbed atoms, amorphous clusters or colloidal, ultrafine particles, of diameter less than 4nm. Similar results were obtained for platinum immobilised in films of DODAC (dioctadecyl-dimethyl-ammonium chloride).

Although no information is presented concerning the stability of the electrode response, this work by Fujihira and Poositisak (1986(a,b)) has shown that the LB technique may provide an important method for immobilizing ultrafine particles of various catalysts at an electrode surface. The ability to minimize and finely control the amount of deposited material, whilst maintaining its activity and accessibility offer important advantages over existing techniques ($ 2). However, it should be noted that no specific spatial orientation of the immobilised species was required for the satisfactory operation of this modified electrode.

The use of LB films to immobilize electroactive species and their correct orientation at the electrode are not synonymous. For example, in immobilisation work with cytochrome c, Yokata et al (1987) found that the electron transfer rate for the cytochrome was less than expected. The discrepancy was attributed to non-ideal orientation of the cytochrome c and to its separation from direct contact with the electrode surface. However, cyclic voltammetric measurements showed that the stability of cytochrome c, immobilised in an LB film at an SnO_2 electrode, is greater than that offered by adsorption.

3.5.5 Photoelectrochemical devices

Interest in solar cell development and photographic science has prompted efforts to sensitize electron transfer at electrode surfaces using immobilized molecules (Fujihira et al, 1985(a,b)). Much of this work has involved the use of surfactant derivatives of ruthenium complexes immobilized on a suitable support, such as gold or tin oxide optically transparent electrodes (OTE's), using the LB technique. Early work by Sprintschnik et al (1977) indicated irradiation of a ruthenium complex derivative could produce hydrogen and oxygen from water (fig 3.7). However, this result was not reproducible. In fact, the properly purified compound was rapidly degraded by ester hydrolysis, resulting in the loss of the ruthenium complex from the electrode surface.

In related studies, Gaines et al (1978), observed that the Ruthenium compound (fig 3.7) undergoes a dark hydrolysis reaction such that ultimately, no surfactant ruthenium complex would remain on the slides, even in the absence of light. In view of the failure of these compounds to catalyze the photodecomposition of water and their instability to hydrolysis, further studies concentrated on hydrolytically stable surfactants.

For example, Fujihira et al (1985b), coated gold and tin oxide, optically transparent electrodes (OTE's) using the surfactant sensitizer $Ru(bpy)_3^{2+}$ (fig 3.8). Dye sensitized photocurrents were observed due to electron transfer from the excited $Ru(bpy)_3^{2+}$ complexes to the conduction band of the OTE. On illumination, the resulting photocurrent decreased gradually after an initial peak. The fall in current with time is attributed to back transfer of electrons, from the electrode to the oxidized complex, rather than loss of the dye. However no detailed information on the long term stability of the electrode response is presented.

In additional studies, Fujihira et al (1985a) constructed an electrochemical

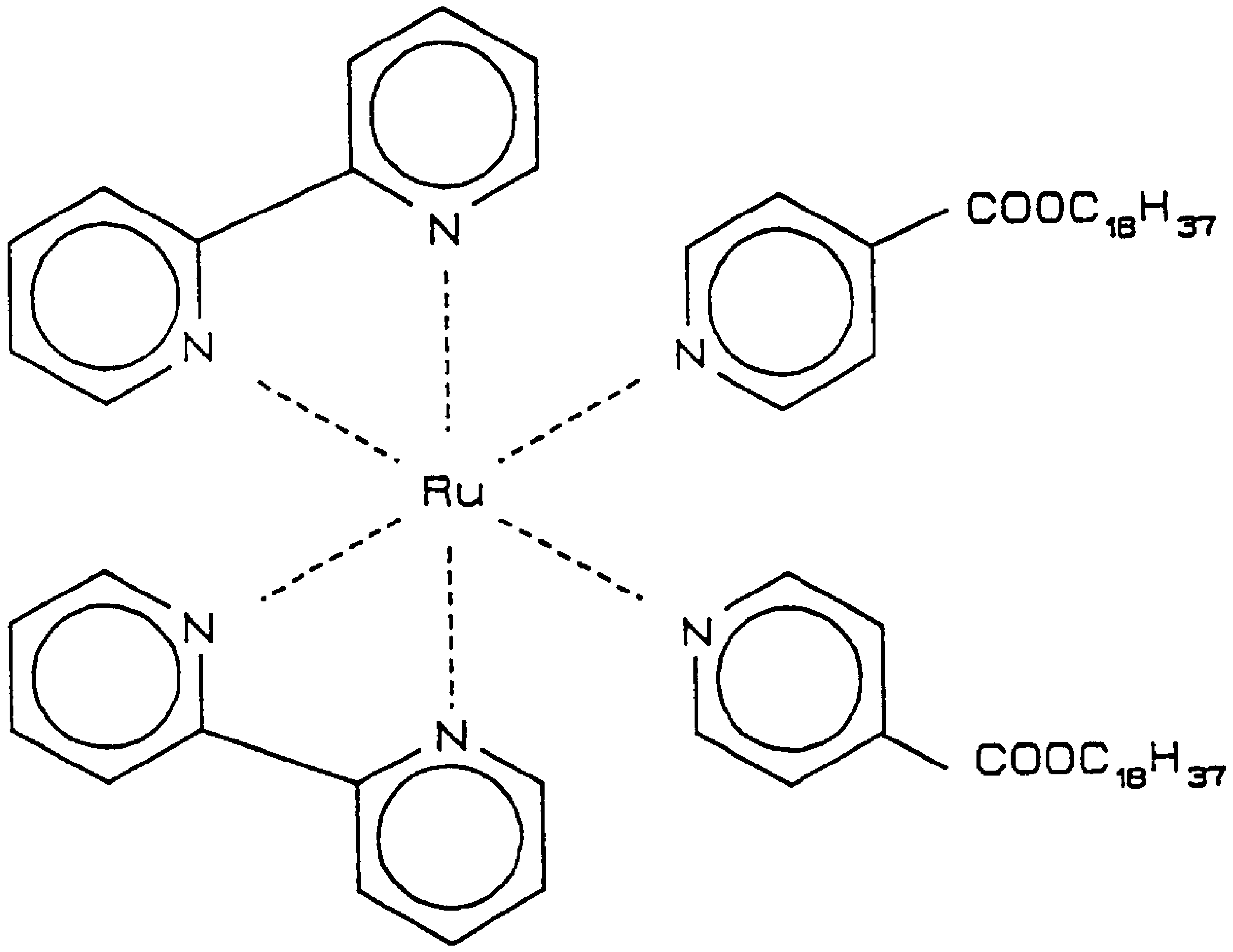

Tris(2,2'-bipyridine)ruthenium(bpy$)_2$ $-Ru^{II}[bpy(COO_{18}H_{37})_2]^{2+}$

Fig 3.7 A ruthenium compound employed in photoelectrochemical studies. (Sprintschnik et al, 1977; Gaines et al, 1978).

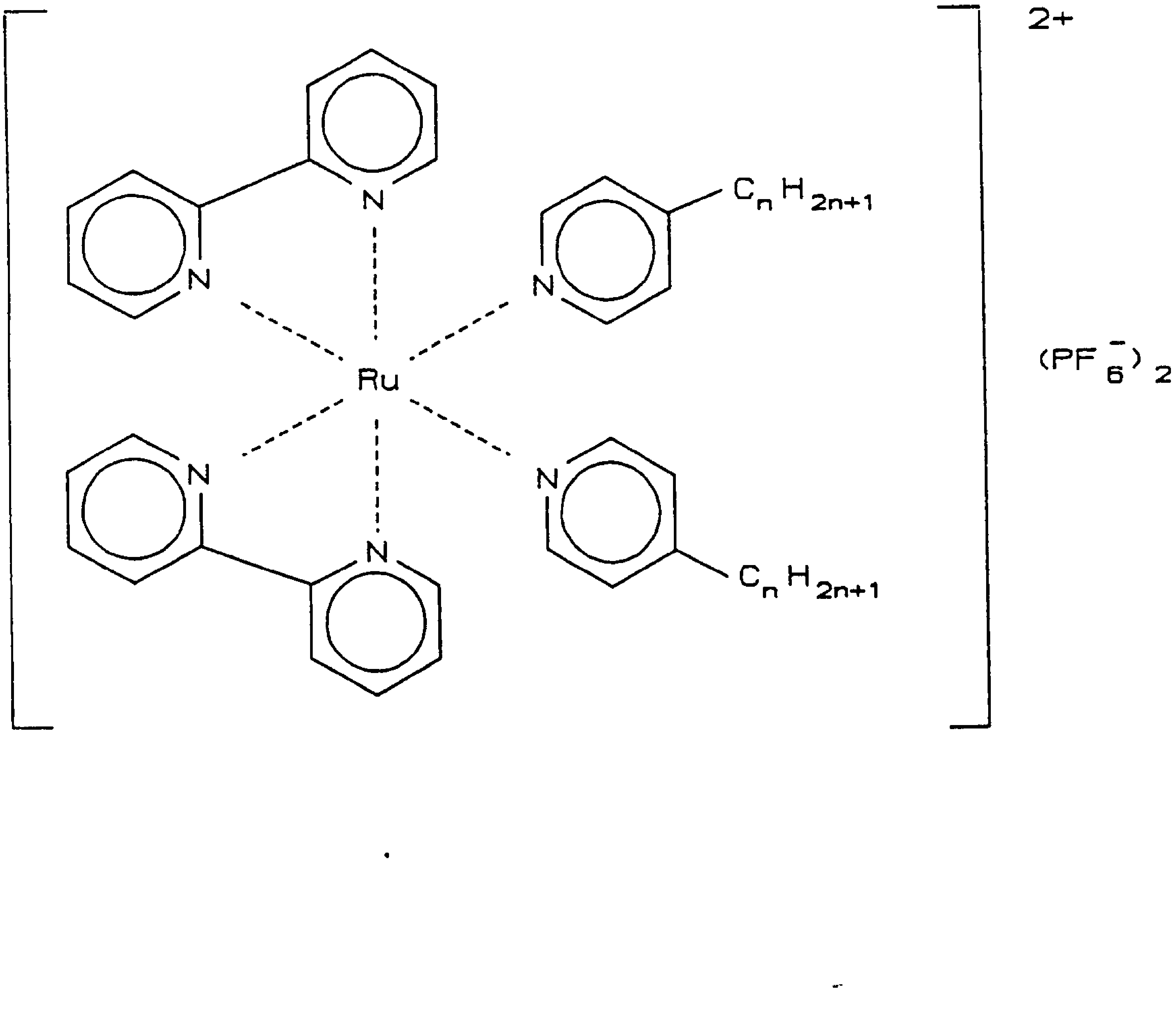

Fig 3.8 Chemical structure of the surfactant derivatives of $Ru(bpy)_3^{2+}$ in the form of PF_6^- salts used as sensitising molecules by Fujihara et al, (1985).

photodiode using special surfactant molecules. In this work, gold OTE's were sensitized using an acceptor (A), spacer (S) and donor (D) arrangement generated by the sequential LB deposition of separate A, S, D moieties (fig 3.9a), or by the deposition of a single triad moiety (fig 3.9 d). The photocurrent for the A/S/D electrode (fig 3.9c) was stable over a period of one hour. The stability of the triad photocurrent response was also reasonable (fig 3.10b). However, the photocurrent for the D/S/A configuration decayed appreciably within ten repetitions of stepped illumination. It is not yet understood why this decay occurred. In both cases, the direction of the photocurrent agreed with that predicted from the energy band diagram for the modified electrode (fig 3.9b). The work also demonstrates that the combination of molecular engineering and LB deposition offer a powerful technique for the development of complex modified electrodes.

Other important compounds employed for photo catalysis include merocyanine dyes. For example, Iriyama et al (1985) synthesised a homologous series of merocyanine dyes, in an attempt to develop a photosynthetic LB film forming pigment with greater chemical stability and photo activity than in-vitro chlorophyll.

3.5.6 Ion selective field effect transistors

Brown (1981) has used LB films of specially synthesized phthalocyanine compounds as the gate sensitizing material in the fabrication of electroactive ISFET gates. However, severe difficulties in encapsulation, poor device yield and low stability were encountered. This work also showed that more complex electrochemical models may be required to describe the behaviour of ISFET structures with ultrathin (<10nm) electroactive gate films. It is of interest to note that the phthalocyanines have been used successfully as the active elements in SAW based gas sensors (Holcroft and Roberts, 1987). When employed in a non-aqueous environment the device stability is no longer a problem.

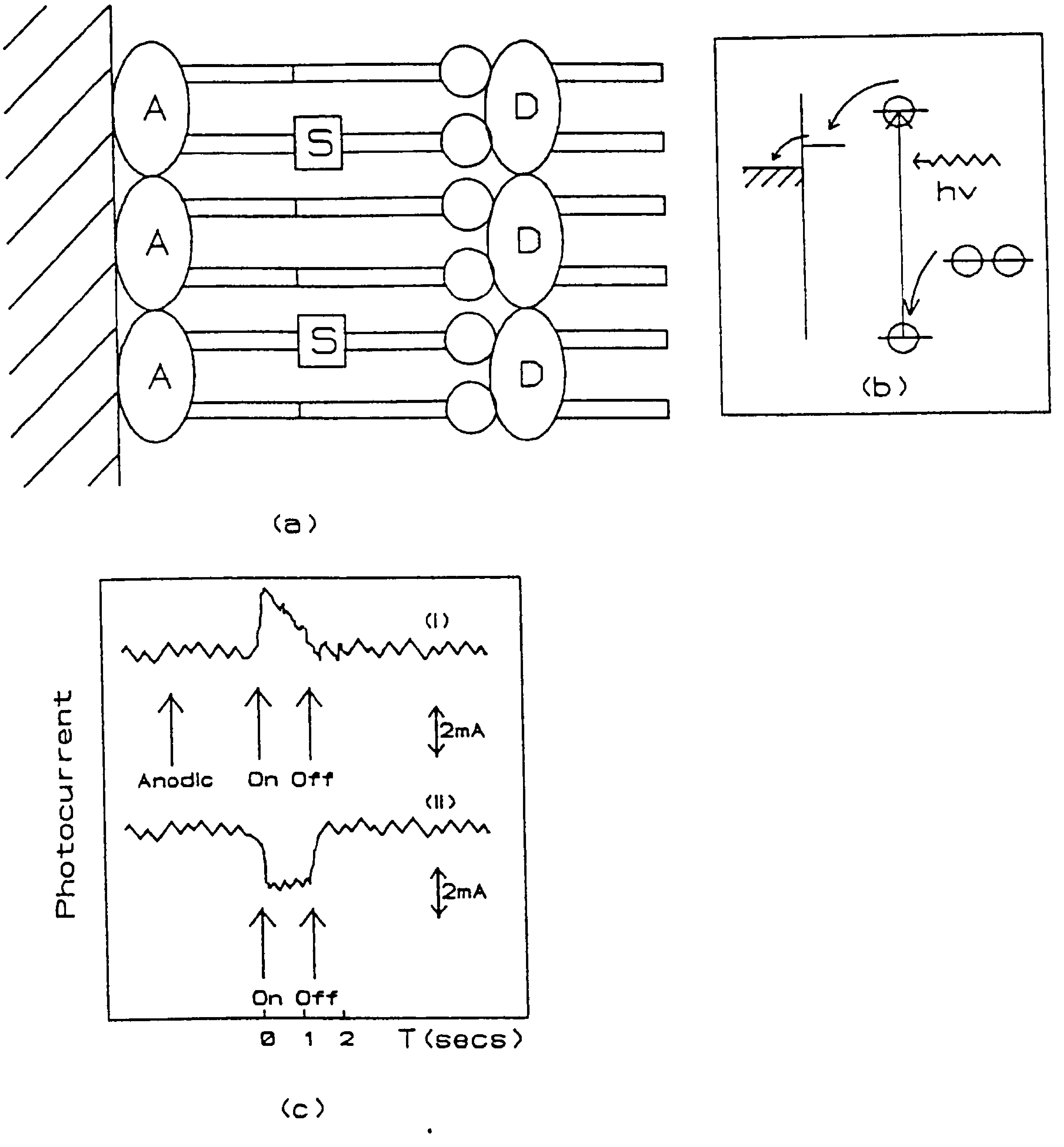

Fig 3.9 (a) Spatial arrangement of A,S and D moieties of functional surfactants in a complex LB film. ○ is the hydrophilic group, □ the hydrophobic functional unit and ▭ the alkyl chain.

(b) Energy diagram for the A/S/D molecular photodiode.

(c) Photocurrent-time curves of A/S/D and D/S/A LB films on gold OTE's in 0.1M KCl, on illumination with 330nm wavelength light.(i)A/S/D (ii)D/S/A (Fujihara et al. 1985).

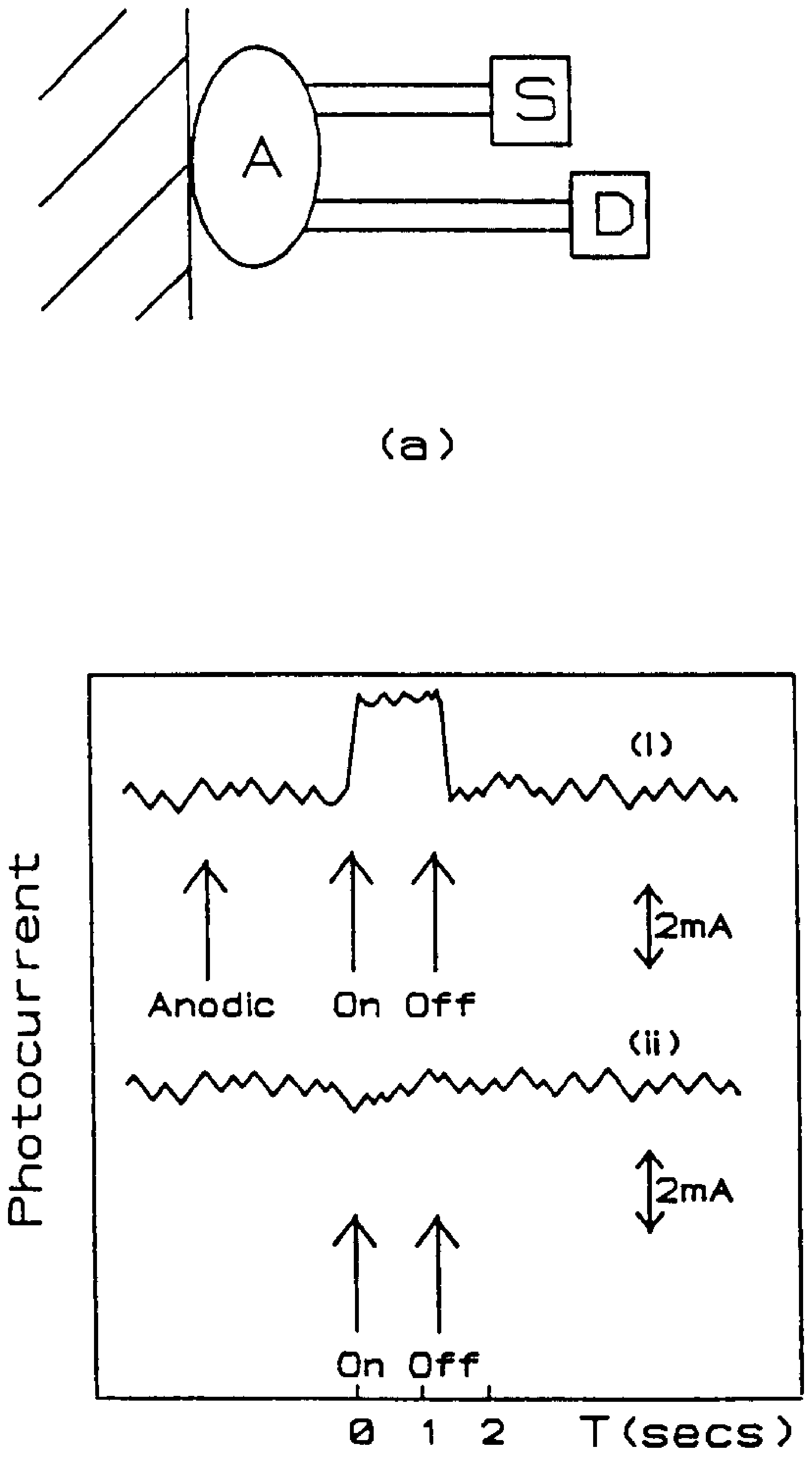

(a)

(b)

Fig 3.10.

(a) Schematic representation of an A/S/D triad molecular photodiode.

(b) Photocurrent-time curves of (i) a mixed triad/arachidic acid film (1:10) and (ii) arachidic acid only, on gold OTE in 0.1M $NaClO_4$. (Fujihara et al 1985).

Interest in the development of ion selective LB coatings has led to studies of the monolayer and transfer characteristics of the ion carrier, valinomycin, both in pure and mixed films. Peng et al (1987) have successfully deposited multilayers of valinomycin onto lead stearate, silver and polymethylmethacrylate. However they found that it was not possible to compress the pure valinomycin monolayer sufficiently to achieve the expected surface area per molecule to obtain a well packed film. In fact, the films were transferred at an approximate surface area of 2.10 to 2.30 nm^2/molecule, compared with a value of 1.68 to 1.88 nm^2/molecule predicted from X-ray data (Abraham and Ketterson, 1984).

Consequently, the transferred films would have had defects covering around 10% of the "film" area. The lack of any definite phase transition point on the valinomycin pi-A curve has been attributed to the stacking of valinomycin molecules beneath the water surface. This model is favoured to that of simple dissolution as the collapse process is reversible (Ries and Swift, 1978). In work related to that of Peng et al (1987), Howarth et al (1987) have successfully deposited multilayers of valinomycin onto single crystal silicon and quartz glass substrates precoated with stearic or tricosanoic acid or their cadmium salts. Infra-red and ultraviolet adsorption measurements indicate that the monolayer transfer is reproducible up to about 60 layers. However, ellipsometry reveals that there is a thickness gradient in the dipping direction which results in an average thickness per monolayer of 0.40nm to 0.66nm. The cause of the gradient is not known, but it may be linked to dissolution in an aqueous environment as it was noted that the effective film thickness was least for that part of the film which had been submerged the longest in the subphase. If this is the case, then it would have serious implications concerning the stability of potassium ion sensing devices which use pure valinomycin multilayers as the active element. Indeed, although preliminary studies have shown that valinomycin can be successfully deposited onto the unmetallized silicon nitride gate areas of transistor structures, no ISFET devices have yet been reported using a valinomycin multilayer LB film that can successfully measure potassium ion concentration in solution.

Furthermore, although the idea of using pure films of valinomycin may seem attractive in terms of simplicity, it is difficult to see how such films could transport potassium ions across a membrane the way they do in natural bilayers. Valinomycin normally acts as an ion carrier. That is, once complexed, it shields the potassium ion with its hydrocarbon periphery. The ion-carrier complex then transports the potassium across the membrane by diffusion. In this way, the valinomycin generates a potassium ion "current" which is a function of the ionic concentration gradient across the membrane (Hille, 1984; Stryer, 1981). However, in a pure monolayer of valinomycin, the valinomycin will be immobile. It would seem then, that the most likely sensing mechanism would be a simple potentiostatic response due to the preferential uptake of potassium ions by the LB film. If this is the case, then for the ions to penetrate the film, it must be porous, but if the film is porous then the ions will short circuit the film and thus nullify any potential effects. Hence, it seems unlikely that LB films of pure valinomycin will provide a means of measuring potassium ion concentration either using potential or current sensing. Although preliminary studies on the transfer of mixed films of valinomycin have been reported, (Howarth et al, 1987) it is clear that further work is required before LB films can be employed satisfactorily to immobilise valinomycin as an ISFET gate sensitizing material.

3.5.7 Enzyme Sensors

An enzyme sensor employing glucose oxidase (GOD) adsorbed onto an LB film has been reported by Morizumii et al (1987). Three film forming materials with different surface charges were investigated to optimise GOD adsorption. These were arachidic acid (C_{20}), arachidic methyl ester ($C_{20}Me$) and a mixture of $C_{20}Me$ with stearyl-methyl-ammonium chloride (4:1), ($C_{18}N_{0.2}$).

The activity of the immobilised GOD was determined by monitoring the optical absorbence of a glucose indigo carmine solution. Active GOD decomposed the glucose to produce hydrogen peroxide which then oxidized the dye, thus changing its colour, which was detected as a change in the optical absorbence of the solution (fig 3.11).

In order to measure the sensitivity of the biosensor, the enzyme adsorbed LB film was first deposited onto a Au-Au hydrogen peroxide electrode to construct a glucose sensor. The electrode current for different glucose concentrations was then measured. As a result of the sensitivity measurements it was found that the $C_{18}N_{0.2}$ film produced the best results and confirmed that ionic interaction between the LB monolayer and the enzyme dominate the adsorption process. Furthermore, by expanding the film and then recompressing it prior to transfer, the enzyme activity was increased, suggesting that a favourable change in enzyme orientation had occurred.

As well as showing that it is feasible to construct an enzyme sensor using the LB technique, this work emphasizes the importance of being able to finely control the spatial orientation of the enzyme to maximize its activity. Such ultrathin film, enzyme devices offer the advantage of shorter response time than is realizable with conventional enzyme sensors (Guibault, 1976). It is also likely that the electrode response will be kinetically, rather than diffusion limited. That is, the speed at which the enzyme can react with the glucose will determine the electrode current rather than the speed at which the glucose can pass through the film, which is the case for conventional membrane immobilized enzyme electrodes (Guibault, 1976). A kinetically limited electrode response is of benefit for in-vivo applications because the response will be rapid and will represent the true surface concentration of glucose.

3.5.8 Immunosensors

Although no immunosensor has yet been fabricated using the LB technique,

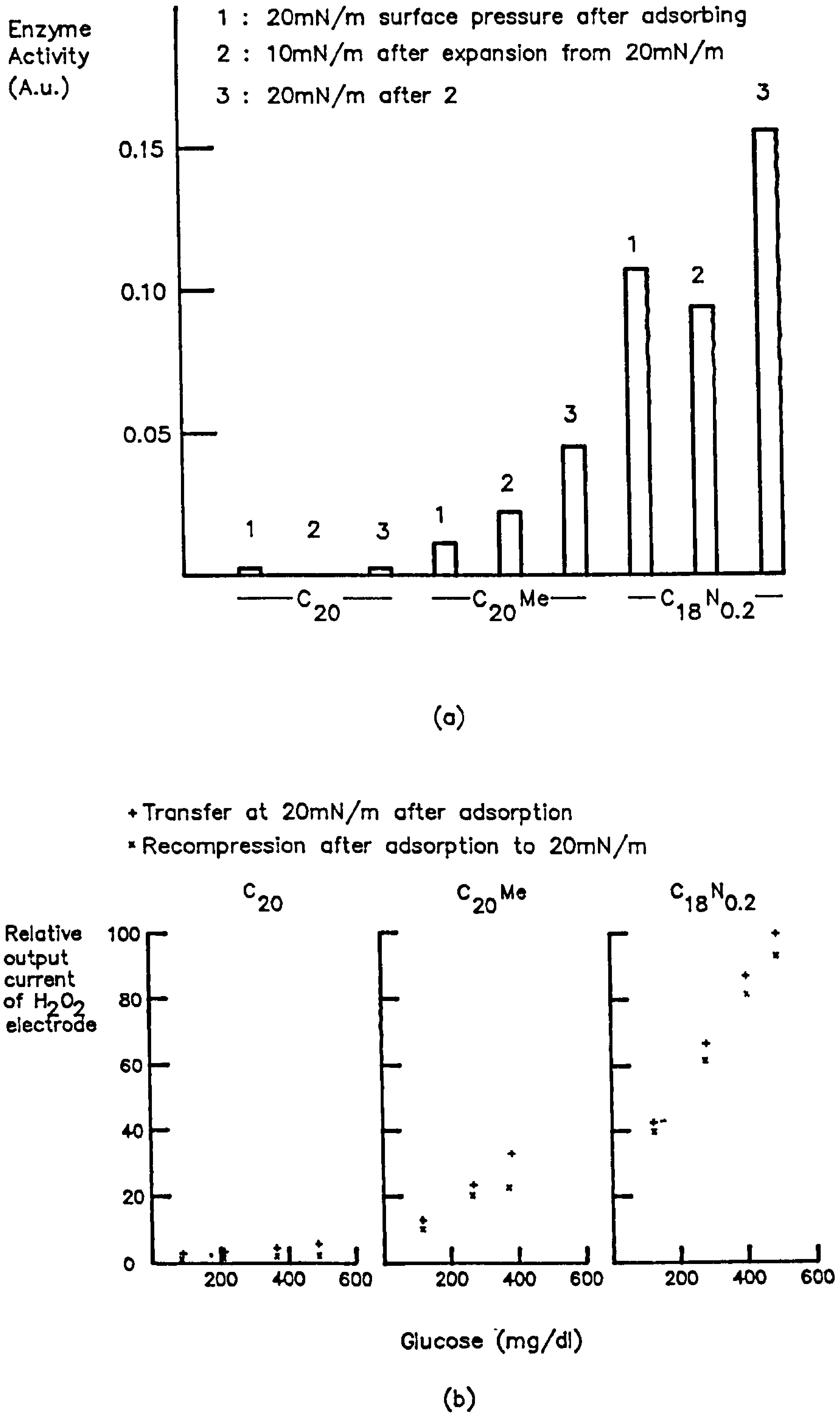

Fig 3.11 a) Graph showing the effects of monolayer preparation on enzyme activity when immoblilsed.

b) A comparison of the sensitivites of the glucose sensors to the three immobilising films and to recompression prior to film transfer. (Morizumii et al, 1987) studies on immunoglobin G(IgG) interaction in lipid monolayers by Akiake et al (1987) show that IgG is adsorbed by the monolayer film. However as lipid-IgG LB films have not yet been transferred to a solid substrate, The ease of film transfer and the stability of the supported LB films have yet to be determined.

3.6 Conclusions

3.6.1 Preparation

The production of LB films is a complex process involving the formation of an ordered monolayer at an air/water interface ($ 3.4.1), followed by transfer to a solid support ($ 3.4.2). In comparison to the methods discussed in $ 2, the LB technique is the most difficult coating method. However, in its favour, LB technology offers considerable flexibility for device applications. For example, the films may be formed using either specially synthesised molecules such as the polyimide precursors developed by Kakimoto et al (1987, $ 3.2) or by mixing the active species with a conventional film forming material (eg the immobilization of GOD in an arachidic acid monolayer; Morizumii et al, 1987 ; $3.5.7) or by a combination of the two techniques (eg the immobilization of a special triad molecule developed by Fujihira et al, (1985a) in a monolayer of arachidic acid $ 3.5.5).

3.6.2 Properties

3.6.2.1 Uniformity of coverage and order within the film

The LB technique can be used to immobilize a high density of functional species in an ultrathin multilayer coating (Fujihira and Poositisak, 1986(a,b)) and permits the orientation of molecules, for example as evidenced by the fabrication of a GOD based enzyme sensor (Morizumii et al, 1987; $ 3.5.7) and by the development of photodiodes (Fujihira et al, 1985a; $ 3.5.5). Although the degree of molecular orientation may not be as high as that achieved using covalent attachment and adsorption ($ 2.2.1; $ 2.2.2; $ 3.4.2), the LB technique offers the unique ability to build up ordered multilayer structures. This facility has been used to advantage in the development of complex structures for photodiode applications (Fujihira et al, 1985a; $ 3.5.5) and permits the build up of thicker films where mechanical robustness is of importance.

The uniformity of coverage can be high although it depends on the monolayer forming molecules ($ 3.5.6) and experimental conditions such as the surface pressure and the dipping speed ($ 3.4.2). Furthermore, characterisation of transferred films reveals the presence of crystalline domains with differing orientations and defects which can develop after deposition ($ 3.4.2) so that the uniformity of coverage is not as high as can be achieved using the best covalent attachment techniques ($ 2.2.2).

3.6.2.2 Site accessibility and Reactivity

The accessibility and reactivity of active sites within the LB film, are in general, similar to those of adsorbed and covalently bound films ($ 2.2.1; $ 2.2.2 ; $ 3.5.4; $ 3.5.7). However, the LB technique offers an important advantage over these techniques for the immobilisation of biological species. This is because it provides a means of immobilizing the species in an environment similar to that found in-vivo which ensures that the molecules will be active. In addition, the ability to use different monolayer forming materials to alter the surface charge can be used to optimise the activity of immobilized species, eg the enzyme GOD (Morizumii et al, 1987). Finally, the ability to immobilize active species, such as platinum, as adsorbed atoms or ultrafine particles, means that the effective electroactivity of the coating may be as high as for 3 dimensional structures such as solvent cast films ($ 2.3).

3.6.2.3 Mechanical/Chemical Stability

LB multilayer films can have greater mechanical and chemical robustness than spin coated films as evidenced by the resistance of 16-8- poly(diacetylene) to plasma etching when used as the gate insulator for an IGFET (Fung and Larkins, 1985; $ 3.5.2) and by the development of electron beam resists ($ 3.5.3). However monomeric LB materials tend to be less robust and various problems have been encountered when the films are exposed to an aqueous environment. For example, Sprintschnik et al (1977) and Gaines et al, (1978) have reported the loss of ruthenium complexes from electrode surfaces ($ 3.5.5).

Problems of stability have been reported by Fujihira et al, (1985a) with reference to the photocurrent of LB film based photodiodes. However, the origin of the instabilities are not understood ($ 3.5.5). Also, in the fabrication of an ISFET using a phthalocyanine as the gate coating material, Brown (1981) encountered severe difficulties due to the instability of the electrode response ($ 3.5.6). Investigations of promising materials for device applications such as valinomycin indicate possible stability problems as evidenced by the thickness gradient of multilayer films observed by Howarth et al, (1987, $ 3.5.6). Furthermore, there is a shortage of information on the stability of electroactive films for use in device applications eg the enzyme sensor developed by Morizumii et al, (1987).

3.6.3 Problems/Future Developments

For device applications, such as electrocatalytic electrodes ($ 3.5.4, 3.5.5) and sensors ($3.5.6, 3.5.7), the LB technique combines the flexibility of solvent casting and polymer electrodeposition for immobilizing electroactive species in a matrix of electroinactive species, with greater control over film dimensions than that provided by covalent attachment and adsorption. However, before the potential of LB technology can be realised in sensor applications such as CME's and ISFET's for the analysis of aqueous solutions, the problems relating to film stability ($ 3.5.5; $3.5.6; $3.6.2.3) in an aqueous environment must be overcome. Consequently, one of the important aims of the present work is to develop a method for characterising LB films in an aqueous environment in order to increase the current understanding of the causes of film instability with the goal of producing stable electroactive electrode coatings for sensor applications.

4.0 Sample preparation

4.1 Introduction

The samples investigated in this work were in the form of thin films deposited onto metallic electrodes. The major part of the work was concerned with films deposited using the Langmuir Blodgett Technique ($3), but early measurements were carried out on thin polymeric films formed by a spinning procedure ($2.2.3). A variety of electrodes were used as substrates eg platinum wire (a noble metal which is well characterized electrochemically), copper clad printed circuit board (PCB, for a large surface area and planar electrode geometry); and glass microscope slides coated in thin metallic films (for a highly smooth surface for good quality LB films). The techniques used for preparing the test samples are described below.

4.2 Substrate preparation

4.2.1 Platinum wire electrodes

The simplest electrodes to prepare were made from 35mm lengths of 0.5mm diameter platinum wire (Johnson Matthey). These electrodes were mounted in PTFE collars (fig 4.1) which served as holders for the electrodes during both deposition and electrical measurements. Prior to coating with film, the platinum wire was polished using an alumina paste (Alumina (BDH) in ultra pure water; 0.3μm initially, 0.075μm in later work to provide a smoother finish). After polishing, the electrodes were carefully rinsed and sonicated three times in ultra pure water (UPW) for 5 minutes. After a final rinse in UPW, the wires were dried in a stream of nitrogen gas (BOC). The platinum wire provided a smooth, reproducible electrode surface which was suitable for both AC admittance ($5) and cyclic voltammetry ($6) measurements. However, as will be seen in

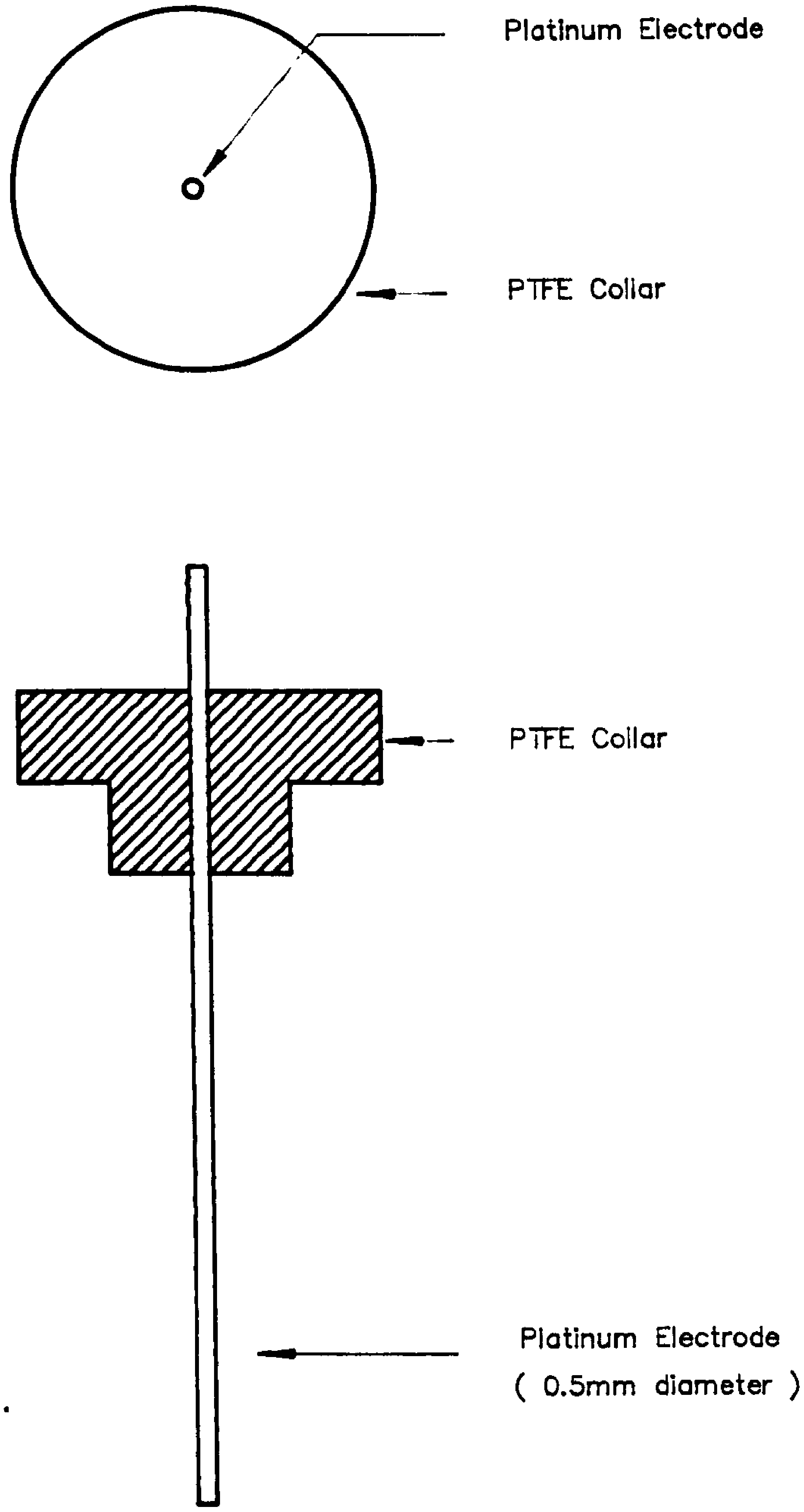

Fig 4.1 Diagram showing the platinum wire electrode and PTFE mounting collar.

section 7, it was difficult to form good quality LB films on platinum and the small surface area of the wires meant that deposition ratios could not be determined accurately. Consequently, several planar electrodes were tested.

4.2.2 Copper printed circuit electrodes

Planar copper electrodes 12mm in diameter, were formed from copper clad, epoxy-bonded glass-fibre printed circuit board using standard photolithographical techniques and a ferric chloride etch. As shown in fig 4.2, contact to the main electrode was via a thin strip, 30mm long and 1mm wide. After preparation and prior to film deposition, the electrodes were soaked in 10% Decon 90 for ca 30 minutes and then in UPW for at least 24 hours, to remove contaminants introduced during the etching process. Immediately prior to coating, surface oxide was removed from the copper using a fine abrasive paper. The electrode was then given a final rinse in UPW and dried in a nitrogen stream.

The main advantages of this electrode were its reproducibility, mechanical and electrical robustness and cheapness to manufacture. The planar electrode geometry facilitates analysis of experimental results, but the use of two coated electrodes can complicate the measurements if the films are of differing quality. The surface roughness and large height difference between the fibre-glass and copper electrode meant that the electrodes proved unsuitable for LB film deposition.

4.2.3 Sputtered copper electrodes

Sputtered copper was used to provide a smooth surface for the deposition of high quality LB films. Great care was required in preparing the glass slides used as the substrate for copper deposition. The final substrate cleaning procedure adopted is outlined

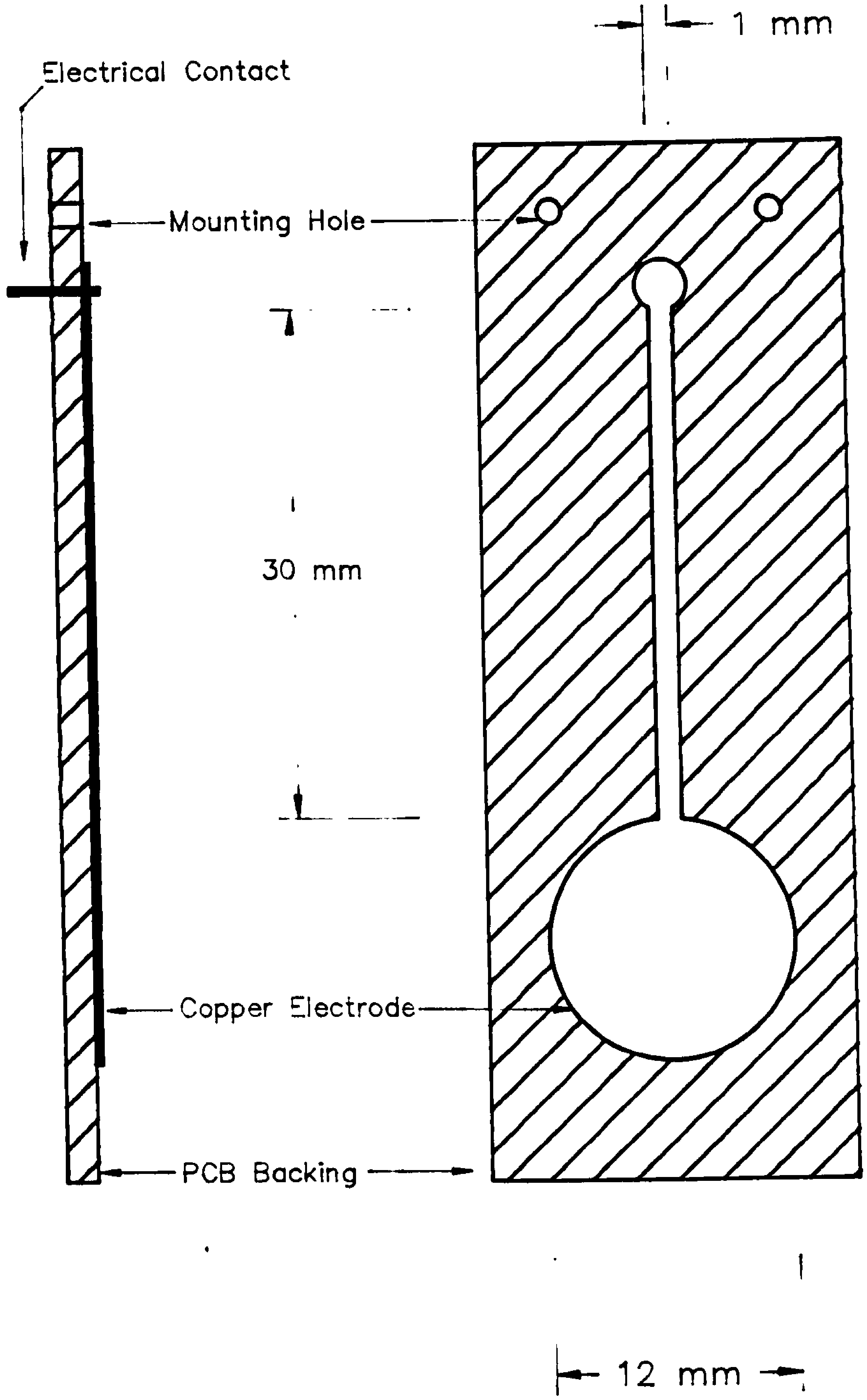

Fig 4.2 Diagram Showing the electrode geometry for the PCB based copper electrode.

below.

4.2.3.1 Slide cleaning procedure

a) Slide preclean and cutting

This step was carried out to remove large contaminant particles and degrease the slides. The slides were degreased using acetone (Scientific Supplies, Chester) in a soxhlet (5 mins), cut and returned to the acetone (10 mins). The slides were then cleaned manually using a commercial cleaning agent before rinsing in tap water (2 mins).

b) Detergent and chemical clean.

This procedure was used to remove finer particles and chemical contamination. The slides were sonicated in 5% Micro (International Products Corporation, UK Branch) in UPW (30 mins) before being rinsed and sonicated (1 min), three times in UPW. Subsequently the slides were soaked in concentrated chromic acid ($4.3.1.4) (60 mins), then rinsed and sonicated (3 mins) twice in UPW.

c) Chemical etching.

This procedure was introduced to improve the adhesion of the metallisation layer by etching the surface of the glass. The slides were soaked for 12 hours in 10% (saturated potassium hydroxide (BDH, Analar Grade) in UPW) +90% ethanol (BDH) before being rinsed and sonicated (2 mins), three times in UPW.

d) Final drying procedure

The slides were sonicated in isopropanol (BDH) (3 mins) and in fresh isopropanol (3 mins) before rinsing and sonicating (2 mins) three times in UPW. The slides were next rinsed in UPW before blow drying in clean nitrogen gas. Finally the slides were baked on a hot plate at $200^{o}C$ for 10 minutes to eliminate the blooming observed initially in the metal films.

4.2.3.2 Sputtering conditions and electrode geometry.

Sputtering was carried out in pure, dry argon at a gas pressure of 5 mTorr in an Edwards High Vacuum Unit. The sputtering rate was ca $4\mu m/hr$. Final film thicknesses were usually in the range $1-3\mu m$. The electrode geometry (fig 4.3) was defined using standard photolithographical techniques. To protect the electrode until required for use, the photoresist layer was left over the copper electrode. Prior to LB film deposition, the electrode was removed from the desiccator and cleaned in acetone.

4.2.4 Evaporated metal electrodes

Very smooth electrodes for LB deposition can also be prepared by vacuum evaporation. Both aluminium (BDH) and silver (BDH) were used in this work. Aluminium was used because it is known that LB films deposit readily onto it (Agarwal, 1975a) and furthermore, the surface oxide is more stable than on copper; an important factor in the AC admittance measurements. For surface plasmon measurements (SPR) LB films were deposited onto evaporated silver films, since these are known to give a sharp, well characterized adsorption minimum in the reflected signal.

In general, the glass slides were cleaned as outlined in $ 4.2.3.1. The vacuum coating system was an Edwards High Vacuum Unit fitted with a liquid nitrogen trap. Clean glass slides were mounted above the filament and evaporation was begun at $\leq 10^{-5}$

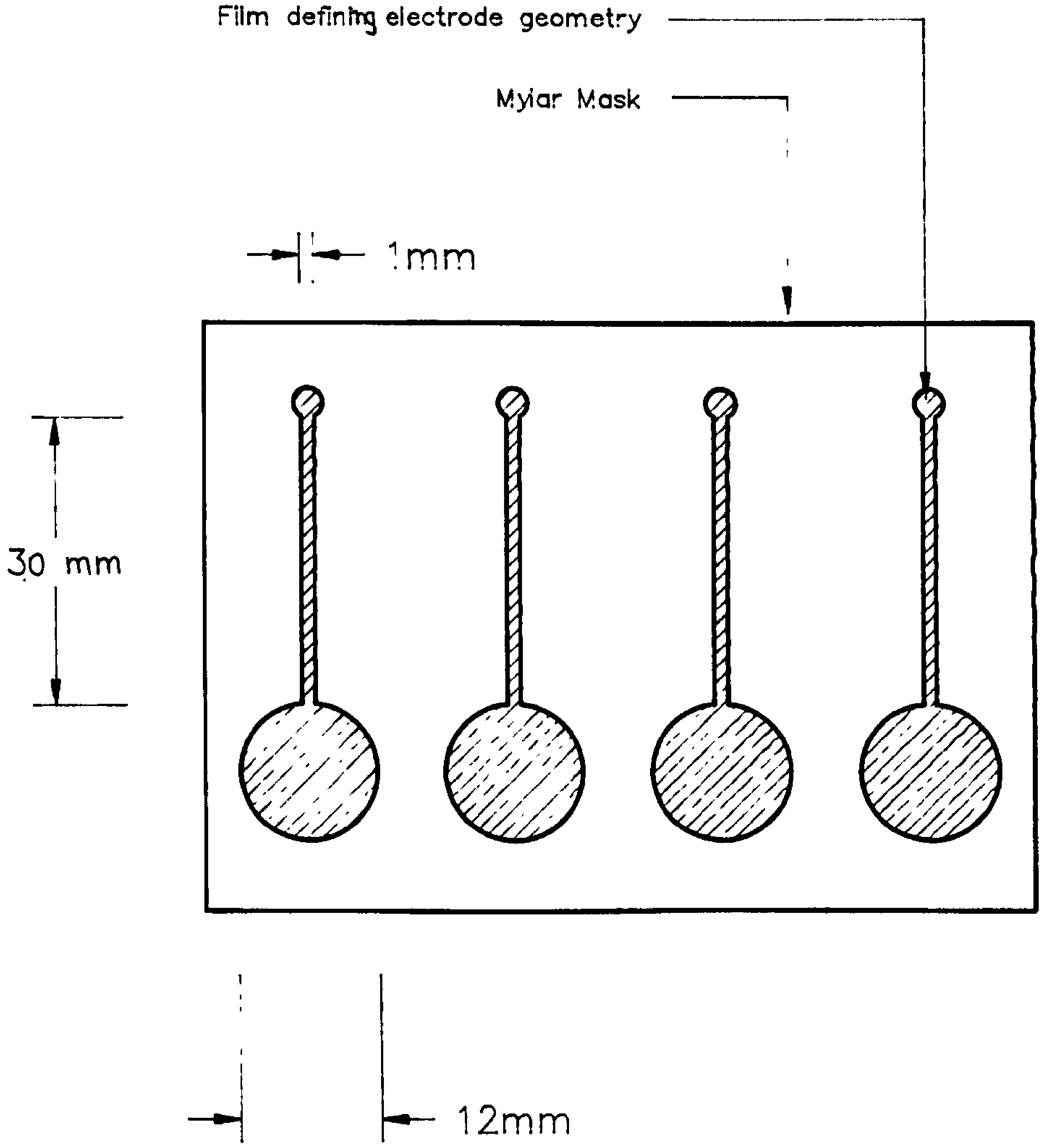

Fig 4.3 Diagram showing the mask used to define the electrode geometry using photolithography.

Torr. Aluminium films of approximately 1000Å were deposited. The thickness of the silver coatings was maesured to be 45Å using a quartz crystal film thickness monitor. 45Å is the optimum thickness of silver for use in SPR.

Although initially the geometry of the aluminium electrode was defined photolithographically, it was soon discovered that evaporation through a mask (fig 4.4) produced better quality films and reduced processing time considerably. Coated slides were stored in a desiccator until required.

4.3 Thin film coating techniques

4.3.1 The Langmuir Blodgett Technique

4.3.1.1 Introduction

The general principles involved in the deposition of mono- and multilayer films by the Langmuir Blodgett Technique have been outlined in Chapter 3. In this section details will be given of the film forming apparatus, deposition procedures and conditions.

4.3.1.2 The Langmuir Trough

The LB troughs used in this work were each enclosed in a cabinet and mounted on an anti-vibration table (Micro G, Technical Manufacturing Corporation). The cabinets were housed in a clean room. The clean room was supplied with doubly filtered air at a positive pressure which was continuously recirculated and filtered by an air conditioning unit. Entry into the room was through an air lock to minimize the ingress of dust.

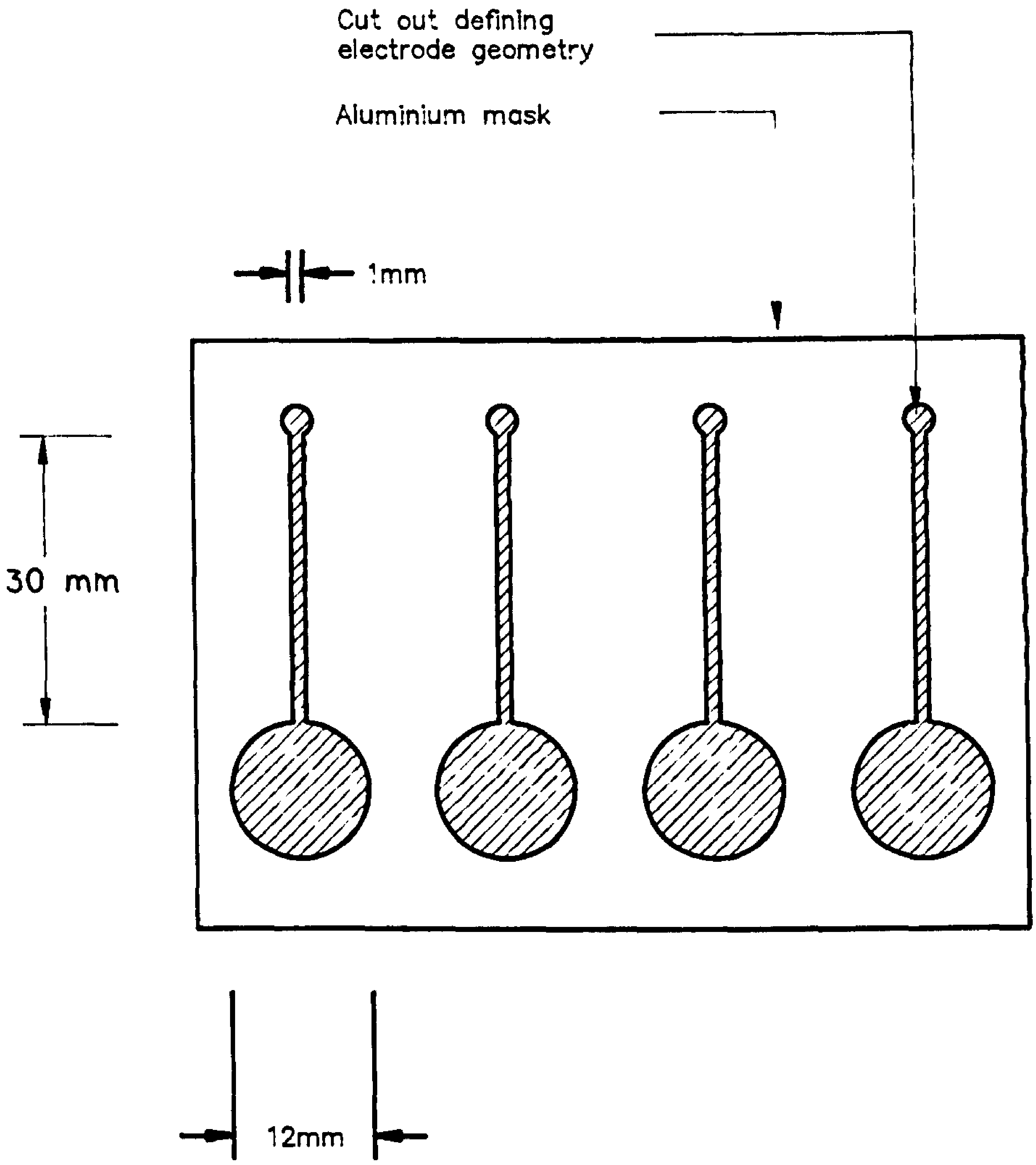

Fig 4.4 Diagram showing the mask used to define the electrode geometry using vapour deposition.

A schematic diagram showing the principles of operation of the Langmuir Trough and the barrier arrangement is shown in fig 4.5 (Blight et al, 1965). The polypropylene trough was mounted on a temperature controlled base plate. A water heater and recirculator (Grant) coupled to a cooling unit (Grant) were used to pump water through the base plate unit. In this way, the subphase temperature, measured using a Brannan Thermometer, was controlled to within ±1.0°C of a set value in the range 0 to 35°C. The surface pressure of the film was measured to an accuracy of ±0.1mN/m using a Wilhelmy plate connected to an electrobalance. The accuracy was later increased to ±0.05mN/m by doubling the width of the Wilhelmy plate.

The barriers are motorized to enable the LB monolayers to be compressed and expanded. A potentiometer, connected to the barrier movement is calibrated to provide a direct measurement of film area. Pressure–Area isotherms were generated by monitoring the surface pressure and barrier position using an xy plotter (HP 7044A or Gould Series 6000). In some of the later work data was collected automatically by computer.

4.3.1.3 Deposition

A dipper motor with associated electronic control circuitry was used to move the substrate vertically through the monolayer film in a steady, controlled manner. Several substrates could be coated simultaneously using a special clamp. The deposition speed could be varied between 1.5 and 9 mm/min. Automatic dipping up to a limit of 99 passes through the monolayer could also be selected.

In general the first monolayer was transferred at a slow speed (1.5mm/min; Agarwal, 1974) and allowed to dry for ca 1 hour. Subsequent layers were applied at a faster rate (9mm/min).

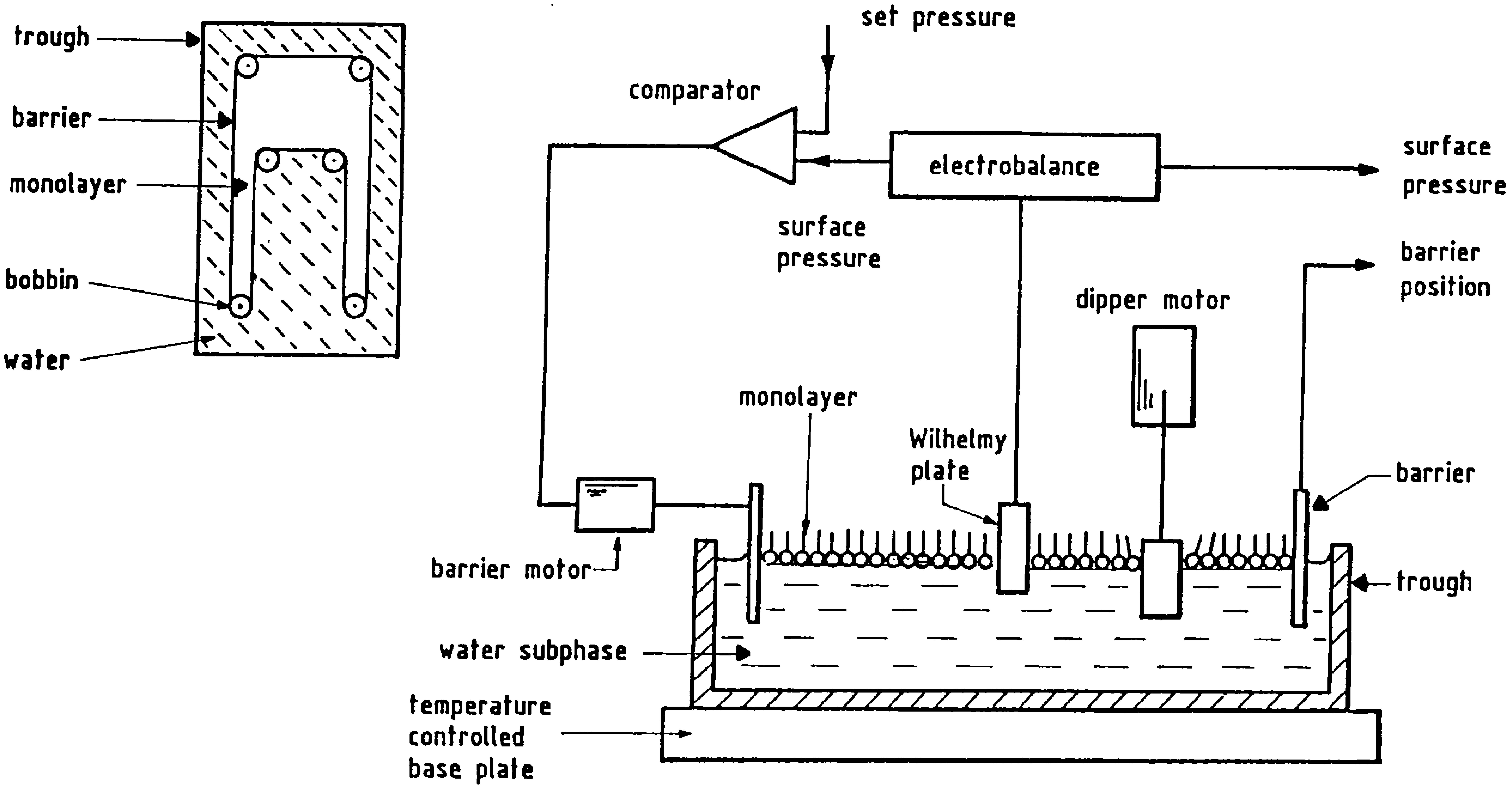

Fig 4.5 (a) Schematic diagram showing the principles of operation of the Langmuir Trough and (b) the barrier arrangement.

During the deposition process the shape and regularity of the meniscus at the substrate/monolayer boundary was used to confirm the type ($3.4) and quality of the deposition. A more quantitative evaluation of the transfer process was provided by the deposition ratio ($3.4).

4.3.1.4 Trough cleaning procedure

In order to maintain the high degree of cleanliness required for monolayer preparation, the trough, barrier and bobbins were cleaned at least every two weeks. The subphase was renewed more frequently. The trough cleaning procedure is outlined below. All internal surfaces of the trough were wiped with chloroform (Koch-Light, Aristar Grade) taking particular care at the joints, followed by rinsing with UPW. If the surfaces were wetted by the UPW, this stage was repeated. The trough was then filled with UPW, to which 100ml of concentrated chromic acid was added slowly, stirring continuously. The concentrated chromic acid comprised of 5 gms of potassium dichromate (Scientific Supplies, Chester) in ≤10ml UPW to which approximately 200ml of concentrated sulphuric acid (Koch Light) was added. The belt and bobbins were then wiped with tissues soaked in chloroform and then UPW, before placing them in the trough in chromic acid. The trough was covered with a perspex sheet and left to soak for between 1 and 12 hours. After soaking, the chromic acid was decanted and the trough, belt and bobbins rinsed several times in UPW. The trough was then refilled with UPW and left to soak for 1 hour to leach out chromate ions before re-rinsing in UPW at least four times.

During this stage the filter paper, Wilhelmy plate was renewed and presoaked to leach out any contaminants. Also the bobbins and belt were carefully replaced and the system recalibrated. Finally, the trough was returned to the cabinet and refilled with UPW.

4.3.1.5 Surface cleaning procedure

Prior to film spreading, the water surface was cleaned using a fine pipette connected to a peristaltic pump. Surface cleaning was continued until there was no change in surface pressure between the maximum and minimum area positions of the barrier.

4.3.1.6 Subphase conditions

All monolayer experiments were performed on a UPW subphase obtained from an Elgastat R01 System (Elga, High Wycombe, Bucks), although the exact subphase conditions depended on the film required. The subphase temperature and pH were measured using a mercury bulb thermometer (Brannan Thermometer) and a pH meter (Philips PW 9409 Digital pH Meter) respectively.

Stearic acid films were spread on either a pure water subphase, pH 5.5-5.7 , or UPW containing hydrochloric acid at pH 3; both with a subphase temperature of 20±2°C. Lowering the subphase pH reduces the influence of impurity ions on film quality. Barium stearate films were spread on a UPW subphase containing 3.10^{-5}M barium chloride (BDH, Analar Grade) and 4.10^{-4}M potassium hydrogen carbonate (BDH, Analar Grade). The latter buffered the subphase at a pH of 7.2; the temperature was maintained in the range 20±2°C.

PBMA films were spread on a UPW subphase at a temperature of 30±1 °C. The higher temperature reduced the monolayer viscosity and improved deposition. At lower temperatures films tend to sink to the bottom of the trough (Stuart, 1986).

4.3.1.7 Monolayer spreading

Spreading solutions were made by dissolving the required compound in chloroform (Koch Light, Aristar Grade). The solutions were generally made up to a concentration of ca 1mg/ml and stored at 0-5 ^{o}C. Prior to spreading, the solutions were allowed to attain room temperature.

The compounds employed were stearic acid (Aldrich) or PBMA (Aldrich) with the addition of gramicidin (Sigma) or valinomycin (Sigma) for the mixed films.

With the barriers open, the spreading solution was applied, either drop-wise or at a constant flow rate, using a micropipette (BCL PDM8) held just above the water surface. The spreading solution was applied at a rate such that the surface pressure did not exceed 5mN/m. After spreading the required volume (typically 50-100μl), the film was kept at zero surface pressure for 20 minutes while the solvent evaporated. The monolayer was then compressed and the pressure-area (π-A) characteristic of the film obtained (\$7, \$8). In general two π-A characteristics were taken at a medium rate of ca 10^{-2}Å^2/molecule/sec for both compression and expansion. A third compression was formed at a slower rate of ca 10^{-3}Å^2/molecule/sec prior to stability and deposition experiments.

Mixed films were produced either by using a spreading solution containing both compounds or by "adding" the second compound to a previously formed monolayer of the immobilizing molecules. The former technique was simple to carry out and ensured that the mixed film was homogeneous. The latter method involved re-expanding the first monolayer until it reached the gas phase, so that the second compound would mix with it as it was applied. The second compound was applied at several points over the monolayer surface to enhance the mixing process. π-A characteristics were then taken as for the pure films.

4.3.2 The spin coating technique

4.3.2.1 Introduction

The technique of spin coating was used to apply materials such as photoresist, polyurethane and PVC to printed circuit board electrodes. These materials were used in the initial studies during which time the AC admittance analysis technique was evaluated.

4.3.2.2 The spinning procedure

The coatings applied by the spinning procedure were photoresist (Iso-electronic grade, iso-poly photoresist K747, MR40; Micro-Image Technology), polyurethane (Woolworth Coverplus, clear finish polyurethane varnish) and PVC dissolved in tetrahyrofuran (High mwt PVC ; Tetrahyrofuran 99%, stabilized with 0.025% butylated hydroxytoluene; both supplied by Aldrich. The PVC based coatings applied were;

a) 1 gm PVC in 10ml tetrahyrofuran
b) 1 gm PVC in 10ml tetrahyrofuran + 5ml Bis-2-ethylhexyladipate
c) 1 gm PVC in 10ml tetrahyrofuran + 5ml Bis-2-ethylhexyladipate + 5 mg Valinomycin

Bis-2-ethylhexyladipate is a plasticizer and valinomycin is a potassium ion selective carrier (both were supplied by Sigma). The electrode, held in a vacuum chuck, was first flooded with the coating solution. The electrode was then spun for 60 seconds, typically at 2500 rpm. The coating was allowed to dry in air for approximately 120 seconds before applying subsequent layers in the same way, as required.

The electrodes coated in polyurethane and pure PVC were dried in the oven for 30 minutes at $80^{o}C$. The PVC films containing Bis-2-ethylhexyladipate were dried at room temperature. This was particularly important with the coatings containing valinomycin because it denatures when overheated. The photoresist films were pre-hardened in an oven at 80°C for 10 minutes before being exposed to UV light for ca 10 minutes to polymerize the coating. The electrode was then returned to the oven at 80°C for at least 30 minutes. Finally, the electrodes were stored in an air tight container until required.

4.4 Concluding Remarks

It was found that several different metallic substrates were required for film deposition to permit complementary investigations of coating properties.

To facilitate cyclic voltammetric and AC admittance measurements, platinum wire electrodes were employed. Whereas for SPR silver was necessary and for AC admittance and optical work, copper and aluminium were needed.

The need for several different materials, although broadening the scope of the work, necessarily complicated and prolonged the experimental work by precluding the use of a single standard process for substrate preparation and processing.

5.0 The AC Admittance Analysis Technique and its application to the characterization of electrode/electrolyte system

AC Admittance Analysis is commonly used to measure the admittance of electrode/electrolyte systems as a function of frequency (eg Brand and Rechnitz, 1969(a,b), 1970; McIntyre and Leidheiser, 1985; Stelzle and Sackmann, 1989). The system under discussion is shown in fig 5.1, and consists of a metal electrode, which may be coated or uncoated, in contact with an electrolyte.

In a series of papers, Brand and Rechnitz, (1969(a,b), 1970), used the technique to characterize ion selective glass, crystal and liquid membrane electrodes in terms of empirically determined equivalent circuits. In corrosion studies McIntyre and Leidheiser (1985) employed the method to evaluate poly-butadiene spin-coated films ($ 2.2.3).

With reference to AC analysis of LB coated electrodes in an electrolyte, the only work reported is that of Buchwald et al (1938), Zahl et al (1938) and Stelzle and Sackmann (1989). Buchwald et al (1938) used a modified Wheatstone Bridge arrangement, where the system under test was balanced by a variable resistance and capacitance. However, measurements were only carried out at 1kHz, with an excitation voltage of 250mV and resistances and capacitances were presented for different numbers of LB layers of barium stearate on chromium electrodes in 0.35M copper sulphate solution. In a continuation of this work, Zahl et al (1938) measured the capacitance and resistance of calcium stearate mono- and multi-layers in a range of electrolytes. A significant variation in capacitance and resistance for different electrolytes and electrolyte concentrations was observed. This factor was considered a severe disadvantage of the technique as they wanted to use an electrolyte contact to replace the conventional mercury drop electrode normally employed in the electrical characterisation of LB films (eg Race and Reynolds, 1935).

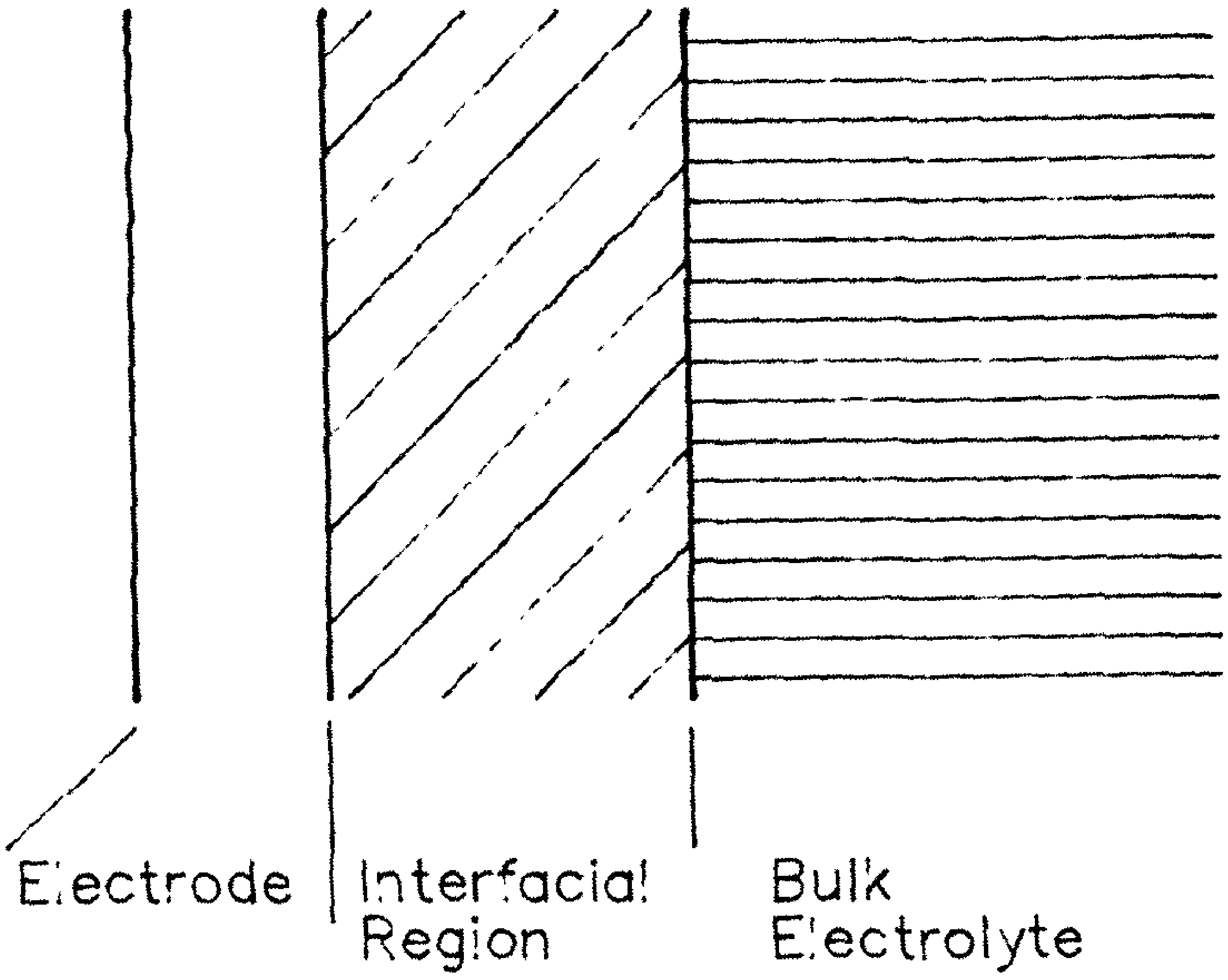

Fig 5.1 Simplified representation of the electrode/electrolyte system.

Very recently, Stelzle and Sackmann, (1989) confirmed that the AC admittance technique can be used to characterise LB film modified electrodes in an aqueous environment. In their work, the capacitance of LB lipid bilayers deposited on cadmium stearate coated, chromium electrodes, was measured as a function of frequency. A value of about 4 was obtained for the dielectric permittivity of the LB film. Stelzle and Sackmann also used the technique to monitor LB film stability and protein adsorption as a function of time.

In the AC analysis technique, a sinusoidal voltage, magnitude V_Y is applied to the system under test (fig 5.2). The magnitude V_X of the measurement voltage is compared to that of the excitation signal. From the ratio V_Y/V_X, the sample admittance is calculated. The admittance is measured for a range of frequencies to produce an admittance vs frequency curve for the system.

To interpret correctly the frequency response of the electrode/electrolyte system it is necessary to identify and account for all the processes that can contribute to the admittance, ie the current- voltage response at a given frequency. Therefore, any factors affecting the movement of charge to the electrode from the bulk of the solution are important. These include (i) diffusion and drift of ions to the electrode ($ 6.5), (ii) the distribution of ions in the interfacial double-layer and (iii) charge exchange between the electrode and the electrolyte.

The purpose of this chapter is to establish the theoretical basis and experimental technique of AC admittance analysis.

5.1 The Theoretical Basis of AC Admittance Analysis

The theoretical analysis of the AC admittance of electrode/electrolyte systems

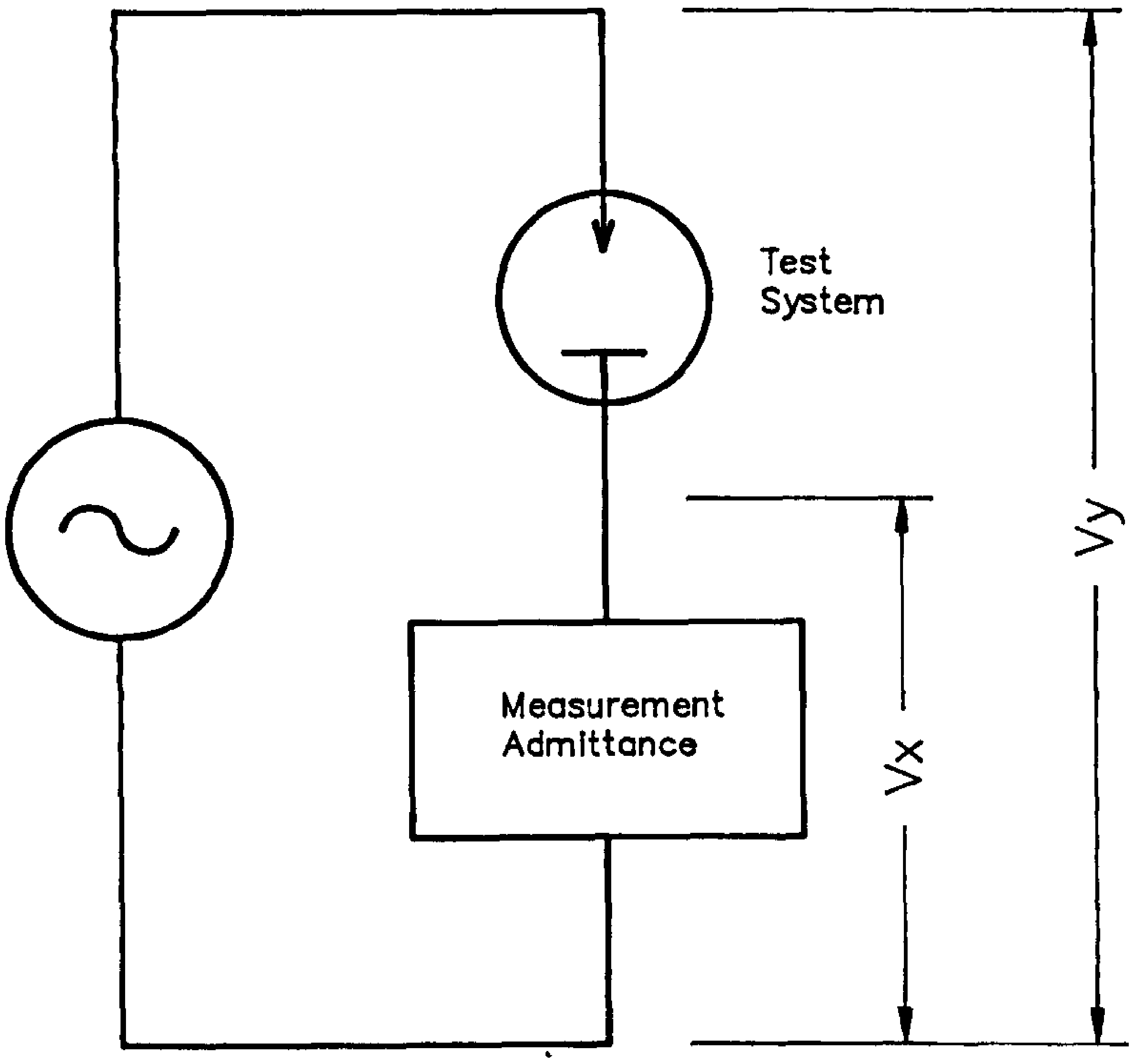

Fig 5.2 Schematic diagram of the experimental arrangement, where Vy is the applied voltage and Vx is the voltage developed across the measurement admittance.

presented below is based on the work of Macdonald (1953, 1971, 1973, 1974, 1976, 1985), Chang and Jaffe (1952) and Franceschetti and Macdonald (1978, 1979). Although the theory was originally developed to explain space charge effects in semi-conductors (Macdonald, 1953), it is equally applicable to a range of electrode/electrolyte systems.

The analysis involves solving idealised transport and Poisson equations, exactly, throughout the system for both positive and negative ions. The equations include the effects of motion under an applied field, recombination and diffusion, although it is assumed that the neutral species do not diffuse. The treatment leads to an equivalent circuit representation (fig 5.3) for the system in which each element is described mathematically in terms of microscopic properties of the electrode/electrolyte arrangement, including ionic valency, (z_n, z_p), mobility (μ_n, μ_p) and concentration (n_i, p_i), electrode discharge rates (r_n, r_p) and the electrolyte dielectric permittivity, ϵ.

In the simplified equivalent circuit of fig 5.3, C_g is the geometric capacitance of the inter-electrode space filled with electrolyte at infinite dilution. The AC response of the ionic double layer is represented by the double layer capacitance C_d which is charged through an electrolyte conductance G_d, while G_t allows for charge transfer across the electrolyte/electrode interface. The circuit representation assumes that the parameters are all frequency independent, although in practice, G_b, C_b, C_d and G_t may show some frequency dependence. A summary of the essential theory is presented in Appendix A, including simplifications appropriate to the present work. (Note that in fig 5.3, the interfacial capacitance, C_{io}, is represented by the double layer capacitance, C_d and it is assumed that the interfacial conductance, $G_{io} << G_d$).

5.2 The modified electrode/electrolyte system

When an electrode is modified by coating with a semi-insulating film, the

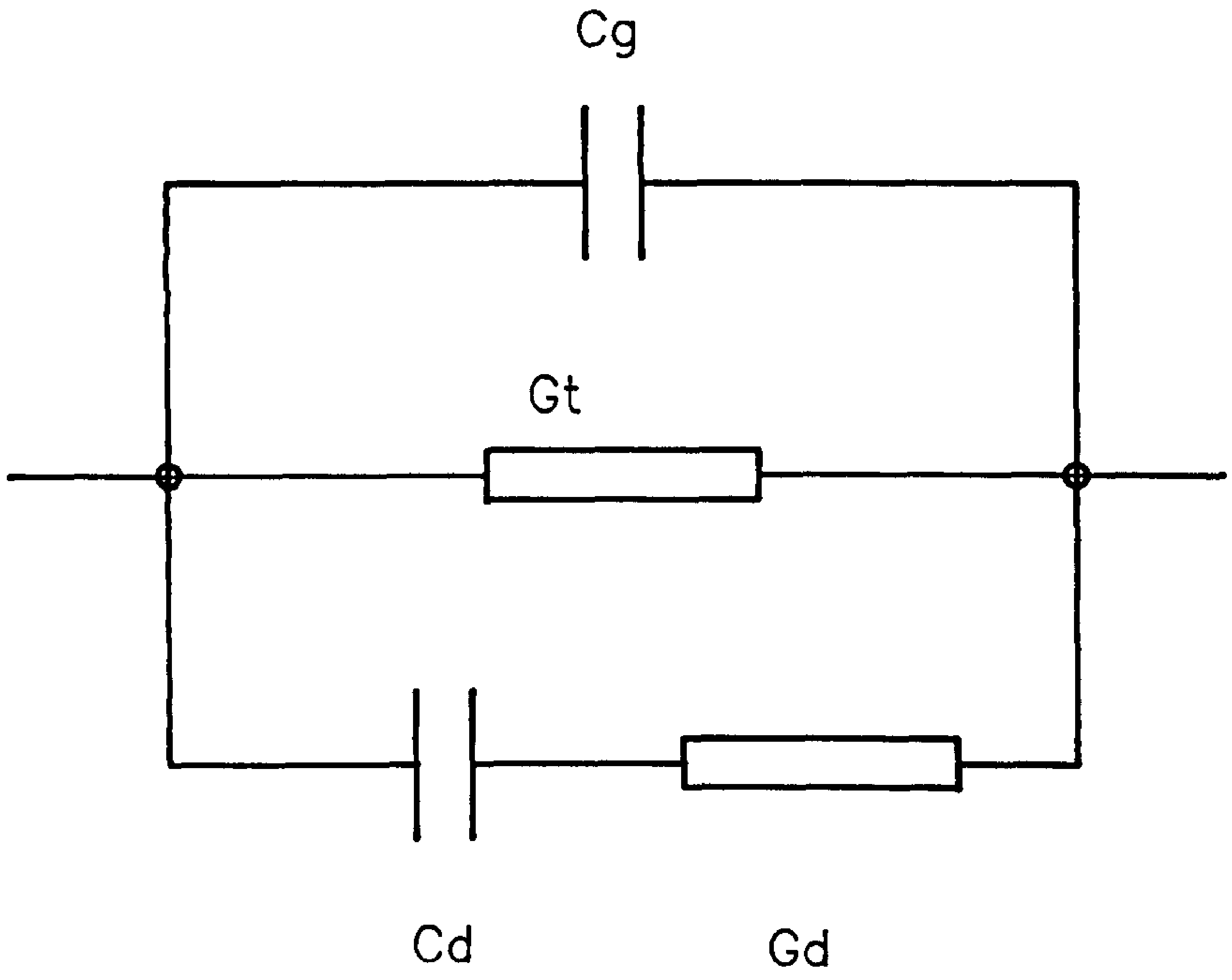

Fig 5.3 Equivalent circuit representation of the electrode/electrolyte system.

distribution of ions within the cell is altered, especially at the electrode/electrolyte interface. The situation is shown schematically in fig 5.4. The coating can be represented by a parallel R-C circuit, (cf Buchwald et al, 1938; Zahl et al, 1938; Stelzle and Sackmann, 1989) resulting in the modified equivalent circuit of fig 5.5(a). However, in practice, the R-C elements describing the coating may need modification to include frequency dependent behaviour.

In the present treatment, it is assumed that the new conditions can be accounted for by defining the ion concentrations in the coating layer by p_i' and n_i' for positive and negative ions with mobilities for ions in the film of μ_p', μ_n' respectively. The layer is therefore treated as a very weak electrolyte. In this way, the coating conductance G_b, can be represented by the parallel combination of an intrinsic conductance G_{bi}, due to the finite conductivity σ, of the film, and a conductance G_{bs}, due to the motion of ions within the film. Therefore G_b is given by;

$$G_b = G_{bi} + G_{bs} = (eA/t_b)[z_p\mu_p'p_i + z_n\mu_n'n_i] + \sigma A/t_b \qquad 5.1$$

An alternative method for evaluating the film conductance is to assume that the electrode coating has defects in an otherwise intact film. If the fraction of electrode covered by intact film is ß, then the fractional defect area is (1-ß) (Stelzle and Sackmann, 1989). Assuming that the conductivity of the defects will be that of the bulk electrolyte σ_d, the effective film conductance, σ_b' can be defined as;

$$\sigma_b' = \beta\sigma_b + (1-\beta)\sigma_d \qquad 5.2$$

where σ_b is the conductivity the coating would have if it was defect-free.

The coating capacitance C_b is essentially the geometric capacitance of the film and can

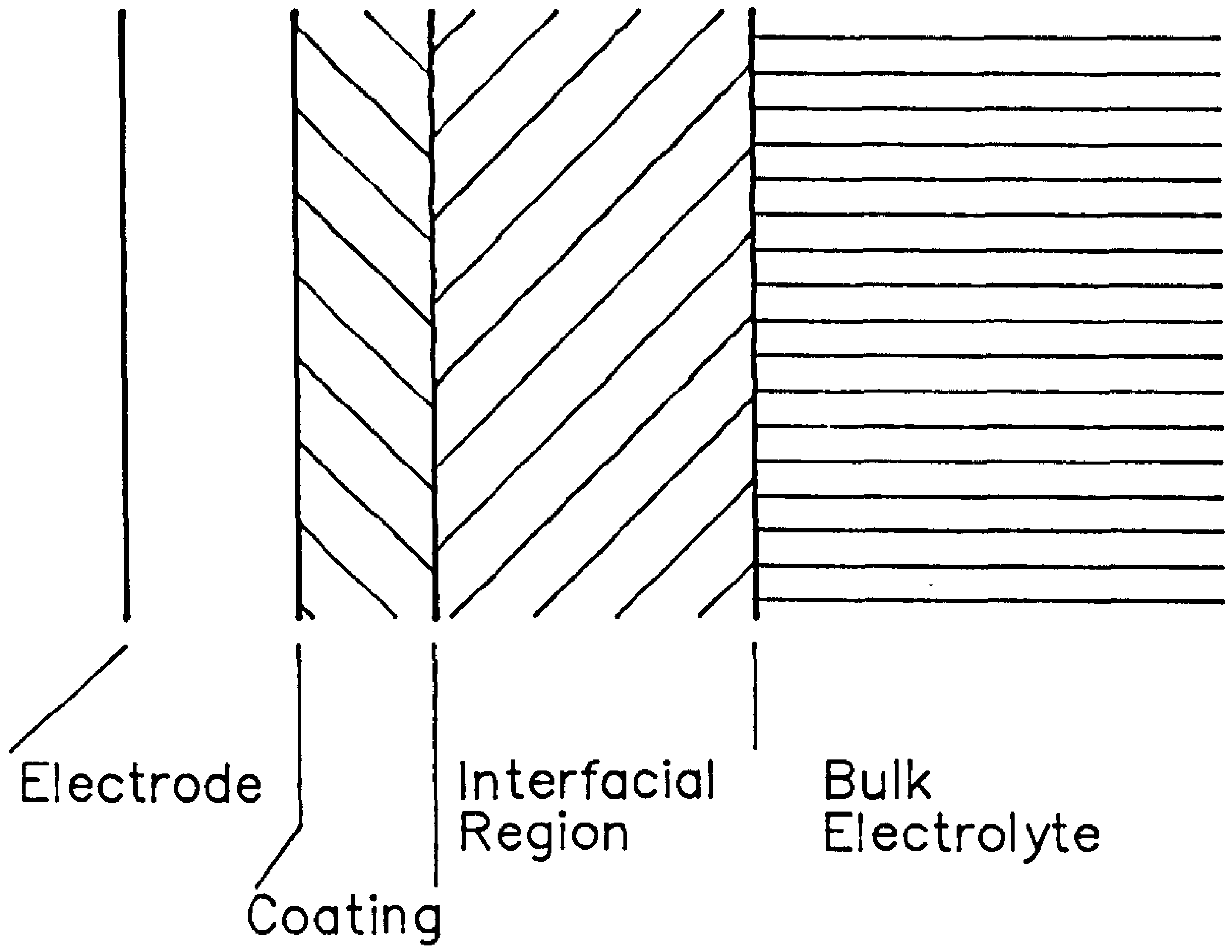

Fig 5.4 Simplified representation of the electrode/coating/electrolyte system.

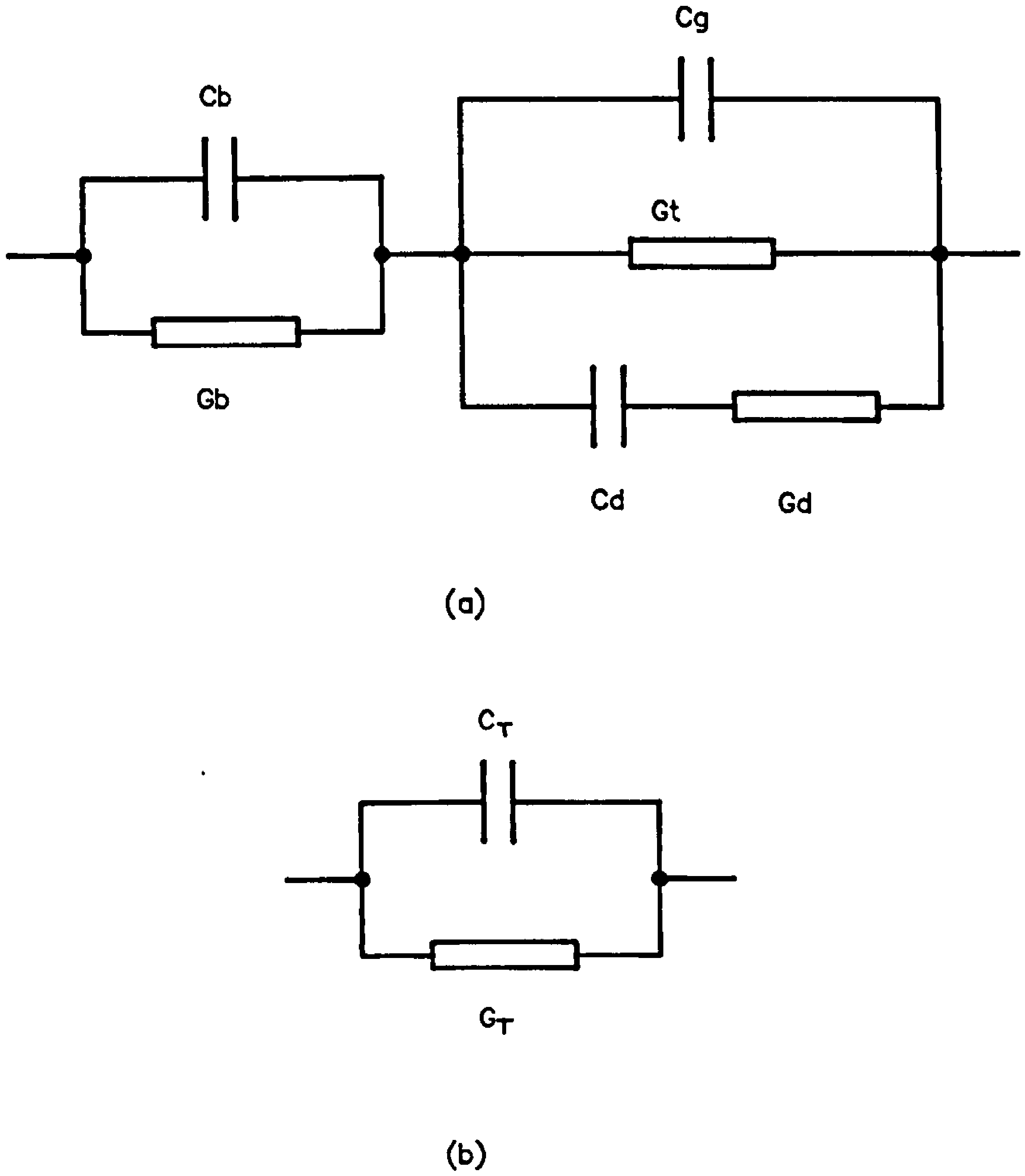

Fig 5.5 a) Simplified equivalent circuit representation of the electrode/coating/electrolyte system using frequency-invariant elements.

b) Circuit assumed by the Frequency Response Analyser.

be defined as;

$$C_b = \epsilon_o \epsilon_b A/t_b \qquad 5.3$$

where ϵ_b is the dielectric permittivity of the coating and t_b is the coating thickness. Again, to allow for the presence of defects and assuming that the effective capacitance of the defects is that of the double layer, the total measured capacitance, C_b' will be the parallel combination of $C_b\beta$ and $C_d(1-\beta)$, therefore;

$$C_b' = \beta C_b + C_d(1-\beta) \qquad 5.4$$

Finally, although the dominant interfacial region will now be at the electrolyte/coating boundary, a modified form of G_t is required. This is because charge transfer now occurs at the coating/electrode interface so that the relevant ionic concentrations and mobilities are those pertaining in the film. For simplicity, the discharge rates, denoted by r_p', r_n' are considered identical to those describing the uncoated case. Therefore the charge transfer conductance G_t', can be defined as;

$$G_{to}' \equiv G_{bi}[\epsilon_n' r_n' + \epsilon_p' r_p' + (r_n' r_p'/2)]/\{2[1+r_n'/2][1+r_p'/2]\} \qquad 5.5$$

where G_{to}' is based on G_{to} (Appendix A, equation A.85), with the substitutions as outlined above so that $\epsilon_p' = (1+\mu_n'/\mu_p')^{-1}$, $\epsilon_n' = (1+\mu_p'/\mu_n')^{-1}$ and the electrolyte conductance G_d has been replaced by G_{bi}.

5.3 The measurement and interpretation of admittance vs frequency plots

The total admittance, Y_T, of the equivalent circuit of fig 5.5(a) can be represented by the circuit shown in fig 5.5(b) in which;

$$Y_T = G_T + jwC_T \qquad 5.6$$

where G_T and C_T were determined experimentally using a frequency response analyser ($ 5.5, fig 5.2). A 30mV peak-to-peak sinusoidal voltage, generated by the FRA was applied across the cell and measurement admittance. A small ac signal was used to minimise the effects of non-linearities (eg Macdonald, 1976). The FRA was used in the ratiometric mode, data being output in terms of a complex number, A+jB, which is characteristic of the cell admittance. In the ratiometric mode;

$$V_Y/V_X = A+jB = (Y_M+Y_T)/Y_M = 1 + Y_T/Y_M \qquad 5.7$$

where the cell admittance, $Y_T=G_T+jwC_T$ and the reference admittance, $Y_M=G_M+jwC_M$. Substituting for Y_M and Y_T in equation 5.7 and rearranging gives;

$$G_T = [G_M(A-1)+wBC_M]/[(A-1)^2+B^2] \qquad 5.8$$

and

$$C_T = [w(A-1)C_M-BG_M]/\{w[(A-1)^2+B^2]\} \qquad 5.9$$

enabling the cell conductance and capacitance to be calculated from A and B. The experimentally determined values of C_T and G_T can then be related to the equivalent circuit parameters using equations 5.10 and 5.11 below.

$$C_T=[(C_bG^2+CG_B^2)+w^2(C_bC^2+C_b^2C)]/[(G_b+G)^2+w^2(C_b+C)^2] \qquad 5.10$$

and the conductance

$$G_T=[(G_b^2G+G_bG^2)+w^2(C_b^2G+C^2G_b)]/[(G_b+G)^2+w^2(C_b+C)^2] \qquad 5.11$$

where

$$C = C_g+\{C_dG_d^2/(G_d^2+w^2C_d^2)\} \qquad 5.12$$

and

$$G = G_t+\{w^2C_d^2G_d/(G_d^2+w^2C_d^2)\} \qquad 5.13$$

Theoretical curves showing the frequency dependence of C_T and $G_T/2\pi f$ over the frequency range 10^{-3} to 10^6 Hz, are given in fig 5.6(a). The curves were calculated using the component values shown in fig 5.6(b). These values were chosen because they give features typical of the systems studied here. In order to estimate the equivalent circuit parameters from experimental curves, it is useful to derive approximate forms for equations 5.10 and 5.11.

(i) Low frequency range

As w->0, $C \approx (C_g+C_d)$ and $G \approx G_t$ so that;

$$C_T \approx C_bG_t^2+(C_g+C_d)G_b^2]/(G_b+G_t)^2 \qquad 5.14$$

and

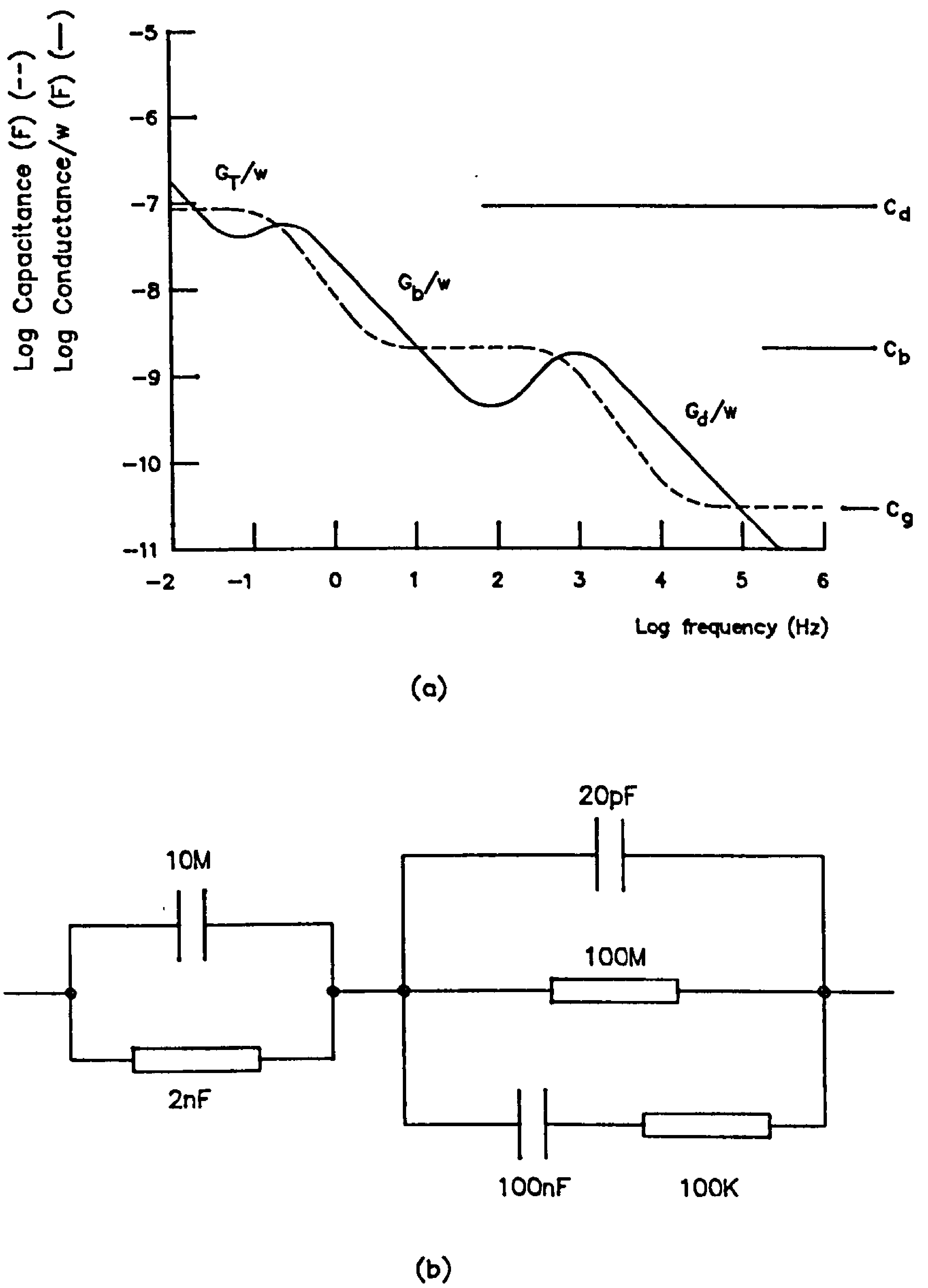

Fig 5.6 a) Idealised capacitance and conductance/w vs frequency curves calculated using the equivalent circuit representation b) of the coated electrode/electrolyte system with the parameter values as indicated.

$$G_T \approx G_bG_t/(G_b+G_t) \qquad 5.15$$

Therefore G_T is approximately the series sum of the charge transfer and the blocking layer conductances. Furthermore, as $C_d>C_b>>C_g$ in the present experimental situation, if $G_b>>G_t$ then $C_T\approx C_d$, the double layer capacitance.

(ii) High frequency range

As w -> ∞,

$$C_T \approx C_bC_g/(C_b+C_g) \qquad 5.16$$

and

$$G_T \approx \{C_b^2(G_d+G_t)+C_g^2G_b\}/(C_b+C_g)^2 \qquad 5.17$$

Again, for the conditions pertaining to the present experimental situation, equations 5.16 and 5.17 can be further reduced to give $C_T\approx C_g$, the geometric capacitance and $G_T\approx G_d$, the electrolyte conductance.

(iii) Mid-frequency range

There are no simplified forms for equations 5.10 or 5.11 for the mid- frequency range. However, the two loss peaks can be used to estimate the coating conductance and capacitance if the electrolyte conductance and double layer capacitance can be determined. It is easily shown that to a first approximation, the loss peak maxima occur at

$$f \approx G_b/(2\pi C_d) = 0.16\text{Hz} \qquad 5.18$$

and

$$f \approx G_d/(2\pi C_b) = 800\text{Hz} \qquad 5.19$$

Therefore, provided that the dispersions are well separated, G_b and C_b can be estimated from equations 5.18 and 5.19 by substituting the values of C_d, G_d estimated as outlined above (i,ii) along with the appropriate value of f. Alternatively, the central plateau of the C_T curve is approximately at C_b and from the negative slope of the mid-frequency portion of the $G_T/2\pi f$ plot, a value for G_b can be obtained.

5.4 Experimental procedure

The measurement cell and temperature control box are shown in fig 5.7. The measurement cell was used with two different electrode arrangements. These were (i) planar, coated electrodes ($ 4.2.2 to $4.2.4), with a surface area of 1.13cm^2, held parallel in a special fixture at a controlled spacing of 3-5mm and (ii) 1mm diameter, platinum wire electrodes ($ 4.2.1), mounted coaxially with a platinum gauze electrode of 10cm^2 surface area. The electrodes under test were placed in the test solution and connected to a frequency response analyser (fig 5.8).

Measurements on spin coated electrodes ($ 4.3.2) were performed after presoaking the electrodes for 24 hours, commencing with the most dilute electrolyte. Measurements on LB film coated electrodes ($ 4.3.1) were performed immediately the electrodes were placed in the electrolyte. In general, freshly coated electrodes were used for each set of experiments.

Experiments were performed at room temperature or at a temperature controlled by passing tap water (20±2°C) or water from a temperature control unit (15.0±0.5°C) through the coil (fig 5.7). The cell temperature was generally measured at the end of each run and the electrolyte pH after each set of experiments.

The cell admittance was measured using a Solartron 1174 Frequency Response Analyser (FRA) (i) as a function of frequency, in the range of 1mHz to 1MHz ($ 5.3) for different times of immersion in the electrolyte and (ii) as a function of time at a fixed frequency. A diagram of the system is shown in fig 5.8. Similar instruments have been used by other workers studying dielectric behaviour (Pugh and Ryan, 1979; Dickinson and Whitfield, 1977; Rudd, 1977; Boukamp, 1984).

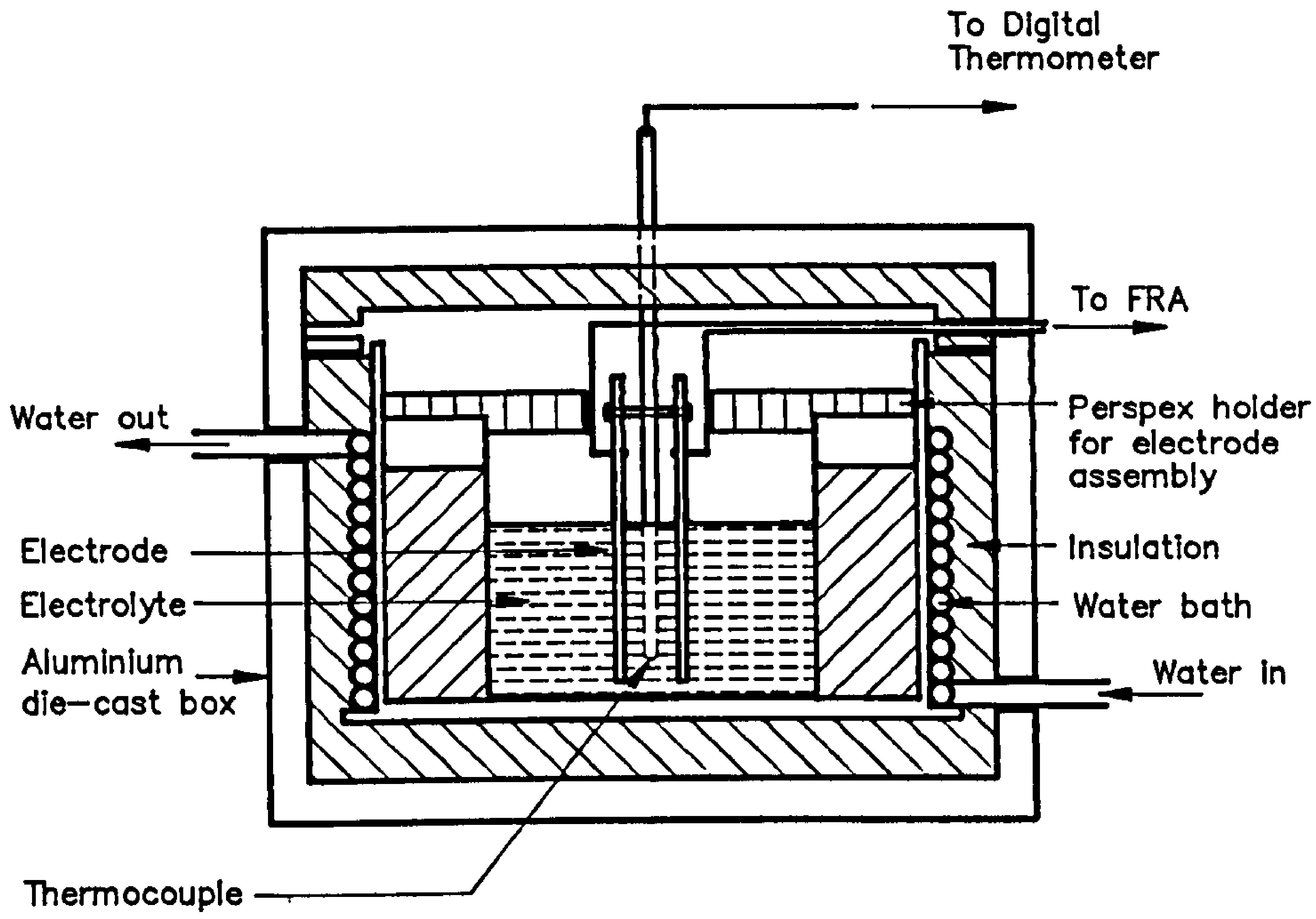

Fig 5.7 Diagram showing the measurement cell and temperature control box

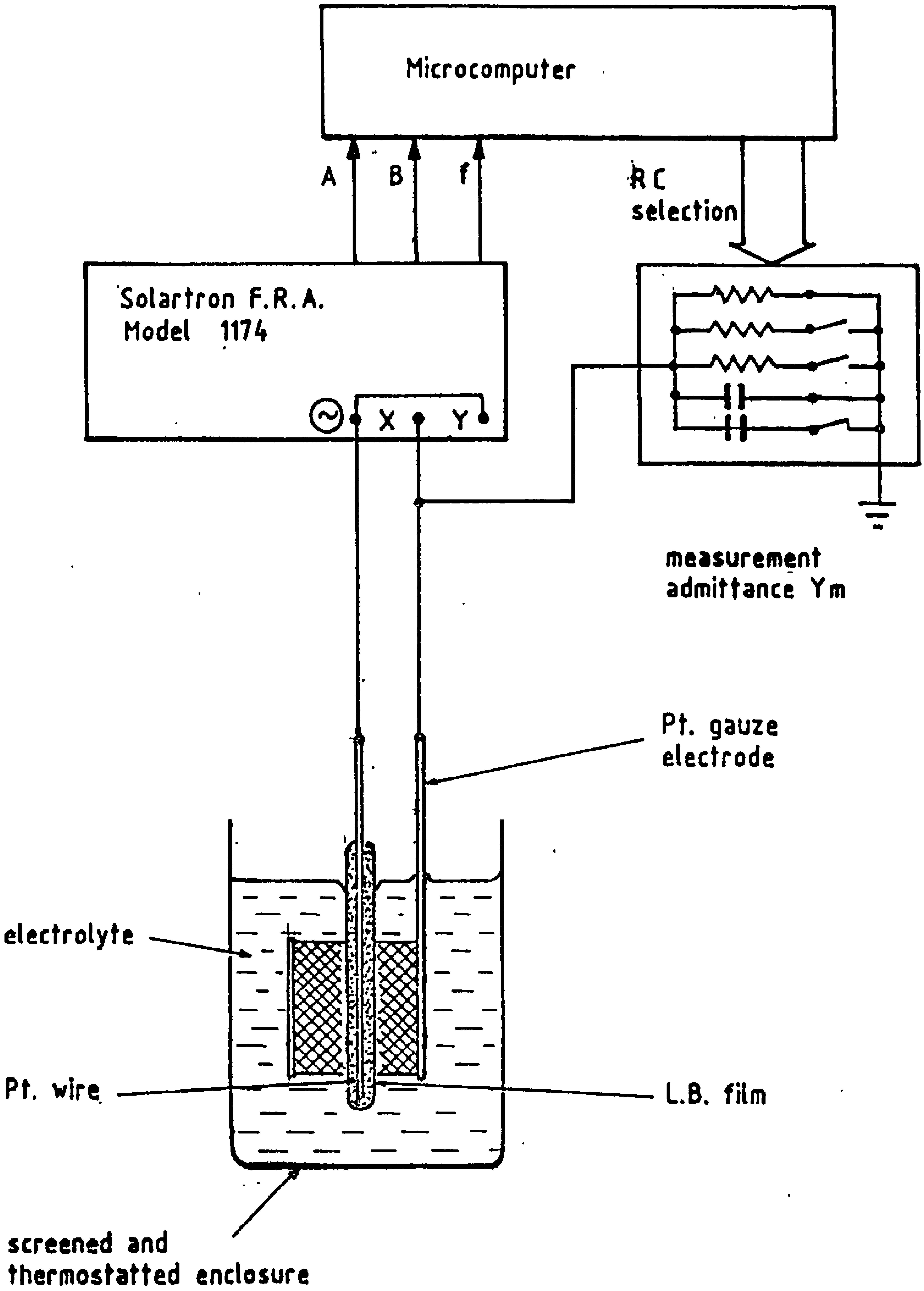

Fig 5.8 The experimental arrangement for the measurement of the AC Admittance of platinum wire electrodes.

The input impedance of the FRA ($\approx 10^6 \Omega$) meant that only impedances up to $\approx 10^7$ Ω could be measured accurately. Also, to improve sensitivity at lower sample impedances, it was necessary to modify the input admittance of the FRA. This was achieved by shunting the input with one of a pair of switchable resistors and capacitors (fig 5.8). The component values were selected so that $|A|$and $|B|$could be kept greater than unity. These shunt components were calibrated using a manual method based on the procedure employed by Pugh and Ryan (1979).

Initially A, B, frequency and an integer representation of the selected measurement components were entered via the keyboard of an Exidy Sorcerer Microcomputer and stored on disc. In order to reduce the measurement time, the FRA was subsequently interfaced to the microcomputer (fig 5.8). Under software control, A, B and frequency data were read by the computer and stored on disc at the end of each run. The software also selected the required measurement admittance to maintain $1.5 \leq |A| \leq 10$ and $1 \leq |B| \leq 10$. The stored data could be printed or plotted with the usual format being log (capacitance) and log (conductance/$2\pi f$) against log (frequency). Automation of the system considerably decreased the experimental run time and permitted the measurement of sample admittance against time at fixed frequency.

5.5 Preliminary results – PVC Coated Electrodes

In sections 5.3 and 5.4, it was shown that within certain limits, the ac admittance technique can be used to measure the conductance and capacitance of thin, semi-insulating films on metal electrodes immersed in electrolyte solutions. To test the validity of the approach, some preliminary measurements were carried out on copper electrodes, spin coated with PVC ($ 4.3.2). The cell admittance was measured as a function of frequency in different concentrations of KCl solution. Curves showing the variation of cell capacitance and (conductance/$2\pi f$) are presented (figs 5.9, 5.10) and discussed with

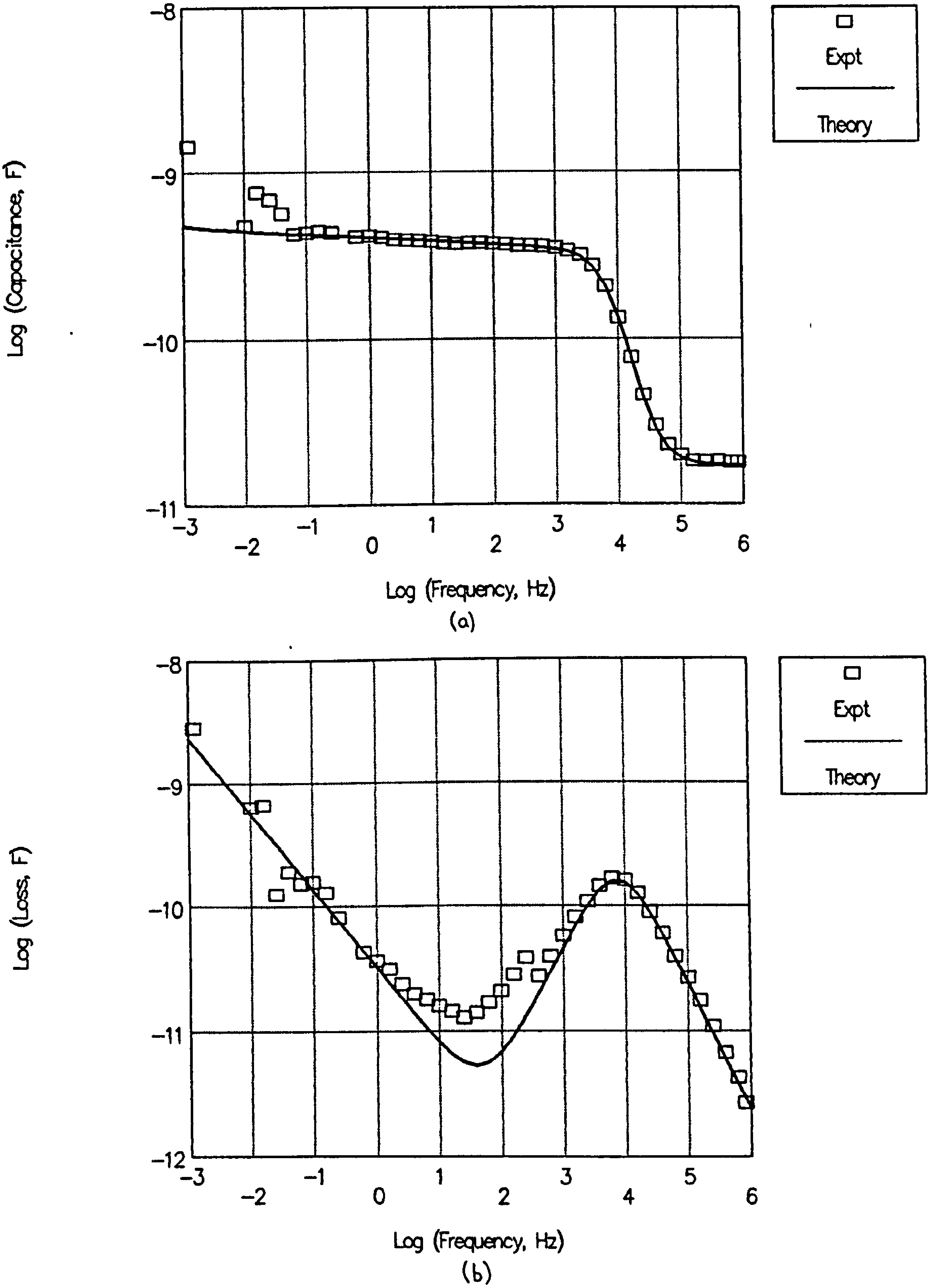

Fig 5.9 (a) Log Capacitance, C_T and (b) Loss ($G_T/2\pi f$) plotted against log frequency, F, for a PCB copper electrode, spin coated with PVC and immersed in 0.2mM KCl at 29.0±2.5°C. The points represent the experimental data whilst the solid lines show a theoretical fit based on the equivalent circuit model shown in Fig 5.5. The parameter values used for the fit are presented in column 1 of Table 5.1.

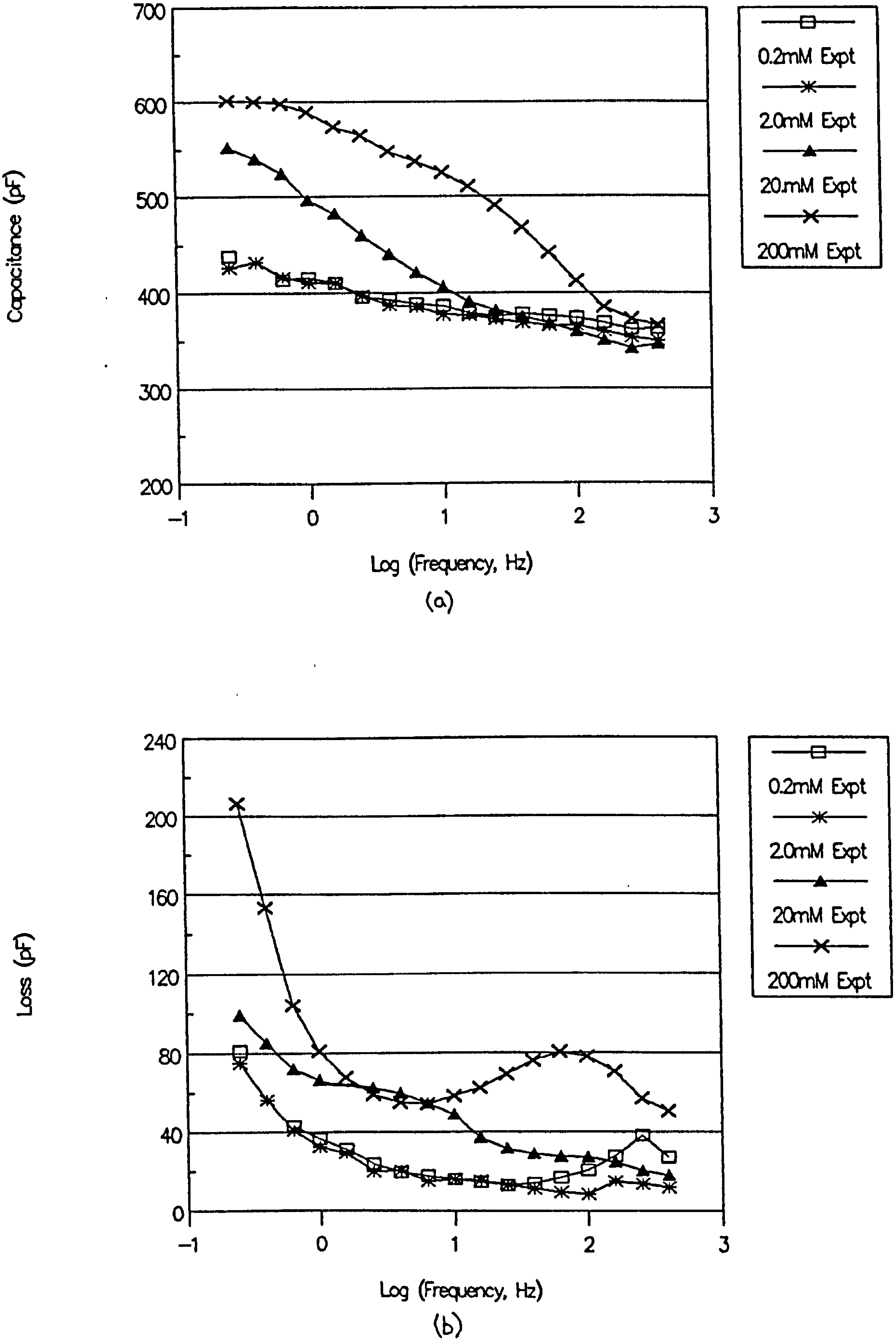

Fig 5.10 (a) Capacitance, C_T and (b) Loss ($G_T/2\pi f$) plotted against log frequency, F, for a PCB copper electrode, spin coated with PVC and immersed in (□) 0.2mM, (*) 2.0mM, (▲) 20mM and (x) 200mM KCl at 29.0±2.5°C.

reference to the equivalent circuit model (fig 5.5(a)). Finally, a summary of equivalent circuit parameter values is presented in Table 5.1.

5.5.1 The variation of cell admittance with frequency

The cell capacitance, C_T and loss, $G_T/2\pi f$ as functions of frequency are shown in the double log plots of fig 5.9 for 0.2mM KCl solution at 29±2.5°C. The points represent the experimental data whilst the solid lines show a theoretical fit based on the equivalent circuit model shown in fig 5.5(a), with the parameter values as given in Table 5.1. n and m are the frequency dependencies of C_b and G_b respectively. Curves for higher molarity solutions are of the same basic shape, although an additional dispersion appears at higher molarities (fig 5.10).

Electrolyte/Parameter	KCl Molarity			
	0.2mM	2mM	20mM	200mM
C_g(F)	1.8x10^{-11}	1.8x10^{-11}	1.8x10^{-11}	1.8x10^{-11}
C_d(F)	5.0x10^{-7}	1.6x10^{-6}	5.1x10^{-6}	1.6x10^{-5}
C_b(F)	4.2x10^{-10}	4.0x10^{-10}	4.2x10^{-10}	4.0x10^{-10}
n	-0.02	-0.02	-0.02	-0.02
G_d(S)	1.7x10^{-5}	5.3x10^{-4}	4.2x10^{-3}	7.2x10^{-2}
G_t(S)	1.0x10^{-11}	1.0x10^{-11}	1.0x10^{-11}	1.0x10^{-11}
G_b(S)	1.0x10^{-10}	1.4x10^{-10}	2.3x10^{-10}	3.3x10^{-10}
m	0.38	0.05	-0.03	0.15

Table 5.1 Summary of parameter values for the equivalent circuit representation of PCB copper electrodes, spin coated with PVC and immersed in a range of KCl molarities at 29.0±2.5°C.

5.5.1.1 Variation of cell capacitance with frequency

At frequencies above 100kHz the cell capacitance reaches a plateau, the geometric capacitance, which from curve fitting is 18pF. The value calculated for the geometric capacitance, C_g, assuming an electrode area of 1.13cm^2, an inter-electrode spacing of 5mm and a relative dielectric permittivity of 78 is 16pF. Allowing for stray capacitances and fringing effects, the calculated and experimental values are in good agreement which confirms that the cell capacitance is dominated by the geometric capacitance at high frequencies.

As the frequency is decreased, the capacitance rises to a second plateau, which from curve fitting is described by the function;

$$C_T = 4.23.10^{-10}.w^{-0.02} \text{ (F)}$$

where the value $4.23.10^{-10}$ F is the capacitance extrapolated to w=1. The dielectric permittivity of PVC is approximately equal to 4 (CRC Handbook of Chemistry and Physics 1986), from which the total film thickness is calculated to be 11.3μm (C_T evaluated at 1kHz), corresponding to a film thickness of 5.65μm per electrode coating. This is of the correct magnitude for the spin coating process and verifies that the mid-frequency capacitance is the electrode coating capacitance. The slight frequency dependence of the capacitance is attributed to the dielectric dispersion of the PVC coating.

At frequencies below 10mHz the cell capacitance begins to rise towards the double layer capacitance, C_d. However, insufficiently low frequencies were attained to accurately determine the limiting low frequency value. Consequently, for the purposes of the theoretical fit, the value of C_d employed was calculated from equation A.83, thus;

$$C_d = C_{io} = MC_g = 5.1.10^{-7} \text{ (F)}$$

5.5.1.2 Variation of cell loss with frequency

The variation of loss, $G_T/2\pi f$ with frequency for the PVC coated copper electrode in 0.2mM KCl is shown in fig 5.9b. At frequencies above 20kHz a straight line region of slope -1 is observed. The value of G_T in this range is estimated at 17μS from curve fitting, which corresponds to an electrolyte molarity of 4.7×10^{-5}, much less than the expected molarity of 2×10^{-4} (A.3.3). This suggests that some of the ions in the electrolyte have been absorbed by the PVC film, possibly occupying pores left in the film as the casting solvent evaporated.

At lower frequencies, the loss curve passes through a dispersion, the peak frequency of which occurs at 7kHz. The peak frequency predicted by the theoretical analysis (equation 5.19), is approximated by;

$$f_{pk} = G_d/(2\pi C_b) \text{ (Hz)}$$

which, for G_d=17μS and $C_b = 4.23 \times 10^{-10}.w^{-0.02}$, gives f_{pk}=5.2kHz. On the low frequency side of the loss peak, the experimental data shows a small step change. This is attributed to the low sensitivity of the measuring circuit in this range. The lack of agreement between the experimental points and theoretical curve at these frequencies is due to this discontinuity. A further contributory factor may be the result of dielectric dispersion in the PVC coating, resulting in an additional small loss. At frequencies below 20Hz, the loss begins to increase, although sufficiently low frequencies were not attained to observe a second loss peak. The coating conductance in the frequency range 20Hz to 1mHz is described by the relationship;

$G_b=1.0.10^{-10}w^{0.5}$ (S)

The loss observed in this frequency range may be due to ionic drift within the film. Based on a film thickness of 5.65μm and for $G_T=1.0.10^{-10}$, t=11.3μm and A=1.13cm^2, the conductivity of the film is estimated from equation 5.1 to be 10^{-11} Sm, assuming that $G_{bs}»G_{bi}$. If the film conductance is the result of ionic flow through small pores, the fraction of the surface covered by such defects would be approximately 1.10^{-8} using the experimentally determined value for G_d. However, if the value for G_d corresponding to the calculated value for a 0.2mM solution of KCl is employed, the fractional coverage is then approximately 1.10^{-9}. A similar figure was given by Glarum and Marshall (1985) for electrodeposited polyphenylene oxide.

5.5.2 Variation of PVC coating admittance as a function of electrolyte molarity.

Capacitance and loss curves as a function of frequency for KCl molarities of 2,20 and 200mM have the same basic curve shape as for 0.2mM KCl (fig 5.9). The parameter values used to generate theoretical curves for the higher molarities are summarised in Table 5.1.

It is noteworthy that the experimental and theoretical plots agree best at high frequencies. For solution molarities above 2mM and at frequencies below 100Hz, the cell capacitance rises to an additional plateau. A corresponding dispersion is observed in the loss curve. These features are shown in fig 5.10(a,b) where the y axis log scale has been replaced by a linear scale. This molarity dependent feature is attributed to ionic drift within the film, leading to a dispersion at frequencies above which the adsorbed ions can no longer follow the sinusoidal waveform. It is suggested that these features are not visible on the capacitance curves for lower molarity electrolytes because the concentration of ions in the film is insufficient to make a marked difference to the film permittivity.

5.6 Conclusions

After considering the theoretical background to AC admittance analysis ($ 5.2), it was shown that within certain limits, the technique can be extended to measure the conductance and capacitance of thin, semi- insulating films on metal electrodes immersed in electrolyte solutions ($5.3 and $5.4). The validity of this approach was verified by carrying out preliminary measurements on copper electrodes, spin coated with PVC ($ 4.3.2).

Admittance data for PVC coated copper electrodes were presented and discussed with reference to an equivalent circuit model for the cell. It was shown that as well as being a useful means of predicting the ideal capacitance and loss behaviour of the cell, observation of areas of discrepancy can provide insight into other phenomena such as ionic drift within the coating.

Therefore by combining the techniques of small signal admittance analysis and equivalent circuit modelling, it is possible to define quantitatively elements included in the model and identify the presence of other mechanisms.

6.0 Cyclic Voltammetry

6.1 Introduction

Cyclic voltammetry is a technique widely used for measuring the current/voltage characteristics of electrode/electrolyte systems. In the technique, a driving potential applied to a working electrode causes oxidation/reduction of the active species to occur at the electrode. This in turn changes the magnitude of currents flowing through the test cell. If the applied potential has a triangular waveform and sweeps periodically between fixed limits, then a dynamic current-voltage characteristic can be obtained for the cell. Such characteristics are known as cyclic voltammograms (Mabbott, 1983).

To obtain a cyclic voltammogram (CV), the aqueous electrolyte containing the electroactive species is placed in a three terminal test cell (fig 6.1). As the potential between the working electrode and the counter electrode is swept between two predetermined limits in a triangular fashion (fig 6.2b), both the current flowing through the working electrode, and its potential with respect to a standard calomel electrode monitored simultaneously and are plotted on an X-Y plotter (Van Benschoten et al, 1983). A typical curve for a reversible, Nernstian process is given in fig 6.2a, for a species O, undergoing the reaction;

$$O + ne \underset{\text{Oxid}}{\overset{\text{Red}}{\rightleftharpoons}} R$$

Where n is the number of electrons transferred per molecule.

The cyclic voltammogram can yield information concerning the electrode material (eg surface area), the surface coating (eg catalytic loading, reactivity (Fujihara and

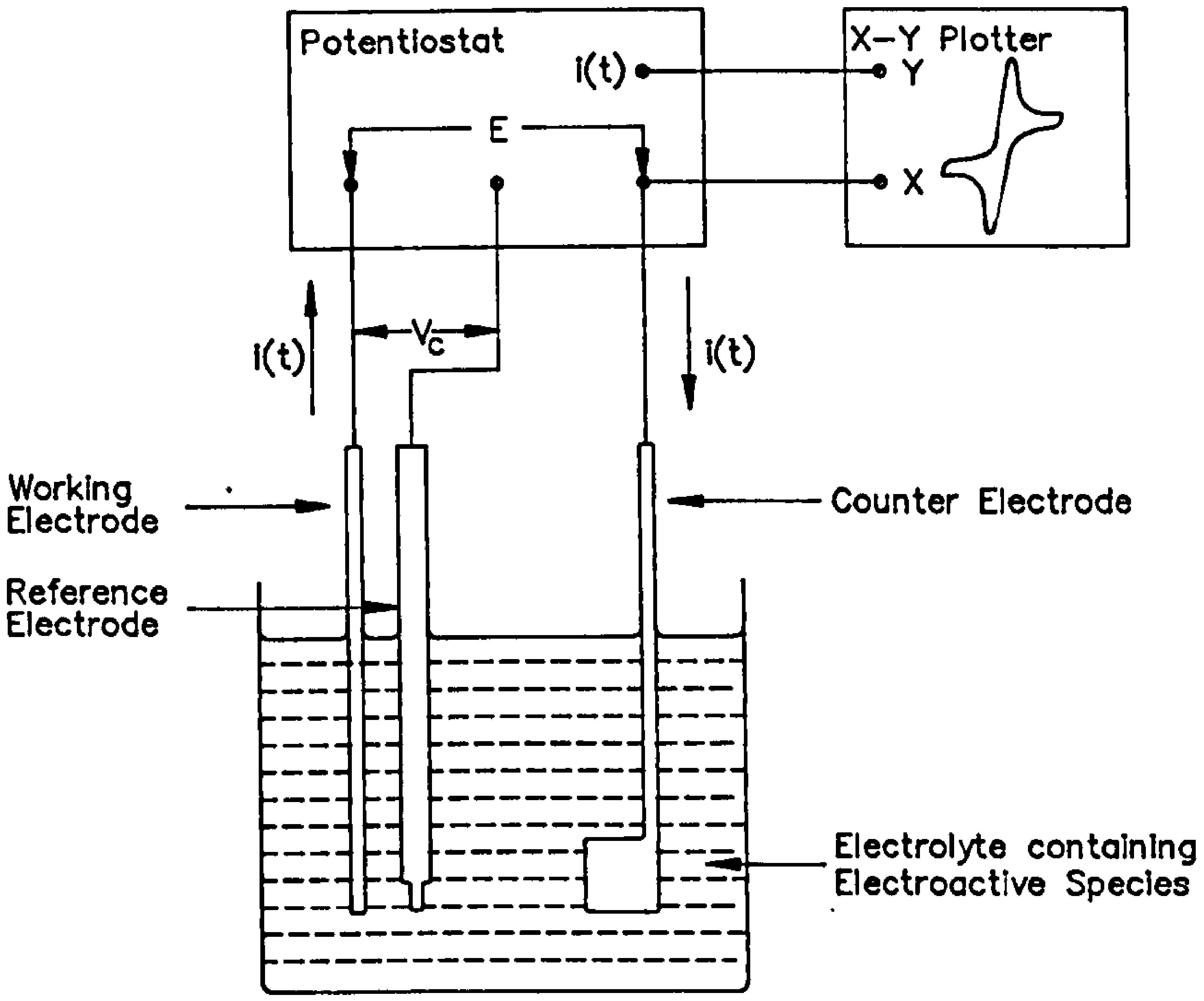

V_c = Controlled potential wrt reference electrode.

$E = E_i + vt$ = Driving potential.

Fig 6.1 Diagram showing the experimental arrangement for Cyclic Voltammetry.

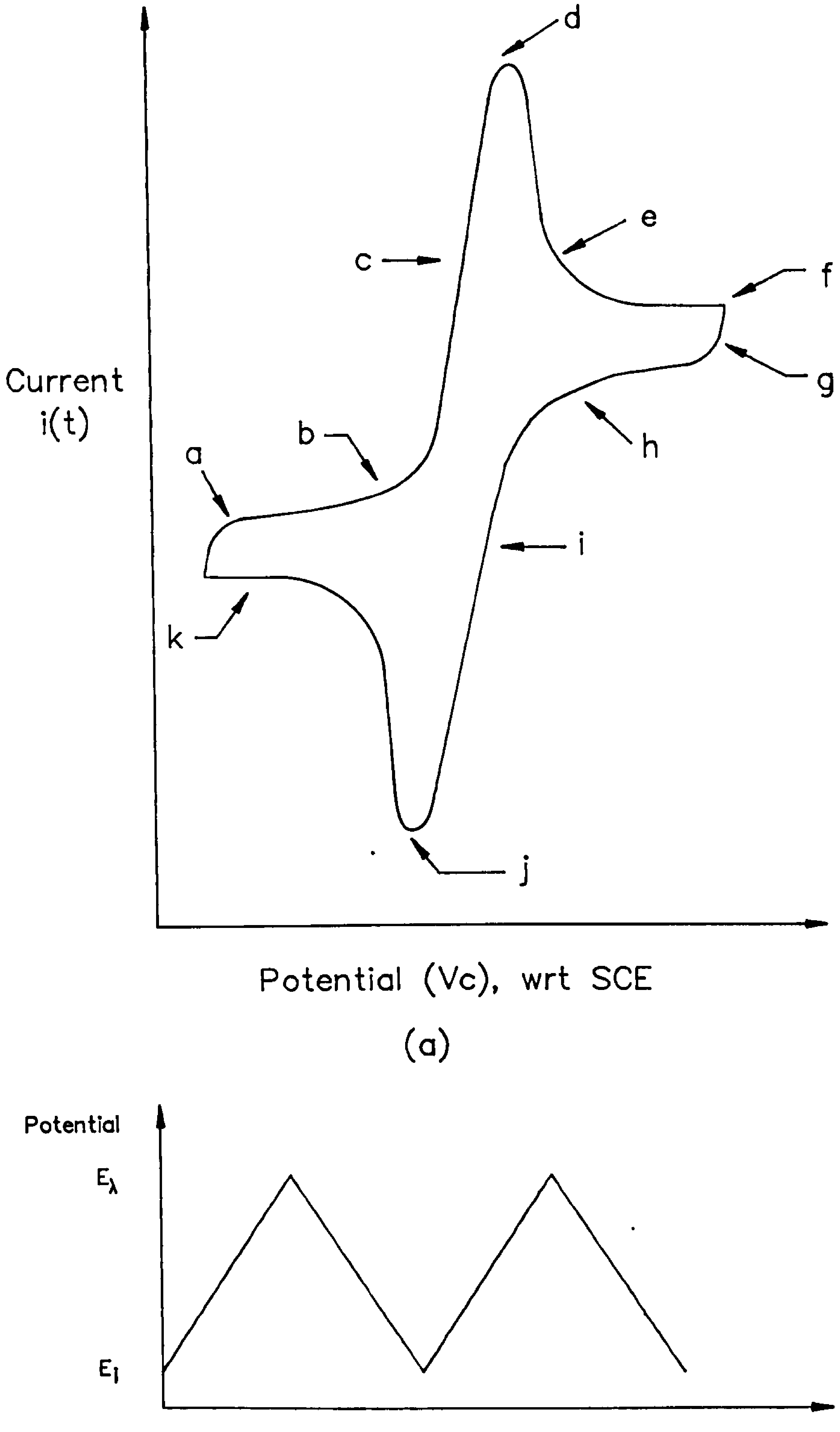

Fig 6.2 a) A typical cyclic voltammogram for a reversible process.

b) A typical triangular switching waveform.

Poosittisak, 1986(a,b)), and permeability to electroactive species (Rubinstein et al, 1987)) and the electroactive species in solution (eg diffusion coefficients, charge, concentration, electrochemical reversibility (Van Benschoten et al, 1983)).

In the following sections, the essential theory relating to voltammetry is presented, followed by a discussion of the factors which determine the shape of the CV. Non-ideal electrode reactions are then considered with reference to bare wire and coated wire electrodes.

6.2 Essential Theory of Voltammetry

Consider again the CV shown in fig 6.2. The total cell current, i is made up of 1) a Faradaic component (ie current due to electron transfer at the electrode) and 2) a non-Faradaic component (ie current due to the physical rearrangement of ions in the double-layer by the charging and discharging of the double layer capacitance (Maloy, 1983; Bard and Faulkner, 1980).

6.2.1 Non-Faradaic Current

The non-Faradaic current may be modelled by considering an electrochemical cell comprising of an ideally polarizable electrode, (IPE) and an ideal reversible electrode (IRE). The cell can be approximated by an electrical circuit of a resistor, R_{sol} in series with a capacitor, C_{dl} (fig 6.3). Then, if a linear potential sweep E, is applied to the circuit;

$$E = E_i + vt \qquad 6.1$$

Where E_i is the initial potential for the sweep and v is the sweep rate in volts/second.

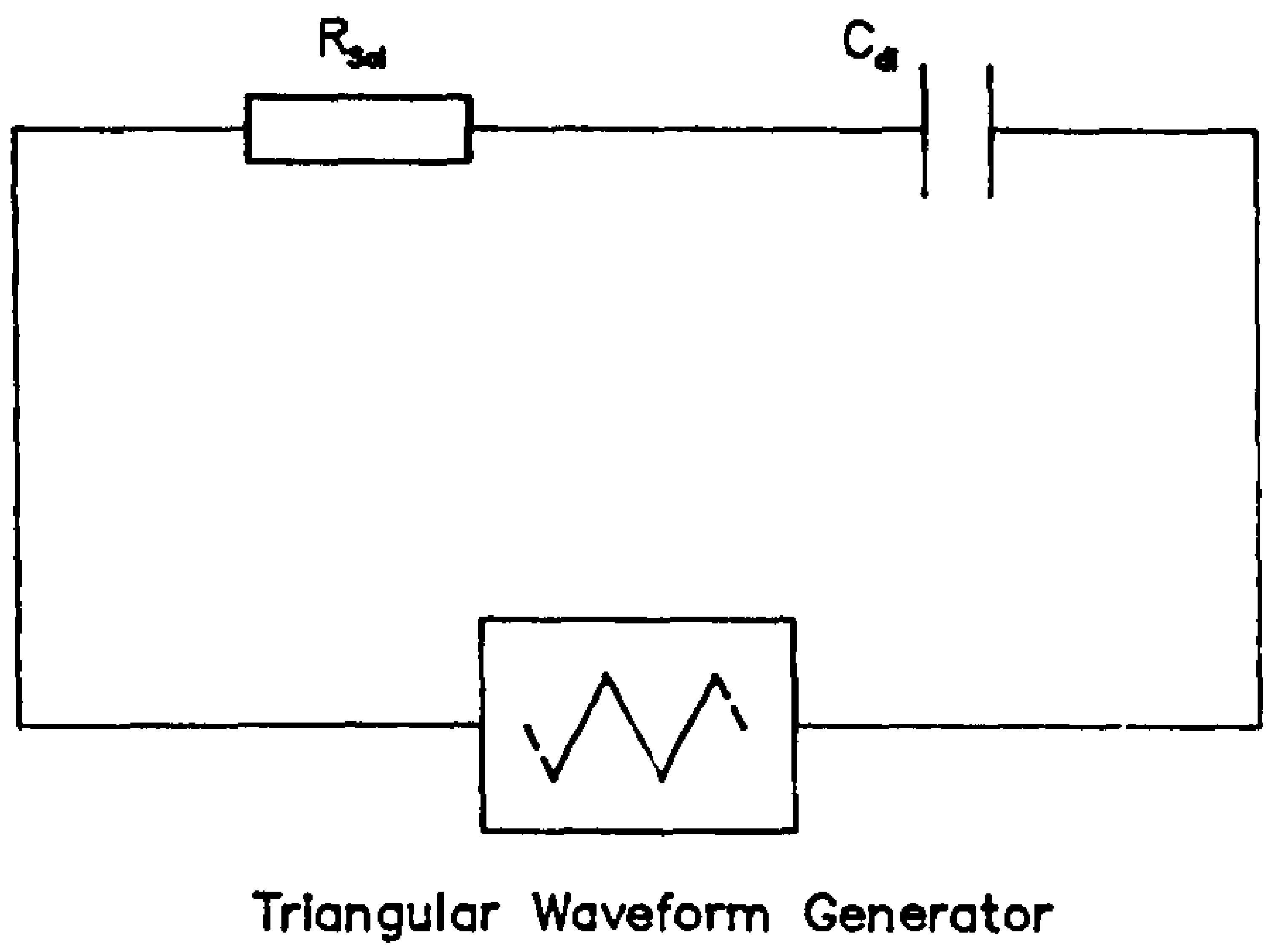

Fig 6.3 Equivalent circuit representation for an electrochemical cell comprising an IPE and an IRE.

Then, assuming that C_{dl} is independent of voltage;

$$E_i + vt = R_{sol}dq/dt + q/C_{dl}$$

From which it follows that;

$$i = i_s + i_t = vC_{dl} + [(E_i/R_{sol} - vC_{dl}) \exp (-t/R_{sol}C_{dl})] \quad 6.2$$

The current contains a steady state component i_s, and a transient part i_t, with time constant $R_{sol}C_{dl}$. Thus, during CV for a triangular waveform which switches from -v to +v, the "cell" current will switch between $-vC_{dl}$ and $+vC_{dl}$. Fig 6.4 shows the non-Faradaic current for the RC circuit model under "steady state" conditions, assuming a small time constant and a potential invariant double layer capacitance (Bard and Faulkner, 1980).

6.2.2 Faradaic Current

In contrast to non-Faradaic processes, Faradaic currents result from charge transfer at the electrode due to reduction and oxidation reactions. Indeed, the Faradaic current that flows at any time is a direct measure of the rate of the electrochemical reaction taking place at the electrode. The rate depends largely on 1) the rate of mass transfer and 2) the rate of charge transfer from electrode to solution and vice versa (Maloy, 1983). This can be seen most easily by considering two extreme cases. These are the application of firstly a slow, linear ramp and secondly, an instantaneous potential step.

6.2.2.1 Steady state voltammetry - Potential controlled current

If an electrode reaction involves only fast heterogeneous charge transfer kinetics

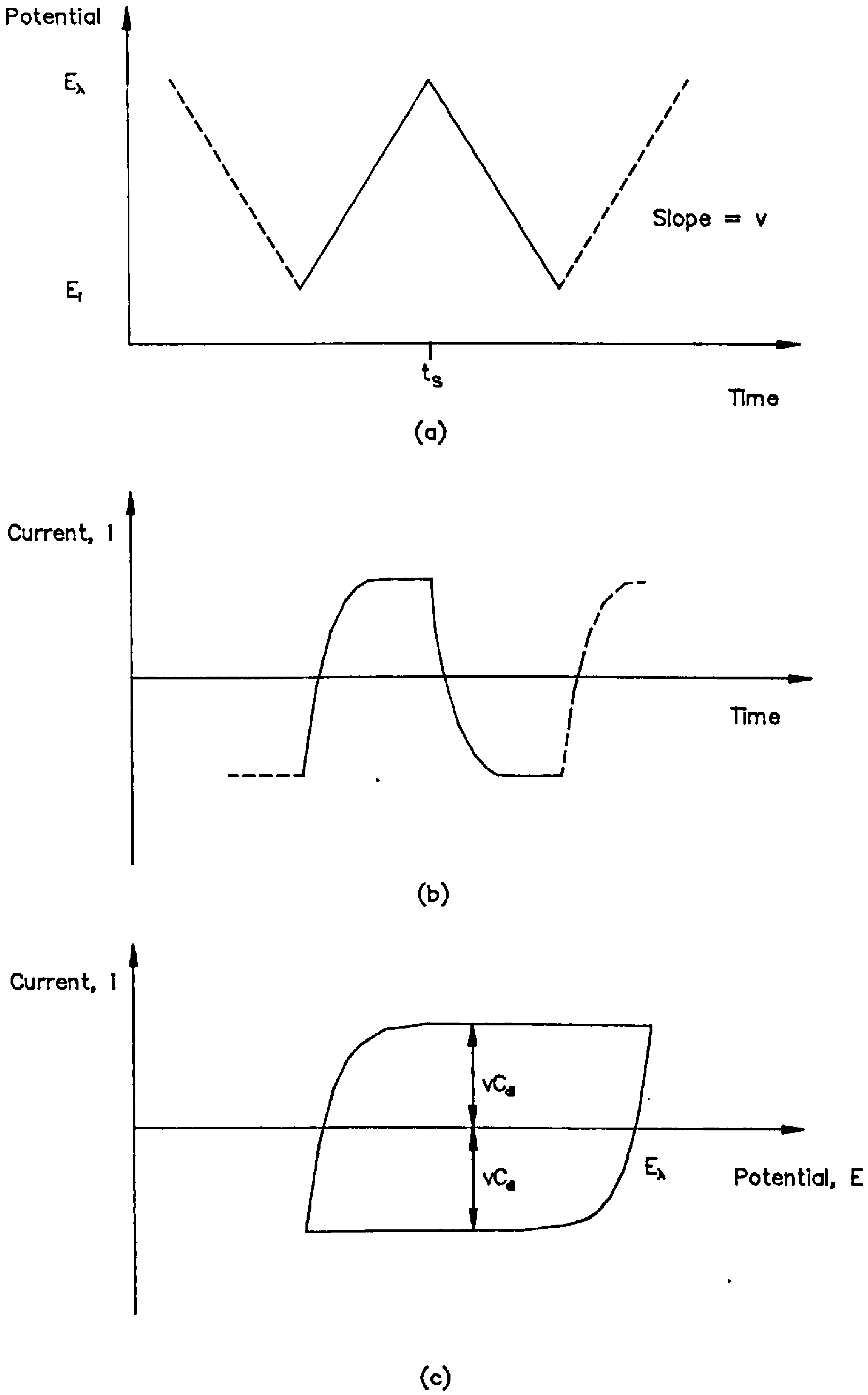

Fig 6.4 Current–Time (b) and Current–Potential (c) plots for a triangular wave (a) applied to an RC circuit (fig 6.3) assuming a time constant $R_{sol}\ C_d$ << switching time, t_s.

and mobile, reversible homogeneous reactions, then the homogeneous reactions can be regarded as being at equilibrium. The surface concentrations of species involved in the Faradaic process are then related to the electrode potential by the Nernst Equation. Furthermore, the net rate of electrode reaction r, is then governed totally by the rate, r_{mt}, at which the electroactive species are brought to the electrode surface by mass transfer and the Faradaic current is then given by;

$$i = rnFA = r_{mt}nFA \tag{6.3}$$

where n is the number of electrons transferred per atom of reactant and A is the electrode area.

The rate of mass transfer of electroactive species r_{mt}, to the electrode surface is governed by migration, convection and diffusion. The total flux per unit area at a distance x from the electrode, $J_i(x)$ is given by the Nernst-Planck equation;

$$J_i(x) = -D_i(dC_i(x)/dx) - (n_iF/RT)(D_iC_id\Phi(x)/dx) + C_iv(x) \tag{6.4}$$

Diffusion Migration Convection

where $J_i(x)$ is the flux of species i at distance x from the electrode surface, D_i is the diffusion coefficient, $dC_i(x)/dx$ is the concentration gradient, $d\Phi(x)/dx$ is the potential gradient, n_i is the valency and C_i the concentration of species i and v(x) is the hydrodynamic velocity (Bard and Faulkner, 1980).

In practice, migrational effects are eliminated by adding to the electrolyte, a compound which will not react at the electrode, at a concentration 100 times greater than that of the electroactive species (Maloy, 1983). The presence of this inert, supporting electrolyte means that to within 1%, any drift current present arises from the added ions not from the electroactive species. The effects of convection are minimised by keeping the measurement cell steady and the solution unstirred (Maloy, 1983). Provided that these precautions are observed, equation 6.4 can be simplified to Fick's First Law of Diffusion;

$$J_i(x) = -D_i(dC_i(x)/dx) \qquad 6.5$$

This means that in the case of steady state mass transfer, the rate of mass transfer is proportional to the concentration gradient at the electrode surface, and in the absence of convection and migration;

$$r_{mt} \propto (dC_o(x)/dx)_{x=0} \qquad 6.6$$

Which can be approximated to;

$$r_{mt} = m_o(C_o^* - C_{o(x=0)})$$

Where C_o^* is the concentration of O in the bulk solution far from the electrode, $C_{o(x=0)}$ is the concentration at the electrode surface and m_o is the mass transfer coefficient of species O. Combining equations 6.3 and 6.6 gives;

$$i = nFAm_o(C_o^* - C_{o(x=0)}) \qquad 6.7$$

For a net cathodic current, R is produced at the electrode which gives;

$$i = nFAm_R(C_R^* - C_{R(x=0)}) \qquad 6.8$$

Where C_R^* is the concentration of R in the bulk solution far from the electrode, $C_{R(x=0)}$

is the concentration at the electrode surface and m_R is the mass transfer coefficient of species R. Furthermore, from equation 6.7 it can be seen that when $C_{o(x=0)}=0$, the current will be at its maximum, i_l, for a given set of mass transfer conditions. This is because it corresponds to all of O being reduced as fast as it can be brought to the electrode surface, thus;

$$i_l = nFAm_oC_o^* \qquad 6.9$$

Then, as stated previously, for a reversible reaction, the equilibrium ratio of reduced O to oxidized R species is determined by the Nernst equation,

$$E = E^{o'} - (RT/nF)\ \ln([O]/[R])_{x=0} \qquad 6.10$$

Where $E^{o'}$ is the formal potential of the electrode. From the Nernst equation it is therefore possible to predict the concentration ratio of [O] to [R] at a given electrode potential. For example, when E=59mV more positive than $E^{o'}$ at a cell temperature of 25°C, the electrode concentration of R is ten times that of O (fig 6.2). It follows that in the simplest case of R initially absent, with $C_R{}^*=0$ and $C_{R(x=0)}$ given by equation 6.8 , then combining equations 6.7 to 6.10 and rearranging gives;

$$E = E^{o'} - RT/nF\ \ln(m_o/m_R) + RT/nF\ \ln((i_l-i)/i) \qquad 6.11$$

Similarly, it can be shown that when both O and R are initially present;

$$E = E^{o'} - RT/nF\ \ln(m_o/m_R) + RT/nF\ \ln((i_{l,c}-i)/(i-i_{l,a}) \qquad 6.12$$

Where $i_{l,c}$ and $i_{l,a}$ are the maximum cathodic and anodic currents respectively. Equations 6.11 and 6.12 are represented graphically in figs 6.4 and 6.5 respectively (Bard and Faulkner, 1980). $E^{1/2}$ is the polarographic half wave potential and is given by;

$$E^{1/2} = E^{o'} + (RT/nF)\ln(D_R/D_O)$$

Where D_R and D_O are the diffusion coefficients of species R and O respectively.

As long as there are sufficient electroactive species at the electrode surface to sustain the equilibrium reaction, the electrode potential will govern the surface concentrations of O and R, in accordance with the Nernst equation. However, in the case of Cyclic Voltammetry, for a range of applied voltages, it is normal for the electrode surface to become depleted of electroactive species. When this occurs, the electrode current/potential characteristic is dominated by diffusion. The situation of a diffusion limited faradaic current can be seen most readily by considering the simple case of a potential step perturbation to an electrochemical system.

6.2.2.2 Potential Step Experiment - Diffusion limited current

The experimental conditions are as previously ($ 6.2.2.1), except that the potential waveform is replaced by an instantaneous potential step of sufficient magnitude to completely reduce all O at the electrode surface. To calculate the diffusion limited current i_d, the linear diffusion equation, Fick's Second Law;

$$C_o(x,t)/dt = D_o d^2C_o(x,t)/dx^2 \qquad 6.13$$

must be solved for the boundary conditions;

$$C_o(x,o) = C_o^* \qquad 6.14$$

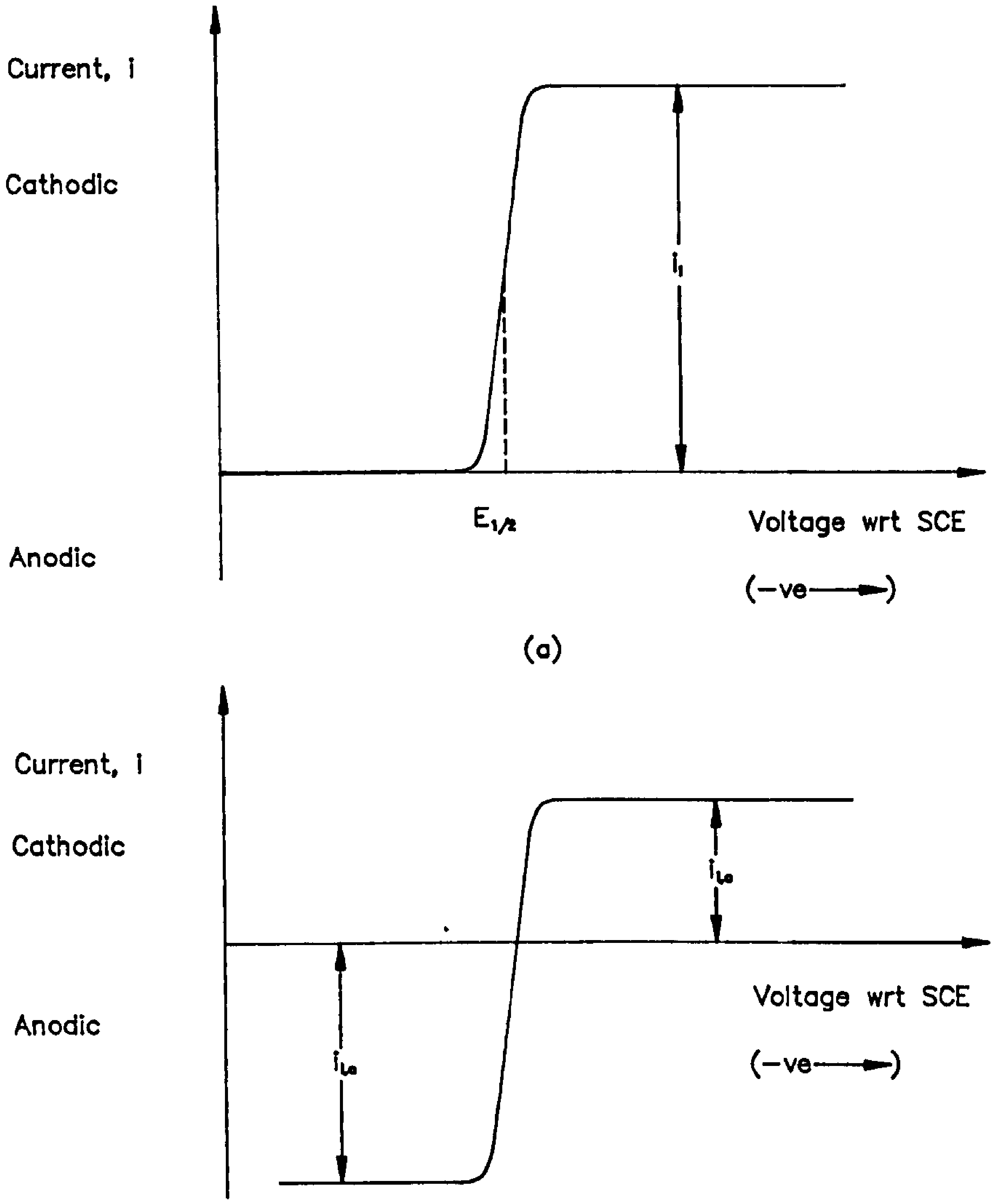

(a)

(b)

Fig 6.5 Current–Potential curves for a reversible reaction with a) only O present initially and b) with both O and R initially present. (Bard and Faulkner, 1980)

$$\lim_{x \to \infty} C_O(x,t) = C_O^* \qquad 6.15$$

$$C_O(0,t) = 0 \text{ (for } t>0) \qquad 6.16$$

Fick's Second Law states that the change in concentration at a location x is given by the difference in flux into and out of an element of width dx at x. The initial condition 6.14, means that the bulk concentration of O extends to the electrode surface. The semi-infinite condition 6.15, asserts that regions sufficiently far from the electrode are unperturbed by the experiment. The third condition 6.16, expresses that the surface concentration of O is zero once the potential step has been applied, which is the definition of the experiment. Then using Laplace transform methods and equations 6.3, 6.5 and 6.13 it can be shown that;

$$i_t = i_d(t) = (nFAD_O^{1/2}C_O^*)/(\pi^{1/2}t^{1/2}) \qquad 6.17$$

Which is known as the Cottrell Equation and is represented graphically in fig 6.6. From the Cottrel Equation it can be seen that when the electrode potential is sufficient to deplete the surface concentration of reactant species, the electrode current falls as $t^{-1/2}$ and is independent of the electrode potential (Bard and Faulkner, 1980).

So far we have considered separately the effects of electrode potential and diffusion on the Faradaic current. In the case of cyclic voltammetry both effects influence the observed CV. A mathematical treatment which models the complete behaviour of a reversible electrochemical system is outlined below.

6.2.2.3 Cyclic Voltammetry

Consider again the reaction O + ne = R, where the experiment commences with only O present and at a potential such that no current flows. Assuming rapid charge

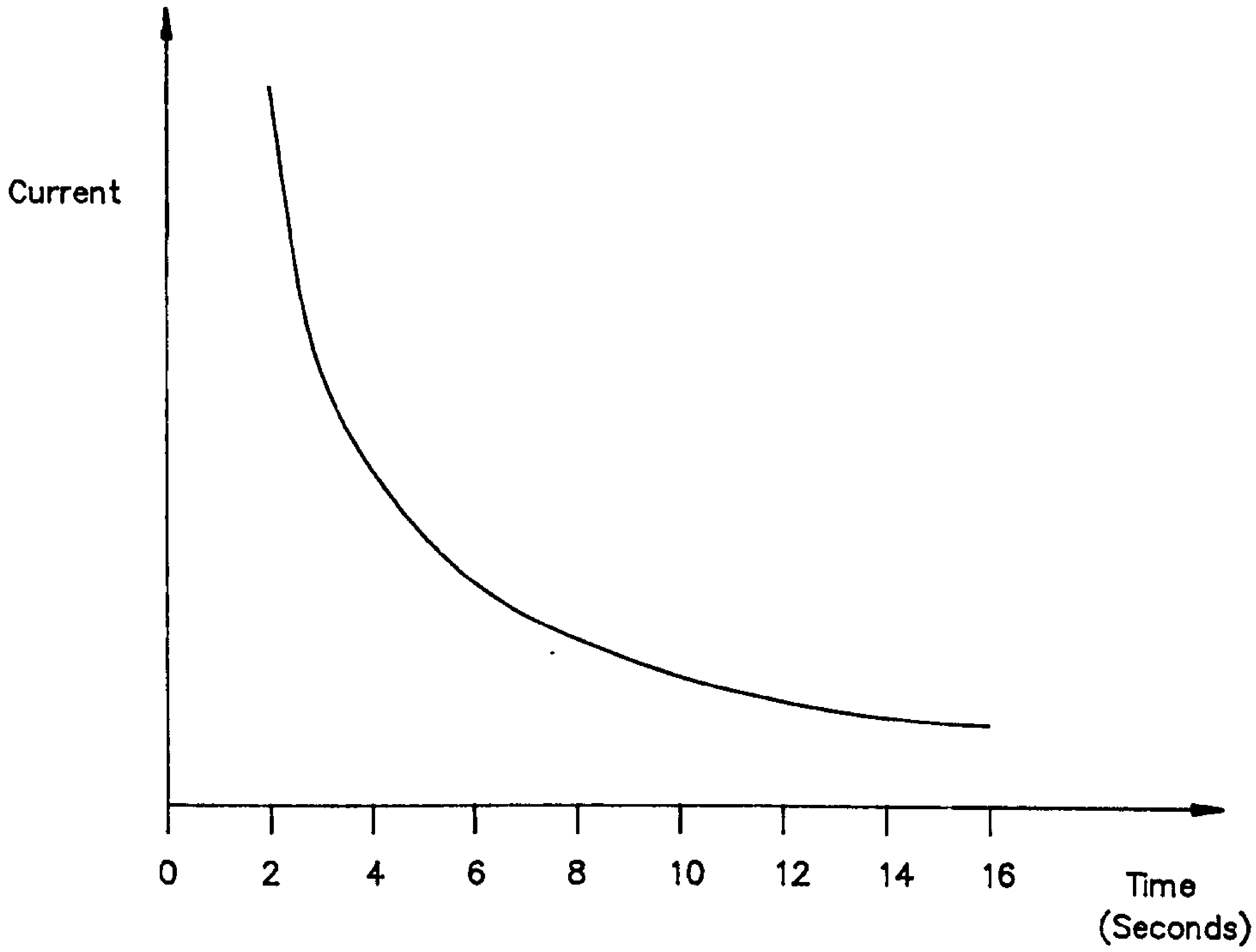

Fig 6.6 Typical current vs time curve for a potential step experiment under limiting current conditions.
(Bard and Faulkner, 1980)

transfer kinetics such that the surface concentrations of O and R are dictated by the Nernst Equation;

$$E(t) = E^{o'} + (RT/nF)\ln\{(C_O(0,t)/C_R(0,t))\} \qquad 6.18$$

where $E(t) = E_i - vt$ for $0 < t \leq \lambda$ 6.19a

and $E(t) = E_i - 2v\lambda - vt$ for $\lambda \leq t$ 6.19b

Where λ is the switching time. Assuming linear diffusion;

$$dC_O(x,t)/dt = D_O d^2C_O(x,t)/dx^2 \ ; \ dC_R(x,t)/dt = D_R d^2C_R(x,t)/dx^2 \qquad 6.20$$

and that at a distance x from the electrode the concentration of O is equal to the bulk concentration, with no R present initially;

$$C_O(x,0) = C_O^* \qquad ;C_R(x,0) = 0 \qquad 6.21$$

$$\lim_{x \to \lambda} C_O(x,t) = C_O^* \qquad ;\lim_{x \to \lambda} C_R(x,t) = 0 \qquad 6.22$$

and the flux balance is

$$D_O\{dC_O(x,t)/dx\}_{x=0} + D_R\{dC_R(x,t)/dx\}_{x=0} = 0 \qquad 6.23$$

Rewriting equation 6.3 gives

$$C_O(0,t)/C_R(0,t) = f(t) = \exp\{(nF/RT)(E_i - E^{o'})\} \qquad 6.24a$$

Substituting 6.19a and b in equation 6.24 gives an abridged form of the boundary condition;

$$C_O(0,t)/C_R(0,t) = \theta S(t) \qquad \text{624b}$$

where $\theta = \exp[(nF/RT)(E_i - E^{o'})]$;

$S(t) = \exp[-\sigma t]$ for $t \leq \lambda$;

$S(t) = \exp[\sigma(t-2\lambda)]$ for $t \geq \lambda$;

and $\sigma = nvF/RT$

Then, noting that $i(t) = nFA\{D_O(dC_O(x,t)/dx)\}_{x=0}$, 6.25

transforming the i(t) notation to i(E) and using equations 6.20, 6.24, 6.25 and the boundary conditions 6.20 to 6.22; it can be shown that ;

$$\int_0^{\sigma t} \chi(z)dz/(\sigma t-z)^{1/2} = 1/(1+\epsilon\theta S(\sigma t)) \qquad 6.26$$

where $\chi(z) = i(\sigma t)/nFAC_O^*(\pi D_O \sigma)^{1/2}$; $z = \sigma t = nF/RT(E_i - E)$;

and $\epsilon = (D_O/D_R)^{1/2}$

The solution to equation 6.26 provides values of $\chi(\sigma t)$ as a function of σt, for a given value of $\epsilon\theta$. From equations 6.24 and 6.25b, the values of σt are related to the potential by;

$$[\ E - E^{1/2}\ ]n = RT/F[\ \ln\epsilon\theta + \ln S(\sigma t)\ ]$$

Therefore, values of $\chi(\sigma t)$ can be regarded as values of $\chi[\ E - E^{1/2}\ ]n$ and will provide values of the current as a function of potential;

$$i = nFAC_O^*(\pi D_O)\sigma^{1/2}\chi(\sigma t) \qquad 6.27$$

It should be noted that as $\chi(\sigma t)$ is a pure number, equation 6.27 gives the functional relationship between the current and any point on the CV curve and the variables. Also, i is proportional to C_O^* and $v^{1/2}$. The numerical solution of equation 6.26 is shown in fig 6.7 (eg Nicholson and Shain, 1964; Bard and Faulkner, 1980).

6.3 Cyclic Voltammograms

Having developed the essential theory to describe the CV wave shape, a CV for a typical reversible system is now discussed. The letters used below in the text refer to positions on the cyclic voltammogram labelled in fig 6.2, and also identify the corresponding concentration–distance profiles in fig 6.8. Consider again the reaction;

$$O + ne \rightleftharpoons R, \text{ represented as } A + ne \rightleftharpoons A^- \qquad 6.28$$

a) At the beginning of the voltage sweep, it is assumed that A is completely oxidized and that the concentrations of the electroactive species at the electrode surface are at their bulk values as shown in fig 6.8a. As the electrode potential is positive with respect to the reference electrode, no Faradaic current (I_F) flows since the energy required to transfer electrons to A is too great. However, the charging of the double layer capacitance C_{dl}, which is a non–Faradaic process, results in a small step increase in current, I_C (cf fig 6.3). The total current I, flowing in the cell is given by equation 6.2.

b) The potential of the electrode is now made increasingly negative with respect to the reference electrode (wrtR). Consequently, the height of the energy barrier for electron transfer to A is lowered resulting in a small cathodic, Faradaic current. The reduction of A to A^- means that the concentration of A at the electrode surface is lower than its bulk value whilst that of A^- is increased (fig 6.8b).

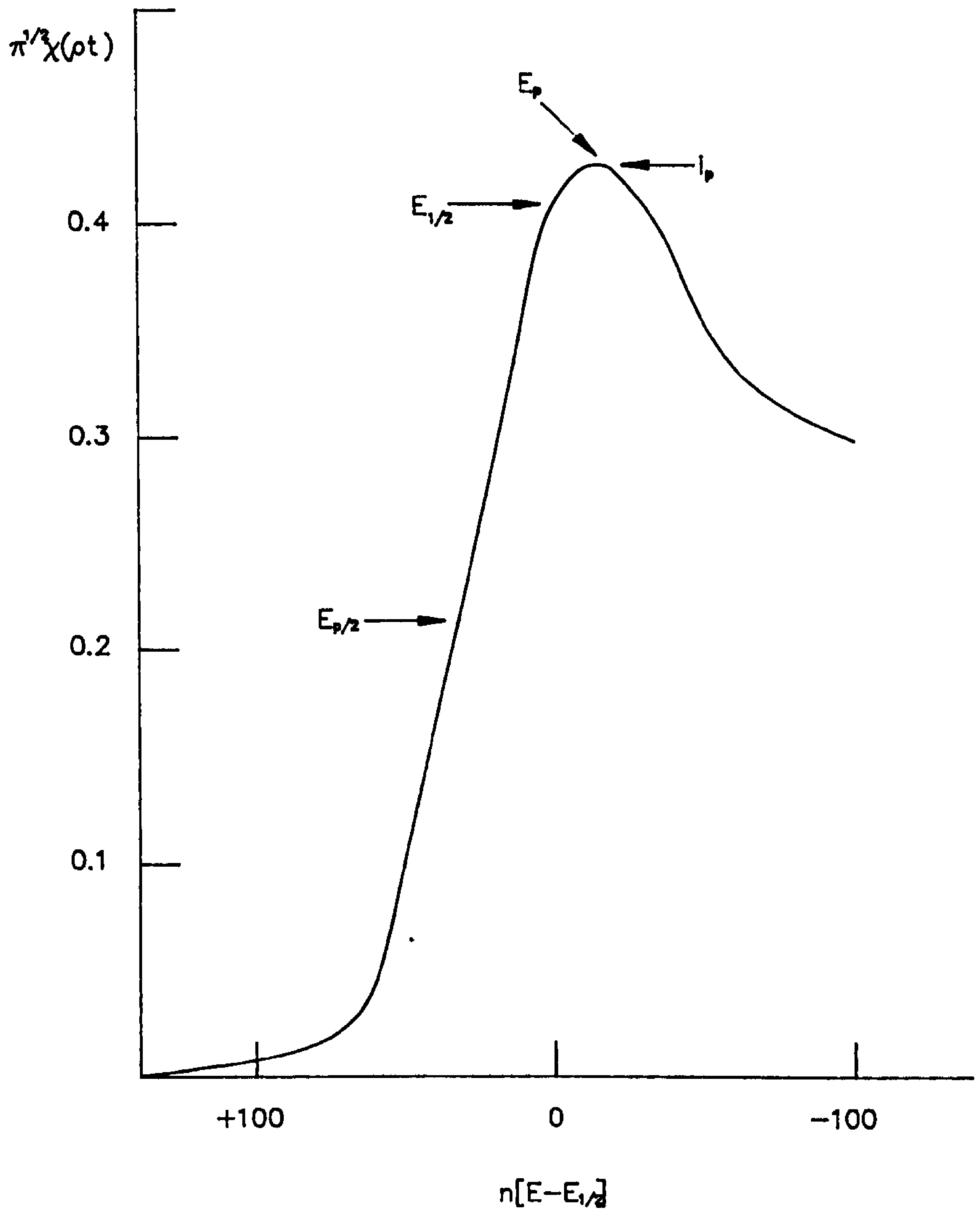

Fig 6.7 Linear Potential Sweep Voltammogram in terms of the dimensionless current function $\pi^{1/2}\chi(\rho t)$.
(Bard and Faulkner, 1980)

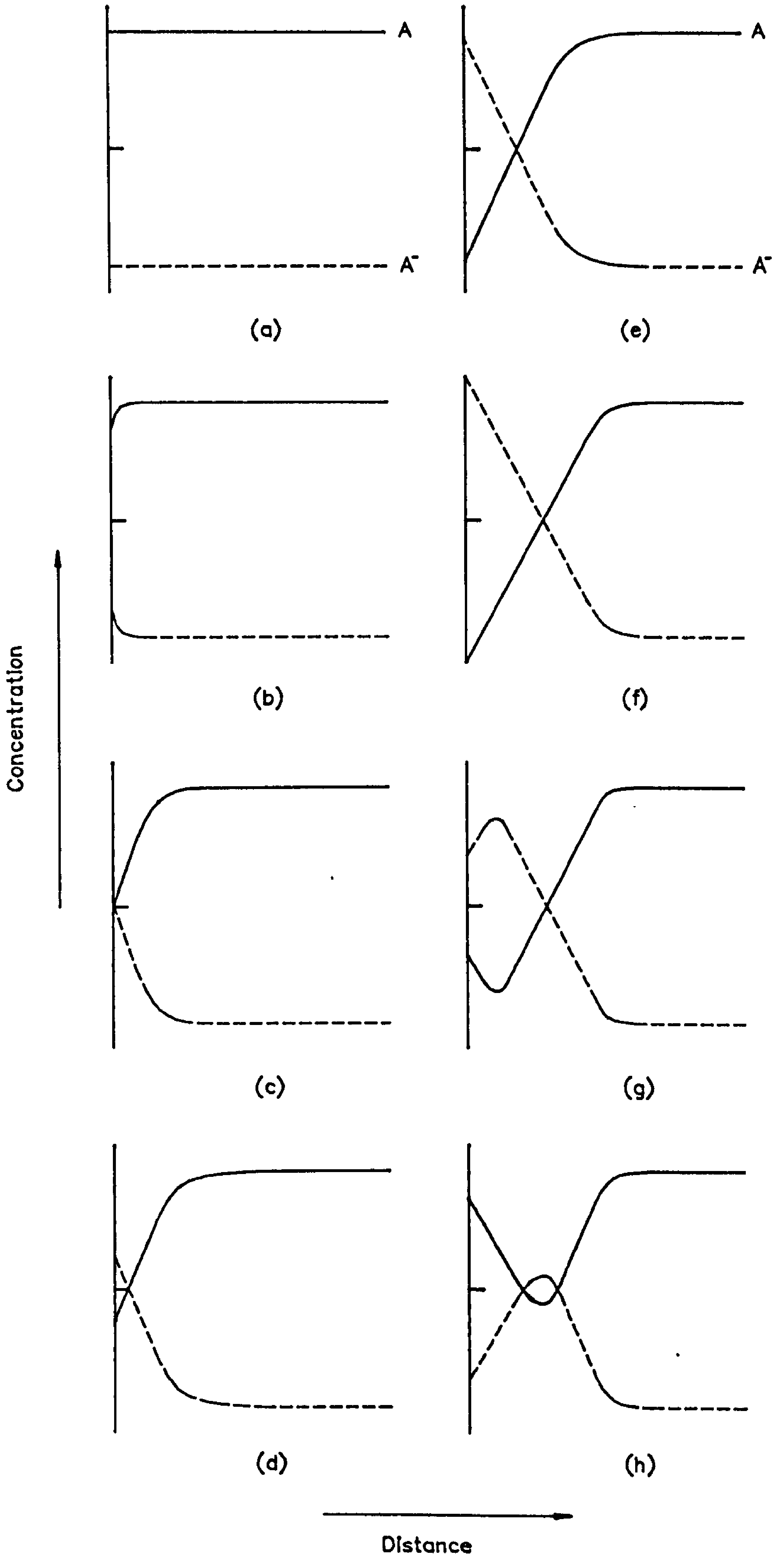

Fig 6.8 Concentration—Distance profiles for a typical, reversible electrode reaction. Each letter indicates the position on the CV curve (fig 6.2), at which the profile occurs. (Kissinger and Heineman, 1983)

c) For increasingly negative electrode potentials (wrtR), electron transfer from the electrode to A becomes even more favourable than at b). As the supply of electroactive species, A, to the electrode surface by diffusion is able to sustain the growing cathodic current, the current rises steeply in agreement with the Nernst equation. Compared to their bulk values, the surface concentration of A is further reduced, widening the region depleted of A, whilst the concentration of A^- is increased (fig 6.8c).

d) Eventually, an electrode potential (wrtR) is reached at which the rate of reduction of A exceeds the rate at which it can be supplied by diffusion through the depletion region and the current peaks.

e) The cathodic current is now limited by diffusion of A to the electrode surface and the current decays exponentially in accordance with Fick's Law of Diffusion (equation 6.5).

f) As at a), a non-Faradaic current flows, although this time it is because the double layer capacitance is discharging rather than charging. The non-Faradaic current results in the step decrease in cathodic current shown on the voltammogram (fig 6.2).

g) Even when the potential sweep is reversed, the electrode current remains cathodic. The reason for this is clear from a consideration of the energy bands, from which it follows that the forward reaction (equation 6.28) is favourable, whereas the reverse, oxidation process is unfavourable. The surface concentrations of A and A^- are the same as those at e), but as the concentration-distance profile is being viewed some time later than at e), the width of the depletion region has increased.

h) The electrode potential is now sufficiently positive for species A^-, concentrated at the electrode surface, to transfer electrons to the electrode. The surface concentration of A increases at the expense of A^- as the electrode reaction proceeds in the reverse direction. As the electrode potential is made more positive (wrtR), the anodic current increases rapidly, as predicted by the Nernst equation.

i) At this potential, the supply of A^- by diffusion is no longer sufficient to sustain the oxidation reaction and the anodic current peaks. The electrode surface is now depleted of A^-, whilst A has regained its bulk concentration value (fig 6.8d).

j) As the electrode potential continues to increase positively (wrtR), the diffusion current falls in accordance with Ficks' Law, and the concentration–distance profiles begin to return to their initial levels (fig 6.8a). However, if the potential sweep is recommenced immediately, the surface conditions at the electrode will not be the same as for the initial voltammogram. Experimentally, this means that unless care is taken to re–initialize the surface concentrations at the electrode (eg by carefully removing the working electrode from the cell and then replacing it), subsequent voltammograms will not be identical to the first sweep (Maloy, 1983; Kissinger and Heineman, 1983).

6.4 Important Parameters and Criteria for Reversibility

The important parameters of a cyclic voltammogram are the peak values of the anodic and cathodic current, i_{pa} and i_{pc} respectively and the potentials E_{pa} and E_{pc} at which they occur (fig 6.9).

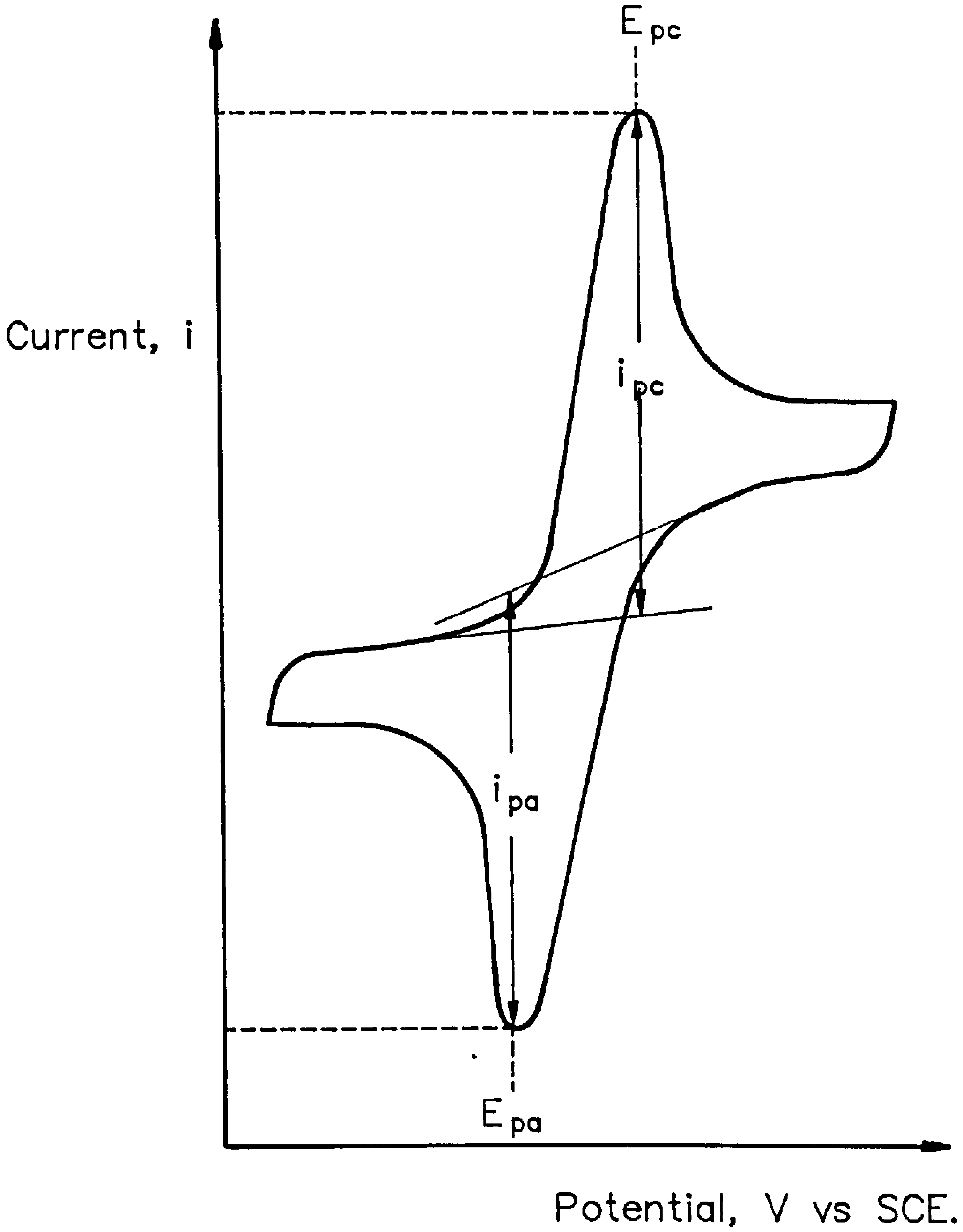

Fig 6.9 A cyclic voltammogram for a typical reversible reaction showing the positions of the peak currents (i_{pa},i_{pc}) and peak potentials (E_{pa},E_{pc}).

6.4.1 Measurement of Peak Currents

From equation 6.27, it follows that when the function $\pi^{1/2}\chi(\sigma t)$ is a maximum, so too is the current. The maximum occurs at $\pi^{1/2}\chi(\sigma t) = 0.4463$, for 25°C, at $n(E_p - E_p^{1/2}) = 28.50$ mV. Hence, the peak current i_p, for a reversible system for the forward sweep of the first cycle is;

$$i_p = 0.4463nFAC_o^*(nF/RT)^{1/2}v^{1/2}D_o^{1/2} \qquad 6.29$$

where v is the scan rate in V/s. For a simple, reversible couple, a plot of i_p vs $v^{1/2}$ yields a straight line from which the diffusion coefficient D, of the system can be determined (fig 6.10) (Bard and Faulkner, 1980 ; Kissinger and Heineman, 1983).

6.4.2 Measurement of the current ratio

Measurement of the current ratio can be used as a check of reversibility and will be unity if the system is reversible, whilst a departure from ideality is evidenced by a current ratio not equal to unity. In practice it can be difficult to measure the peak currents accurately because the true baseline can be hard to locate. This is because of the non-Faradaic currents. However, Nicholson (1966, 1964) has developed a semi-empirical method to measure the current ratio which eliminates baseline errors and is particularly useful for analysing voltammograms of non-ideal systems. The current ratio is given by;

$$\frac{i_{pa}}{i_{pc}} = \frac{(i_{pa})_o}{(i_{pc})_o} + \frac{0.485(i_{ps})_o}{(i_{pc})_o} + 0.086 \qquad 6.30$$

Where $(i_{pa})_o$ and $(i_{pc})_o$ are the anodic and cathodic peak currents and $(i_{ps})_o$ is the current at the switching potential, all measured with respect to the zero current axis. The relationship (equation 6.30), is accurate to within 1% for ;

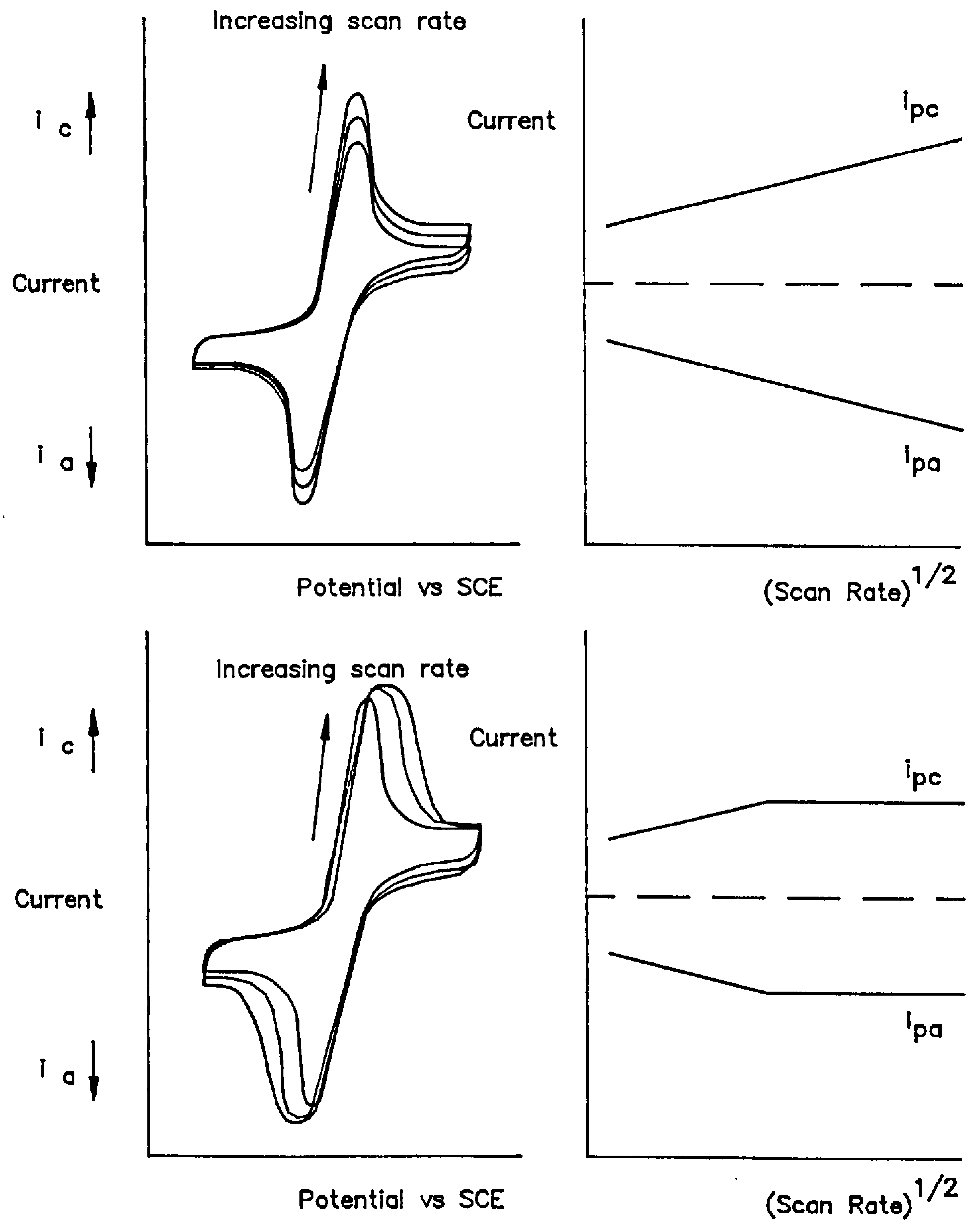

Fig 6.10 Cyclic voltammograms and corresponding current vs (Scan Rate)$^{1/2}$ plots for a) a reversible and b) a quasi-reversible redox process.

$0.05 \leq k\tau \leq 1.25$

and for switching potentials $E\lambda$, in the range ;

$E_{\lambda} \leq E_{pc} - 0.06/n$

where k is the rate constant for the reaction, τ is the time from $E^{1/2}$ to the switching potential, E_{λ}. k is in cm/sec, E_{λ} and E_{pc} are in volts.

6.4.3 Formal Reduction Potential

The peak separation may also be used as a check of reversibility. The formal reduction potential, E^o for a reversible couple is centred between E_{pa} and E_{pc} such that;

$$E^o = (E_{pa}+E_{pc})/2 \qquad 6.31$$

The number n, of electrons transferred per atom in the electrode reaction, for such a couple can be determined from the separation, ΔE_p between the peak potentials, since

$$\Delta E_p = E_{pa}-E_{pc} = 0.059/n \qquad 6.32$$

In the case of an ideal, reversible system, E_{pa} and E_{pc} are equally and oppositely spaced, 28.5/n mV from the voltage axis cross-over. Redox couples whose peaks shift further apart with increasing scan rate are categorized as quasi-reversible (Bard and Faulkner, 1980; Kissinger and Heineman, 1983; Mabbott, 1983).

6.5 Quasi Reversible Electrode Reactions

So far, only ideal systems have been considered for which the rate of charge transfer is sufficient to maintain the equilibrium concentration of O and R at the electrode surface, as predicted by the Nernst Equation. In practice, the rate of charge transfer can be insufficient to maintain equilibrium at the electrode surface and the current values are then less than those predicted by the Nernst equation for a given electrode potential. The peak separation is increased and the rate of current rise with potential decreased, with respect to the reversible system as shown by fig 6.11. However, as predicted by equation 6.29, the peak separation is sweep dependent and if the sweep rate is made sufficiently low, the process becomes reversible. That is, it is possible to reduce the sweep rate to permit equilibrium conditions to be attained at the electrode surface in accordance with the Nernst equation. Based on this qualitative analysis, a quantitative method for estimating the standard rate constant for a quasi reversible reaction has been determined by Matsuda and Ayabe (1955) and Nicholson (1965). Before detailing their work, it is first necessary to consider the kinetic representation of equation 6.3. Consider the relationship;

$$\mathrm{O} + ne \underset{k_b}{\overset{k_f}{=}} \mathrm{R}$$

where k_f and k_b represent the forward and reverse rate constants respectively. The forward component proceeds at a rate r_f, which is proportional to the surface concentration of O, thus;

$$r_f = k_f C_O(0,t) = i_c/nFA \qquad 6.33$$

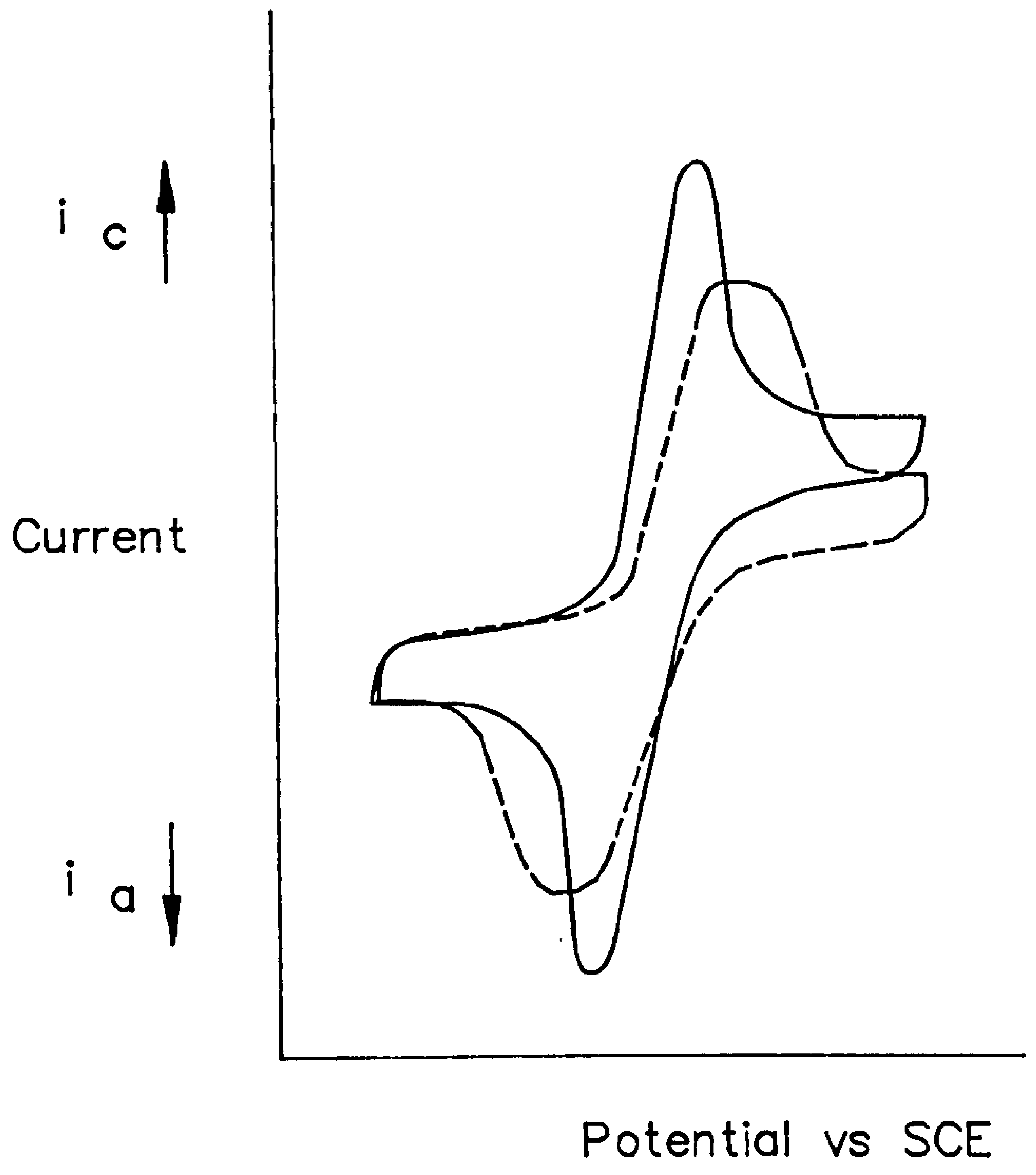

Fig 6.11 Cyclic voltammograms comparing a typical reversible (—) and quasi–reversible (- -) redox process.

Similarly, for the reverse reaction;

$$r_r = k_b C_R(0,t) = i_a/nFA \quad 6.34$$

The net reaction rate is then given by;

$$r_{net} = r_f - r_r = k_f C_O(0,t) - k_b C_R(0,t) \quad 6.35$$

$$= (i_c - i_a)/nFA \quad 6.36$$

Or rearranging;

$$i = i_c - i_a = nFA[k_f C_O(0,t) - k_b C_R(0,t)] \quad 6.37$$

Based on a free energy curve model it can be shown that;

$$k_f = k^o \exp-[\alpha nF(E - E^{o'})] \quad 6.38$$

$$k_b = k^o \exp[(1-\alpha)nF(E - E^{o'})] \quad 6.39$$

Where k^o is the standard rate constant, that is the value of k when $k_f = k_b$, which occurs when the electrode reaction is at equilibrium and $C_O^* = C_R^*$.

Substituting for k_f and k_b in equation 6.37 leads to the Butler-Volmer Equation;

$$i = nFAk^o(C_O(0,t)\exp[-\alpha nF(E-E^{o'})] - C_R(0,t)\exp[(1-\alpha)nF(E-E^{o'})] \quad 6.40$$

Where k^o is a measure of kinetically how facile the redox reaction is and α is a measure of the symmetry of the energy barrier to the oxidation and reduction reactions (Bard and Faulkner, 1980).

Nicholson (1965) has derived a relationship from which the standard rate constant can be calculated for a quasi-reversible reaction. The theory applies strictly to the first sweep for planar electrode systems with mass transfer by diffusion only and where the solution resistance can be ignored. Furthermore, it is assumed that R is generated in-situ and that both O and R are soluble. The boundary conditions for this case are;

$$dC_O/dt = D_O d^2C_O/dx^2 \qquad 6.41$$

$$dC_R/dt = D_R d^2C_R/dx^2 \qquad 6.42$$

For $t = 0$, $x \geq 0$

$$C_O = C_O^* \; ; C_R = C_R^* \qquad 6.43$$

At $t \geq 0$

$$\lim_{x \to 0} C_O = C_O^* \; ; \qquad \lim_{x \to 0} C_R = C_R^* \qquad 6.44$$

$t \geq 0$, $x = 0$

$$D_O dC_O/dx + D_R dC_R/dx = 0 \qquad 6.45$$

$$D_O dC_O/dx = k_f C_O - k_b C_R \qquad 6.46$$

Finally, the sweep waveform is defined as;

$$E = E_i - vt \text{ for the first reduction} \tag{6.47}$$

and $$E = E_i + vt - 2v\lambda \text{ for the first oxidation} \tag{6.48}$$

where E_i is the initial equilibrium potential and λ is the period of the triangular wave. Using equation 6.40 with the above boundary conditions gives;

$$D_O(dC_O(x,t)/dx)_{x=0} =$$

$$k^o \{ \exp[-(\alpha nF/RT)(E(t)-E^{o'})] \{ C_o(0,t) - \exp[(nF/RT)(E(t)-E^{o'})]C_R(0,t) \} \} \tag{6.49}$$

By application of Laplace transform methods, the above boundary value problem can be converted to a linear integral equation;

$$\{\chi(y)[(\gamma(Co^*/C_R^*)S_{a\lambda}(y)]^{\alpha}\}/\psi =$$

$$1 - S_{a\lambda}(y) - \int_0^y \chi(z)dz/(y-z)^{1/2} -$$

$$\gamma(C_o^*/C_R^*)S_{a\lambda}(y) \int_0^y \chi(z)dz/(y-z)^{1/2} \tag{6.50}$$

Where $\gamma = (D_O/D_R)^{1/2}$; $y = at$; $\chi(y) = D_O(dC_O/dx)/(C_O^*(\pi D_O)^{1/2})$

$a = nFv/RT$;

$S_\lambda(t) = \exp(-at)$; $t < \lambda$;

$S_\lambda(t) = \exp(at-2a\lambda)$; $t > \lambda$;

and $$\psi = \gamma^{\alpha}k_o/(\pi a D_O)^{1/2} \tag{6.51}$$

from which it follows that the wave shape and ΔE_p are functions of v,k^o,σ and E_λ. If E_λ is at least 90mV beyond the cathodic peak, the effect of E_λ is small such that the curves can be regarded as a function of the dimensionless parameter ψ and α.

6.5.1 Dependence on α of the theoretical curves

A value of $\alpha = 0.5$ is taken as the normal, symmetrical case. For $\alpha > 0.5$ the cathodic peak is more rounded and the peak heights occur at more negative values of current (fig 6.12). A slight displacement of both peaks along the potential axis also occurs. When $\alpha < 0.5$ the converse holds. This means that in the range $0.3 < \alpha < 0.7$, ΔE_p is independent of α.

6.5.2 Dependence on ψ of the theoretical curves

When $\psi > 7$ the curves are Nernstian and for $\psi < 0.001$, the reaction is completely irreversible. For intermediate values of ψ, the form of the curve depends markedly on the exact values of ψ and α. The dependence on ψ of the theoretical CV curves is shown is fig 6.13. As ψ decreases from 7, which corresponds to the reversible case, both anodic and cathodic peaks reduce in height and increase in separation.

In practice, a scan rate is used which gives an experimental ΔE_p in the useful range of fig 6.14. From the experimental $n\Delta E_p$ and if the scan rate is known, the corresponding value of k^o can be obtained from equation 6.51, which is valid for $\Gamma^\alpha = 1.0$.

6.6 Modification of electrode processes by an electrode coating

As previously stated in $6.2.2, the Faradaic current for a bare electrode is influenced by two major mechanisms, namely charge transfer at the electrode surface and

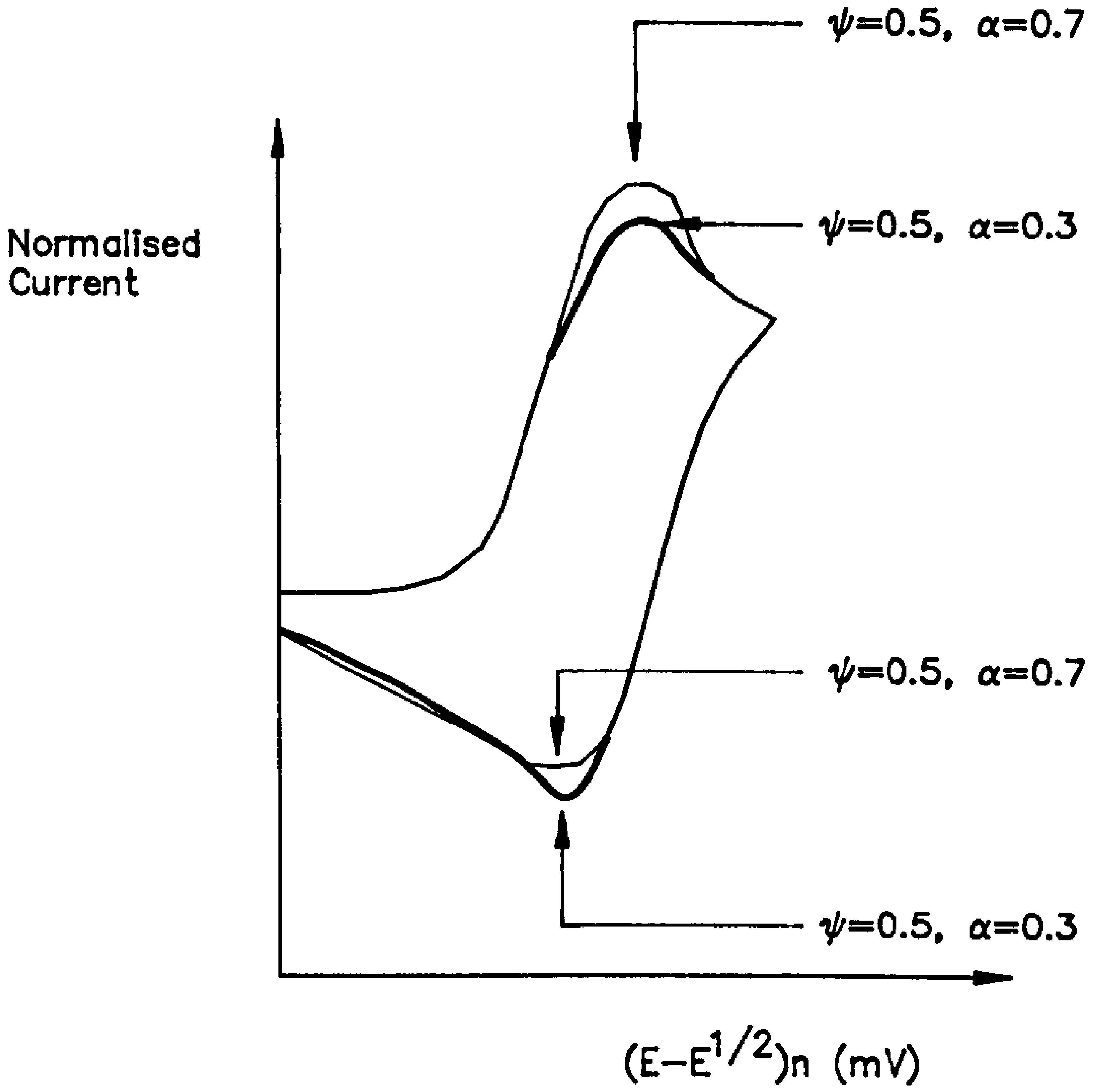

Fig 6.12 Cyclic voltammogram showing the effect of the charge transfer coefficient, α on curve shape. (Nicholson, 1965)

/

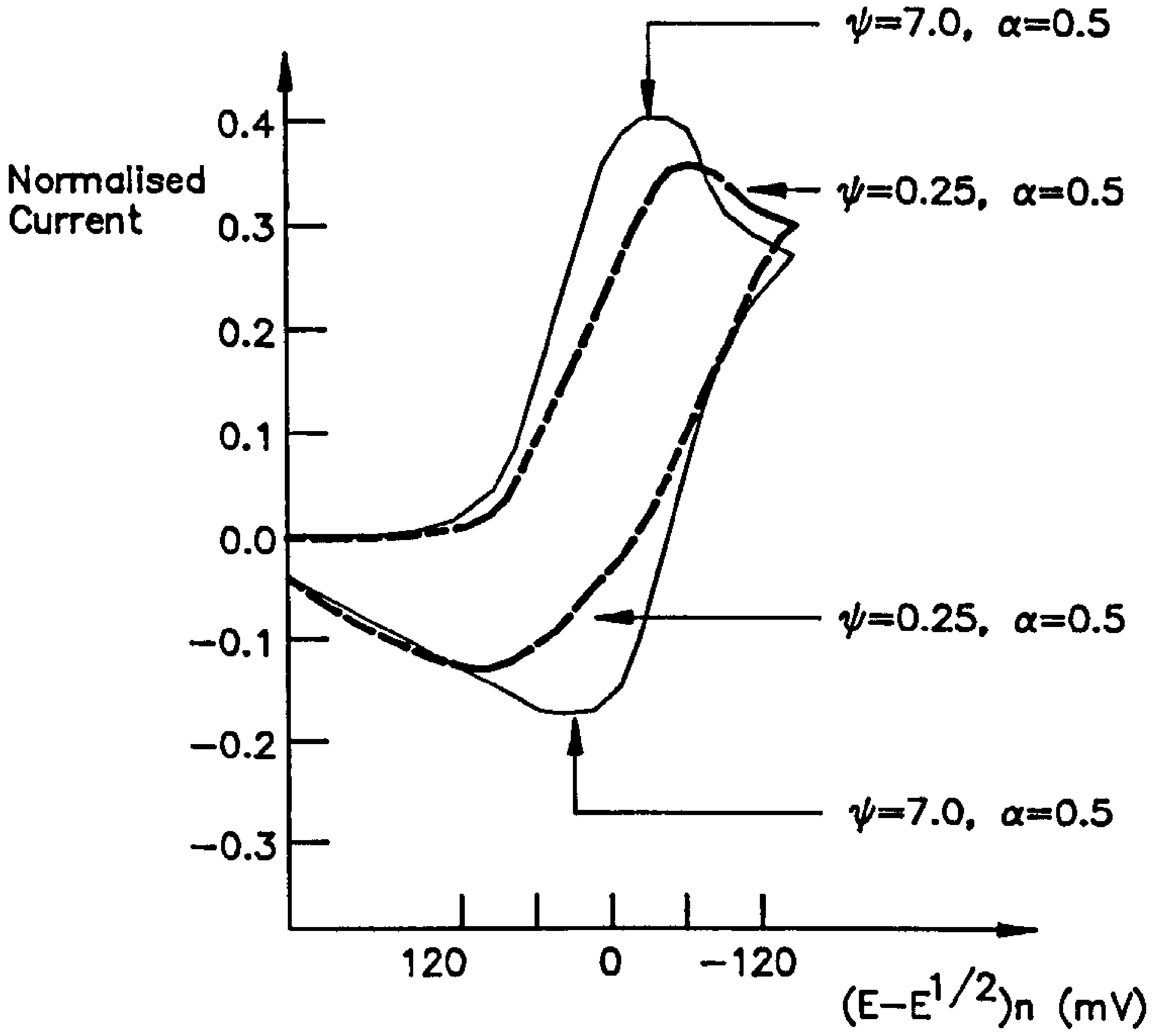

Fig 6.13 Cyclic voltammogram showing the effect of the charge transfer parameter, ψ on curve shape.
(Nicholson, 1965)

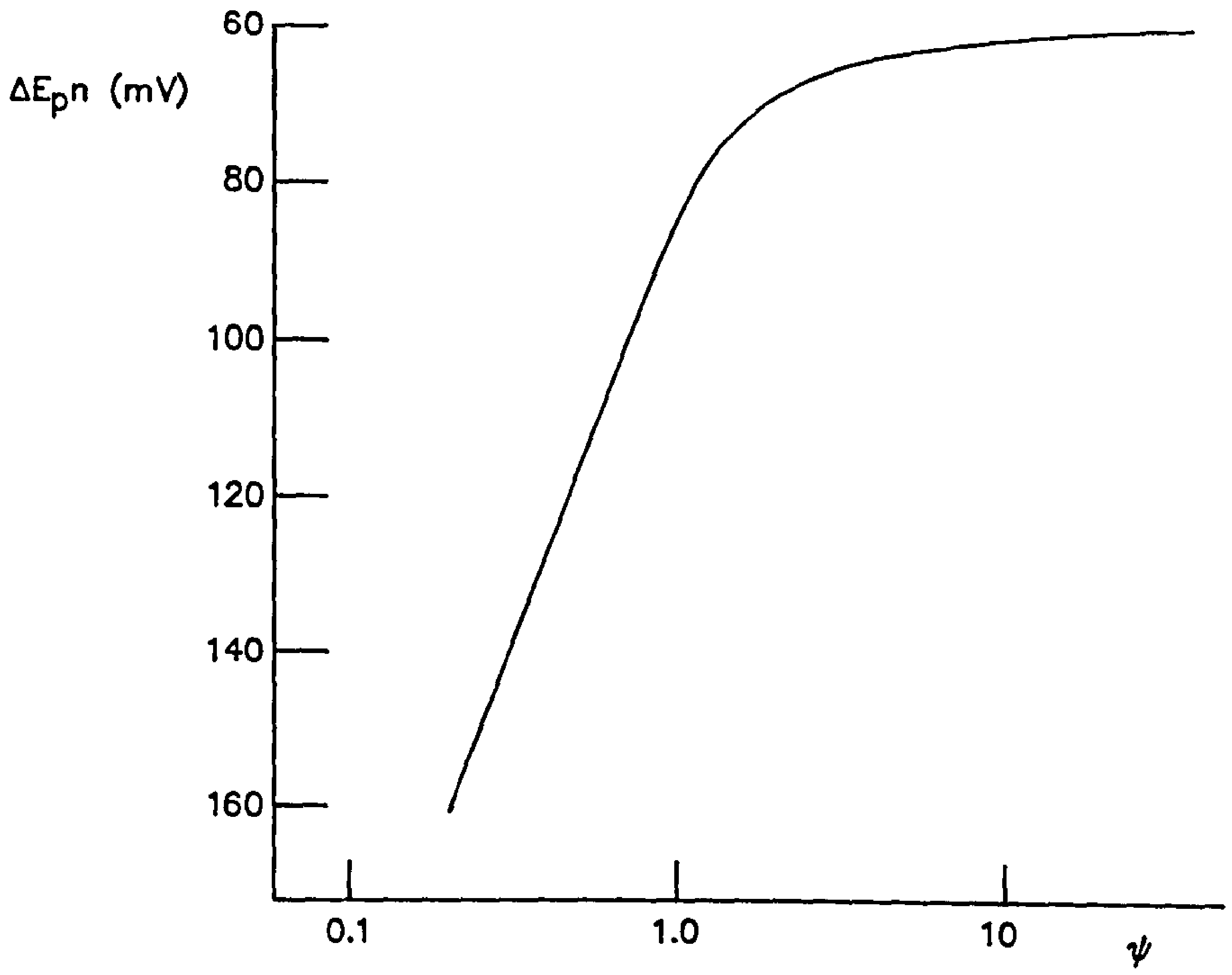

Fig 6.14 The variation of peak potential separation, $\Delta E_p n$ with ψ. (Nicholson, 1965)

mass transfer of electroactive species to and from the electrode surface. It therefore follows that any coating on the electrode may change the electrode current by 1) restricting mass transfer of electroactive species to and from the electrode surface and/or 2) alter charge transfer at the electrode.

6.6.1 Mass transfer effects

6.6.1.1 Reduced electrode area

The simplest case to consider is that of incomplete coverage with an impervious, insulating coating. Mass transfer is blocked at the coated regions of the electrode but unhindered over the bare areas. The effective electrode area is simply reduced to the uncoated electrode area. Therefore the resulting voltammogram will show reduced peaks but will otherwise be unchanged with respect to the uncoated electrode for all sweep rates (fig 6.15).

6.6.1.2 Coating with diffusion coefficient less than the bulk solution

If the electrode is coated uniformly with a material which has a diffusion coefficient D_c, which is lower than that of the bulk solution D_{sol}, for the electrochemical species of interest, the electrode current peaks will be reduced as the diffusion coefficient of the electrode will dominate the diffusion limited currents of the cell. In the case of a potential step, the current will be reduced by a factor of $(D_c/D_{sol})^{1/2}$. For CV, equation 6.28 predicts a similar result (fig 6.16; Diaz et al, 1981).

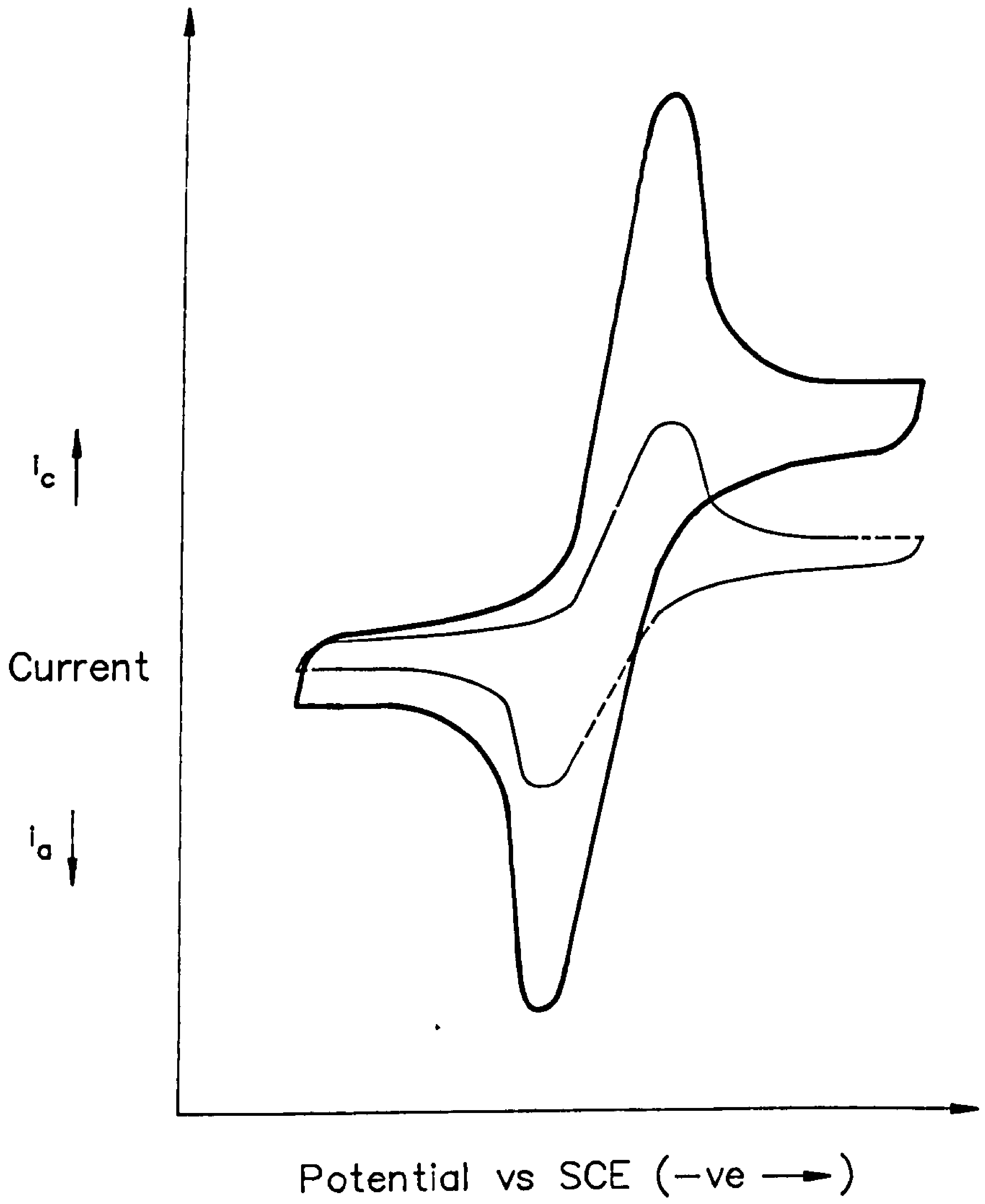

Fig 6.15 Cyclic Voltammograms showing an uncoated electrode (—) and an electrode partially coated with a blocking layer (--).

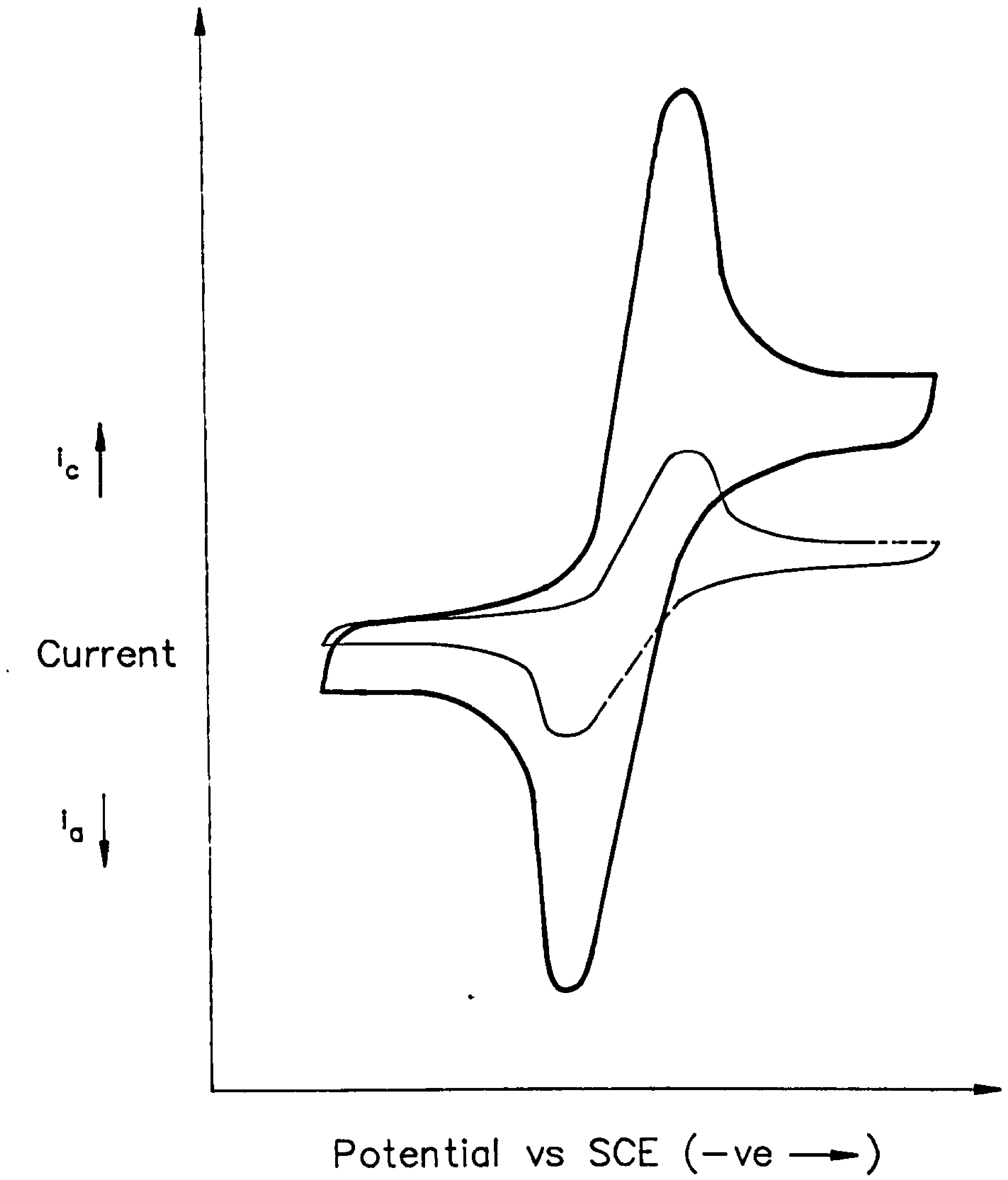

Fig 6.16 Cyclic Voltammograms showing an uncoated electrode (—) and an electrode coated with a porous layer (--) with a diffusion coefficient < diffusion coefficient of the solution.

6.6.2 Charge transfer effects

The electrode coating may alter charge transfer processes at the electrode either because 1) the coating is charged and so alters the potential profile near the electrode or 2) the coating is impermeable to the electrochemical species but charge transfer is mediated by the coating.

6.6.2.1 Electrode coating charged

If the electrode coating has a charge of equal polarity to the reactant species then the electrode potential must be increased by an amount equal to the effective coating potential to maintain the same electrode current as was previously measured for a bare electrode.

Conversely, if the coating charge is of the opposite sign ~~as~~ to the reactant species, then the species will be preconcentrated at the electrode surface and the current will be higher than observed at the same electrode potential for an uncoated electrode (fig 6.17).

6.6.2.2 Charge transfer mediated by electrode coating

If charge transfer from electrochemical species to the film and subsequent charge transport through the film are slower than the charge transfer for the uncoated electrode, then the kinetics of the coating will be rate limiting and the peak separation distance will be increased whilst the peak heights are decreased for a given sweep rate compared to the uncoated electrode (fig 6.18).

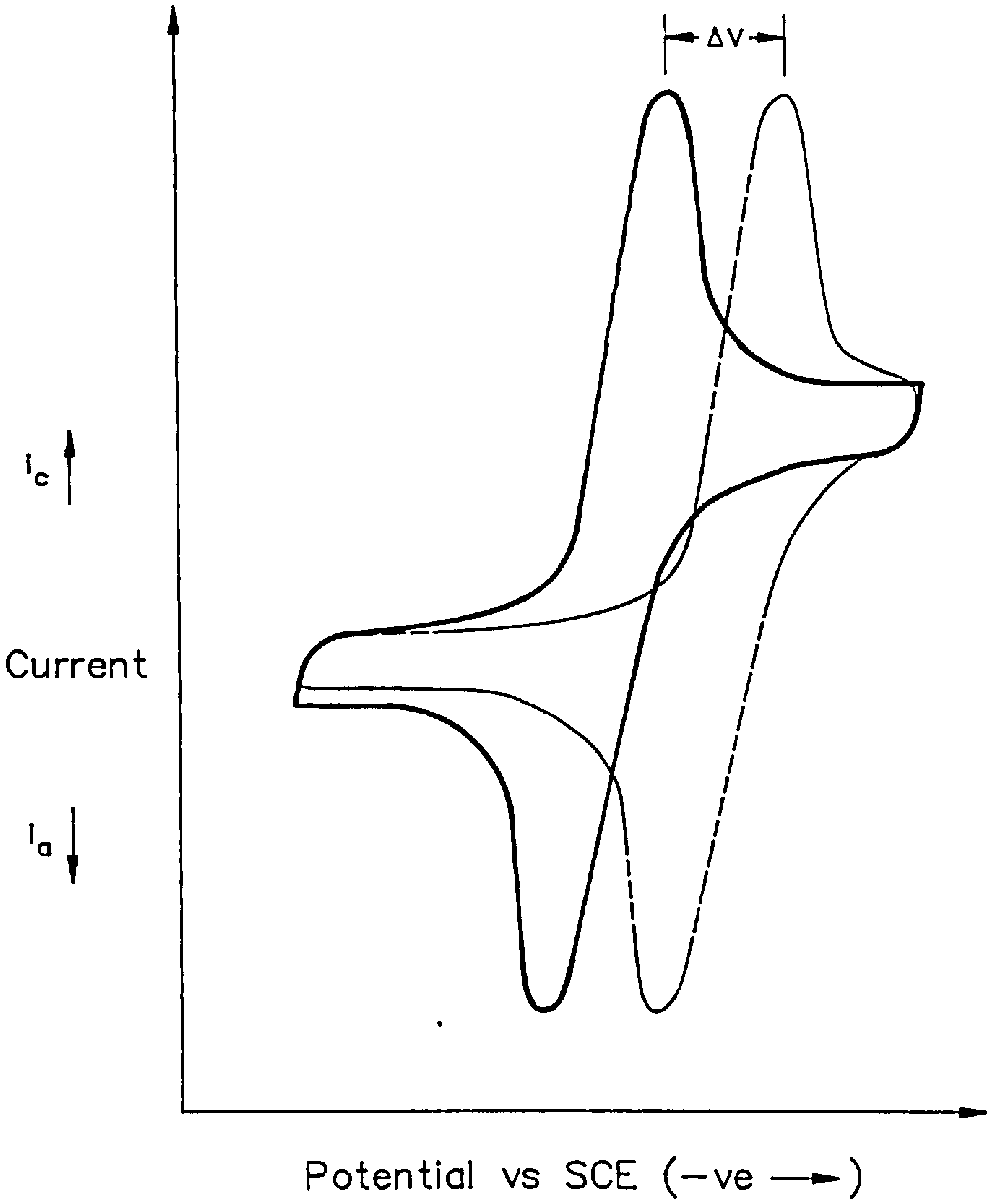

Fig 6.17 Cyclic Voltammograms showing an uncoated electrode (—) and an electrode coated with a negatively charged material of surface potential ΔV (– –).

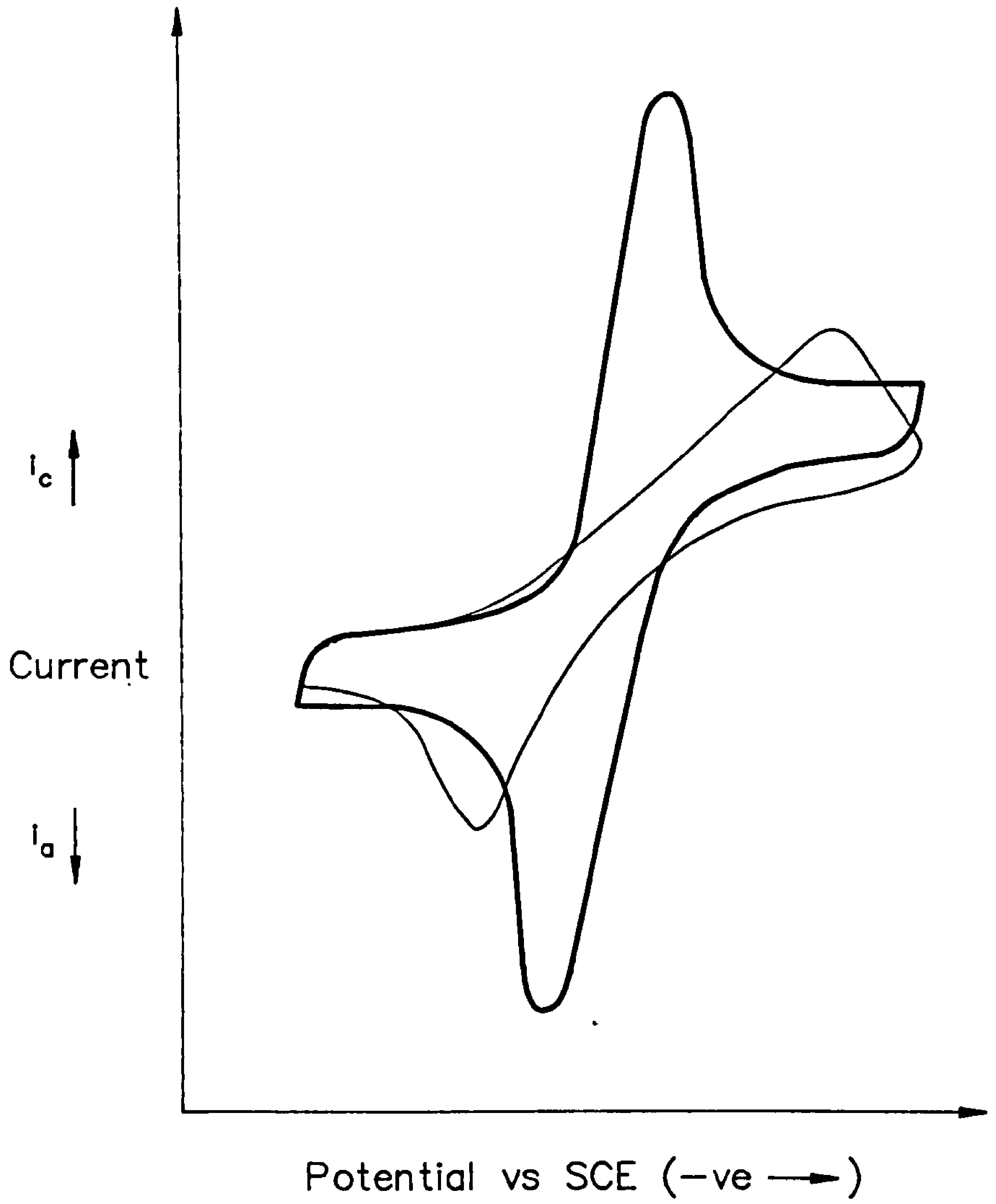

Fig 6.18 Cyclic Voltammograms showing an uncoated electrode (—) and an electrode coated in a material which reduces charge transfer to the electrode surface (--).

6.7 Conclusions

Cyclic voltammetry is a powerful tool for investigating redox processes at an electrode. By comparing the CV for a bare electrode with a CV for a coated electrode obtained using the same experimental conditions it is possible to gather information about the electrode coating. Such information includes coating porosity, surface charge, reactivity and diffusion coefficients for redox species ($ 6.6).

CV can therefore be employed to determine the suitability of materials for use as immobilising layers prior to incorporating electroactive species. Furthermore, CV may also be used to assess the resulting electroactive coating.

7 The characterisation of Barium Stearate and Barium Stearate/Gramicidin LB multilayers on metal substrates

7.1 Introduction

Monolayers of stearic acid and its salts, such as barium and cadmium stearate have been thoroughly characterised at the air/water interface ($3.3). The relative ease of preparation of Barium Stearate (fig 7.1) and in particular the lack of need for any special safety procedures makes Barium Stearate more attractive as a film forming material than the more "ideal" cadmium salt (eg Kopp et al, 1975). Furthermore, as stearic acid was used to check the cleanliness and calibration of the trough, it was logical to use its barium salt for deposition work (fig 7.1).

The deposition of Barium Stearate onto substrates such as aluminium, gold and silver has been well covered in the literature ($3.4). Its ability to form multilayers on a range of materials meant that it was suitable for depositing onto platinum, copper and aluminium. However, the lack of data on the stability of Barium Stearate multilayers in an aqueous environment meant that it was essential to characterise the multilayers in a range of electrolytes. Without such information, it was impossible to determine if Barium Stearate was suitable for immobilising ion selective species to produce ion sensors. Consequently, the characterisation of Barium Stearate multilayers in an aqueous environment is the subject of this chapter.

The chapter commences with details of the preparation of the Barium Stearate monolayers ($7.2.1) and their subsequent deposition onto platinum, copper and aluminium electrodes ($7.2.2). This is followed by a discussion of the results for the ac admittance ($7.3.1) and cyclic voltammetric ($7.3.2) characterisation of Barium Stearate deposited onto platinum wire electrodes. The problems encountered in obtaining stable, good quality

Barium Stearate coatings on platinum necessitated the use of a different electrode material. To begin with, sputtered copper electrodes were employed for deposition. The results for the ac admittance characterisation of Barium Stearate on sputtered copper electrodes is covered in $7.4. These studies showed that copper was also unsuitable and subsequently, deposition was carried out onto evaporated aluminium electrodes ($7.5). The good quality and stability of Barium Stearate deposited onto aluminium suggested that this combination would be suitable for immobilising ion selective species. Consequently, initial efforts to develop an ion selective electrode were concerned with the ac admittance analysis of mixed Barium Stearate/Gramicidin films deposited onto evaporated aluminium electrodes ($7.6). The chapter ends with a review of the important findings, detailed in the preceding sections ($7.7).

7.2 Barium Stearate Multilayers

7.2.1 Preparation of films

The cleanliness of the trough and accuracy of the calibration ($4.3.1.4) was routinely checked by producing monolayers of stearic acid ($4.3.1.7) using spreading solutions containing ca 1.0mg Stearic Acid/ml chloroform. Fig 7.2(a) shows a typical π-A curve for Stearic Acid. The surface area decreases monotonically with increasing surface pressure with a characteristic knee at ca $25 mN/m^2$. The monomer molecular areas were estimated to be 23.9 ± 0.7 $Å^2$ and 20.4 ± 0.6 $Å^2$ at 19 ± 1 °C, at the liquid and solid phase transitions respectively. These values are in good agreement with the literature (eg Stuart, 1986; Gaines, 1986).

Monolayers of Barium Stearate were produced in the same way as for stearic acid, except that $3x10^{-5}M$ $BaCl_2$ and $4x10^{-4}M$ $KHCO_3$ were added to the subphase ($4.3.1.6). Fig 7.2(b) shows typical π-A curves for $BaSt_2$ (Fig 7.1). As the surface pressure is increased, the surface area decreases monotonically to produce the characteristic knee at between 5 and 10mN/m^2. The monomer molecular areas were estimated to be 21.4±0.7 Å^2 and 20.3±0.7 Å^2 in the liquid and solid phase respectively, at 19±1 ^{o}C, again the values agree well with the literature (eg Gaines, 1986; Roberts, 1990).

7.2.2 Deposition onto substrates

Platinum wire electrodes ($4.2.1) were used as substrates for deposition as they permitted both ac admittance ($5.0, $7.3) and cyclic voltammetric characterisation ($6.0, $7.4) of the Barium Stearate multilayers to be carried out. In addition, they were relatively easy to prepare for deposition and could be reused.

Prior to deposition, the platinum wire electrodes, mounted in PTFE collars ($4.2.1, fig 4.1), were polished using a paste of 0.3μm aluminium oxide powder in ultra pure water. After polishing, the electrodes were rinsed thoroughly in ultra pure water and dried in a stream of nitrogen. Between one and eight such electrodes were then mounted in a special fixture for deposition. It is estimated that ratios in the range 1.2–2.4 were achieved, with an average ratio of 1.8±0.4. Even when eight electrodes were dipped simultaneously, their total surface area was still too low to accurately measure the area of film deposited. This problem arose because the change in surface area per dipping cycle of about 1cm^2/dipping cycle/electrode, was of the same order of magnitude as the minimum area change that could be detected by the barrier control system. Therefore, area changes due to film collapse and deposition both appeared as a step change on the deposition charts. Consequently, it was not possible to separate the change in area due to film collapse from the change in area due to deposition. This is reflected by the high values for the deposition ratios which include both contributions to the changes in film area. In order to obtain measurable deposition ratios and to improve the stability of the deposited films, copper electrodes were used for deposition and subsequent ac admittance analysis.

Initially, Barium Stearate was deposited onto copper substrates similar to those used in the polymer studies ($5.5), but deposition was found to be poor because of the poor surface quality of the copper layer. However, good quality deposition was achieved onto electrodes prepared by sputtering a 3μm thick layer of copper onto clean microscope slides ($4.2.3). Immediately prior to deposition, these electrodes were also polished with 0.3μm alumina powder and rinsed thoroughly in ultra-pure water. LB films of Barium Stearate were then deposited with good deposition ratios in the range 0.97-1.03.

Finally, deposition was carried out onto aluminium electrodes. Aluminium was used because of the relative stability of its surface oxide and its ability to enhance film stability. The electrodes were prepared by evaporating aluminium onto clean microscope slides ($4.2.4). Barium Stearate multilayers were deposited with deposition ratios in the range 1.17±0.14 (fig 7.3).

7.3 Barium Stearate Multilayers on Platinum Wire Electrodes

The admittance properties of platinum electrodes ($4.2.1) coated with between one and eleven monolayers of Barium Stearate using the Langmuir Blodgett Technique ($4.3.2) were characterised in a range of electrolytes and electrolyte molarities.

As will be seen below, the film coverage was found to be poor, indicating patchy electrode coatings. Consequently, a thorough modelling of the Barium Stearate films on platinum was unwarranted. Instead, the discussion of the ac admittance results is confined to the experimental plots and estimates from these curves of coating capacitance, conductance, dielectric permittivity, conductivity and defect coverage.

7.3.1 Admittance Measurements

AC admittance data is presented in double log plots of capacitance (C_T) and loss ($G_T/2\pi f$). These plots represent the raw experimental data. In order to identify trends in the results, the data is summarised using a range of additional plots. To identify molarity dependent trends the coating capacitance, C_b at 0.16Hz, 10Hz and at the cross-over point between the C_T and loss curves, and G_b estimated at 0.16Hz and 10Hz, are presented as a function of the electrolyte molarity. At 0.16Hz (w=1), the coating capacitance and conductance can be represented by $C_b=C_b'.w^n$ and $G_b=G_b'.w^m$. Plots of n and m as a function of electrolyte molarity are given to show any trends in the frequency dependence of C_b and G_b. Thickness dependent trends are shown in plots of inverse capacitance and conductance plotted as a function of the number of coating layers or deposition cycles. Where appropriate, C_b and G_b are presented as a function of the electrolyte to determine if the properties of the coating are sensitive to the anion or cation present in solution. To gain further insight into the molarity and electrolyte dependence of the coatings, plots of dielectric permittivity, ϵ_r and conductivity σ, are presented.

In order to quantify the quality of the films, defect coverages were estimated from the capacitance and conductance data. The estimates assume that the coating consists of regions of intact film and defects filled with electrolyte. The measured capacitance, C_b' is then that of areas of intact film, βC_b and double layer regions, $(1-\beta)C_d$, where the ~~film~~ electrode is in contact with the electrolyte (equation 5.4). Similarly, the measured conductivity, σ' is that of regions of intact film, $\beta\sigma_b$ and defects filled with electrolyte, $(1-\beta)\sigma_{\underset{d}{b}}$ (equation 5.2). To evaluate equation 5.4, C_b is taken to be equal to either the lowest normalised value, the mean value of the measured data or the theoretical value, whichever is most appropriate. In order to evaluate equation 5.2, σ_b is taken to be equal to the minimum film conductivity measured for the given coating/substrate combination. Defect estimates less than zero are represented by --- in the data tables and arise when the measured value is less than the value assumed for C_b or σ_b.

The analysis of the admittance data is based on the following principles ;

1) A full theoretical fit was ruled out due to time restrictions. All analysis is therefore necessarily approximate.

2) It is desirable to use the same criteria for all curves to facilitate comparison of results. However, because of the two electrode geometries employed, features do not necessarily appear at the same range of frequencies. Furthermore, depending on the relative magnitudes of the coating capacitance and conductance, the low frequency part of the curves sometimes exhibit the double layer capacitance dispersion and sometimes do not. Many of the C_T curves for coated platinum exhibit 3 linear portions at frequencies below the C_g dispersion. However, the break points vary from sample to sample, making it difficult to use the same frequency(/ies) for quoting C_b values.

3) The frequency dependence of C_b and G_b in the experimental results means that the frequency at which values are quoted is of importance. If the coating capacitance and conductance could be defined using an equation of the form $X_b = X_b(w=1)w^n$, where X is C_b or G_b, then all coatings could be described satisfactorily in terms of X(w=1) and n. Unfortunately, this is not possible for all the results. It is therefore necessary to quote values of C_b and G_b at several frequencies to try and describe the coating. The possible frequencies which could be used are restricted by the low and high frequency dispersions (C_d and C_g respectively). Therefore, frequencies above the C_d dispersion, and below the C_g dispersion must be used.

To add to these complications, by comparing the ideal curves for C_T and $G_T/2\pi f$, it is apparent that the frequency range over which C_b is represented by the C_T is different from that over which G_b is represented by $G_T/2\pi f$.

4) Bearing in mind all the above points it is considered that the following frequencies should be used to describe C_T data ;

i) C_b at high frequencies from the cross over point in C_T and $G_T/2\pi f$ curves, at the peak in the C_g dispersion. $C_b=2xC_T$ at this point. This should approximate to the film capacitance at frequencies above that at which the permeant ions can effect it. In theory, the values of capacitance evaluated at this point should then be independent of electrolyte and electrolyte molarity and should reflect the dielectric permittivity of the dry film.

ii) C_b at mid frequencies at 10Hz. If there is an additional dispersion in the curves, due to the presence of ions in the film, then this usually peaks at around 10Hz. Therefore the effect of ions on the coating will be best detected at this frequency.

iii) C_b at low frequency at w=1 as a means of describing the film using the equation $C_b=C_b(w=1)w^n$. Only to be used if this is above the C_d dispersion and if the C_T curve is a straight line for 2 or more decades. If the C_d dispersion is affecting the curve at this frequency point, for a particular set of data, a corrected value of C_b, extrapolated from the C_T curve at higher frequencies, could be presented.

5) G_b must be measured beyond the minima in $G_T/2\pi f$ occurring after the C_g dispersion. Comparing experimental curves with the ideal, it is even more difficult to arrive at sensible frequencies at which to define G_b. However ;

i) G_b at high frequencies could be measured at the point just above the minima, assuming that in this region the ions have minimal effect on the measured film conductance. However, as this point is often poorly defined, this possibility is ruled out.

ii) G_b at 10Hz for reasons as presented in 4(ii). In addition, this frequency is sufficiently low to ensure that we are on the "straight" portion of the $G_T/2\pi f$ curve (cf theoretical curve).

iii) G_b at w=1 for reasons as given in 4(iii). This assumes that the "correct" film conductance is that measured at w=1. Based on the argument that ions in pin-holes contribute a frequency dependent conductivity, it seems likely that their contribution to the film conductance will be greatest at low frequencies. As it is not practical to measure G_b at high frequencies, it will not be possible to evaluate the film conductance in the absence of ions (see 5.1).

6) It should be noted that 4(i) implies taking measurements at unique frequencies for each admittance plot (ie the values will be measured at a different frequency for each electrolyte molarity). This is obviously in contrast to 4(ii), 4(iii), 5(ii) and 5(iii) where all values are quoted at the same frequency. This may raise the question of trying to normalise the data with respect to frequency. However, plots of C_T vs $G_T/2\pi f$ in the complex plane, which is a way of representing the data independently of frequency, for example, for 10 dip PBMA in NaCl at different molarities, reveals that increasing the molarity introduces an additional dispersion (as observed in the double log plots) and depresses the low frequency arcs. This means that the observed molarity dependent behaviour of the film is effectively independent of frequency, so there is no advantage in performing such normalisation. In addition, as this linear representation of the data necessitates at least two plots to show all parts of the curve clearly, its use was considered

impractical. In contrast, the double log plots enable all the data to be shown clearly on one graph and facilitates measurement of power law frequency dependency.

The cell capacitance, C_T and loss, $G_T/2\pi f$ are shown as functions of frequency in the double log plots of figs 7.4 and 7.5 for an uncoated platinum electrode and a similar electrode coated in 9 monolayers of Barium Stearate in 0.2, 2, 20 and 200mM KCl solutions at 15°C.

As observed earlier for PVC coated electrodes ($5.5), at high frequencies in 0.2mM KCl, the capacitance falls as expected to reach the geometric capacitance of the electrode arrangement (fig 7.5a). C_g is estimated to be 25±2pF from the high frequency capacitance plateau. As the electrode geometry is coaxial, the theoretical value for C_g can be calculated from the equation;

$$C_g = 2\pi\epsilon_0\epsilon_r d/\ln(r_2/r_1)$$

where r_2 is the radius of the gauze electrode, r_1 is the radius of the platinum wire electrode and d is the length of platinum electrode in the electrolyte. The other symbols are as defined in Appendix A. In the experiments, r_2 = 5mm and r_1 = 0.25mm, so that for a 10mm length of electrode, the geometric capacitance is 14.8pF/cm of wire. Therefore, for a dipped length of 16mm, C_g= 23.7pF, in good agreement with the measured value of 25±2pF.

Also at frequencies above 1000Hz, depending on the electrolyte molarity, the loss curves are of slope -1, corresponding to the electrolyte molarity (fig 7.5b, $A.3.3). For the coaxial electrode geometry, the electrode area A, in equation A.86 is replaced by the expression $2\pi d$ and L by $\ln(r_2/r_1)$. The values of electrolyte molarity calculated from the loss curves of fig 7.5 are summarised in Table 7.1. The mean value of the electrolyte molarity, normalised with respect to the nominal solution molarity for all the data presented on Barium Stearate coated platinum wire electrodes, is 1.0±0.1. The close agreement between the experimental and theoretical values for the geometric capacitance and solution conductance confirm the validity of these results ($5.5.1).

Nominal Molarity	Molarity From Expt	Expt/Nominal Molarity
2.0×10^{-4}	1.6×10^{-4}	0.8
2.0×10^{-3}	2.2×10^{-3}	1.1
2.0×10^{-2}	2.1×10^{-2}	1.0
2.0×10^{-1}	1.6×10^{-1}	0.8

Table 7.1 A comparison of the nominal and experimentally determined electrolyte molarities, obtained during ac admittance analysis of platinum electrodes coated with 9 monolayers of barium stearate and immersed in KCl at 15±1°C.

Comparing figs 7.4 and 7.5, the presence of the 9 monolayer film is apparent from the general reduction in both capacitance and loss and the shift of the main dispersion to higher frequencies. The frequency of this dispersion also moves to higher frequencies as the molarity increases, as noted previously for PVC coated copper electrodes ($ 5.5.2). However, unlike the PVC coated electrodes, the frequency dependence of the capacitance for the coated electrodes is quite marked and greater than for the uncoated electrodes. It should be noted though, that the capacitance plateaus for the coated electrodes do become more horizontal with higher molarities. At frequencies below 1Hz, both C_T curves and $G_T/2\pi f$ curves begin to merge.

The film capacitance estimated from i) the cross over point of the C_T and $G_T/2\pi f$ curves, ii) at 10Hz and iii) at $1/2\pi$Hz is shown as a function of electrolyte molarity in fig 7.6a. A similar plot of coating conductance at $1/2\pi$Hz is presented in fig 7.6b. The reasons for using these frequencies are outlined in $7.3.1. From fig 7.6a it is clear that at

$1/2\pi$Hz and 10Hz, the film capacitance and loss increase with increasing molarity. In contrast, the capacitance at the cross-over frequency appears to be independent of electrolyte molarity. This suggests that electrolyte ions are able to penetrate the film, increasing its admittance at frequencies below the C_T, $G_T/2\pi f$ cross-over point. Then, at and above this frequency, the electrolyte ions within the film are unable to follow the applied electric field.

To gain further insight into the quality of the films, the coating conductivity and permittivity were calculated from the values of coating capacitance and conductance shown in Fig 7.6 and summarised in Table 7.2, using equations 5.3 and 5.1 respectively, assuming a monolayer thickness of 2.5nm (Handy and Scala, 1966; Srivastava and Verma, 1962, 1966; Fankuchen, 1938, Table 7.3). The values of film permittivity range from 23 in 0.2mM KCl at 10Hz to 805 in 200mM KCl at $1/2\pi$Hz (Table 7.3) and are obviously high compared to the expected value of 3 (eg Porter and Wyman, 1938; Race and Reynolds, 1939; Zahl et al, 1939; Sugi et al, 1979; Millany and Jonscher, 1979), even for the low molarity solution. This suggests that film coverage is poor and that there may be regions of either very thin coverage including areas of uncoated platinum wire where the electrolyte can form double layer regions in contact with the electrode. If this is the case, then molarity dependent changes in the double layer capacitance could explain the increase in film permittivity with molarity (Equation A.83, Table 7.3). Assuming that this is so, the defect coverage can be estimated from equation 5.4, $5.2 (Stelzle and Sackmann, 1989) using values of C_d estimated at $1/2\pi$Hz from fig 7.4a. The values of defect coverage are given in Table 7.4 and range from 20% down to 0.3%, assuming that an intact film would have a dielectric permittivity of 3. Even at the cross-over frequency, beyond which it is suggested the electrolyte ions no longer contribute to the coating capacitance,

C_b (μF) estimates at given frequency			
Molarity/ Frequency	0.16Hz	10Hz	Cross-Over Frequency
$2.0\text{x}10^{-4}$	2.6	0.3	1.9
$2.0\text{x}10^{-3}$	3.4	0.9	0.6
$2.0\text{x}10^{-2}$	6.9	2.8	1.3
$2.0\text{x}10^{-1}$	9.2	4.0	1.3

(a)

G_b (μS) estimates at given frequency			
Molarity/ Frequency	0.16Hz	10Hz	Cross-Over Frequency
$2.0\text{x}10^{-4}$	2.1	23	--
$2.0\text{x}10^{-3}$	2.1	36	--
$2.0\text{x}10^{-2}$	6.3	71	--
$2.0\text{x}10^{-1}$	6.3	71	--

(b)

Table 7.2 (a) Film capacitance, C_b and (b) Conductance, G_b, for 9 monolayers of Barium Stearate deposited onto platinum electrodes and immersed in a range of KCl molarities. The capacitance data were estimated from the curves shown in fig 7.5a and are given at 0.16Hz, 10Hz and the loss/capacitance cross over points. The conductance data are given at 0.16 and 10Hz only, estimated from the loss curves of fig 7.5b. (The capacitance and conductance values are shown in fig 7.6, plotted against electrolyte molarity).

the defect coverage is still around 7%. Thus it seems that large areas of the platinum electrode were uncoated. The patchy nature of the deposition is likely to give rise to the curved "plateau" region, although the concentric eletrode geometry could also have been responsible for this effect.

ϵ_r estimates at given frequency			
Molarity/ Frequency	0.16Hz	10Hz	Cross-Over Frequency
$2.0\text{x}10^{-4}$	210	23	154
$2.0\text{x}10^{-3}$	306	81	53
$2.0\text{x}10^{-2}$	640	260	117
$2.0\text{x}10^{-1}$	805	350	110

(a)

$\sigma(\text{nSm}^{-1})$ estimates at given frequency			
Molarity/ Frequency	0.16Hz	10Hz	Cross-Over Frequency
$2.0\text{x}10^{-4}$	1.5	17	--
$2.0\text{x}10^{-3}$	1.7	29	--
$2.0\text{x}10^{-2}$	5.2	58	--
$2.0\text{x}10^{-1}$	4.9	55	--

(b)

Table 7.3 (a) Dielectric permittivities and (b) conductivities for barium stearate coated platinum electrodes, immersed in KCl. The values were calculated from the data in Table 7.2, assuming a monolayer thickness of 2.5nm.

A further indication of poor coverage is given by analysis of monolayer conductivities, which range from 1.5nSm^{-1} in 0.2mM KCl at $1/2\pi$Hz to 58nSm^{-1} in 20mM KCl at 10Hz. Assuming the film conductance arises from the presence of electrolyte filled pin holes and regions of defect free coating, then the defect coverage can be estimated from equation 5.2 (§5.4, Table 7.3b). Assuming that σ_{bs} is equal to the lowest measured film conductivity of 1.5nSm^{-1}, the percentage area occupied by such defects ranges from $2.1\text{x}10^{-8}\%$ at $1/2\pi$Hz in 0.2mM KCl up to $2.9\text{x}10^{-4}\%$ in 20mM KCl at 10Hz (Table 7.4b). It seems unlikely that the pin hole coverage can be molarity and frequency dependent, as suggested by these estimates. Futhermore, these figures are much

Percentage defect coverage estimates from C_b			
Molarity/ Frequency	0.16Hz	10Hz	Cross-Over Frequency
2.0×10^{-4}	24	2	17
2.0×10^{-3}	28	7	5
2.0×10^{-2}	45	18	8
2.0×10^{-1}	47	20	6

(a)

Percentage defect coverage estimates from G_b			
Molarity/ Frequency	0.16Hz	10Hz	Cross-Over Frequency
2.0×10^{-4}	2.1×10^{-8}	7.9×10^{-5}	--
2.0×10^{-3}	8.8×10^{-7}	1.4×10^{-4}	--
2.0×10^{-2}	1.9×10^{-5}	2.9×10^{-4}	--
2.0×10^{-1}	1.7×10^{-5}	2.7×10^{-4}	--

(b)

Table 7.4 Percentage defect coverages for barium stearate coated platinum wire electrodes in KCl. The defect coverages were estimated from (a) the experimentally determined coating capacitance and double layer capacitance, assuming that an intact film would have a dielectric permittivity of 3 (equation 5.3) and (b) the experimentally determined coating conductance using equation 5.2 (Stelzle and Sackmann, 1989). In order to evaluate equation 5.2, it was assumed that an intact 9 monolayer film of $BaSt_2$ would have a conductivity of $1.5nSm^{-1}$, which was the lowest value measured for $BaSt_2$ deposited onto platinum wire electrodes.

lower than the defect coverage indicated by the capacitance measurements.

Additional experiments were carried out in 2mM solutions of KI and NaCl to determine whether the film admittance was dependent either on the cation or anion present in the electrolyte. The results of these measurements, again with 9 monolayer films of Barium Stearate on platinum are given in the double log plots of fig 7.7 and 7.8. Fig 7.7(a) and (b) show that the nature of the anion has only a small effect on the capacitance and loss curves of the bare electrode. The presence of the iodide ion appears to have the largest effect, increasing both C_T and G_T. For the coated electrode, the presence of the iodide ion has an even larger effect, producing a systematic increase in C_T and G_T for all frequencies below ≈100Hz. This effect is also seen clearly from the plots of coating capacitance and conductance shown as a function of electrolyte in Fig 7.9. It is of interest that as previously (Fig 7.6), the variations in C_b and $G_b/2\pi f$ are most marked at $1/2\pi$Hz. At the cross-over frequency there is little difference between the values of C_b, reinforcing the observation that the electrolyte ions no longer affect the film capacitance at high frequencies.

The double log plots of fig 7.10, show C_T and $G_T/2\pi f$ as functions of frequency for 1, 3, 5, 7 and 11 monolayer films of Barium Stearate on platinum, in 20mM KCl. The curves of fig 7.10 have the same basic features as those described earlier (figs 7.5 and 7.7) and show the expected decrease in coating conductance and capacitance with increasing numbers of monolayers. The data given here apply to the highest quality films deposited at each thickness.

The inverse of the coating capacitance and loss are shown against the number of Barium Stearate monolayers in fig 7.11. The values were estimated from the curves in fig 7.10 at 0.16Hz, 10Hz, and additionally, for $1/C_b$, at the capacitance/loss cross over point. As expected, the data points for the uncoated platinum electrode in fig 7.11 are seen to be close to the values obtained by extrapolating the straight line to zero layers. Furthermore, from the plots of inverse capacitance and loss against the number of coating monolayers, a linear dependence is observed as predicted by equations 5.1 and 5.3 (fig 7.11). It is noteworthy that there are no significant break points on either of the curves (fig 7.11) indicating that there is no marked improvement in film quality as the film thickness increases from 1 to 11 monolayers. This suggests that the first monolayer governs the quality of subsequent layers. Similar findings have been reported for other LB films (eg Peterson, 1984). Monolayer permittivities were calculated from the gradients of the lines of best fit to the data points in fig 7.11a. The values range from 82 at the cross-over frequency to 912 at 1/2πHz. The effective dielectric permittivity is again high compared to values of between 2 and 8 for dry films (eg Porter and Wyman, 1938; Race and Reynolds, 1939; Zahl et al, 1939; Sugi et al, 1979; Millany and Jonscher, 1979). As previously, it is suggested that the electrolyte forms a double layer in contact with the uncoated areas of the electrode, producing the observed increase in permittivity. Based on this model, the defect coverage is estimated to be between 5% and 61% at the cross-over frequency and at 1/2πHz respectively (Table 7.5, equation 5.4). Following a similar approach to that used above to analyse the capacitance data, the film conductivity was estimated to range from 4.4 to 67 nSm^{-1}.

Parameter/ Frequency	Monolayer C_b (μF)	ϵ_r	% defect coverage
X-over	0.8±0.1	82	5
10Hz	3.4±0.3	334	22
0.16Hz	9.3±0.2	912	61

(a)

Parameter/ Frequency	Monolayer G_b (μS)	σ (nSm^{-1})	% defect coverage
10Hz	77	67	3.4×10^{-4}
0.16Hz	5.1	4.4	1.5×10^{-5}

(b)

Table 7.5 Barium Stearate monolayer permittivities and conductivities estimated from the plots of reciprocal capacitance and loss (fig 7.11), assuming a monolayer thickness of 2.5nm. The corresponding defect coverages are also presented. The defect coverages in (a) were estimated from the experimental values of C_b and a theoretical estimate of the double layer capacitance (equation 5.3, Stelzle and Sackmann, 1989) and assuming a dielectric permittivity of 3. The values of defect coverage in b) were estimated from equation 5.2, assuming that electrolyte filled defects and intact regions of the film contribute to the measured conductance. σ_{bs} (equation 5.2), was assumed to be equal to the lowest measured value of conductivity of 1.5nSm^{-1}.

The corresponding defect coverage is 3.4×10^{-4}% at 10Hz, assuming that both the film and electrolyte contribute to the measured film conductance (equation 5.2, Table 7.5b).

The results indicate that although the capacitance and loss curves show the expected trends with increasing molarity and film thickness, the coating coverage is nonetheless poor. To investigate the possible reasons for the poor coverage, time dependent changes in the film admittance were measured. Data from these experiments are presented as cell capacitance and loss after exposures of 0 and 20 minutes, to 20mM KCl at 15°C and are shown in the double log plots of figs 7.12 to 7.16 for 3, 5, 7, 9 and 11 monolayers of Barium Stearate on platinum. Curves obtained at greater exposure times were generally similar to those at twenty minutes, indicating that the film ageing processes are practically complete after 20 minutes immersion in the electrolyte. The increase in capacitance and loss seen in these figures shows that Barium Stearate films on platinum are unstable, either the layers are peeling off or significant rearrangement is occurring.

In order to determine the extent of the film desorption, admittance curves were measured for i) a platinum electrode E_C, coated in 5 monolayers of Barium Stearate after 0, 20, 50 and 1140 minutes, ii) a freshly polished platinum electrode E_P and iii) a platinum electrode which was dipped but with no monolayer on the trough, E_D. The latter being used to check what effects the dipping procedure had on the admittance of the bare platinum (fig 7.17). It is apparent that within 20 minutes the capacitance and loss of the coated electrode, E_C has increased to values observed for the sub-phase dipped electrode, E_D. As time progresses, the capacitance and loss of E_C increases even further. However, after 1140 minutes, the capacitance and loss of E_C were still lower than that of the freshly polished electrode, E_P.

The implication here is that an oxide film grows on the platinum and that the rate of growth of this oxide is significantly reduced by the presence of the LB film. Then, as the Barium Stearate desorbs, the exposed platinum gradually oxidises so that after 1140 minutes the electrode is almost devoid of Barium Stearate, being covered in platinum oxide instead. Further evidence of the time dependency of the Barium Stearate films on platinum is provided by curves showing the variation of coating capacitance and conductance measured at 10Hz in 20mM KCl for 3, 7 and 11 monolayer films on platinum (fig 7.18a). Equivalent data for a freshly polished, uncoated platinum electrode is given for comparison in fig 7.18b.

It is interesting that for the 11 monolayer film, there is no distinct peak in capacitance or loss, only a gradual increase in their values with immersion time. In contrast, the curves for the 3 and 7 monolayer films, (fig 7.18a) show a rapid increase in capacitance and loss during the first 6 minutes of immersion in the electrolyte, followed by a gradual decrease over the remainder of the measurement period. (This time dependent behaviour was also observed occasionally during the measurement of cell admittance as a function of frequency taken at discrete time intervals (eg fig 7.17)). A decrease in measured capacitance due to oxide growth was measured during dielectric studies of dry metal-insulator-metal structures by Polymeropoulos et al, (1980). (Capacitance and loss data estimated at the initial, peak and final values from fig 7.18 are shown in fig 7.19 as a function of their position on the curve). The initial values of C_b compare well with the previous results obtained in 0.2mM KCl (Table 7.2). Indeed, the estimates of ϵ_r from the film capacitance measured when the electrodes were first immersed in the electrolyte are in the range of 19-24. These values are generally lower than those obtained previously for Barium Stearate LB films deposited onto platinum electrodes. However, the film permittivity roughly doubles as the immersion time increases before falling in value. This trend suggests that even when the initial film quality is reasonable, hydration and desorption processes quickly lead to an increase in the measured coating capacitance. The initial desorption of Barium Stearate is then followed by the growth of protective oxide on the exposed regions of the electrode.

7.3.2 Cyclic Voltammetry

In addition to the ac admittance measurements described above, cyclic voltammetry was also used to characterise the Barium Stearate multilayers. Fig 7.20 shows cyclic voltammograms (CV's) obtained using a sweep rate of 0.1V/second, for a platinum foil electrode in 5mM $K_3Fe(CN)_6$ with 0.1M KCl as the supporting electrolyte. The solid line is for an uncoated electrode and the dashed lines represent CV's for the same electrode coated in 7 monolayers of Barium Stearate after 0.5 and 8 minutes exposure to the electrolyte. Similarly shaped CV's were obtained for 3 and 5 monolayer films of Barium Stearate on platinum. The presence of Barium Stearate on the electrode results in a time dependent reduction in electrode current compared to the uncoated electrode (fig 7.20).

The dependence of the peak currents upon film thickness and (sweep rate)$^{1/2}$ are shown in the Levich plots of fig 7.21 ($6.4.1). The current does not fall as one might expect as the number of coating monolayers is increased. This means that the 7 monolayer film was of poorer quality than the 5 monolayer film. This is consistent with the admittance studies which show that it is very difficult to obtain good quality films of barium stearate onto platinum ($7.3.1). The observation that the current does vary with film thickness suggests that rather than modifying charge transfer at the electrode, which would require only the presence of a monolayer coating, the film is instead restricting movement of dye molecules to or from the electrode. At the same time, the reasonable symmetry of the currents about the x-axis indicates that the reaction is reversible for the range of sweep rates employed. This is confirmed by the variation of peak separation with (sweep rate)$^{1/2}$ which is close to that of bare platinum (fig 7.22, $6.4.2).

The observed reduction in peak currents could be caused by electro-static repulsion and/or mechanical blocking of the dye molecules by the Barium Stearate film

($6.5). However, electro-static repulsion can be ruled out because it would cause a shift in the CV characteristic along the voltage axis ($6.6.2.1).

From figs 7.20 it is apparent that the coating is becoming less blocking with increasing electrolyte exposure time. This effect is seen more clearly in the plots of peak anodic and cathodic current as a function of time for a 3 and 7 monolayer film of Barium Stearate on a platinum foil electrode (fig 7.23). The solid lines represent the current at a bare platinum electrode. Again, the symmetry of the plots about the x-axis shows that the electrode process is reversible at a sweep rate of 0.1V/sec, even in the presence of the coating.

The gradual increase in peak currents with time may indicate the penetration of water and supporting electrolyte ions through pin hole defects and/or desorption of the film. Comparing the time dependent changes shown in the cyclic voltammograms and ac admittance studies, after only 15 minutes, the anodic and cathodic peak currents, i_{pa} and i_{pc} have increased by a factor of 3.5 to reach 70% of the bare electrode values (fig 7.20 and 7.23), whereas for a similar film thickness, ϵ_r has only doubled (fig 7.18a). This indicates that desorption was slower during ac admittance measurements than CV which may be a consequence of the smaller perturbing voltage and lower electrolyte concentration. In addition, it is important to remember that the ac admittance measurements were performed in the absence of redox species. Also of note is the rapid convergence of the current versus time curves for 3 and 7 monolayer Barium Stearate films (fig 7.23). This suggests that desorption is more rapid for a thicker film, indicating the importance of inter-layer adhesion which is seemingly greater close to the electrode surface. These non-bulk properties are well known in dielectric studies where the dielectric permittivity for a monolayer is 1.6 to 2.1, but for multilayers 2.1 to 4.2 or higher (eg Khana and Srivastava, 1972; Handy and Scala, 1966; Millany and Jonscher, 1979). Under the deposition conditions employed, mixed Barium Stearate/stearic acid multilayers will have been formed. In this case, we may be observing dissolution of the stearic acid, which is known to occur at the air/water interface. However, studies on multilayers indicate that transferred films have greater stability and the strong association between stearic acid and stearate is indicated by both skeletonisation experiments and infra-red spectra (Hasmonay et al, 1980). The results suggest that initially the Barium Stearate acts as an effective blocking layer, preventing ferricyanide ions from approaching the metal surface. However, as time progresses, the Barium Stearate film desorbs and the ferricyanide has easier access to the electrode.

In order to investigate further any charge dependent effects of Barium Stearate on platinum electrodes, cyclic voltammograms were measured for electrodes using the positively charged dye, benzyl viologen (fig 7.24). With 5 monolayers of Barium Stearate, the standard redox peaks are still observed at A and A'. In addition, there is a pair of new peaks, B and B', indicating a second process is occurring at -480mV vs SCE.

Although the peak separation for the standard reaction, A-A', is greater than the expected value of 59mV for a reversible redox reaction at 25°C, ($6.4.3) the new reaction (B-B'), has a peak separation of 61mV which is close to 59mV. The variation of peak height (B-B'), with sweep rate also indicates that the new reaction is reversible (fig 7.25, $6.4.1). In addition, peak enhancement increases with film thickness, indicating that rather than producing a simple charge residence effect, the Barium Stearate is actually involved in the reaction, although not as a mediator ($6.6.2.2).

The shift in background current level at -300mV may be a consequence of the new redox process. This is because the positive and negative voltage limits are normally chosen to ensure that the background current has decayed before reversing the sweep voltage. For example, the negative sweep potential is normally set to not less than ca 35/n mV past the cathodic peak, where n is the number of electrons involved in the redox process

(Nicholson and Shain, 1964). The new process will generate more oxidised species at the electrode and since the new process is at a more positive voltage than that of the standard redox reaction, the current will have less time to decay.

From fig 7.24, the peaks attributable to the benzyl viologen reaction grow rapidly while the additional peaks disappear. A possible explanation for the observed results is that the Barium Stearate introduces a new chemical into the cell which undergoes a redox reaction. This may be a reaction involving the stearate chain itself, or the reaction of a new compound formed by the film combining chemically with benzyl viologen. The sharp peaks indicate rapid electron transfer resulting in depletion of the redox species at the electrode. If the reaction is due to the film, the redox species will be present initially at the electrode surface but as the film desorbs, the species are released into the electrolyte where they will be very dilute. Therefore the effect will disappear while the standard benzyl viologen reaction is no longer hindered.

AC admittance and CV studies show that $BaSt_2$ deposited onto platinum results in coverage which deteriorates with time when the electrode was immersed in electrolyte. In addition, the inability to obtain accurate deposition data for Barium Stearate on platinum meant that it was extremely difficult to monitor film deposition. Therefore, deposition and ac admittance analysis of Barium Stearate on larger area, copper electrodes was performed.

7.4 Barium Stearate Multilayers on Sputtered Copper Electrodes

Cell capacitance, C_T and loss, $G_T/2\pi f$, plotted as a function of frequency, are presented in the double log plots of fig 7.26 for 3 monolayers of Barium Stearate on sputtered copper electrodes in 2mM KCl solution at 19±2°C. For the curve obtained immediately after immersing the electrode in the electrolyte (t=0), a theoretical fit was attempted, based on the equivalent circuit model (§A.3). As can be seen, a good fit was obtained between theory and the experimental curves provided that two of the components (C_d and G_t) were assumed to be frequency-dependent. The values employed in the theoretical fit were $C_d=10^{-4}w^{0.9}F$; $C_b=1.8x10^{-7}F$; $C_g=1.6x10^{-11}F$; $G_d=7.5x10^{-4}S$; $G_b=1.25x10^{-5}S$; $G_t=10^{-5}w^{0.7}S$. Curves for uncoated copper are given for comparison.

The presence of the LB film is clearly detected, giving rise to i) the expected plateau of almost constant capacitance between 1 and 500Hz; ii) a high frequency loss peak at around 10^3Hz; and iii) a significant reduction in both capacitance and conductance in the frequency range below ≈100Hz. It is obvious though, that the film capacitance and loss increase markedly with time of immersion in the electrolyte. This trend is also seen clearly in the plots of capacitance and loss against time, estimated from the curves in fig 7.26 at 10Hz and shown in fig 7.27 (Table 7.6).

Parameter/ Immersion Time(mins)	3m $BaSt_2$ on Copper		Uncoated Copper	
	$C_b(\mu F)$	$G_b(nS)$	$C_b(\mu F)$	$G_b(nS)$
0	0.18	1.81	18	139
19	0.94	1.79	154	672
49	1.54	1.91	286	674

Table 7.6 Coating capacitance, C_b, conductance, G_b and uncoated electrode capacitance, C_b and conductance G_b, at immersion times of 0, 19 and 49 minutes for sputtered copper electrodes coated in three LB monolayers of $BaSt_2$ in 2mM KCl at 20±1°C.

The capacitance at the high frequency plateau (not shown) was 16pF which is close to the expected value. In addition, the electrolyte molarity, calculated from the high frequency slope of the $G_T/2\pi f$ curve is 2.5mM, in reasonable agreement with the expected value of 2mM, if allowance is made for fringe electric fields.

From curve fitting, the film capacitance is estimated to be 0.18μF and arises from the presence of three monolayers on each of the two electrodes. Therefore, the effective film thickness is 15nm (2.5nm per monolayer) so that the relative permittivity is calculated to be 2.7. (If the presence of the oxide layer is taken into account, the figure would be reduced to 2.4). The value obtained is well within the range of 1.9 to 3.7 reported for both wet and dry LB films of Barium Stearate by Porter and Wyman (1938), Race and Reynolds (1939) and Zahl et al (1939) and within the range 2.64–2.77 presented by Sugi et al (1979) for dry cadmium stearate films, though much lower than the 4–8 quoted more recently by Millany and Jonscher (1980). The relative permittivity obtained here is also consistent with the values reported for black lipid membranes (BLM) which suggests that the general quality of the LB films is good. Also from curve fitting, the conductance of the layer is estimated to be 12.5μS, giving a conductivity of $2x10^{-9}$ Sm^{-1}. This should be compared with values in the range $5x10^{-10}$ to $5x10^{-13}$ Sm^{-1} quoted by Tien (1974) and Wei and Woo (1973) for a phospholipid BLM assuming that the thickness of such a membrane is 5nm.

As the time for which the electrode has been exposed to the electrolyte increases, the coating capacitance gradually increases and the curve tends towards that of the uncoated copper electrode. Similarly, for the loss curves, the coating conductance gradually increases with time (fig 7.27). The observed changes are attributed to electrolyte ions penetrating the film followed by growth of the copper oxide. This is supported by corrosion studies of nickel, coated with 9 microns of polybutadiene and immersed in a 3% solution of NaCl by McIntyre and Leidheiser (1986) who reported that the oxide growth produced blisters which disrupted the coating and enhanced the rate of corrosion ($2.2.3). It is therefore suggested that as the copper is oxidised, initially through pin-hole defects in the LB film, its growth disrupts the nearby intact LB film.

The fractional defect coverage can be estimated by assuming that double layer regions are formed in contact with the electrode in pin- holes filled with electrolyte ($7.3). Based on the experimental value of 2.7 for the dielectric permittivity and a theoretical value of 15.3μF for the double layer capacitance ($A.3.1), the defect coverage after 19 minutes, is estimated to be 5% and by 49 minutes this value has increased to 9%. These figures contrast with $6x10^{-5}$% and $1x10^{-4}$% if the defect coverage is calculated, assuming electrolyte conduction through pin-holes in the film, ($5.4, equation 5.2), much lower than the values estimated from the capacitance measurements.

Although the initial film quality was good, as evidenced by the value of 2.7 estimated for the dielectric permittivity of the film, the instability of the coating meant that an alternative substrate was required. Consequently, experiments were performed on aluminium electrodes.

7.5 Barium Stearate Monolayers on Evaporated Aluminum Electrodes

The cell capacitance, C_T and loss, $G_T/2\pi f$ as functions of frequency are shown in the double log plots of figs 7.28 and 7.29 for a 3 and 9 monolayer film of Barium Stearate respectively on evaporated aluminium electrodes, in 0.2, 2, 20 and 200mM KCl solutions at 21±1°C. Similar curves were obtained during tests in $CaCl_2$ and NaCl solutions (fig 7.30 and fig 7.31).

The capacitance plateaus in the frequency range 1 to 100Hz are relatively flat and well defined, similar to the results for PVC but without the dispersion which arose from ions in the film. The slight rise in capacitance below 100mHz, which was observed in some of the curves was probably due to the double layer capacitance ($5.3, figure 5.6). The expected loss peaks are also clearly defined, as is the increase in loss below 1 Hz, arising from the coating conductance ($5.3).

At frequencies above 100kHz and for electrolyte molarities of 0.2mM and 2mM, the cell capacitance reaches a plateau at 20±2pF, corresponding to the geometric capacitance, C_g (figs 7.28 to 7.31). The calculated value for C_g, assuming an electrode area of $1.13cm^2$ and inter-electrode spacing of 4mm is also 20pF, in excellent agreement with the experimental result. In addition, good agreement was obtained between actual electrolyte molarity and values deduced from the high frequency slopes of the loss plots. The mean ratio of experimental to nominal electrolyte molarity was 1.1±0.2 for all the data obtained on Barium Stearate coated aluminium electrodes with the exception of the anomalous results obtained for 0.2M KCl ($A.3.3, Table 7.7). The reason for the large discrepancy is not known, but cannot arise from limitations of theory or loss of accuracy of the measurement system, since good agreement was obtained at the same molarity using the platinum electrode ($7.3.1, Table 7.2).

Nominal Molarity	Molarity From Expt	Expt/Nominal Molarity
$2.0x10^{-4}$	$2.2x10^{-4}$	1.1
$2.0x10^{-3}$	$1.9x10^{-3}$	1.0
$2.0x10^{-2}$	$1.4x10^{-2}$	0.7
$2.0x10^{-1}$	$0.3x10^{-1}$	0.2

Table 7.7 A comparison of the nominal and experimentally determined electrolyte molarities, obtained during ac admittance analysis of barium stearate coated evaporated aluminium electrodes in KCl at 21±1°C.

At frequencies below 10^2 and 10^4Hz, depending on solution molarity, the capacitance rises to a second plateau which can be described by the equation;

$$C_T=C_b w^n \text{ (F)}$$

Nominal Molarity	KCl		NaCl		$CaCl_2$	
	$C_b(\mu F)$	n	$C_b(\mu F)$	n	$C_b(\mu F)$	n
2.0×10^{-4}	0.25	-0.08	0.25	-0.13	0.24	-0.08
2.0×10^{-3}	0.20	-0.10	0.19	-0.17	0.20	-0.07
2.0×10^{-2}	0.15	-0.05	0.16	-0.14	0.17	-0.09
2.0×10^{-1}	0.15	-0.05	0.13	-0.10	0.16	-0.08

(a)

Nominal Molarity	KCl		NaCl		$CaCl_2$	
	G_b(nS)	m	G_b(nS)	m	G_b(nS)	m
2.0×10^{-4}	32	0.52	64	0.46	56	0.47
2.0×10^{-3}	34	0.50	58	0.40	37	0.42
2.0×10^{-2}	37	0.42	33	0.39	31	0.36
2.0×10^{-1}	56	0.35	43	0.38	74	0.21

(b)

Electrolyte /Molarity	C_b (μF) estimated at 10Hz		
	KCl	NaCl	$CaCl_2$
2.0×10^{-4}	0.20	0.18	0.20
2.0×10^{-3}	0.16	0.16	0.18
2.0×10^{-2}	0.13	0.15	0.16
2.0×10^{-1}	0.13	0.13	0.15

(c)

Electrolyte /Molarity	C_b (μF) estimated at X-over		
	KCl	NaCl	$CaCl_2$
2.0×10^{-4}	0.13	0.19	0.19
2.0×10^{-3}	0.13	0.13	0.14
2.0×10^{-2}	0.12	0.13	0.13
2.0×10^{-1}	0.12	0.12	0.13

(d)

Electrolyte /Molarity	G_b (μS) estimated at 10Hz		
	KCl	NaCl	$CaCl_2$
2.0×10^{-4}	1.51	2.70	0.28
2.0×10^{-3}	0.59	0.66	0.52
2.0×10^{-2}	0.49	0.33	0.52
2.0×10^{-1}	0.47	0.49	0.44

(e)

Table 7.8 Film capacitance, C_b, Conductance, G_b n and m for 3 monolayers of Barium Stearate deposited onto evaporated aluminium electrodes and immersed in a range of electrolytes and electrolyte molarities. The capacitance and n data were estimated from the curves shown in fig 7.28a to 7.31a and are given at (a) 0.16Hz (c) 10Hz and (d) the loss/capacitance cross over points. The conductance and m data are given at (b) 0.16 and (e) 10Hz only, estimated from the loss curves of fig 7.28b to 7.31b. (The capacitance, conductance, n and m are shown in fig 7.32 to 7.34, plotted against electroltye molarity).

Similarly the coating conductance, in the approximate frequency range of 10Hz to 10mHz may be defined by the relationship ;

$$G_T=G_b w^m \text{ (S) (\$5.5.1)}$$

The values of C_b, G_b, n and m estimated at 1/2πHz from figs 7.28 to 7.31 are summarised in Table 7.8 and shown as a function of electrolyte and electrolyte molarity in figs 7.32 and 7.33. In addition, values of C_b estimated at 10Hz and from the high frequency cross-over point of the C_T and $G_T/2\pi f$ curves are also given (fig 7.34, Table 7.8). From figs 7.32a and 7.34, a clear trend of decreasing capacitance with increasing electrolyte molarity is observed, although the trend is independent of the electrolyte cation.

It should be noted that as the electrodes were tested first in the lowest molarity electrolyte, progressing to the highest molarity, the x-axis may be considered as an approximate time axis. Furthermore, as the film capacitance normally increases with time ($7.3, $7.4), the trend of decreasing coating capacitance with increasing molarity must reflect the presence of an additional mechanism. The only explanation that can be offered at present is that the repeated action of removing the electrodes from the electrolyte and replacing them in a different electrolyte may have accelerated the growth of aluminium oxide, leading to a reduction in the measured capacitance.

From fig 7.32b, the molarity dependence of the coating conductance at 1/2π Hz is less clear than that of the coating capacitance. Again, noting that the molarity axis is also an approximate time axis, for results using $CaCl_2$ and NaCl electrolyte, the initial fall in coating conductance with increasing molarity may be due to growth in the aluminium oxide, whereas the eventual increase in conductance occurring at 0.2M concentrations may be caused by an increase in the number of film defects. This could have arisen from the rearrangement of crystalline regions or actual loss of film. Inspection of the coatings using a phase contrast microscope support both explanations (fig 7.35).

The photographs in fig 7.35 suggest that initially, the film is reasonably homogenous, as evidenced by the smoothness of the "background" surface. Defects apparently arise from b), c) movement of domains including d) the folding back of areas of film and a) actual loss of film. Similar phenomena were reported by Kopp et al (1975) from studies of the stability of LB films using electron microscopy and infra-red spectroscopy. In particular Kopp et al (1975) noted that small aggregates and holes formed in 3 and 5 monolayer coatings of $BaSt_2$ soon after deposition onto carbon film. In the case of $BaSt_2$ deposited onto germanium substrates, larger defects such as patches and islands were observed. In addition, when $BaSt_2$ was deposited onto glass, flat islands and holes were reported with areas of the film occasionally folding back on adjacent regions. In all cases, the changes in film structure progressed with time. Consequently, even if the rearrangement of the dry $BaSt_2$ films on aluminium was complete, exposure to the electrolyte would have induced further changes (Kopp et al, 1975).

As the film capacitance was observed to decrease as the length of immersion time increased, the growth of the oxide must have dominated any capacitance changes. Therefore, it is unlikely that the number of holes through the film increased significantly during this time. Instead it is suggested that changes in film structure during immersion were mainly restricted to movement of domains including folding back of the film, rather than desorption. This is consistent with the observed changes in coating capacitance, because provided reasonable monolayer coverage of the electrode is maintained and neglecting any interfacial effects, any reorganisation of the additional layers would not result in a change in the measured film capacitance. The eventual increase in film conductance could be attributed to film desorption at the longer exposure times.

The effective dielectric permittivity and conductivity of the films were calculated as described previously ($7.3). The values thus obtained are summarised in Table 7.9. The dielectric permittivity ranges from 1.0 to 11.8 with a mean of 3.0±2.0, including the 9 monolayer film, or 2.4±0.6 excluding the 9 monolayer film. The generally higher values of permittivity for the 9 layer film are indicative of poor coverage. However, the mean value of 2.4±0.6 is in good agreement with values quoted in the literature (eg Porter and Wyman, 1938; Race and Reynolds, 1939; Zahl et al, 1939; Sugi et al, 1979; Millany and Jonscher, 1979). Values of between 4.5 and 8.5 pSm^{-1} at $1/2\pi$Hz for the film conductivity support the fact that the film coverage is good.

Indeed, the conductivity is around 3 orders of magnitude lower than for Barium Stearate films on platinum and copper ($7.3, $7.4). The difference could be due to a significant improvement in film quality or the presence of an insulating aluminium oxide layer. The absence of an insulating oxide in the case of the Barium Stearate coated platinum and copper electrodes would result in direct pathways for charge transfer through pinholes, and consequently, higher film conductivities. It is noteworthy that in dielectric studies on dry metal–insulator (LB film)–metal structures, Millany and Jonscher (1979) reported that the film conductance was high when tin was used as the electrode material.

The values of fractional defect coverage based on the coating capacitance for the 3 monolayer films at $1/2\pi$Hz are given in Table 7.9 and range from 2.6% to less than 0.1%, with a mean value of 1.0%, again indicating good quality deposition. In contrast with these values, assuming that the film conductance is the result of ionic flow through small pores, the fraction of the surface covered by such defects is estimated to be less than

Nominal Molarity	ϵ_r from C_b at 0.16Hz			ϵ_r from C_b at 10Hz			ϵ_r from C_b at X-over		
	KCl	NaCl	$CaCl_2$	KCl	NaCl	$CaCl_2$	KCl	NaCl	$CaCl_2$
2.0×10^{-4}	3.7	3.2	3.6	3.0	2.7	3.0	1.9	2.8	2.8
2.0×10^{-3}	2.9	2.8	3.0	2.4	2.4	2.7	1.9	1.9	2.1
2.0×10^{-2}	2.2	2.4	2.6	1.9	2.2	2.4	1.8	1.9	1.9
2.0×10^{-1}	2.2	2.0	2.4	1.9	1.9	2.2	1.8	1.7	1.0

(a)

Nominal Molarity	% defects from C_b at 0.16Hz			% defects from C_b at 10Hz			% defects from C_b at X-over		
	KCl	NaCl	$CaCl_2$	KCl	NaCl	$CaCl_2$	KCl	NaCl	$CaCl_2$
2.0×10^{-4}	6.9	4.9	6.4	4.0	2.8	4.0	0.0	3.2	3.2
2.0×10^{-3}	1.1	0.9	1.2	0.5	0.5	0.8	0.0	0.0	0.1
2.0×10^{-2}	0.1	0.1	0.2	0.0	0.1	0.1	---	0.0	0.0
2.0×10^{-1}	1.7	0.0	0.0	0.0	0.0	0.0	---	---	---

(b)

Nominal Molarity	σ(pSm^{-1}) from G_b at 0.16Hz			σ(pS^{-1}) from G_b at 10Hz		
	KCl	NaCl	$CaCl_2$	KCl	NaCl	$CaCl_2$
2.0×10^{-4}	4.5	8.5	7.5	200	359	38
2.0×10^{-3}	4.5	7.7	4.9	78	88	68
2.0×10^{-2}	4.9	4.4	4.0	65	44	68
2.0×10^{-1}	7.5	7.8	9.8	62	65	58

(c)

Nominal Molarity	% defects ($\times 10^9$) from G_b at 0.16Hz			% defects ($\times 10^9$) from G_b at 10Hz		
	KCl	NaCl	$CaCl_2$	KCl	NaCl	$CaCl_2$
2.0×10^{-4}	140	290	120	63	120	6
2.0×10^{-3}	15	31	10	3	4	1
2.0×10^{-2}	2	3	2	0.3	0.3	0.3
2.0×10^{-1}	2	3	2	0.1	0.2	0.1

(d)

Nominal Molarity	% defects from G_b at 0.16Hz			% defects from G_b at 10Hz		
	KCl	NaCl	$CaCl_2$	KCl	NaCl	$CaCl_2$
2.0×10^{-4}	0.1	0.1	0.0	1.7	3.3	0.2
2.0×10^{-3}	0.0	0.0	0.0	0.1	0.1	0.0
2.0×10^{-2}	0.0	0.0	---	0.0	0.0	0.0
2.0×10^{-1}	0.0	0.0	0.0	0.0	0.0	0.0

(e)

Table 7.9 (a) Dielectric permittivities and (c) conductivities for barium stearate coated aluminium electrodes, immersed in KCl, NaCl and $CaCl_2$. The values were calculated from the data in Table 7.8, assuming a monolayer thickness of 2.5nm. (b, d, e) Percentage defect coverages for barium stearate coated aluminium electrodes. The defect coverages were estimated from (b) the experimentally determined coating capacitance and double layer capacitance, assuming that an intact film would have a dielectric permittivity of 1.8 (equation 5.3) and (d,e) the experimentally determined coating conductance using (d) equation 5.1 and (e) equation 5.2 (Stelzle and Sackmann, 1989). In order to evaluate equation 5.2, it was assumed that a film of $BaSt_2$ would have a conductivity of 4.0pSm^{-1}, which was the lowest value measured.

1.5×10^{-9} at $1/2\pi$Hz. This indicates considerably higher film quality than achieved with Barium Stearate on copper (§7.4) and comparable quality to that obtained with electrodeposited polyphenylene oxide where a figure of 10^{-9} was given by Glarum and Marshall (1985).

In addition to characterising the molarity and electrolyte dependence of Barium Stearate multilayers on aluminum, the effect of coating thickness was also investigated. C_T and $G_T/2\pi f$ as functions of frequency for 5, 13 and 19 monolayer films of Barium Stearate in 2mM KCl are shown in the double log plots of fig 7.36. The presence of the Barium Stearate is clearly demonstrated by the reduction in C_T and $G_T/2\pi f$ with increasing numbers of coating layers. Coating conductance, conductivity, capacitance, dielectric permittivity and defect coverages at $1/2\pi$Hz, estimated as outlined previously are summarised in Table 7.10.

The inverse of the coating conductance and capacitance measured at $1/2\pi$Hz are shown as a function of the number of LB monolayers in fig 7.37. Neither curve shows the expected inverse dependence on coating thickness. The largest discrepancy occurs for the 19 monolayer film, suggesting that below 14 monolayers, pin hole defects can still bridge the coating. From the inverse capacitance plot the capacitance of the aluminium oxide is estimated to be 0.62μF which corresponds to an oxide thickness of 25nm, this contrasts with a value of 2.8nm reported by Millany and Jonscher, (1979). However, the value of 2.8nm was from studies on dry films, so that a value of 25nm is reasonable for measurements in an aqueous environment.

Parameter/ Number of Monolayers	Data for $BaSt_2$ on aluminium at 0.16Hz			
	C_b(nF)	ϵ_r	G_b(nS)	σ(pSm^{-1})
3	0.20	2.9	34	4.5
5	0.20	4.9	69	15
9	0.15	6.6	12	4.8
13	0.10	6.5	18	10
19	0.03	3.2	3.4	2.8

(a)

Parameter/ Number of Monolayers	% defect coverages	
	from C_b	from G_b
3	0.6	$5.7x10^{-9}$
5	1.8	$4.6x10^{-8}$
9	1.6	$8.4x10^{-9}$
13	1.1	$2.9x10^{-8}$
19	0.1	$1.2x10^{-10}$

(b)

Table 7.10 (a) Capacitance, conductance, dielectric permittivity and conductivity for barium stearate coated aluminium electrodes, immersed in KCl. (b) Percentage defect coverages estimated from (i) the experimentally determined coating capacitance and double layer capacitance, assuming that an intact film would have a dielectric permittivity of 2.4 (equation 5.3) and (ii) the experimentally determined coating conductance using (ii) equation 5.2 (Stelzle and Sackmann, 1989). In order to evaluate equation 5.2, it was assumed that a film of $BaSt_2$ would have a conductivity of $2.8pSm^{-1}$.

In addition to the experiments performed to characterise the molarity, electrolyte and thickness dependence of Barium Stearate films on aluminium, experiments were also carried out to determine the stability of the films. Capacitance and loss data from one such experiment are shown in fig 7.38 plotted against time of immersion in 0.2mM KCl at 23±1°C measured at 10Hz. (Similar curves were obtained in 2mM KCl measured at 80Hz). Both capacitance and loss increase steadily, reaching maximum values after ca 90 minutes, after which their values decrease gradually for the remainder of the measurement period. This trend was observed for Barium Stearate coated onto platinum ($7.3, fig 7.18a) but on aluminium, the films are more stable. The percentage increases in C_b and $G_b/2\pi f$ for Barium Stearate on platinum were 63% and 96% compared to 43% and 44% respectively on aluminium (Table 7.11). More significantly, the peak values were reached after only 6 minutes compared to 90 minutes for the same coating on aluminium. It is unlikely that the difference in electrolyte molarity could account for this variation, particularly as the capacitance and loss of the $BaSt_2$ films on aluminium was observed to fall as the KCl molarity was increased from 0.2mM to 20mM (fig 7.32).

Material	KCl mol	% from C_b	% from G_b	Time (mins)
Platinum	20	63	96	8
Copper	2	500	1833	>50
Aluminium	0.2	43	44	90

Table 7.11 A summary of stability data for 3 monolayers of Barium Stearate on Platinum, Copper and Aluminium, measured at 10Hz in KCl. The percentage values represent the increase in C_b and G_b from the initial to peak values. The immersion time required to reach the peak values is given in the last column.

These results contrast with those observed earlier for $BaSt_2$ coated aluminium electrodes characterised in different electrolyte molarities, where C_b and G_b decreased with immersion time (fig 7.32, 7.34). This again suggests that the repeated removal, air exposure and re-immersion of the electrodes during the tests in different electrolytes accelerated the growth of the aluminium oxide. The accelerated oxide growth then dominated any underlying increase in C_b and G_b due to ionic penetration and/or film desorption. However, when the electrodes were tested continuosly in the same 0.2mM KCl solution, the dominant change in C_b and G_b was initially due to ionic penetration and desorption. The eventual reduction in capacitance and loss is thought to be caused by the gradual growth of aluminium oxide.

7.6 Mixed Barium Stearate / Gramicidin multilayers on evaporated aluminium electrodes

7.6.1 Introduction

Gramicidin has been studied extensively as a model pore (Hille, 1984). It can provide a fixed channel across membranes through which cations can pass. Geometrically, it has an inner channel of 0.4nm diameter but externally, is shaped like a rod of triangular cross section with sides of ca 0.74nm and length 2.5nm (Hille, 1984).

The basic mechanism by which Gramicidin transports ions can be explained by considering that the barrier to movement of a heavily hydrated ion into a narrow pore is the energy required to dehydrate the ion. If the pore provides solvation of similar magnitude, the energy barrier is greatly reduced. Therefore, as long as the pore diameter exactly matches the diameter of the cation in one of its levels of hydration, the ion will be able to enter the pore and traverse the membrane. Consequently, a small degree of cation selectivity is provided by the requirement that the diameters of the pore and hydrated cation must match. For example, Gramicidin-A, with a pore diameter of 0.4nm, when incorporated into lipid bilayers formed from glyceryl mono-oleatedecane, shows conductance ratios;

$\sigma(H^+)/\sigma(Na^+) = 14$ and $\sigma(K^+)/\sigma(Na^+) = 1.8$ (Hille, 1984).

It was therefore anticipated that by incorporating Gramicidin in an LB film and measuring the film admittance in a range of KCl and NaCl solutions, a cation dependent conductance would be observed. Previous experiments had established that aluminium appeared to provide the best substrate for stable layers and so the first attempts at making an ion selective sensor consisted of incorporating Gramicidin into Barium Stearate LB films on aluminium.

7.6.2 Surface behaviour of Gramicidin/Barium Stearate Monolayers.

Mixed monolayers of Gramicidin and Barium Stearate were prepared firstly by producing a monolayer of Barium Stearate ($3.3), expanding the monolayer to zero surface pressure and then adding a solution of Gramicidin-D in chloroform (0.5 to 1.2mg/ml), drop wise at a number of points on the monolayer surface using a micro-pipette. After allowing time for the solvent to evaporate and for the Gramicidin to mix, the monolayer was compressed in readiness for deposition. Pressure-Area isotherms for the pure Barium Stearate and mixed Barium Stearate/Gramicidin monolayers are shown in fig 7.39. Similar curves were carried out for a range of Gramicidin solution volumes.

The average surface area per Gramicidin molecule was estimated to be 298±45 $Å^2$, which is in good agreement with the value of ca 336$Å^2$/molecule based on the space filling model for Gramicidin-A (Urry, 1971a,b). There is no correlation between the gramicidin surface areas and the ratio of gramicidin to barium stearate molecules. This means that for the concentrations used there was no siginficant interaction between Gramicidin molecules.

Parameter/ Number of Experiment	Conditions			Surface Area (/$Å^2$)	
	Temp (^oC)	pH	($BaSt_2$:Gr) Molecules	$BaSt_2$	Gramicidin
1	22.0	7.2	177:1	20.9	246
2	20.2	8.5	70:1	20.8	271
3	20.0	7.7	140:1	20.2	365
4	20.1	7.5	47:1	20.4	311
5	20.3	7.9	35:1	20.4	297

Table 7.12 Subphase conditions and surface areas for Barium Stearate and Gramicidin. The mean area/molecule for Gramicidin is 298±45$Å^2$/molecule.

7.6.3. Deposition onto substrates

The electrodes were prepared as previously, by evaporating aluminium onto clean microscope slides ($4.2.4). Mixed LB films of Barium Stearate and Gramicidin were deposited with deposition ratios in the range 1.04±0.11. It should be noted that three different pairs of coated aluminium electrodes were dipped concurrently and that a different pair was used for each set of experiments. Any comparison between the different admittance curves of figs 7.40, 7.41 and 7.42 therefore assumes that the coatings were of equal quality.

7.6.4 AC admittance of mixed Gramicidin/Barium Stearate LB films

The cell capacitance, C_T and loss, $G_T/2\pi f$ as functions of frequency are shown in the double log plots of figs 7.40 and 7.41 for a 3 monolayer film, tested using the sequence 0.2, 2, 20, 200, 0.2mM for KCl and NaCl solutions respectively. Curves of a similar shape to those in fig 7.40 were obtained during similar tests in KCl solutions on a monolayer film.

Initial confirmation of the validity of the data is again provided by the close agreement between the experimental and calculated values of geometric capacitance and solution molarity ($7.3, $7.4, $7.5). The geometric capacitance is measured to be 19±2pF, compared to the expected value of 20pF, while the normalised solution molarity is 1.0±0.3, excluding data for 0.2M electrolytes ($7.5).

The coating capacitance and loss at $1/2\pi$ Hz, and the corresponding values of n and m, estimated from figs 7.40 and 7.41 are shown as a function of electrolyte molarity in figs 7.42 and 7.43 respectively. Additional capacitance data measured at 10Hz and the high frequency cross-over point of the $G_T/2\pi f$ and C_T curves is presented in fig 7.44. (The reasons for choosing these frequencies are outlined in $7.3.1). The film conductance was not estimated at 10Hz from the $G_T/2\pi f$ curves because horizontal plateaus were reached before this frequency so that at 10Hz, $G_T/2\pi f$ is no longer representative of the electrode coating ($7.5). The decrease observed in the coating capacitance with increasing electrolyte molarity is attributed, as previously ($7.5), to the growth of aluminium oxide at the coating defects.

It is noteworthy that the capacitance of the coating measured in NaCl is lower than that for the coating measured in KCl. This suggests that the coatings tested in NaCl are of higher quality than those tested in KCl. However, the conductance measurements suggest that the opposite is true. It is interesting to compare the variation of film capacitance with electrolyte molarity for Barium Stearate and Gramicidin/Barium Stearate films on aluminium (figs 7.32a, 7.34 and figs 7.42a, 7.43). For example, whilst the capacitance of the mixed film is similar to that of the Barium Stearate films on aluminium and the trend of decreasing capacitance with increasing electrolyte molarity is less distinct. In addition, for Barium Stearate on aluminium, (figs 7.32a, 7.34), the film capacitance roughly halved as the electrolyte molarity was increased from 0.2 to 200mM. The corresponding change for the mixed film was generally less than 30% (fig 7.42a, 7.44). These results suggest that the introduction of Gramicidin could have increased the stability of the film. A similar enhancement of film stability was reported as a result of the incorporation of cytochrome-B_5 in phospholipid (Wilkinson et al, 1986).

Further evidence of the quality of the Barium Stearate/Gramicidin films was obtained by calculating the effective dielectric permittivity of the coating from the estimates of film capacitance (figs 7.42a and 7.44). The values of permittivity range from 1.8 to 3.4 with a mean of 2.3±0.5, in good agreement both with literature (eg Porter and Wyman, 1938; Race and Reynolds, 1939; Zahl et al, 1939; Sugi et al, 1979; Millany and Jonscher, 1979) and experimentally determined values for pure Barium Stearate on aluminium (\$7.5). The average defect coverage was 0.4%, estimated from the film capacitance as previously (\$7.3, \$7.4, \$7.5), indicating that the film quality is high. The film capacitance, permittivity and defect coverages are summarised in Table 7.13.

In fig 7.42b, the initial fall in coating conductance with increasing molarity during tests in KCl may be due to growth in the aluminium oxide (\$7.5). It is apparent that the conductance of the mixed film shows little molarity dependence, although an electrolyte dependence is clearly discernable, based on the average values of 150nS and 50nS for the film conductance in NaCl and KCl solutions respectively. This is opposite to the expected trend based on the conductivity ratio for $\mathrm{Na^+}$ and $\mathrm{K^+}$ for Gramicidin (\$7.6.1). It is therefore unlikely that the Gramicidin can be conferring any conductivity to the film. This is probably because only a very small proportion of the gramicidin molecules will be in line across the thickness of the 3 layer film. The average values of film conductance compare with values of 48nS and 40nS for pure Barium Stearate films in NaCl and KCl respectively (\$7.5, fig 7.3.2b).

The average defect coverage, assuming that the measured conductivity is due to conduction through electrolyte filled pinholes was $\approx 2\mathrm{x}10^{-7}\%$. The corresponding values for pure Barium Stearate were $2\mathrm{x}10^{-9}\%$ at 0.16Hz. Therefore, although the stability of the mixed film appears higher than that of the pure film, the quality of the mixed film is apparently ~~higher~~ lower than that for pure Barium Stearate deposited onto evaporated aluminium electrodes.

Values of n and m, presented as a function of electrolyte molarity in fig 7.43 show no significant molarity or electrolyte dependence. Indeed, the scatter in these results, especially the variation between the initial and final estimates in 0.2mM electrolyte, means that it is more appropriate to consider the average values of n and m in each electrolyte rather than to analyse the results in more detail. The average values for n in KCl and

Nominal Molarity	KCl		NaCl	
	C_b(μF)	n	C_b(μF)	n
2.0×10^{-4}	0.242	-0.10	0.196	-0.12
2.0×10^{-3}	0.200	-0.09	0.196	-0.06
2.0×10^{-2}	0.171	-0.12	0.154	-0.09
2.0×10^{-1}	0.158	-0.10	0.100	-0.02
$2.0\times10^{-4*}$	0.242	-0.10	0.100	-0.02

(a)

Nominal Molarity	KCl		NaCl	
	ϵ_r	% defect	ϵ_r	% defect
2.0×10^{-4}	3.6	4.9	2.9	2.2
2.0×10^{-3}	3.0	0.7	2.9	0.6
2.0×10^{-2}	2.6	0.1	2.3	---
2.0×10^{-1}	2.4	---	1.5	---
$2.0\times10^{-4*}$	3.6	4.9	1.5	---

(b)

Nominal Molarity	KCl		NaCl	
	C_b(μF)	ϵ_r	C_b(μF)	ϵ_r
2.0×10^{-4}	0.122	1.8	0.150	2.3
2.0×10^{-3}	0.123	1.8	0.163	2.4
2.0×10^{-2}	0.118	1.8	0.136	2.0
2.0×10^{-1}	0.127	1.9	0.141	2.1
$2.0\times10^{-4*}$	0.124	1.9	0.123	1.8

(c)

Nominal Molarity	KCl		NaCl	
	C_b(μF)	ϵ_r	C_b(μF)	ϵ_r
2.0×10^{-4}	0.116	1.7	0.140	2.1
2.0×10^{-3}	0.116	1.7	0.148	2.2
2.0×10^{-2}	0.110	1.6	0.110	1.6
2.0×10^{-1}	0.128	1.9	0.128	1.9

(d)

$BaSt_2$/Gramicidin/Al at 0.16Hz in KCl				
Nominal Molarity	G_b(nS)	m	σ(pSm^{-1})	% defects
2.0×10^{-4}	269	0.08	35.7	7.8×10^{-7}
2.0×10^{-3}	62	0.41	8.3	1.8×10^{-8}
2.0×10^{-2}	40	0.44	5.3	1.2×10^{-9}
2.0×10^{-1}	52	0.44	6.9	4.9×10^{-10}
$2.0\times10^{-4*}$	42	0.50	5.5	7.9×10^{-8}

(e)

$BaSt_2$/Gramicidin/Al at 0.16Hz in NaCl				
Nominal Molarity	G_b(nS)	m	σ(pSm^{-1})	% defects
2.0×10^{-4}	133	0.44	18	5.5×10^{-7}
2.0×10^{-3}	211	0.29	28	1.1×10^{-7}
2.0×10^{-2}	169	0.36	23	1.3×10^{-8}
2.0×10^{-1}	181	0.36	24	6.3×10^{-9}
$2.0\times10^{-4*}$	79	0.46	11	2.8×10^{-7}

(f)

Table 7.13 A summary of the ac admittance data for evaporated aluminium electrodes coated in 3 monolayers of $BaSt_2$/Gramicidin. (a) Film capacitance, C_b, and n at 1/2πHz for electrodes immersed in KCl and NaCl, estimated from figs 7.40a and 7.41a. (b) Dielectric permittivity, ϵ_r and percentage defect estimates based on the data in (a). (c) C_b, ϵ_r at 10Hz from the curves in figs 7.40a and 7.41a. (d) C_b, ϵ_r at the cross over point of the capacitance and loss curves in figures 7.40a and 7.41a. NB The defect coverages estimated from the capacitance data in (c,d) were all less than 0% and are therefore not shown. (e) G_b, m, conductivity, σ and percentage defect coverages estimated at 1/2πHz from the KCl curves in figs 7.40b and 7.41b. (f) G_b, m, conductivity, σ and percentage defect coverages estimated at 1/2πHz from the NaCl curves in figs 7.40b and 7.41b. The dielectric permittivity and film conductivity was calculated assuming a monolayer thickness of 2.5nm. The defect coverages in (b),(c) and (d) assumed an ideal coating permittivity 2.4 whilst those in (e, f) assumed an intact film conductivity of $2.8pSm^{-1}$.

NaCl were -0.10±0.01 and -0.06±0.04 for the mixed Gramicidin/$BaSt_2$ films compared to -0.08±0.03 and -0.14±0.03 for the pure film. The only significant difference in these results is for n in NaCl but even here, the disparity amounts to only 10% when the standard deviations are taken into account. Consequently, it is apparent that the incorporation of Gramicidin into Barium Stearate does not produce a marked change in n or m.

Based on Ohm's Law and the Diffusion equation, it is possible to estimate the channel conductance from which the conductance increase produced by the Gramicidin can be calculated (Hille, 1984). Using this approach, the film conductance in 0.2mM KCl would be around 0.04 S, assuming all the Gramicidin molecules lined up across the width of the film. In practice the values would be much less. It should also be noted that as Gramicidin is a pore, it normally passes ions across a membrane where there is a bathing solution on both sides to supply and sink the ionic flux. The situation of a coated electrode is more like a single sided membrane with no sink. Consequently, any ions entering the pores would have nowhere to go and would block the entry of further ions by electrostatic repulsion. Any effect would only be transient but should have been detectable using ac admittance analysis.

In addition to characterising the mixed Gramicidin/Barium Stearate multilayers in KCl and NaCl, measurements were performed at different pH. The double log plots of fig 7.45 show C_T and $G_T/2\pi f$ as functions of frequency for a 3 monolayer film in 20mM KCl at pH 3, 5, 7 and 9. The features of the curves are essentially the same as those described earlier. The main differences to note are the presence of a small dispersion in the $G_T/2\pi f$ curves at pH 7 and 9 with a corresponding step in capacitance at about 10Hz. At frequencies below 1Hz, the film conductance changes with pH, although no trend is discernible (fig 7.45). The coating capacitance and loss at $1/2\pi$ Hz, estimated from fig 7.45, are shown in fig 7.46 as a function of electrolyte pH. (As a result of the close proximity of the capacitance and loss curves in fig 7.45, it was considered unnecessary to repeat the analysis at other frequencies). These investigations were performed to make use of the large conductance ratio for H^+ ions with respect to Na^+ ions. A large increase in film conductivity was therefore expected as the solution pH decreased from pH 9 to pH 3. However no such trend is discernible.

7.7 Conclusions

Barium Stearate was deposited onto platinum wire, sputtered copper and evaporated aluminium electrodes. The coated electrodes were then characterised in a range of electrolytes and electrolyte molarities using ac admittance analysis and for the coatings on platinum, cyclic voltammetry. The analysis permitted the coatings to be characterised in terms of monolayer permittivity, conductivity and defect coverage. Based on this information, electrolyte interaction with the electrode coating, including suggested reasons for the variations in electrode admittance with time of immersion in the electrolyte have been discussed qualitatively.

AC admittance and CV studies both showed that $BaSt_2$ deposited onto platinum results in patchy coverage which deteriorated with time when the electrode was immersed in electrolyte. Furthermore, the inability to obtain accurate deposition data for Barium Stearate on platinum necessitated the use of larger surface area electrodes. Therefore, deposition and ac admittance analysis of Barium Stearate on copper electrodes was performed ($7.2.2).

Admittance data for sputtered copper electrodes coated in Barium Stearate indicate that although it is possible to obtain good quality films, as evidenced by the initial values of 2.7 for the dielectric permittivity and 7×10^{-8} for the fractional defect coverage, the films quickly deteriorate when exposed to an electrolyte. This is attributed to the disruptive action of the copper oxide. Consequently, it is concluded that sputtered copper electrodes are unsuitable as a substrate for LB film coated devices required to operate in the presence of water. To overcome the problems encountered in using copper as the electrode material it was decided to use aluminium instead.

Barium Stearate deposited onto aluminium resulted in good quality films with an average dielectric permittivity of 2.4±0.6 for the 3 monolayer coatings, corresponding to an average defect coverage of only 1.0%. The film conductivity of 4.5 to 8.5 pSm^{-1} at $1/2\pi Hz$ was further evidence of high quality. In addition, the $BaSt_2$ films on aluminium showed greater stability than when deposited onto platinum or copper. Consequently, the Barium Stearate deposited onto aluminium was considered to be a suitable system for the development of an ion selective electrode. Initially, work was carried out to immobilise Gramicidin in Barium Stearate and to deposit the monolayers onto evaporated aluminium electrodes.

Mixed monolayers of Barium Stearate and Gramicidin were successfully deposited onto aluminium electrodes. Pressure area characteristics indicated that the Gramicidin was correctly oriented in the LB film. However, subsequent admittance characterisation of the coated electrodes showed no conclusive behaviour to indicate that Gramicidin was functioning as a pore. This was probably due to the non alignment of the channels across the three layer film. In future experiments, the ion-carrier valinomycin was employed instead.

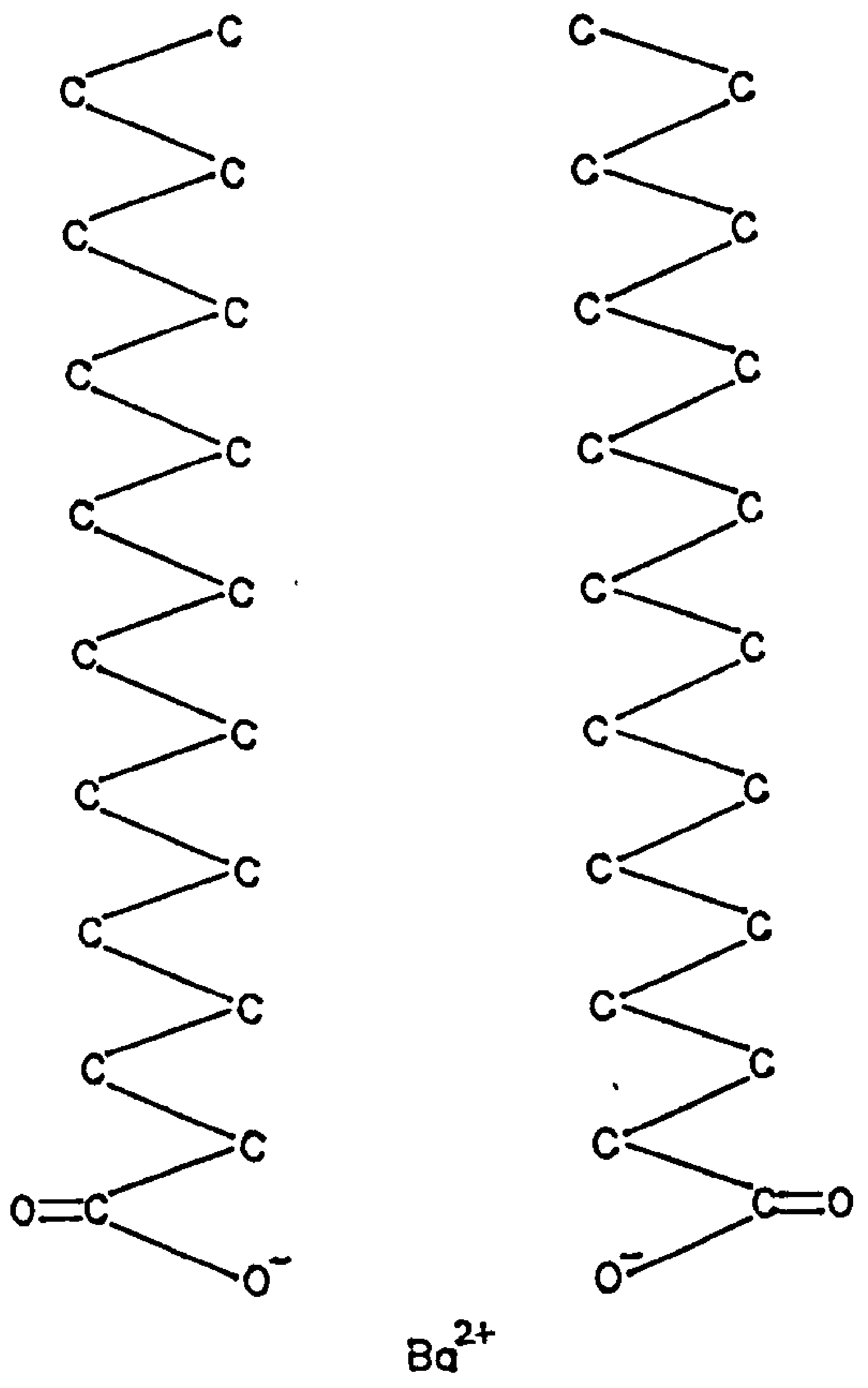

Fig 7.1 Molecular Structure of Barium Stearate (H atoms omitted for clarity).

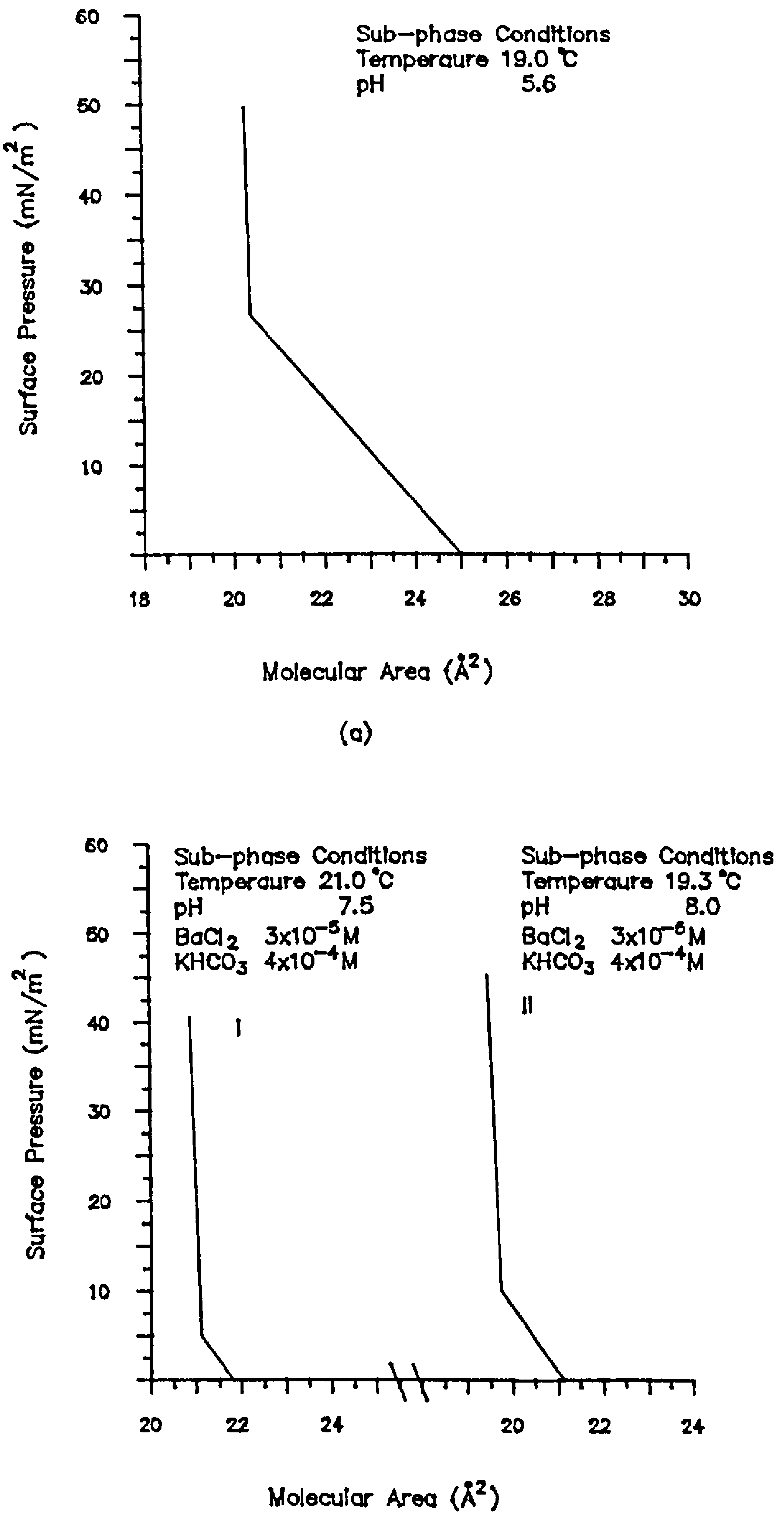

(a)

(b)

Fig 7.2 Pressure–Area Curves for (a) Stearic Acid and (b) Barium Stearate.

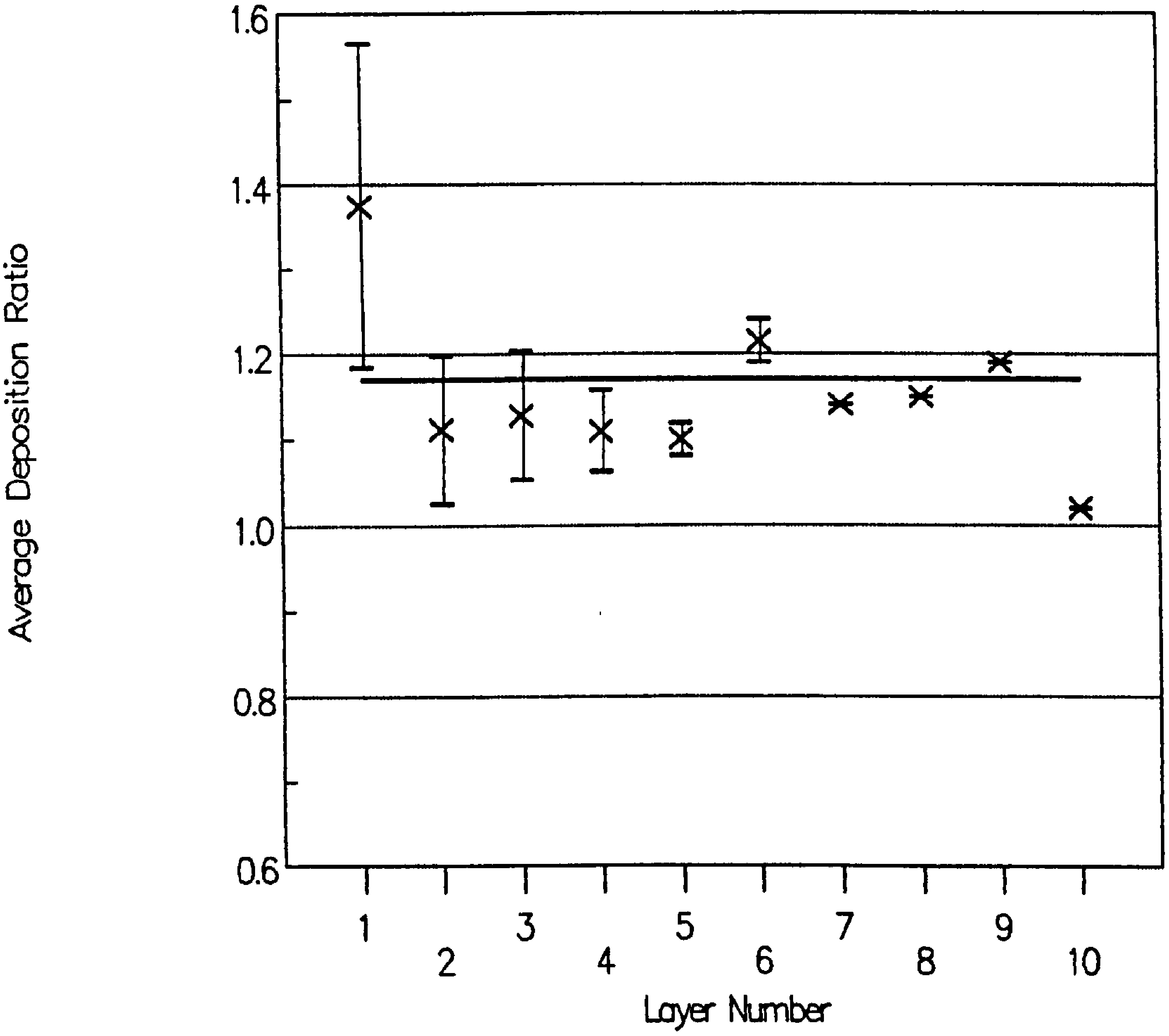

Fig 7.3 Deposition ratios for Barium Stearate onto evaporated aluminium electrodes plotted as a function of the number of the monolayer . (x) is the average value and (–) represents (±) standard deviation at that point. The average deposition ratio overall, is 1.17±0.14.

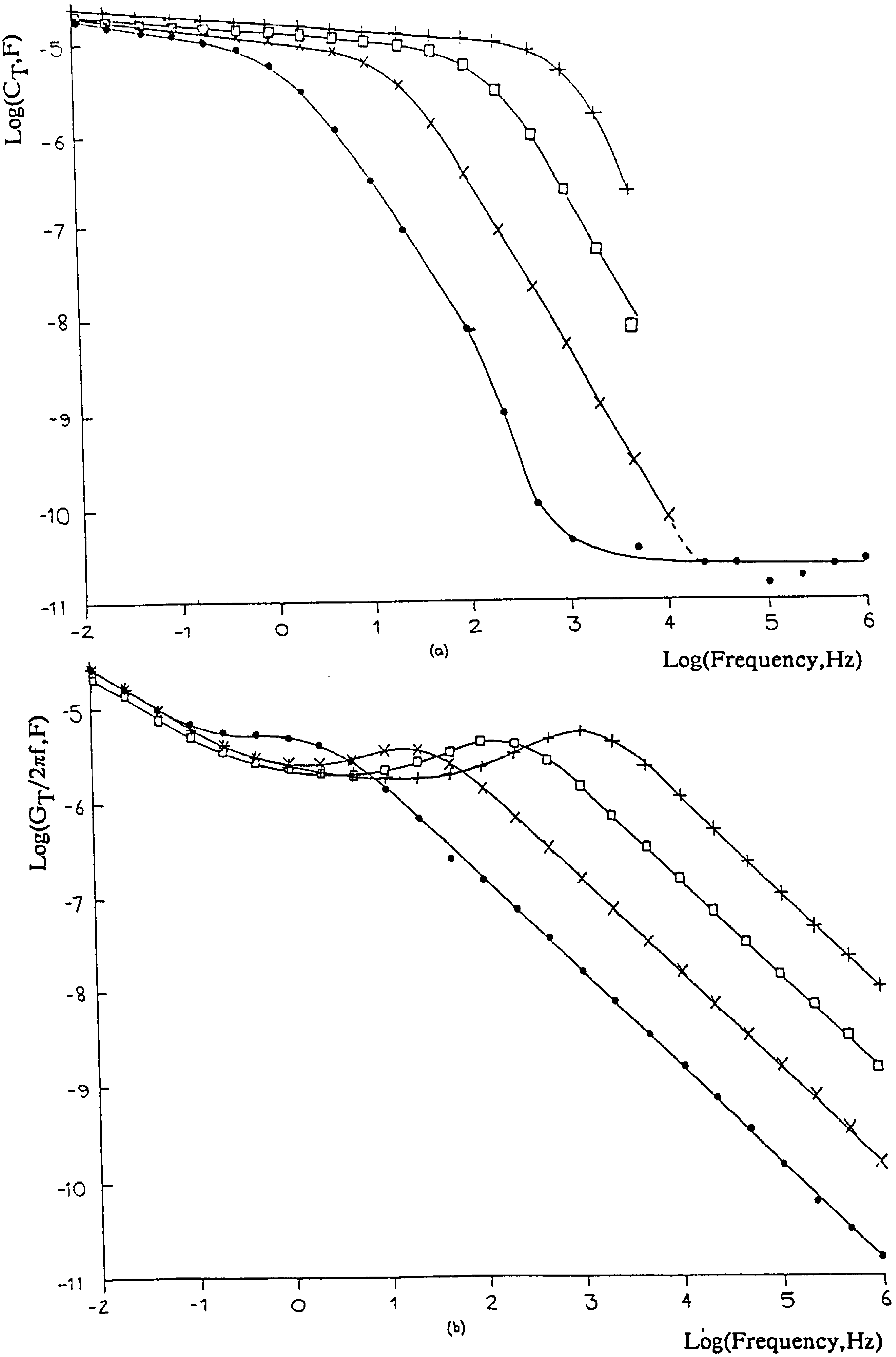

Fig 7.4 (a) Log Capacitance, C_T and (b) Loss ($G_T/2\pi f$) plotted against log frequency, F, for an uncoated platinum electrode immersed in (•) 0.2mM, (x) 2.0mM, (□) 20mM and (+) 200mM KCl at 15°C.

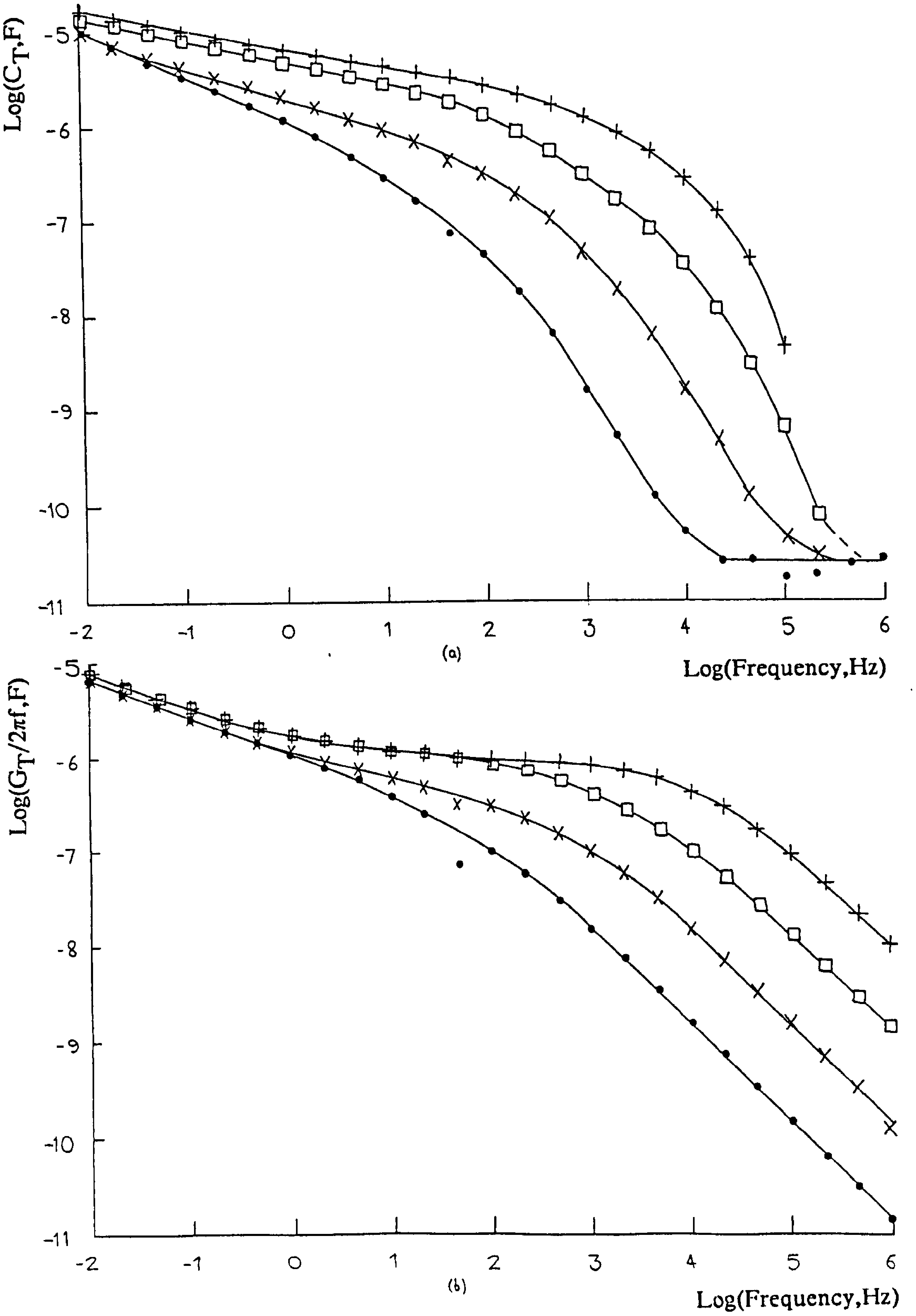

Fig 7.5 (a) Log Capacitance, C_T and (b) Loss ($G_T/2\pi f$) plotted against log frequency, F, for a platinum electrode coated in 9 monolayers of $BaSt_2$ and immersed in (•)0.2mM, (x) 2.0mM, (□) 20mM and (+) 200mM KCl at 15^oC.

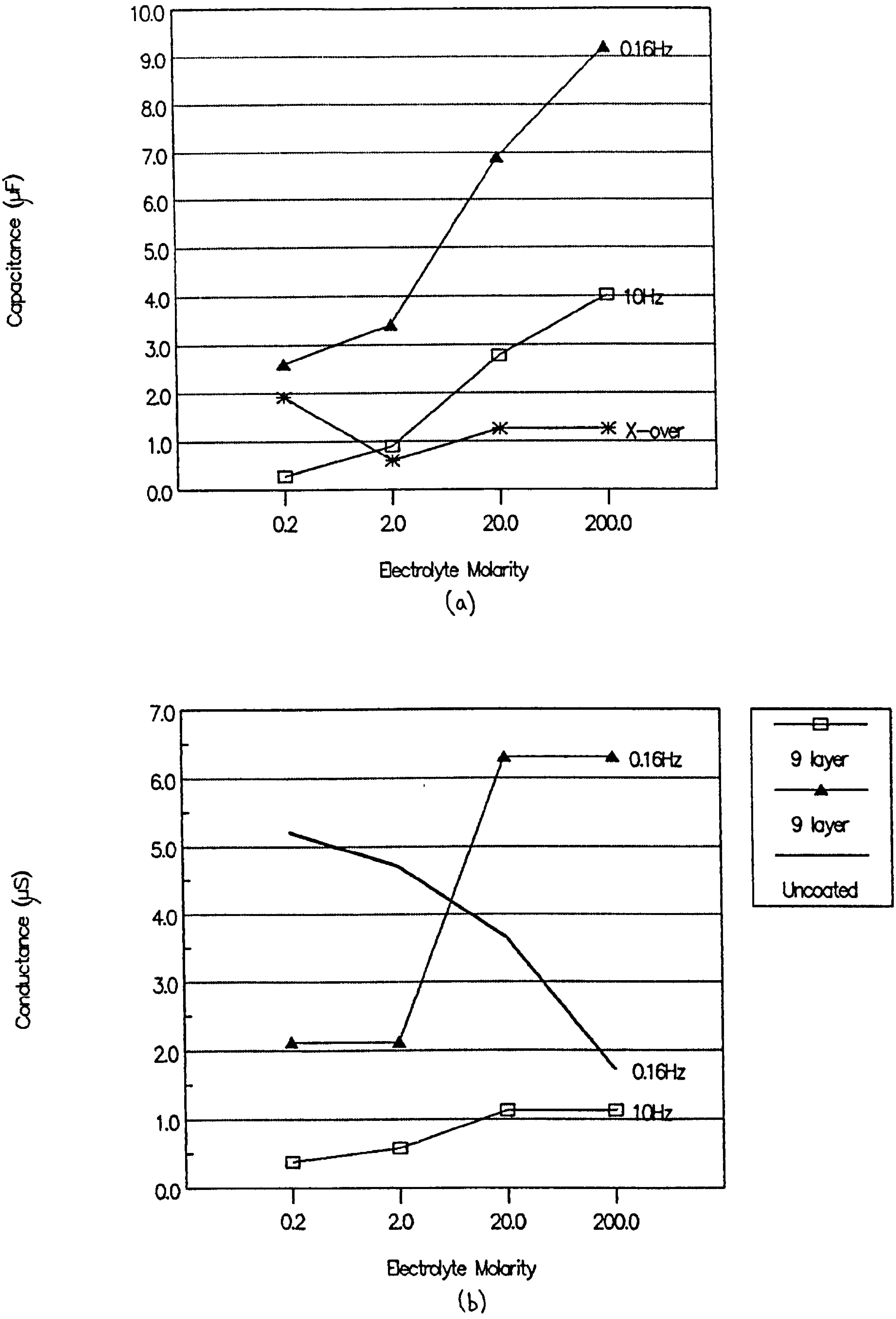

Figure 7.6 (a) Capacitance C_b, and Conductance G_b, for a platinum electrode coated with 9 monolayers of $BaSt_2$, plotted as a function of KCl molarity at 15°C. Capacitance values were estimated from fig 7.5a at (▲) 0.16Hz, (□) 10Hz and (*) the capacitance/loss cross-over point. Conductance data were estimated from fig 7.5b at (▲) 0.16Hz and (□) 10Hz. Conductance data for the uncoated platinum electrode was estimated from fig 7.4b at 0.16Hz (-) and is given for comparison.

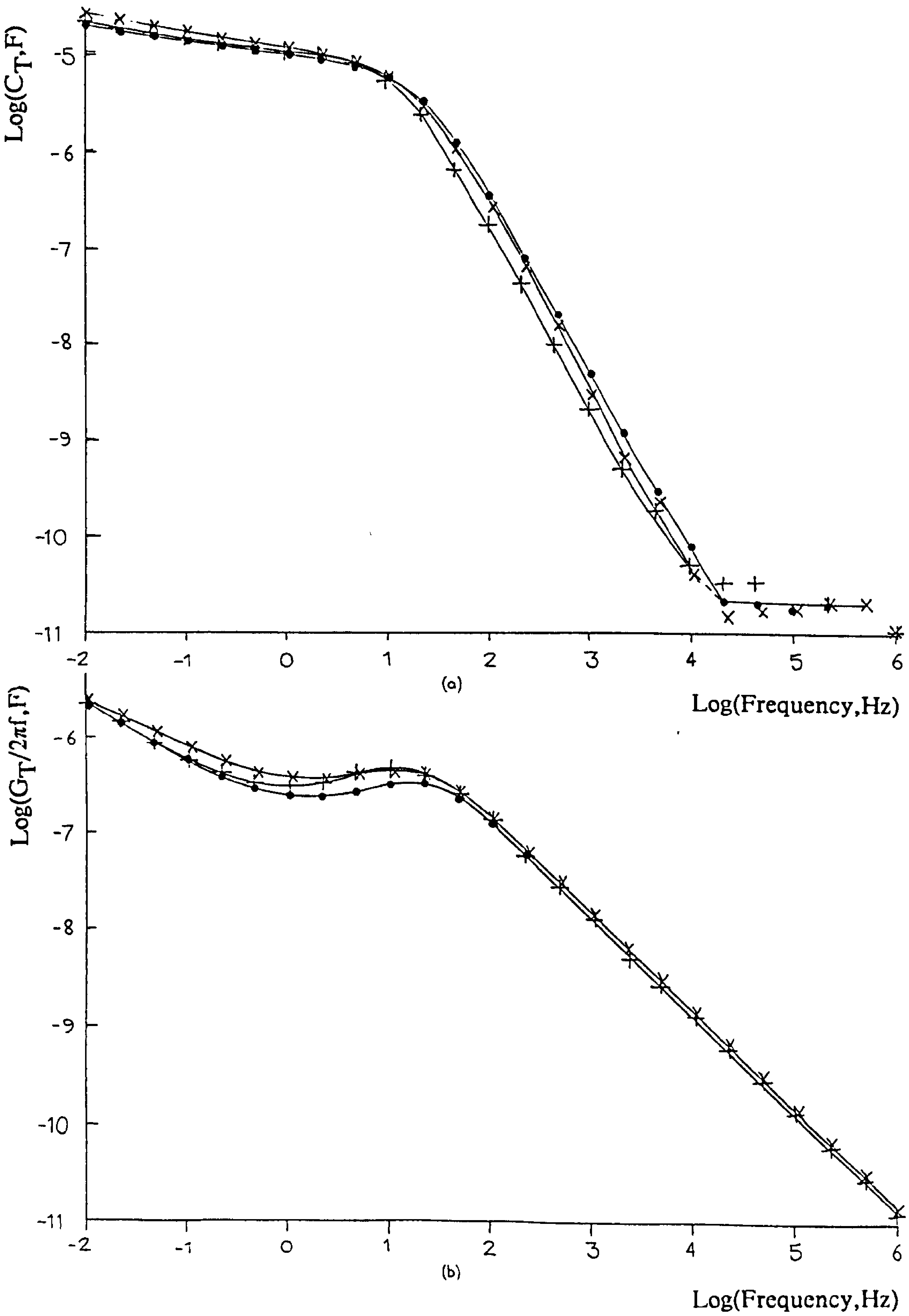

Fig 7.7 (a) Log Capacitance, C_T and (b) Loss ($G_T/2\pi f$) plotted against log frequency, F, for an uncoated platinum electrode immersed in 20mM (•)KCl, (x) KI, and (+) NaCl at 15°C.

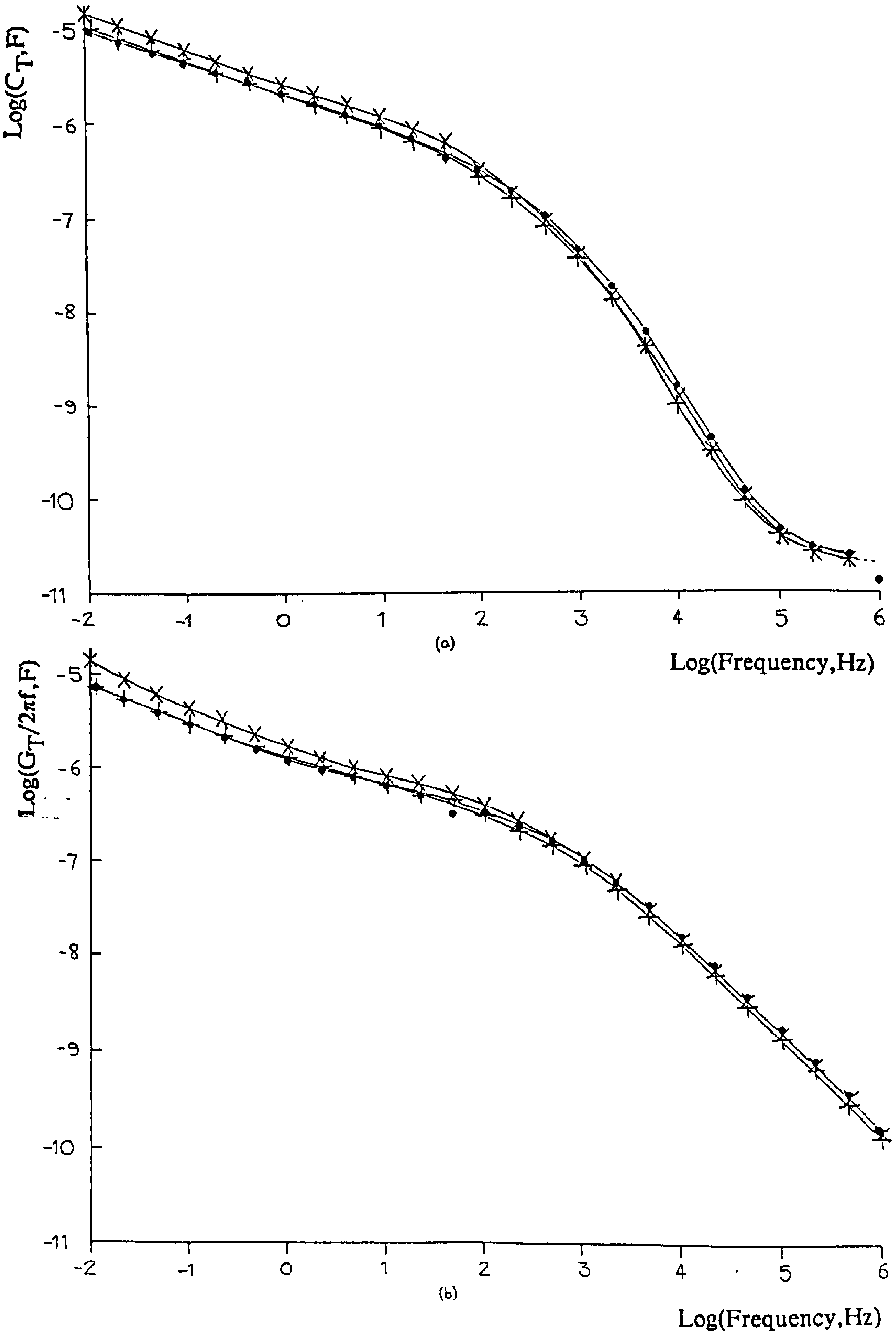

Fig 7.8 (a) Log Capacitance, C_T and (b) Loss ($G_T/2\pi f$) plotted against log frequency, F, for a platinum electrode coated in 9 monolayers of $BaSt_2$ and immersed in 20mM (•)KCl, (x) KI, and (+) NaCl at 15°C.

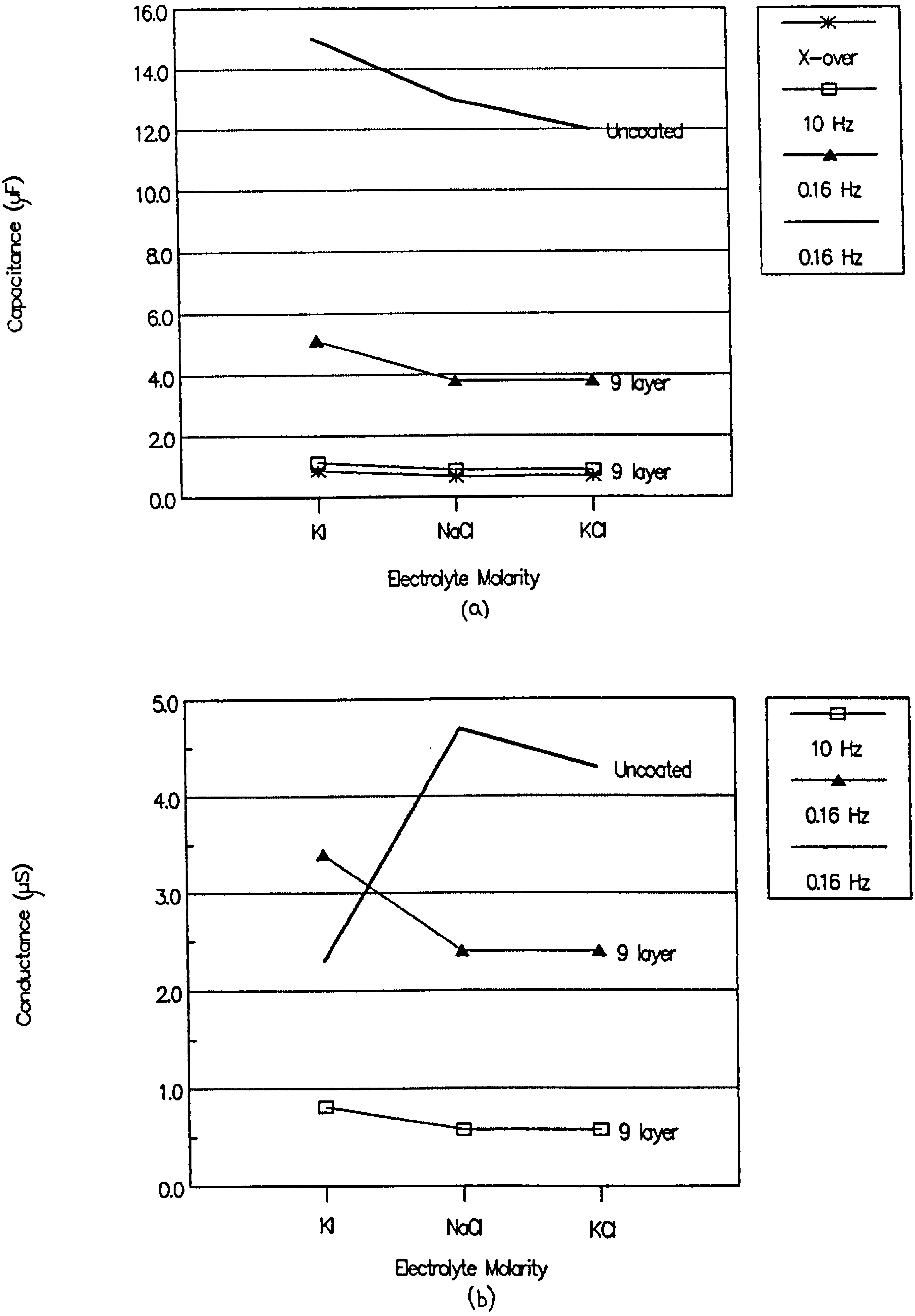

Fig 7.9 (a) Capacitance C_b, and Conductance G_b, for a platinum electrode coated with 9 monolayers of $BaSt_2$, plotted as a function of 20mM electrolyte at 15°C. Capacitance values were estimated from fig 7.8a at (▴) 0.16Hz, (□) 10Hz and (*) the capacitance/loss cross-over point. Conductance data were estimated from fig 7.8b at (▴) 0.16Hz and (□) 10Hz. Capacitance and conductance data for an uncoated platinum electrode, estimated from the curves of fig 7.7 at 0.16Hz (–) are given for comparison.

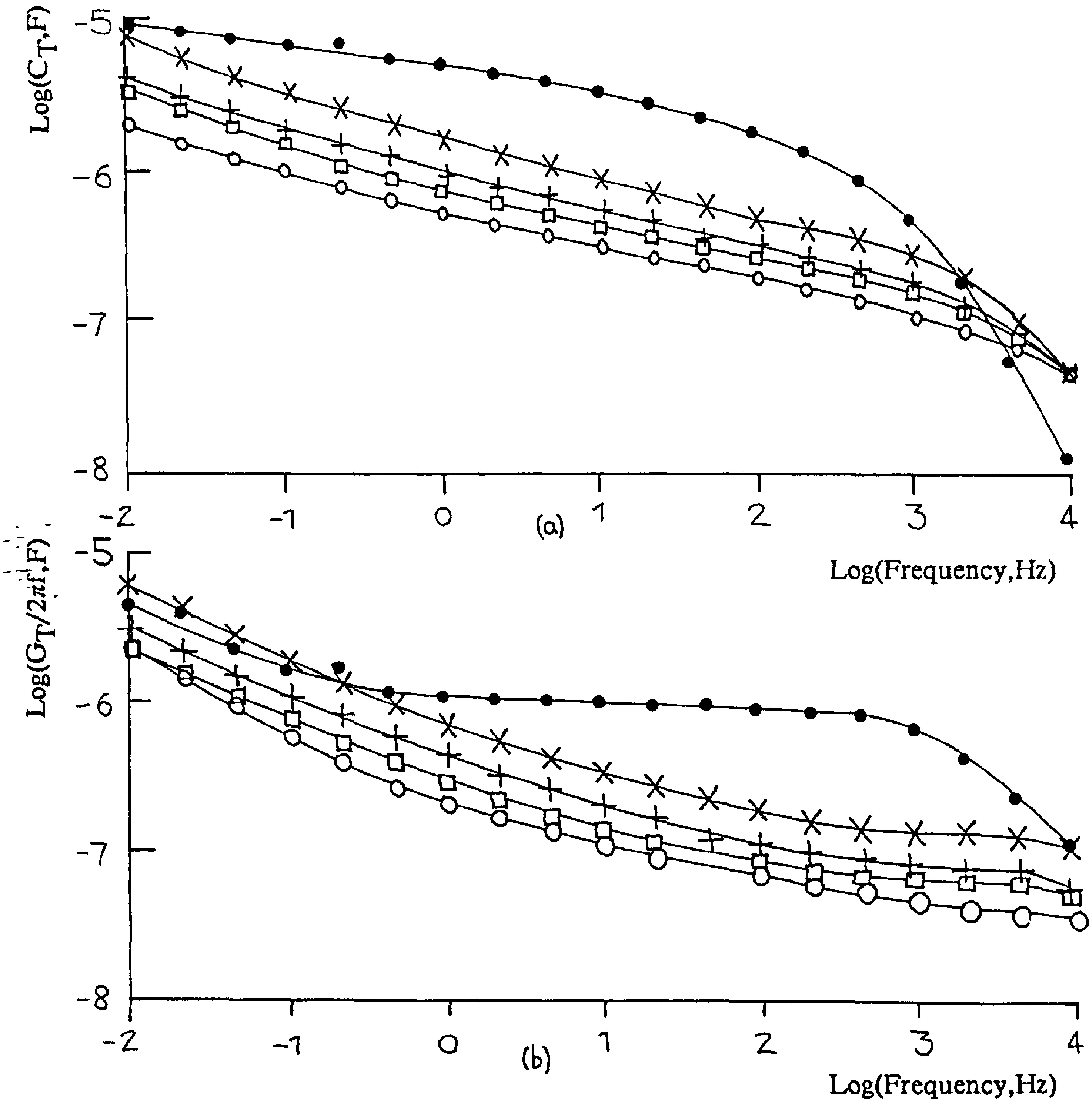

Fig 7.10 (a) Log Capacitance, C_T and (b) Loss ($G_T/2\pi f$) plotted against log frequency, F, for a platinum electrodes coated in (•) 1, (x) 3, (+) 5, (□) 7 and (o) 11 monolayers of $BaSt_2$, immersed in 20mM KCl at 15°C.

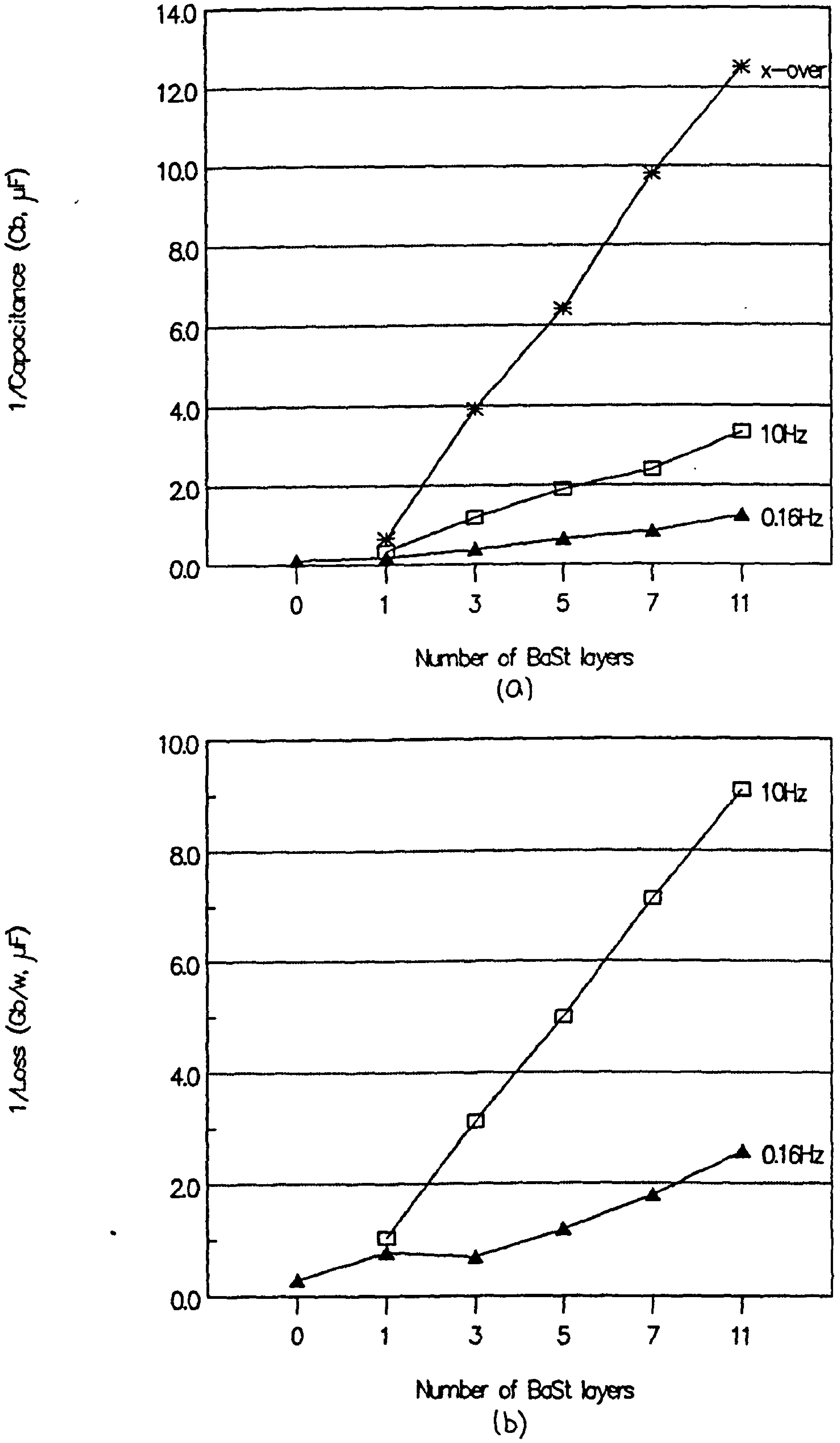

Fig 7.11 (a) Reciprocal capacitance ($1/C_b$), and (b) loss ($1/[G_b/2\pi f]$), for a platinum electrode coated with 1, 3, 5, 7 and 11 monolayers of $BaSt_2$ immersed in 20mM KCl at 15°C, plotted as a function of the number of monolayers. Reciprocal capacitance values were estimated from fig 7.10a at (▲) 0.16Hz, (□) 10Hz and (*) the capacitance/loss cross-over point. Reciprocal conductance data were estimated from fig 7.10b at (▲) 0.16Hz and (□) 10Hz.

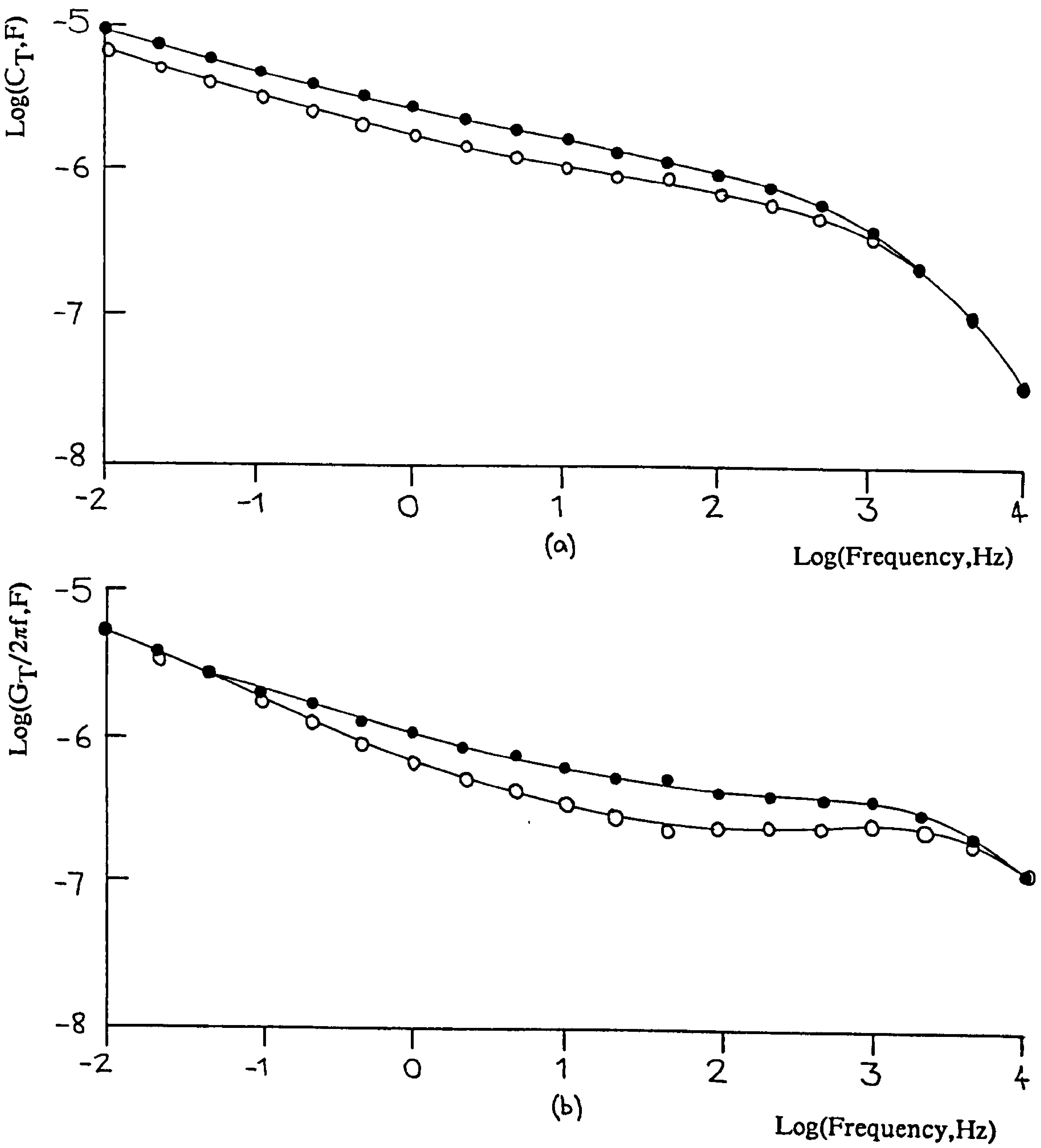

Fig 7.12 (a) Log Capacitance, C_T and (b) Loss ($G_T/2\pi f$) plotted against log frequency, F, for a platinum electrode coated in 3 monolayers of $BaSt_2$ on (o) initial immersion and (•)after 20 minutes exposure to 20mM KCl at 15°C.

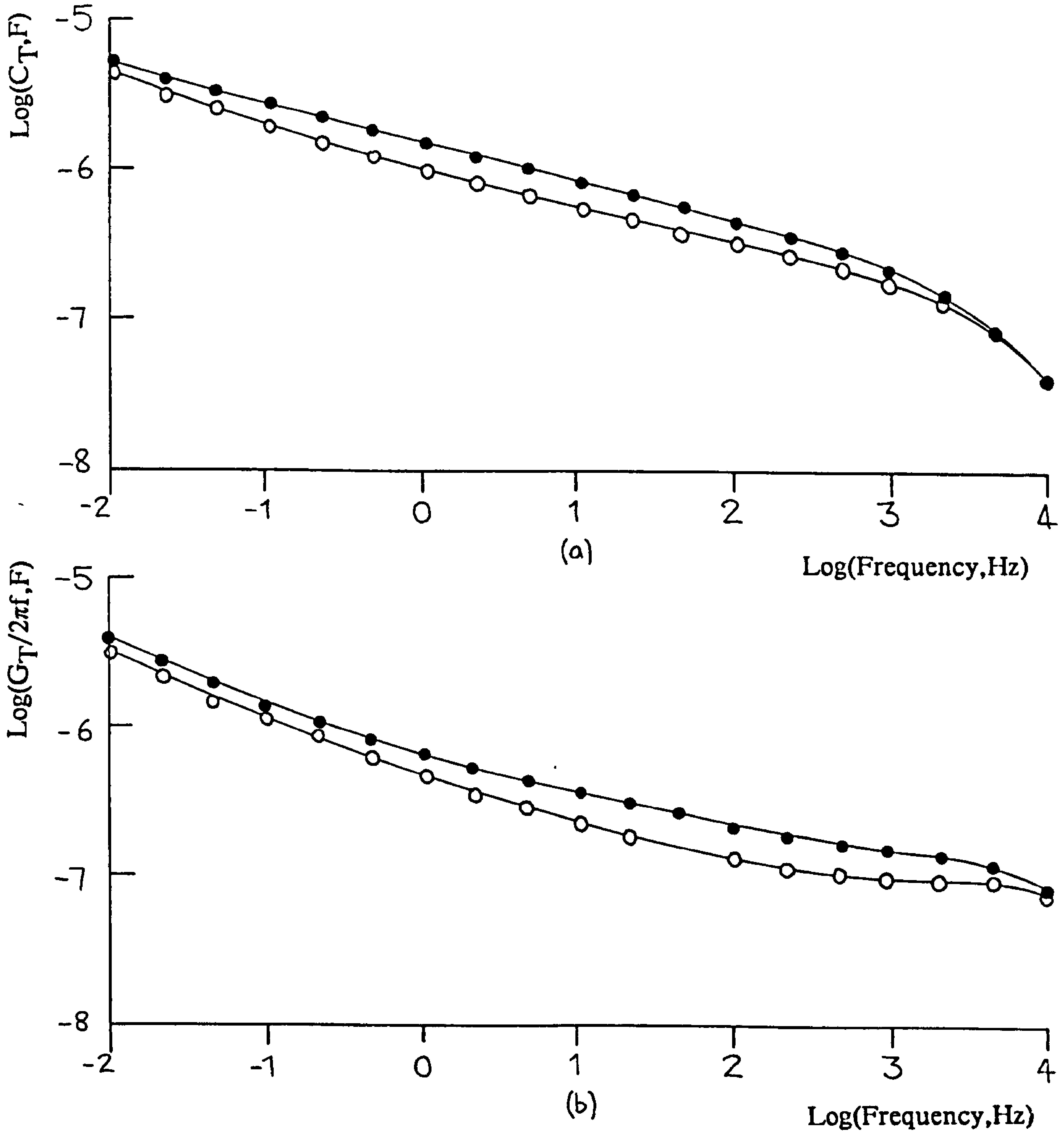

Fig 7.13 (a) Log Capacitance, C_T and (b) Loss ($G_T/2\pi f$) plotted against log frequency, F, for a platinum electrode coated in 5 monolayers of $BaSt_2$ on (o) initial immersion and (•)after 20 minutes exposure to 20mM KCl at 15°C.

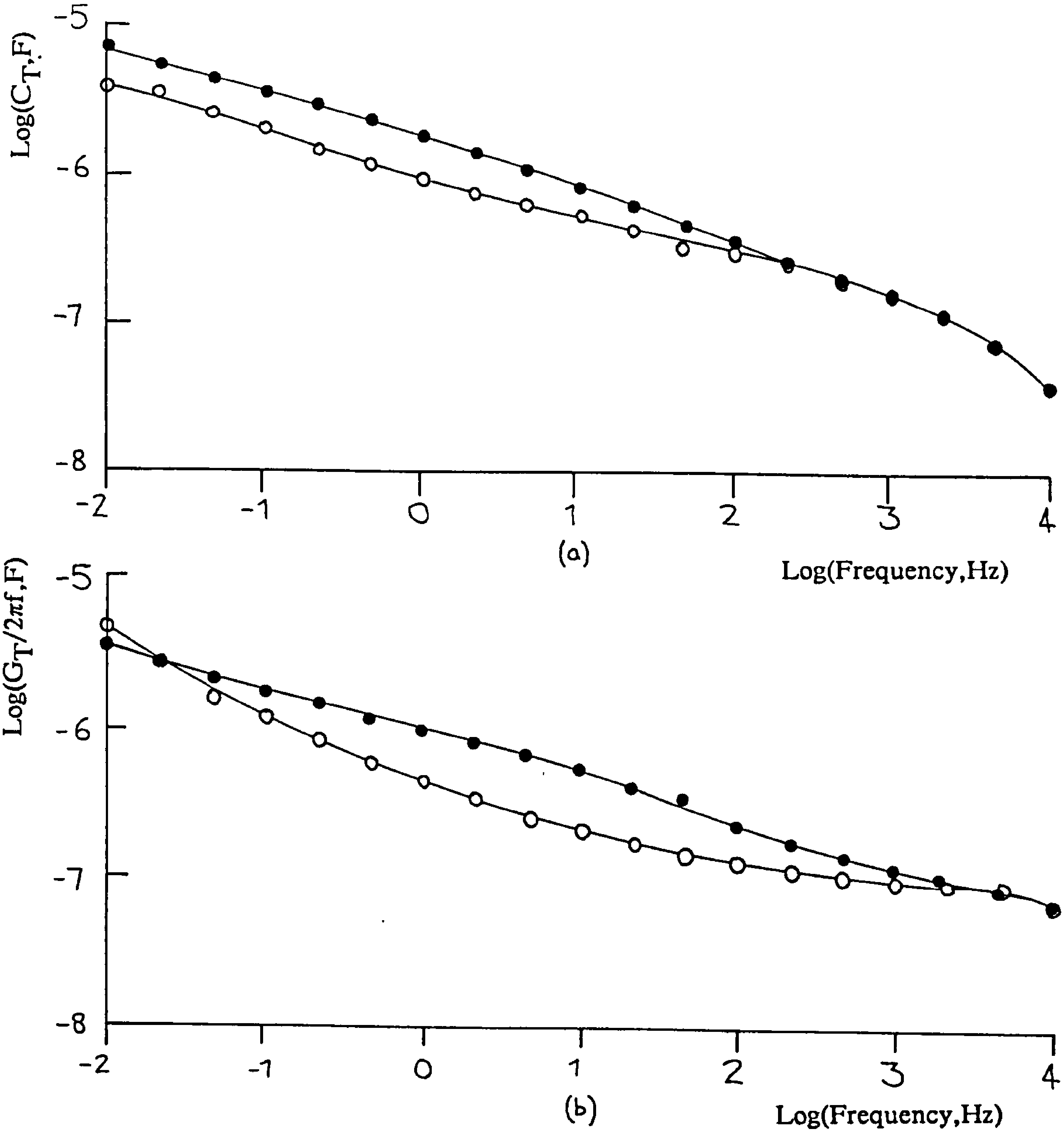

Fig 7.14 (a) Log Capacitance, C_T and (b) Loss ($G_T/2\pi f$) plotted against log frequency, F, for a platinum electrode coated in 7 monolayers of BaSt$_2$ on (o) initial immersion and (•)after 20 minutes exposure to 20mM KCl at 15°C.

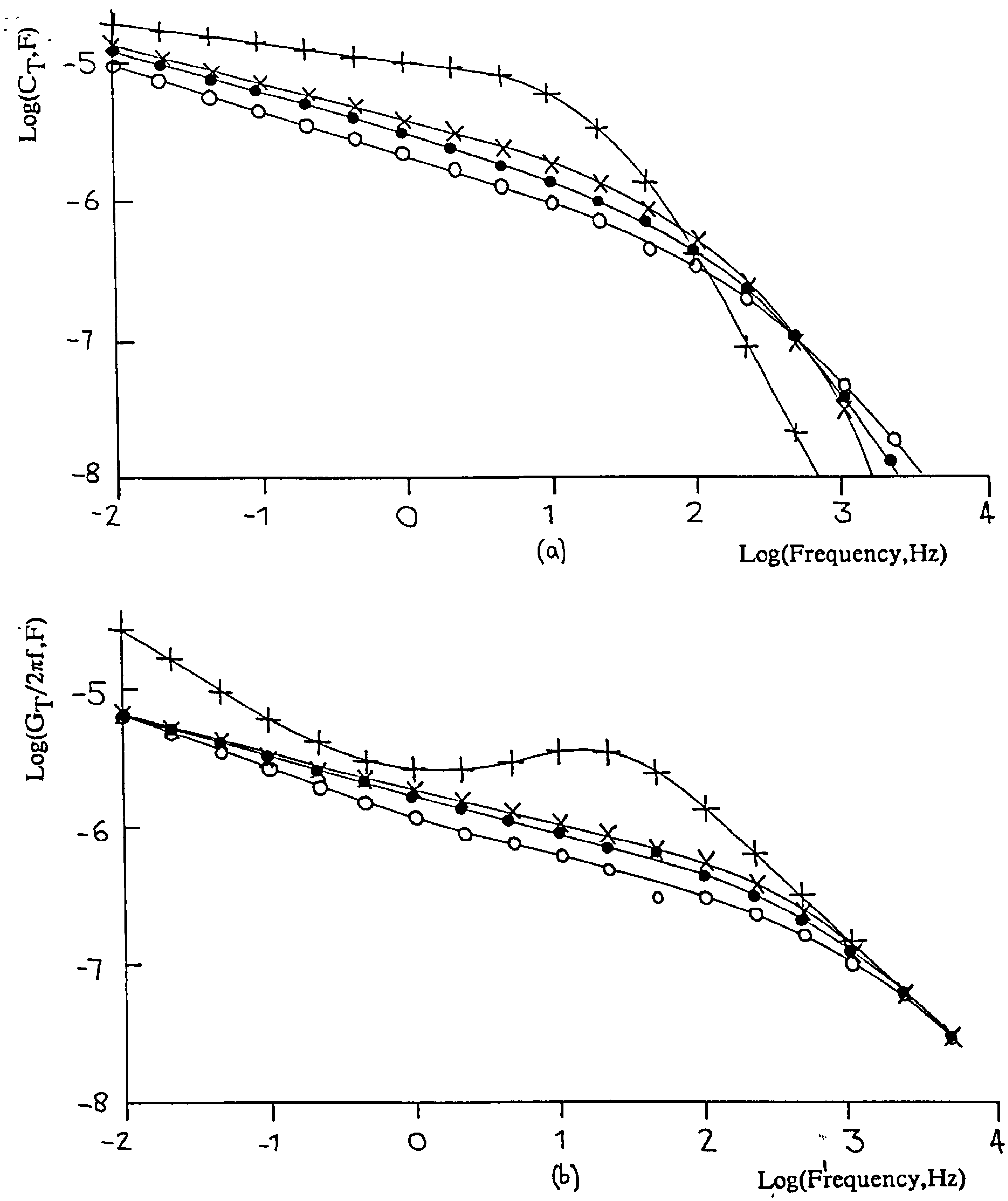

Fig 7.15 (a) Log Capacitance, C_T and (b) Loss ($G_T/2\pi f$) plotted against log frequency, F, for a platinum electrode coated in 9 monolayers of $BaSt_2$ on (o) initial immersion and after (•)32 and (x) 240 minutes in 20mM KCl at 15°C. For comparison, similar curves are shown for an uncoated platinum electrode (+).

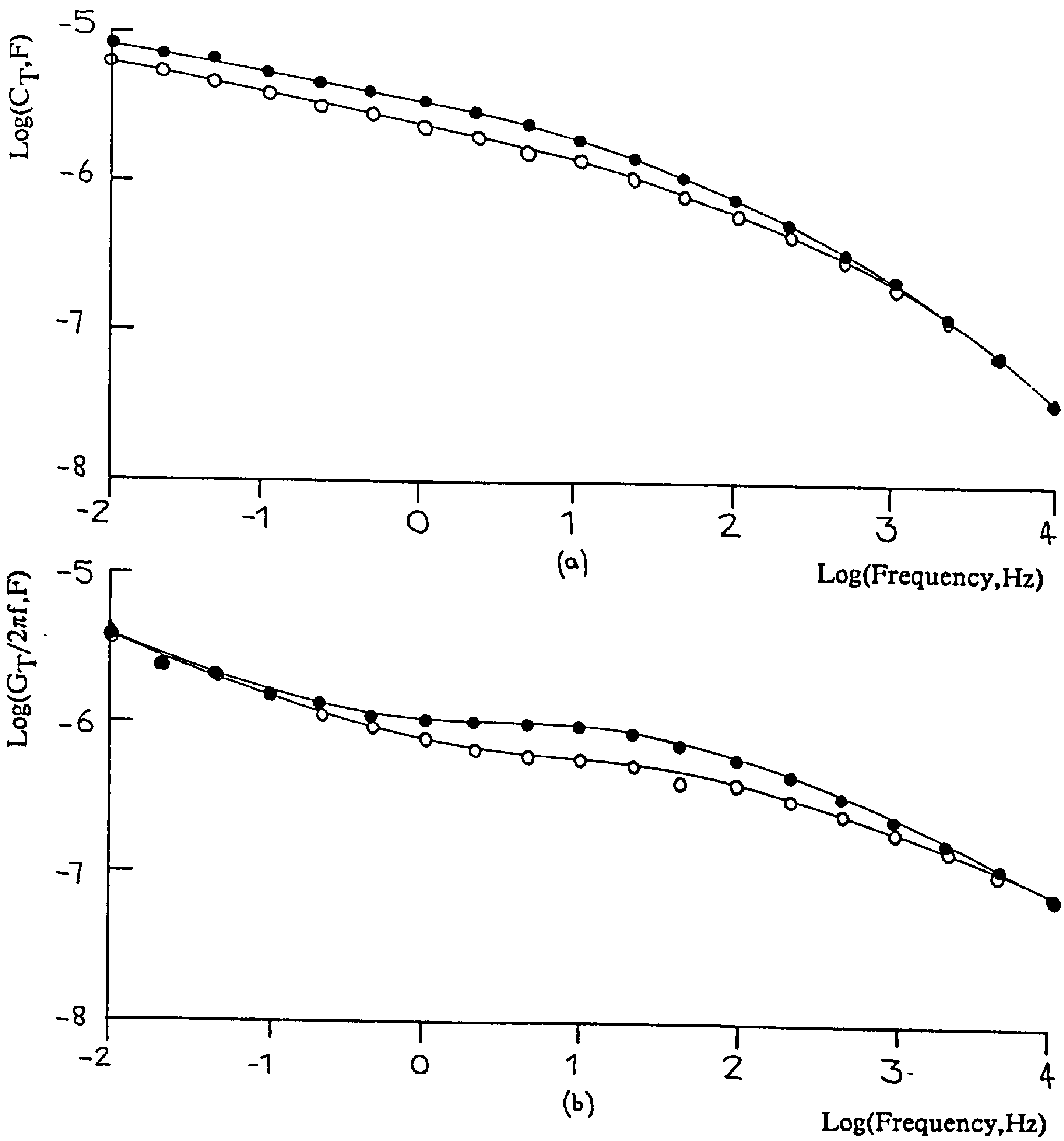

Fig 7.16 (a) Log Capacitance, C_T and (b) Loss ($G_T/2\pi f$) plotted against log frequency, F, for a platinum electrode coated in 11 monolayers of $BaSt_2$ on (o) initial immersion and (•)after 20 minutes exposure to 20mM KCl at 15°C.

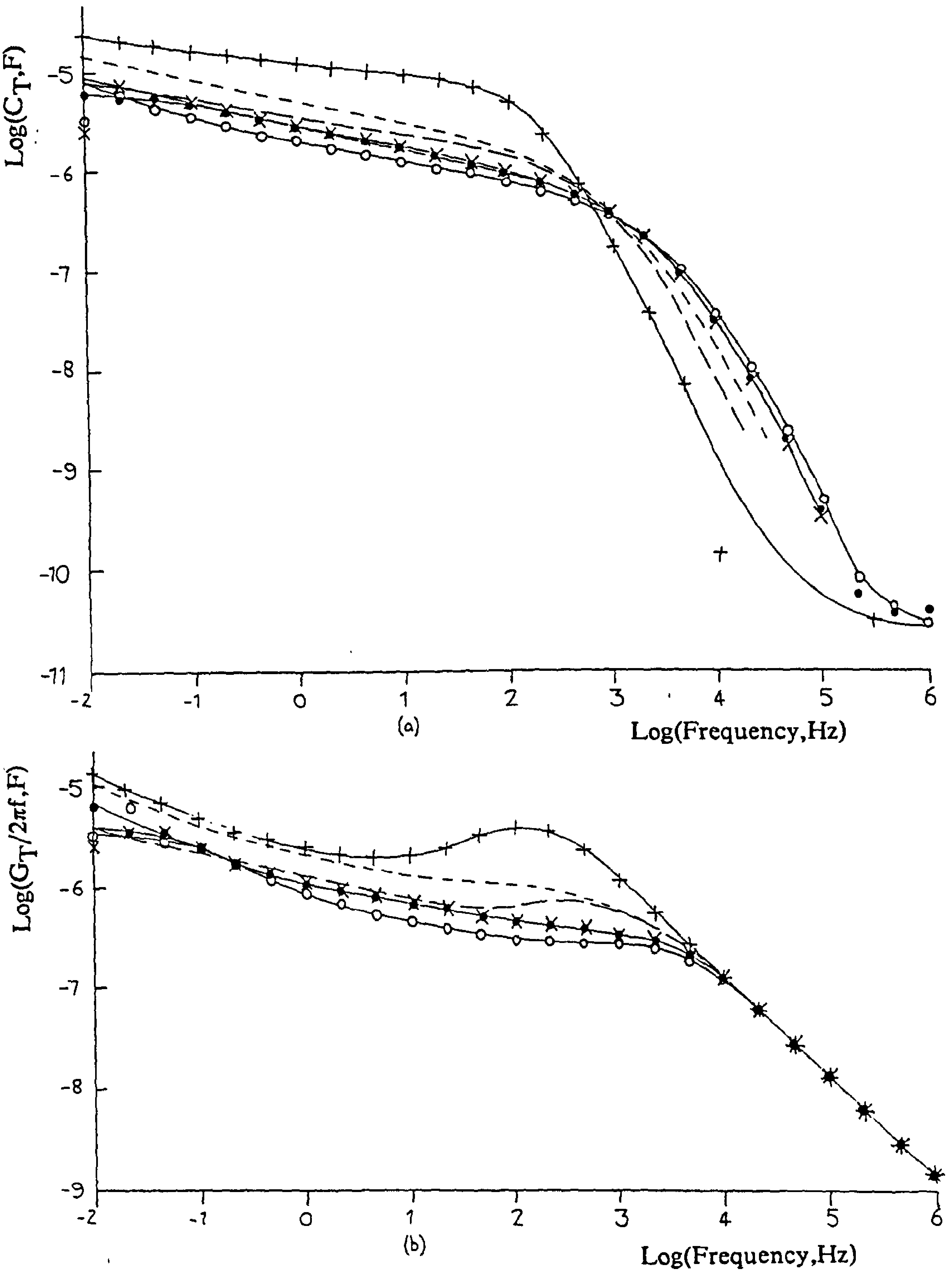

Fig 7.17 (a) Log Capacitance, C_T and (b) Loss ($G_T/2\pi f$) plotted against log frequency, F, for i) a platinum electrode E_C, coated in 5 monolayers of barium stearate after (o) 0, (•) 20, (x) 50 and (- - -) 1140 minutes, ii) (-+-) a freshly polished platinum electrode E_P and iii) (———) platinum electrode which was dipped but with no monolayer on the trough, E_D, immersed in 20mM KCl at 15°C.

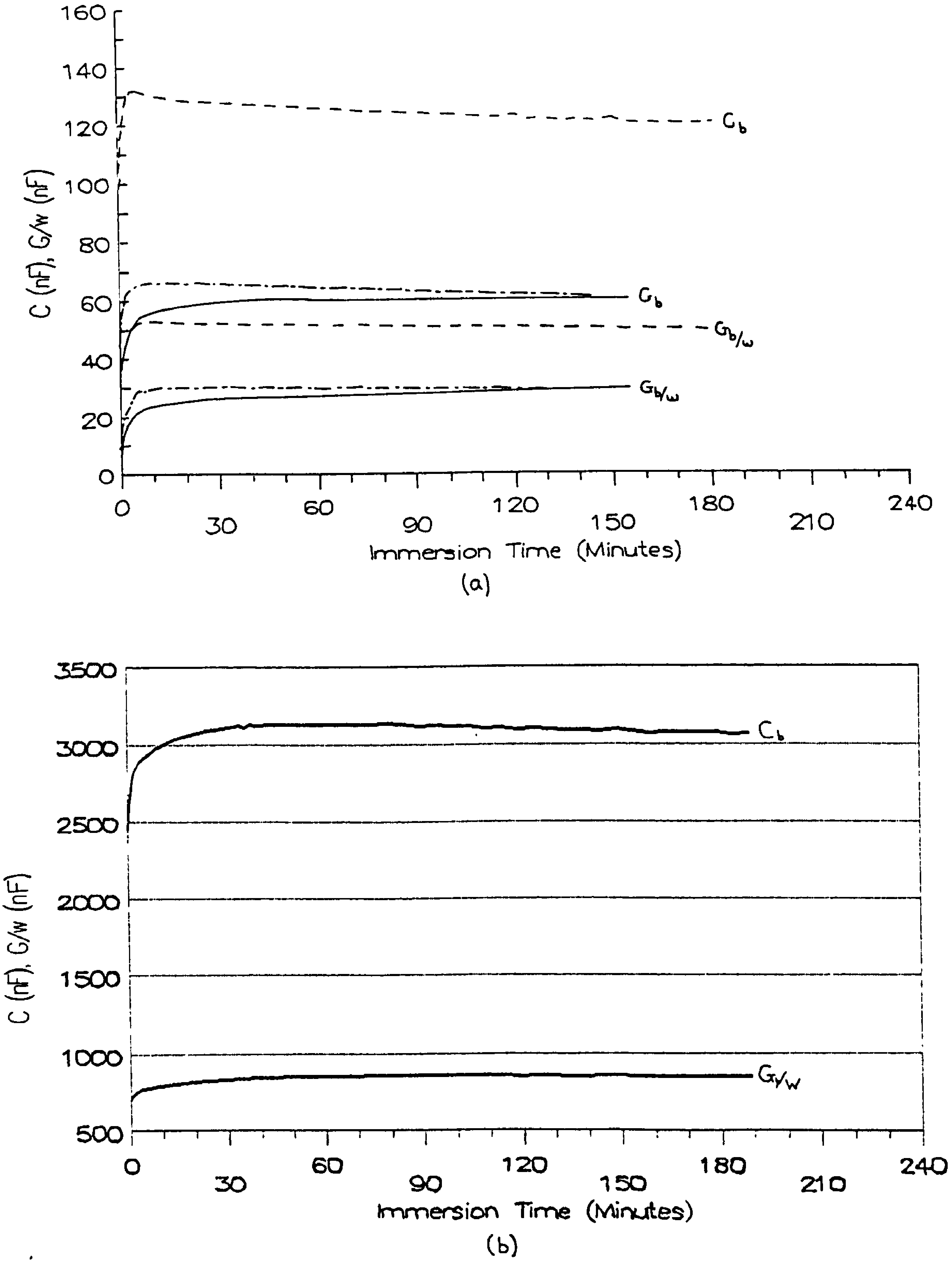

Fig 7.18 (a) Capacitance, C_T and Loss ($G_T/2\pi f$) plotted against immersion time in 20mM KCl at 15°C, measured at 10Hz for (– – –)3, (– · – · –)7 and (——)11 layer Barium Stearate films on platinum (fig 7.18a). (b) Equivalent data for a freshly polished, uncoated platinum electrode.

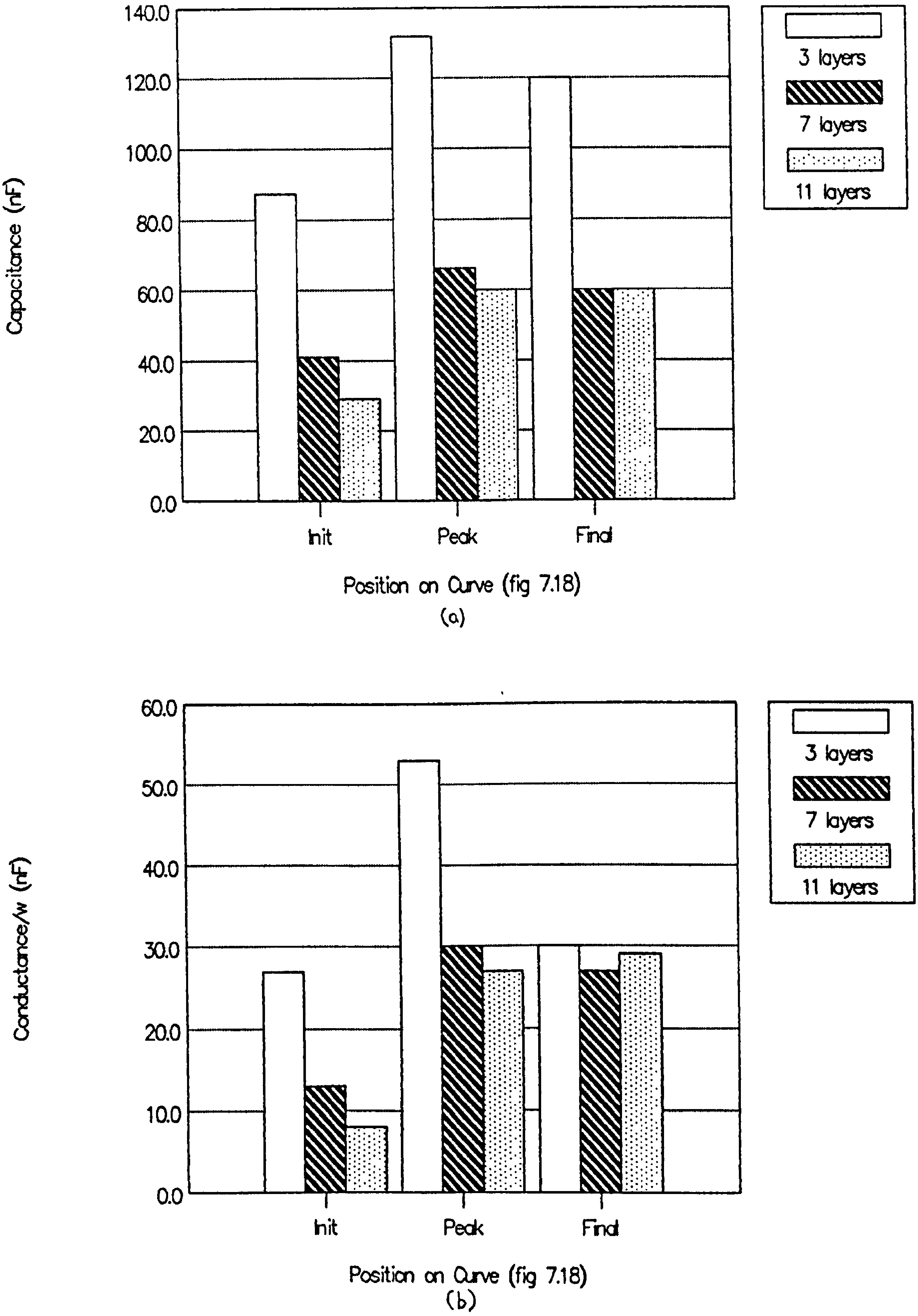

Fig 7.19 (a) Capacitance (C_T) and (b) Loss ($G_T/2\pi f$), plotted as a function of immersion time, for a platinum electrode coated with □ 3, ▨ 7 and ░ 11 monolayers of $BaSt_2$, measured at 10Hz in 20mM KCl at 15°C.

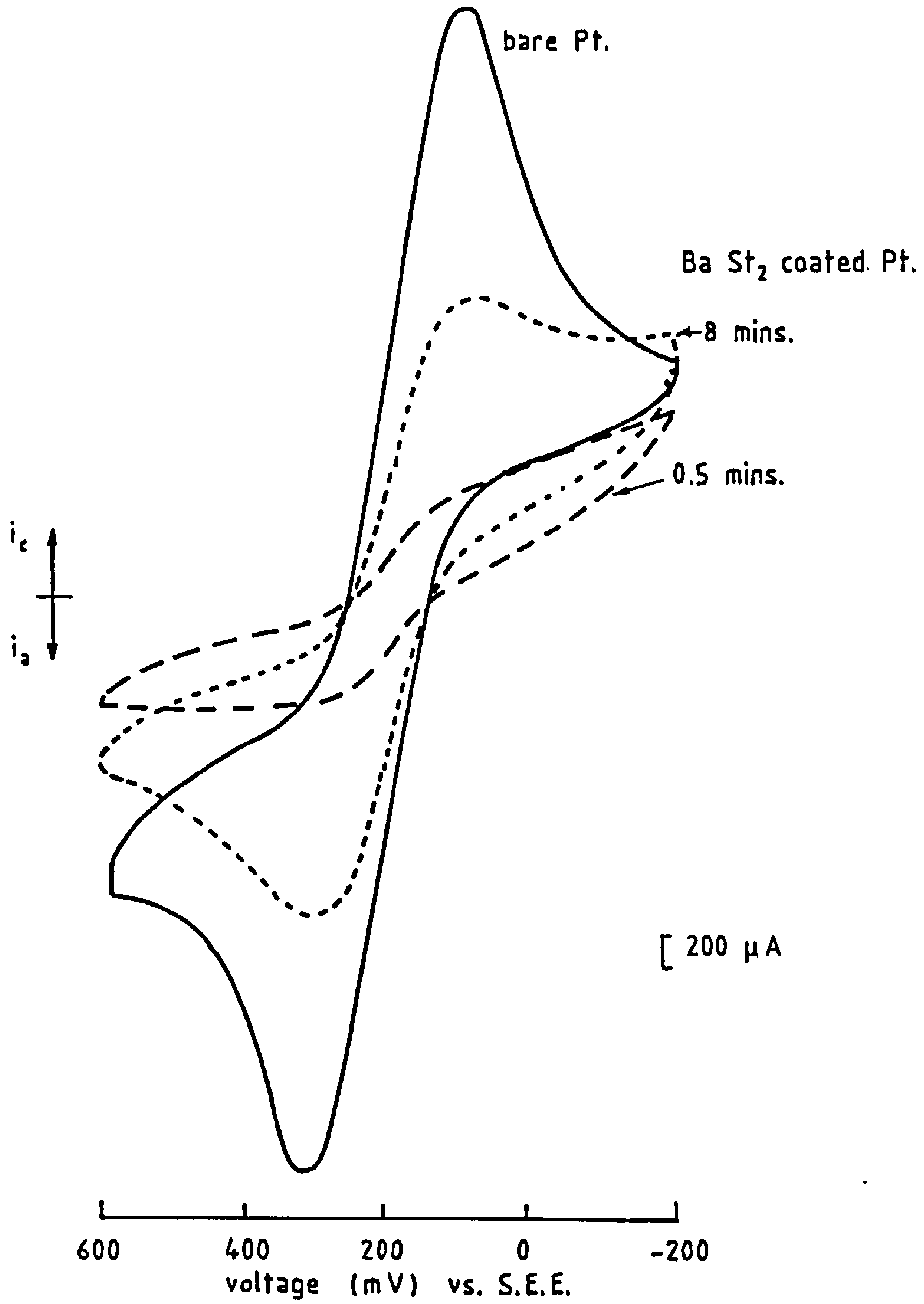

Fig 7.20 Cyclic voltammograms for i) an uncoated platinum foil electrode (——) and ii) the same electrode coated in 7 monolayers of $BaSt_2$ in 0.1M KCl and 5mM $K_3Fe(CN)_6$ with a sweep rate of 0.1V/sec. Curves for the coated electrode are shown after (———)0.5 and (– – –)8 minutes immersion.

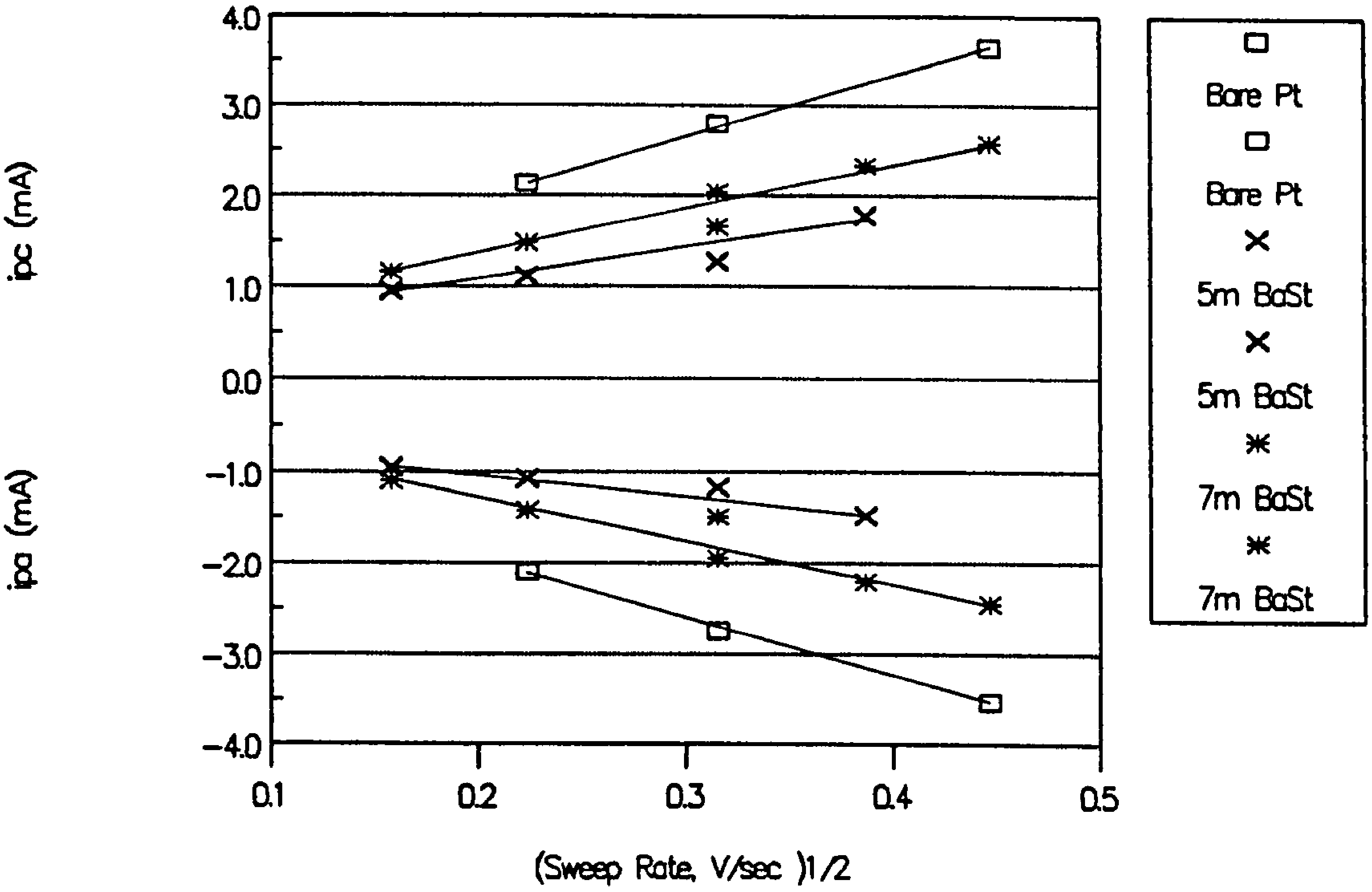

Fig 7.21 Peak anodic and cathodic currents, i_{pa} and i_{pc}, for (□) an uncoated platinum foil electrode and the same electrode coated with (x) 5 and (*) 7 monolayers of $BaSt_2$ plotted as a function of (sweep rate)$^{1/2}$. The peak currents were estimated from cyclic voltammograms measured during immersion of the electrodes in 0.1M KCl and 5mM $K_3Fe(CN)_6$ (eg fig 7.20).

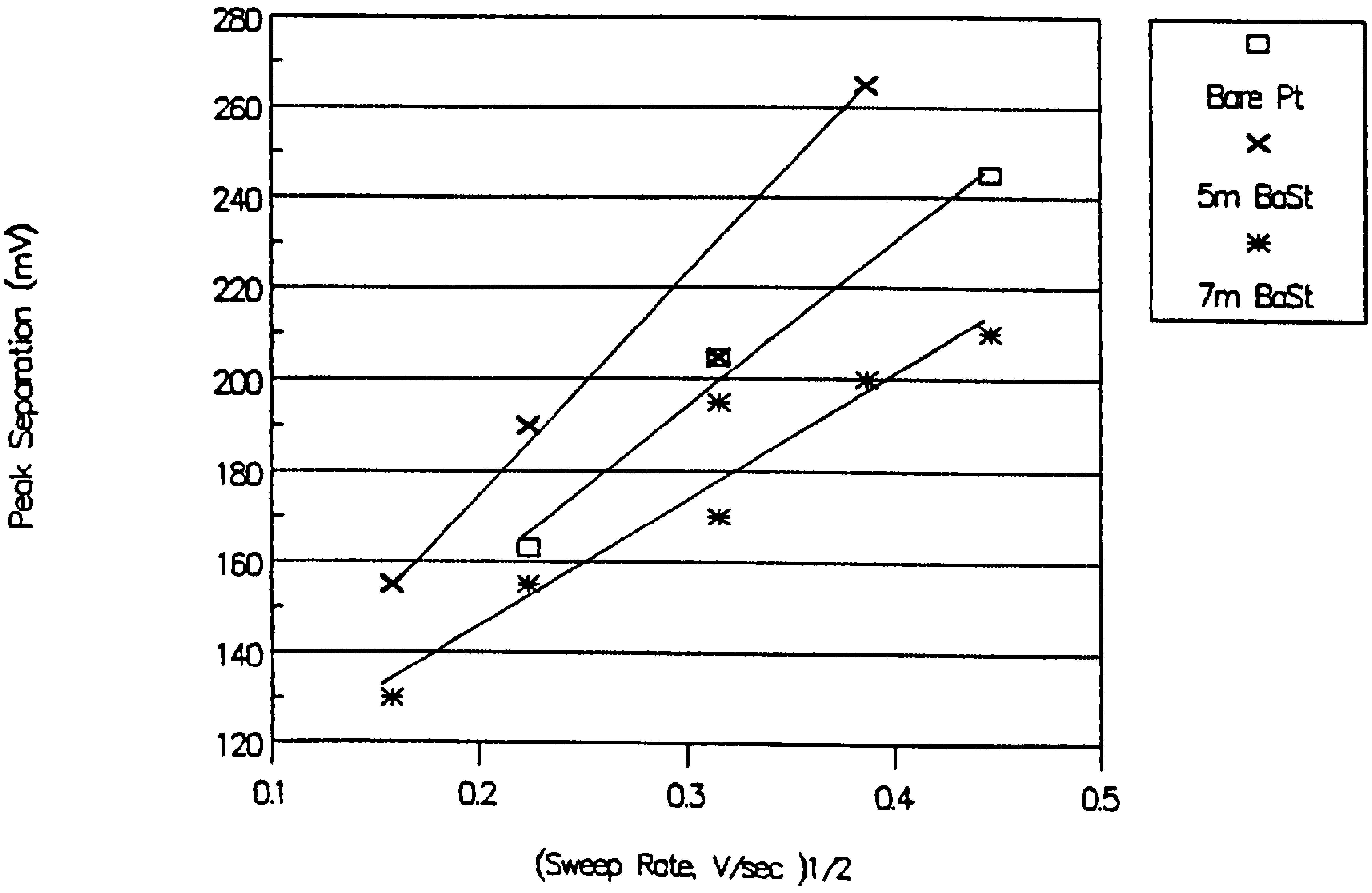

Fig 7.22 Peak separation for (□) an uncoated platinum foil electrode and the same electrode coated with (x) 5 and (*) 7 monolayers of $BaSt_2$ plotted as a function of (sweep rate)$^{1/2}$. The peak separations were estimated from cyclic voltammograms measured during immersion of the electrodes in 0.1M KCl and 5mM $K_3Fe(CN)_6$ (eg fig 7.20).

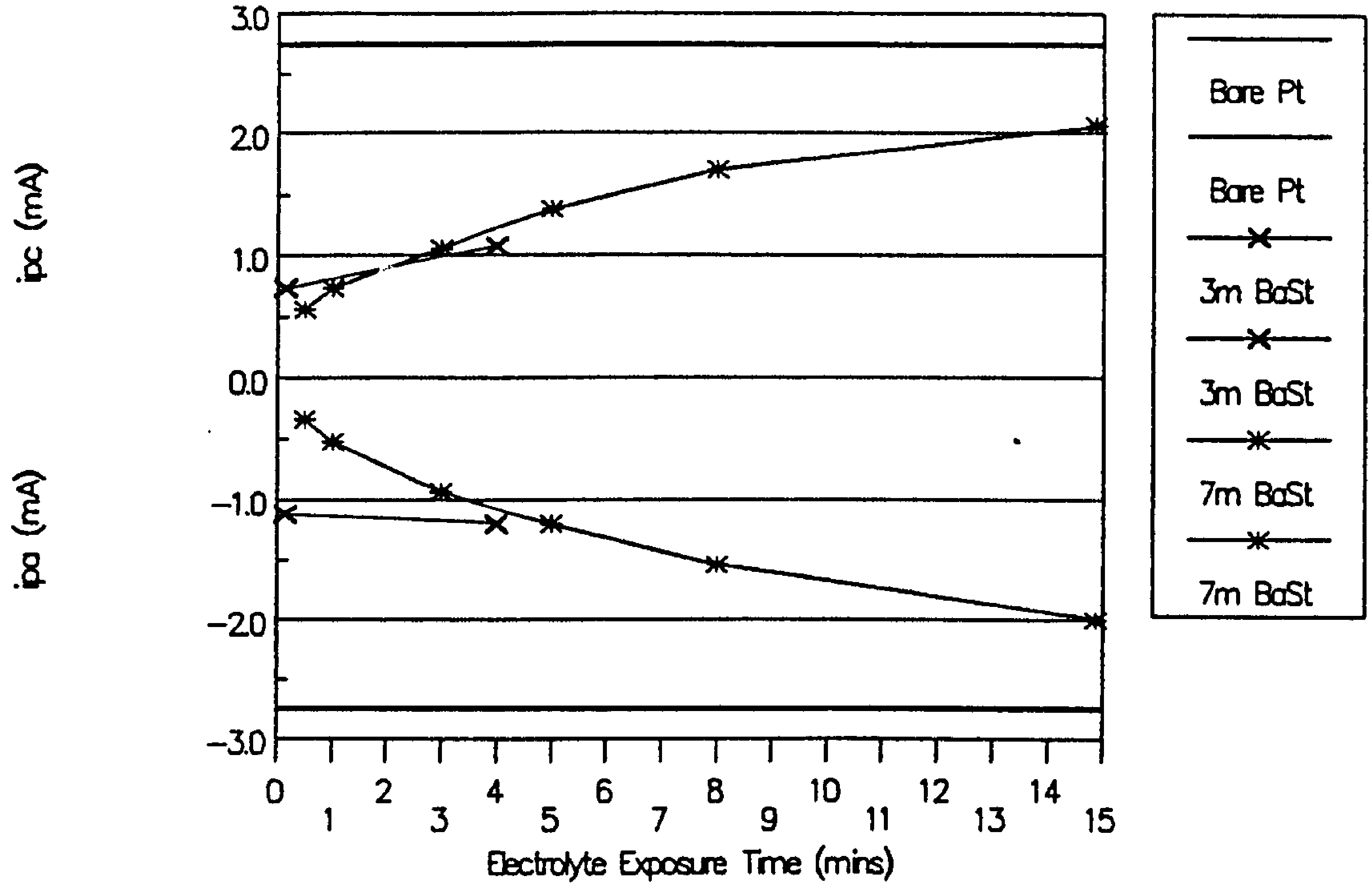

Fig 7.23 Peak anodic and cathodic currents, i_{pa} and i_{pc}, for (——)an uncoated platinum foil electrode and the same electrode coated with (x) 3 and (*) 7 monolayers of $BaSt_2$ plotted as a function of electrolyte immersion time. The peak currents were estimated from cyclic voltammograms measured during immersion of the electrodes in 0.1M KCl and 5mM $K_3Fe(CN)_6$ (eg fig 7.20).

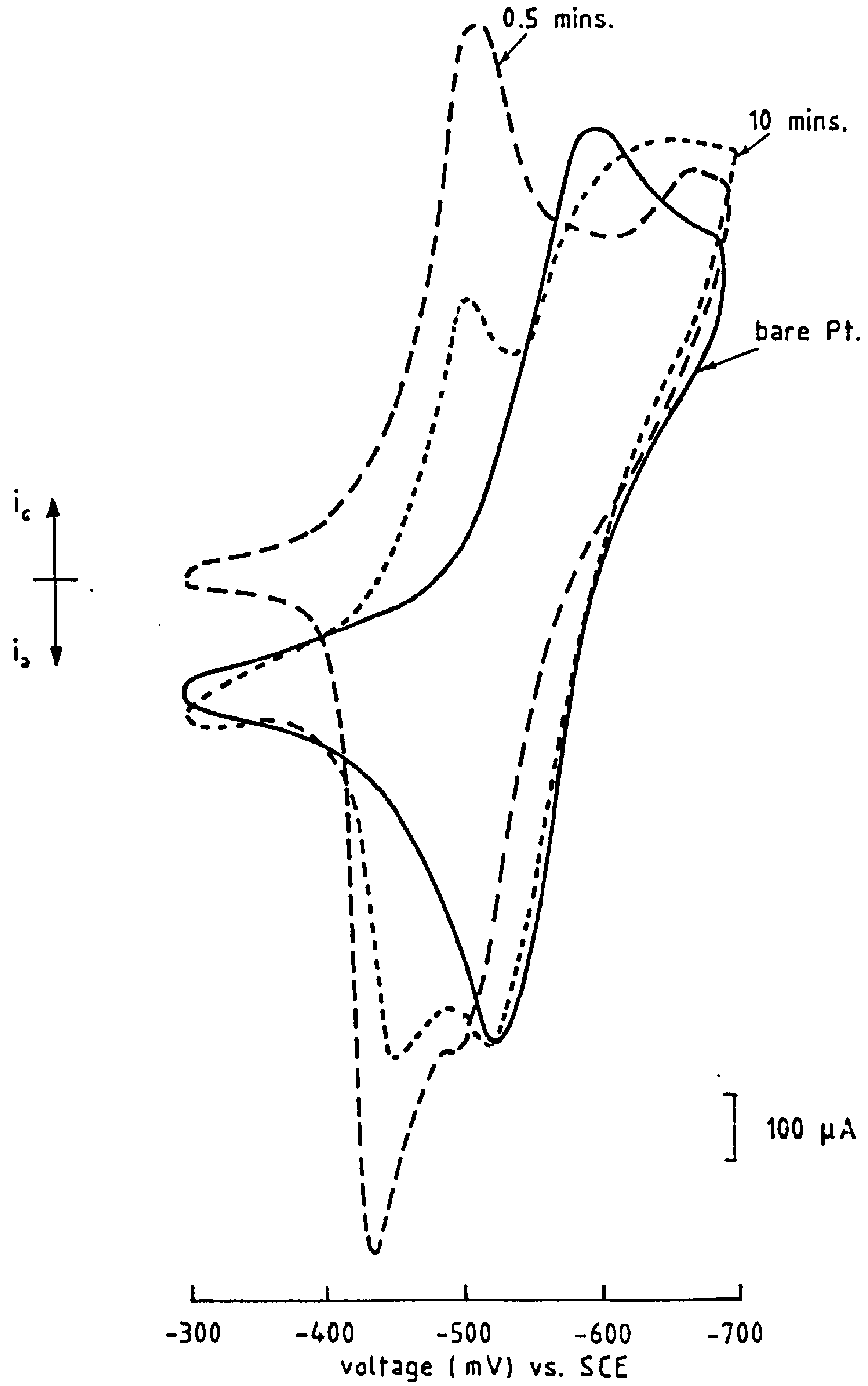

Fig 7.24 Cyclic voltammograms for i) an uncoated platinum foil electrode (——) and ii) the same electrode coated in 5 monolayers of $BaSt_2$ in 0.1M KCl and 1mM Benzyl Viologen with a sweep rate of 0.1V/sec. Curves for the coated electrode are shown after (———)0.5 and (---)10 minutes immersion.

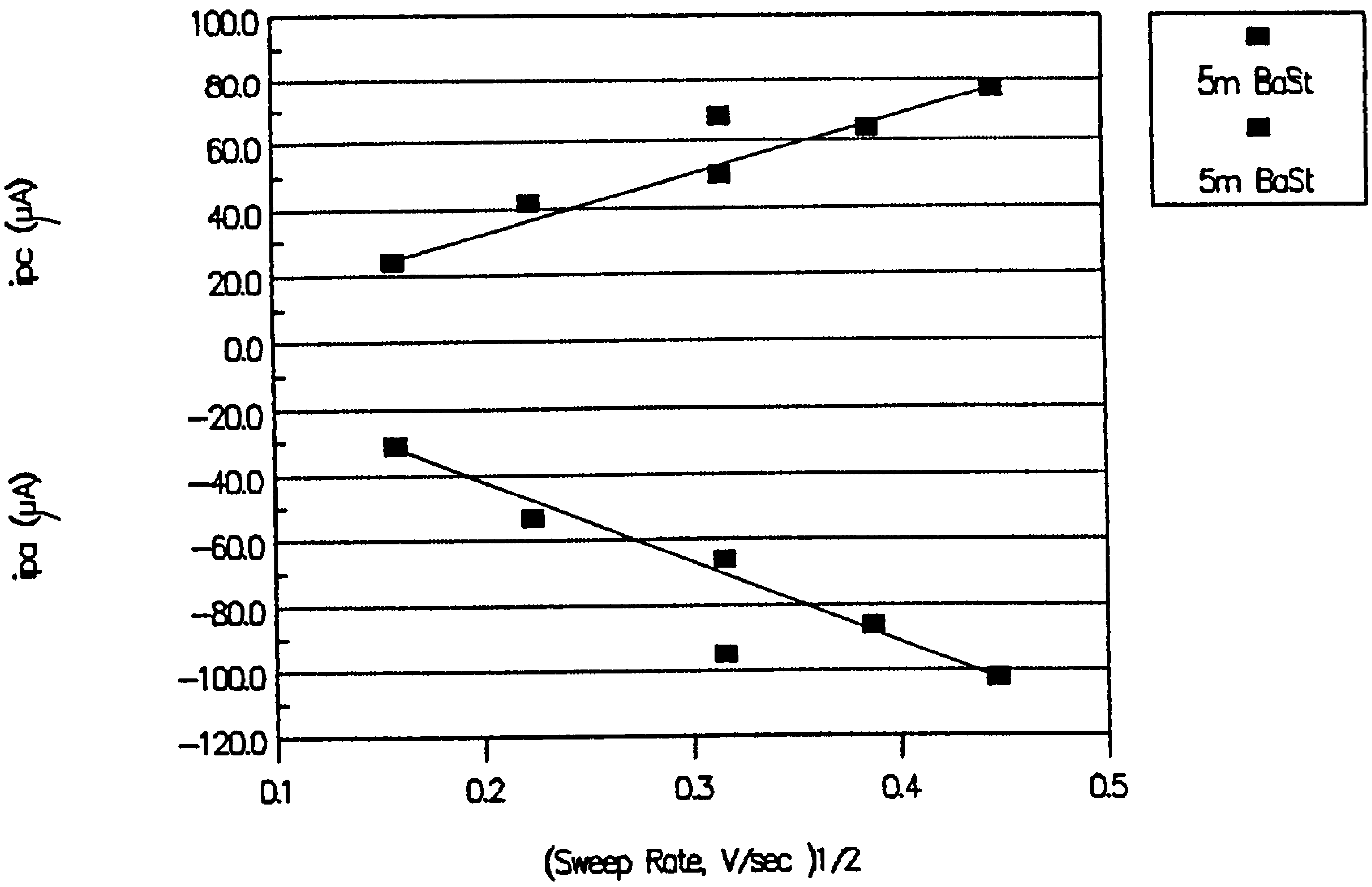

7.25 Peak anodic and cathodic currents, i_{pa} and i_{pc}, for a platinum foil electrode coated with (■) 5 monolayers of $BaSt_2$ plotted as a function of (sweep rate)$^{1/2}$. The peak currents were estimated from cyclic voltammograms measured during immersion of the electrodes in 0.1M KCl and 1mM Benzyl Viologen (eg fig 7.24).

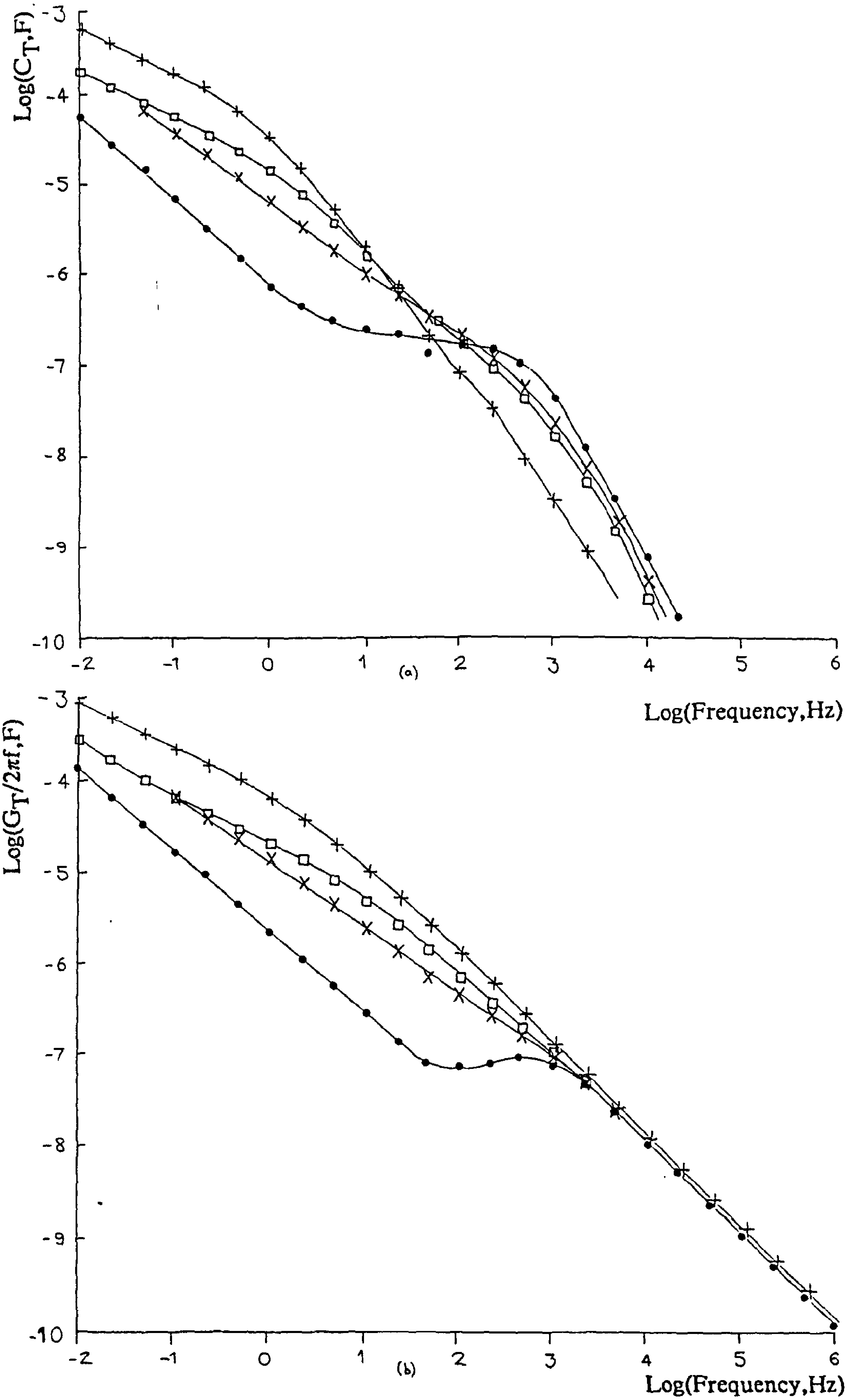

Fig 7.26 (a) Log Capacitance (C_T) and Loss ($G_T/2\pi f$) of a sputtered copper electrode coated with 3 monolayers of $BaSt_2$ plotted as a function of log frequency. Curves are shown i) (•)immediately after immersion ii) (x) after 19 mins and iii) (□) after 49 minutes in 2mM KCl at 19±2°C. For comparison, the corresponding curves for an uncoated sputtered copper electrode are also shown (+). The solid line, through the data points (•) measured immediately after immersion shows a theoretical fit where $C_d=10^{-4}w^{0.9}F$; $C_b=1.8x10^{-7}F$; $C_g=1.6x10^{-11}F$; $G_d=7.5x10^{-4}S$; $G_b=1.25x10^{-5}S$; $G_t=10^{-5}w^{0.7}S$.

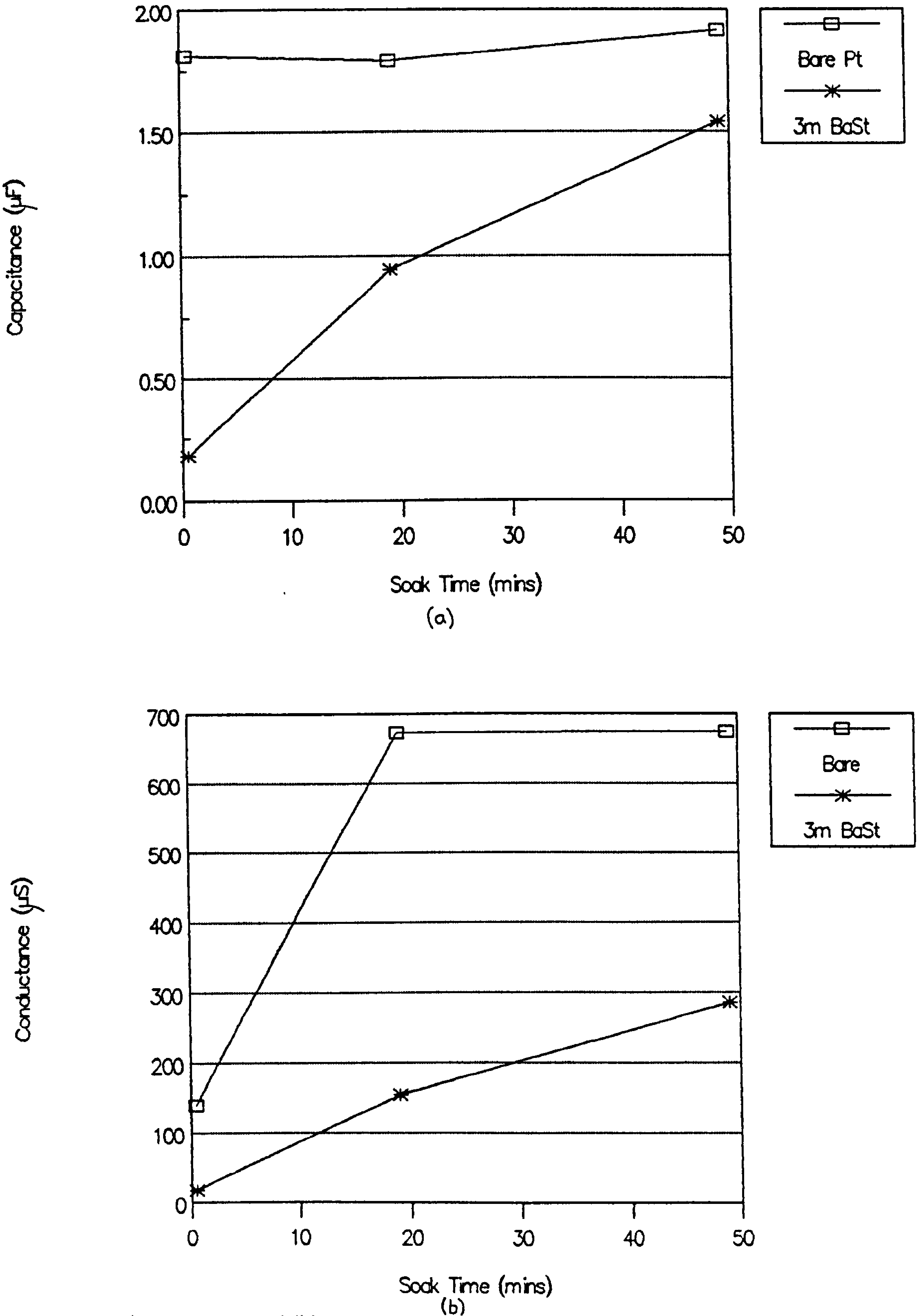

Fig 7.27 (a) Capacitance and (b) conductance for (*) an uncoated sputtered copper electrode and (□) a similar electrode coated in 3 monolayers of $BaSt_2$ and immersed in 2mM KCl at 19±2°C, estimated from the curves in fig 7.26 and plotted as a function of immersion time.

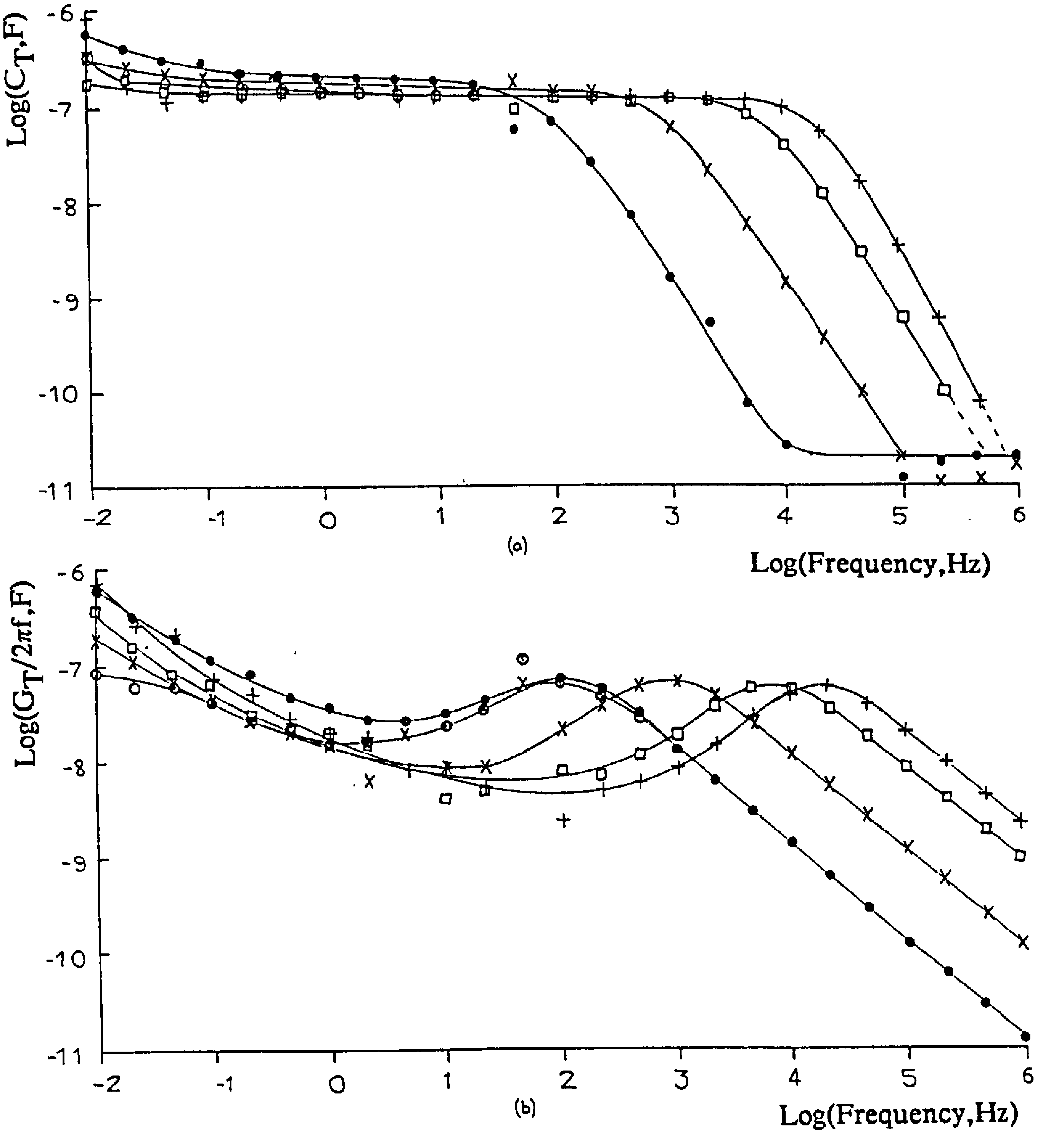

Fig 7.28 (a) Log Capacitance, C_T and (b) Loss ($G_T/2\pi f$) plotted against log frequency, F, for an evaporated aluminium electrode coated with 3 monolayers of $BaSt_2$ and immersed in (•)0.2mM, (x) 2.0mM, (□) 20mM and (+) 200mM KCl at 21±1°C.

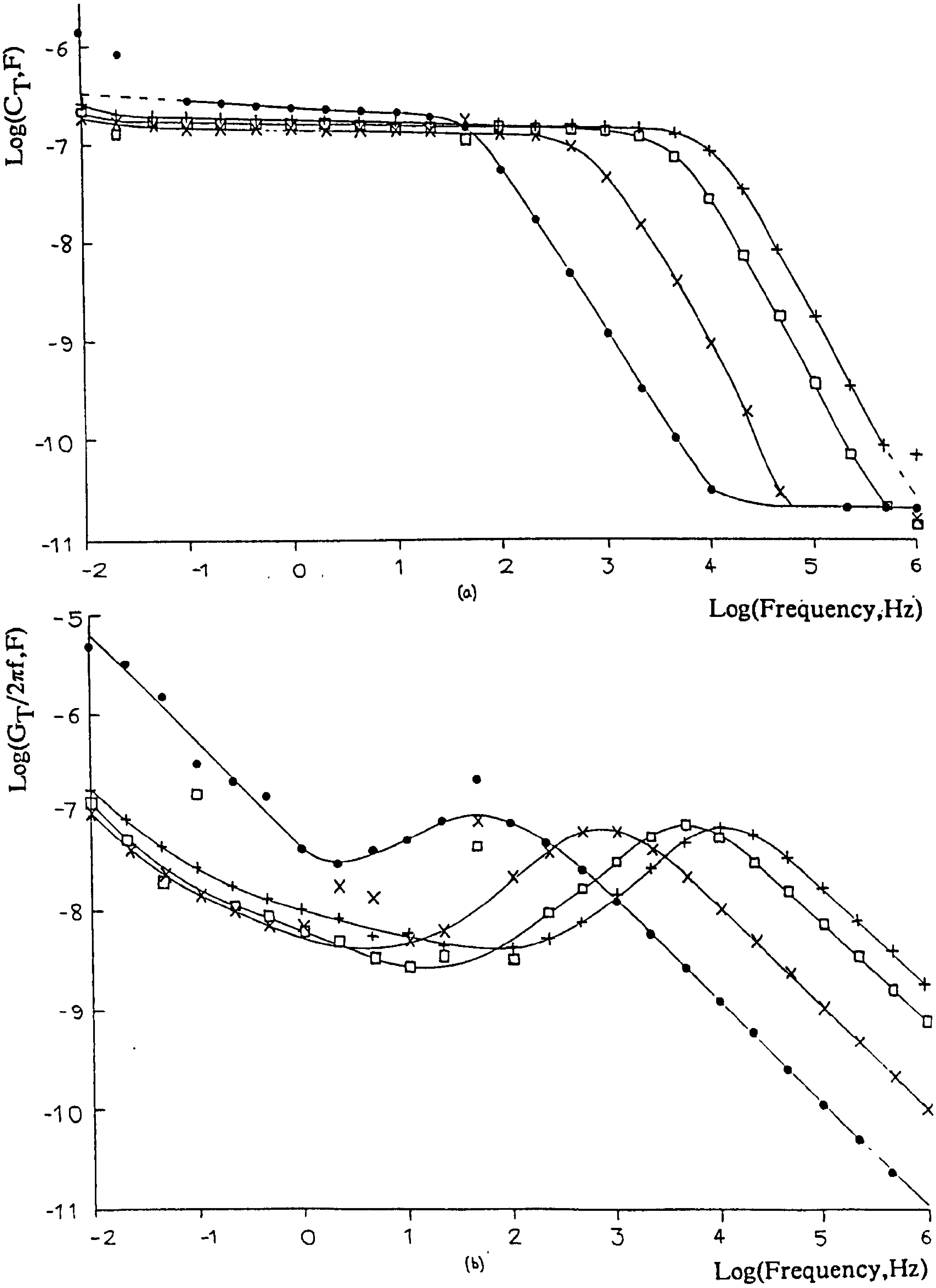

Fig 7.29 (a) Log Capacitance, C_T and (b) Loss ($G_T/2\pi f$) plotted against log frequency, F, for an evaporated aluminium electrode coated with 9 monolayers of $BaSt_2$ and immersed in (•)0.2mM, (x) 2.0mM, (☐) 20mM and (+) 200mM KCl at 21±1°C.

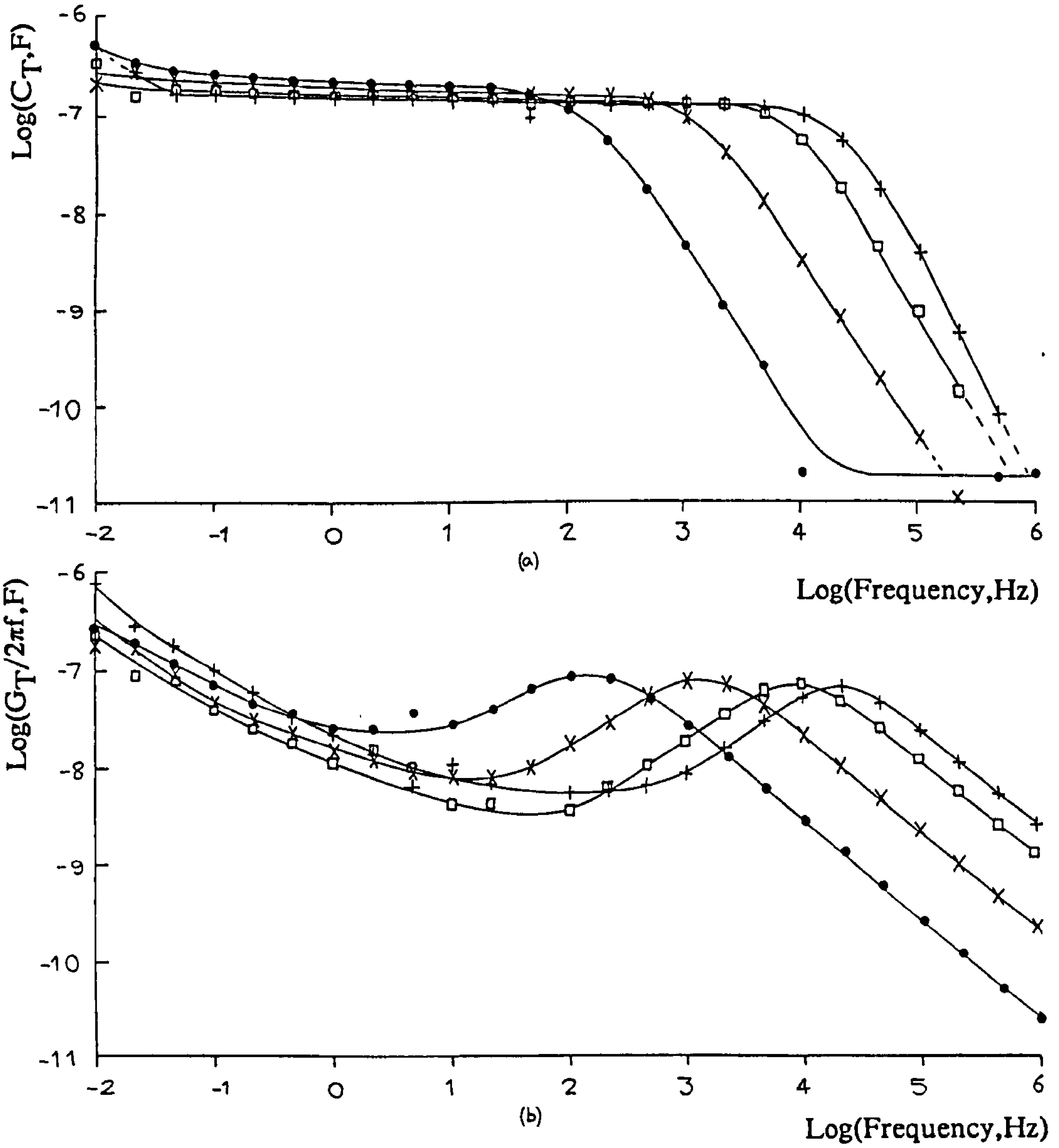

Fig 7.30 (a) Log Capacitance, C_T and (b) Loss ($G_T/2\pi f$) plotted against log frequency, F, for an evaporated aluminium electrode coated with 3 monolayers of $BaSt_2$ and immersed in (•)0.2mM, (x) 2.0mM, (□) 20mM and (+) 200mM $CaCl_2$ at 21±1°C.

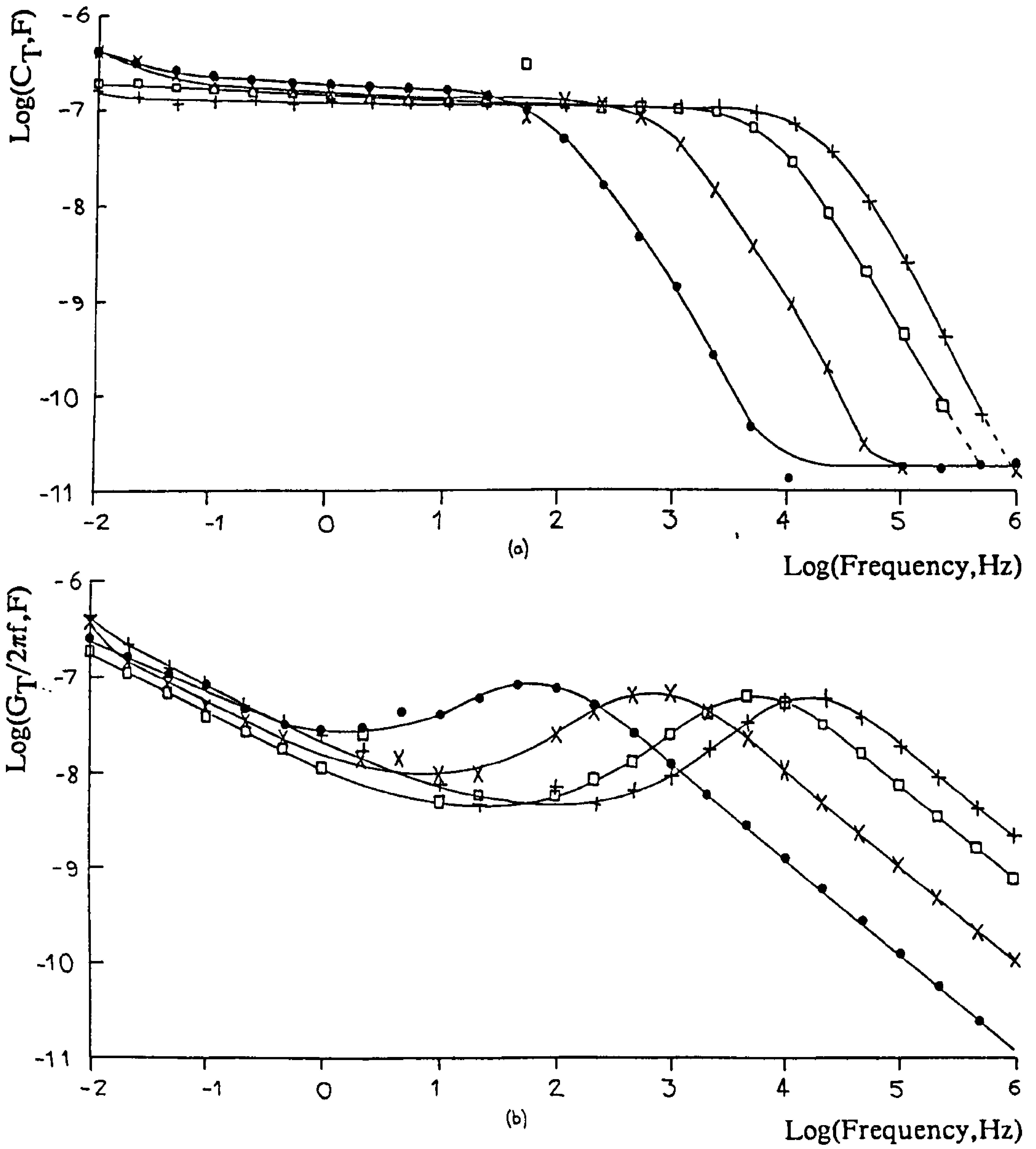

Fig 7.31 (a) Log Capacitance, C_T and (b) Loss ($G_T/2\pi f$) plotted against log frequency, F, for an evaporated aluminium electrode coated with 3 monolayers of $BaSt_2$ and immersed in (•)0.2mM, (x) 2.0mM, (□) 20mM and (+) 200mM NaCl at 21±1°C.

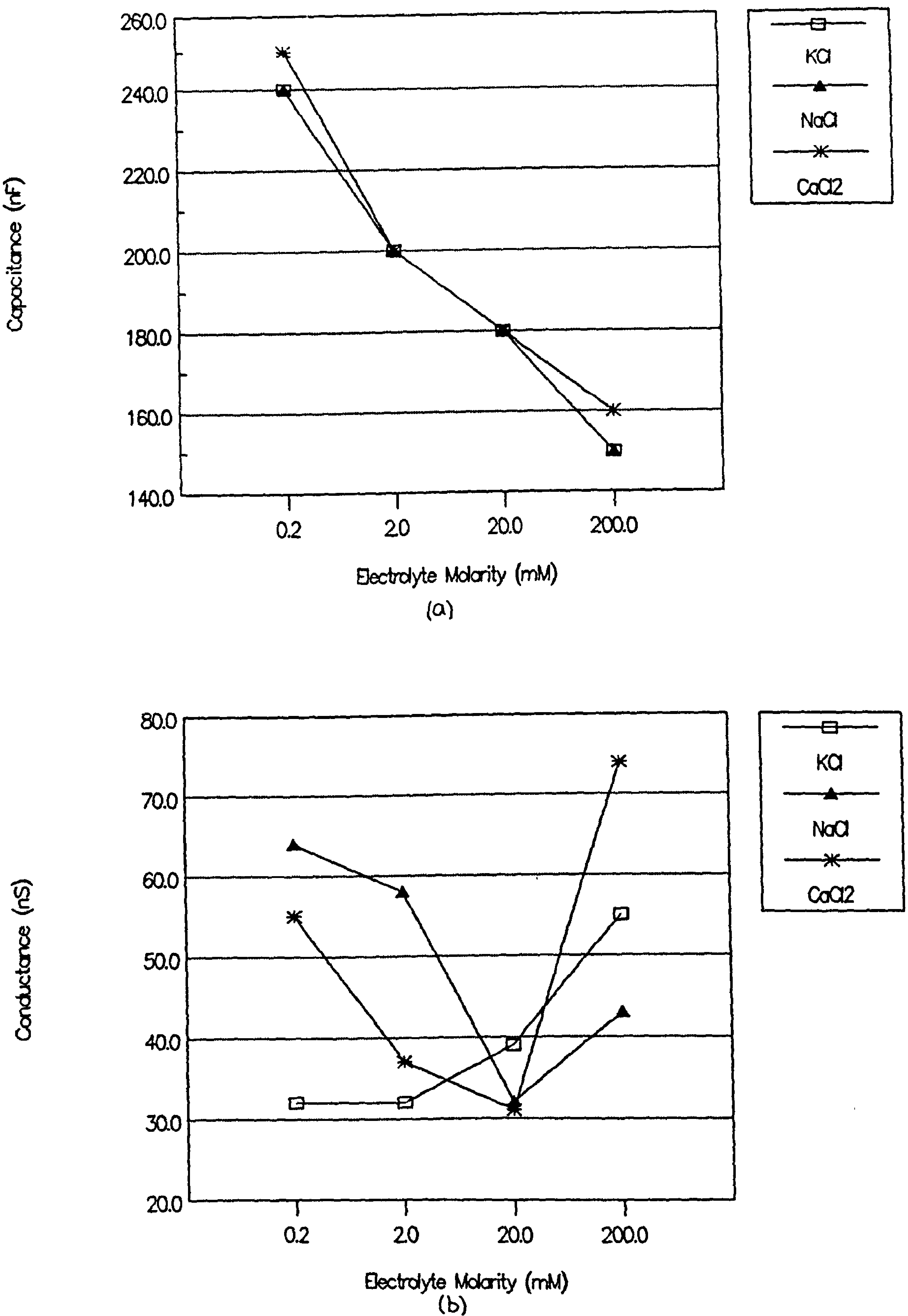

Fig 7.32 (a) Capacitance C_b, and conductance G_b at $1/2\pi$Hz and 21±1°C, for an evaporated aluminium electrode coated with 3 monolayers of $BaSt_2$ and plotted as a function of electrolyte molarity. Results are shown for immersion in (□) KCl, (▲) NaCl and (*) $CaCl_2$. (Capacitance and conductance values were estimated from figs 7.28 to 7.31).

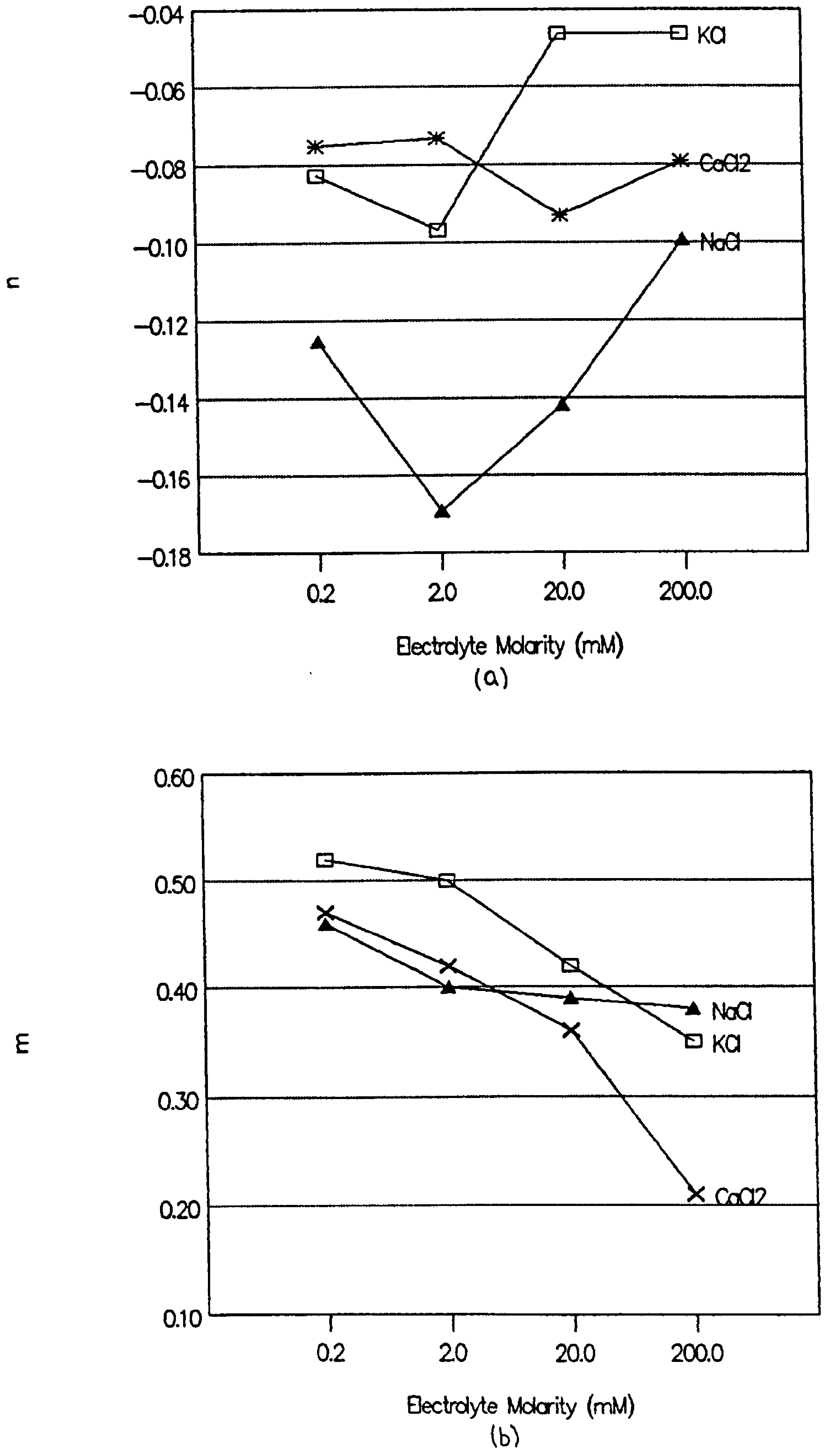

Fig 7.33 (a) n and (b) m for an evaporated aluminium electrode coated with 3 monolayers of $BaSt_2$ and plotted as a function of electrolyte molarity. Results are shown for immersion in (□) KCl, (▴) NaCl and (*) $CaCl_2$. (n and m values were estimated from figs 7.28 to 7.31).

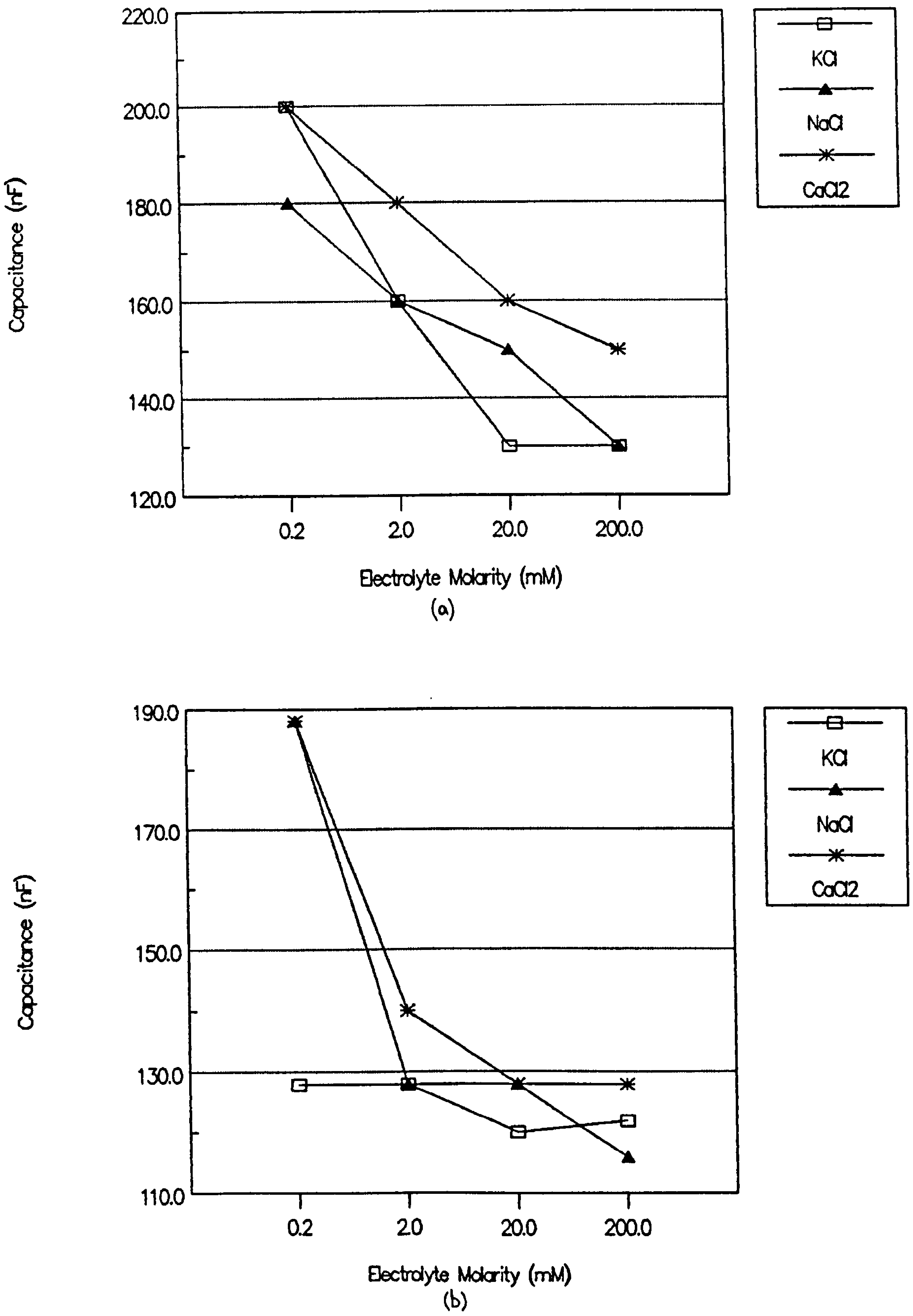

Fig 7.34 Capacitance C_b at (a) 10Hz and (b) the cross over point of the capacitance/loss curve, for an evaporated aluminium electrode coated with 3 monolayers of $BaSt_2$ and plotted as a function of electrolyte molarity. Results are shown for immersion in (□) KCl, (▲) NaCl and (*) $CaCl_2$ at $21 \pm 1^{\circ}C$. (Capacitance values were estimated from figs 7.28 to 7.31).

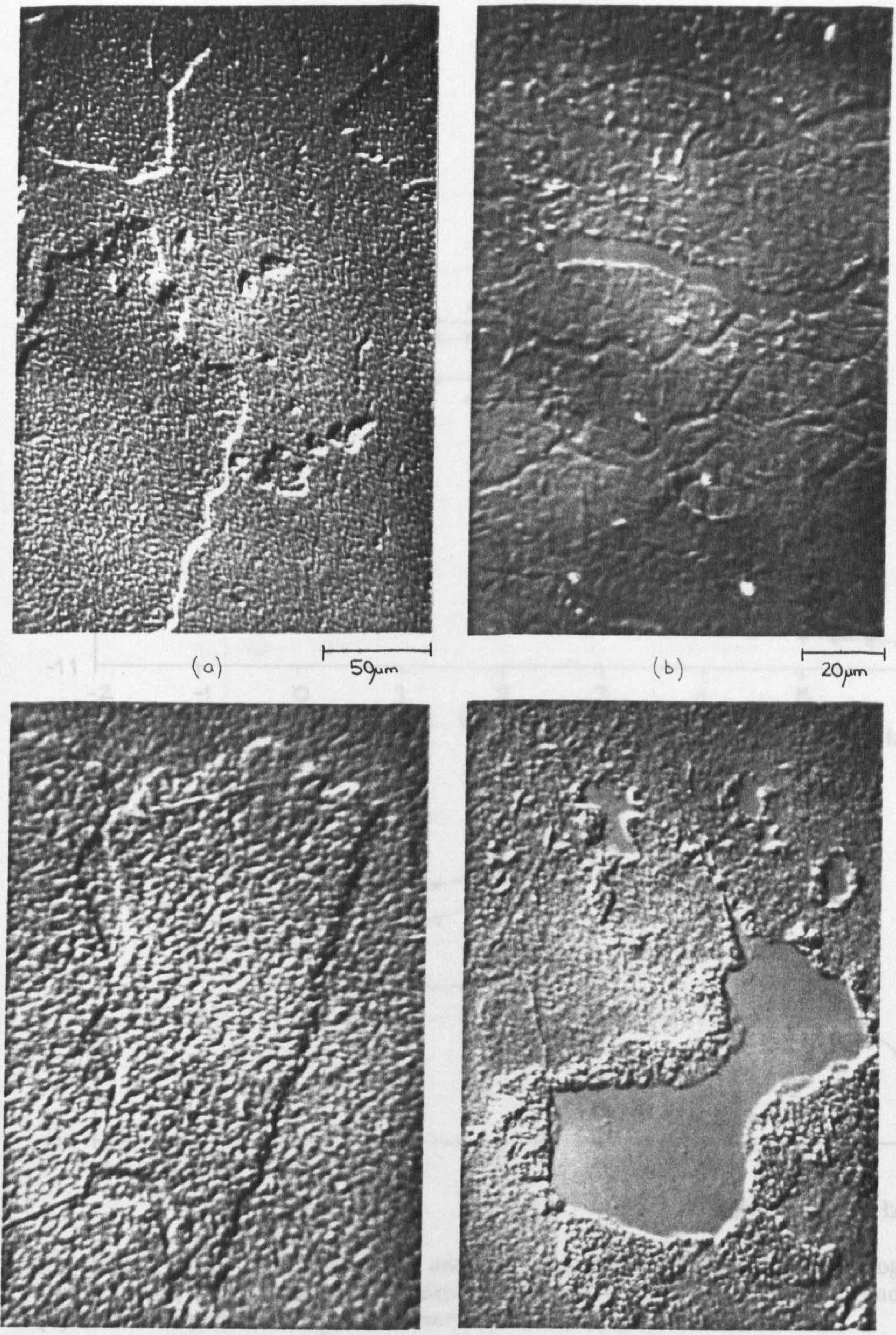

Fig 7.35 Photographs of 5 monolayers of Barium Stearate deposited onto evaporated aluminium electrodes. Photographs (a, b) were taken prior to and (c, d) after immersion in electrolyte. The photographs were taken from images produced by a phase contrast microscope.

(a) The lowered regions provide evidence of uneven coverage, probably arising from loss of film. (b) The smooth regions are taken to represent areas of uncoated or monolayer coated electrode resulting from movement of domains in subsequent layers. (c) Further evidence that the domains can move is shown by the clear shift in position of the region in the centre of the photograph. (d) As well as relocation occuring in the plane of the film, regions can also fold back on to newer layers.

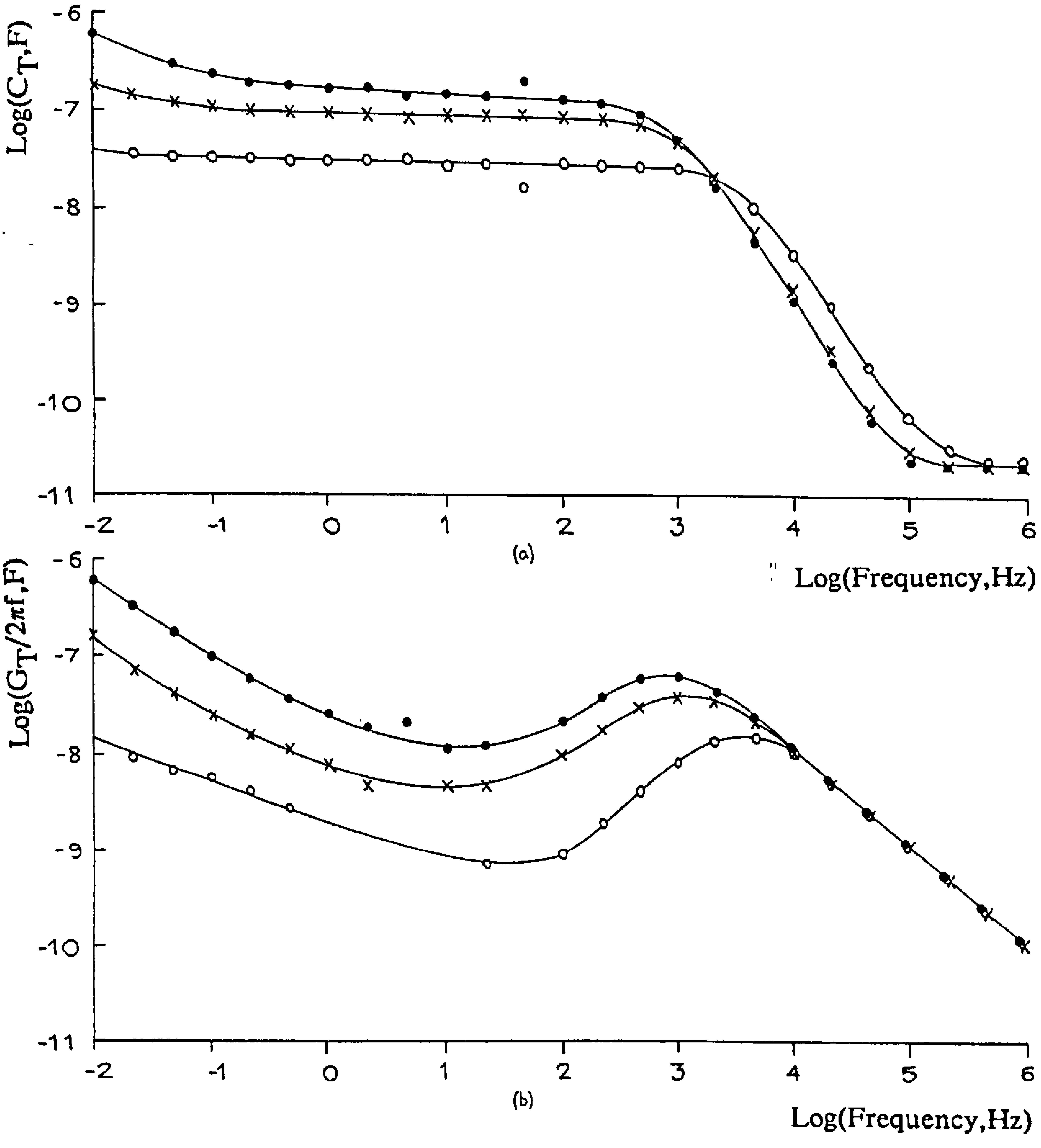

Fig 7.36 (a) Log Capacitance, C_T and (b) Loss ($G_T/2\pi f$) plotted against log frequency, F, for an evaporated aluminium electrode coated with (•)5, (x) 13 and (o) 19 monolayers of $BaSt_2$ and immersed in 2mM KCl at 21±1°C.

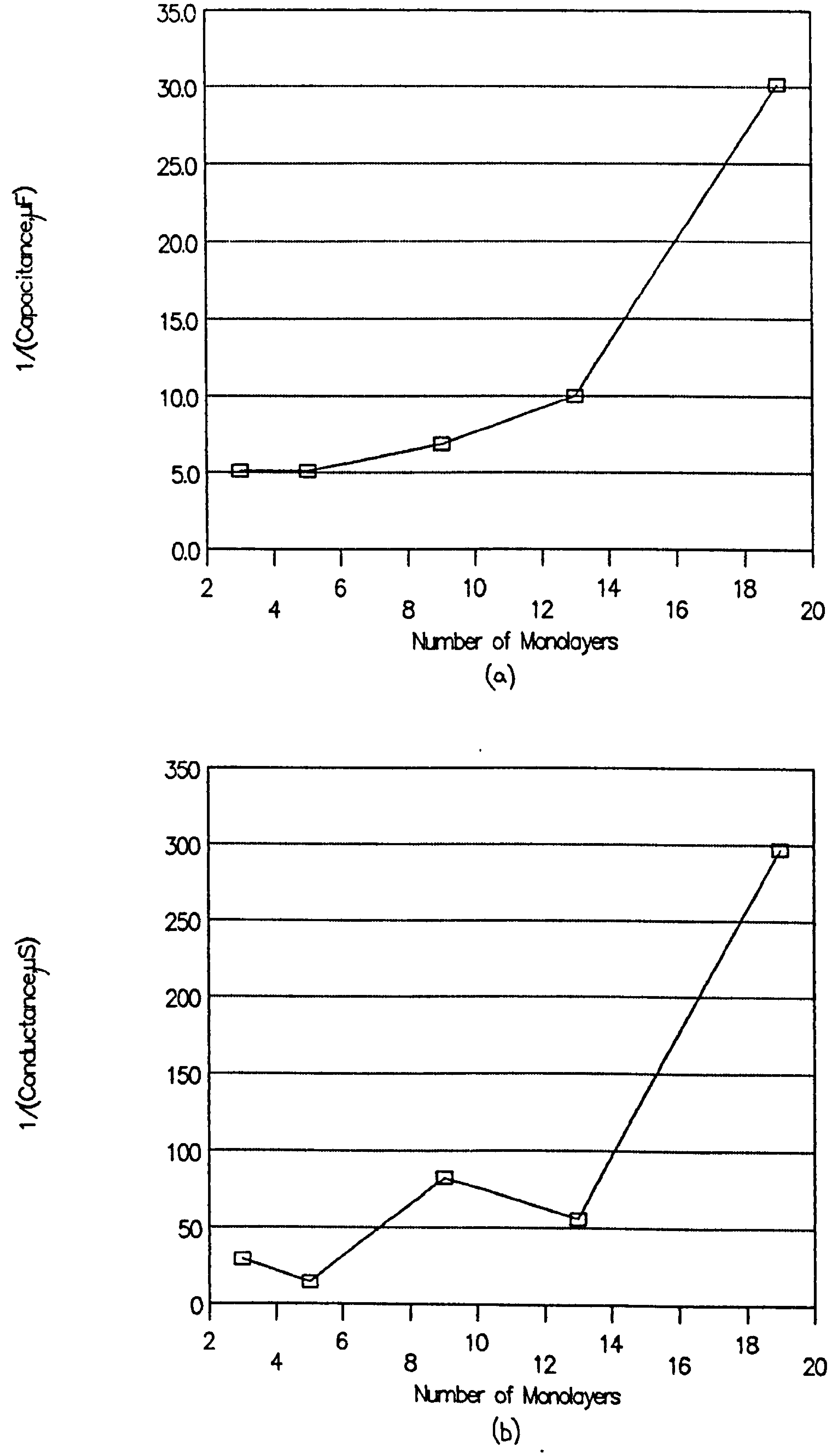

Fig 7.37 (a) Reciprocal capacitance ($1/C_b$), and (b) conductance ($1/G_b$), measured at $1/2\pi$ Hz, for an evaporated aluminium electrode coated with 1, 3, 9, 13 and 19 monolayers of $BaSt_2$ immersed in 2mM KCl at 22±1°C, plotted as a function the number of monolayers.

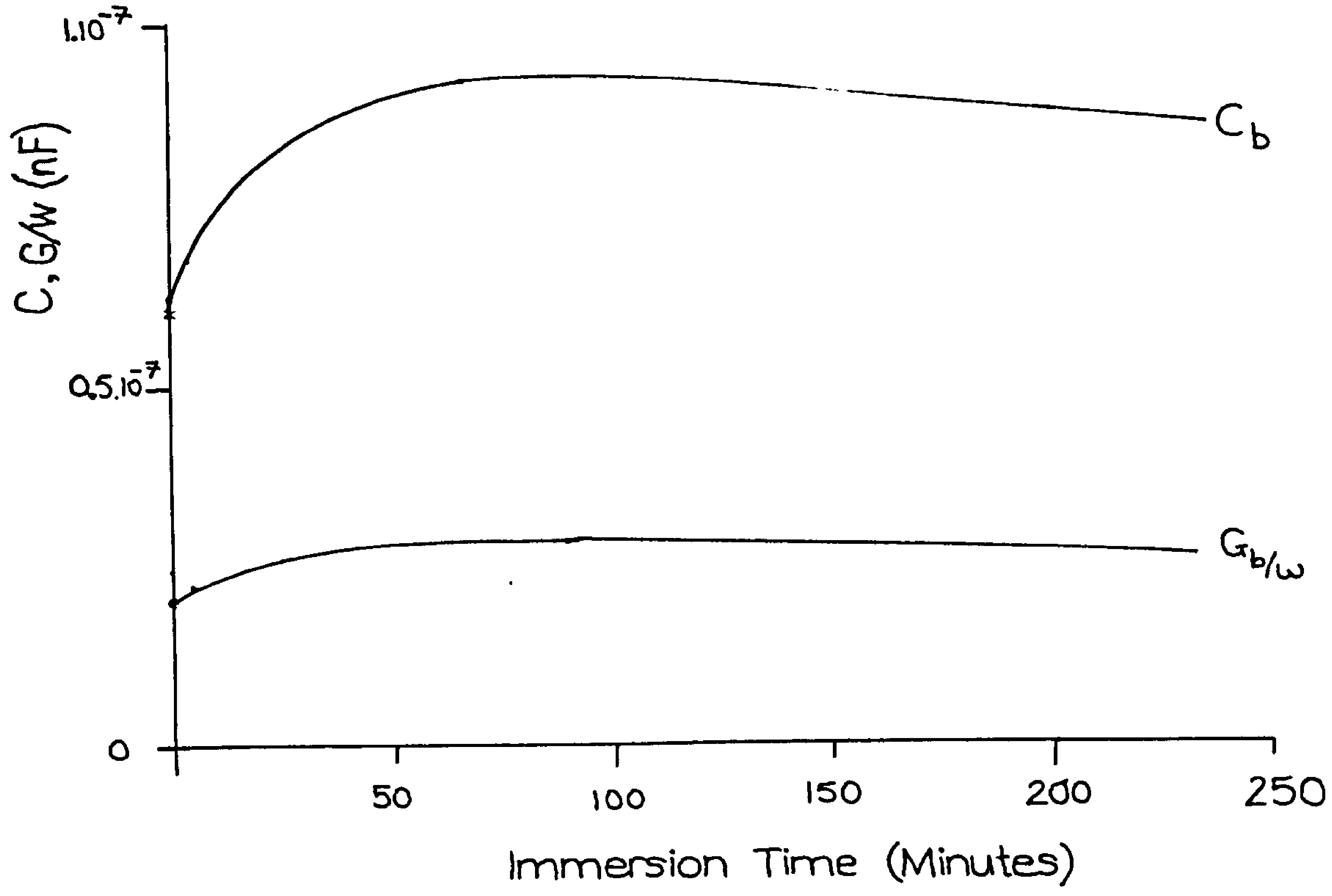

Fig 7.38 (a) Capacitance (C_T) and Loss ($G_T/2\pi f$) for an evaporated aluminium electrode coated with 3 monolayers of $BaSt_2$, measured at 10Hz and plotted as a function of immersion time in 0.2mM KCl at 23±1°C and pH 6.0.

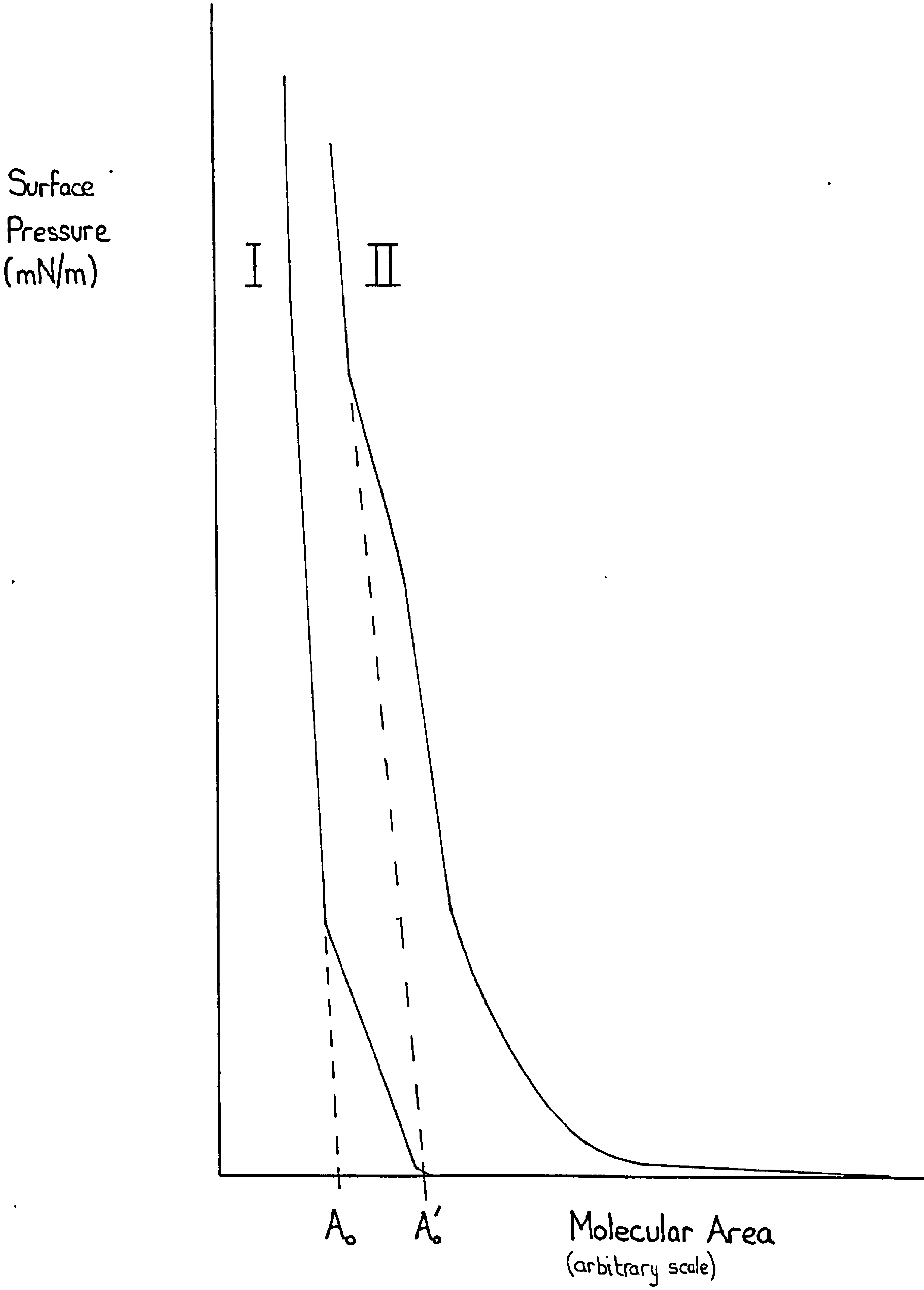

Fig 7.39 Pressure–Area Curves for I) $BaSt_2$ and II) mixed $BaSt_2$/Gramicidin (180:1) monolayers at 20±1°C and pH 7.9, where A_o = 20.6±0.3Å^2 and A_o' = 298±40Å^2.

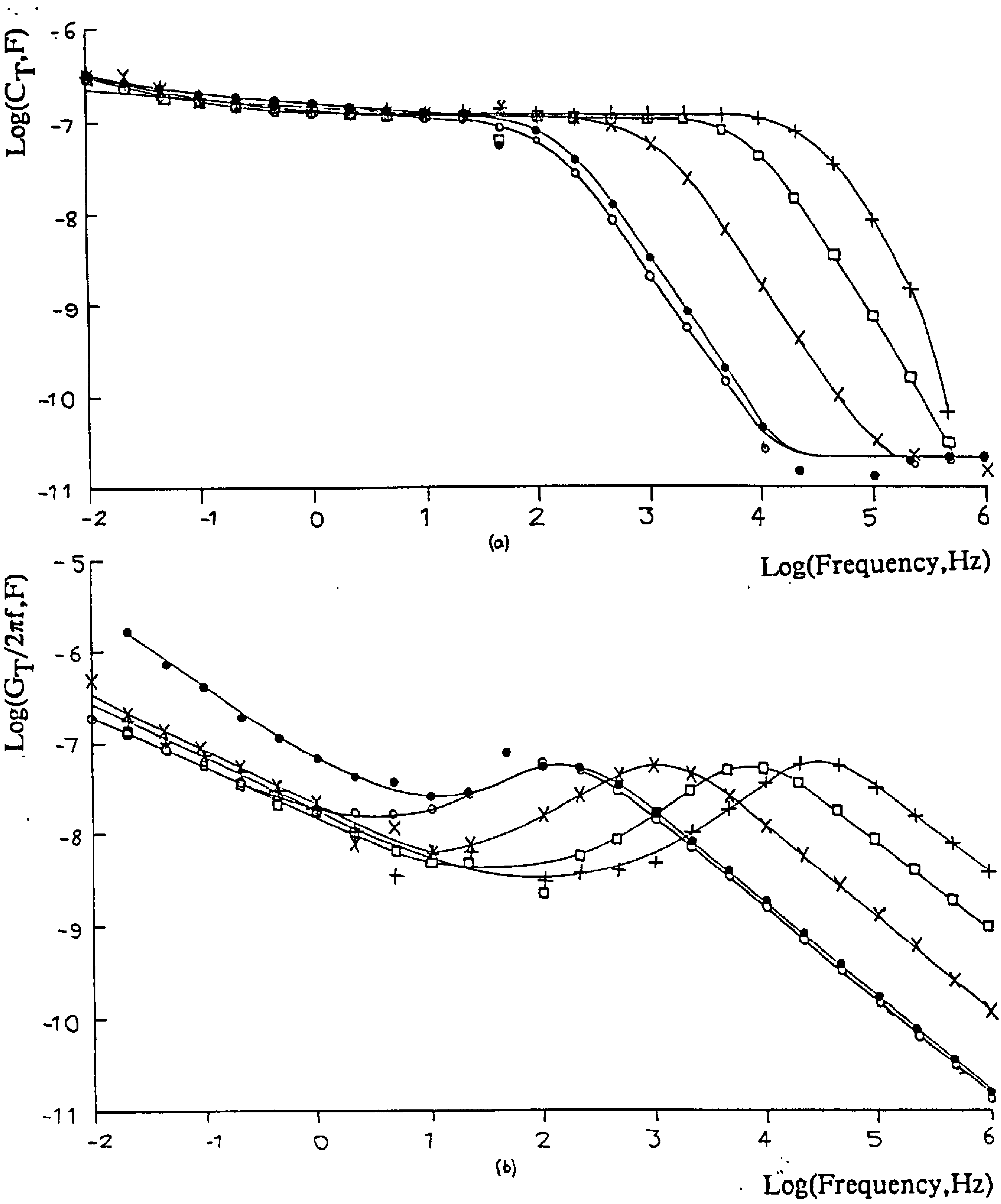

Fig 7.40 (a) Log Capacitance, C_T and (b) Loss ($G_T/2\pi f$) plotted against log frequency, F, for an evaporated aluminium electrode coated in 3 monolayers of $BaSt_2$/Gramicidin and immersed in (•)0.2mM, (x) 2mM, (□) 20mM (+) 200mM and again in (o) 0.2mM KCl at 22.0±0.6°C and pH 5.3.

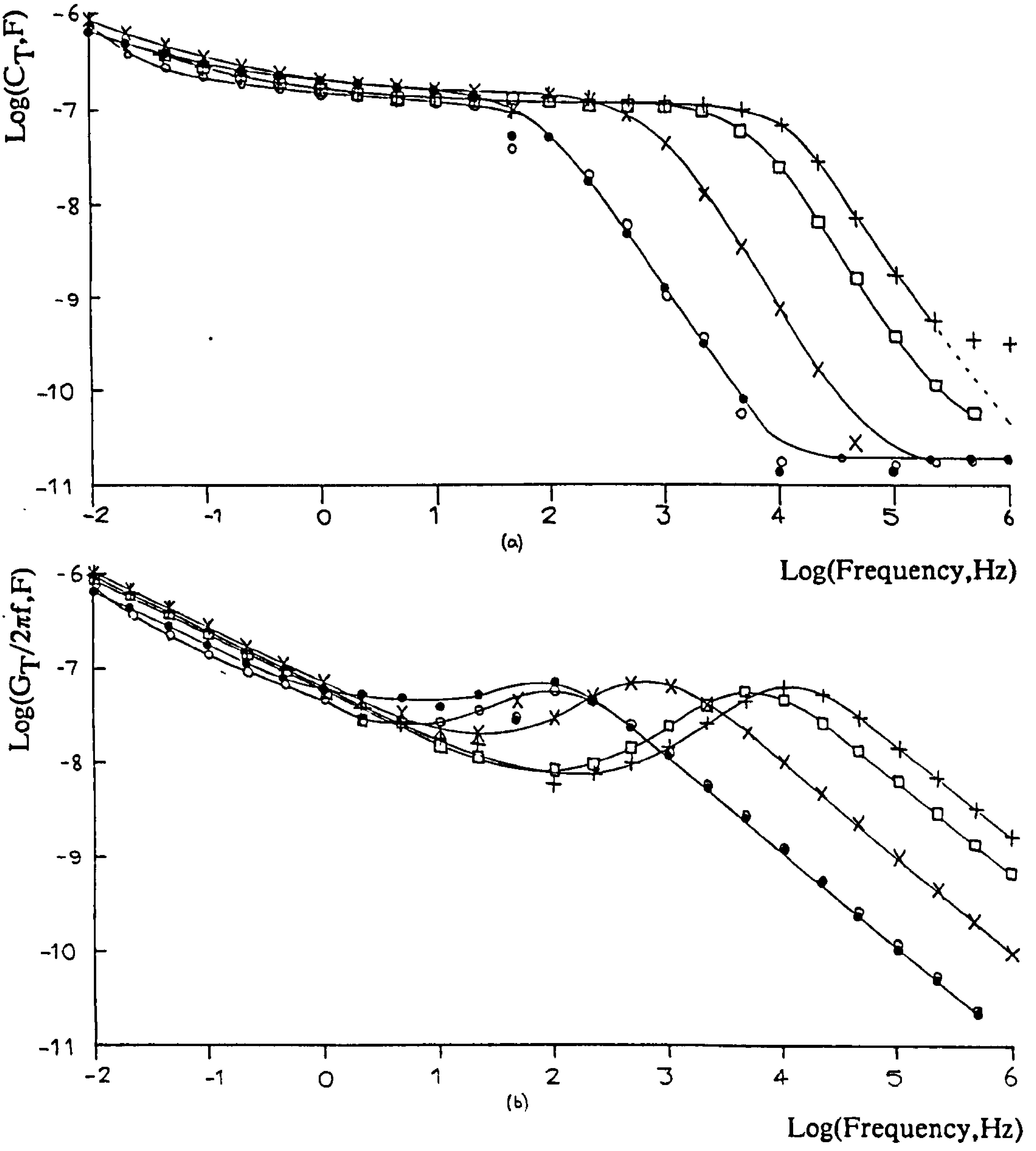

Fig 7.41 (a) Log Capacitance, C_T and (b) Loss ($G_T/2\pi f$) plotted against log frequency, F, for an evaporated aluminium electrode coated in 3 monolayers of $BaSt_2$/Gramicidin and immersed in (•)0.2mM, (x) 2mM, (□) 20mM (+) 200mM and again in (o) 0.2mM NaCl at 22.0±0.6°C and pH 5.7.

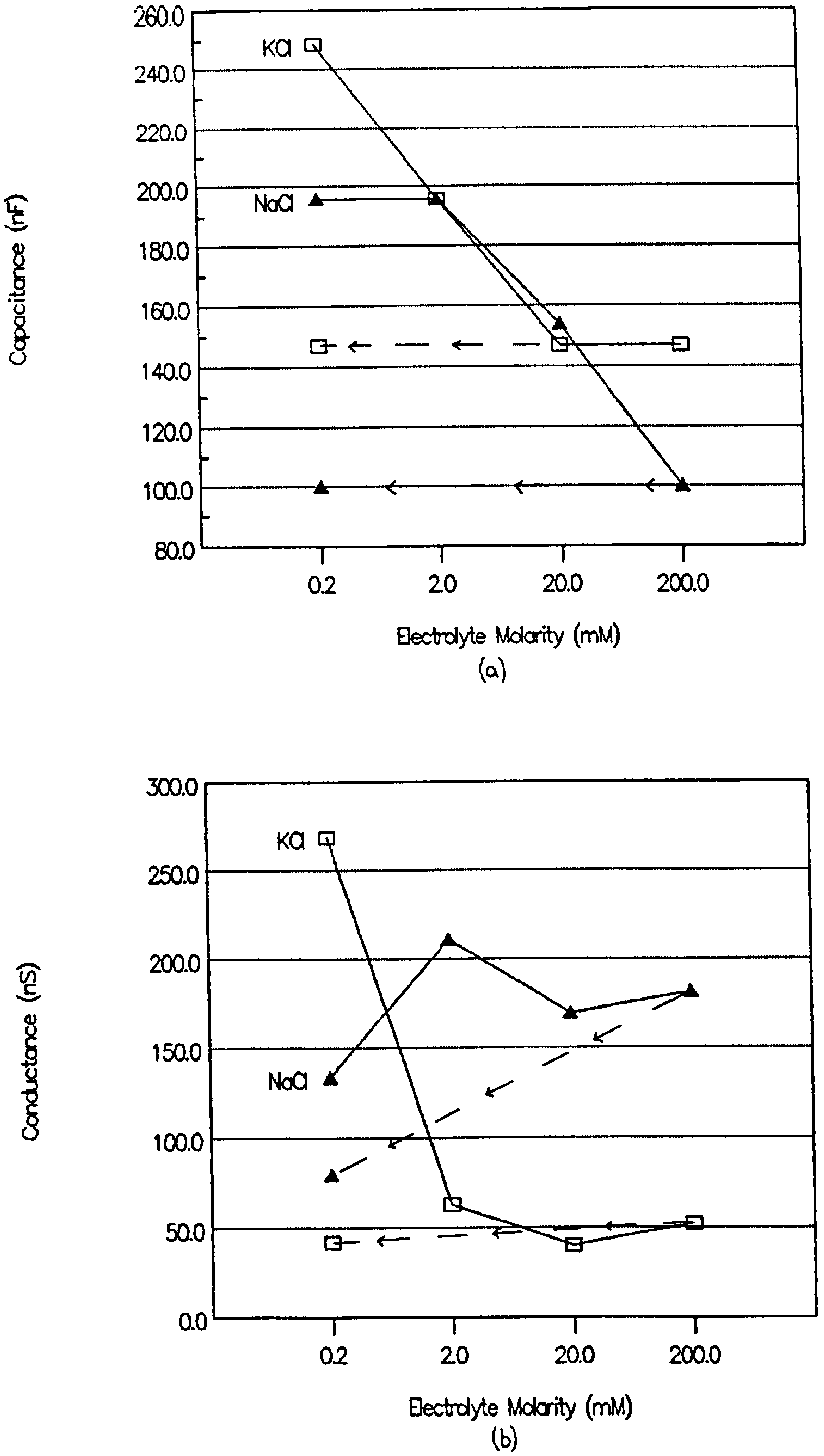

Fig 7.42 (a) Capacitance C_b, and conductance G_b at $1/2\pi$Hz and 21±2°C, for an evaporated aluminium electrode coated with 3 monolayers of $BaSt_2$/Gramicidin and plotted as a function of electrolyte molarity. Results are shown for immersion in (□) KCl and (▲) NaCl. (Capacitance and conductance values were estimated from figs 7.40 and 7.41).

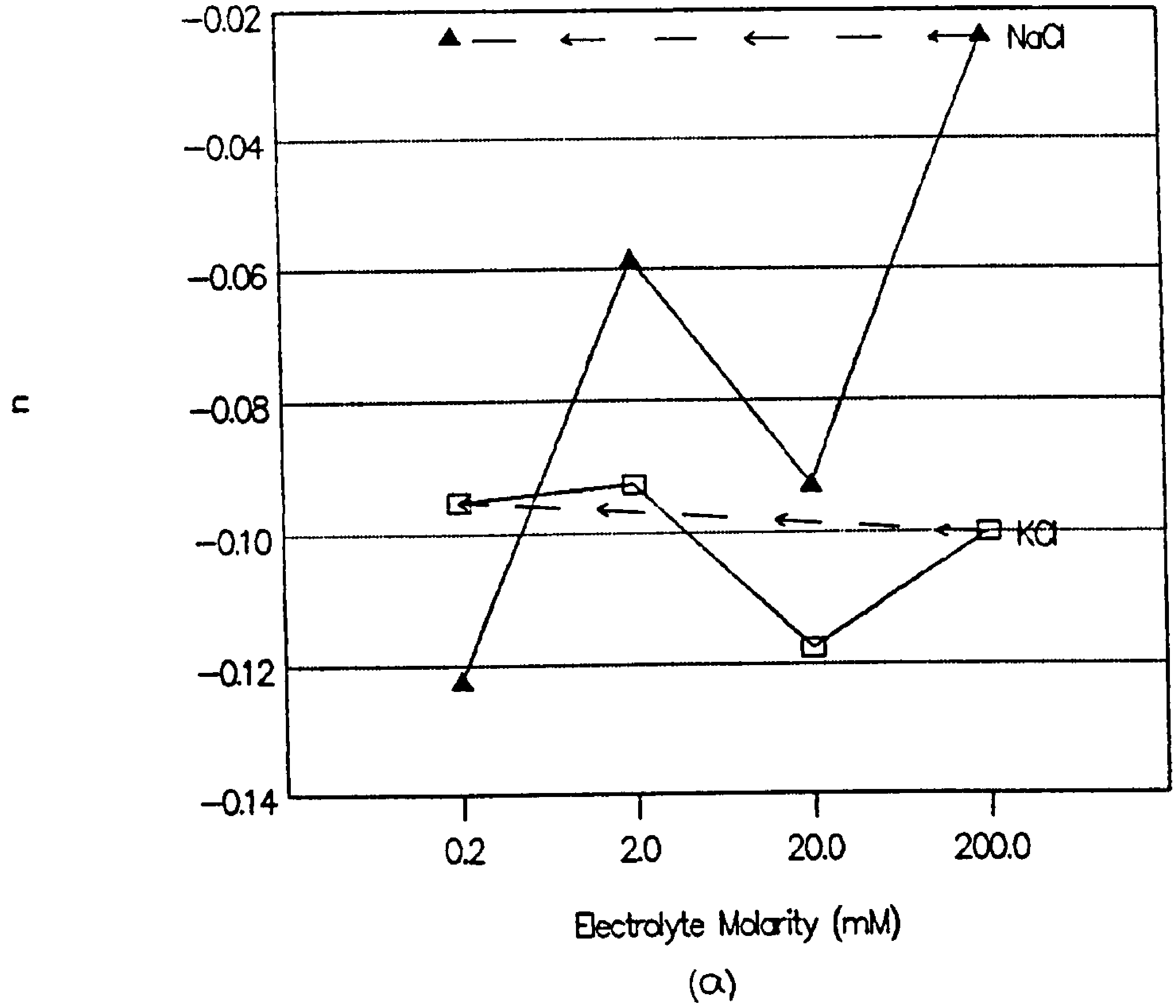

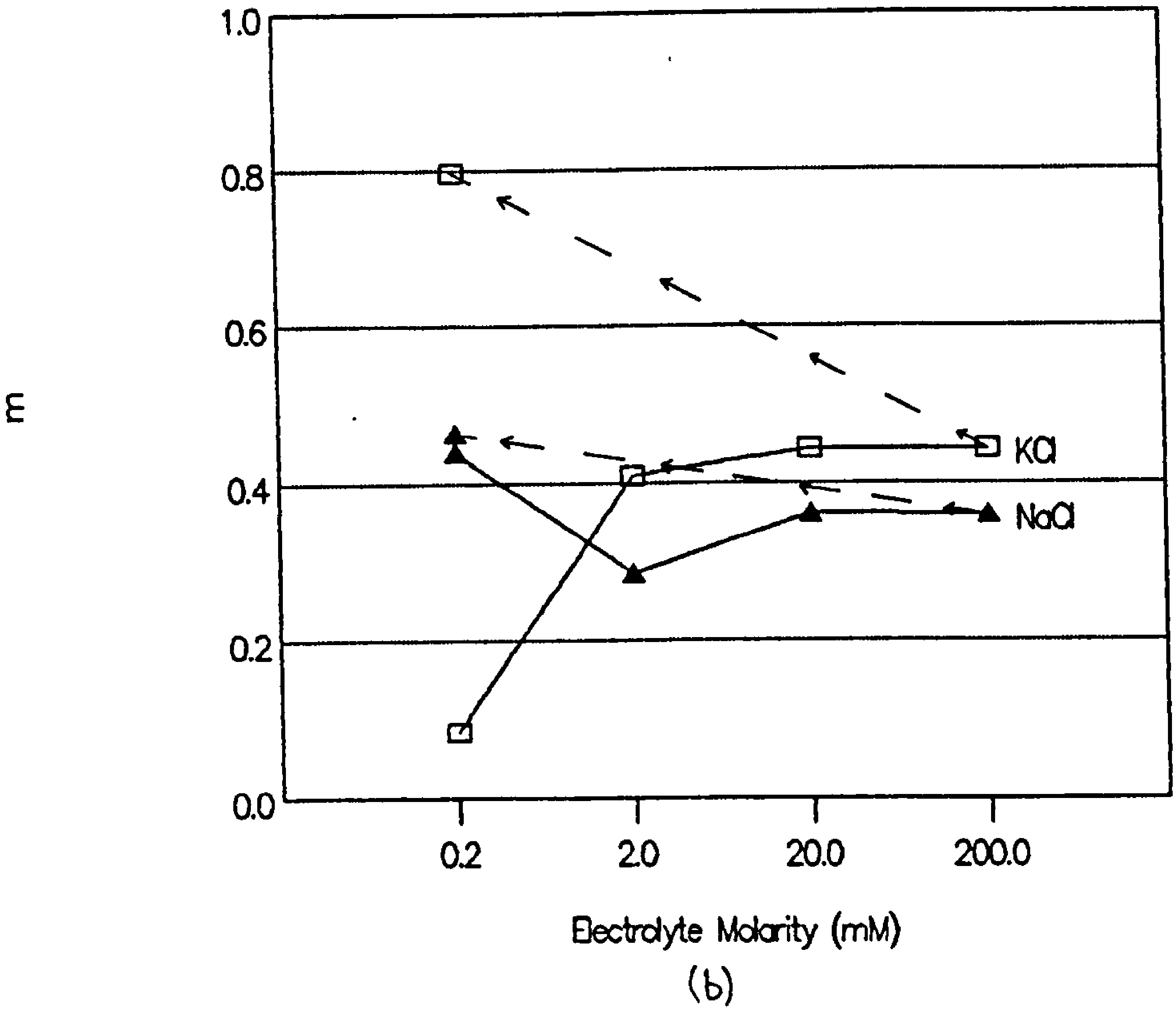

Fig 7.43 (a) n and (b) m for an evaporated aluminium electrode coated with 3 monolayers of $BaSt_2$/Gramicidin and plotted as a function of electrolyte molarity at 21±2°C. Results are shown for immersion in (□) KCl and (▲) NaCl. (n and m values were estimated from figs 7.40 and 7.41).

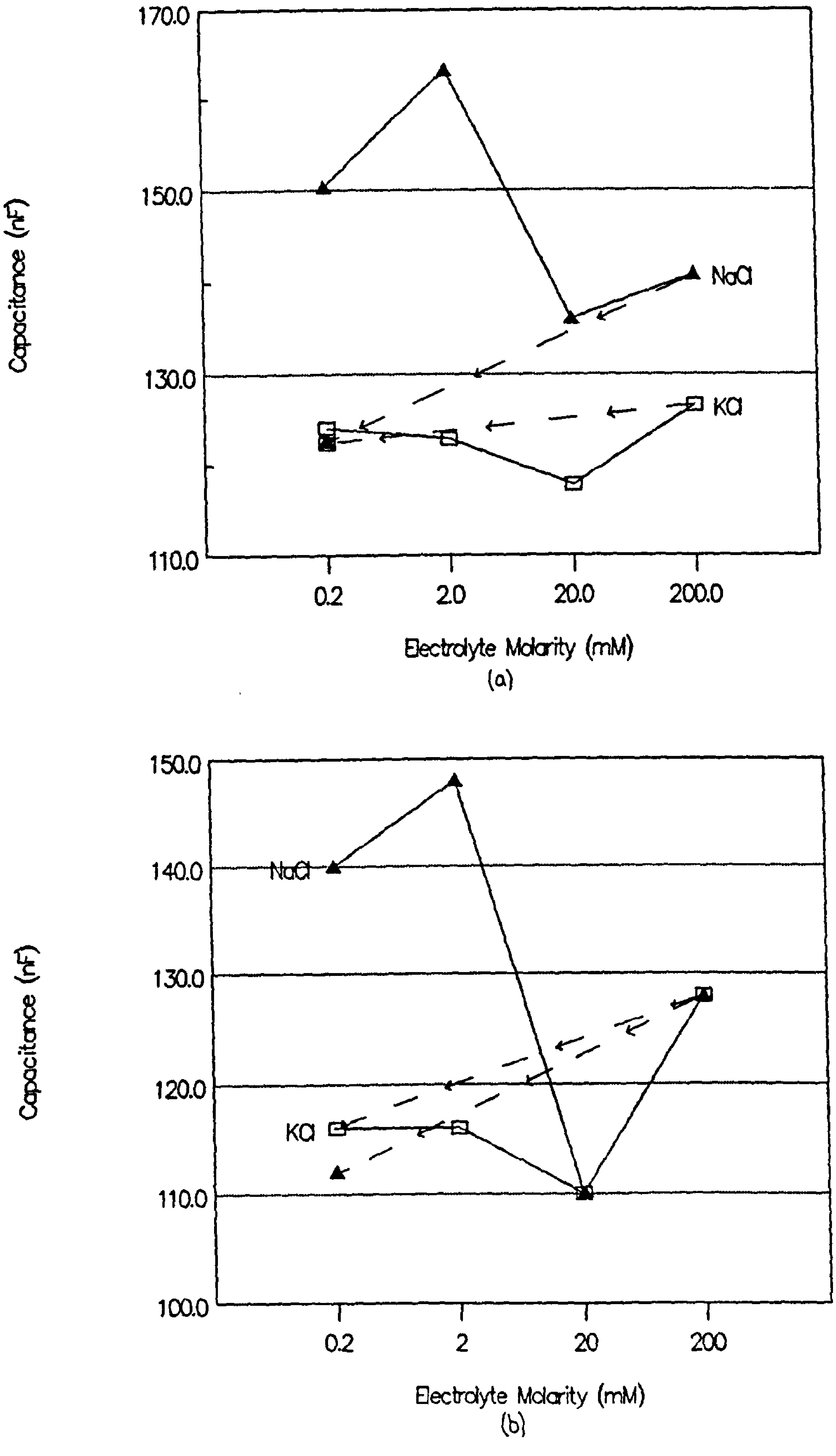

Fig 7.44 Capacitance C_b at (a) 10Hz and (b) the cross over point of the capacitance/loss curve, for an evaporated aluminium electrode coated with 3 monolayers of BaSt$_2$/Gramicidin and plotted as a function of electrolyte molarity. Results are shown for immersion in (□) KCl and (▲) NaCl at 21±1°C. (Capacitance values were estimated from figs 7.40 and 7.41).

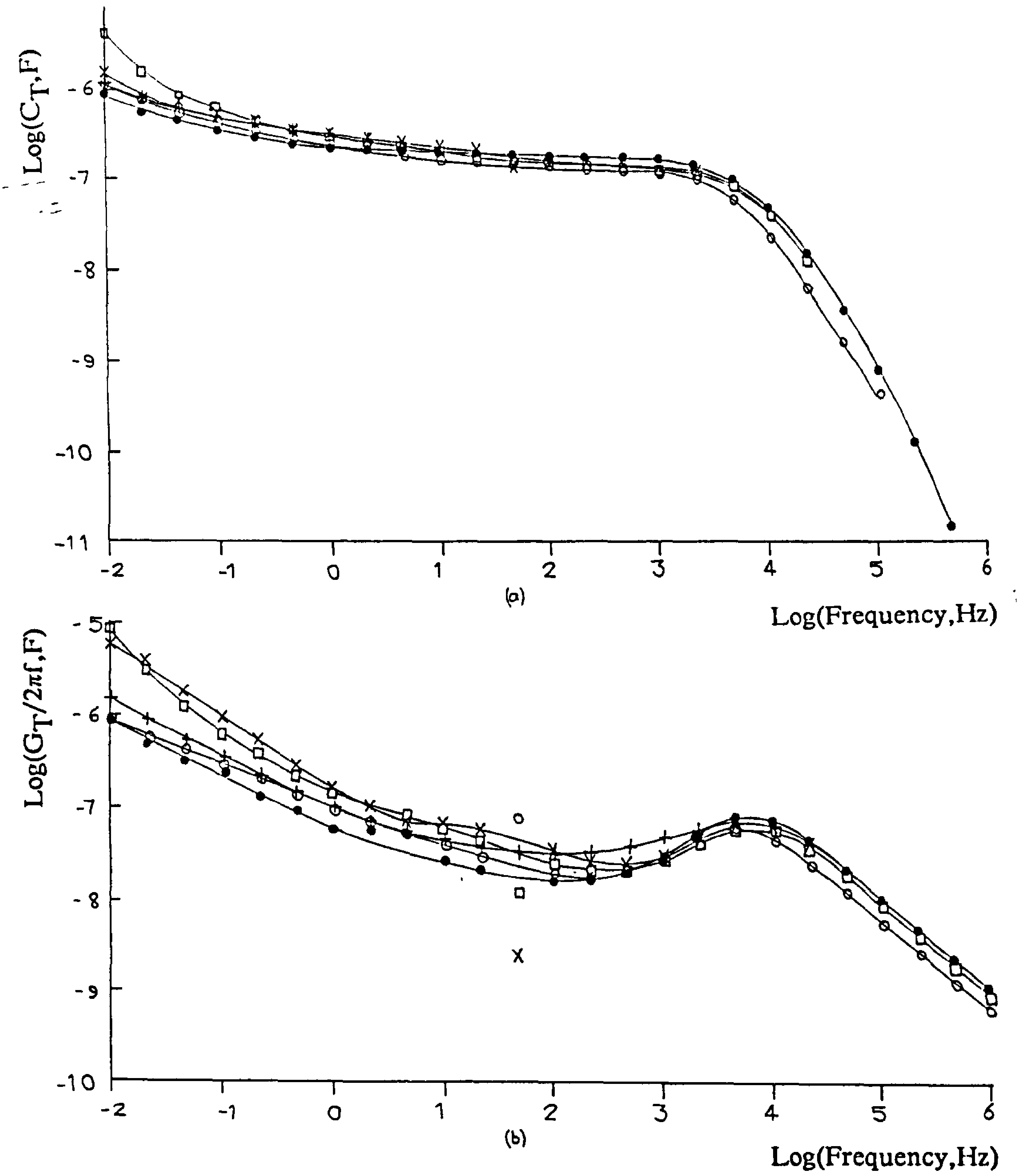

Fig 7.45 (a) Log Capacitance, C_T and (b) Loss ($G_T/2\pi f$) plotted against log frequency, F, for an evaporated aluminium electrode coated with 3 monolayers of $BaSt_2$/Gramicidin and immersed in KCl at pH (•)5, (x) 7, (□) 9, (+) 3 and again at pH (o) 5 at 22.0±0.6°C.

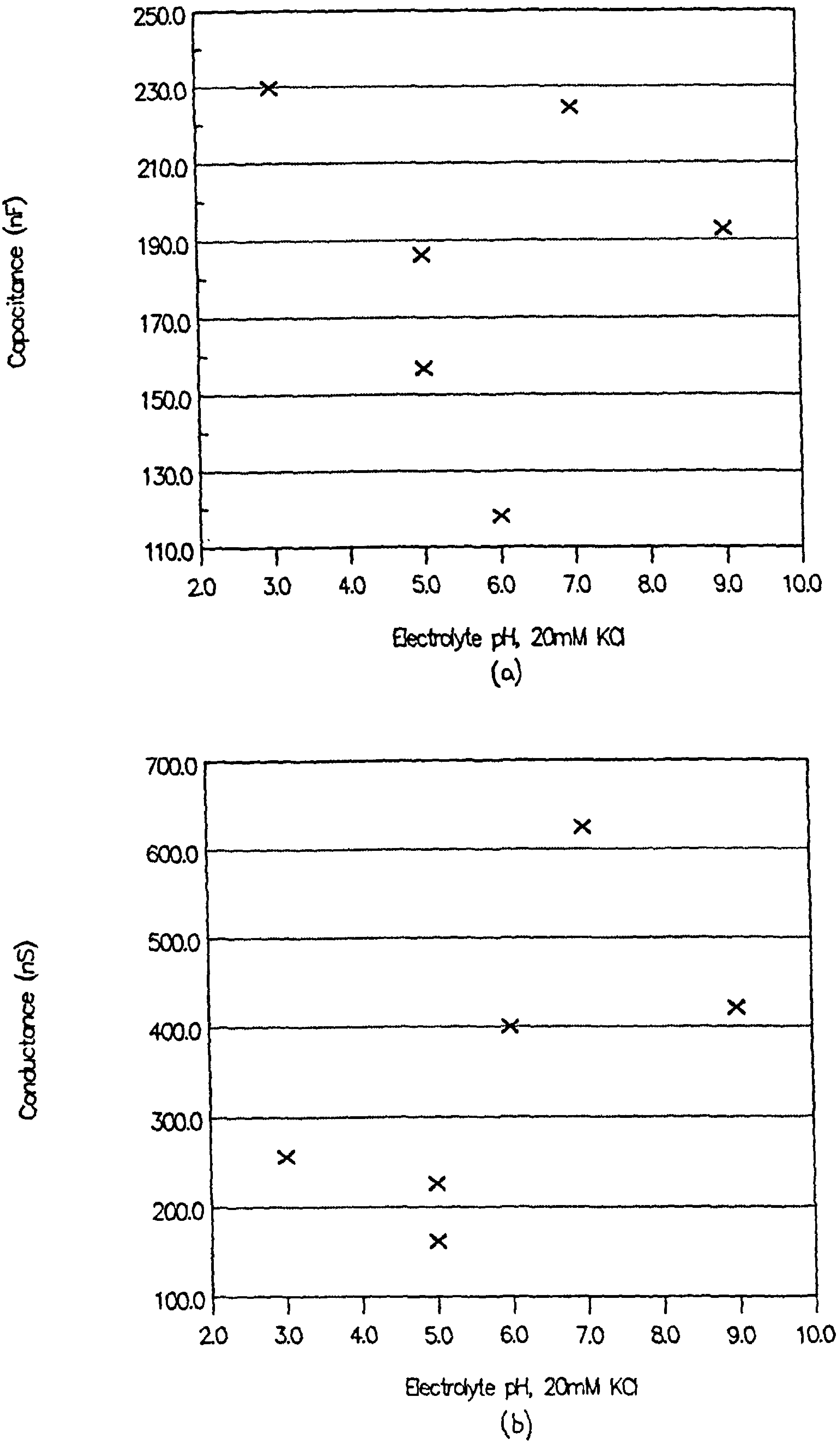

Fig 7.46 (a) Capacitance C_b, and conductance G_b at $1/2\pi$Hz and 22.0±0.6°C, for an evaporated aluminium electrode coated with 3 monolayers of BaSt$_2$/Gramicidin and plotted as a function of KCl electrolyte pH. (Capacitance and conductance values were estimated from figs 7.45).

8.0 The characterisation of PBMA coated electrodes

8.1 Introduction

Admittance and cyclic voltammetry studies of barium stearate coated platinum electrodes revealed that the coatings were unstable in an electrolyte environment ($ 7). Consequently, LB film forming compounds, capable of forming more stable multilayers were considered. Work reported on polymers indicated that such compounds can provide more robust coatings (eg Fung and Larkins, 1985). However, as discussed previously ($ 3.4), the polymer must be chosen carefully to obtain a good quality multilayer film. For example, if a monomer film is polymerised after transfer to the substrate, conformational changes can produce voids in the coating (eg acid diacetylene; Sarkar and Lando, 1983). The use of preformed polymers avoids this problem, consequently, poly-butyl-methacrylate (PBMA) was used (fig 8.1). PBMA has already been employed in work to immobilise dyes (Stuart, 1986). Furthermore, the chemical passivity of PBMA means it is suitable for immobilising ion selective molecules (Billmeyer, 1984).

8.2 PBMA Multilayers

8.2.1 Preparation of Films

Monolayers of PBMA were produced as described in section 4.3.2 using spreading solutions containing ca 1.0mg PBMA/ml chloroform. Fig 8.2a shows a typical π-A curve for PBMA, at 20°C at pressures below the collapse region. The surface area decreases monotonically with increasing surface pressure without any distinct changes of phase. From the initial π-A curves, the monomer molecular area was estimated to be 22 $Å^2$ at 20 °C. This figure is in reasonable agreement with the value of 24.4 $Å^2$ at 20 °C reported by Stuart (1986). In subsequent deposition work, the monomer surface area at 10mN/m, is estimated to be 31.2±2.3 Å^2 at a temperature of 30.6± 0.5°C and a pH of 4.8±0.3. Assuming that the PBMA monomer lies flat on the surface of the water, the molecular area is estimated to be 34 Å^2 per monomer. This would suggest that one of the methyl groups has left the water surface. (The area estimation was based on standard bond lengths, ionic radii (Huheey, 1978) and bond angles (Morrison and Boyd, 1983)).

As the surface pressure is increased beyond 15mN/m (fig 8.2b), the monolayer passes through 2 plateau regions before a "solid-phase" is encountered. If the monolayer is cycled from low to high pressure, a gradual decrease in film area is observed (fig 8.2b). For example, if the film is cycled from 0 to 22mN/m, 0 to 32mN/m and 0 to 32mN/m a loss of 3% of the film area is observed on each return to 0mN/m. In work with mixed PBMA/dye films, Stuart (1986) noted that the fall in monolayer surface area coincided with the appearance of dye in the subphase and attributed this to the loss of film to the subphase. For this reason, in all the deposition work reported here, monolayer surface pressures were kept to below 15mN/m and deposition was carried out at 10mN/m.

The temperature dependence of the π-A curves for PBMA are shown in fig 8.3. From this figure, the initial part of the π-A curves appears to be largely independent of temperature. However, below ca 15Å^2/molecule, the surface pressure begins to increase with temperature. This suggests that it is not until pressures beyond the collapse region are reached that the monomer units are sufficiently packed for their thermal energy to influence the surface pressure. The rise in surface pressure with temperature may also reflect the reduction in film collapse at higher temperatures.

8.2.2 Deposition onto substrates

Deposition experiments were carried out onto platinum wire, evaporated silver and aluminium and onto sputtered copper on glass, all substrates prepared as described in section 4.2. Deposition ratios of PBMA onto copper are presented in fig 8.4. In Table 8.1 the average figures for the deposition ratios per cycle for all substrates are given. Several features are apparent from fig 8.4;

i) The deposition ratios were greater during withdrawal of the substrate than on entry.

ii) The amount of film deposited increases during the first 6 dipping cycles before reaching a steadier value.

iii) The amount of film deposited is quite variable, indicating that it is difficult to obtain reproducible films on copper/glass substrates, using PBMA. This may be because the ester side group is only weakly hydrophilic (Hodge et al, 1985).

Material	Coating	Deposition Ratio
Copper	PBMA	1.20±0.14
Copper(1)	PBMA	1.48
Silver	PBMA	1.29
Aluminium	PBMA	1.76
Platinum	PBMA	1.98
Platinum	PBMA/Valinomycin	1.74

Table 8.1 Summary of average deposition ratios per dipping cycle for PBMA onto various substrates. (1) Glass slide completely covered in sputtered copper.

From the average values for the deposition ratio per cycle on platinum, aluminum, silver and copper electrodes (Table 8.1), deposition quality appears highest on platinum. For the other substrates, the poor deposition ratios may have been caused by poor adhesion onto the glass substrate (the metal electrode covered only 16% of the total substrate area). To check this, dipping was attempted onto slides that were completely covered in metal. The deposition ratio per dipping cycle rose to 1.48, which is well short of the expected value of 2 for good quality Y type films.

Despite the difficulties in obtaining regular film deposition, the high stability of the films deposited on platinum electrodes justified the use of PBMA. In the following sections, the results of the electrical characterisation of PBMA coated electrodes are presented and discussed.

8.2.3 Admittance Measurements

The admittance properties of platinum electrodes ($4.2.1) coated with between 20 and 60 monolayers of PBMA, using the Langmiur Blodgett Technique ($4.3.2), were characterised in a range of electrolytes and electrolyte molarities. The admittance results show that the films are stable and of high quality. The main variables employed during the presentation and discussion of the admittance data are described in $7.3.1.

8.2.3.1 PBMA multilayers on platinum wire electrodes

Fig 8.5(a,b) shows double log plots of capacitance (C_T) and loss ($G_T/2\pi f$) as a function of frequency, (f) for a platinum wire electrode dipped 10 times through an LB film of PBMA ($4.3.1.3, $8.1). The electrode was characterised in NaCl solutions of molarity 0.2, 2, 20, 200mM and again in 0.2mM at 22.5±1.5°C. The results obtained in the two experiments with 0.2mM solution show that the PBMA films are stable in NaCl.

At frequencies below 1 Hz, the loss curve is linear and largely independent of electrolyte molarity. Between 1 and 1000Hz a dispersion appears which becomes broader and shifts to higher frequencies as the electrolyte molarity increases. A similar dispersion was observed with PVC coated electrodes (\$5.5). Above 1000Hz the normal electrolyte/geometric capacitance dispersion is observed. The corresponding C_T curves increase in height with increasing molarity. At frequencies above 1000Hz the normal decrease in C_T is observed as the geometric capacitance C_g, is approached. C_g is estimated to be 21pF, in good agreement with the theoretical value of 18pF for a 12mm dipped length (\$7.3.1). The values of electrolyte molarity, calculated from the high frequency portion of the loss curves of fig 8.5 are summarised in Table 8.2. The good agreement between the experimental and theoretical values confirm the validity of these results (\$5.5.1, \$7.3.1).

Nominal Molarity	Molarity From Expt	Expt/Nominal Molarity
2.0×10^{-4}	2.5×10^{-4}	1.27
2.0×10^{-3}	2.2×10^{-3}	1.10
2.0×10^{-2}	1.7×10^{-2}	0.85
2.0×10^{-1}	2.4×10^{-1}	1.21

Table 8.2 A comparison of the nominal and experimentally determined electrolyte molarities, obtained during ac admittance analysis of platinum electrodes coated with a 10 dip coating of PBMA and immersed in NaCl at 22.5±1.5°C.

When the electrolyte was changed to KCl (figs 8.6 to 8.8), the double log plots of $G_T/2\pi f$ and C_T vs frequency for 10, 20 and 30 dip coated platinum wires respectively, tested in 0.2, 2, 20, 200 and again in 0.2mM solutions showed the same main features as fig 8.5, including good film stability. Comparing figs 8.5 to 8.8, it is clear that the film capacitance and conductance decrease with increasing film thickness, as expected (\$5.1, equations 5.3 and 5.1 respectively). In addition, the low frequency dispersions in the loss curves become broader (figs 8.6 to 8.8).

To facilitate comparison of film properties, the film capacitance estimated at i) $1/2\pi f$ Hz, ii) 10Hz and iii) the cross-over point of the C_T and $G_T/2\pi f$ curves is shown as a function of electrolyte molarity in figures 8.9a, 8.11a and 8.12 respectively. Similar plots of coating conductance at i) $1/2\pi$ Hz and ii) 10Hz are shown in figs 8.9b and 8.11b respectively. The film admittance can be further characterised by the frequency coefficients, n and m, if it is assumed that in the frequency range 1 to 0.01Hz, the film capacitance, C_b and conductance, G_b can be approximated by the expressions $C_b=C_b(w=1)w^n$ and $G_b=G_b(w=1)w^m$. Values of n and m are plotted as a function of electrolyte molarity in fig 8.10. The estimates of C_b, G_b, n and m are summarised in Table 8.3.

The plot of coating capacitance at $1/2\pi$ Hz as a function of electrolyte molarity (fig 8.9a) shows that C_b is clearly molarity dependent. Indeed, at this frequency, the film capacitance may be described by the equation;

$$\log(\text{Capacitance}) = A \times \log(\text{Molarity}) + B$$

where values for A and B, determined empirically from fig 8.9a are given below.

	A	B	10^B(μF)
10 dip film in NaCl	0.08±0.02	-6.42±0.04	0.38
10 dip film in KCl	0.08±0.02	-6.38±0.04	0.42
20 dip film in KCl	0.12±0.01	-6.70±0.02	0.20
30 dip film in KCl	0.12±0.01	-6.99±0.02	0.10

From the above equation, B is the log of the film capacitance in a 1 molar solution. It should be noted that as the molarity dependence of the double layer capacitance is given by;

log(double layer capacitance) = 0.5xlog(molarity) + constant

it is possible that the increase in capacitance with molarity is because of the influence of the double layer capacitance on the value of C_T at $1/2\pi$ Hz (equation 5.14, $5.3). However, even at 10Hz (fig 8.11a), the film capacitance is still clearly dependent on electrolyte molarity. In contrast, at the cross-over frequency (fig 8.12), the film capacitance no longer shows a clear dependence on the molarity of the electrolyte.

In addition to considering the dependence of film capacitance on the electrolyte and coating thickness, further information about the film can be obtained from the loss data. Indeed, the initial fall in $G_T/2\pi f$ (figs 8.5b to 8.8b) with frequency in the range 0.01 to 1 Hz, can be attributed to the low frequency conductance of the electrode coating ($5.3).

At 0.16Hz (fig 8.9b), the conductance values are largely independent of electrolyte molarity, (figs 8.10b and 8.13b). This suggests that at low frequencies, the film is essentially saturated with electrolyte ions even at 0.2mM concentration. Consequently the higher molarities produce no increase in conductance at $1/2\pi$ Hz. Alternatively, it could indicate that the effects of film hydration dominate any ion-dependent influence on film conductivity at low frequencies. A similar phenomenon was observed in the molarity dependence of PVC coatings on copper electrodes ($5.5).

Although largely independent of the molarity of the electrolyte, it is clear that the film conductance is cation dependent. The rise in average conductance at $1/2\pi$Hz, in changing from NaCl electrolyte to KCl respectively, could be due to the different mobilities of the K^+ and Na^+ ions. As the mobilities of K^+, Na^+ and Cl^- ions are 7.62, 5.19 and $7.91\times10^{-8}m^2/V.sec$ respectively, in aqueous solution (Bard and Faulkner, 1980), the presence of K^+ rather than Na^+ ions in the film could produce a 20% increase in film

Values at 0.16Hz Nominal Molarity	10 dip NaCl		10 dip KCl	
	C_b(μF)	n	C_b(μF)	n
2.0×10^{-4}	0.19	-0.39	0.22	-0.32
2.0×10^{-3}	0.24	-0.33	0.22	-0.32
2.0×10^{-2}	0.25	-0.29	0.30	-0.32
2.0×10^{-1}	0.35	-0.28	0.37	-0.28
2.0×10^{-1}	0.18	-0.39	0.19	-0.31

(a)

Values at 0.16Hz Nominal Molarity	20 dip KCl		30 dip KCl	
	C_b(μF)	n	C_b(μF)	n
2.0×10^{-4}	0.075	-0.23	0.040	-0.24
2.0×10^{-3}	0.100	-0.21	0.048	-0.24
2.0×10^{-2}	0.119	-0.18	0.065	-0.24
2.0×10^{-1}	0.172	-0.23	0.088	-0.22
2.0×10^{-1}	0.059	-0.23	0.034	-0.22

(b)

Values at 10 Hz Nominal Molarity	10 dip NaCl	10 dip KCl	20 dip KCl	30 dip KCl
	C_b(nF)	C_b(nF)	C_b(nF)	C_b(nF)
2.0×10^{-4}	38	43	19	7.7
2.0×10^{-3}	58	51	28	11.3
2.0×10^{-2}	78	76	40	18.7
2.0×10^{-1}	113	118	66	31.0
2.0×10^{-1}	38	40	16	7.7

(c)

Values at Cross-over Nominal Molarity	10 dip NaCl	10 dip KCl	20 dip KCl	30 dip KCl
	C_b(nF)	C_b(nF)	C_b(nF)	C_b(nF)
2.0×10^{-4}	8.8	10.4	2.9	1.3
2.0×10^{-3}	7.5	7.5	2.4	1.2
2.0×10^{-2}	6.9	6.6	2.1	1.3
2.0×10^{-1}	8.1	8.1	3.0	---
2.0×10^{-1}	8.8	8.8	2.7	1.3

(d)

Values at 0.16Hz Nominal Molarity	10 dip NaCl		10 dip KCl	
	G_b(nS)	m	G_b(nS)	m
2.0×10^{-4}	134	0.58	160	0.64
2.0×10^{-3}	134	0.64	170	0.65
2.0×10^{-2}	100	0.55	226	0.62
2.0×10^{-1}	134	0.58	180	0.64
2.0×10^{-1}	115	0.62	160	0.64

(e)

Values at 0.16Hz Nominal Molarity	20 dip KCl		30 dip KCl	
	G_b(nS)	m	G_b(nS)	m
2.0×10^{-4}	55	0.55	21	0.75
2.0×10^{-3}	55	0.55	27	0.80
2.0×10^{-2}	62	0.63	30	0.79
2.0×10^{-1}	70	0.68	30	0.79
2.0×10^{-1}	46	0.62	23	0.85

(f)

Values at 10 Hz Nominal Molarity	10 dip NaCl	10 dip KCl	20 dip KCl	30 dip KCl
	G_b(μS)	G_b(μS)	G_b(μS)	G_b(μS)
2.0×10^{-4}	1.19	1.17	0.32	0.13
2.0×10^{-3}	1.44	1.28	0.81	0.34
2.0×10^{-2}	1.56	1.70	0.98	0.51
2.0×10^{-1}	2.07	2.00	1.12	0.89
2.0×10^{-1}	1.09	1.17	0.30	0.21

(g)

Table 8.3 Film capacitance, C_b conductance, C_b, n and m for PBMA deposited onto platinum electrodes and immersed in a range of NaCl and KCl molarities. The capacitance data were estimated from the curves shown in fig 8.5a to 8.8a and are given at (a,b) 0.16Hz, (c) 10Hz and (d) the loss/capacitance cross over points. The conductance data are given at (c,f) 0.16Hz and (g) 10Hz only, estimated from the loss curves of fig 8.5b to 8.8b.

conductivity, ie a value of 1.5×10^{-7} S, which, to within experimental error, is equal to the value of conductivity measured in KCl of $1.8\pm0.3\times10^{-7}$ S. This assumes that the film conductivity is dominated by the presence of electrolyte ions and that the relative ionic mobilities are the same in the film as in the bulk electrolyte. It is noteworthy that by 10Hz there is little difference between the film conductance measured in NaCl and KCl solutions, although at 10Hz the film conductance now shows some dependence on electrolyte molarity (fig 8.11b).

As previously discussed for barium stearate coated platinum electrodes ($7.3.1), these results suggest that electrolyte ions are also able to penetrate the PBMA film, producing an increase in its capacitance at frequencies below the $C_T/(G_T/2\pi f)$ cross-over point. It is suggested that the low frequency dispersion observed in $G_T/2\pi f$ may be due to the migration of ions within pinholes in the film in response to the applied ac field. However, as the excitation frequency increases, the ions become less able to follow the field. Therefore, the finite mobility of the ions in the coating results in a frequency dependent contribution to the measured dielectric permittivity of the film. This model would explain why, by 10Hz the nature of the electrolyte no longer influences the film conductance. A similar model was proposed to explain the dispersions in the PVC curves ($5.5) and would explain the observed dependence of the dispersions in the PBMA loss on electrolyte, electrolyte molarity and film thickness. In addition, the smaller molarity dependence exhibited by the thicker films could reflect a reduction in the number of film defects, allowing fewer ions to penetrate the film.

Although there is no clear trend of increasing m with molarity, there is a thickness dependency (fig 8.10). Interestingly for conductances, the thicker film shows the strongest power law dependence ($m\approx0.8$ for the 30 dip sample whereas for the thinner samples $m\approx0.60\pm0.05$). This may indicate that for the thinner films, the dominant conductance mechanism is due to the movement of ions in pin hole defects, whereas for the thicker films, the reduced number of pin hole defects, as shown by the lower film conductances (fig 8.10b), means that the conductance of the film is more important. From the plots of n as a function of electrolyte molarity, it can be seen that the power law dependence of C_b on frequency is relatively weak for the thicker films, $n \approx 0.23 \pm 0.02$ but is much stronger for the thinner films. If the double layer capacitance, C_d, contributes to the frequency dependence of C_T in the frequency range 1 to 1000Hz, the fall in frequency dependence of C_T with increasing film thickness could be because the influence of C_d on C_T decreases as the ratio C_d:C_b increases (equation 5.10, $5.3).

Further insight into thickness dependent trends of the PBMA coated platinum electrodes is provided by the plots of reciprocal capacitance and conductance in figures 8.13 to 8.15. The decrease in film conductance and capacitance with increasing film thickness is as expected from the dependence of C_b and G_b on the inverse of the film thickness (equations 5.1 and 5.3, figs 8.13 to 8.15). The reasonable agreement between these plots and theory indicates that PBMA deposition onto platinum is reproducible and results in a multilayer film structure (Roberts, 1985).

In order to compare monolayer film properties, the film conductivity σ, and permittivity ϵ_r per monolayer, were estimated from the capacitance and conductance data (Table 8.3) assuming a PBMA monolayer thickness of 0.7nm. This figure was calculated from the mole volume of PBMA ($1.35 \times 10^{-4} m^3$/mole in rubbery, amorphous form at 25°C, Van Krevelen and Hoftyzer, 1976) and the experimentally determined molecular area for PBMA. Therefore;

$$\text{PBMA monomer thickness} \approx 1.35 \times 10^{-4} / (6.023 \times 10^{23} \times 31 \times 10^{-20}) \approx 0.7\text{nm}$$

The variation of the monolayer film permittivity at i) 0.16Hz, ii) 10Hz and iii) the cross-over frequency and conductivity per monolayer, at i) 0.16Hz and ii) 10Hz, as a function of electrolyte molarity are shown in fig 8.16 to fig 8.18 respectively. The error bars in figs 8.16 and 8.18 represent the uncertainties in ϵ_r and σ, based on the lines of best fit to the points in figs 8.13 to 8.15. Interestingly, a similar expression to that relating the coating capacitance to electrolyte molarity can be used for the film permittivity at $1/2\pi$ Hz;

$$\log(\text{Permittivity}) = D\log(\text{Molarity}) + E$$

where, from fig 8.15a, $D = 0.10 \pm 0.01$ and $E = 1.70 \pm 0.02$. As D was evaluated from the gradients of the capacitance vs coating thickness curves of fig 8.13a, it is reasonable that it should equal the average value of A given earlier. The values of ϵ_r and σ are summarised in Table 8.4.

From the plots of dielectric permittivity ϵ_r, as a function of KCl concentration, it is clear that at 0.16Hz, (fig 8.16a) and 10Hz (fig 8.17a), ϵ_r is molarity dependent. However, at the higher cross-over frequencies this dependence has disappeared (fig 8.18). As observed for barium stearate coated substrates (§7), ϵ_r is highest at low frequencies, having an average value of ca 20 at 0.16Hz and ca 6 at 10Hz. By the cross-over frequencies, the average value of ϵ_r has fallen to around 1. This is lower than the expected value of 3 for PBMA and suggests that either a dispersion has occurred in the PBMA or that the true thickness of the film is greater than that used in the calculations.

The film conductivity shows no clear dependence on electrolyte molarity at 0.16Hz. However, by 10Hz, a marked increase in σ occurs as the concentration of the electrolyte is raised. This corresponds to the low frequency dispersion on the double log plots (figures 8.5 to 8.8). The film conductivity is ca 90pSm^{-1} at 0.16Hz and 1100pSm^{-1} at 10Hz. These values compare favourably with Barium Stearate coatings on platinum and are indicative of good quality coverage (§7.5).

Data for 10 dip PBMA/Pt electrode in NaCl					
	Permittivity			Conductivity	
Molarity/ Frequency	0.16Hz	10Hz	Cross-Over Frequency	0.16Hz pS/m	10Hz pS/m
2.0x10^{-4}	15.9	3.2	1.5	100	883
2.0x10^{-3}	20.1	4.9	1.3	100	1070
2.0x10^{-2}	21.0	6.5	1.2	74	1160
2.0x10^{-1}	29.4	9.5	1.4	100	1540
2.0x10^{-4}	15.1	3.2	1.5	85	813

(a)

Data for 10 dip PBMA/Pt electrode in KCl					
	Permittivity			Conductivity	
Molarity/ Frequency	0.16Hz	10Hz	Cross-Over Frequency	0.16Hz pS/m	10Hz pS/m
2.0x10^{-4}	18.1	3.6	1.7	119	869
2.0x10^{-3}	18.7	4.3	1.3	126	951
2.0x10^{-2}	25.5	6.4	1.1	168	1260
2.0x10^{-1}	31.1	9.9	1.4	134	1490
2.0x10^{-4}	16.1	3.4	1.5	119	869

(b)

Data for 20 dip PBMA/Pt electrode in KCl					
	Permittivity			Conductivity	
Molarity/ Frequency	0.16Hz	10Hz	Cross-Over Frequency	0.16Hz pS/m	10Hz pS/m
2.0x10^{-4}	12.6	3.1	1.0	82	469
2.0x10^{-3}	16.8	4.8	0.8	82	1200
2.0x10^{-2}	20.0	6.7	0.7	93	1460
2.0x10^{-1}	28.9	11.0	1.0	104	1670
2.0x10^{-4}	9.9	2.7	0.9	69	450

(c)

Data for 30 dip PBMA/Pt electrode in KCl					
	Permittivity			Conductivity	
Molarity/ Frequency	0.16Hz	10Hz	Cross-Over Frequency	0.16Hz pS/m	10Hz pS/m
2.0x10^{-4}	10.0	1.9	0.7	46	401
2.0x10^{-3}	12.1	2.8	0.6	61	758
2.0x10^{-2}	16.4	4.7	0.6	68	1140
2.0x10^{-1}	22.1	7.8	---	68	1980
2.0x10^{-4}	8.4	1.9	0.7	51	468

(d)

Table 8.4 (a) Dielectric permittivities and (b) conductivities for PBMA coated platinum electrodes, immersed in KCl. The values were calculated from the data in Table 8.3, assuming a monolayer thickness of 0.7nm.

The combination of high but stable molarity dependent ϵ_r values at 0.16Hz and 10Hz and the molarity dependence of σ at 10Hz suggest that electrolyte ions are able to diffuse into the film. As discussed previously for $BaSt_2$ coated platinum electrodes ($7.3.1), it is suggested that below the high frequency dispersion, ions within the film respond to the applied electric field, producing an increase in the effective conductivity and permittivity of the coating. At and beyond the high frequency dispersion, the frequency of the electric field becomes too great for the ions to respond to and the measured ϵ_r becomes that of the film in the absence of electrolyte ions.

Further information concerning the quality of the PBMA films can be obtained by estimating the percentage of defects in the films (Table 8.5). Assuming that the measured capacitance is the combination of defect free regions of PBMA and pinholes filled with electrolyte forming double layers (equation 5.4), the defect coverages range from 27% for a 10 dip coated electrode in 0.2mM KCl at 0.16Hz to 0.0% for 20 and 30 dip coated electrodes at 10Hz and the cross-over frequencies. Furthermore, the defect coverage clearly falls with increasing film thickness. If the defect coverage is estimated from the film conductivity, assuming that the measured conductivity is due to regions of "intact" film with pin holes filled with electrolyte, the percentage coverage in such defects ranges from 2.5×10^{-5}% for 10 dip films in 0.2mM electrolyte down to 1.6×10^{-9}% for a 30 dip film in 200mM KCl. As previously ($7), these estimates are much lower than those based on the capacitance measurements. It is noteworthy that the estimates of defect coverage show a marked dependence on electrolyte molarity. This is because the molarity dependence of the coating conductivity and permittivity is lower than that for the electrolyte conductivity and double layer capacitance.

To further characterise the PBMA films, a 10 dip coated platinum electrode was tested in a range of 20mM electrolytes in the sequence; $CaCl_2$, KI, NaCl, KCl, $CaCl_2$. The results are presented in the double log plots of figs 8.19 to 8.21, each showing

% defect coverages at 0.16Hz from C_b data				
Molarity/ Frequency	10 dip NaCl	10 dip KCl	20 dip KCl	30 dip KCl
$2.0x10^{-4}$	27.0	31.5	9.8	4.7
$2.0x10^{-3}$	10.9	10.0	4.3	1.9
$2.0x10^{-2}$	3.6	4.4	1.7	0.9
$2.0x10^{-1}$	1.6	1.8	0.8	0.4
$2.0x10^{-4}$	25.3	27.3	7.0	3.6

(a)

% defect coverages at 10 Hz from C_b data				
Molarity/ Frequency	10 dip NaCl	10 dip KCl	20 dip KCl	30 dip KCl
$2.0x10^{-4}$	0.4	1.3	0.1	---
$2.0x10^{-3}$	1.2	0.8	0.6	---
$2.0x10^{-2}$	0.7	0.7	0.4	---
$2.0x10^{-1}$	0.4	0.4	0.3	---
$2.0x10^{-4}$	0.4	0.7	---	---

(b)

% defect coverages at 0.16Hz from G_b data				
Molarity/ Frequency	10 dip NaCl	10 dip KCl	20 dip KCl	30 dip KCl
$2.0x10^{-4}$	$1.6x10^{-6}$	$2.2x10^{-6}$	$1.1x10^{-6}$	---
$2.0x10^{-3}$	$1.9x10^{-7}$	$2.4x10^{-7}$	$1.1x10^{-7}$	$4.4x10^{-8}$
$2.0x10^{-2}$	$1.3x10^{-8}$	$4.3x10^{-8}$	$1.6x10^{-8}$	$7.5x10^{-9}$
$2.0x10^{-1}$	$4.0x10^{-9}$	$6.6x10^{-9}$	$4.4x10^{-9}$	$1.6x10^{-9}$
$2.0x10^{-4}$	$1.2x10^{-6}$	$2.2x10^{-6}$	$6.9x10^{-7}$	$1.5x10^{-7}$

(c)

% defect coverages at 10 Hz from G_b data				
Molarity/ Frequency	10 dip NaCl	10 dip KCl	20 dip KCl	30 dip KCl
$2.0x10^{-4}$	$2.5x10^{-5}$	$2.5x10^{-5}$	$1.3x10^{-5}$	$1.1x10^{-5}$
$2.0x10^{-3}$	$3.6x10^{-6}$	$2.7x10^{-6}$	$3.5x10^{-6}$	$2.2x10^{-6}$
$2.0x10^{-2}$	$5.3x10^{-7}$	$4.3x10^{-7}$	$5.0x10^{-7}$	$3.8x10^{-7}$
$2.0x10^{-1}$	$1.1x10^{-7}$	$1.1x10^{-7}$	$1.2x10^{-7}$	$1.5x10^{-7}$
$2.0x10^{-4}$	$2.4x10^{-5}$	$2.5x10^{-5}$	$1.2x10^{-5}$	$1.3x10^{-5}$

(d)

Table 8.5 Percentage defect coverages for PBMA coated platinum wire electrodes in NaCl and KCl. The defect coverages were estimated from i) (a,b) the experimentally determined coating capacitance assuming that an intact film would have a dielectric permittivity of 3 (equation 5.3) and ii) (c,d) the experimentally determined coating conductance using (b) equation 5.2 (Stelzle and Sackmann, 1989). In order to evaluate equation 5.2, it was assumed that an intact film of PBMA would have a conductivity of $23pSm^{-1}$, which was the lowest value measured. NB There were no valid defect coverage estimates based on ϵ_r data at the cross-over frequencies because $\epsilon_r < 3$.

capacitance, C_T and loss, $G_T/2\pi f$ as a function of frequency for the two measurements in $CaCl_2$, along with curves for one of the other electrolytes. It is noteworthy that the coatings appear less stable when tested in a range of 20mM electrolytes than when tested in one electrolyte at different molarities (figs 8.5 to 8.8). Even so, at frequencies below about 100Hz, where the cell admittance is characteristic of the electrode coating, only the loss curve for the 10 dip coated electrode in KI falls outside the two results in $CaCl_2$.

The electrolyte dependent behaviour of the film is shown clearly by the plots of coating capacitance at i) 0.16Hz, ii) 10Hz, iii) the high frequency cross over point of the C_T and $G_T/2\pi f$ curves and conductance at i) 0.16Hz, ii) 10Hz and n, m as a function of electrolyte (figs 8.22 to 8.25). The data is summarised in Table 8.6.

From fig 8.22b, it is again apparent that only the film conductance in KI lies outside the values measured in $CaCl_2$, being about 12% higher. It is interesting that the power law frequency dependencies, n and m also reveal electrolyte dependent behaviour (fig 8.23). The values of n for KI and KCl are both more negative than the lowest value estimated from the curves in $CaCl_2$, being ≈ -0.31 and ≈ -0.33 compared to ≈ -0.30 respectively. However, the differences between these values are small, particularly in comparison to the difference of ≈ 0.2 between m in KI and the other electrolytes (m in KI is ≈ 0.62, compared to ≈ 0.42 in the other electrolytes). From these results it is apparent that the PBMA film conductance shows a slight dependence on I^- ions, the importance of which is discussed more fully in section 8.3.3. The dielectric permittivities of the film, estimated in the different electrolytes range from 32 at 0.16Hz to 1.1 at the cross over frequency and are similar to those obtained for 10, 20 and 30 dip coated platinum electrodes (Table 8.7). Conductivities and defect coverages are also similar in magnitude to those discussed previously.

Electrolyte	10 dip PBMA/Pt at 0.16Hz			
	C_b(μF)	n	G_b(μS)	m
$CaCl_2$	0.272	-0.23	0.142	0.61
KI	0.340	-0.32	0.257	0.42
NaCl	0.333	-0.28	0.222	0.61
KCl	0.362	-0.33	0.200	0.61
$CaCl_2$	0.386	-0.30	0.226	0.62

(a)

Electrolyte	10 dip PBMA/Pt		
	C_b(nF) 10 Hz	C_b(nF) X-over	G_b(μS) 10 Hz
$CaCl_2$	92	15	2.61
KI	100	13	3.22
NaCl	104	21	3.16
KCl	96	18	3.36
$CaCl_2$	104	18	3.36

(b)

Table 8.6 Film capacitance, C_b, Conductance, G_b, n and m for a 10 dip coated platinum electrode immersed in a range of 20mM electrolytes. The capacitance and n data were estimated from the curves shown in fig 8.19a to 8.21a and are given at (a) 0.16Hz (b) 10Hz and (b) the loss/capacitance cross over points. The conductance and m data are given at (a) 0.16 and (b) 10Hz only, estimated from the loss curves of fig 8.19b to 8.21b.

Data for 10 dip PBMA/Pt electrode in a range of 20mM electrolytes					
	Permittivity			Conductivity	
Molarity/ Frequency	0.16Hz	10Hz	Cross-Over Frequency	0.16Hz pS/m	10Hz pS/m
$CaCl_2$	22.8	7.7	1.3	105	1940
KI	28.5	8.4	1.1	168	2390
NaCl	27.9	8.7	1.7	165	2350
KCl	30.4	8.1	1.5	149	2490
$CaCl_2$	32.4	8.7	1.5	168	2490

(a)

Electro- lyte	% defects based on C_b			% defects based on G_b	
	0.16Hz	10Hz	X-over	0.16Hz	10Hz
$CaCl_2$	2.6	0.6	---	2.4x10^{-8}	7.6x10^{-7}
KI	5.0	1.1	---	4.3x10^{-8}	8.3x10^{-7}
NaCl	4.9	1.1	---	5.7x10^{-8}	1.1x10^{-6}
KCl	5.4	1.0	---	3.6x10^{-8}	8.6x10^{-7}
$CaCl_2$	3.9	0.8	---	4.9x10^{-8}	9.9x10^{-7}

(b)

Table 8.7 (a) PBMA monolayer permittivities and conductivities estimated from the data in Table 8.6, assuming a monolayer thickness of 0.7nm. (b) The defect coverages were estimated from the experimental values of C_b and a theoretical estimate of the double layer capacitance, (equation 5.3, Stelzle and Sackmann, 1989) assuming a dielectric permittivity of 3. The values of defect coverage were estimated from the conductance data using equation 5.2, and the lowest measured value of conductivity for PBMA coated onto platinum of 23pSm^{-1}.

Figs 8.26 shows cyclic voltammograms for a bare and PBMA coated platinum wire in a 1mM solution of potassium ferricyanide, obtained using a sweep rate of 0.1V/second at a temperature of 21°C and with 200mM KCl as the supporting electrolyte. The solid line is for an uncoated electrode and the dashed lines represent CV's for the same electrode with a 10 dip coating of PBMA after 0 and 30 minutes exposure to the electrolyte. The marked reduction in electrode current indicates that the PBMA film blocks significantly the electrode reaction, whilst the small increase in electrode current with time confirms the stability of the film.

The dependence of the peak electrode currents, i_{pa} and i_{pc}, on (sweep rate)$^{1/2}$ are shown in the Levich plots of fig 8.27 ($6.4.1). The roughly equal reduction in electrode current about the x-axis suggests that the reaction, although markedly reduced, is still reversible for the range of sweep rates employed. However, the increase in peak separation with (sweep rate)$^{1/2}$ (fig 7.28) indicates that the reaction is at least restricting diffusion of the redox species to and from the electrode surface.

To determine if the PBMA exhibits any charge dependent effects, CV's were also measured for electrodes using benzyl viologen ($7.3.2). Fig 8.29 shows CV's for bare and PBMA coated platinum wire electrodes in 1mM benzyl viologen, obtained using a sweep rate of 0.1V/second at 21°C and with a supporting electrolyte of 200mM KCl. As previously, the solid line is for an uncoated electrode and the dashed lines are for CV's measured using the same electrode with a 10 dip coating of PBMA after 0 and 30 minutes exposure to the electrolyte. The marked reduction in electrode current indicates that the PBMA coating is blocking access of the redox species to the electrode surface. This is also shown clearly by plots of electrode currents as a function of (sweep rate)$^{1/2}$ (fig 8.30). The approximate symmetry of the electrode currents indicates that the electrode reaction is still reversible. Finally, the difference between the peak currents measured for the coated electrodes in potassium ferricyanide and benzyl viologen may reflect differences in the quality of the electrode coverage.

It is apparent that the permittivity and conductivity of PBMA show some molarity dependence. This is attributed to the influence of the double layer capacitance on C_T at

$1/2\pi$Hz and at higher frequencies, to the presence of ions in the film. The dependence of film conductivity on ionic species suggests that ions are free to move within pin hole defects in the film. This means that if PBMA is used as an immobilising matrix, site access will not be restricted. Furthermore, the ability of PBMA to reduce the redox reaction at a platinum electrode during CV studies, using both positive and negative redox species, indicates that PBMA is suitably passive. Consequently it is concluded that PBMA is suitable for use as an immobilising matrix for ion selective species.

8.2.3.2 PBMA coated copper electrodes

Capacitance, C_T and loss ($G_T/2\pi f$) curves are shown in the double log plots of fig 8.31, as a function of frequency for copper electrodes dipped 10, 20 and 30 times through an LB film of PBMA ($ 8.2.1). The average deposition ratios were calculated to be 1.34, 1.07 and 0.94 respectively ($ 8.2.2) assuming X type deposition. Each electrode was tested in a 2mM KCl solution at exposure times of approximately 0, 30, 60 and 120 minutes. Results are presented for the electrodes when initially immersed in electrolyte ie an exposure time equal to zero. Reciprocal values for C_b estimated at i) 0.16Hz ii) 10Hz and iii) the $C_T/(G_T/2\pi f)$ high frequency crossing point and G_b at i) 0.16Hz ii) 10Hz, plotted as a function of coating thickness are shown in fig 8.32 and summarised in Table 8.8.

As expected, the mid-frequency plateau, which is representative of the coating capacitance, decreases in magnitude as the coating thickness increases (equation 5.3). Similarly, at frequencies below the high frequency loss peak, the coating conductance decreases, as the coating thickness increases (equation 5.1, Table 8.3). Based on a monolayer thickness of 0.7nm ($ 8.3.1), the dielectric permittivity is estimated to range from ≈25 at 0.16Hz for a 20 dip film down to 1.4 for a 30 dip film at the cross-over frequency. The dielectric permittivity is expected to be 3.0±0.3, based on literature values for poly-ethyl-methacrylate (Billmeyer, 1984). It is surprising that the value of ϵ_r is higher for the 20 dip film than for the 10 dip film at 0.16Hz. This may reflect the lower deposition ratio of 1.07 per dipping cycle estimated for the 20 dip film. The values of film conductivity range from $4.7 \times 10^{-9}Sm^{-1}$ down to $4.4 \times 10^{-11}Sm^{-1}$ at 0.16Hz. These values compare well with the value of $2 \times 10^{-9}Sm^{-1}$ for barium stearate coated copper electrodes and are indicative of high quality films.

If the higher than expected values of coating capacitance are due to regions of electrolyte double layer in contact with the electrode surface, the fractional coverage in such defects would be from 0 up to ca 9%. Whereas, if the film conductivity is due to regions of "intact" film containing pin hole defects filled with electrolyte, the fractional coverage is ca 1×10^{-5}% at 0.16Hz (Table 8.8).

Obviously, the values of fractional defect coverage are much lower, based on values of film conductance rather than capacitance. The difference between these estimates could be because patchy coverage gives rise to thin, high capacitance areas that are still sufficiently thick to result in only a small number of pin hole defects bridging the film. Furthermore, as the values of conductivity/monolayer and fractional defect coverage are markedly lower when calculated from the conductance of the 30 dip film than from the conductance of the thinner films, it appears that a nominal film thickness of around 30 layers is required to produce a significant reduction in the number of electrolyte pathways across the film (fig 8.31). Interestingly, a similar observation was made for PBMA coated platinum electrodes where m was significantly higher for the 30 dip film compared to the thinner films.

Coating Thickness	Capacitance			Conductance	
	0.16Hz (μF)	10Hz (nF)	Cross-Over (nF)	0.16Hz (μS)	10Hz (μS)
10	1.23	251	156	38	21
20	0.88	118	55	14	9.2
30	0.10	61	34	0.12	0.38

(a)

Coating Thickness	Permittivity			Conductivity	
	0.16Hz	10Hz	Cross-Over	0.16Hz	10Hz
10	17.2	3.5	2.2	4.7×10^{-9}	2.6×10^{-9}
20	24.7	3.3	1.5	3.5×10^{-9}	2.3×10^{-9}
30	4.4	2.5	1.4	4.4×10^{-11}	1.4×10^{-10}

(b)

Coating Thickness	% defects from C_b			% defects from G_b	
	0.16Hz	10Hz	Cross-Over	0.16Hz	10Hz
10	9.0	0.3	---	1.3×10^{-5}	7.0×10^{-6}
20	6.8	0.1	---	9.3×10^{-6}	6.0×10^{-6}
30	0.3	---	---	---	2.7×10^{-7}

(c)

Table 8.8 (a) Film capacitance, C_b, and Conductance, G_b for PBMA deposited onto sputtered copper electrodes and immersed in 2mM KCl. The capacitance data were estimated from the curves shown in fig 8.31a and are given at 0.16Hz, 10Hz and the loss/capacitance cross over points. The conductance data are given at 0.16Hz and 10Hz, estimated from the loss curves of fig 8.31b. (b) Dielectric permittivities and conductivities for PBMA coated platinum electrodes immersed in KCl. The values were calculated from the data in (a) assuming a monolayer thickness of 0.7nm. (c) Percentage defect coverages for PBMA coated sputtered copper electrodes. The defect coverages were estimated from (a) the experimentally determined coating capacitance assuming that an intact film would have a dielectric permittivity of 3 (equation 5.3) and the experimentally determined coating conductance using equation 5.2 (Stelzle and Sackmann, 1989). In order to evaluate equation 5.2, it was assumed that an intact film of PBMA would have a conductivity of 89pSm^{-1}, which was the lowest value measured for PBMA deposited onto sputtered copper electrodes.

An indication of film stability is given in the double log plots of ($G_T/2\pi f$) and C_T vs f for a copper electrode dipped 10 times through an LB film of PBMA (fig 8.33(a,b) and $ 8.2.1), with an average deposition ratio of 1.34 per dipping cycle ($ 8.2.2). The electrode was tested using a 2mM KCl solution at exposure times of 1.5, 35, 60, 125, 245 and 302 minutes. A gradual decrease in film conductance and capacitance is observed with increasing exposure time. This trend is shown clearly in fig 8.34 by the plots of C_b and G_b estimated at 10Hz from the curves in fig 8.33. It should be noted that this decrease contrasts with the normal increase in admittance observed for an uncoated copper electrode over a similar period of electrolyte exposure time (Table 7.6). The values of C_b, G_b, ϵ_r, σ estimated at 10Hz are presented in Table 8.9 along with the corresponding estimates of defect coverage. The defect coverages range from 0.7% after 1.5 minutes exposure down to 0% after 302 minutes, based on the capacitance measurements. The corresponding values based on the conductance measurements range from 5.9x10^{-6}% down to 1.3x10^{-6}% using equation 5.2. These results suggest that copper oxide is forming on the areas of exposed copper but does not disrupt the PBMA coating. Further support for

Data for PBMA/Cu at 10Hz						
Immersion Time	C_b (nF)	G_b (μS)	ϵ_r	σ (nS/m)	C_b % def	G_b % defects
1.5	296	18.0	4.1	2.23	0.7	5.9x10^{-6}
35	239	5.5	3.4	0.68	0.2	1.7x10^{-6}
60	228	4.9	3.2	0.61	0.1	1.5x10^{-6}
125	205	4.6	2.9	0.57	---	1.4x10^{-6}
245	171	4.5	2.4	0.55	---	1.4x10^{-6}
302	171	4.3	2.4	0.54	---	1.3x10^{-6}

Table 8.9 Coating capacitance, C_b, conductance, G_b, permittivity, ϵ_r, conductivity, σ, and defect coverages for a PBMA coated sputtered copper electrode as a function of electrolyte immersion time, estimated from the curves in fig 8.33. The defect coverages were estimated as outlined in Table 8.8.

this suggestion is provided by the variation in film capacitance and conductance with time shown in fig 8.35. The upper and lower traces show C_T and $G_T/2\pi f$ vs time, measured at a frequency of 220 Hz, in 2mM KCl. A frequency of 220 Hz was chosen to ensure that the admittance measurements were performed at a position on the capacitance plateau representative of the coating. This was later verified by measuring the cell admittance as a function of frequency. The resulting double log plot of capacitance as a function of frequency showed that at 220Hz, C_T was on that part of the curve characteristic of C_b. The initial increase in conductance and capacitance is followed by a steady decrease in their values. In general, similar results were obtained for 15, 20 and 30 dip films. In addition, a few admittance vs frequency results, measured at discrete time intervals showed this time-dependence. However, due to the relatively long time intervals between the admittance measurements, this trend was not always detected.

It is suggested that the initial increase in coating admittance is due to electrolyte ions penetrating the film when the electrode is first immersed in the electrolyte solution. Then, once through the film, the ions react at the electrode surface to produce copper oxide. The copper oxide formed in this way increases the effective thickness of the electrode coating, leading to the observed decrease in film capacitance and conductance with time (fig 8.35). That this does not produce an increase in the measured admittance, as in the case of $BaSt_2$ deposited onto copper electrodes, is due to the greater robustness of the polymer coating. Visual inspection of the electrode surface, before and after exposure of the electrode to the electrolyte solution, indicated that oxide growth increased with time.

As the time dependent behaviour of the electrodes was dominated by the oxide, rather than the PBMA film, it was concluded that experiments to consider the electrolyte and molarity dependence of the coating admittance were not practical on copper substrates. Subsequently, work was carried out on aluminium electrodes to couple the advantages of a large surface area electrode, with a reactive but self passivating oxide forming material ($7.5).

8.2.3.3 PBMA coated aluminium electrodes

Fig 8.36(a,b) shows double log plots of capacitance, C_T and loss, $(G_T/2\pi f)$ as a function of frequency for an aluminium electrode dipped 10 times through an LB film of PBMA ($ 8.2.1). An average deposition ratio per dipping cycle of 1.76 was calculated. The electrode was tested using a 2mM KCl solution at exposure times of approximately 0, 23, 40 and 60 minutes. A gradual increase in film conductance and capacitance is observed with increasing exposure time. The variation of C_b and G_b, estimated from fig 8.36, are shown as a function of electrolyte exposure time in fig 8.37. These values are summarised in Table 8.10. It should be noted that the increases in capacitance and conductance of the PBMA coated electrodes are greater than those observed for an uncoated aluminium electrode over the same period of electrolyte exposure time. This trend is opposite to that for the copper electrodes, where a decrease in admittance with time was observed ($ 8.2.3.2).

From the low frequency region of the C_T curves, the film capacitance is calculated to be $0.96\mu F/cm^2$ at $1/2\pi$ Hz. Based on a 20 layer film with a monolayer thickness of 0.7nm, the dielectric permittivity of the film is 9.0. By 10Hz, ϵ_r has fallen to 6.2, which is still higher than the expected value of 3 (Billmeyer, 1984). If the film and double layer capacitance are known, the fractional defect coverage can be estimated using equation 5.4. For example, using a value of $11.1\mu F/cm^2$ for the double layer capacitance, calculated from the Debye Length, the coverage by defects would be from 1.9% up to 3.4% after 60 minutes exposure to the electrolyte. This figure is much lower than the 12% based on the average deposition ratio of 1.76 per dipping cycle.

The value of G_b at $1/2\pi$ Hz is 5.6×10^{-8} S. Again assuming a 20 layer film, the film conductivity can be estimated from equation 5.1, to be 1.4×10^{-11} Sm^{-1}. If the film conductivity is assumed to be due to areas of "intact" film containing pin hole defects filled with electrolyte, the coverage in defects would be between 8.3×10^{-8} and 1.2×10^{-7}%. Again this figure is much lower than that suggested from the capacitance, indicating a similar situation to that seen for copper ($ 8.2.3.2).

The gradual increase in C_b and G_b with time is indicative of electrolyte ions penetrating the film (Table 8.10). As the observed changes in C_b and G_b exceed those measured for a bare aluminium electrode, the variations must be due to time dependent properties of the coating/electrolyte system. It is suggested that the time dependent changes in C_b and G_b are due to ion penetration rather than desorption of the film.

Data for PBMA/Al electrode in KCl					
	Capacitance			Conductance	
Immersion Time	0.16Hz (μF)	10Hz (μF)	Cross-Over (μF)	0.16Hz (μS)	10Hz (μS)
0	0.32	0.22	0.02	0.06	0.19
23	0.40	0.27	0.10	0.18	0.29
40	0.40	0.29	0.10	0.24	0.32
60	0.49	0.33	0.10	0.24	0.32

(a)

Data for PBMA/Al electrode in KCl					
	Permittivity			Conductivity	
Immersion Time	0.16Hz	10Hz	Cross-Over	0.16Hz	10Hz
0	9.0	6.2	1.3	1.4×10^{-11}	4.7×10^{-11}
23	11.2	7.6	5.6	4.5×10^{-11}	7.2×10^{-11}
40	11.2	8.1	5.6	6.0×10^{-11}	7.9×10^{-11}
60	11.7	9.2	5.6	6.0×10^{-11}	7.9×10^{-11}

(b)

Data for PBMA/Al electrode in KCl					
	% defects from C_b			% defects from G_b	
Immersion Time	0.16Hz	10Hz	Cross-Over	0.16Hz	10Hz
0	1.9	1.0	---	---	9.0×10^{-8}
23	2.6	1.4	0.8	8.3×10^{-8}	1.6×10^{-7}
40	2.6	1.6	0.8	1.2×10^{-7}	1.8×10^{-7}
60	3.4	2.0	0.8	1.2×10^{-7}	1.8×10^{-7}

(c)

Table 8.10 (a) Film capacitance, C_b, and Conductance, G_b for PBMA deposited onto evaporated aluminium electrodes and immersed in 2mM KCl. The capacitance data were estimated from the curves shown in fig 8.36a and are given at 0.16Hz, 10Hz and the loss/capacitance cross over points. The conductance data are given at 0.16 and 10Hz, estimated from the loss curves of fig 8.36b. (b) Dielectric permittivities and conductivities for PBMA coated aluminium electrodes immersed in KCl. The values were calculated from the data in (a) assuming a monolayer thickness of 0.7nm. (c) Percentage defect coverages for PBMA coated evaporated aluminium electrodes. The defect coverages were estimated from (a) the experimentally determined coating capacitance and double layer capacitance, assuming that an intact film would have a dielectric permittivity of 3 (equation 5.3) and the experimentally determined coating conductance using equation 5.2 (Stelzle and Sackmann, 1989). In order to evaluate equation 5.2, it was assumed that a film of PBMA would have a conductivity of $14pSm^{-1}$, which was the lowest value measured for PBMA deposited onto evaporated aluminium electrodes.

8.3 PBMA/Valinomycin Multilayers

Polymeric materials such as PVC have been used to immobilise valinomycin to produce potassium sensitive electrodes (eg Band and Kratochvil, 1974; Band et al, 1976; Cattrall and Tribuzio, 1974; \$2.3.3). Compared to such block polymers, LB films offer distinct advantages such as high molecular order for the immobilized species in an ultrathin coating (Fujihira and Poositisak, 1986(a,b); Fujihira and Araki, 1986a; \$3.6). Therefore, valinomycin was incorporated into a LB film of PBMA in order to fabricate a potassium ion sensor.

8.3.1 Preparation and characterisation of monolayer films at the air/water interface

Monolayers of valinomycin were prepared using a spreading solution of approximately 1.8mg/ml in chloroform (\$4.3.1.7). π-A characteristics for the valinomycin monolayers (fig 8.38) exhibited an S shaped curve with no distinct phase change, similar to those reported in the literature (Abraham and Ketterson, 1984; Peng et al, 1987; Howarth et al, 1987, although premature pressure saturation occurred as observed by Kemp and Wenner, (1972).

The PBMA/valinomycin monolayers showed similar characteristics to monolayers of pure valinomycin (fig 8.39). The mixed monolayers were formed with a spreading solution containing 1.07mg/ml PBMA and ca 0.3mg/ml valinomycin (\$ 4.3.1.7). Because of difficulties in weighing the valinomycin, its concentration was estimated from the π-A curve, assuming a molecular area of 2.7nm^2/molecule (Abraham and Ketterson, 1984). On this basis, the molar ratio of PBMA to valinomycin was estimated to be 30:1. The importance of the molar ratio of PBMA to valinomycin is discussed later with reference to the molecular packing of the monolayer film (\$ 8.3.2).

8.3.2 Deposition onto substrates

Mixed films of PBMA/Valinomycin were deposited onto platinum wire electrodes using both machine and hand dipping. It was found that the latter resulted in higher quality films. This is attributed to the higher dipping speeds achieved by hand deposition. In addition, the tip of each electrode was coated with a sphere of epoxy to eliminate the possibility of end effects. The average deposition ratio per cycle was estimated to be 1.74, compared to a value of 1.98 measured for pure PBMA films (8.2.2). This suggests that the presence of valinomycin has no seriously deleterious effect on the deposition process.

8.3.3 Admittance Measurements

Fig 8.40 shows admittance results for a 20 dip PBMA/valinomycin coated platinum electrode tested in 0.2, 2, 20, 200, 0.2mM NaCl solutions. The curves are similar in shape to those observed earlier (fig 8.6 to 8.9) for pure PBMA coated electrodes. Although, whilst the stability of the mixed film is high, as indicated by the good agreement between results for the initial and final test in 0.2mM NaCl, the conductance and capacitance per monolayer are higher for the mixed film than for the pure PBMA films of equivalent thickness.

When the same electrode was tested in KCl solutions of molarity 0.2, 2, 20 and 200mM the double log plots (fig 8.41), showed that $G_T/2\pi f$ and C_T rose in value at frequencies below 1kHz as the electrolyte molarity was increased. Consequently, there are marked differences between the film conductances and capacitances, measured in KCl and NaCl in this frequency range. The largest differences occur at and above 2mM concentrations, with the coating conductance in KCl being significantly higher than in NaCl. This is in marked contrast to the results for the pure PBMA films, where no significant differences in film admittance were observed ($8.3.1, figs 8.5 to 8.8).

Therefore, these results provide the first proof that the valinomycin is imparting ion selectivity to the electrode response.

The molarity and cation dependence of the film can be seen more clearly in the plots of film capacitance, measured in NaCl and KCl at (i) $1/2\pi$ Hz, (ii) 10Hz and (iii) the high frequency cross over point of the capacitance and loss curves, shown as a function of electrolyte molarity in figs 8.42a, 8.44a and 8.45. The equivalent conductance data, measured at $1/2\pi$Hz and 10Hz, are given in fig 8.42b and 8.44b, whilst values of n and m are shown in fig 8.43. The data is summarised in Table 8.11.

At $1/2\pi$Hz, the film capacitance increases more rapidly with electrolyte molarity in KCl than in NaCl. This contrasts with the pure film where there was no significant difference between the curves for the two electrolytes (fig 8.9a). There are also differences in values for n, which in the case of the pure film are reasonably stable at around -0.30, whereas for the PBMA/Val film n falls from -0.30 to -0.47 as the molarity is increased (fig 8.10a). The conductance of the mixed film measured in NaCl is comparable to that of a 10 dip PBMA film and therefore shows no significant molarity dependence ($8.3.1). In the case of the PBMA film, at 0.16Hz the conductance is higher in KCl than in NaCl but again shows no molarity dependence ($8.3.1). This is in marked contrast to the conductance of the PBMA/Val coating where a very significant molarity dependence is observed. The film conductance rises from 0.14μS to 0.63μS as the KCl concentration is increased from 0.2 to 200mM, providing clear evidence that the electrode coating conductance is $[K^+]$ dependent. There are no clear trends of m dependence on electrolyte molarity, with values of ≈0.63 in NaCl and ≈0.54 in KCl. By 10 Hz, the cation dependency of C_b and G_b are less marked. However, C_b and G_b are still clearly molarity dependent, with both the film capacitance and conductance being slightly greater in KCl

Nominal Molarity	NaCl		KCl	
	C_b(µF)	n	C_b(µF)	n
2.0×10^{-4}	0.15	-0.30	0.18	-0.29
2.0×10^{-3}	0.19	-0.31	0.22	-0.38
2.0×10^{-2}	0.23	-0.32	0.31	-0.44
2.0×10^{-1}	0.36	-0.27	0.55	-0.47
2.0×10^{-1}	0.16	-0.31	---	---

(a)

Nominal Molarity	NaCl		KCl	
	G_b(nS)	m	G_b(nS)	m
2.0×10^{-4}	143	0.62	143	0.61
2.0×10^{-3}	127	0.56	191	0.51
2.0×10^{-2}	148	0.67	358	0.47
2.0×10^{-1}	203	0.63	631	0.54
2.0×10^{-1}	127	0.66	---	---

(b)

Nominal Molarity	Data at 10Hz				Data at X-over	
	NaCl	KCl	NaCl	KCl	NaCl	KCl
	C_b(nF)	C_b(nF)	G_b(pS)	G_b(pS)	C_b(nF)	C_b(nF)
2.0×10^{-4}	43	51	833	890	25	23
2.0×10^{-3}	56	66	833	940	19	21
2.0×10^{-2}	75	78	1070	1230	20	18
2.0×10^{-1}	100	123	1490	1910	19	21
2.0×10^{-1}	43	---	833	---	21	---

(c)

Table 8.11 Film capacitance, C_b conductance, G_b, n and m for a 20 dip coating of PBMA/Valinomycin on platinum and immersed in a range of NaCl and KCl molarities. The capacitance data were estimated from the curves shown in fig 8.40a and 8.41a and are given at (a) 0.16Hz, (c) 10Hz and (c) the loss/capacitance cross over points. The conductance data are given at (b) 0.16 and (c) 10Hz only, estimated from the loss curves of fig 8.40b and 8.41b.

than in NaCl as observed for the PBMA films ($8.2.3.1). As expected from previous discussions, there is no apparent molarity or cation dependence in the film capacitance at the cross-over frequencies ($8.2.3.1).

The values of film permittivity and conductivity are summarised in Table 8.12.

Data for 20 dip PBMA/Val/Pt electrode in NaCl					
	Permittivity			Conductivity	
Molarity/ Frequency	0.16Hz	10Hz	Cross-Over Frequency	0.16Hz pS/m	10Hz pS/m
$2.0x10^{-4}$	24.8	7.2	2.1	212	1670
$2.0x10^{-3}$	32.5	9.3	1.6	188	1670
$2.0x10^{-2}$	38.8	12.5	1.7	220	2140
$2.0x10^{-1}$	60.1	16.8	1.6	302	2980
$2.0x10^{-4}$	27.2	7.2	1.7	188	1670

(a)

Data for 20 dip PBMA/Val/Pt electrode in KCl					
	Permittivity			Conductivity	
Molarity/ Frequency	0.16Hz	10Hz	Cross-Over Frequency	0.16Hz pS/m	10Hz pS/m
$2.0x10^{-4}$	30.3	8.6	1.9	212	1780
$2.0x10^{-3}$	37.0	11.0	1.7	284	1870
$2.0x10^{-2}$	51.5	13.1	1.5	532	2460
$2.0x10^{-1}$	93.0	20.6	1.7	937	3820

(b)

Table 8.12 Dielectric permittivities and conductivities for PBMA/Val coated platinum electrodes, immersed in (a) NaCl and (b) KCl. The values were calculated from the data in Table 8.11, assuming a monolayer thickness of 0.7nm.

Comparing these figures with those in Table 8.6 for a platinum electrode coated with a 10 dip film of PBMA, it is apparent that in NaCl at 0.16Hz and 10Hz, both ϵ_r and σ are approximately half those measured for the PBMA/Val film. By the cross-over frequencies, the difference is only around 25%. These results suggest that the mixed film has a greater number of defects than pure film, in spite of the reasonably close deposition ratios (§8.2.2).

From similar tests performed in KCl, at 0.16Hz the ϵ_r values ranged from 30.3 to 93.0, compared to 18.1 to 31.1 for the pure film. The film conductance values increased from 212pSm^{-1} to 937pSm^{-1} compared to a variation of only 119 to 168pSm^{-1} for the pure film. The valinomycin is clearly producing a [K$^+$] dependent response at 0.16Hz. Once again, at higher frequencies the differences in film conductance are much less marked.

Assuming ϵ_r=3, the defect coverages are estimated to range from ca 0.4% up to 28% for the PBMA/Val film based on the measured values of film capacitance. Similar values were obtained for the pure films. If, on the other hand, the defect coverages are estimated from the film conductance, assuming that an intact film would have a conductivity of 2.3x10^{-11}Sm^{-1}, the percentages are 2.5x10^{-4} down to 1.9x10^{-8} (Table 8.13). These values are higher than those estimated for the pure films and again suggest that the defect coverage is higher in the mixed film. This is attributed to the effect of the valinomycin molecules upon the packing of the PBMA polymer chains (fig 8.46) and also explains the difference in $G_T/2\pi f$, C_T between the mixed film and pure PBMA films tested in NaCl solutions. Based on the molecular areas of the PBMA monomer and valinomycin molecule, it was estimated that 11 PBMA monomer units are required to surround a valinomycin molecule. The actual mole ratio was 30:1 ($ 8.1). Even so it is likely that the addition of valinomycin to the monolayer will disrupt the packing of the PBMA chains. Any small cavities between PBMA and valinomycin molecules will increase the pinhole density in the multilayer coating, producing an increase in the film conductivity and capacitance. If the pinhole penetration by electrolyte is time dependent, the above model could also explain the gradual increase of coating admittance observed in fig 8.40.

To investigate further the electrolyte dependence of the mixed film, the same electrode was tested in various 20mM electrolytes in the sequence $CaCl_2$, KI, NaCl, KCl, $CaCl_2$. The results of these measurements are shown in the double log plots of fig 8.47. A comparison of the results for the initial and final test in $CaCl_2$ shows that there is a slow increase in C_T and $G_T/2\pi f$ with electrolyte exposure time. A similar time dependence was observed for a 10 dip PBMA coated platinum electrode ($8.3.1, fig 8.22 to 8.25). However, as the low frequency admittance of the electrode, when tested in KI and KCl solutions is higher than in the final $CaCl_2$ test, it is evident that the coating admittance is still measurably higher when the K^+ ions are present in the electrolyte. The decrease in coating admittance when a K^+ containing electrolyte is replaced by an electrolyte with a different cation shows that the processes giving rise to the increase in coating admittance are reversible. It should be noted that although the electrode was rinsed thoroughly in UPW before being replaced in a different electrolyte, it is possible that some K^+ ions have remained in the film, contributing to the apparent increase in coating admittance with time.

The electrolyte dependence of the film is summarised in terms of the coating capacitance, conductance, n and m, plotted as a function of electrolyte in figs 8.48 to 8.51 (Table 8.14). Similar data for a platinum electrode coated in a 10 dip film of PBMA are given for comparison. From fig 8.47, it is clear that the film conductance and

Data for PBMA/Val/Pt electrode in NaCl					
	% defects from C_b			% defects from G_b	
Molarity	0.16Hz	10Hz	Cross-Over	0.16Hz	10Hz
2x10^{-4}	22.1	4.3	---	5.0x10^{-6}	4.9x10^{-5}
2x10^{-3}	9.3	2.0	---	5.0x10^{-7}	5.8x10^{-6}
2x10^{-2}	3.5	0.9	---	8.3x10^{-8}	1.0x10^{-6}
2x10^{-1}	1.8	0.4	---	1.9x10^{-8}	2.2x10^{-7}
2x10^{-4}	24.5	4.3	---	4.5x10^{-6}	5.1x10^{-5}

(a)

Data for PBMA/Val/Pt electrode in KCl					
	% defects from C_b			% defects from G_b	
Molarity	0.16Hz	10Hz	Cross-Over	0.16Hz	10Hz
2x10^{-4}	27.6	5.6	---	2.5x10^{-4}	5.2x10^{-5}
2x10^{-3}	10.7	2.5	---	3.6x10^{-5}	5.5x10^{-6}
2x10^{-2}	4.8	1.0	---	8.5x10^{-6}	8.5x10^{-7}
2x10^{-1}	2.8	0.5	---	3.4x10^{-6}	2.8x10^{-7}

(b)

Table 8.13 Percentage defect coverages for PBMA/Val coated platinum wire electrodes in (a) NaCl and (b) KCl. The defect coverages were estimated from the experimentally determined coating capacitance and double layer capacitance, assuming that an intact film would have a dielectric permittivity of 3 (equation 5.3) and the experimentally determined coating conductance using equation 5.2 (Stelzle and Sackmann, 1989). In order to evaluate equation 5.2, it was assumed that an intact film of $BaSt_2$ would have a conductivity of 23pSm^{-1}, which was the lowest value measured. NB There were no valid defect coverage estimates based on ϵ_r data at the cross-over frequencies because $\epsilon_r < 3$.

capacitance are higher in KI and KCl than in $CaCl_2$ or NaCl, with the most significant differences arising in the film conductances. At $1/2\pi$Hz, G_b is 40% higher in KI and KCl than the highest value measured in $CaCl_2$. This compares to a difference of only 12% between the conductance of the pure film in KI and $CaCl_2$. By 10Hz, the ion dependent changes in film conductance are no greater than the difference between the initial and final tests in $CaCl_2$. n and m follow similar trends to those observed for the pure PBMA film. However, it should be noted that the average value of n for the mixed film is about -0.65, compared to -0.3 for the 10 dip PBMA film, while the values of m are lower for the mixed film than for the pure film. From these results it is clear that the conductance of the PBMA/valinomycin film is K^+ dependent. In addition, the close proximity of the film conductance in KI and KCl electrolytes, indicates that any I^- dependence of the pure film ($ 8.2.3.1) is insignificant compared to the K^+ dependence imparted by the presence of valinomycin.

The K^+ dependence of the film is seen clearly in the values of ϵ_r and σ summarised in Table 8.13. For example, at 0.16Hz, ϵ_r is ≈118 in KCl compared to an initial value of ≈75 in $CaCl_2$. The corresponding values of σ are 1040 and 401 pSm^{-1}. These values contrast with data for the pure PBMA film where ϵ_r ranged from 30.4 in KCl to 22.8 in $CaCl_2$ with corresponding conductivity data of 149 pSm^{-1} and 105 pSm^{-1}. Once again, the valinomycin is clearly imparting a K^+ selective response. If, as previously, it is assumed that an intact film of PBMA/Val should have a dielectric permittivity of 3, the defect coverage is estimated to range from ca 7% to 11% at 0.16Hz. The equivalent estimates based on the coating conductivity are $1.7x10^{-7}$ to $4.8x10^{-7}$%.

Further evidence of the potassium ion concentration $[K^+]$ dependent response of the electrode is presented in fig 8.52. The upper and lower traces show capacitance, C_T and loss, $G_T/2\pi f$ vs time, measured at a frequency of 1.0 Hz, as a function of electrolyte ionic composition. A valinomycin/PBMA electrode was immersed in a 20mM NaCl solution and allowed to come into equilibrium for ca 5 minutes. Then 2ml of the electrolyte was removed and replaced by 2ml of a 2M KCl solution, giving a final K^+ concentration of 200mM. Within 20 seconds, both C_T and $G_T/2\pi f$ increased rapidly to a new steady state, in response to the injection of potassium ions. It should be noted that

Data for 20 dip PBMA/Val/Pt electrode					
	C_b			G_b	
Molarity/ Frequency	0.16Hz (μF)	10Hz (nF)	Cross-Over (nF)	0.16Hz (μS)	10Hz (μS)
$CaCl_2$	0.45	113	61	0.27	3.8
KI	0.63	134	61	0.70	5.3
NaCl	0.52	113	61	0.35	4.1
KCl	0.70	140	61	0.70	5.3
$CaCl_2$	0.59	165	61	0.49	6.3

(a)

Data for 20 dip PBMA/Val/Pt electrode					
	Permittivity			Conductivity	
Molarity/ Frequency	0.16Hz	10Hz	Cross-Over Frequency	0.16Hz pS/m	10Hz pS/m
$CaCl_2$	74.7	19.0	10.2	401	5650
KI	105.7	22.5	10.2	1040	7890
NaCl	87.3	19.0	10.2	520	7900
KCl	117.5	23.5	10.2	1040	6140
$CaCl_2$	99.0	27.7	10.2	728	9330

(b)

Electro-lyte	% defects based on C_b			% defects based on G_b	
	0.16Hz	10Hz	X-over	0.16Hz	10Hz
$CaCl_2$	7.1	1.6	0.7	1.7×10^{-7}	2.7×10^{-6}
KI	10.1	1.9	0.7	4.8×10^{-7}	3.8×10^{-6}
NaCl	8.3	1.6	0.7	2.3×10^{-7}	2.9×10^{-6}
KCl	11.3	1.9	0.7	4.8×10^{-7}	3.8×10^{-6}
$CaCl_2$	9.5	2.4	0.7	3.3×10^{-7}	4.4×10^{-6}

(c)

Table 8.14 (a) Film capacitance, C_b, Conductance, G_b n and m for a 20 dip PBMA/Val coated platinum electrodes immersed in a range of 20mM electrolytes. The capacitance data were estimated from the curves shown in fig 8.46a and are given at 0.16Hz, 10Hz and the loss/capacitance cross over points. The conductance data are given at 0.16 and 10Hz only, estimated from the loss curves of fig 8.46b. (b) PBMA/Val monolayer permittivities and conductivities estimated from the data in (a), assuming a monolayer thickness of 0.7nm. (c) The defect coverages were estimated from the experimental values of C_b and a theoretical estimate of the double layer capacitance (equation 5.3, Stelzle and Sackmann, 1989) and assuming a dielectric permittivity of 3. The values of defect coverage were estimated from the conductance data using equation 5.2, assuming that the conductivity of an intact PBMA/Val film is $23pSm^{-1}$.

the electrode response time is probably dominated by the time taken for the NaCl and KCl solutions to mix properly.

At time t_3, the electrolyte was removed from the test cell and replaced with 20ml NaCl. The decrease in C_T and $G_T/2\pi f$ between t_3 and t_4 again shows that the electrode processes are reversible. The test cycle was repeated from t_4 to t_7. The dashed line shows $G_T/2\pi f$ and C_T when 2ml of 2M NaCl was added in place of the 2M KCl added previously. This result is a control to allow for the change in electrode admittance due to the increase in electrolyte concentration from 20mM to 200mM. Therefore the difference between the solid and dashed lines gives the dependence of the electrode coating on potassium ion concentration alone.

There are two possible reasons for the observed dependence of electrode coating admittance on $[K^+]$ (figs 8.41, 8.42, 8.47 and 8.52). The first is based on the assumption that the molecular area of the complexed valinomycin (val/K^+) is less than that of the uncomplexed valinomycin. That is, in the absence of K^+ ions, the valinomycin would be uncomplexed and the film pin hole density would be low. When K^+ ions are introduced into the electrolyte, some of the valinomycin molecules will become complexed with a concomitant reduction in area (Table 8.15), leaving gaps in the coating. As the $[K^+]$ is increased, so too would the number of complexed valinomycin molecules. Therefore the film capacitance and conductance would increase with increasing $[K^+]$. This model is supported by both X-ray data on crystalline valinomycin (Neupert-Laves and Dobler, 1975) and CPK space filling models (Kemp and Wenner, 1972; Abraham and Ketterson, 1984), which show that the molecular area of valinomycin is approximately 20% lower when complexed (Table 8.15). In monolayer studies, Kemp and Wenner (1972) calculated molecular areas from π-A curves for valinomycin and found that uncomplexed valinomycin has a molecular area 185–190Å^2 compared to 165Å^2 when complexed. Based on these values, the maximum change in area due to complexation would be 25Å^2. If this

Molecular Area ($Å^2$)	X-ray	Bond-lengths and angles	π-A LB monolayer	CPK Space Model	Cell Constants
Complexed Valinomycin	145(1)	---	266±32(3) 165 (4)	149(3)	---
Uncomplexed Valinomycin	188(2)	188(3)	266±32 (3) 185-190(4)	190(3)	168(3)

Table 8.15 Summary of molecular area estimates for valinomycin. (1) Neupert-Laves and Dobler (1975); (2) Smith et al (1975) ; (3) Abraham and Ketterson (1985); (4) Kemp and Wenner (1972).

resulted in a single, spherical defect in the film per molecule, its radius would be ≈4Å. Such a defect would be too small to permit penetration of hydrated K^+ ions.

In contrast to these findings, studies on monolayers of valinomycin by Abraham and Ketterson, (1984) suggest that the molecular area of valinomycin is independent of subphase conditions. The authors present π-A curves for valinomycin spread on NaCl and KCl subphases and state that both can be fitted by a molecular area at the point of inflexion of 2.66±0.32 nm^2/molecule. (These areas were projected from the CPK space-filling atomic model to give values of 1.5 to 1.9nm^2/molecule for the most and least compressed conformations respectively). No explanation of the different findings was presented by Abraham and Ketterson (1984). This means that if (i) the experimental conditions were such that the valinomycin was complexed when spread on a K^+ containing subphase and (ii) the monolayer properties of valinomycin better represent the valinomycin/PBMA multilayer than data on crystalline valinomycin, then it is unlikely that the molecular area of the valinomycin molecules entrapped in a multilayer of PBMA will be dependent upon the ionic composition of the test electrolyte.

Therefore, the second possible explanation of the observed results is that, when complexed, valinomycin molecules migrate through the multilayer film under the influence of the applied ac signal. This is analogous to the way in which valinomycin transports K^+ ions in biological membranes (Hille, 1984; $ 3.5.6). The finite mobility of the charged val/K^+ complex will result in a frequency dependent dielectric permittivity similar to that described earlier for ions (eg $8.2.3.1). As the number of complexed valinomycin molecules is a function of [K^+], the change in coating admittance would be too. It is interesting to note that the dependence of the mixed PBMA/Val film's conductance on the cation concentration is already markedly reduced by 10Hz, although a molarity dependence is still apparent. This suggests that the complex is unable to follow the electric field, even by around 10Hz because of its low mobility and provides further evidence that the complexed valinomycin is contributing to the film conductance.

8.4 Conclusions

Admittance and cyclic voltammetric analysis of PBMA coated platinum electrodes showed that the films are stable in an electrolyte environment. The PBMA films were passive in all the electrolytes used, with the exception of KI, where a slight increase in film conductance was observed, apparently induced by I^- ions. It was concluded that the stability and passivity of the PBMA films on platinum were sufficient for it to be used to immobilise ion selective species.

The only disadvantage in using platinum wire electrodes was their small surface area, which made it difficult to determine deposition ratios accurately ($7.2.2). The use of sputtered copper electrodes overcame this problem. However, it was not possible to obtain high reproducibility of deposition ratios, indeed, deposition ratios in the range 1.34 to 0.94 were measured during deposition experiments with quite large variations between coating layers. The variable quality of the deposition is reflected in the results as admittance measurements suggest that the films were patchy, although the σ values were low. The use of copper proved a disadvantage as the oxide growth dominated the time dependent behaviour of the electrodes ($7.4). This meant that experiments to consider the electrolyte and molarity dependence of the coating admittance were not practical on copper substrates. Subsequent work was therefore carried out on aluminium electrodes.

Preliminary admittance results for PBMA coated aluminium electrodes suggest that although the coating conductance is low, which is indicative of a good quality film, the relatively high dielectric permittivity implies that the coating is in fact of uneven thickness (§8.2.3.3). The increase in admittance with time shows that the electrolyte ions are able to gradually penetrate the film. Further work is required to improve film quality before investigating the properties of mixed films on aluminium electrodes.

Material	% change in ϵ_r at 0.16Hz		% change in σ at 0.16Hz	
	NaCl	KCl	NaCl	KCl
PBMA	46	42	26	29
PBMA/Valinomycin	59	67	29	77

Table 8.16 Summary of the maximum percentage changes in PBMA and PBMA/ Valinomycin permittivity and conductivity estimated from the admittance data during immersion in 0.2 to 200mM electrolyte.

Investigations of the PBMA/Valinomycin coated electrode show a [K^+] dependent response at frequencies below 10Hz. Proof that the incorporation of valinomycin in the PBMA film produces a [K^+] selective response may be provided by comparing the percentage increases in ϵ_r and σ with NaCl and KCl concentration (Table 8.16). For example, whilst there is only a 26-29% increase in σ for both films in NaCl and for the pure film in KCl, the conductivity of the mixed film increases by 77% for the same change in electrolyte concentration. It is probable that this response is due to the migration of complexed val/K^+ within the PBMA film. It may therefore be considered that the entrapped valinomycin molecules are active in transporting K^+. The sensitivity of a K^+ sensor using the film could be improved using compensation techniques. As the pure PBMA film shows a similar molarity dependent trend in NaCl and KCl to the mixed film in NaCl, this would provide a means of correcting for the influence of the "background" electrolyte. Such techniques, involving "subtraction" of the response of an active and control electrode have been reported for enzyme sensors (Morizumii et al, 1987, Rennenburg, 1986).

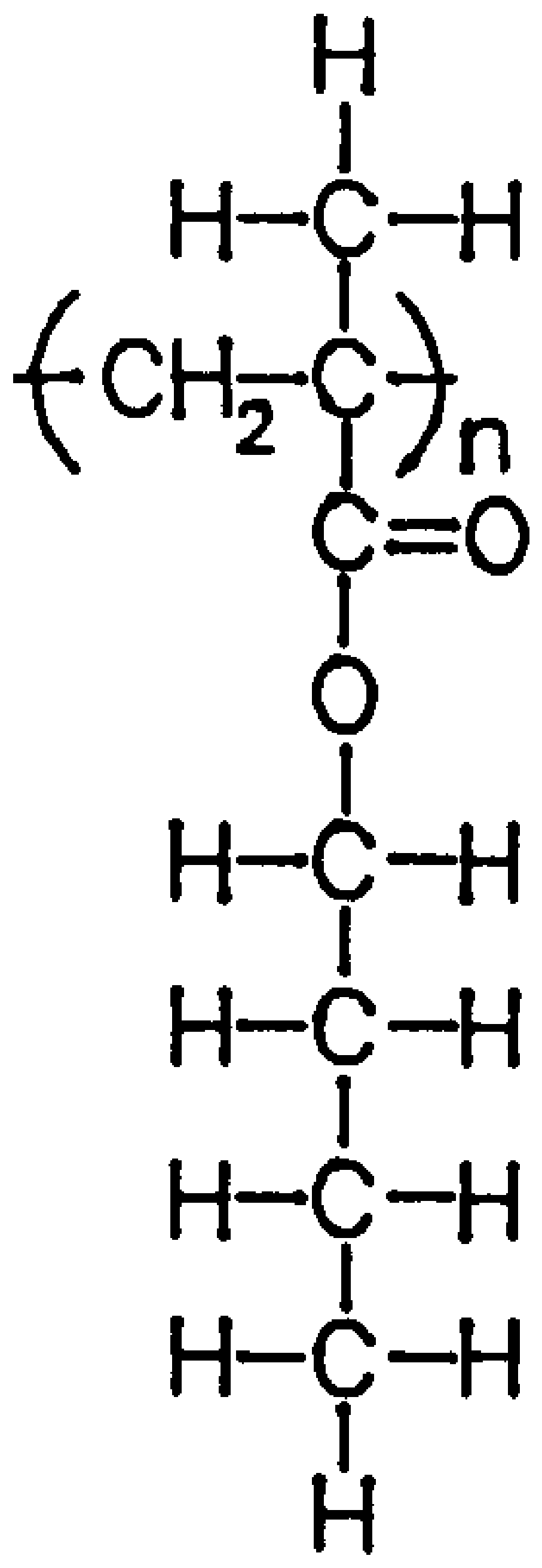

Fig 8.1 Structural formula for Poly-butyl-methacrylate (PBMA).

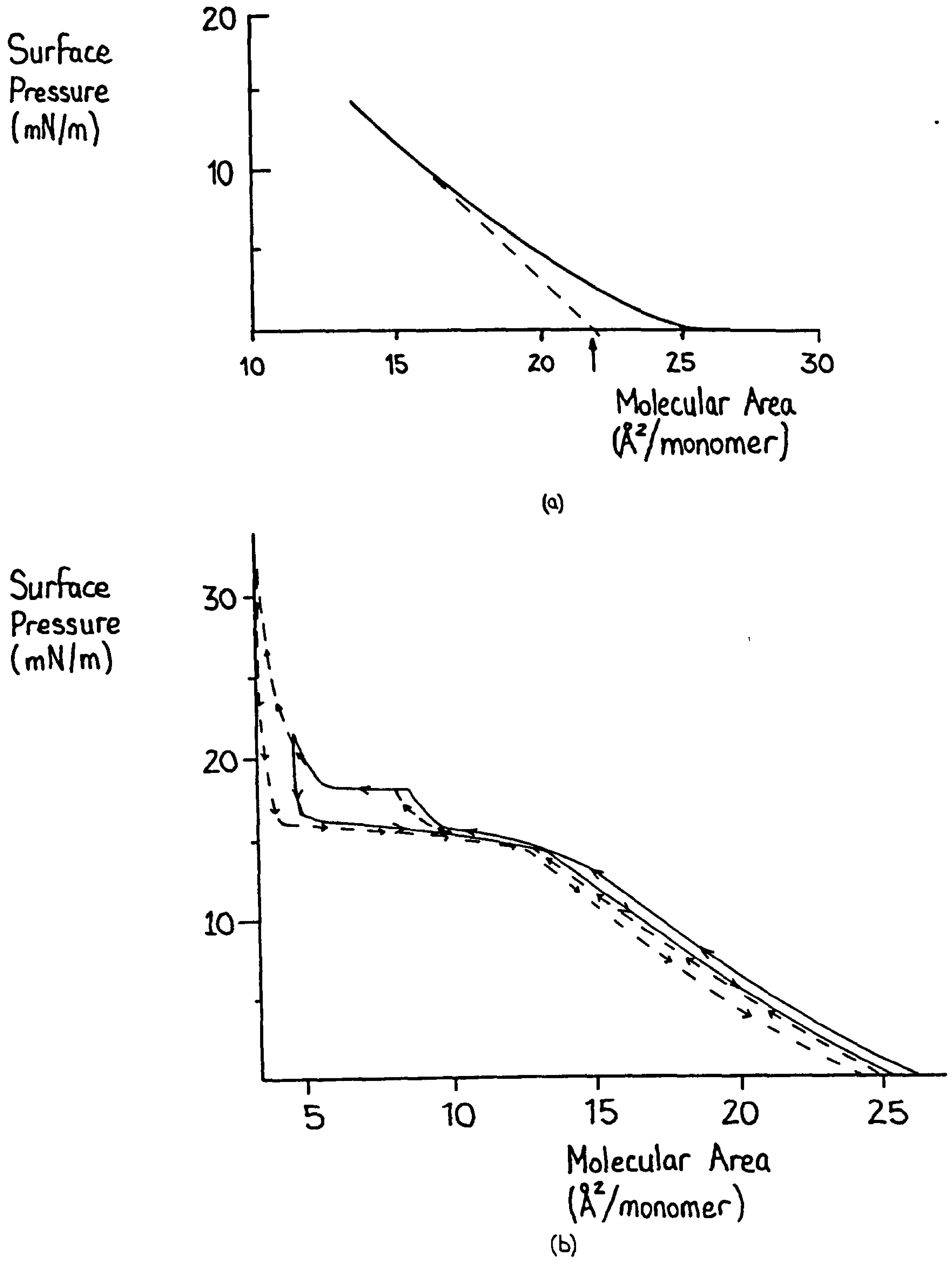

Fig 8.2 Pressure-Area Curves for PBMA (a) at 20°C ($A_0 = 22Å^2$) and (b) at 37°C ($31.2 \pm 2.3Å^2$). The dashed lines in (b) show the variation in curve shape during pressure cycling.

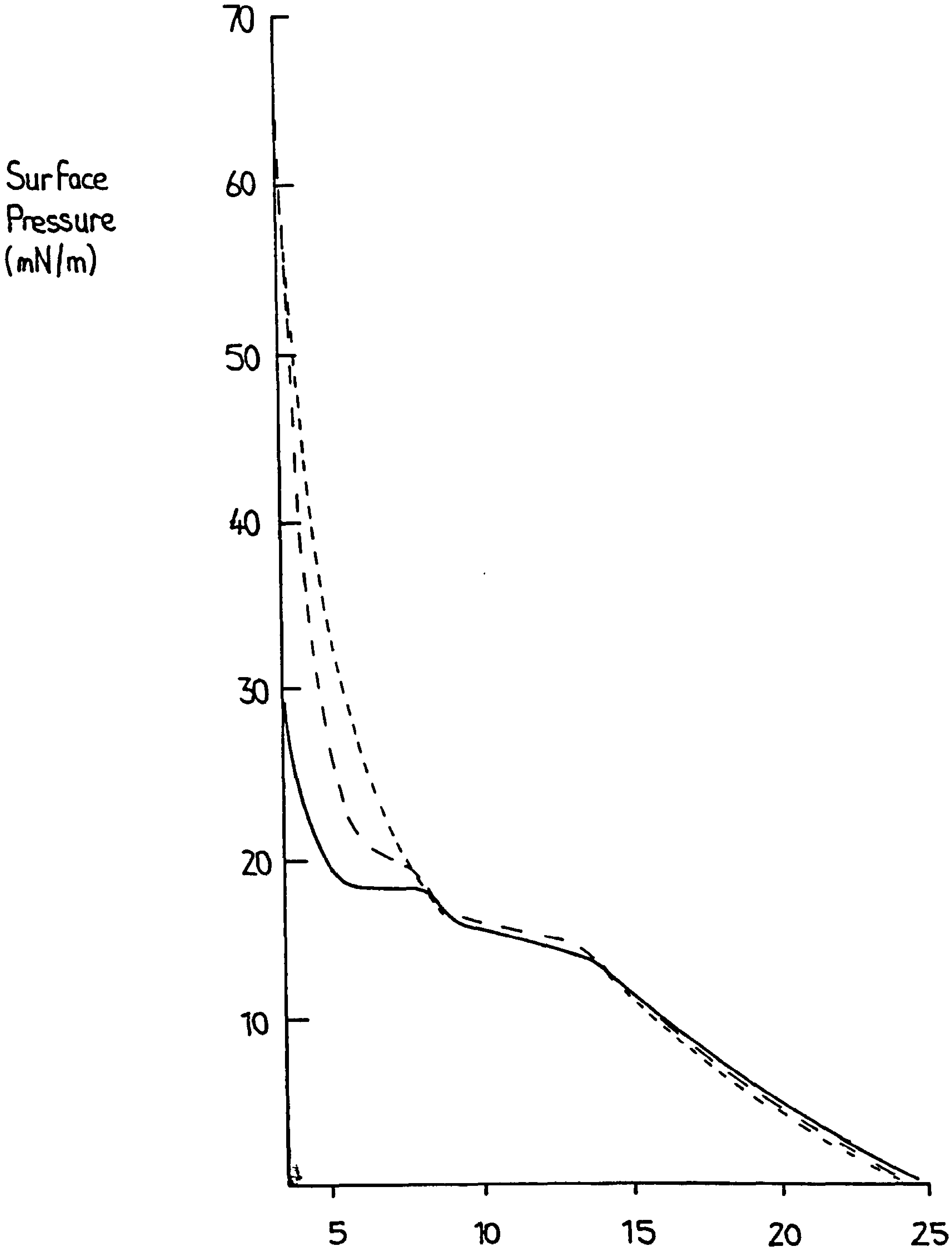

Fig 8.3 Pressure–Area Curves for PBMA at (—)20°C, (——)28°C and (- -) 37°C.

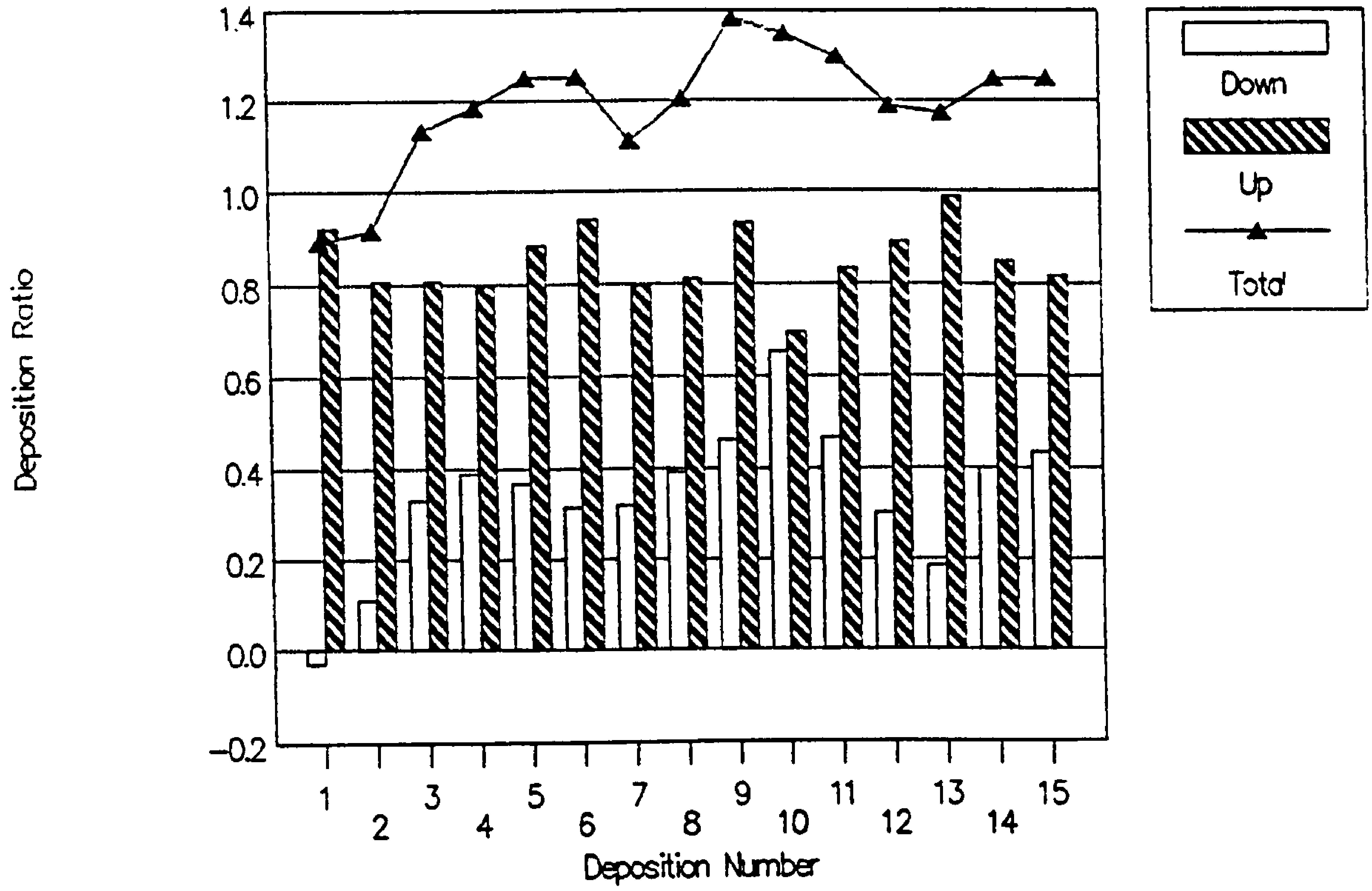

Fig 8.4 Deposition ratios for successive PBMA monolayers deposited onto sputtered copper electrodes plotted as a function of the number of the monolayer. The average deposition ratio overall, is 1.20±0.14.

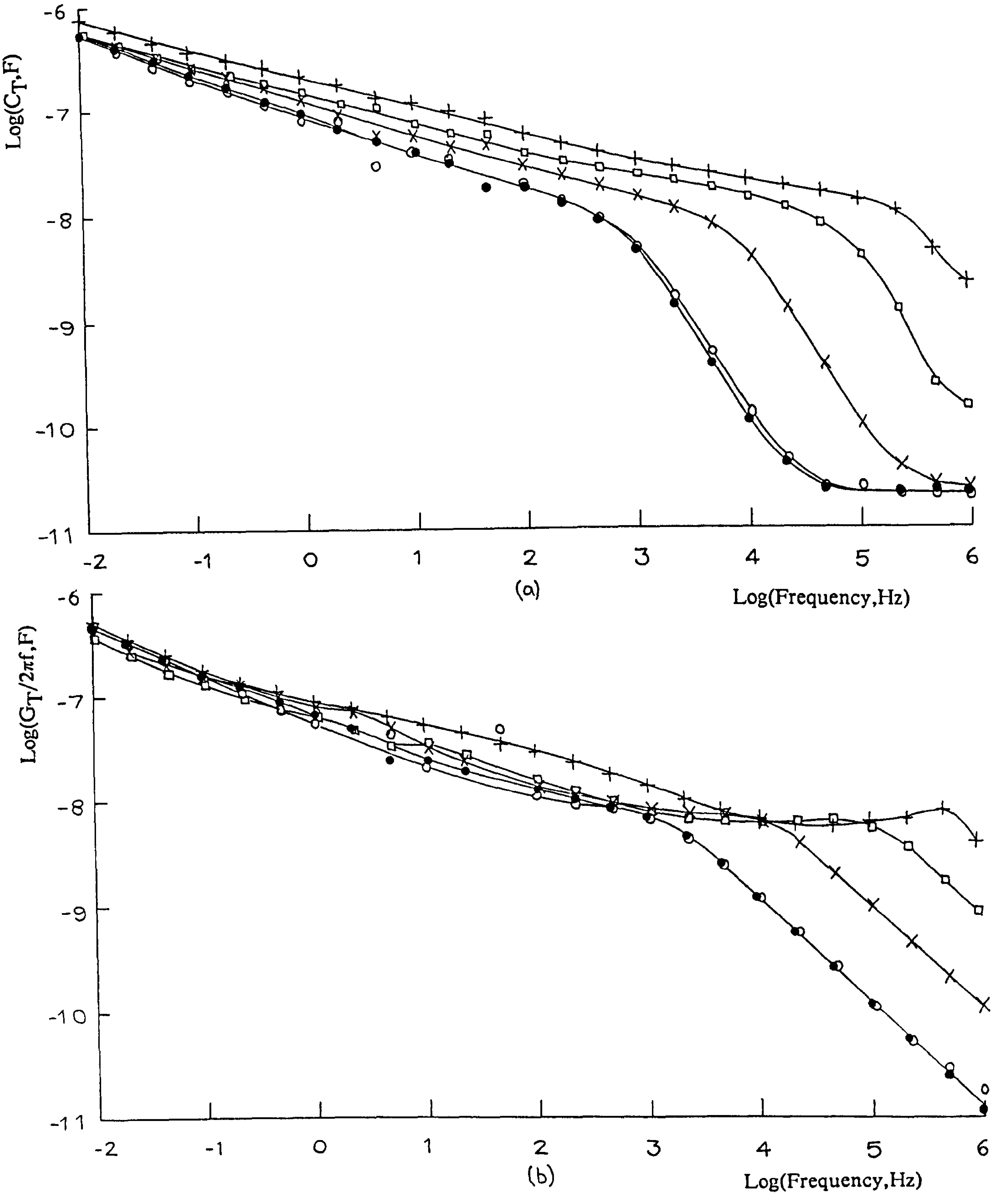

Fig 8.5 (a) Log Capacitance, C_T and (b) Loss ($G_T/2\pi f$) plotted against log frequency, F, for a platinum electrode coated in 20 monolayers of PBMA and immersed in (•)0.2mM, (x) 2.0mM, (□) 20mM and (+) 200mM NaCl at 22.5±1.5°C.

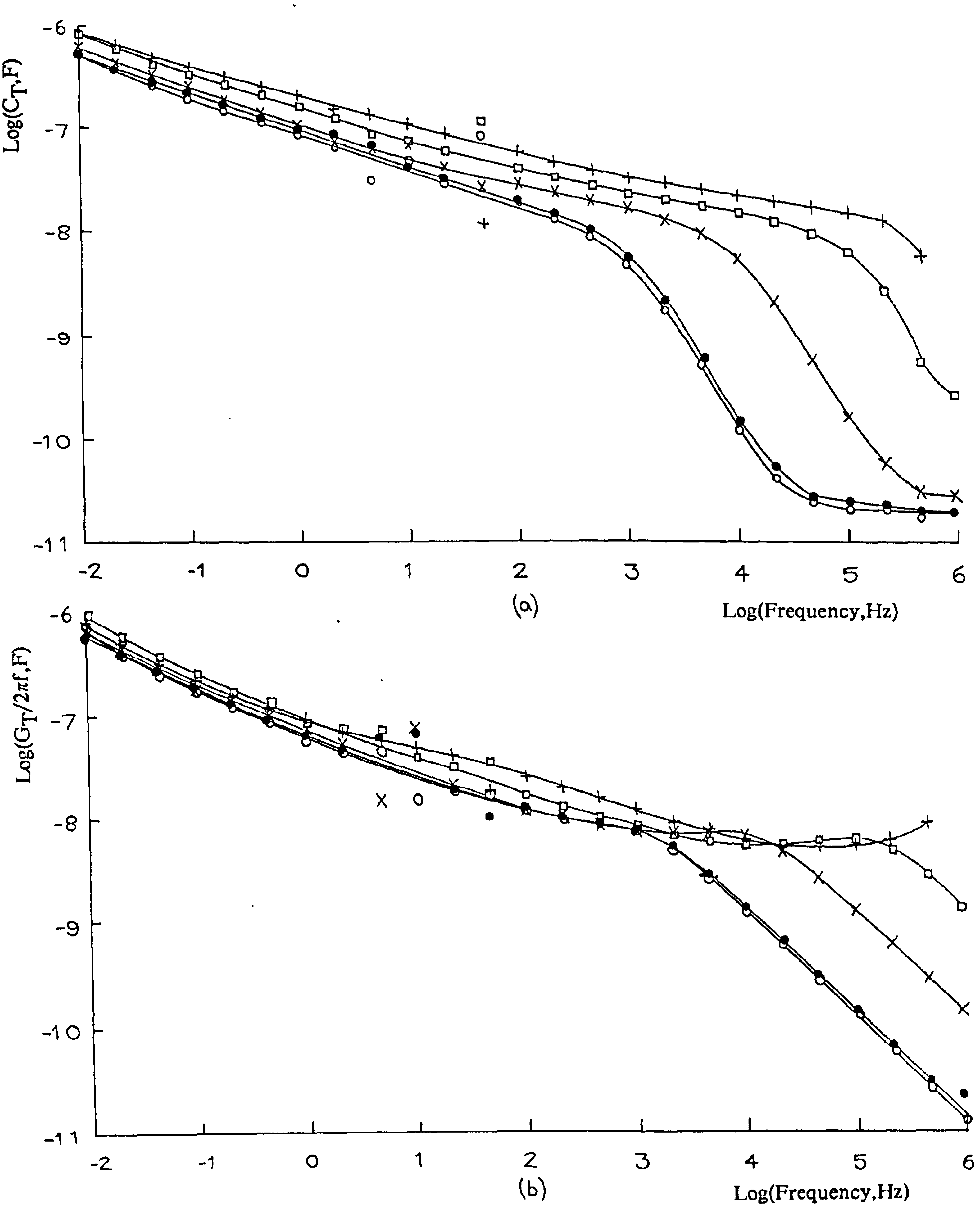

Fig 8.6 (a) Log Capacitance, C_T and (b) Loss ($G_T/2\pi f$) plotted against log frequency, F, for a platinum electrode coated in 20 monolayers of PBMA and immersed in (•)0.2mM, (x) 2.0mM, (□) 20mM and (+) 200mM KCl at 23.5±0.5°C.

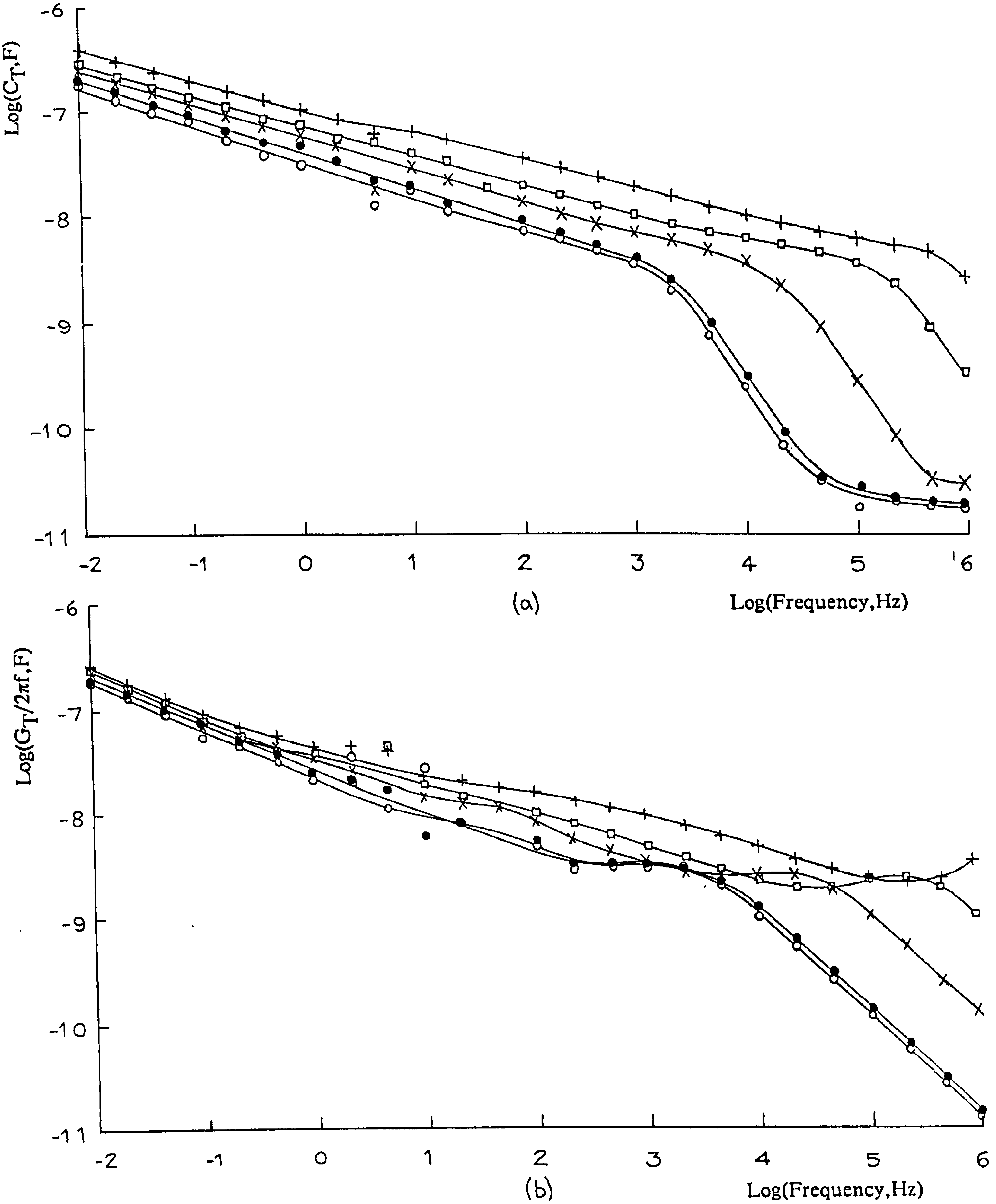

Fig 8.7 (a) Log Capacitance, C_T and (b) Loss ($G_T/2\pi f$) plotted against log frequency, F, for a platinum electrode coated in 40 monolayers of PBMA and immersed in (•)0.2mM, (x) 2.0mM, (□) 20mM and (+) 200mM KCl at 23.5±0.5°C.

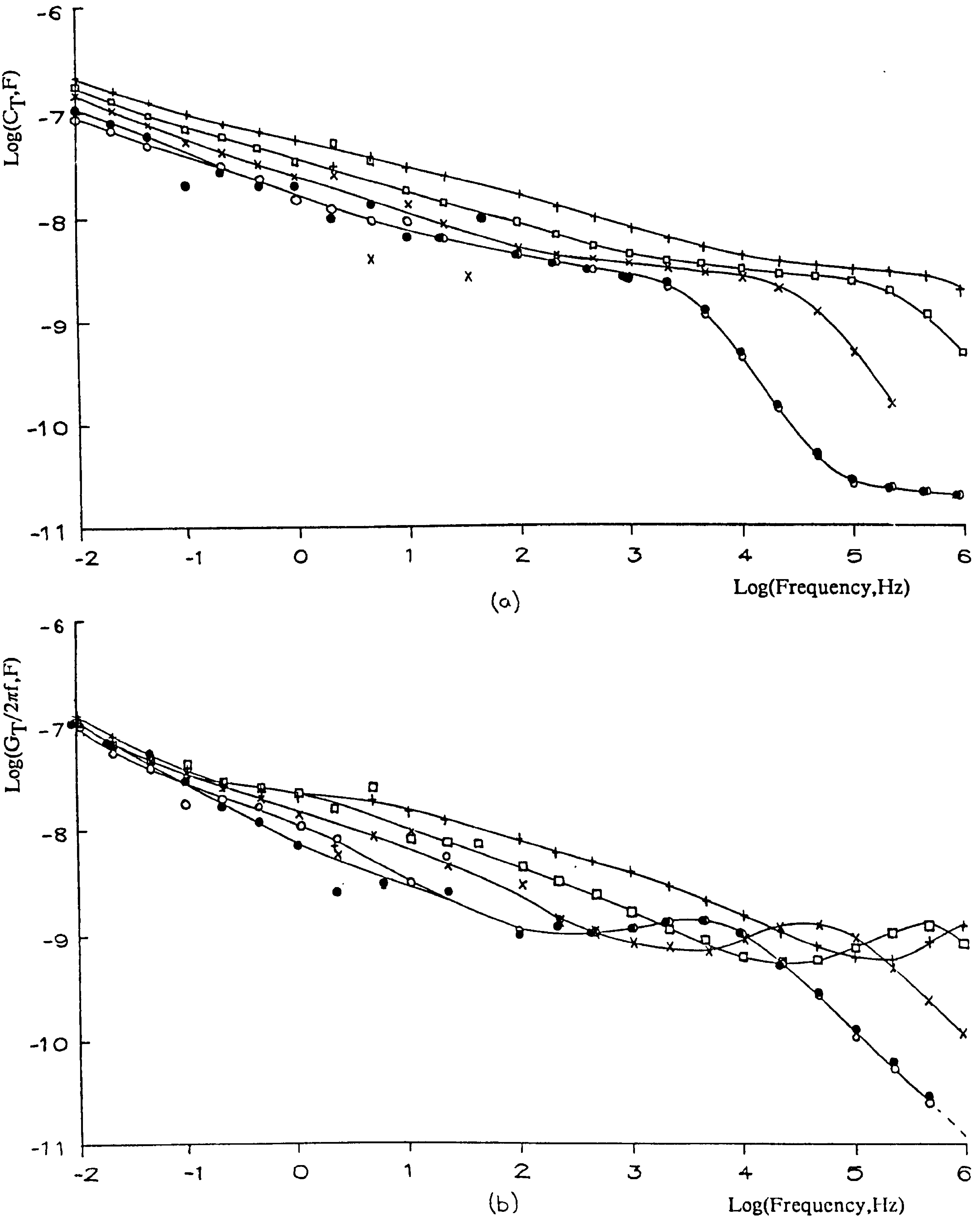

Fig 8.8 (a) Log Capacitance, C_T and (b) Loss ($G_T/2\pi f$) plotted against log frequency, F, for a platinum electrode coated in 60 monolayers of PBMA and immersed in (·)0.2mM, (x) 2.0mM, (□) 20mM and (+) 200mM KCl at 23.5±0.5°C.

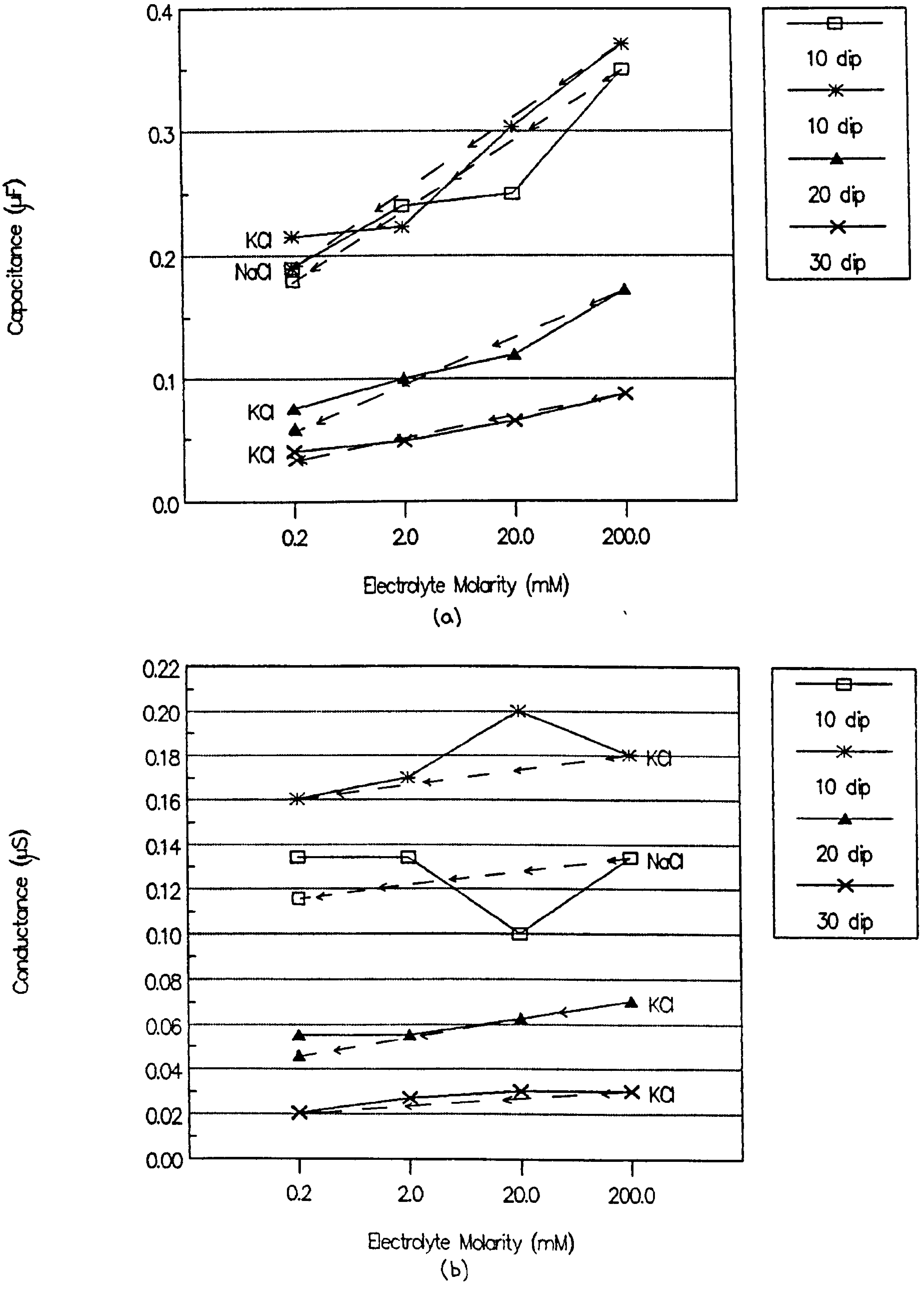

Fig 8.9 (a) Capacitance C_b, and (b) Conductance G_b, for a platinum electrode coated with 20, 40 and 60 monolayers of PBMA, plotted as a function of electrolyte molarity. Capacitance and conductance values were estimated from fig 8.5a to 8.8a and fig 8.5b to 8.8b respectively at 0.16Hz.

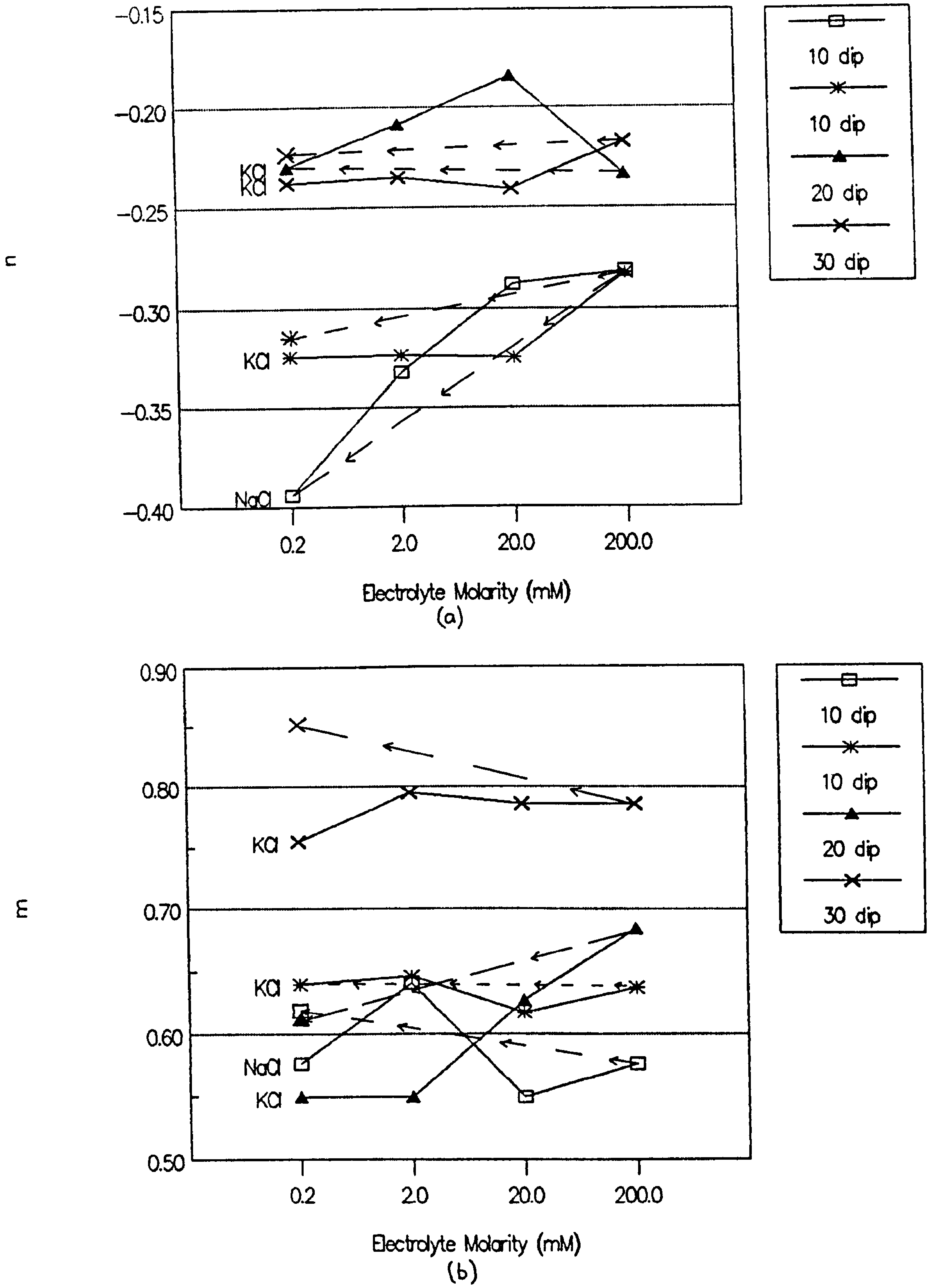

Fig 8.10 (a) n and (b) m for a platinum electrode coated with 20, 40 and 60 monolayers of PBMA, plotted as a function of electrolyte molarity. n and m values were estimated from fig 8.5a to 8.8a and fig 8.5b to 8.8b respectively.

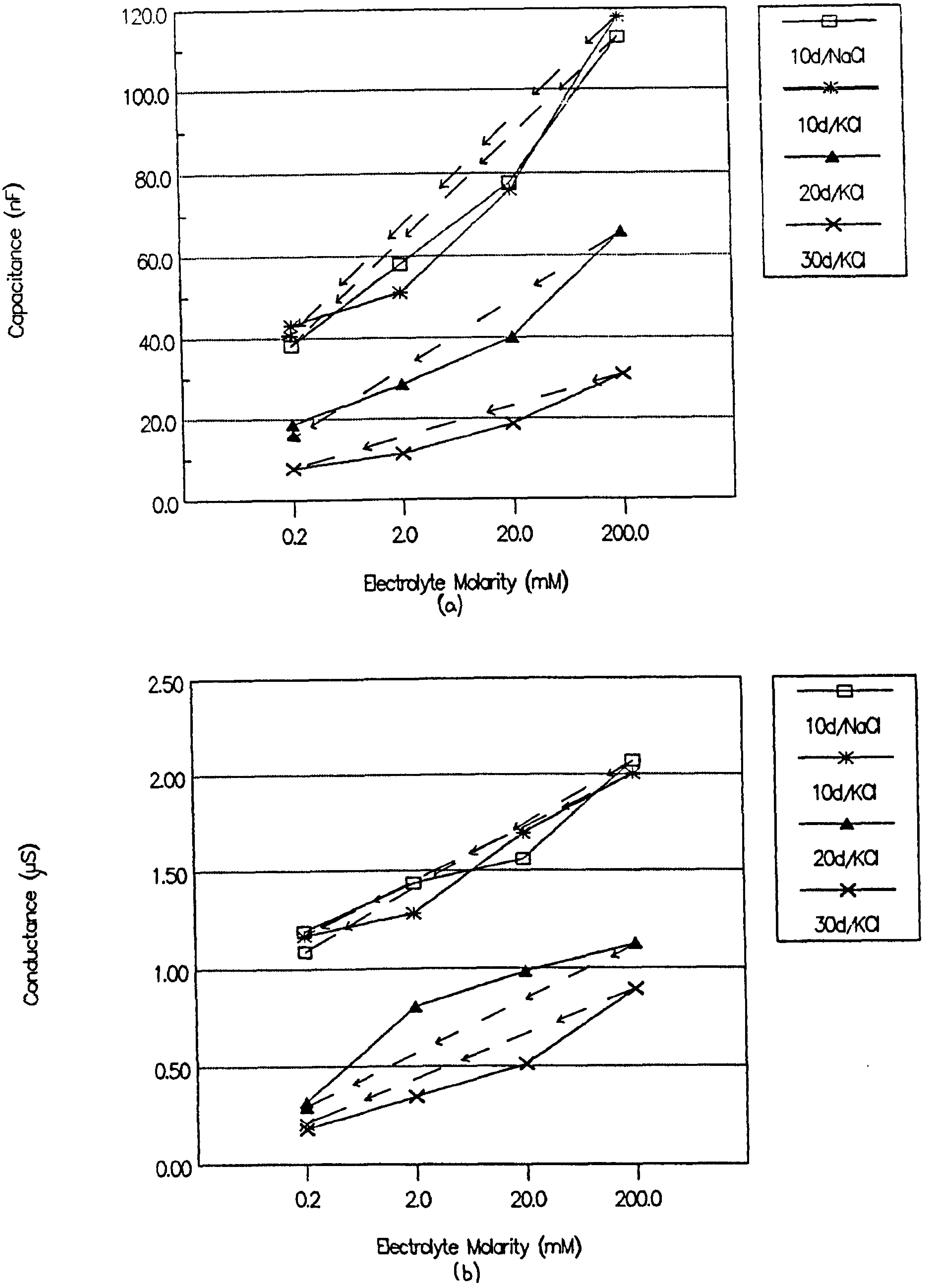

Fig 8.11 (a) Capacitance C_b, and (b) Conductance G_b, for a platinum electrode coated with 20, 40 and 60 monolayers of PBMA, plotted as a function of electrolyte molarity. Capacitance and conductance values were estimated from fig 8.5a to 8.8a and fig 8.5b to 8.8b respectively at 10Hz.

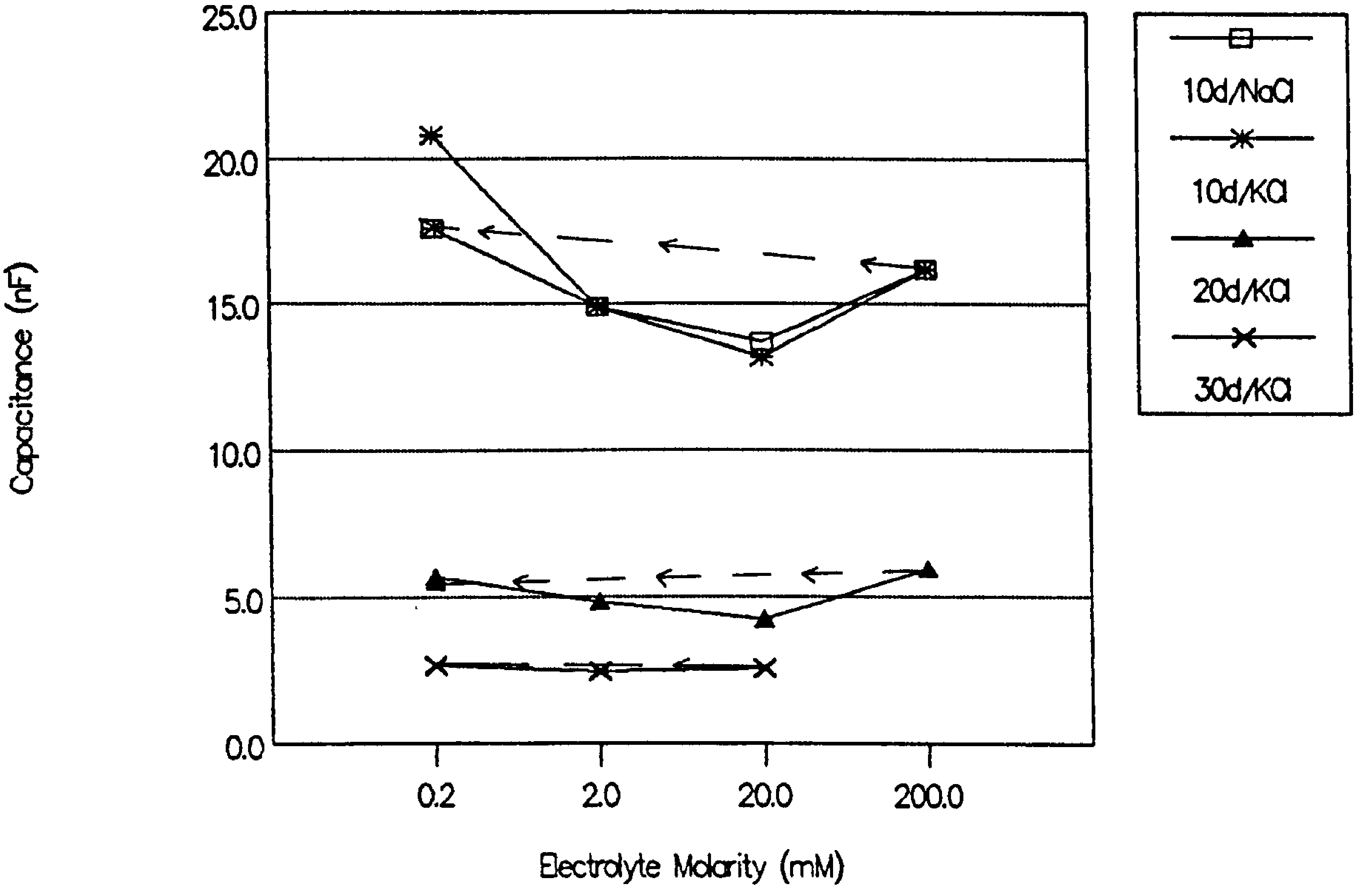

Fig 8.12 Capacitance C_b for a platinum electrode coated with 20, 40 and 60 monolayers of PBMA, plotted as a function of electrolyte molarity. Capacitance values were estimated from fig 8.5a to 8.8a at the cross over point of the C_T and $G_T/2\pi f$ curves.

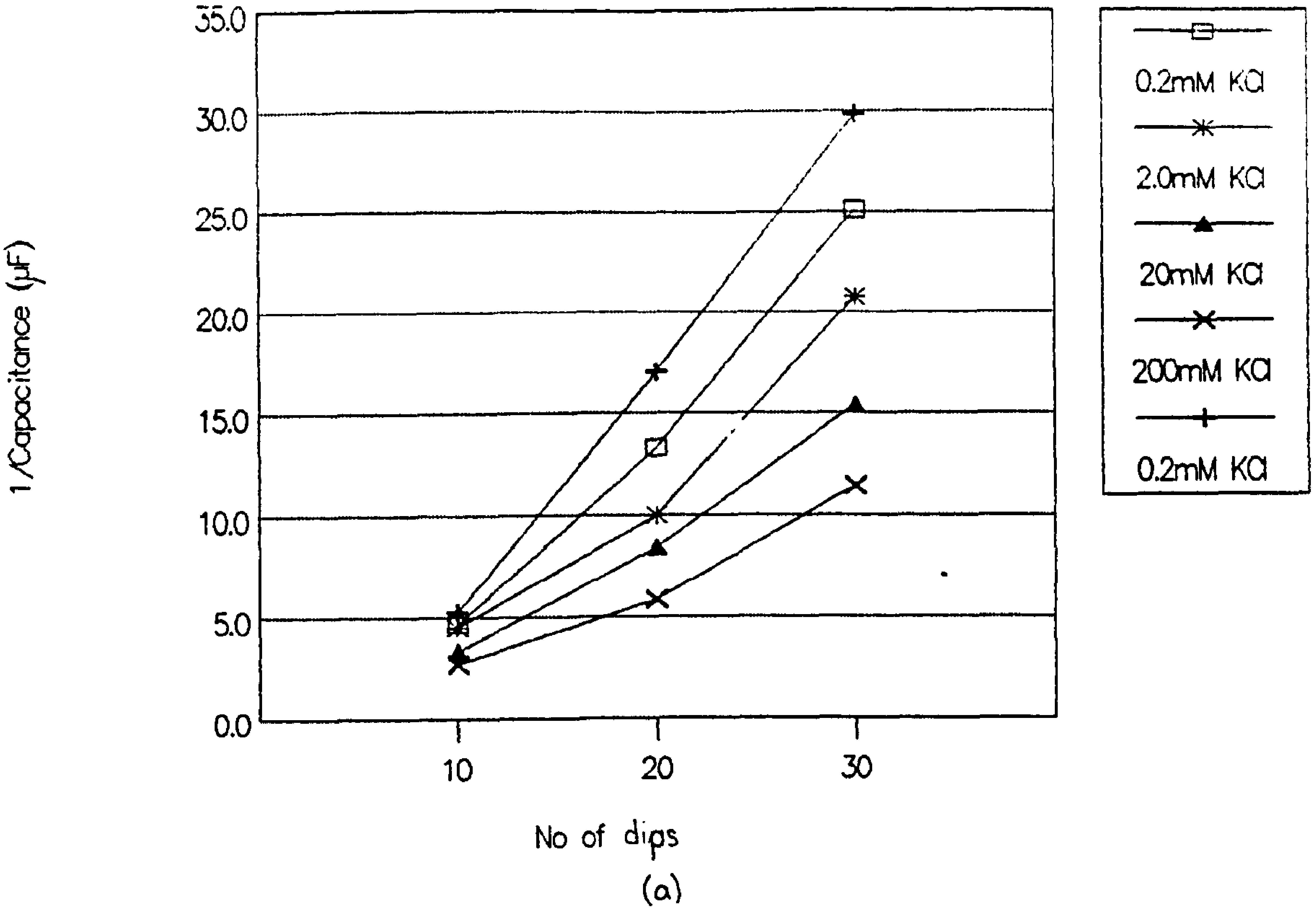

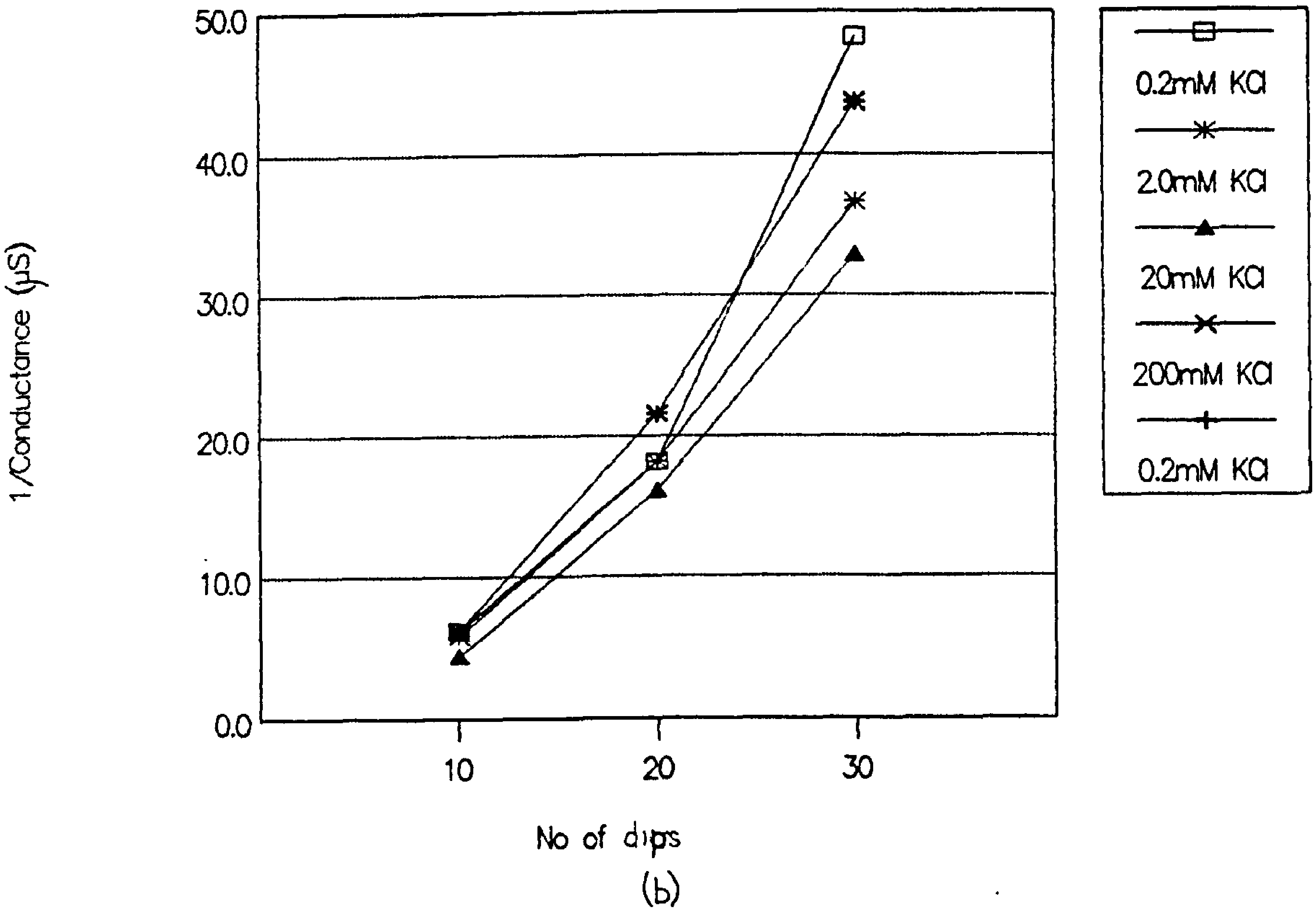

Fig 8.13 (a) Reciprocal capacitance ($1/C_b$), and (b) conductance ($1/G_b$), for a platinum electrode coated with 20, 40 and 60 monolayers of PBMA immersed in (□) 0.2, (*) 2, (▲) 20, (x) 200 and again in (+) 0.2mM KCl at 23.5±0.5°C, plotted as a function the number of dipping cycles. Reciprocal capacitance and conductance values were estimated from fig 8.6a to 8.8a and fig 8.6b to 8.8b respectively at 0.16Hz.

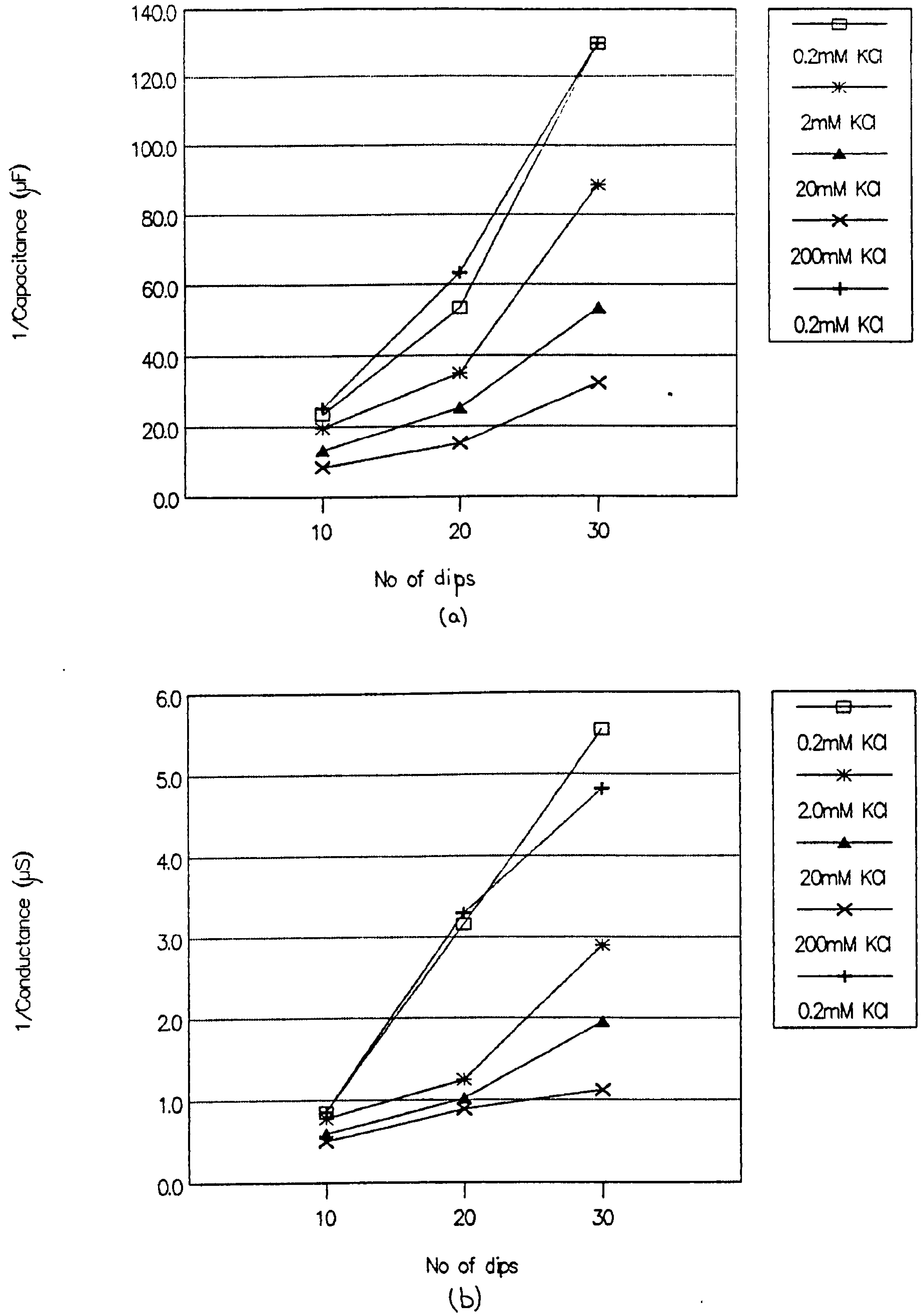

Fig 8.14 (a) Reciprocal capacitance ($1/C_b$), and (b) conductance ($1/G_b$), for a platinum electrode coated with 20, 40 and 60 monolayers of PBMA immersed in (□) 0.2, (*) 2, (▲) 20, (x) 200 and again in (+) 0.2mM KCl at 23.5±0.5°C, plotted as a function the number of dipping cycles. Reciprocal capacitance and conductance values were estimated from fig 8.6a to 8.8a and fig 8.6b to 8.8b respectively at 10Hz.

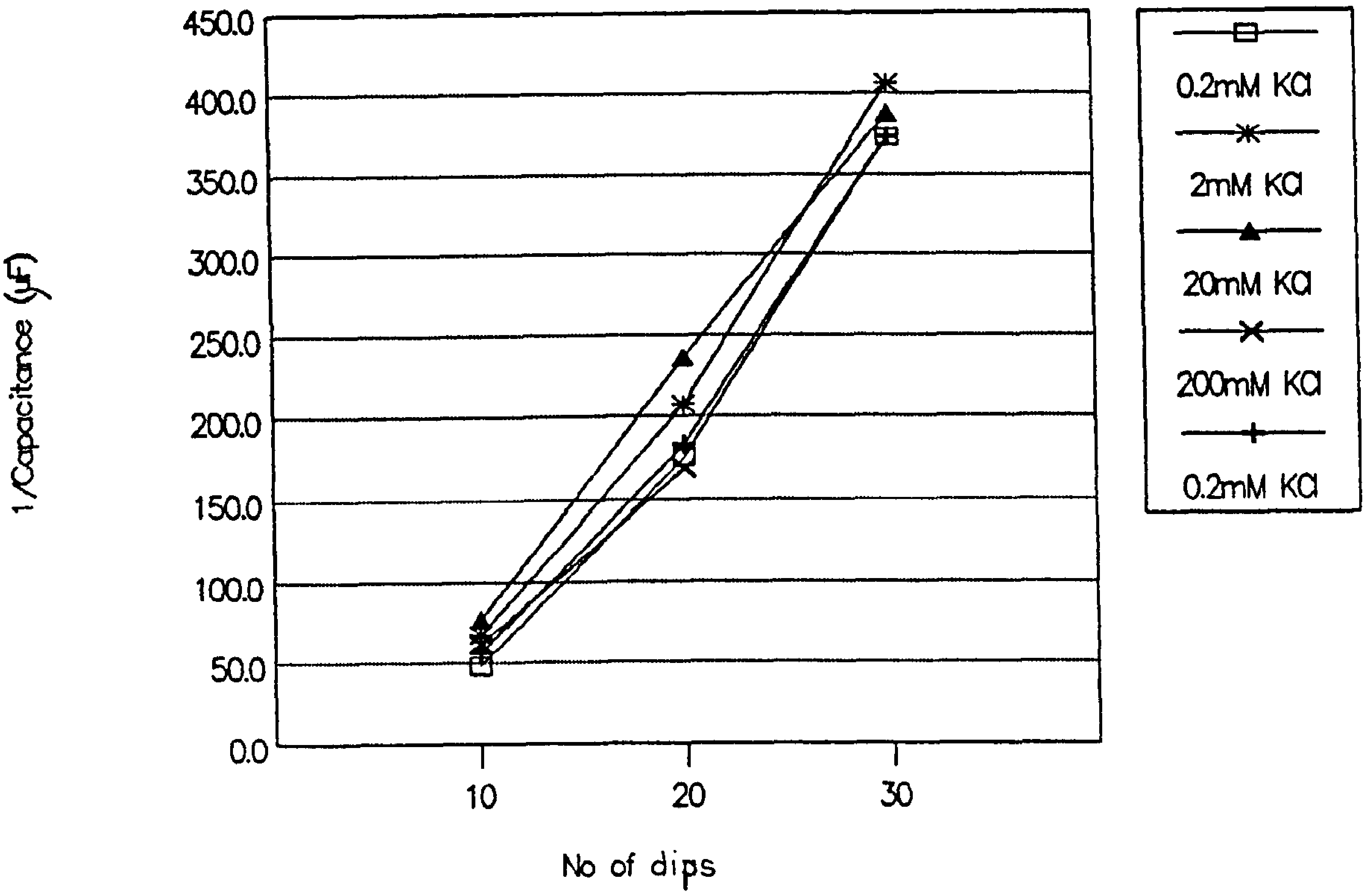

Fig 8.15 Reciprocal capacitance ($1/C_b$) for a platinum electrode coated with 20, 40 and 60 monolayers of PBMA immersed in (□) 0.2, (*) 2, (▲) 20, (x) 200 and again in (+) 0.2mM KCl at 23.5±0.5°C, plotted as a function the number of dipping cycles. Reciprocal capacitance values were estimated from fig 8.6a to 8.8a at the cross over point of the C_T and $G_T/2\pi f$ curves.

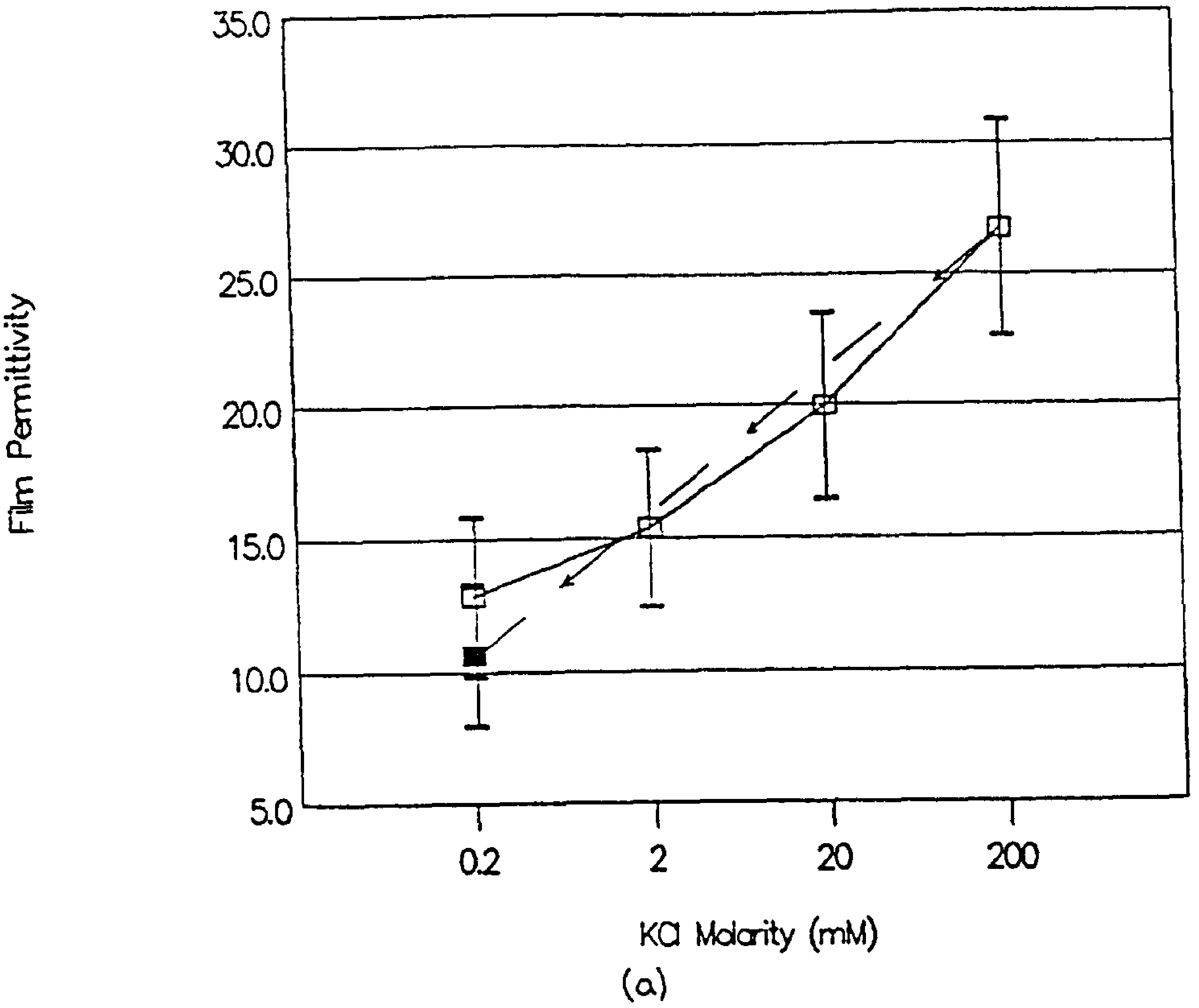

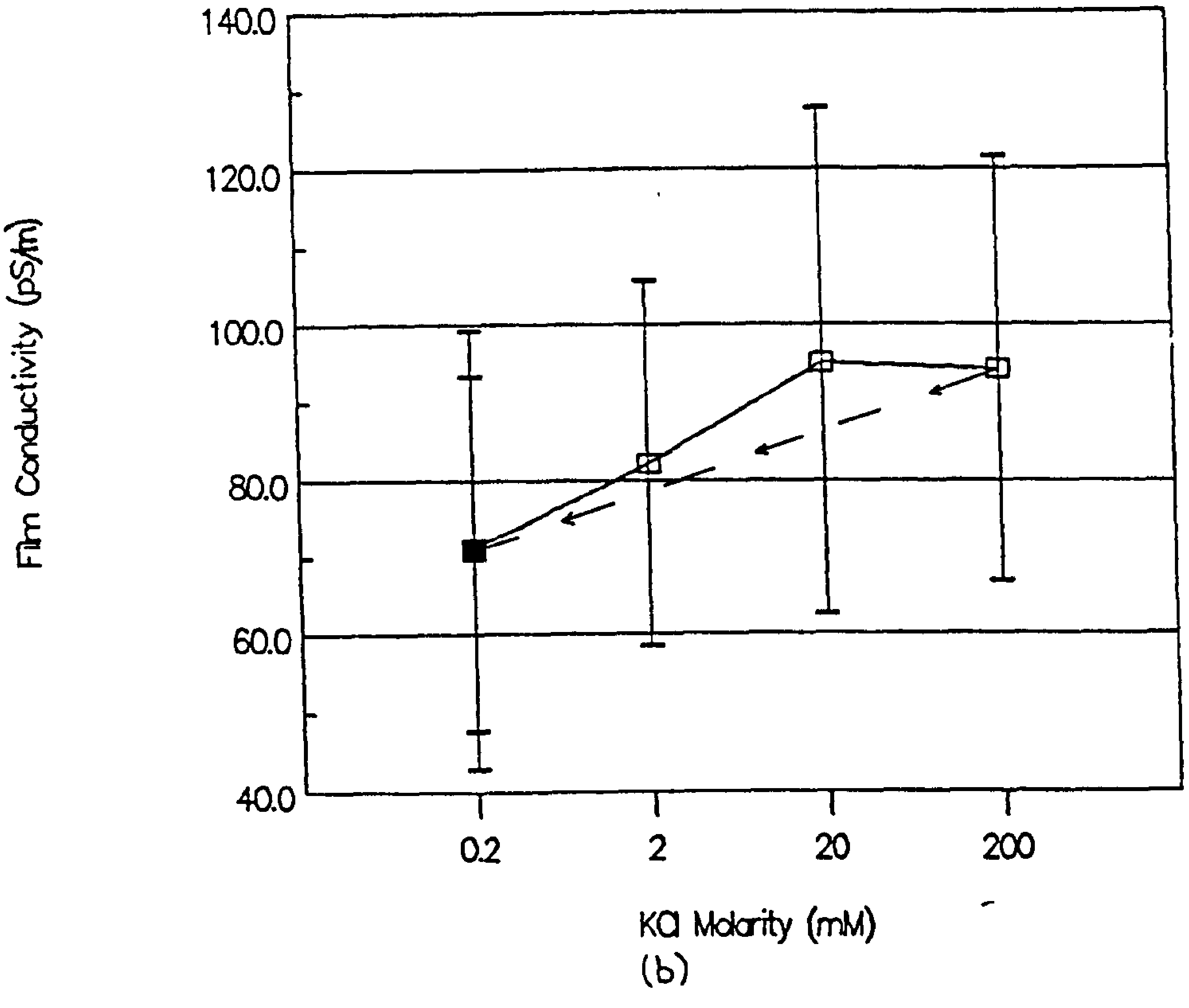

Fig 8.16 (a) Film permittivity, ϵ_r and (b) conductivity, σ, at 0.16Hz for a platinum electrode coated with 20, 40 and 60 monolayers of PBMA immersed in KCl at 23.5±0.5°C, plotted as a function of KCl molarity. The values were caluclated assuming a monolayer thickness of 0.7nm.

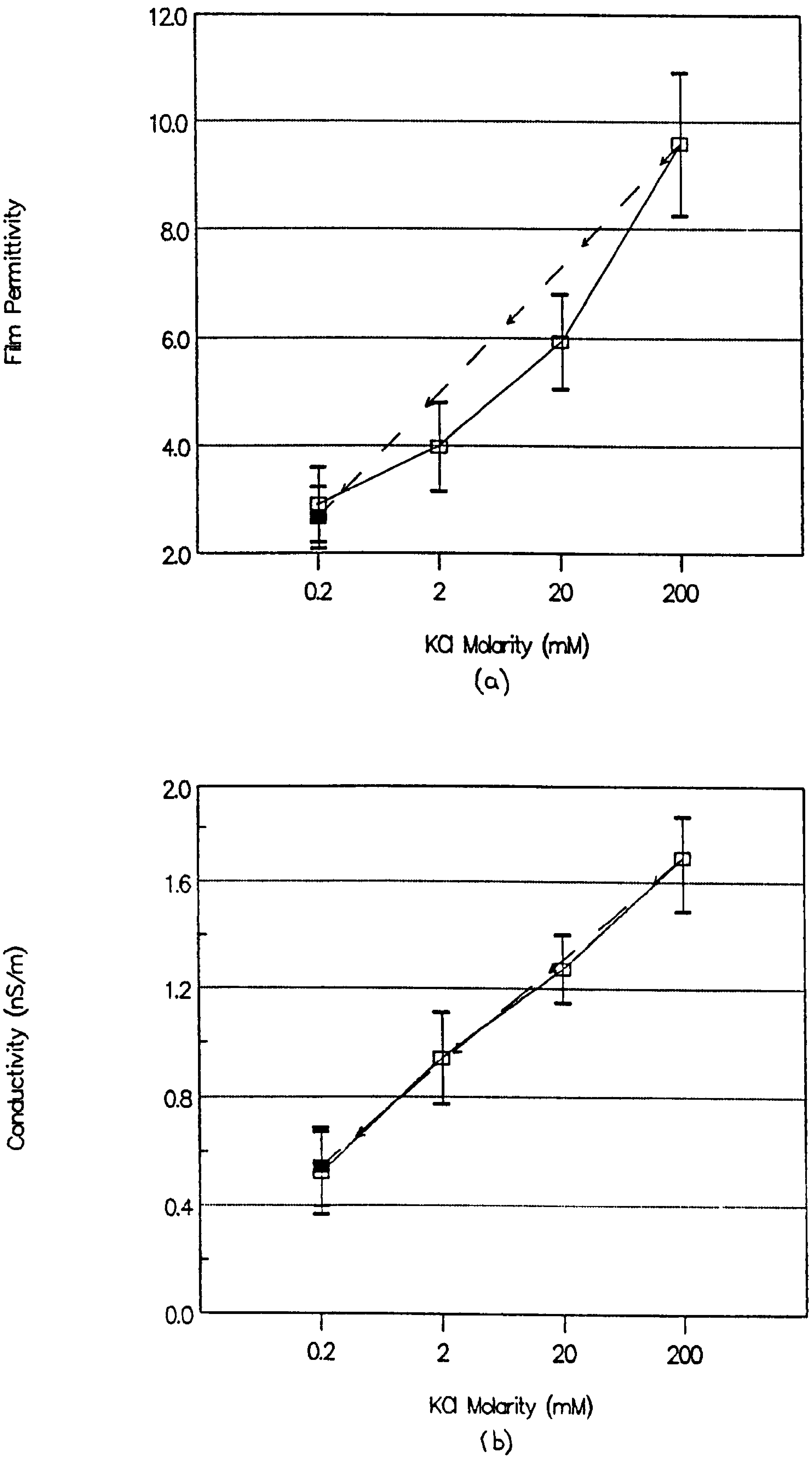

Fig 8.17 (a) Film permittivity, ϵ_r and (b) conductivity, σ, at 10Hz for a platinum electrode coated with 20, 40 and 60 monolayers of PBMA immersed in KCl at 23.5±0.5°C, plotted as a function of KCl molarity. The values were caluclated assuming a monolayer thickness of 0.7nm.

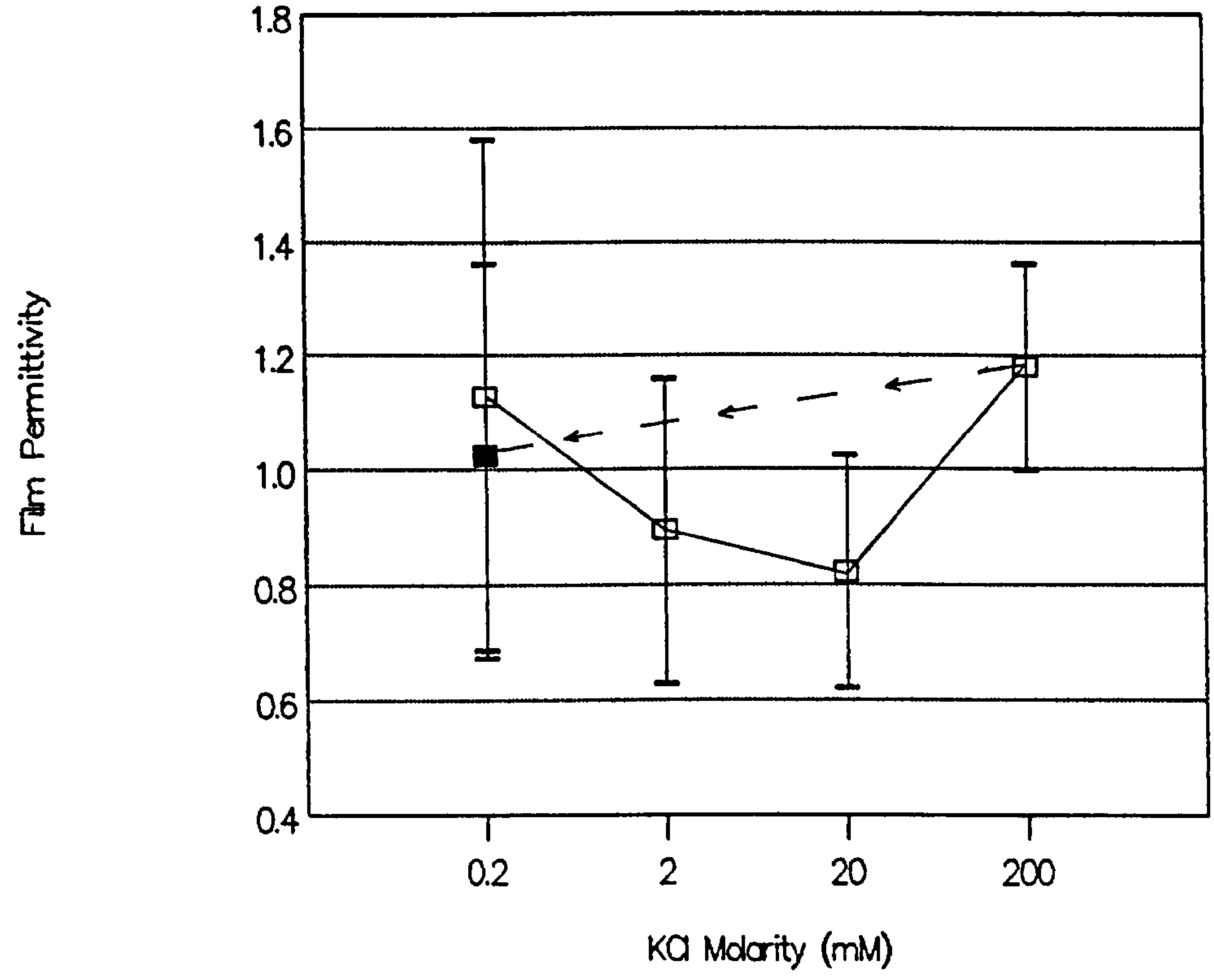

Fig 8.18 Film permittivity, ϵ_r at the cross over frequencies for a platinum electrode coated with 20, 40 and 60 monolayers of PBMA immersed in KCl at 23.5±0.5°C, plotted as a function of KCl molarity. The values were calculated assuming a monolayer thickness of 0.7nm.

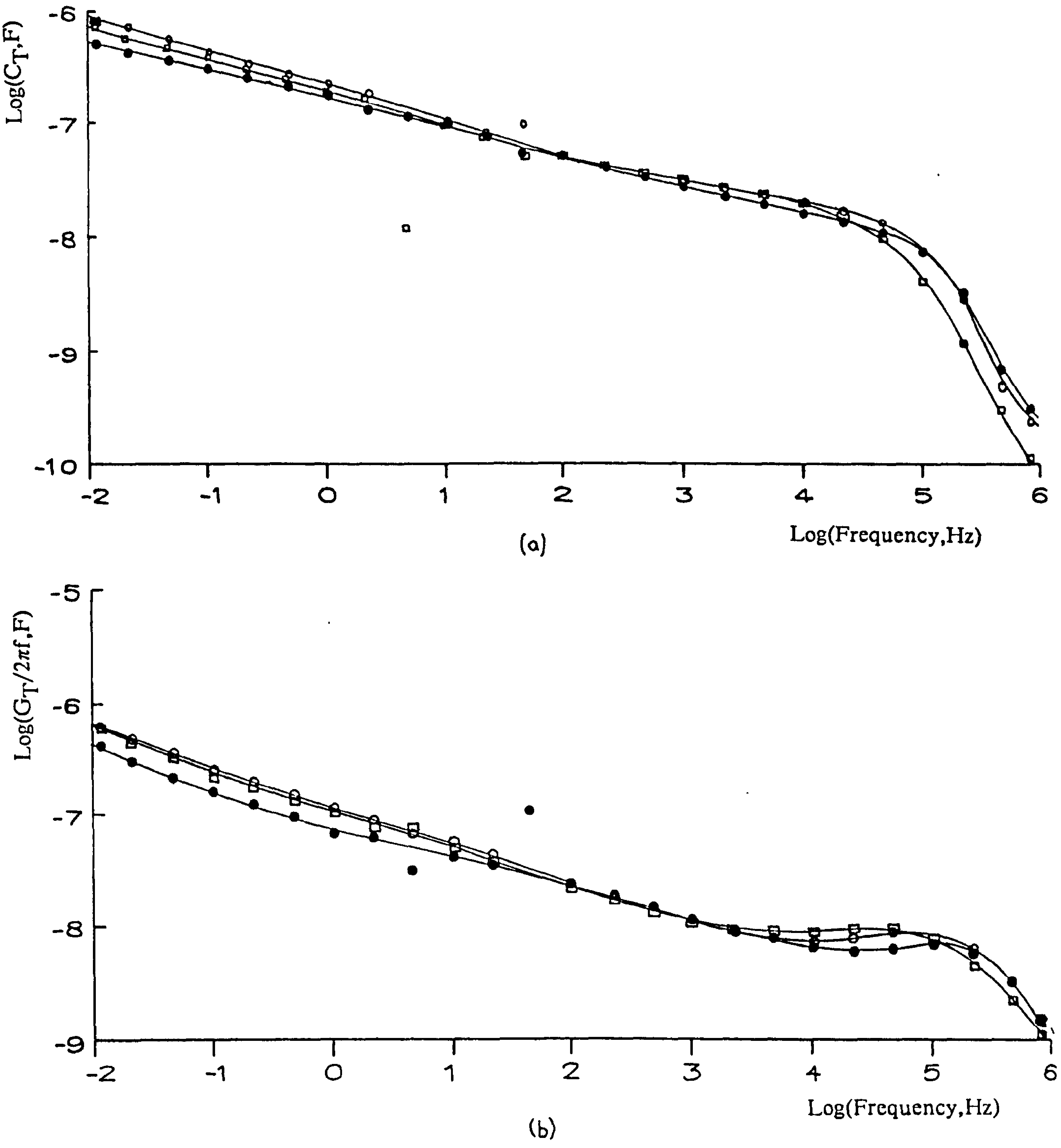

Fig 8.19 (a) Log Capacitance, C_T and (b) Loss ($G_T/2\pi f$) plotted against log frequency, F, for a platinum electrode coated in 20 monolayers of PBMA and immersed in 20mM (•)$CaCl_2$, (□) NaCl and again in (o) $CaCl_2$ at 22°C.

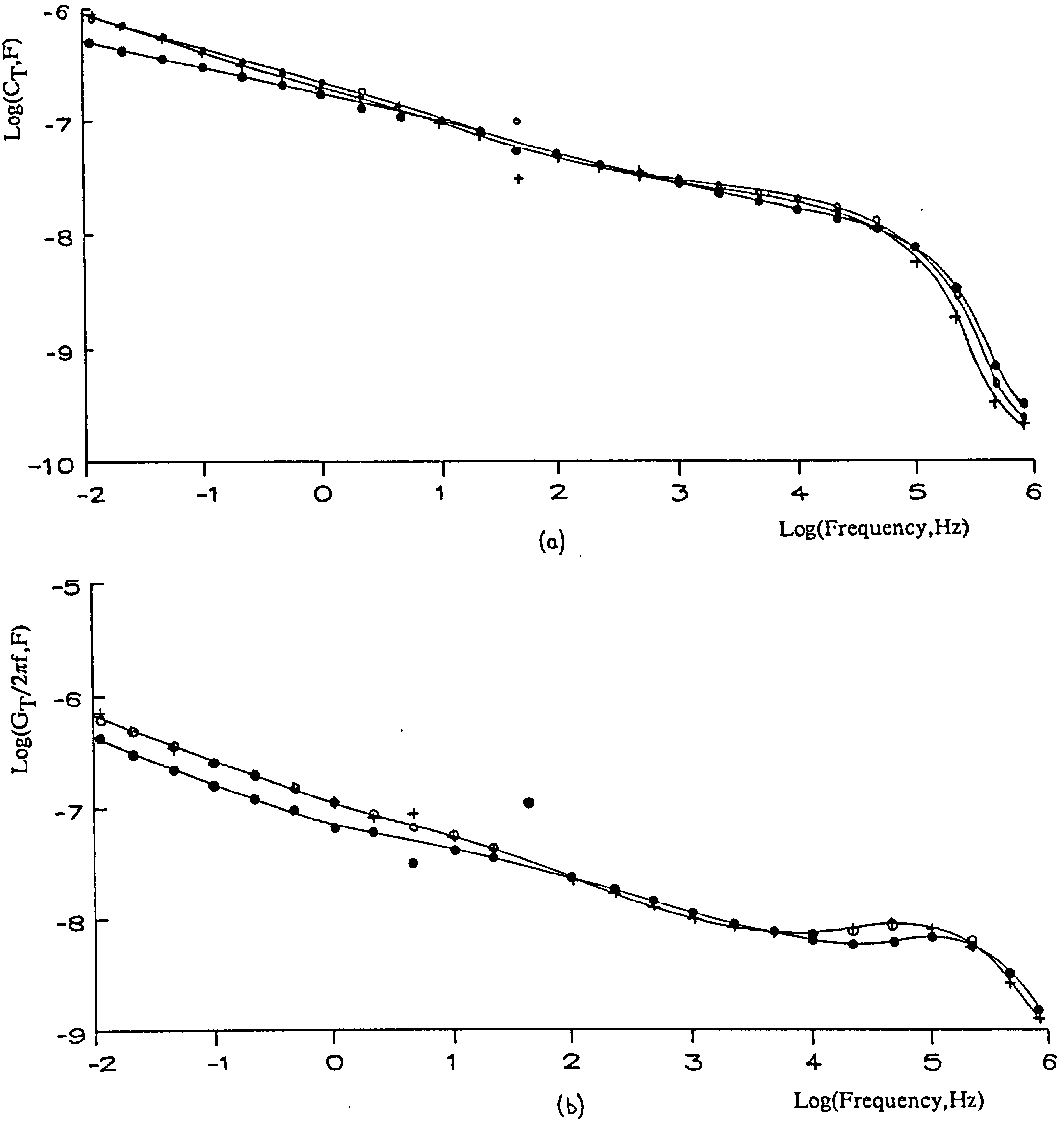

Fig 8.20 (a) Log Capacitance, C_T and (b) Loss ($G_T/2\pi f$) plotted against log frequency, F, for a platinum electrode coated in 20 monolayers of PBMA and immersed in 20mM (•)$CaCl_2$, (+) KCl and again in (o) $CaCl_2$ at 22°C.

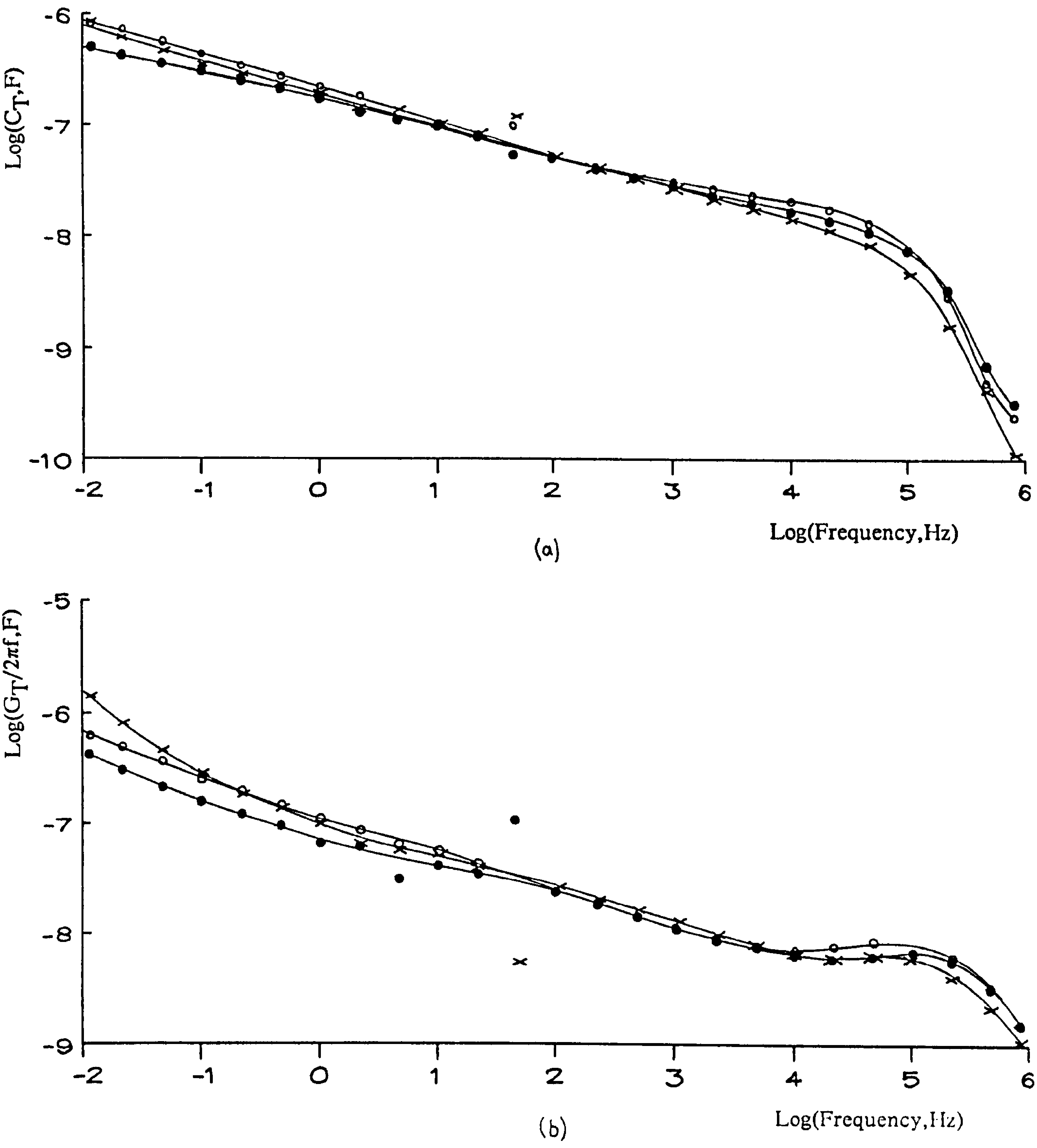

Fig 8.21 (a) Log Capacitance, C_T and (b) Loss ($G_T/2\pi f$) plotted against log frequency, F, for a platinum electrode coated in 20 monolayers of PBMA and immersed in 20mM (•)$CaCl_2$, (x) KI and again in (o) $CaCl_2$ at 22°C.

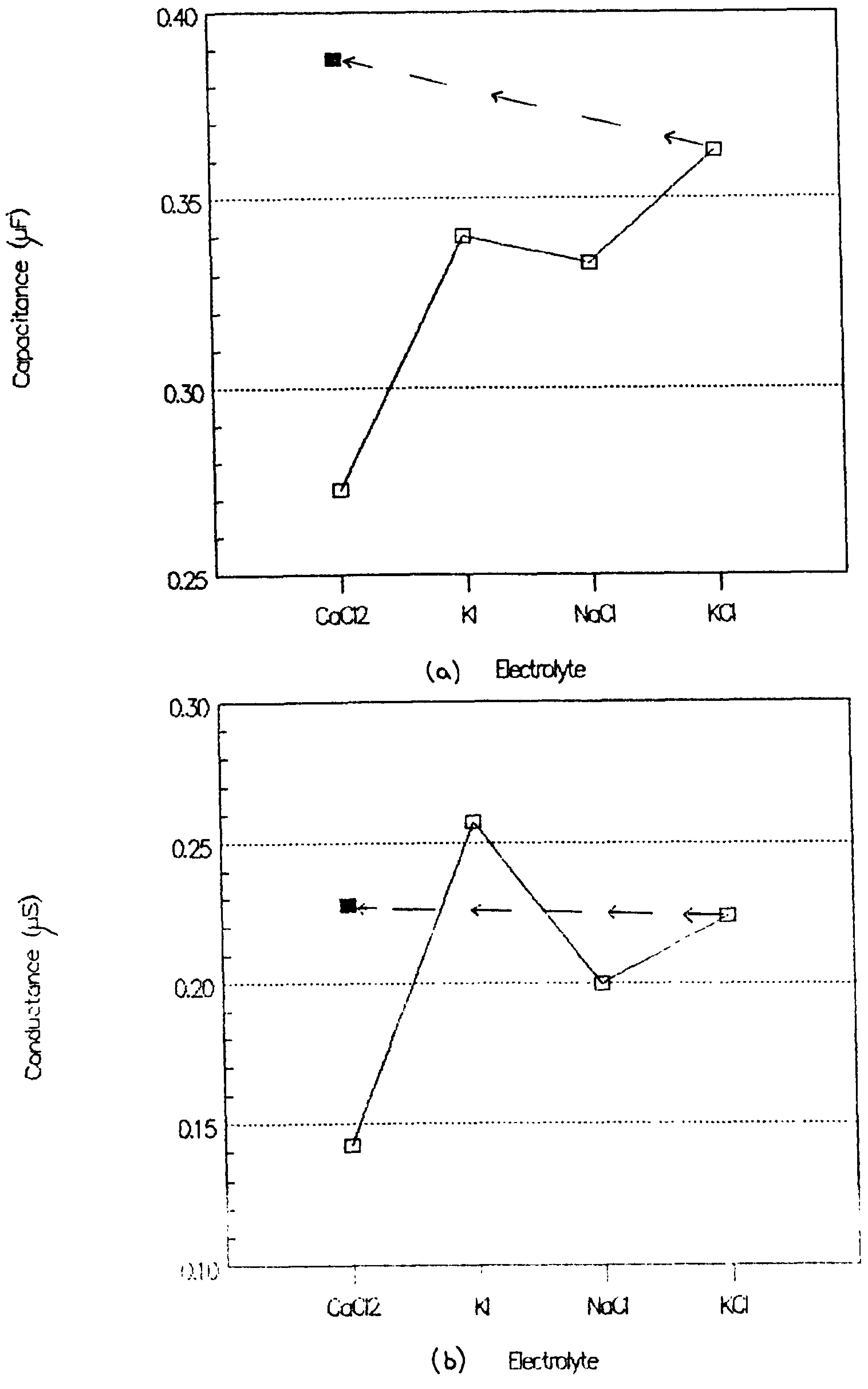

Fig 8.22 (a) (□,■) Capacitance C_b, and (b) (□,■) Conductance G_b, for a platinum electrode coated with 20 monolayers of PBMA immersed in a range of electrolytes and plotted as a function of electrolyte. Capacitance and conductance values were estimated from fig 8.19a to 8.21a and fig 8.19b to 8.21b respectively at 0.161Hz.

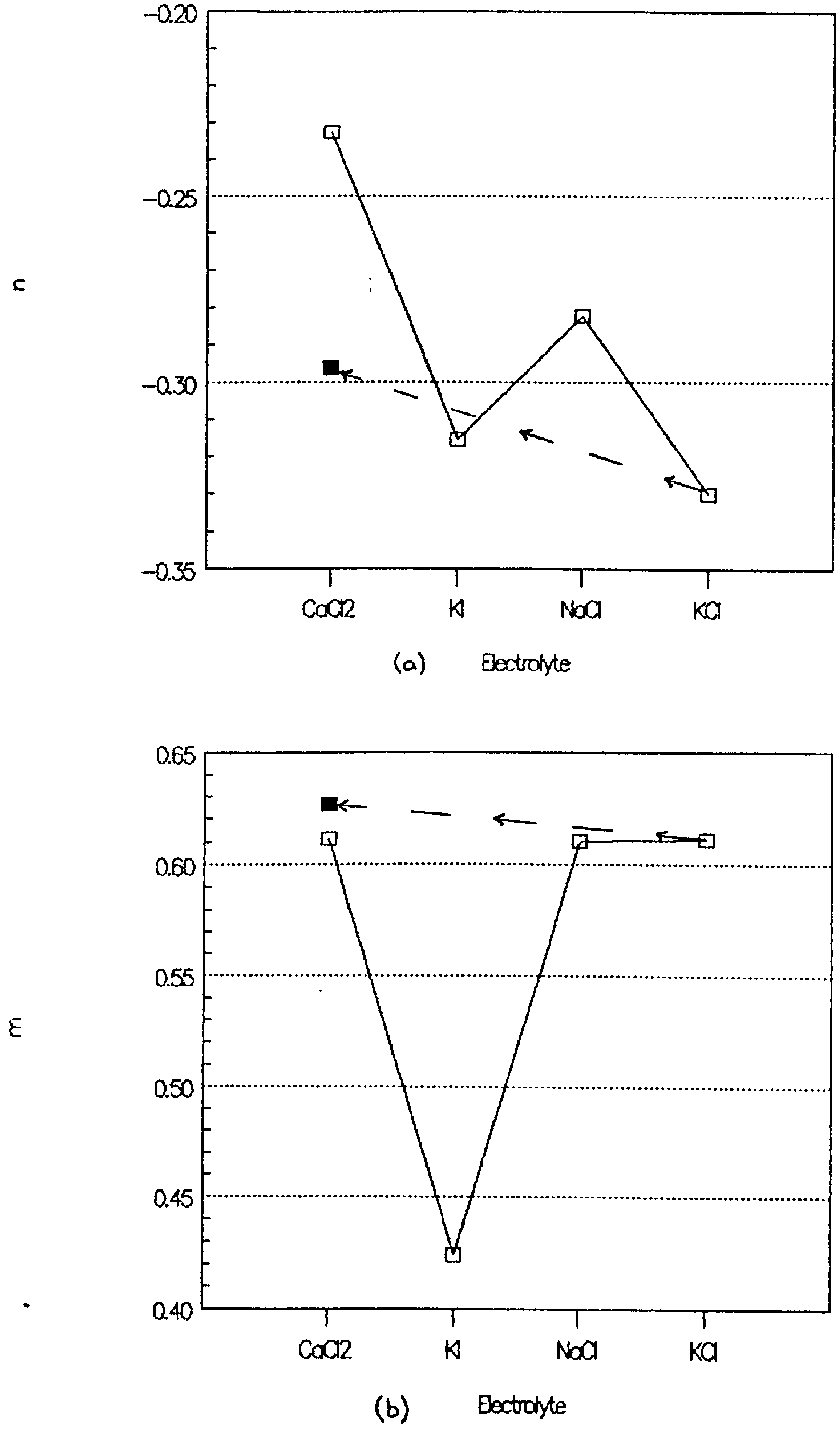

Fig 8.23 (a) (□,■) n and (b) (□,■) m for a platinum electrode coated with 20 monolayers of PBMA immersed in a range of electrolytes and plotted as a function of electrolyte. n and m values were estimated from fig 8.19a to 8.21a and fig 8.19b to 8.21b respectively.

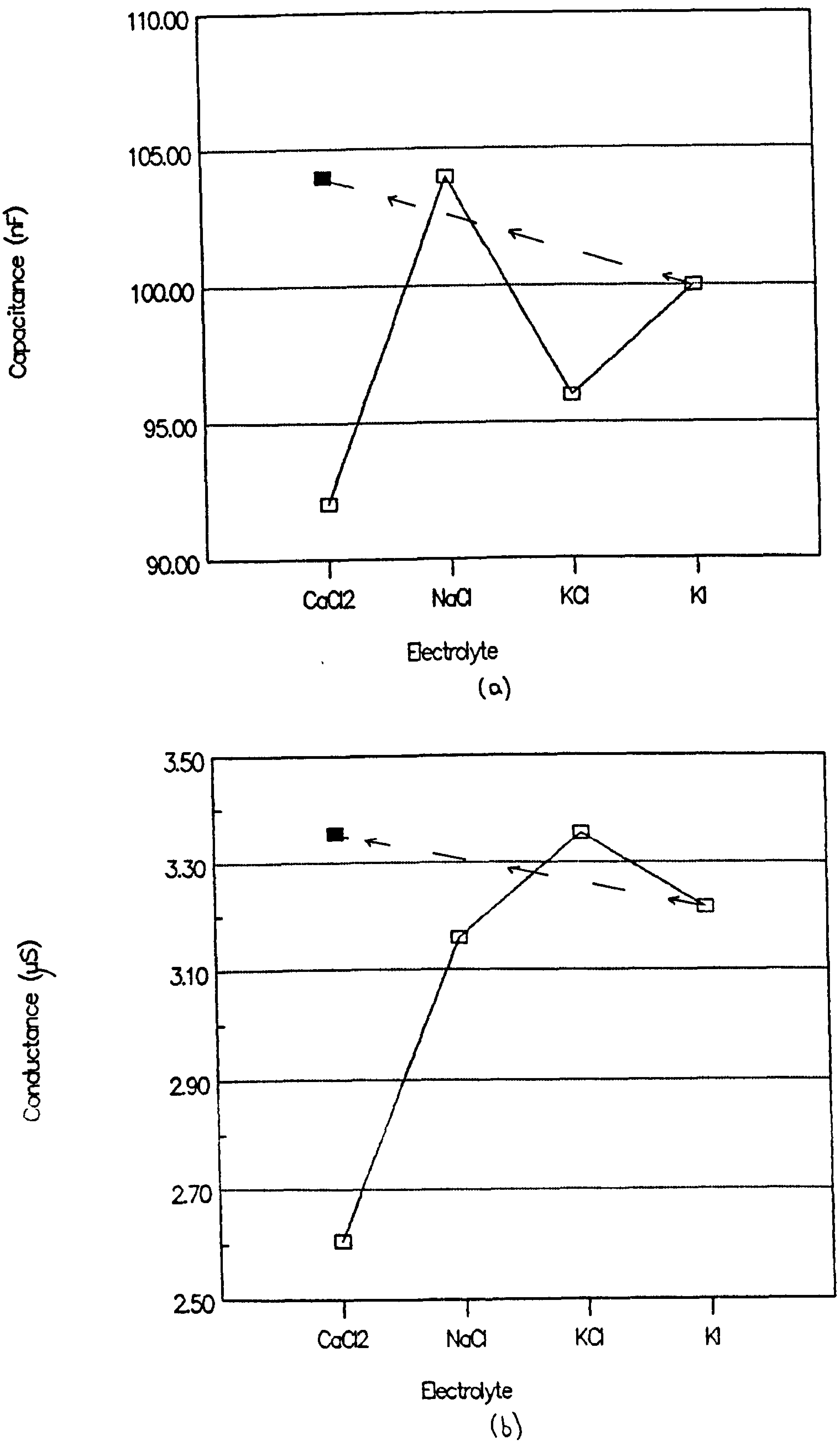

Fig 8.24 (a) (□,■) Capacitance C_b, and (b) (□,■) Conductance G_b, for a platinum electrode coated with 20 monolayers of PBMA immersed in a range of electrolytes and plotted as a function of electrolyte. Capacitance and conductance values were estimated from fig 8.19a to 8.21a and fig 8.19b to 8.21b respectively at 10Hz.

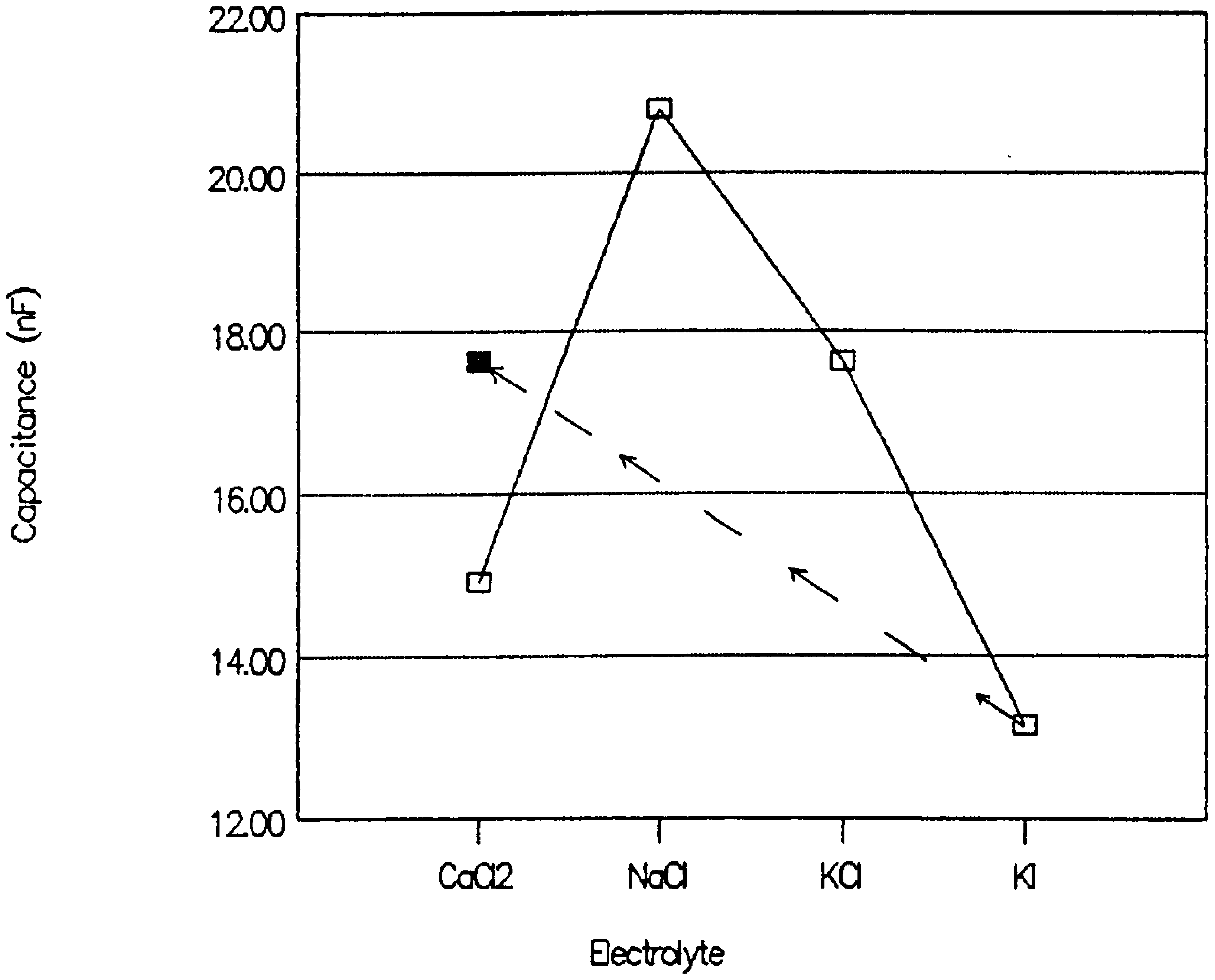

Fig 8.25 (□,■) Capacitance C_b for a platinum electrode coated with 20 monolayers of PBMA immersed in a range of electrolytes and plotted as a function of electrolyte. Capacitance values were estimated from fig 8.19a to 8.21a.

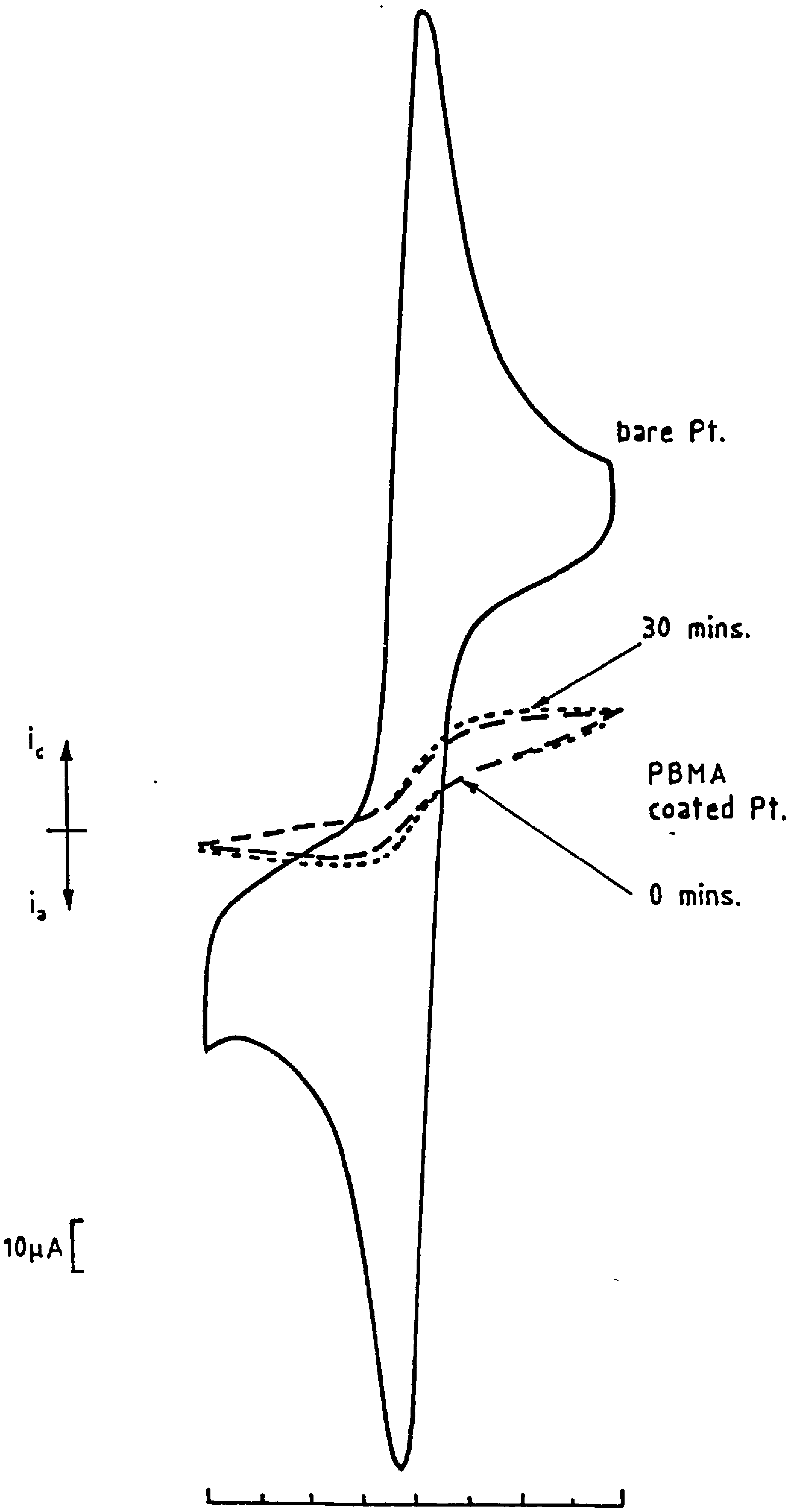

Fig 8.26 Cyclic voltammograms for i) an uncoated platinum wire electrode (——) and ii) the same electrode coated in 20 monolayers of PBMA in 0.1M KCl and 1mM $K_3Fe(CN)_6$ with a sweep rate of 0.1V/sec at 21°C and pH=5.7. Curves for the coated electrode are shown after (———)0 and (– – –) 30 minutes immersion.

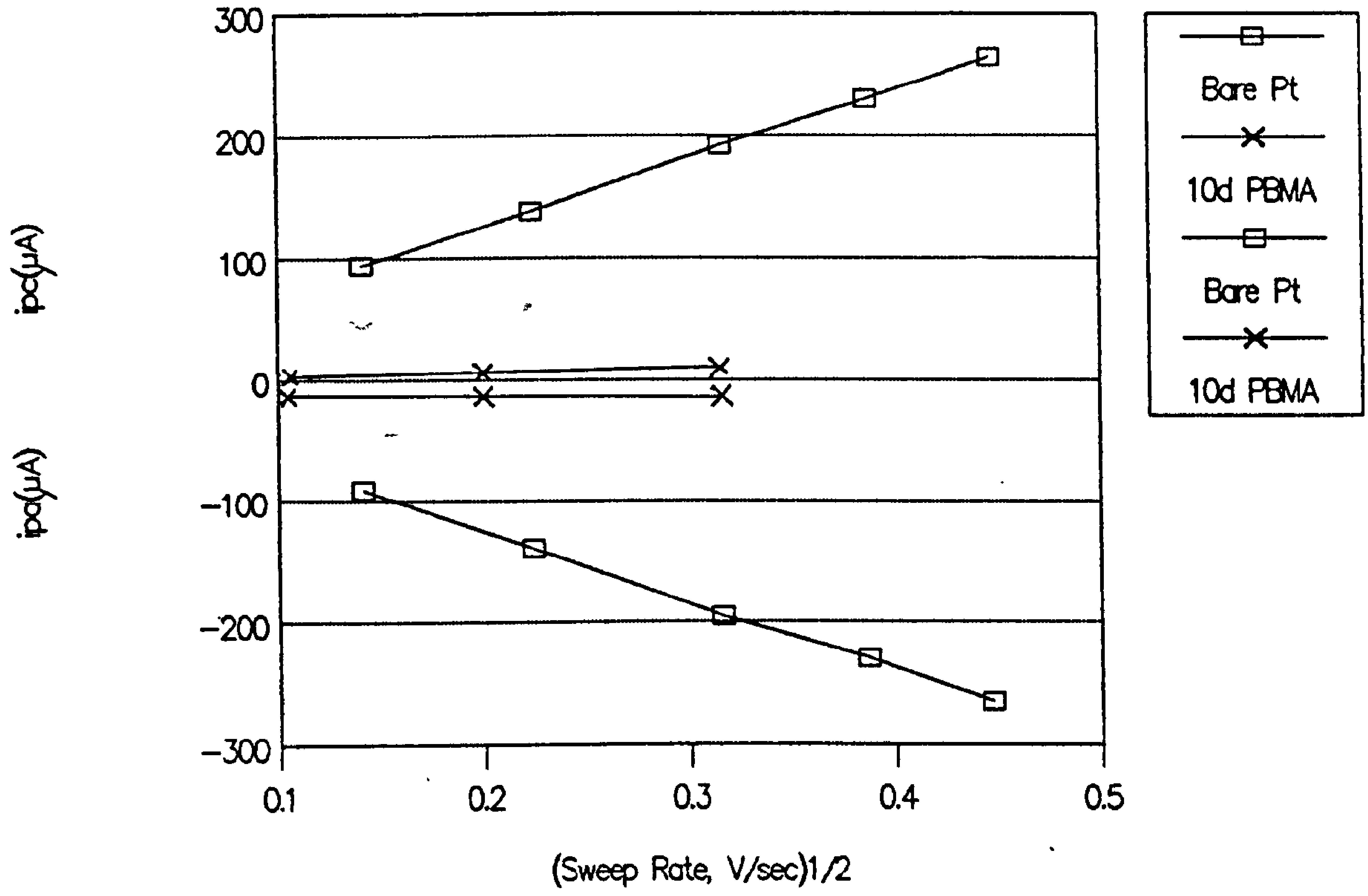

Fig 8.27 Peak anodic and cathodic currents, i_{pa} and i_{pc}, for (□) an uncoated platinum wire electrode and the same electrode coated with (x) 20 monolayers of PBMA plotted as a function of (sweep rate)$^{1/2}$. The peak currents were estimated from cyclic voltammograms measured during immersion of the electrodes in 0.1M KCl and 1mM $K_3Fe(CN)_6$ (eg fig 8.26).

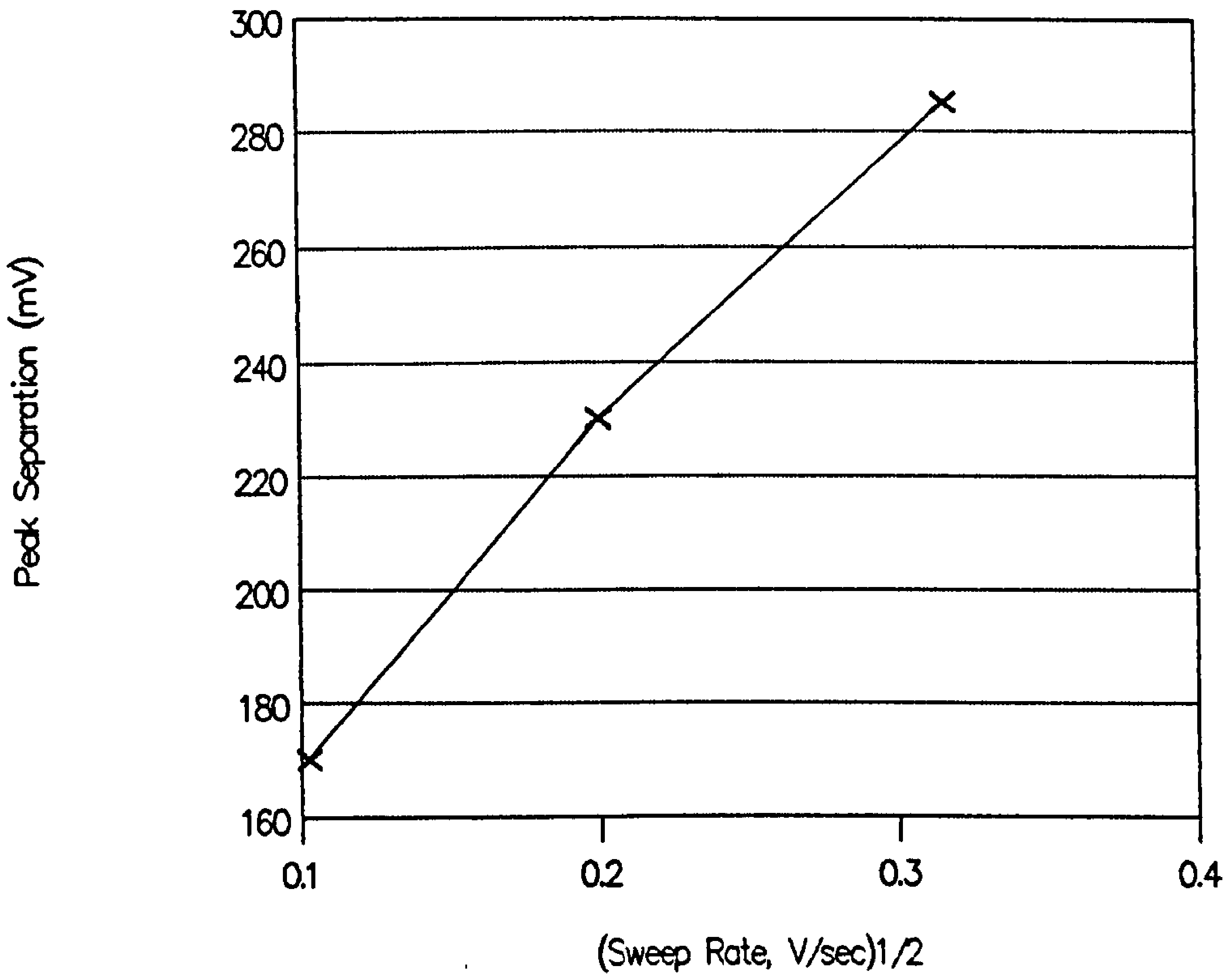

Fig 8.28 Peak separation for a platinum wire electrode coated with (x) 20 monolayers of PBMA plotted as a function of (sweep rate)$^{1/2}$. The peak separations were estimated from cyclic voltammograms measured during immersion of the electrodes in 0.1M KCl and 1mM $K_3Fe(CN)_6$ (eg fig 8.26).

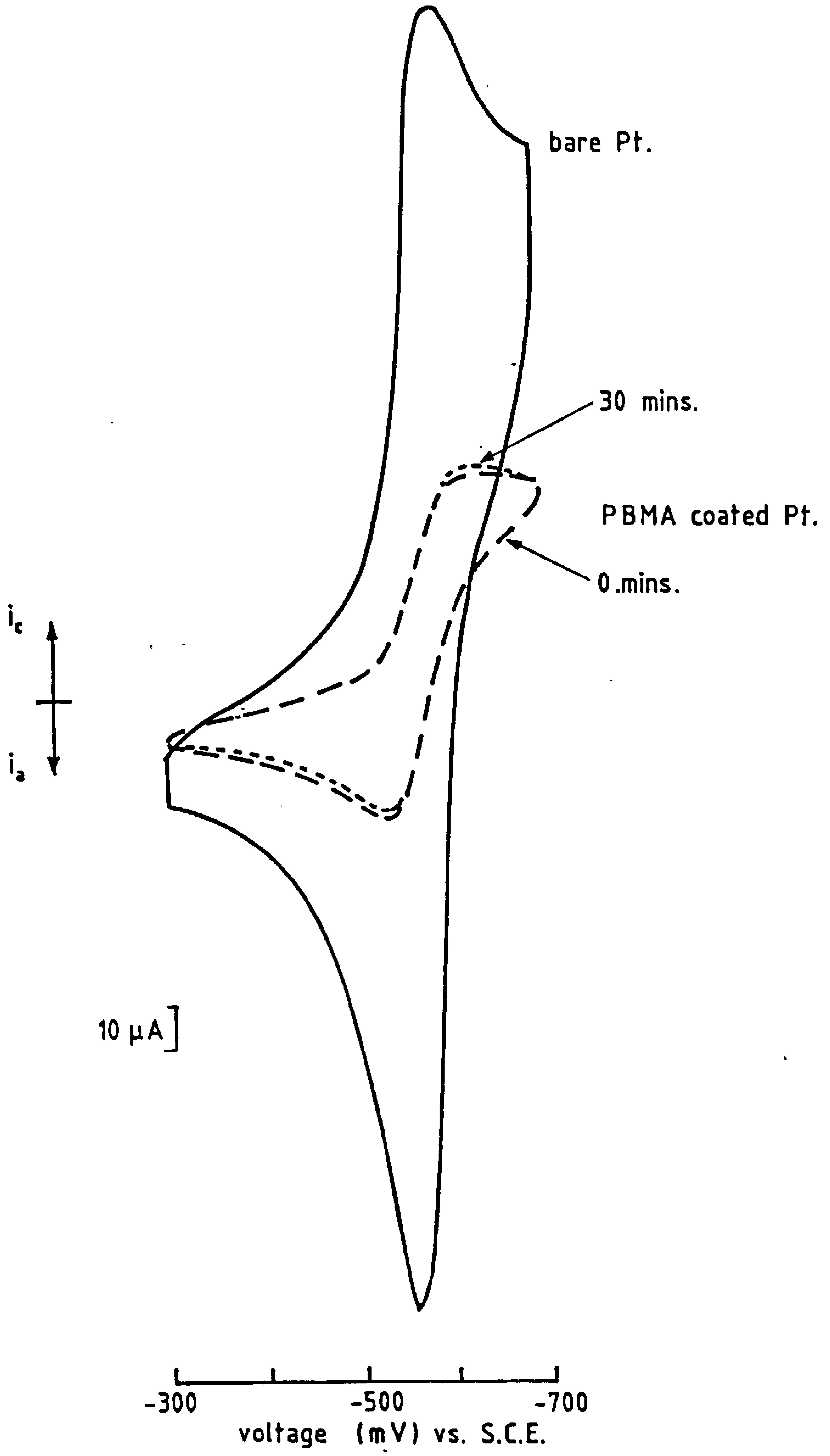

Fig 8.29 Cyclic voltammograms for i) an uncoated platinum wire electrode (——) and ii) the same electrode coated with 20 monolayers of PBMA in 0.1M KCl and 1mM Benzyl Viologen with a sweep rate of 0.1V/sec at 21°C and pH=6.5. Curves for the coated electrode are shown after (— —) 0 and (– – –) 30 minutes immersion.

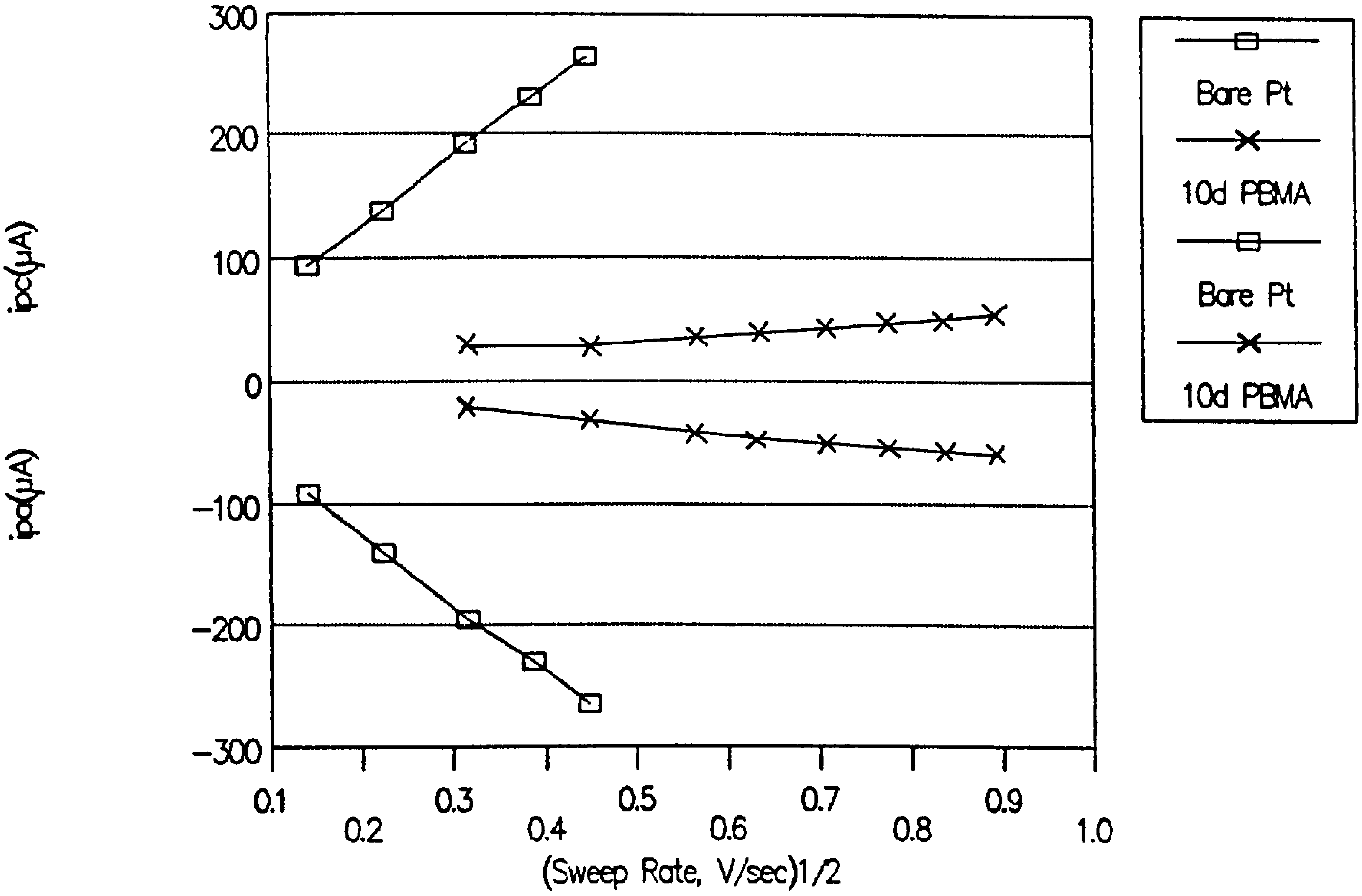

Fig 8.30 Peak anodic and cathodic currents, i_{pa} and i_{pc}, for (□) an uncoated platinum wire electrode and the same electrode coated with (x) 20 monolayers of PBMA plotted as a function of (sweep rate)$^{1/2}$. The peak currents were estimated from cyclic voltammograms measured during immersion of the electrodes in 0.1M KCl and 1mM Benzyl Viologen (eg fig 8.29).

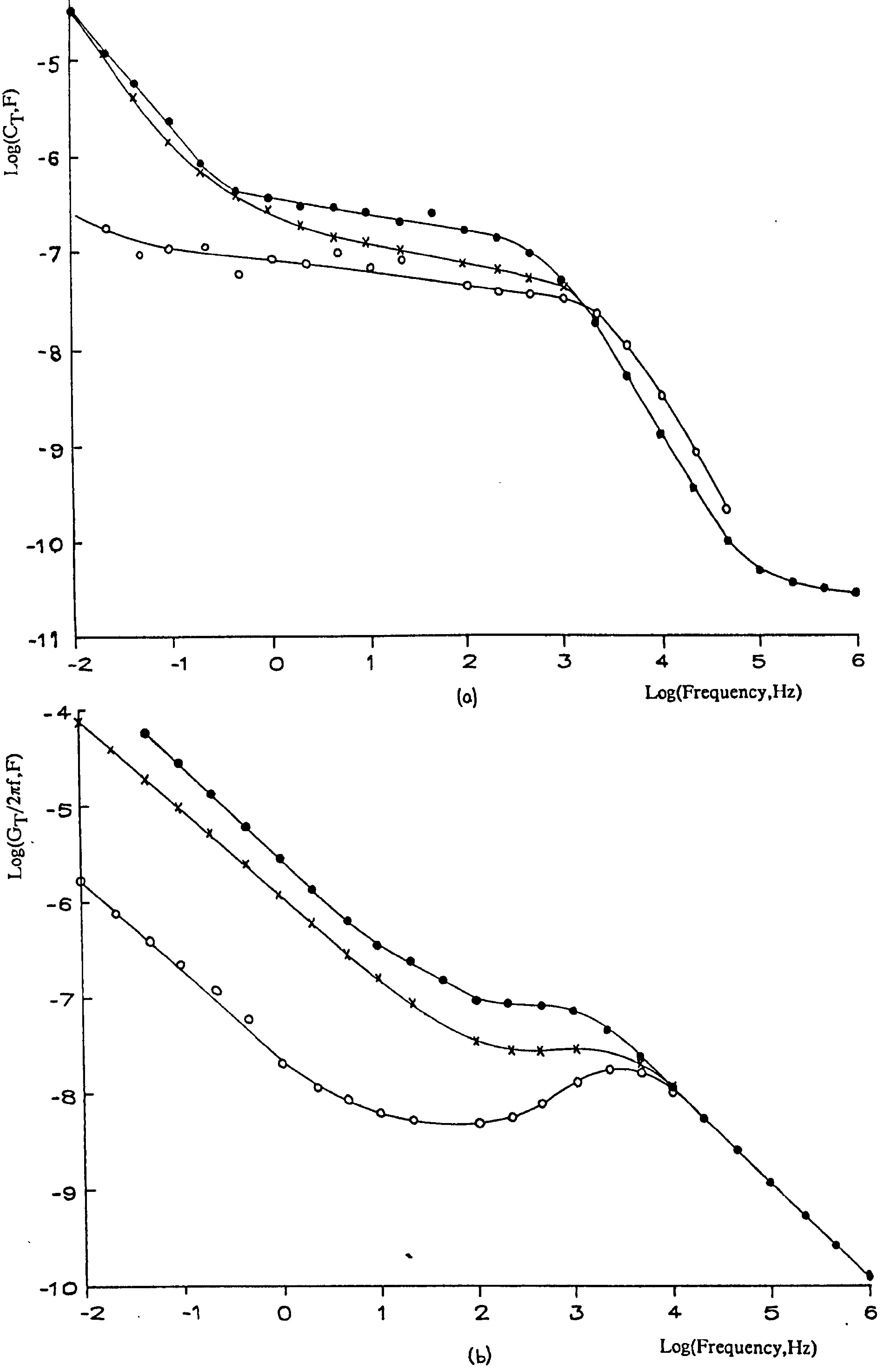

Fig 8.31 (a) Log Capacitance (C_T) and Loss ($G_T/2\pi f$) of a sputtered copper electrode with a (●) 10, (x) 20 and (o) 30 dip coating of PBMA plotted as a function of log frequency in 2mM KCl at 19±2°C.

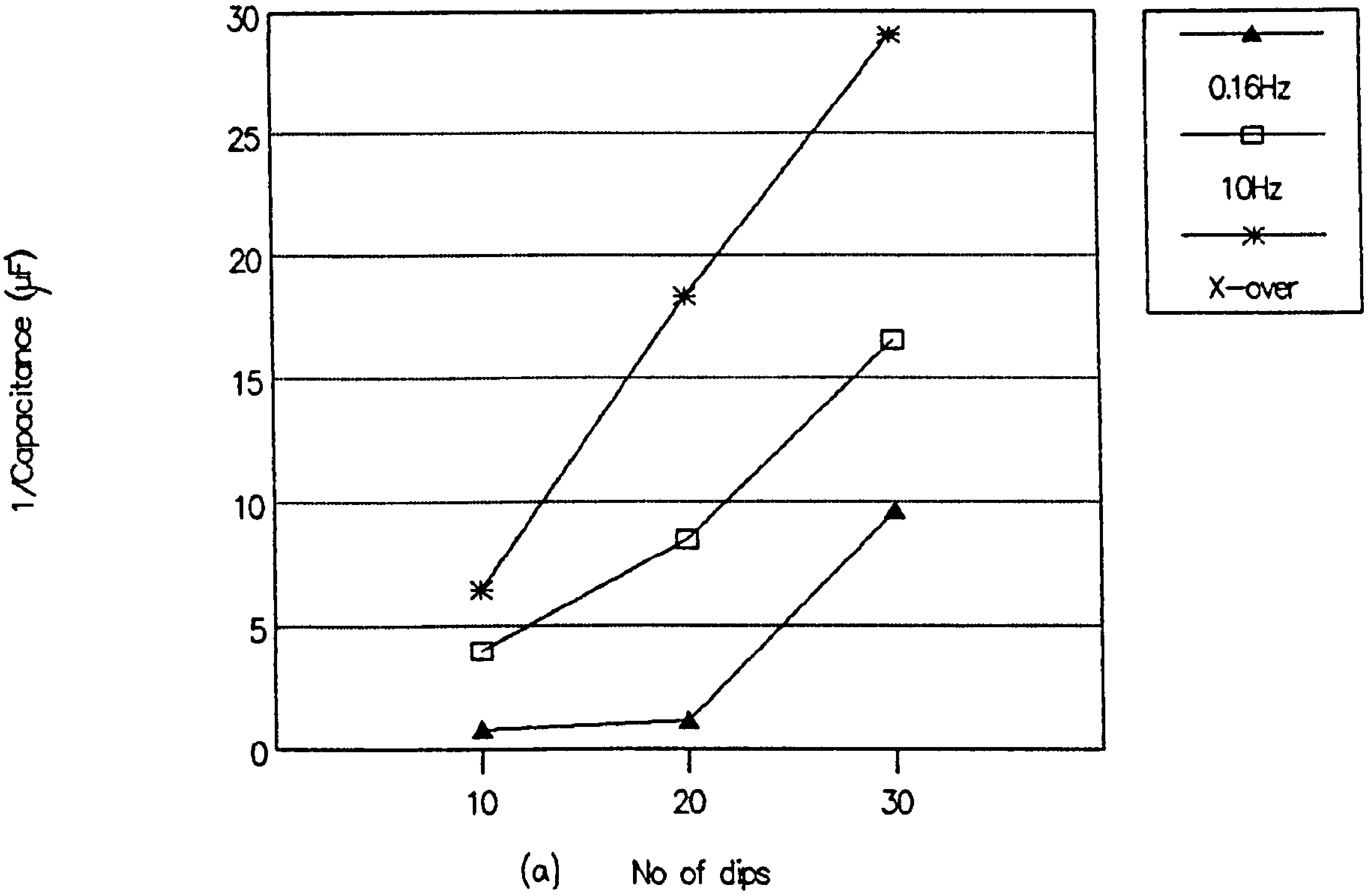

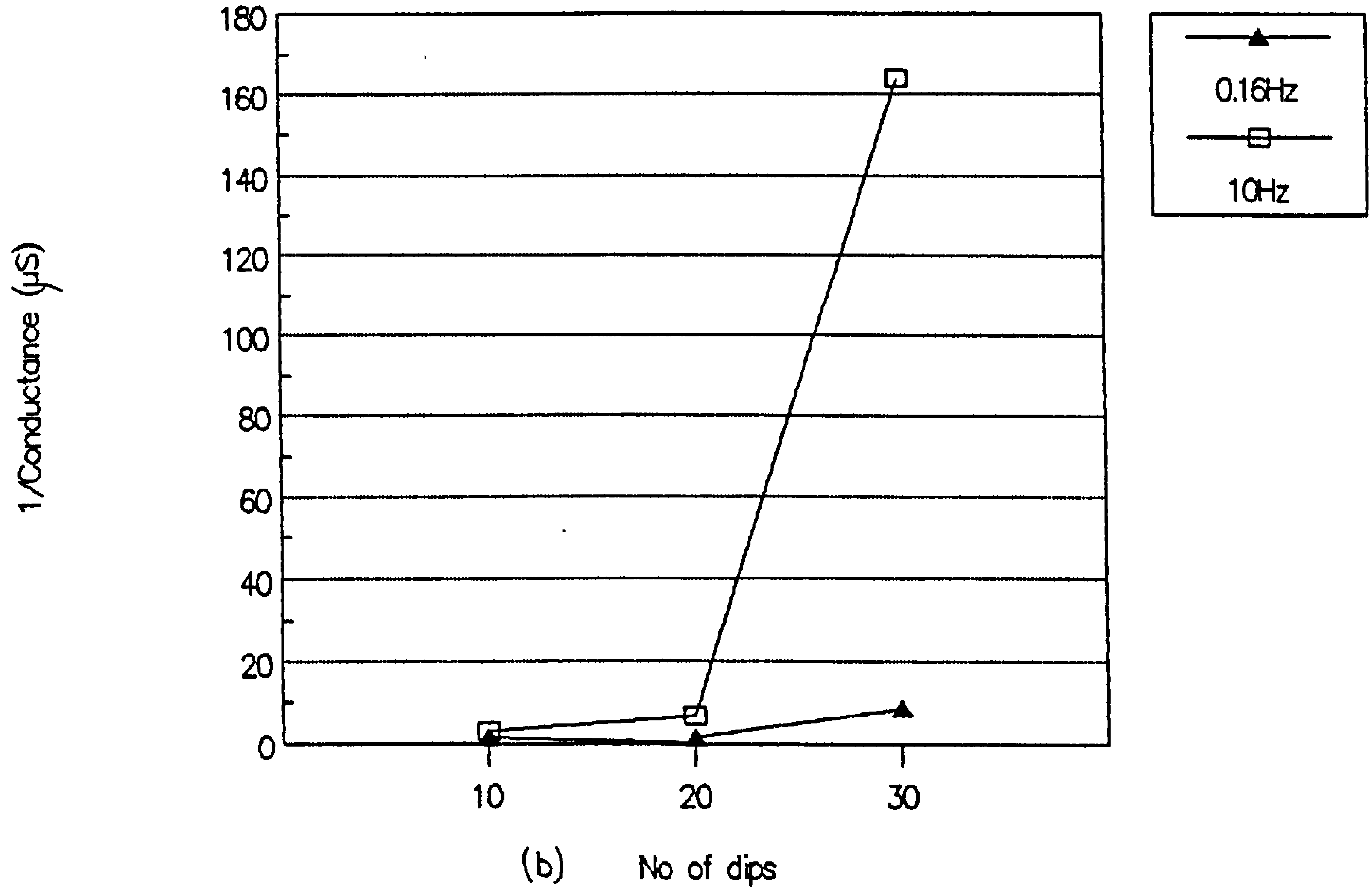

Fig 8.32 (a) Reciprocal capacitance ($1/C_b$) and (b) conductance ($1/G_b$) for a platinum electrode with a 10, 20 and 30 dip coating of PBMA immersed in 2mM KCl at 23°C, plotted as a function the number of dipping cycles. Reciprocal capacitance values were estimated from fig 8.31a at (▲) 0.16Hz, (□) 10Hz and (*) the cross over frequencies. Reciprocal conductance values were estimated from fig 8.31b at (▲) 0.16Hz and (□) 10Hz.

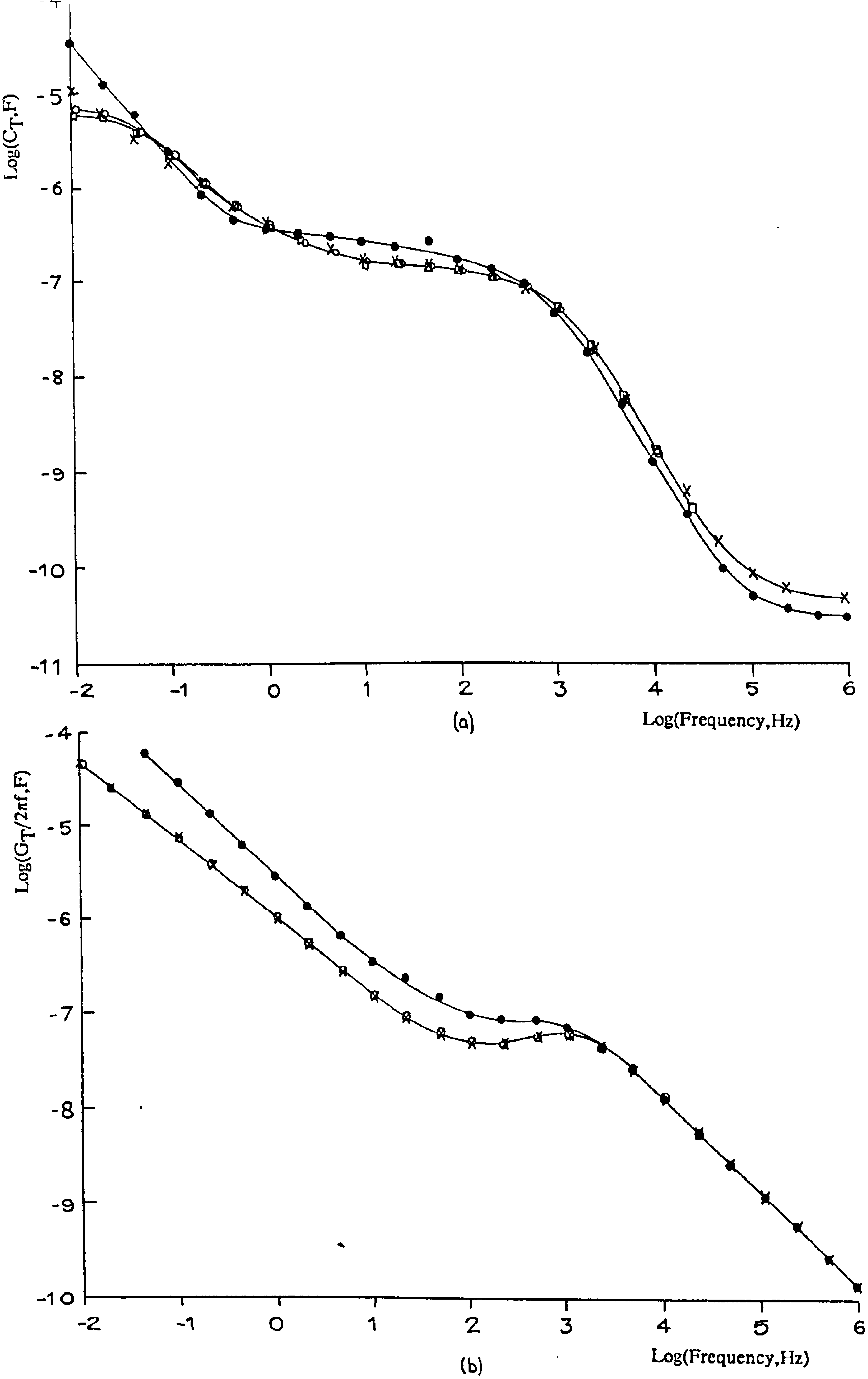

Fig 8.33 (a) Log Capacitance, C_T and (b) Loss ($G_T/2\pi f$) plotted against log frequency, F, for a sputtered copper electrode with a 10 dip coating of PBMA after (●) 1.5, (x) 60, (□) 245 and (o) 302 minutes exposure to 2mM KCl at 23°C.

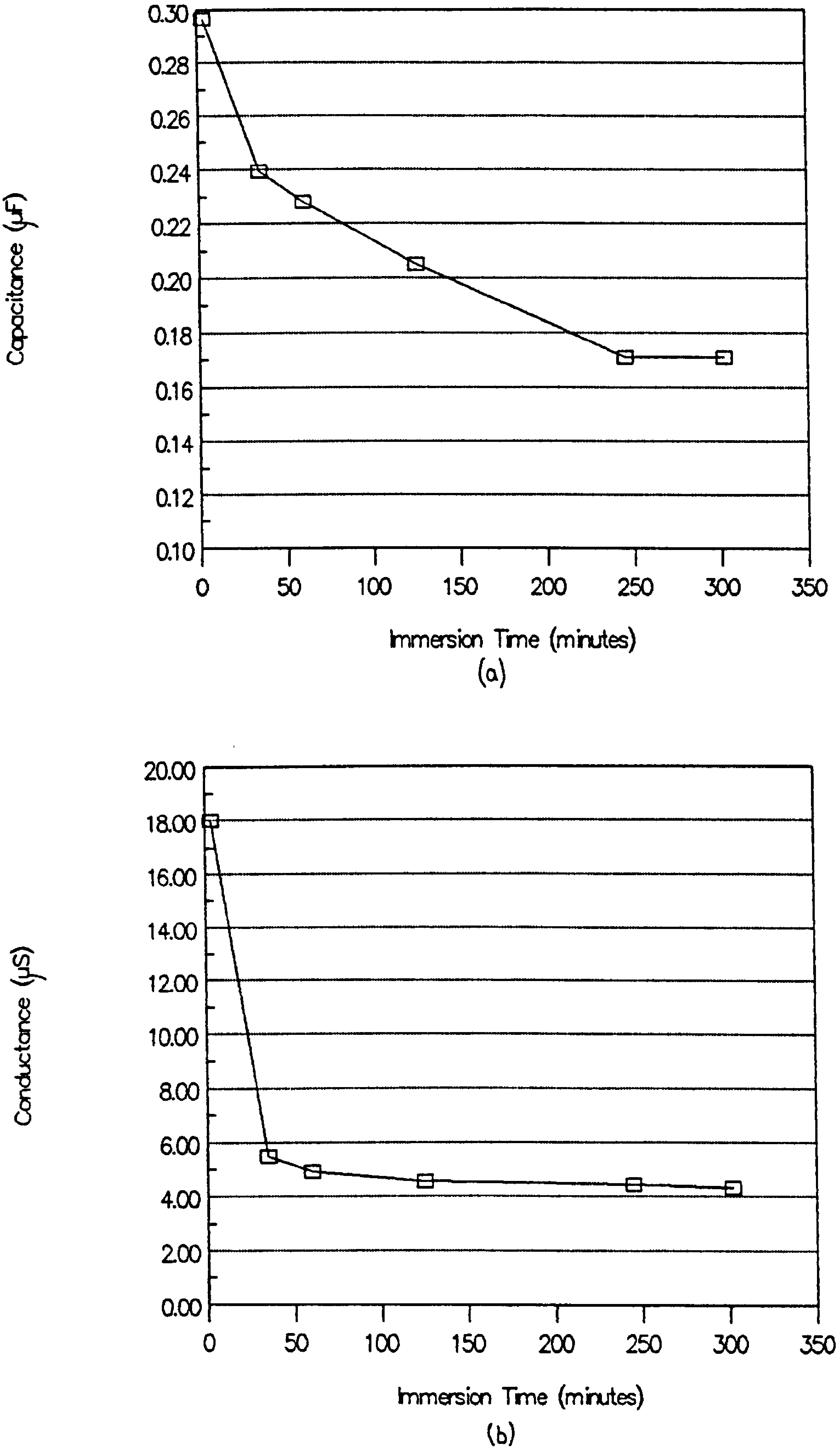

Fig 8.34 (a) Capacitance C_b and (b) conductance G_b for a 10 dip coated sputtered copper electrode plotted as a function of immersion time in 2mM KCl at 23°C. The capacitance and conductance data were estimated from the curves in fig 8.33 at 10Hz (and from additional curves not shown in fig 8.33).

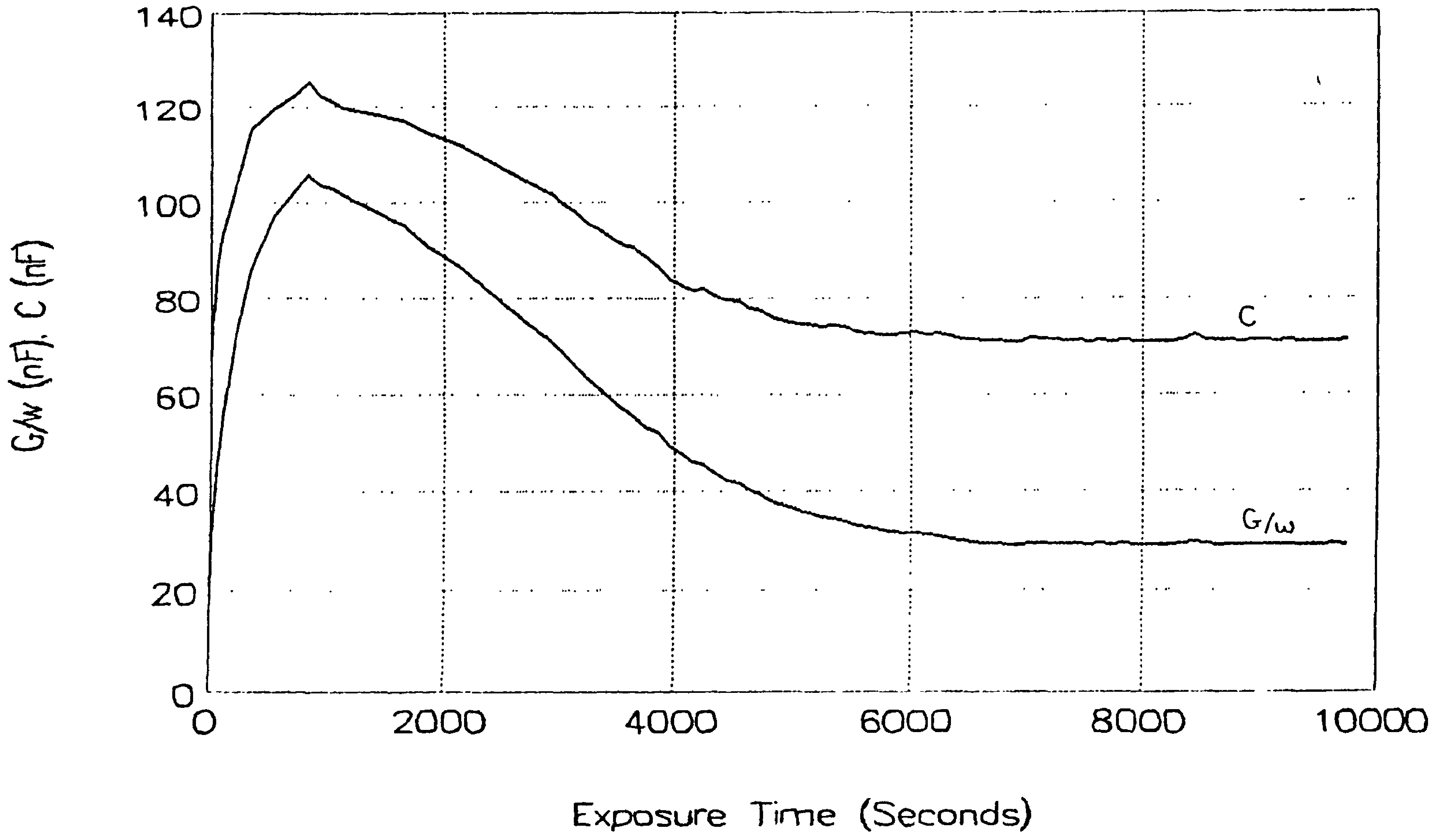

Fig 8.35 Capacitance, C_T and loss, $G_T/2\pi f$ for a sputtered copper electrode with a 15 monolayers of PBMA, immersed in 2mM KCl at 22±2°C and plotted as a function of immersion time.

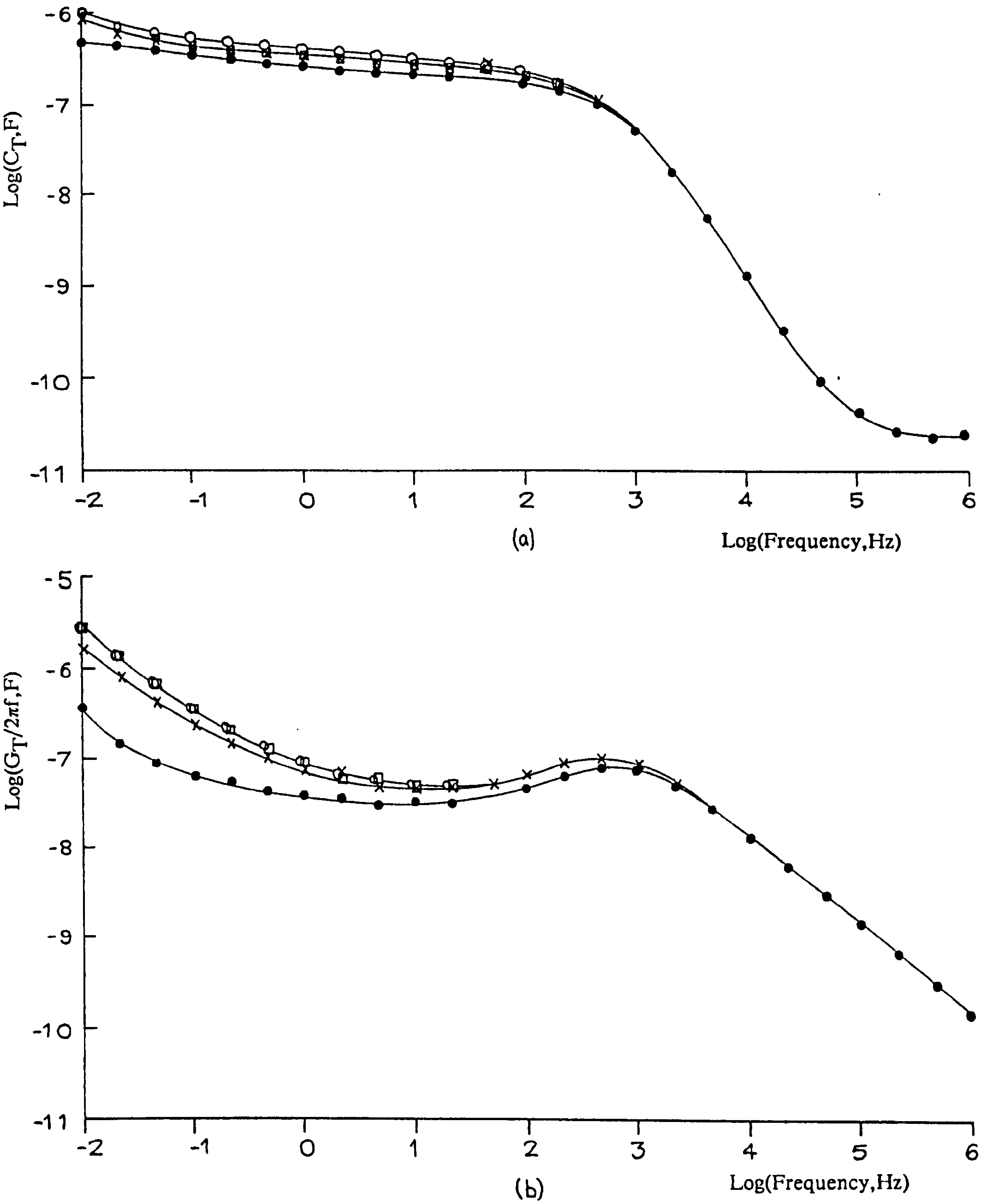

Fig 8.36 (a) Log Capacitance, C_T and (b) Loss ($G_T/2\pi f$) plotted against log frequency, F, for an evaporated aluminium electrode with a 10 dip coating of PBMA after (●) 0, (x) 23, (□) 40 and (o) 60 minutes exposure to 2mM KCl at 23°C.

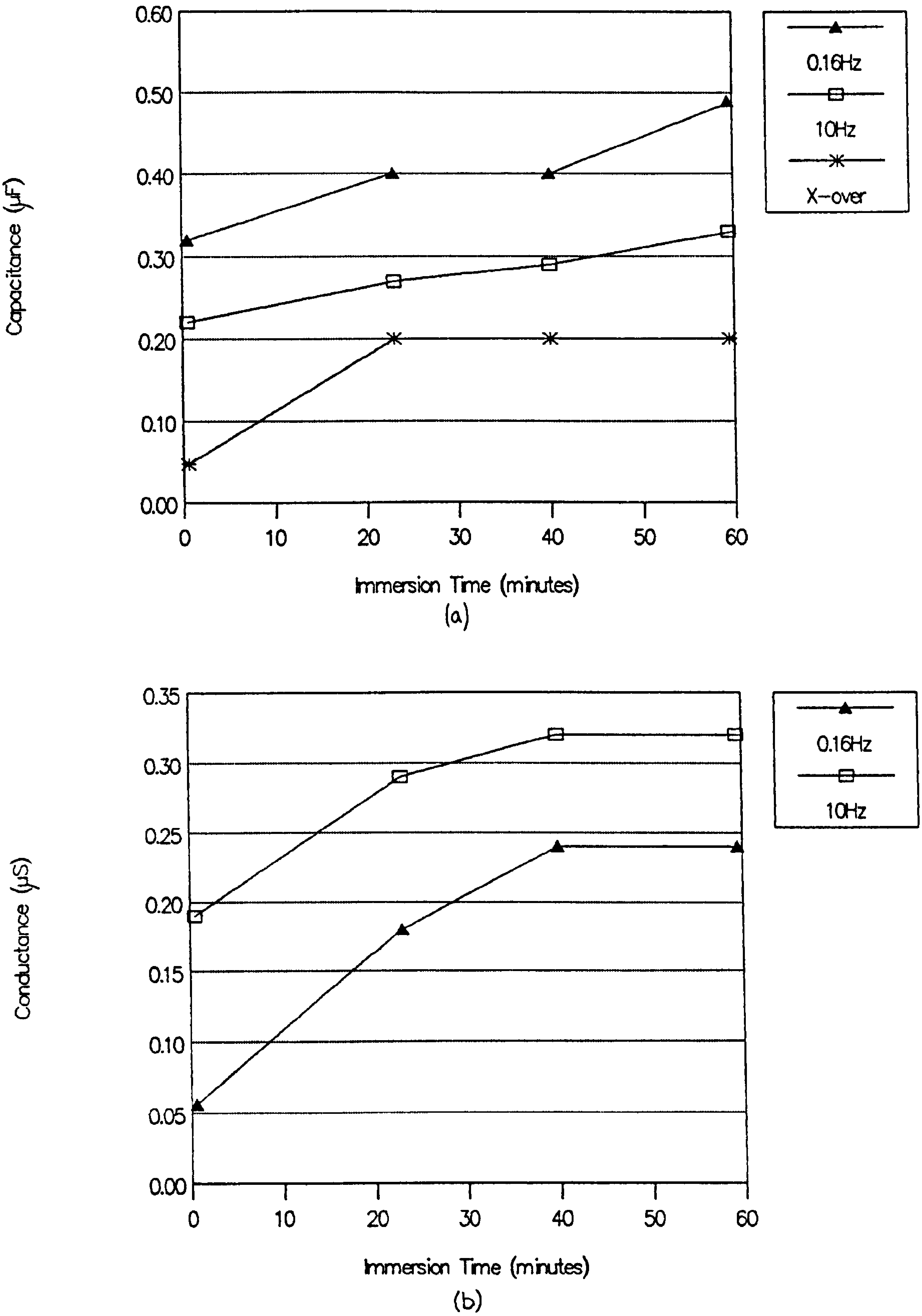

Fig 8.37 (a) Capacitance C_b and (b) conductance G_b for a 10 dip coated sputtered copper electrode plotted as a function of immersion time in 2mM KCl at 23°C. The capacitance data were estimated from the curves in fig 8.36a at (▲) 0.16Hz, (□) 10Hz and (*) the cross over frequencies. Conductance values were estimated from fig 8.36b at (▲) 0.16Hz and (□) 10Hz.

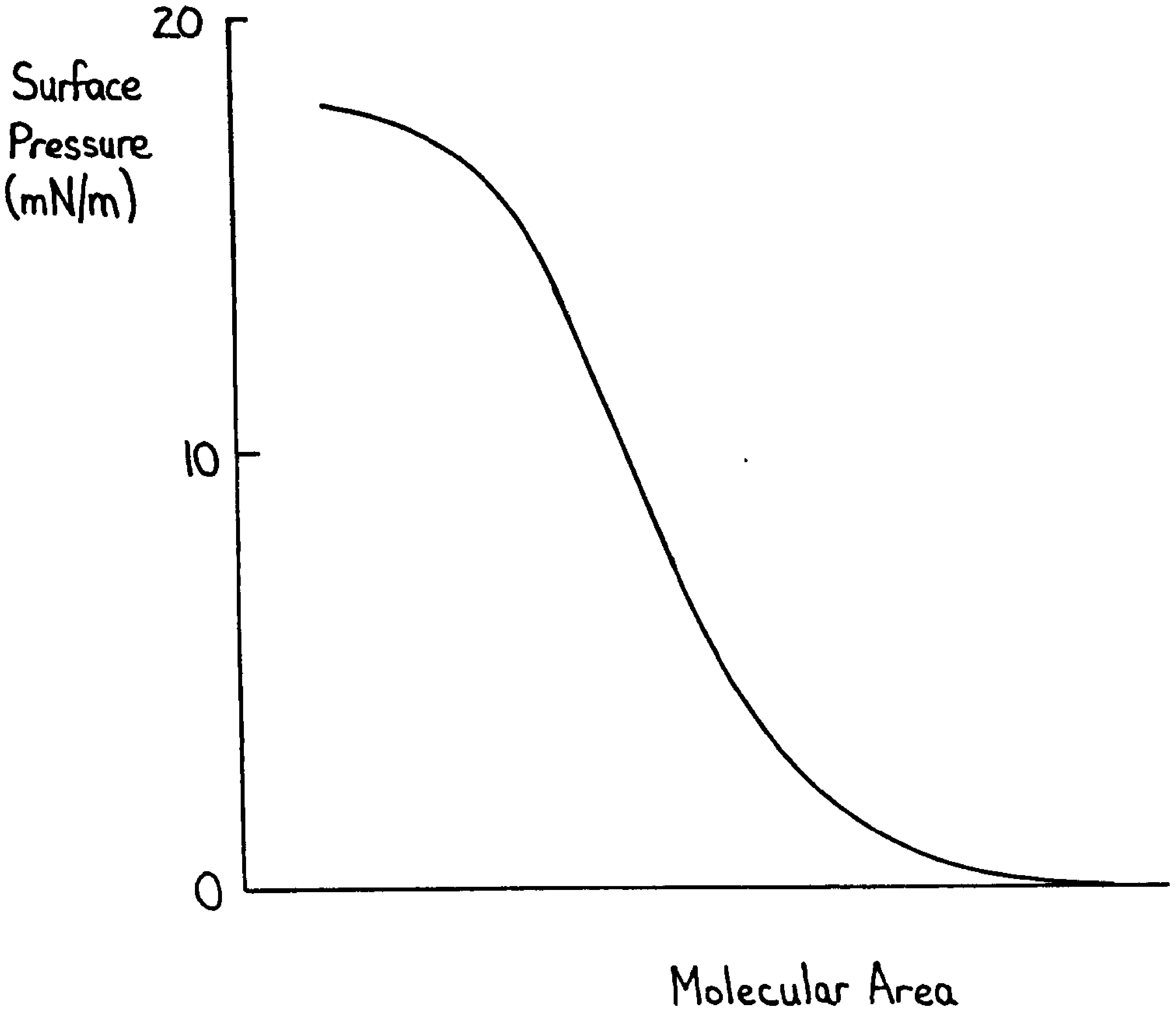

Fig 8.38 Pressure-Area Curve for valinomycin at 21.5°C and pH 5.3.

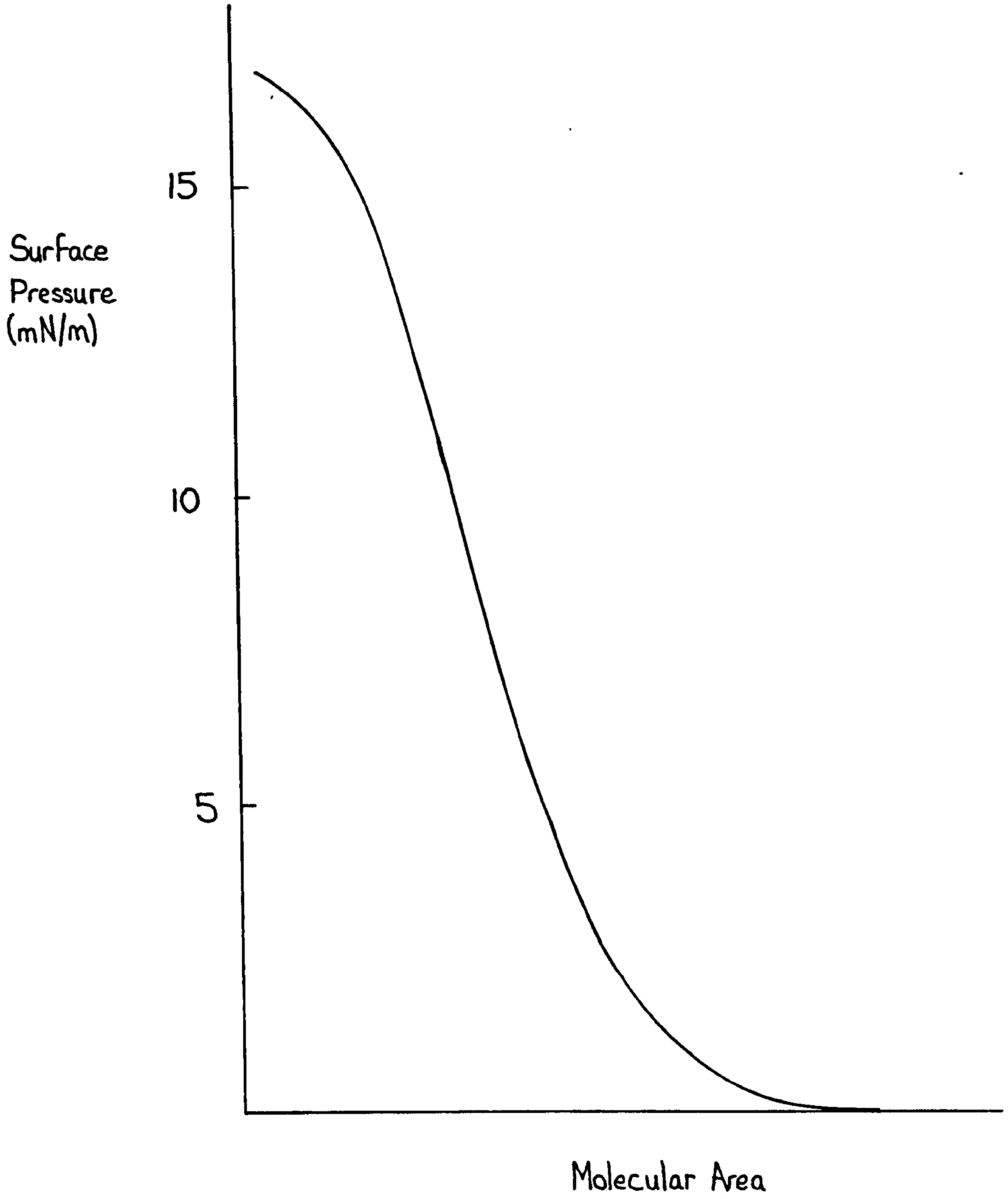

Fig 8.39 Pressure–Area Curve for a mixed monolayer of PBMA and Valinomycin at 22.4^{o}C and pH 5.8.

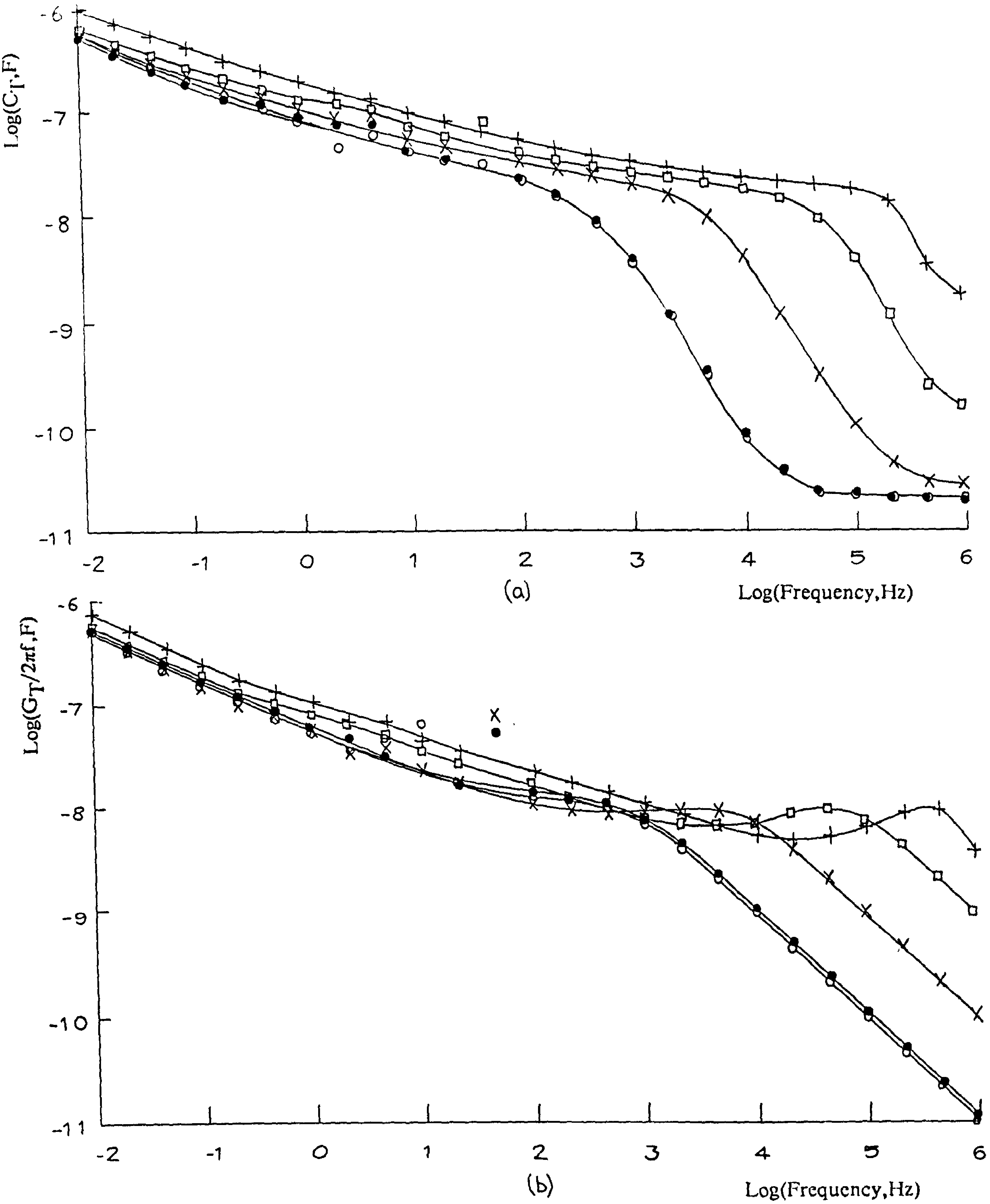

Fig 8.40 (a) Log Capacitance, C_T and (b) Loss ($G_T/2\pi f$) plotted against log frequency, F, for a platinum electrode coated in 40 monolayers of PBMA/Valinomycin and immersed in (•)0.2mM, (x) 2.0mM, (□) 20mM and (+) 200mM NaCl at 23.2±0.1°C.

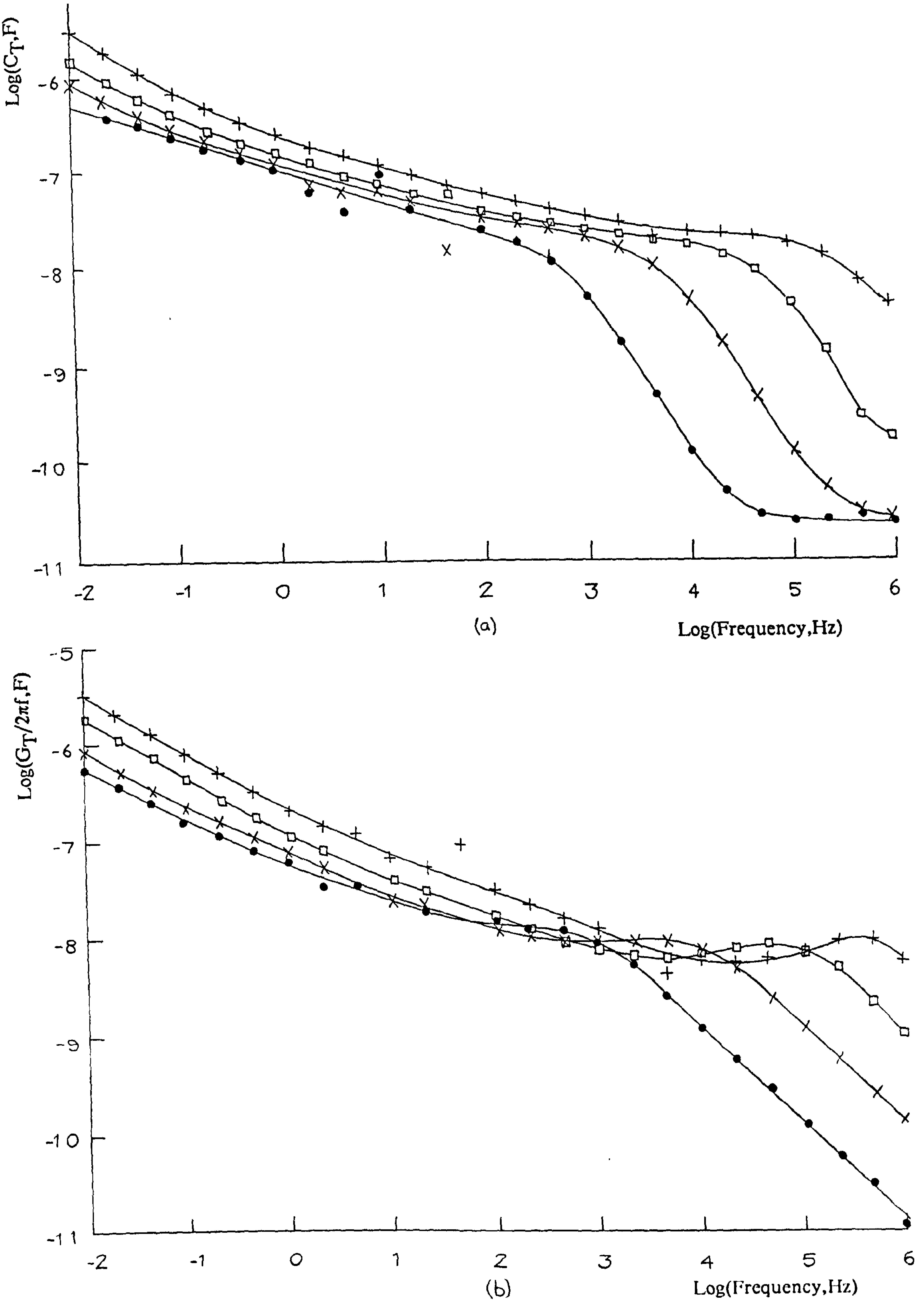

Fig 8.41 (a) Log Capacitance, C_T and (b) Loss ($G_T/2\pi f$) plotted against log frequency, F, for a platinum electrode coated in 40 monolayers of PBMA/Valinomycin and immersed in (·) 0.2mM, (x) 2.0mM, (□) 20mM and (+) 200mM KCl at 23.2±0.1°C.

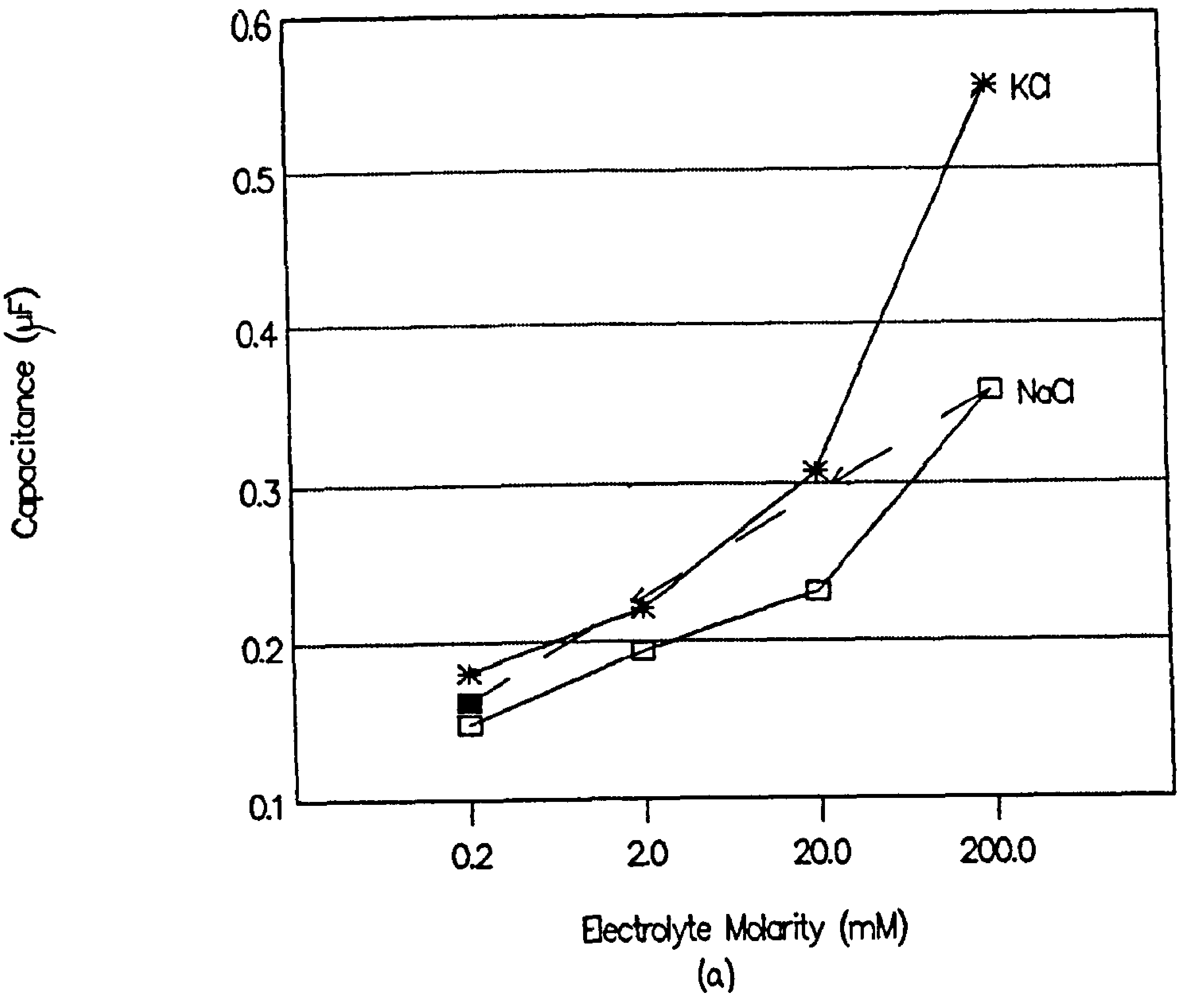

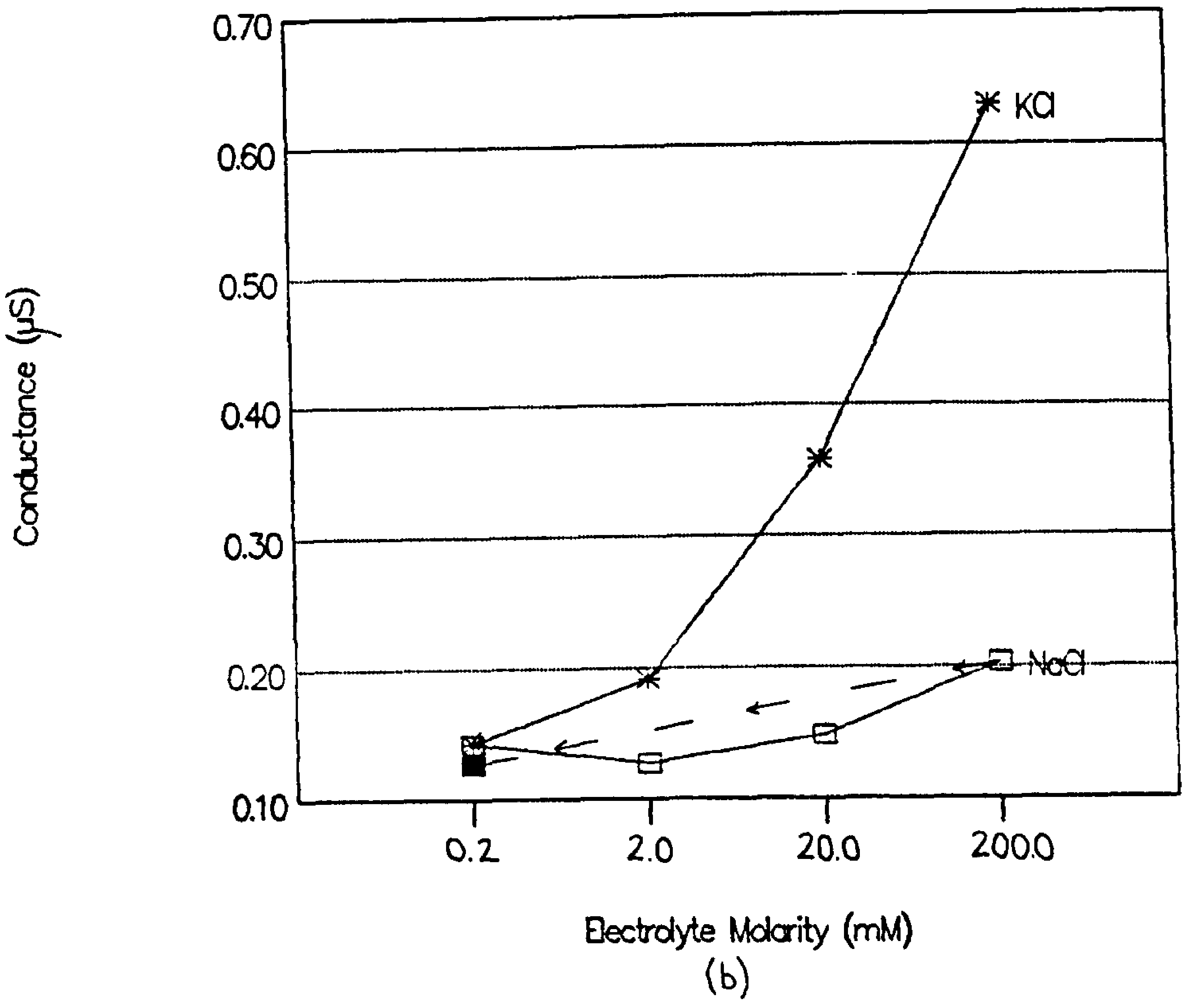

Fig 8.42 (a) Capacitance C_b, and (b) Conductance G_b, for a platinum electrode coated with 40 monolayers of PBMA/Valinomycin, plotted as a function of electrolyte molarity. Capacitance and conductance values were estimated from figs 8.40a, 8.41a and figs 8.40b, 8.41b respectively at 0.16Hz.

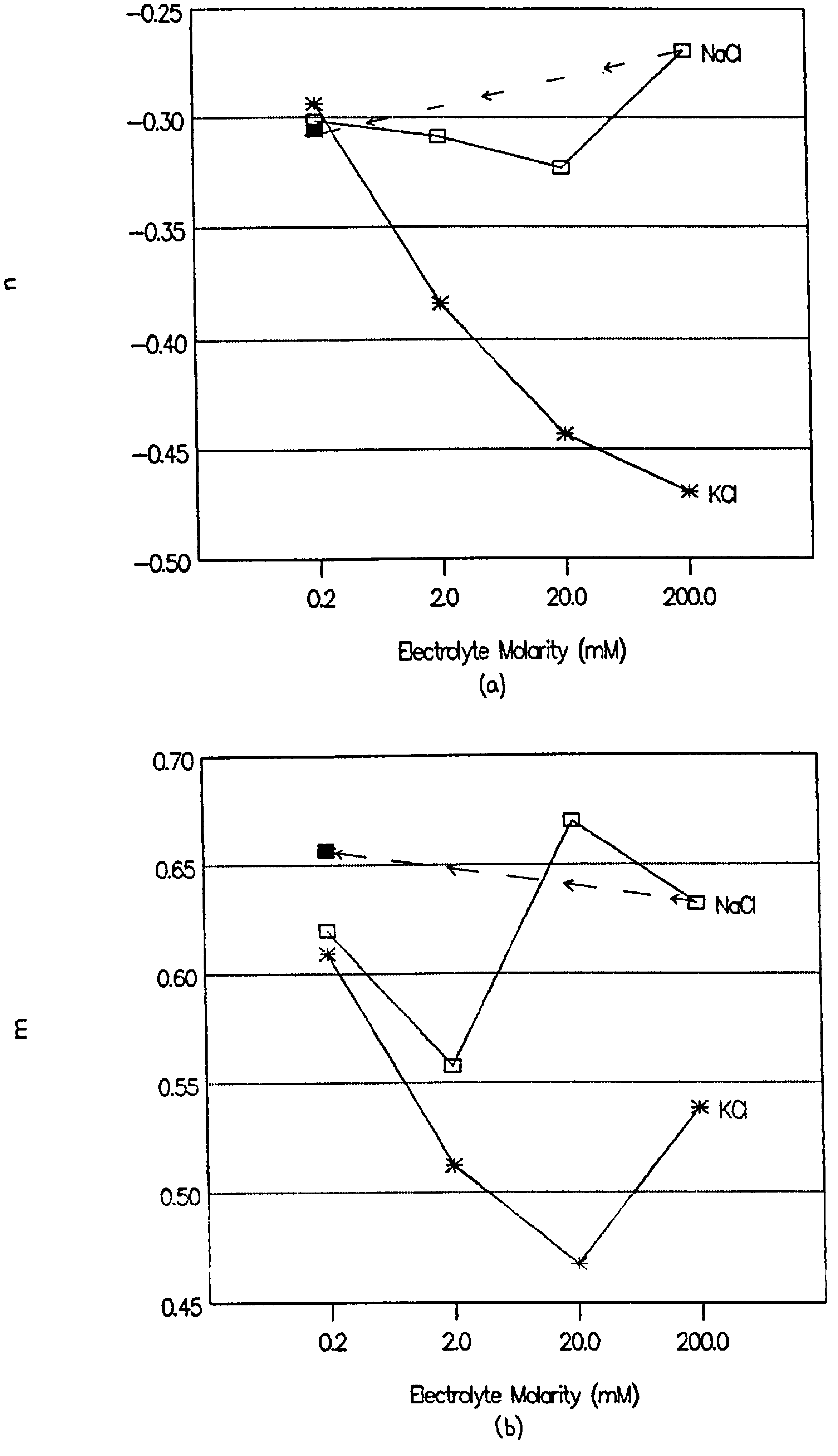

Fig 8.43 (a) n and (b) m for a platinum electrode coated with 40 monolayers of PBMA/Valinomycin, plotted as a function of electrolyte molarity. n and m values were estimated from figs 8.40a, 8.41a and figs 8.40b, 8.41b respectively.

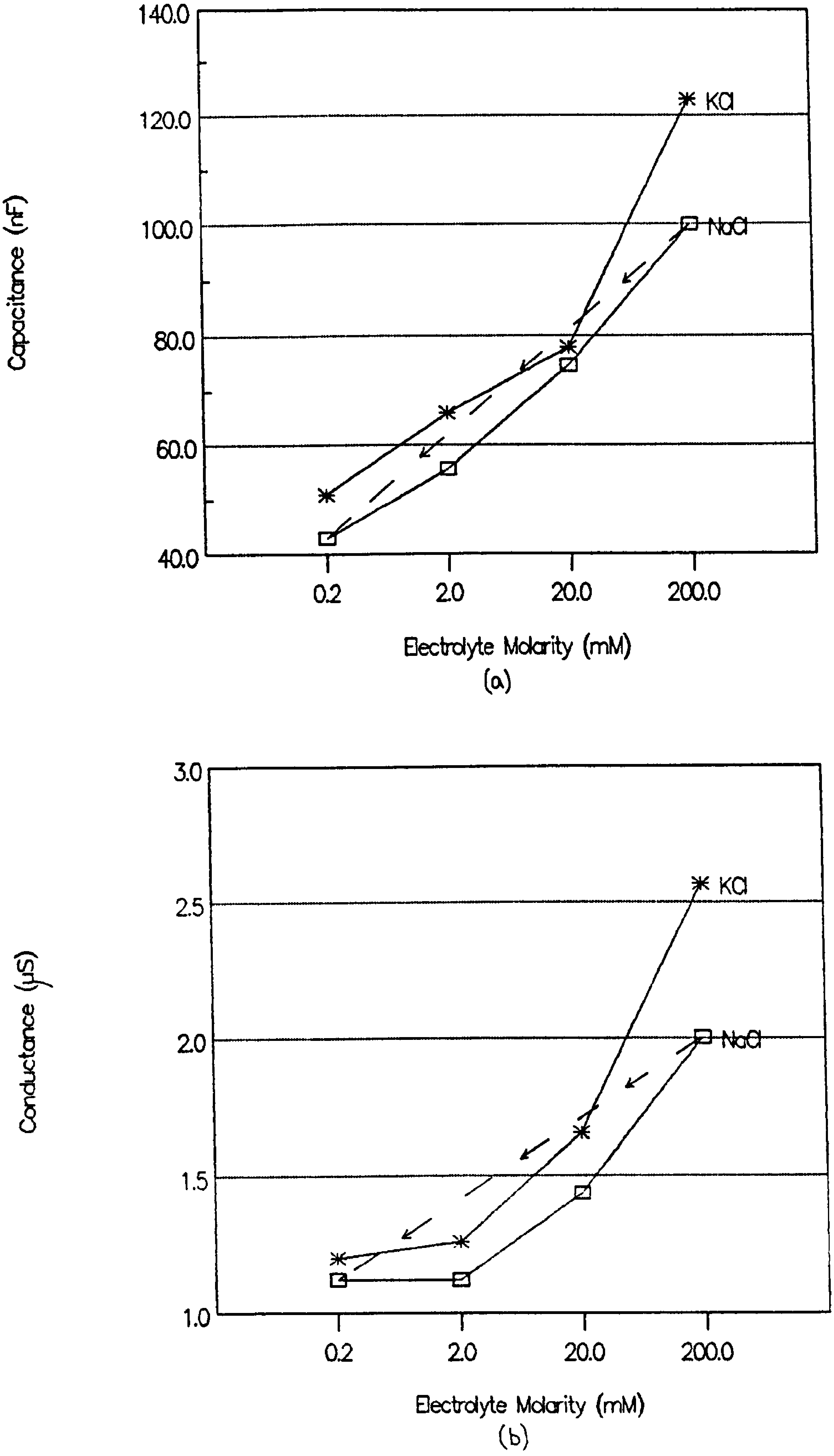

Fig 8.44 (a) Capacitance C_b, and (b) Conductance G_b, for a platinum electrode coated with 40 monolayers of PBMA/Valinomycin, plotted as a function of electrolyte molarity. Capacitance and conductance values were estimated from figs 8.40a, 8.41a and figs 8.41b, 8.42b respectively at 10Hz.

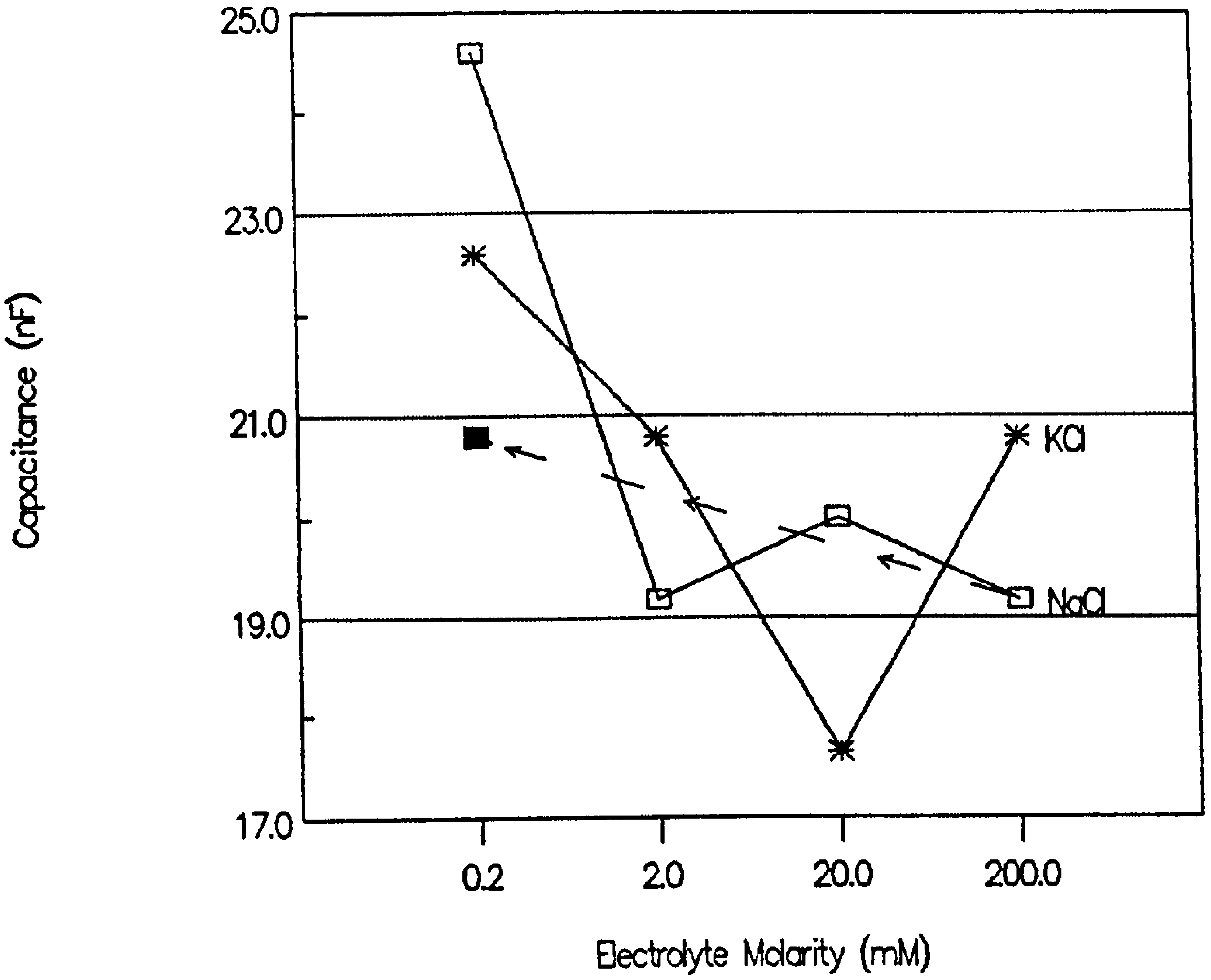

Fig 8.45 Capacitance C_b for a platinum electrode coated with 40 monolayers of PBMA/Valinomycin, plotted as a function of electrolyte molarity. Capacitance values were estimated from figs 8.40a and 8.41a at the cross over point of the C_T and $G_T/2\pi f$ curves.

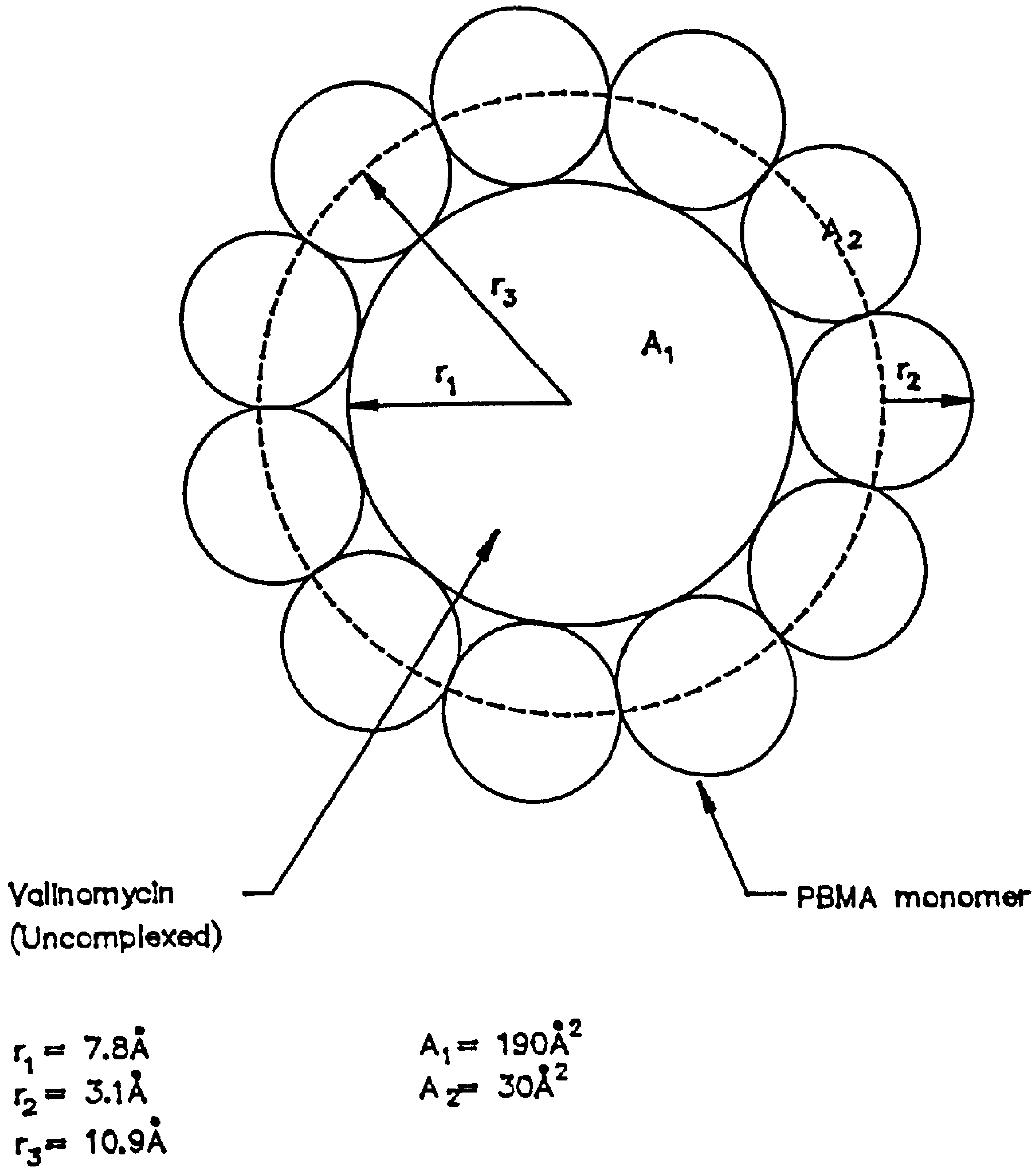

Fig 8.46 Simplified representation of valinomycin and PBMA molecules, based on their estimated monomer areas. The diagram shows that a minimum of 11 PBMA molecules are required to surround each valinomycin molecule.

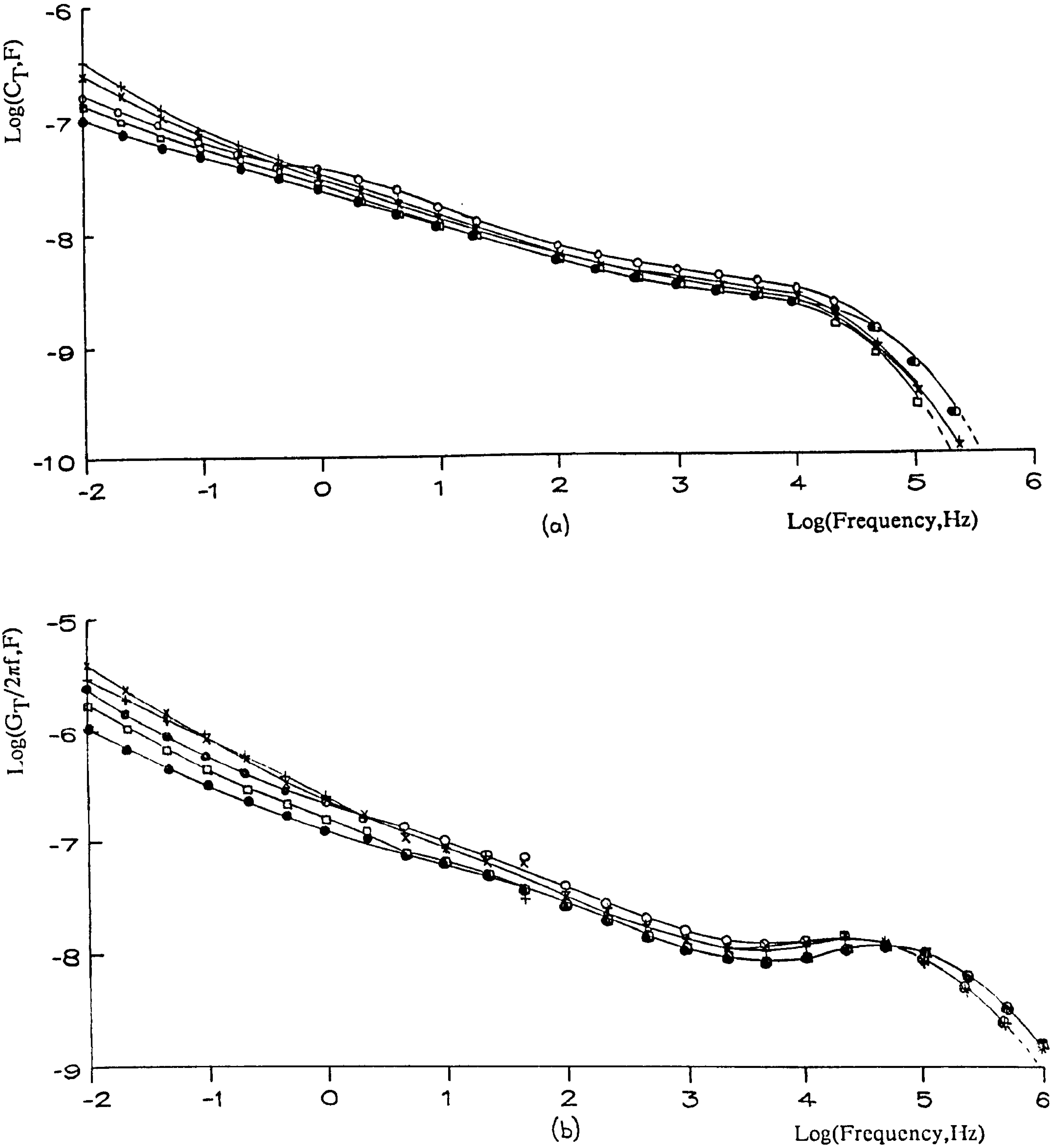

Fig 8.47 (a) Log Capacitance, C_T and (b) Loss ($G_T/2\pi f$) plotted against log frequency, F, for a platinum electrode coated in 40 monolayers of PBMA/Valinomycin and immersed in the 20mM electrolytes (●) $CaCl_2$, (x) KI, (□) NaCl, (+) KCl and again in (o) $CaCl_2$ at 22°C.

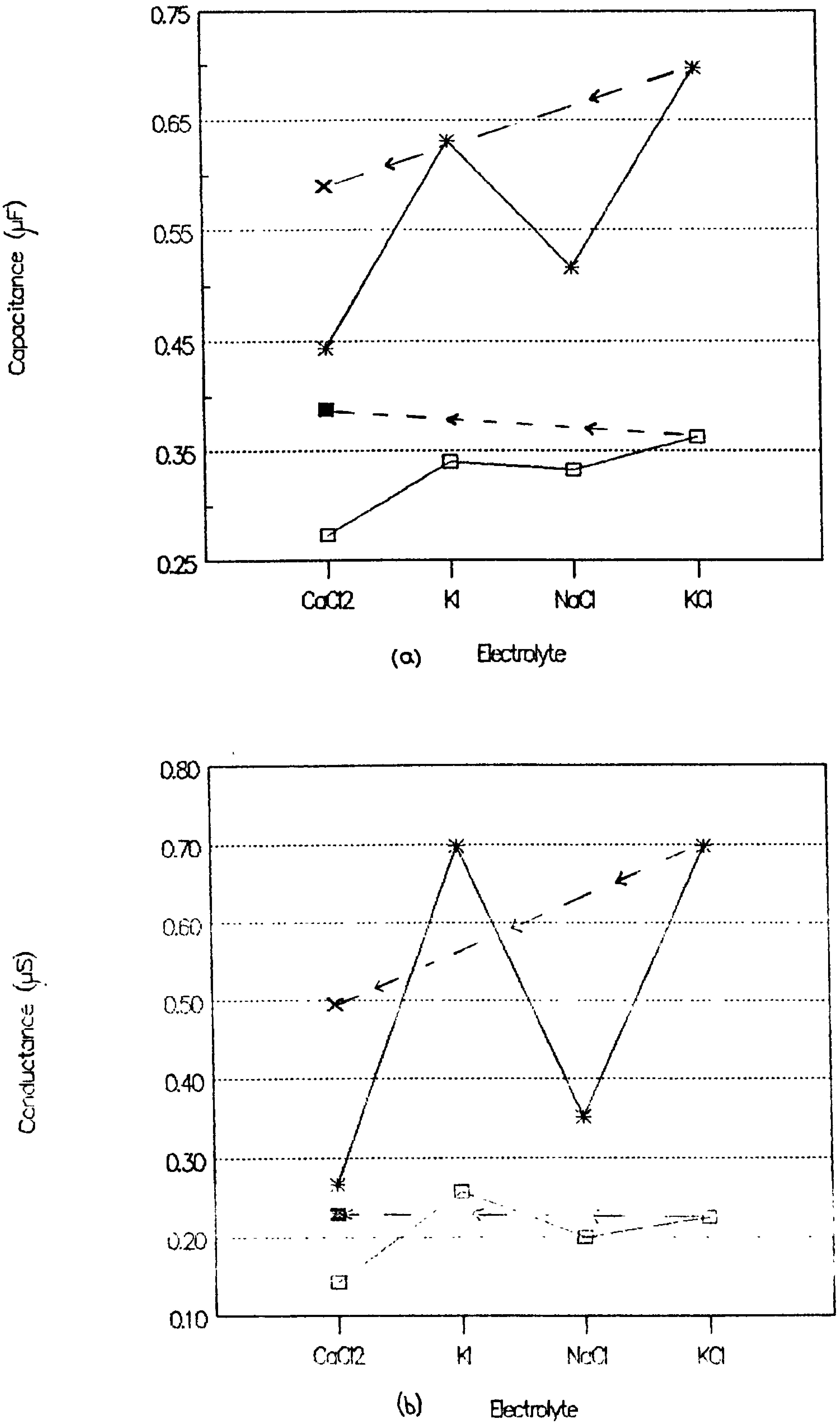

Fig 8.48 (a) (*,x) Capacitance C_b, and (b) (*,x) Conductance G_b, for a platinum electrode coated with 40 monolayers of PBMA/Valinomycin immersed in a range of electrolytes and plotted as a function of electrolyte. Capacitance and conductance values were estimated from fig 8.47a and 8.47b respectively at 0.16Hz. Corresponding data (□,■) for a similar platinum electrode coated in 20 monolayers of PBMA are given for comparison.

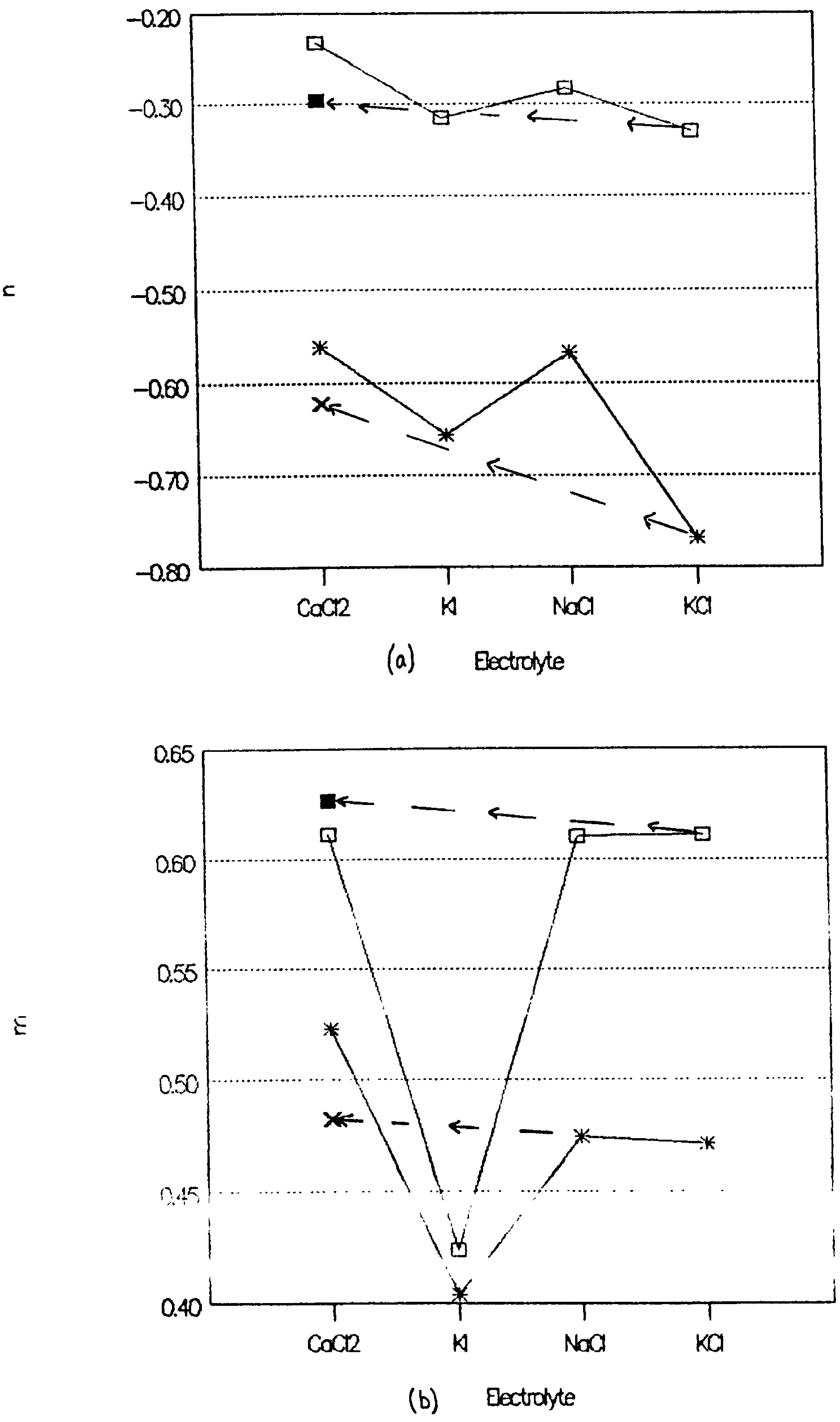

Fig 8.49 (a) (*,x) n and (b) (*,x) m for a platinum electrode coated with 40 monolayers of PBMA/Valinomycin immersed in a range of electrolytes and plotted as a function of electrolyte. n and m values were estimated from fig 8.47a and 8.47b respectively. Corresponding data (□,■) for a similar platinum electrode coated in 20 monolayers of PBMA are given for comparison.

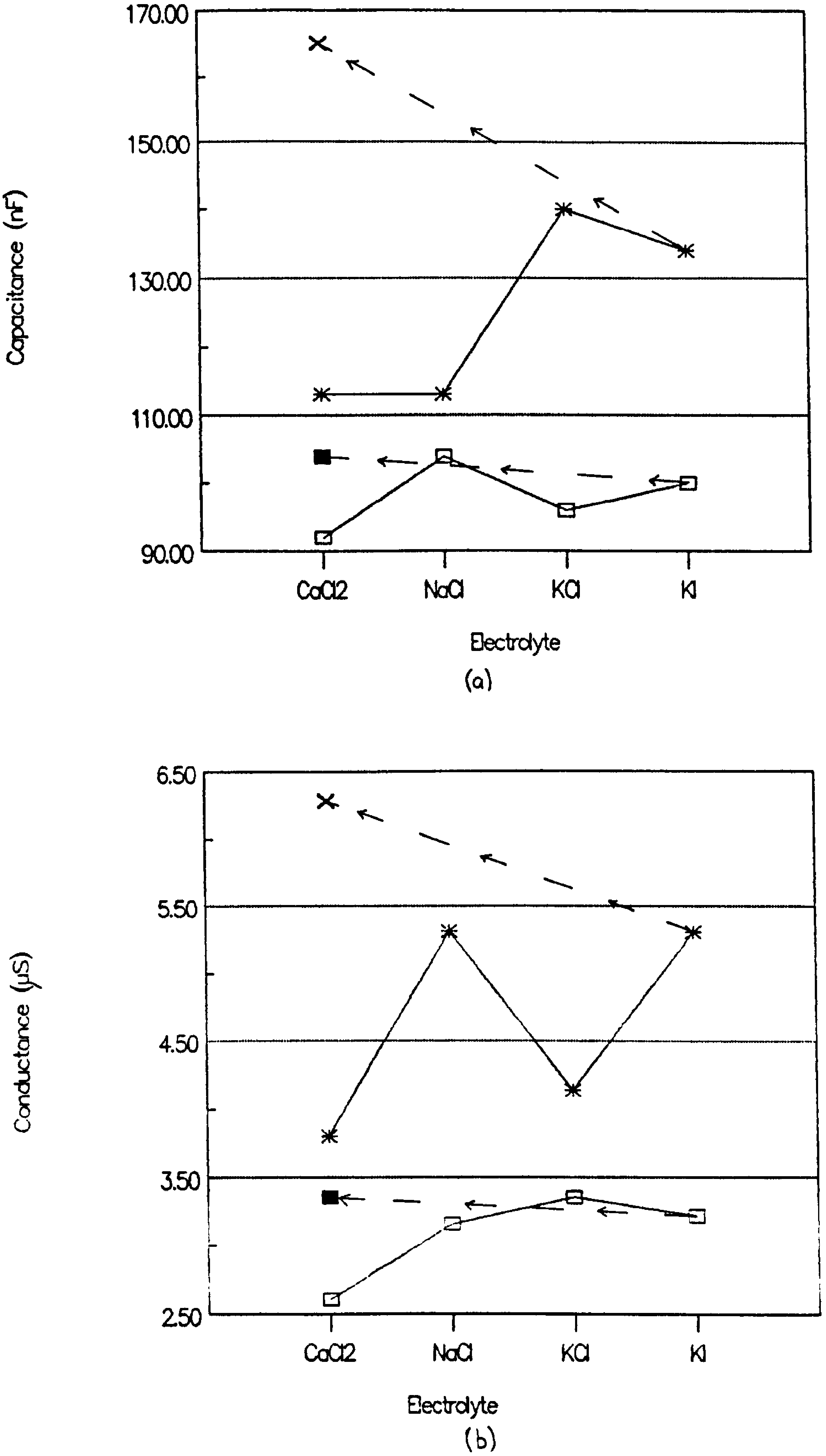

Fig 8.50 (a) (*,x) Capacitance C_b, and (b) (*,x) Conductance G_b, for a platinum electrode coated with 40 monolayers of PBMA/Valinomycin immersed in a range of electrolytes and plotted as a function of electrolyte. Capacitance and conductance values were estimated from fig 8.47a and 8.47b respectively at 10Hz. Corresponding data (□,■) for a similar platinum electrode coated in 20 monolayers of PBMA are given for comparison.

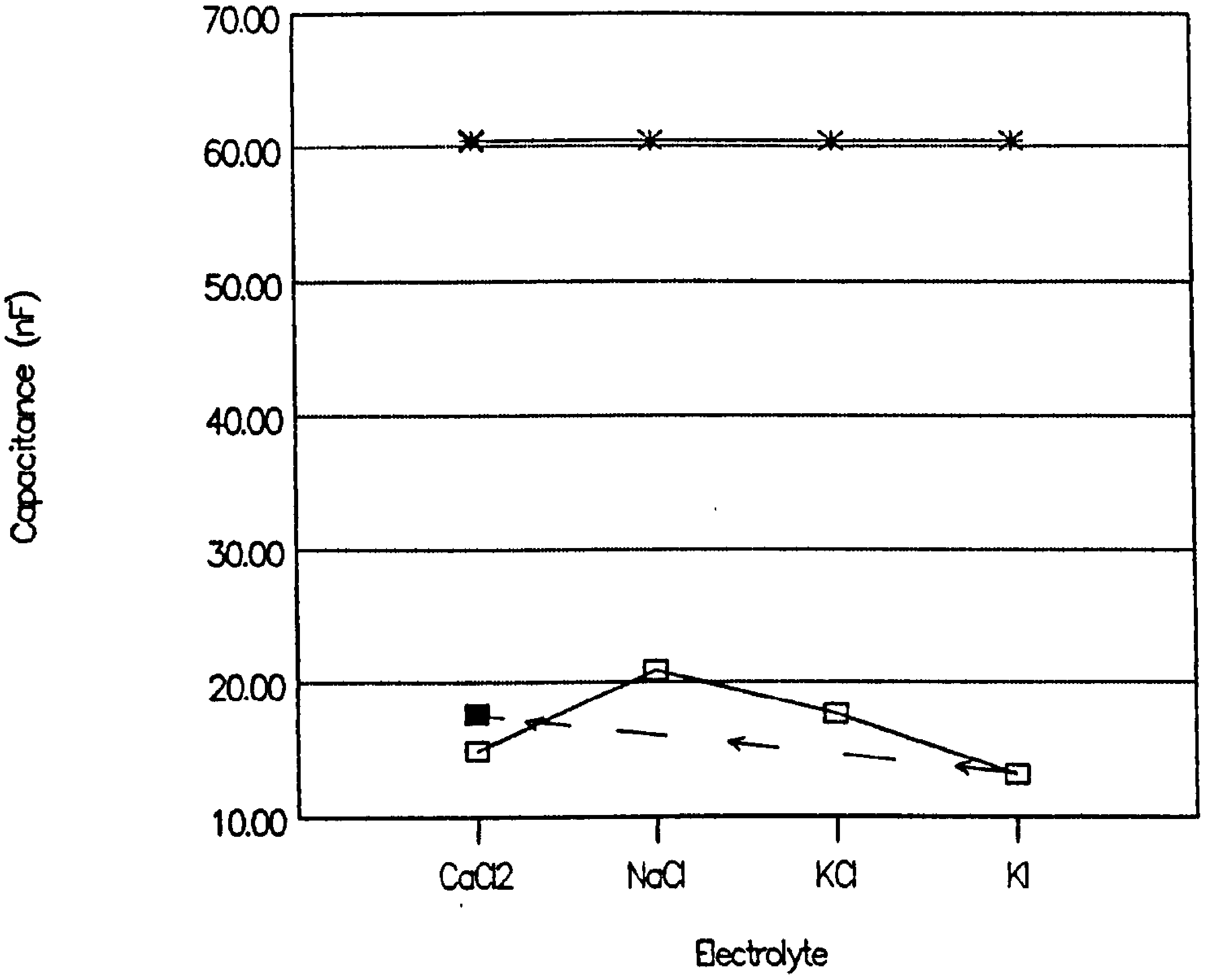

Fig 8.51 (*,x) Capacitance C_b for a platinum electrode coated with 40 monolayers of PBMA/Valinomycin immersed in a range of electrolytes and plotted as a function of electrolyte. Capacitance values were estimated from fig 8.47a at the cross over frequencies of the C_T and $G_T/2\pi f$ curves. Corresponding data (□,■) for a similar platinum electrode coated in 20 monolayers of PBMA are given for comparison.

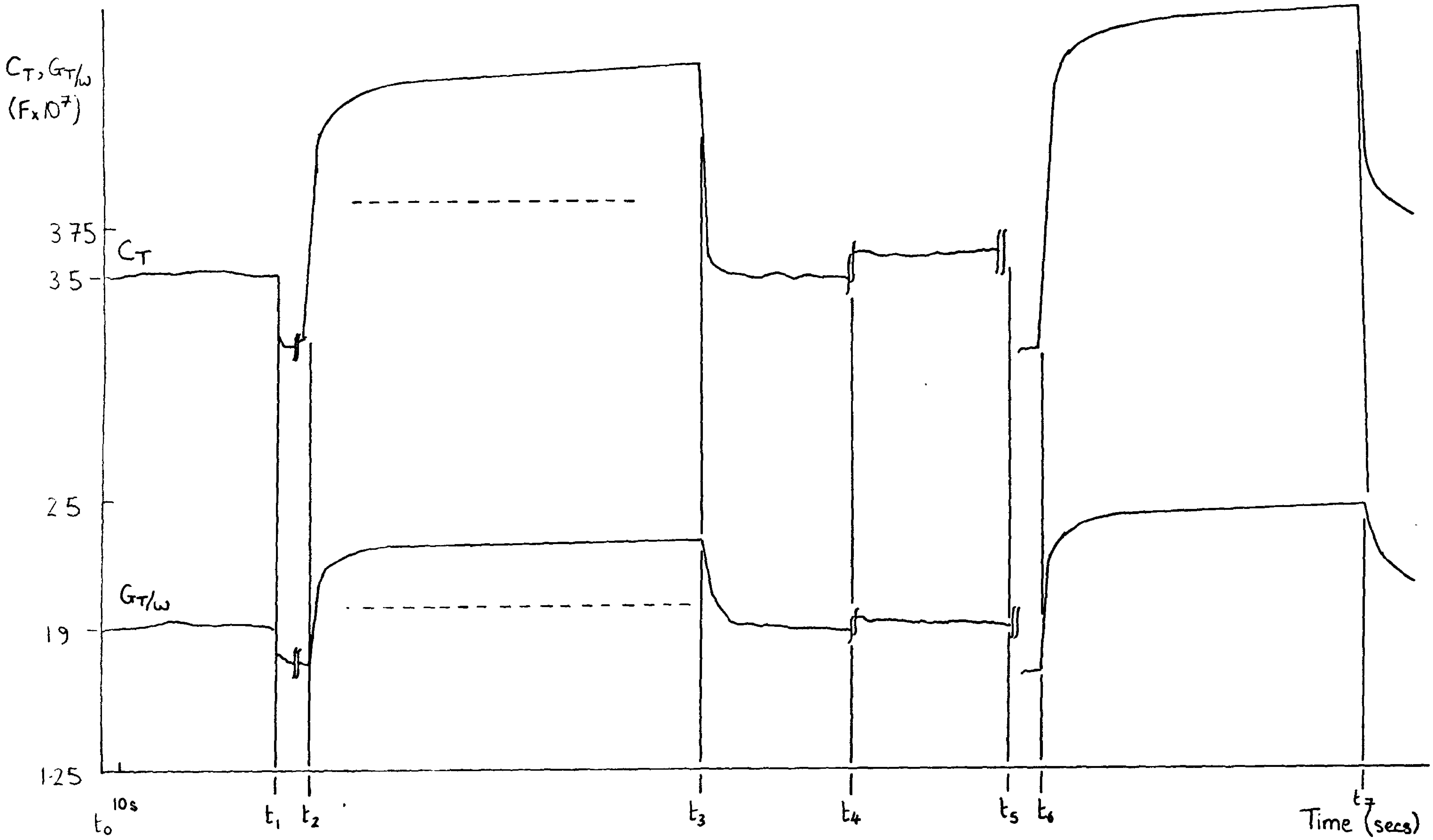

Fig 8.52 Capacitance and loss for a platinum electrode coated with 40 monolayers of PBMA/Valinomycin plotted as a function of electrolyte immersion time for a range of electrolyte compositions.

9.0 Conclusions

The technique of AC admittance analysis has been successfully adapted for the characterisation of thin films on electrodes in an electrolyte environment. The theoretical basis of the method was developed from the work of Macdonald (1953, 1971, 1973, 1974, 1976, 1985; $5; Appendix). Based on this treatment, an equivalent circuit was developed to model the behaviour of the cell. The soundness of the method was first established by measurements on copper electrodes, spin coated with PVC ($4.3.2). Detailed studies of Langmuir Blodgett coated electrodes were then carried out ($7; $8). The evaluation of the equivalent circuit parameters for PVC and barium stearate coatings on copper has shown the potential offered by such detailed analysis. For example, as well as being a useful means of predicting the ideal capacitance and loss behaviour of the cell, observation of areas of discrepancy can provide insight into other phenomena such as ionic drift within the coating.

During the course of the work, deposition was carried out onto platinum, copper, aluminium and silver. Platinum wire electrodes were the most versatile as they could be used for cyclic voltammetry and ac admittance studies. In addition they were reusable which meant that sample preparation time was lowest for coatings deposited onto platinum. It is also worth noting that platinum is an ideal material for in-vivo applications. Unfortunately, the small surface area of these electrodes meant that it was not possible to accurately determine the deposition ratios. Furthermore, the electrode geometry meant that the use of phase contrast microscopy to examine the coating was of limited value.

As deposition ratios provide a useful measure of deposition quality, larger surface area, sputtered copper electrodes were used in place of the platinum wire electrodes. The initial quality of films deposited onto copper was high as evidenced by dielectric permittivities of 2.7 and 4.1 respectively for barium stearate and PBMA. However, the growth of copper oxide around pin hole defects in the barium stearate film disrupted the coating, leading to a 2% increase in permittivity per minute. The PBMA coatings showed greater robustness, as evidenced by the slow decrease in capacitance of -0.2% per minute. In the case of PBMA, it appears that rather than disrupting the PBMA coating adjacent to defects in the film, the oxide has increased the effective electrode coating thickness at those points. It is suggested that the relatively high reactivity of copper is the reason for the high conductivities measured for both Barium Stearate and PBMA coatings. In order to obtain more stable barium stearate coatings, aluminium electrodes were next used for deposition. Coatings deposited onto these electrodes were of good initial quality and exhibited good long term stability.

In addition to the dependence of the coating quality and stability on the electrode material, a range of molarity, electrolyte and thickness dependent trends were observed. For example, the coating capacitance and loss showed an overall increase with molarity for barium stearate, PBMA and PBMA/Val deposited onto platinum. This is attributed to penetration of the coating by ions and, in the case of barium stearate, desorption of the coating. The latter was confirmed by the cyclic voltammetry studies which showed that although the barium stearate film initially reduced the electrode currents, this passivating effect quickly diminished as the film desorbed.

In the case of barium stearate and mixed barium stearate/gramicidin LB films deposited onto aluminium, there was an overall decrease in coating capacitance with increasing electrolyte molarity and total electrolyte exposure time. This is attributed to a combination of the good stability of the barium stearate coatings on aluminium and the growth of the aluminium oxide, accelerated by the repeated removal and re-immersion of the electrode in the different molarity electrolytes. Consequently, any ionic penetration of the film and/ or desorption was masked by the growth of the aluminium oxide. It is suggested that the gradual increase in the coating admittance of the PBMA coated aluminium electrode with time was because of the slower growth in the aluminium oxide as the electrode was kept in the same electrolyte during this test. In this case therefore, the dominant factor was ionic penetration, as observed in the case of PBMA deposited onto platinum.

The possible mechanisms which contribute to the observed admittance behaviour of the coated electrodes are :-

i) Penetration of the film by ions leading to a frequency dependent rise in coating conductivity and permittivity. When the film quality is good, this can produce a marked dispersion in the loss curve.

ii) Re-organisation and desorption of the coating leading to an increase in the coating admittance.

iii) Growth of oxide on the electrode leading to a decrease in the measured admittance unless the oxide disrupts the film, as in the case of barium stearate deposited onto copper.

Defect coverages have been estimated using the method of Stelzle and Sackmann (1989), and have revealed significant differences between the estimates based on capacitances and conductances. This may be due to the difficulties of estimating the value of the "ideal" film conductance/capacitance or may point to the need to develop a more complex model.

The first attempt to produce an ion selective coating proved unsuccessful. Even though the π-A curve indicated that the Gramicidin molecules were correctly oriented, admittance studies of the Barium Stearate/Gramicidin coatings showed that the gramicidin was not imparting the expected ion selectivity. This was attributed to the use of a 3 layer film which meant that the Gramicidin molecules only contributed to the measured admittance where they lined up to form a channel through the coating.

After establishing that LB coatings of PBMA deposited onto platinum electrodes were stable and porous to small ions, it was decided to incorporate valinomycin into the PBMA LB film to produce a potassium ion sensitive coating. The results show clearly that the admittance of the PBMA/valinomycin coating depends on the potassium ion concentration. Furthermore, the electrode response was shown to be reversible.

The main objective of this research, namely the development of a technique for the characterisation of thin electrode coatings in a electrolyte environment has been achieved. The technique has been employed to characterise spin coated PVC films on copper electrodes and LB films of Barium Stearate and PBMA on a range of substrates. Furthermore, based on the characterisation of PBMA films on platinum, a mixed PBMA/Valinomycin LB film has been produced and shown to be $[K^+]$ sensitive. Now that the essential ground work has been carried out, there are several areas for further work including methods for improving the instrumentation and for investigating other coating/substrate combinations.

The collection and analysis of data could be greatly enhanced by the use of an up to date frequency response analyser suitably interfaced to a stand alone IBM PC. This would permit data collection under complete software control and permit the use of high quality commercial software for data analysis and presentation. The development of a Non-Linear Least Squares Fit program would also be valuable as a means of obtaining equivalent circuit values for coating characterisation. Such a system would significantly reduce the time required for data collection, analysis and presentation and equally importantly, would provide a more accurate means of characterising the coatings.

The coating characterisation using AC admittance was complemented by cyclic voltammetry in the case of films deposited onto platinum. However, as both techniques are essentially electrical they provide information about the macroscopic properties of the coating from which microscopic properties must be deduced. It is therefore suggested that, for example, surface plasmon resonance and AC admittance analysis be employed concurrently to obtain detailed information on the variation of coating thickness during the course of the admittance analysis. In addition, the use of radio actively labelled salts such as KI, could provide a means of estimating the degree of ionic uptake by the coatings.

Now that the AC admittance technique has been used to show that a PBMA/Valinomycin coating is K^+ sensitive, it would be interesting to characterise this coating more fully and to investigate other coating/substrate combinations. These could include the incorporation of valinomycin into phospholipid bilayers which would provide a more natural environment for the valinomycin (cf Wilkinson et al, 1986). However, as the stability and robustness of a phospholipid coating could be low, it would be useful to try some of the recently developed LB film forming polymers such as the polymerisable phospholipid reported by Singh et al (1987). Such polymers, which possess long chains, would produce a more ordered film than PBMA for immobilising electroactive species. In addition to characterising ion selective coatings on platinum wire electrodes, it would also be of interest to investigate the properties of enzymes immobilised in LB films (Morizumii et al 1987).

To develop electroactive coatings further using the LB technique, it will be necessary to measure their time response and selectivity. This information is required to compare the electrodes to those fabricated using conventional techniques (§2). To facilitate the accurate measurement of the response of the electrode it will be necessary to modify the design of the test cell to ensure that the electrolyte mixing time is much less than the electrode response time.

Finally, in order to develop a practical sensor using LB technology, the use of planar electrodes, with one active and one inactive coating, would enhance the sensitivity and stability of the electrode response. To fabricate such a device it will be necessary to deposit the coating successfully onto gold or platinum evaporated electrodes on glass.

Appendix A

Theoretical basis of the AC Admittance Analysis Technique for the characterization of electrode/electrolyte systems

A.1 Assumptions and restrictions governing the theoretical treatment

The theory was originally developed by Ross Macdonald (1953, 1971, 1973, 1974, 1985) to explain space charge effects in semiconductor materials but is equally applicable to a range of electrode/electrolyte systems. In fact, the theory applies for any extrinsic-intrinsic case and for any values of mobile-charge mobilities and valencies. Although in the theory presented here, charge carrier size effects and compact double layer effects, including specific adsorption are neglected, it should be noted that some of these effects can now be accounted for. For example, a complex rate constant may be employed to account for the presence of an adsorbed intermediate (Macdonald, 1976) and the system impedance can be separated to give compact and bulk-diffuse double layer effects (Franceschetti and Macdonald, 1978).

In the final AC solution, zero charge conditions are assumed at the electrode and the boundary conditions are those employed by Chang and Jaffe (1952) as defined by equations A.36 to A.39. Finally, as strong electrolytes were used in the experimental work, only results for this intrinsic case are presented.

The system under consideration is taken to consist of a homogeneous material, held at constant, spatially uniform temperature, between two, plane parallel electrodes, separated by a distance, d (fig A.1). The analysis assumes unit electrode area. Finally, it is assumed that the mobile charge concentrations always have their steady state or equilibrium values, as determined by the electrode potential ($ 6.2.2.1).

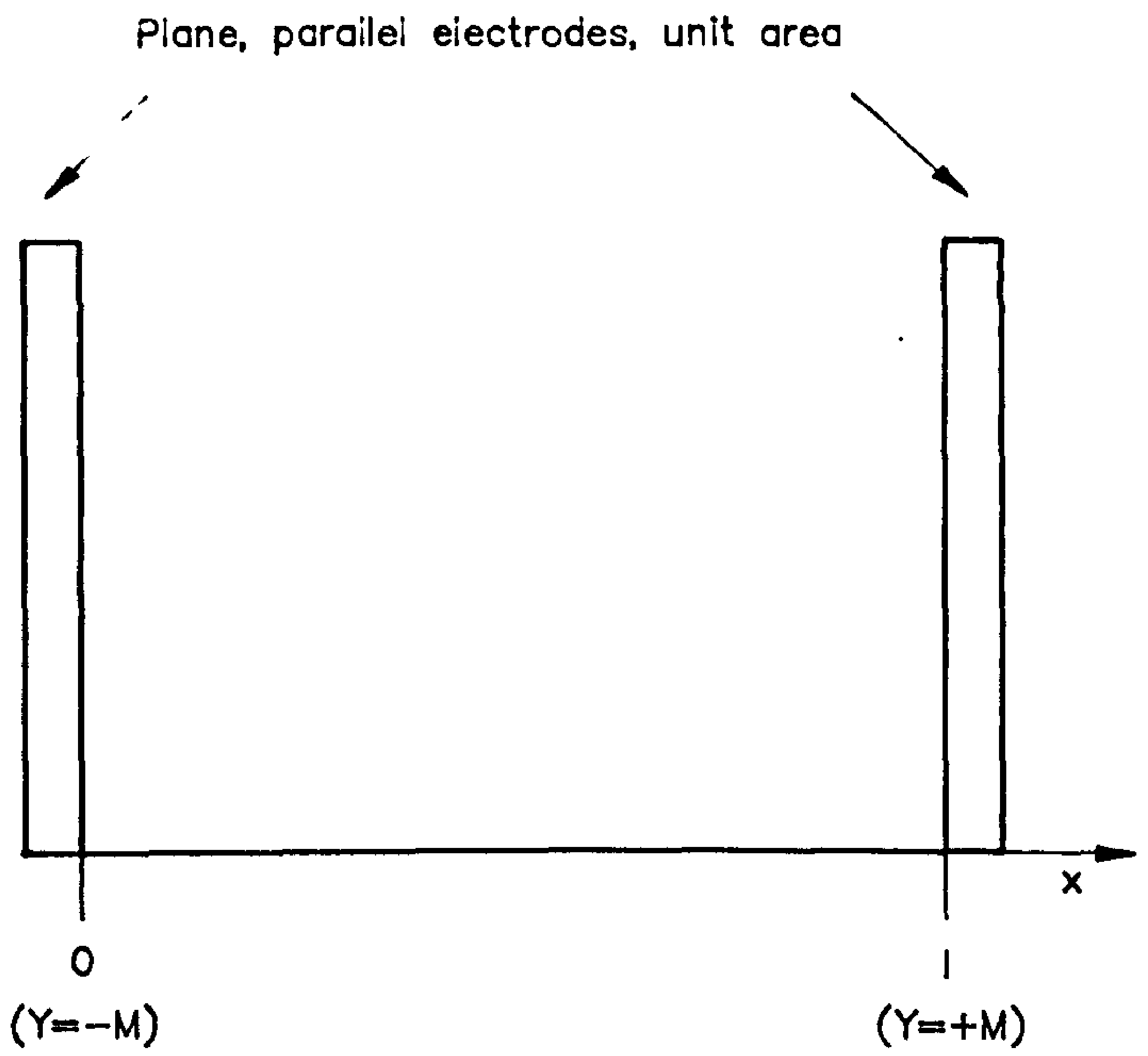

Fig A.1 Diagram showing the electrode geometry assumed for the theoretical treatment of the electrode/electrolyte system.

The usual transport equations for a one dimensional system are ;

$$\delta p/\delta t = - \delta(j_p)/\delta x \qquad A.1$$

$$\delta n/\delta t = - \delta(j_n)/\delta x \qquad A.2$$

Where the flux due to positive and negative ions is given by j_p and j_n respectively;

$$j_p \equiv (\mu_p pE - D_p\delta p/\delta x) \qquad A.3$$

$$j_n \equiv - (\mu_n nE - D_n\delta n/\delta x) \qquad A.4$$

where E is the electric field and the first term on the right hand side is the flux component due to ionic drift under the influence of the electric field E, and the second term is the flux due to diffusion of the ions caused by a concentration gradient. The resulting currents are then given by I_p and I_n respectively, where ;

$$I_p \equiv ez_p j_p \qquad A.5$$

$$I_n \equiv ez_n j_n \qquad A.6$$

and the total current I ;

$$I = I_n + I_p + (\epsilon\epsilon_o)(\delta E/\delta t) \qquad A.7$$

The Einstein equation ;

$$D_i = (kT/ez_i) \mu_i \qquad A.8$$

and the Poisson equation ;

$$\delta E/\delta x = (e/\epsilon\epsilon_o) (z_p p - z_n n) \qquad A.9$$

are also required. Where i = n or p, D_i and μ_i are the diffusion coefficient and mobility of species i, respectively. ϵ is the dielectric constant of the basic material in the absence of mobile charge effects; that is, the solvent in the absence of the solute.

The negative and positive mobile charge concentrations are defined as n_e and p_e respectively for zero current equilibrium. This situation corresponds to the field free, $V_D = V_o = 0$, zero–electrode–charge case for electrolytes. These static quantities are then the unperturbed bulk values, denoted n_i and p_i respectively. When V_D is not intrinsically zero, the potential measured with respect to a reference electrode which yields I_o=0 corresponds to the V_o=0 equilibrium condition. Therefore, the present V_o is actually the electrolyte overpotential. When a single working electrode is involved, $V_o = 0$, corresponds to the condition of zero electrode charge. Then using the unperturbed bulk values for the electrolyte ion concentrations, from equations A.3 to A.7 it follows that the high frequency limiting conductance, G_d may be written as ;

$$G_d = (e/d)(z_p\mu_p p_i+z_n\mu_n n_i) \qquad A.10$$

and the intrinsic Debye length, L is given by ;

$$L = [(\epsilon\epsilon_o kT/e^2)(z_n{}^2 n_i+z_p{}^2 p_i)]^{\frac{1}{2}} \qquad A.11$$

In order to simplify subsequent work, the normalised expressions given below are introduced;

$$\pi_m \equiv \mu_n/\mu_p \quad \text{A12}$$

$$\epsilon_p \equiv G_p/G_d \equiv (1+\pi_m)^{-1} \quad \text{A13}$$

$$\epsilon_n \equiv G_n/G_d \equiv (1+\pi_m{}^{-1})^{-1} \quad \text{A14}$$

It should be noted that $\epsilon_p+\epsilon_n = \delta_p+\delta_n = 1$

$$\pi_z \equiv z_n/z_p \quad \text{A15}$$

$$\delta_p \equiv (1+\pi_z)^{-1} \quad \text{A16}$$

$$\delta_n \equiv (1+\pi_z{}^{-1})^{-1} \quad \text{A17}$$

Consider a one dimensional system with x measured from the left hand electrode and $0 \le x \le d$ (fig A.1). Let X represent the number of Debye lengths in distance x, then ;

$$X \equiv x/L \quad \text{A18}$$

and define the normalised electric field as E^* ;

$$E^* \equiv (eL/kT)E \quad \text{A19}$$

Also let $\tau \equiv wt$ A20

$$P \equiv p/z_p p_i \quad \text{A21}$$

$$N \equiv n/z_n n_i \quad \text{A22}$$

and the normalised frequency, Ω is given by ;

$$\Omega \equiv wC_g/G_d \qquad \text{A23}$$

where $C_g \equiv \epsilon\epsilon_o/d$, is the geometric capacitance per unit area, and w is the radial frequency. The dielectric relaxation time τ_D is given by ;

$$\tau_D \equiv \epsilon\epsilon_o/[e(z_p\mu_p p_i + z_n\mu_n n_i)] \qquad \text{A24}$$

$$\equiv C_g/G_d \qquad \text{A25}$$

Therefore, from equations A.23 and A.24, it follows that;

$$\Omega \equiv w\tau_D \qquad \text{A26}$$

It should be noted that most measurable space charge and discharge effects of interest occur in the normalised frequency range, $0 \leq \Omega < 1$.

Equations A.1 to A.7 may now be re-written in normalised form. Combining A.1 and A.3, A.2 and A.4 and using equations A.8 and A.9 gives ;

$$\delta^2 P/\delta X^2 = \Omega\delta_p\epsilon_p^{-1}\delta P/\delta\tau + z_p[E^*\delta P/\delta X + (\delta_p P - \delta_n N)P] \qquad \text{A27}$$

$$\delta^2 N/\delta X^2 = \Omega\delta_n\epsilon_n^{-1}\delta N/\delta\tau - z_n[E^*\delta N/\delta X + (\delta_p P - \delta_n N)N] \qquad \text{A28}$$

$$\delta E^*/\delta X = \delta_p P - \delta_n N \qquad \text{A29}$$

$$I_p = (\, 2kT/e)\, G_d\epsilon_p M \,(\, z_p P E^* - \delta P/\delta X \,) \qquad \text{A30}$$

$$I_n = (2kT/e)\, G_d \epsilon_n M\, (z_n N E^* - \delta N/\delta X) \qquad \text{A31}$$

$$\text{and } I = I_n + I_p + (2kT/e)(G_d \Omega M)\delta E^*/\delta\tau \qquad \text{A32}$$

where $M \equiv (1/2L)$ and is the number of Debye lengths contained in d/2. The normalised potential Φ^*, may be written as ;

$$\Phi^* = e\Phi/kT \qquad \text{A33}$$

and

$$\Phi^*(Y) = - \int_{-M}^{Y} E^*(Y)dY \qquad \text{A34}$$

where $Y = X - M$ and $\Phi^*(Y) = 0$ at $Y = -M$ (fig A.1).

Using the subscripts M and -M to denote $Y = M$ and $Y = -M$ respectively, the normalised, applied potential may be rewritten as $V^* = \Phi^*$. Furthermore the applied potential for the case of interest may be defined as ;

$$V^* = V_0^* + V_1^* \sin\tau \qquad \text{A35}$$

In order to obtain the total current I, as a function of applied potential, boundary conditions are required. The treatment is limited to frequency and time independent parameters. It should be noted that as the boundary condition parameters depend on V_0^*, the parameter values may need to be different at the two electrodes. Furthermore, even if the two electrodes are identical, the equilibrium condition does not necessarily correspond to zero charge on the surfaces. This is because electrochemical differences between the electrode material and electrolyte and/or differences in the free energy of formation of positive and negative mobile carriers will lead to a contact potential V_D which perturbs the concentration of the mobile charges near the electrodes even when no direct current flows. It is therefore necessary to specify the equilibrium perturbation as part of the initial and boundary conditions.

Following the work of Chang and Jaffe (1952), simple boundary conditions are defined for the small signal ac response for the linear regime around equilibrium. Therefore, at the boundaries $Y = \pm M$ (ie $x=0,d$);

$$I_{p\text{-}M} = -r_p(ez_pD_p/d)(p_{-M}-p_{e\text{-}M})$$

$$= -r_p(kT/e)(G_d\epsilon_p)\Delta P_{-M} \tag{A36}$$

$$I_{pM} = r_p(ez_pD_p/d)(p_M-p_{eM})$$

$$= r_p(kT/e)(G_d\epsilon_p)\Delta P_M \tag{A37}$$

$$I_{n\text{-}M}= r_n(ez_nD_n/d)(n_M-n_{eM})$$

$$= r_n(kT/e)(G_d\epsilon_n)\Delta N_M \tag{A38}$$

$$I_{nM} = -r_n(ez_nD_n/d)(n_{-M}-n_{e\text{-}M})$$

$$= -r_n(kT/e)(G_d\epsilon_n)\Delta N_{-M} \tag{A39}$$

where $\Delta P_{-M}\equiv P_{-M}-P_{e\text{-}M}$ and $\Delta N_M\equiv N_M-N_{eM}$ etc, and r_p, r_n are dimensionless discharge parameters. It is assumed that the rate of discharge of the ions at the electrode is proportional to the difference between the instantaneous values at the electrode $p_{\pm M}$,

$n_{\pm M}$, and the equilibrium values p_e, n_e. This means that the time independent values, p_e, n_e need not be identical to the undisturbed bulk concentrations, n_i, p_i. Furthermore, r_p and r_n can be related to a symmetrical, free energy barrier at the electrodes and to specific reaction rate constants, k_f and k_b which are the forward and reverse reaction rate constants respectively ($ 6.5). In the case of cyclic voltammetry for example, a current-voltage relationship can be derived which relates the overall electrode response to the reaction rate constants ($ 6.5).

In the case of complete blocking, which corresponds to an infinite potential barrier at the electrode, r_p and $r_n = 0$. Whilst at the other extreme of an infinite reaction rate;

$$\Delta P_{-M} \equiv \Delta P_M \equiv \Delta N_{-M} \equiv \Delta N_M \equiv 0$$

Explicit boundary conditions are obtained by evaluating equations A.30, A.31 at $Y = \pm M$ and using equations A.36 to A.39. Also using the fact that $I(Y)$ is independent of Y in a one dimensional situation gives $\delta I/\delta Y=0$. Consequently $I_{-M} = I_M$. Therefore ;

$$(r_n\epsilon_n/2M)(\Delta N_M+\Delta N_{-M})-(r_p\epsilon_p/2M)(\Delta P_M+\Delta P_{-M})=\Omega(\delta E_M^*/\delta\tau - \delta E_{-M}^*/\delta\tau) \quad \text{A40}$$

At equilibrium, both sides of equation A.40 are identically zero, and in the $V^* = V_o^*$ static situation, where I_o may be zero or non zero, equation A.40 becomes ;

$$(r_n\epsilon_n)(\Delta N_{oM}+\Delta N_{o-M})-(r_p\epsilon_p)(\Delta P_{oM}+\Delta P_{o-M})=0 \qquad \text{A41}$$

Now, assuming that $V^* = V_o^* + V_1^*\exp(i\tau)$ for $V_1^* < 1$, P and N can be split into static and time varying quantities and any harmonics in P, I etc can be neglected. In this way the response to $V_1^*\exp(i\tau)$ represents a small perturbation to the system about its equilibrium at V_o^*. Equations are now presented separately for the static and dynamic perturbations respectively.

$$\delta^2P/\delta X^2 = z_p[E_o^{*}\delta P_o/\delta X+(\delta_pP-\delta_nN)P_o] \tag{A42}$$

$$\delta^2N/\delta X^2 = -z_n[E_o^{*}\delta N_o/\delta X+(\delta_pP-\delta_nN)N_o] \tag{A43}$$

$$\delta E^{*}/\delta X = \delta_pP_o-\delta_nN_o \tag{A44}$$

$$I_{po} = (2kT/e)G_d\epsilon_pM(z_pP_oE_o^{*}-\delta P_o/\delta X) \tag{A45}$$

$$I_{no} = (2kT/e)G_d\epsilon_nM(z_nN_oE_o^{*}-\delta N_o/\delta X) \tag{A46}$$

$$I_o = I_{no}+I_{po} \tag{A47}$$

$$z_pP_{o-M}E_{o-M}^{*}-\delta P_{o-M}/\delta X = -(r_p/2M)\Delta P_{o-M} \tag{A48}$$

$$z_pP_{oM}E_{oM}^{*}-\delta P_{oM}/\delta X = (r_p/2M)\Delta P_{oM} \tag{A49}$$

$$z_nN_{o-M}E_{o-M}^{*}+\delta_{No-M}/\delta X = (r_n/2M)\Delta N_{o-M} \tag{A50}$$

$$z_nN_{oM}E_{oM}^{*}+\delta N_{oM}/\delta X = -(r_n/2M)\Delta N_{oM} \tag{A51}$$

and

$$V_o^{*}(Y) = -\int_{-M}^{M} E_o^{*}(Y)dY \tag{A52}$$

It should be noted that when $V^{*} = V_o^{*} = 0$, $I_o = 0$ and the static solution reduces to the equilibrium condition independently of r_p and r_n values. However, for the complete blocking case, where $r_p = r_n = 0$, $I_o = I_{o-M} = I_{oM} = 0$ for any applied V_o^*. This means that the final equilibrium state reached in the completely blocking situation will not be the same as in the original case unless $V_o^* = 0$. Furthermore, when $|V_o^*| > 0$ and r_p and/or r_n are/is non zero, the final condition is the static steady state but is not a condition of equilibrium.

The linearised perturbative equations are ;

$$\delta^2 P_1/\delta X^2 = i\Omega\delta_p\epsilon_p^{-1}\delta P_1 + z_p[E_o^*\delta P_1/\delta X + E_1^*\delta P_o/\delta X$$

$$+(\delta_p P_1 - \delta_n N_o)P_o + (\delta_p P_o - \delta_n N_o)P_1] \qquad \text{A53}$$

$$\delta^2 N_1/\delta X^2 = i\Omega\delta_n\epsilon_n^{-1}\delta N_1 - z_n[E_o^*\delta N_1/\delta X + E_1^*\delta N_o/\delta X$$

$$+(\delta_p P_1 - \delta_n N_1)N_1 + (\delta_p P_o - \delta_n N_o)N_1] \qquad \text{A54}$$

$$E_1^*/\delta X = \delta_p P_1 - \delta_n N_1 \qquad \text{A55}$$

$$I_p 1 = (2kT/e)G_d\epsilon_p M(z_p(P_o E_1^* + P_1 E_o^*) - \delta P_1/\delta X) \qquad \text{A56}$$

$$I_n 1 = (2kT/e)G_d\epsilon_n M(z_n(N_o E_1^* + N_1 E_o^*) - \delta N_1/\delta X) \qquad \text{A57}$$

$$I_1 = I_n 1 + I p_1 + (2kT/e)(G_d i\Omega M)\delta E_1^* \qquad \text{A58}$$

$$z_p(P_{o-M}E_{1-M}^* + P_{1-M}E_{o-M}^*) - \delta P_{1-M}/\delta X = -(r_p/2M)\Delta P_{1-M} \qquad \text{A59}$$

$$z_p(P_{oM}E_{1M}^* + P_{1M}E_{oM}^*) - \delta P_{1M}/\delta X = (r_p/2M)\Delta P_{1M} \qquad \text{A60}$$

$$z_n(N_{o-M}E_{1-M}^{*}+N_{1-M}E_{o-M}^{*})+\delta N_{1-M}/\delta X = (r_n/2M)\Delta N_{1-M} \qquad \text{A.61}$$

$$z_n(N_{oM}E_{1M}^{*}+N_{1M}E_{oM}^{*})+\delta N_{1M}/\delta X = -(r_n/2M)\Delta N_{1M} \qquad \text{A.62}$$

and finally ;

$$V_1^{*}(Y) = - \int_{-M}^{M} E_1^{*}(Y)dY \qquad \text{A.63}$$

In order to solve equations A.42 to A.63, equations A.42 to A.52 are used to solve for the spatial dependence of the static quantities and the equilibrium solution. These results are then used in equations A.53 to A.62. However, as such solutions can only be carried out numerically, only results for special cases are presented here.

For convenience, the six main parameters of the present problem are represented in the following way; (r_p, r_n ; π_m , π_z ; X , M), where X is zero for the present, electrolyte case. The parameter values used in the experimental work are summarised in table A.1. It should be noted that in terms of impedances, the (A,B;C,D;E,F) and (A,B;C^{-1},D^{-1};-E,F) cases are identical, where A is a specific value of r_p, B of r_n etc.

A.2 Specific Solution

To make an analytic solution in the general $V_o^{*}=0$, (r_p,r_n;π_m,π_z;X,M) case, it is assumed that $V_D^{*} = \delta E_o^{*}(Y)/\delta X = E_o^{*}(Y) \equiv 0$ for all Y. The static situation is then that for zero–electrode–charge where the steady state concentrations are the bulk values, n_i and p_i. It follows that $\delta^2P/\delta X^2 = \delta^2N/\delta X^2 = \delta P/\delta X = \delta N/\delta X = I_o \equiv 0$ for all Y. Under these conditions, $p_o - p_{ef}$, $P_o - P_{ef} \equiv z_p^{-1}$, $n_o - n_{ef}$, and $N_o = N_{ef} \equiv z_n^{-1}$. The equilibrium neutrality condition which applies for $\delta E_o^{*}(Y)/\delta X = 0$ may be rewritten as ;

$$z_p p_i - z_n n_i = 0 \quad \text{A64}$$

$$\delta_p P_i - \delta_n N_i = 0 \quad \text{A65}$$

$$\delta_p p_i - \delta_n n_i + [(z_n n_i + z_p p_i)/2] = 0 \quad \text{A66}$$

The zero electrode charge condition leads to the simplification of equations A.53 to A.62;

$$\delta^2 P_1/\delta X^2 = a_{11}P_1 + a_{12}N_1 \quad \text{A67}$$

$$\delta^2 N_1/\delta X^2 = a_{21}P_1 + a_{22}N_1 \quad \text{A68}$$

where

$$a_{11} = \delta_p(1 + i\Omega\epsilon_p{}^{-1}) \quad \text{A69}$$

$$a_{12} = -\delta_n \; ; \; a_{21} = -\delta_p \quad \text{A70}$$

and $a_{22} = \delta_n(1 + i\Omega\epsilon_n{}^{-1})$ A71

and ;

$$I_{p1} = (2kT/e)G_d\epsilon_p M(E_1{}^* - \delta P_1/\delta X) \quad \text{A72}$$

$$I_{n1} = (2kT/e)G_d\epsilon_n M(E_1{}^* + \delta N_1/\delta X) \quad \text{A73}$$

$$E_{1M}{}^* - \delta P_{1-M}/\delta X = (r_p/2M)P_{1M} \quad \text{A74}$$

$$E_{1M}^{*}+\delta N_{1M}/\delta X = -(r_n/2M)N_{1M} \qquad A75$$

It should be noted that as P_1 and N_1 are antisymmetric about $Y = 0$, the other boundary conditions are not required. Furthermore, as the total current amplitude is independent of x, I_1 can be averaged to yield ;

$$I_1 = 1/2M \int_{-M}^{M} [\, I_{p1}(Y) + I_{n1}(Y) + \{\, 2kTG_d i\Omega M/e \,\}E_1^{*}(Y) \,]\, dY$$

$$= (kT/e)G_d \int_{-M}^{M} [\, (\epsilon_n N_i/\delta X + \epsilon_p P_i/\delta X) + (\epsilon_p + \epsilon_n + i\Omega)E_1^{*}(Y) \,]\, dY \qquad A76$$

The total admittance Y_T, is then given by $Y_T = I_1/(-V_1)$, which can be written as ;

$$Y_T = -eI_1/kTV_1^{*}$$

$$= G_d(1+(2/V_i^{*})(\epsilon_p P_{1M} - \epsilon_n N_{1M})) + iwC_g \qquad A77$$

Where G_d and C_g are the components of Y_T at the high frequency limit; $Y_{T\infty} \equiv G_d + iwC_g$. Note that equation A.77 follows from equation A.76 and A.63 and the antisymmetry of P_1 and N_1.

Using matrix manipulations and calculus, a complex expression for Y_T can be derived as a function of the basic parameters r_p, r_n, π_m, π_z, X, M and Ω. However, because of the complexity of the solution it is more meaningful to consider results for specific cases. Results pertaining to the experimental work carried out here are discussed below (Table A.1), with reference to the equivalent circuit representation based on the theoretical treatment (fig A.2).

A.3 Equivalent Circuit Representation of the Electrode/Electrolyte System

A.3.1 Interfacial Admittance

At low frequencies, the cell response is determined by the interfacial admittance, $Y_i(w)$. The processes contributing to $Y_i(w)$ include diffusion limited transport and charge separation. A large "pseudo capacitance" can result from diffusion limited transport if positive and negative species discharge unequally at the electrode; charge separation at the interface leads to a double layer capacitance.

The general form of $Y_i(w)$ is complex so only simplified results applicable for w ->0, are given here.

In the limit w→0,

$$Y_i(w)\Big|_{w\to 0} = Y_{i0} = 1/((G_{i0})^{-1} + (jwC_{i0})^{-1}) \qquad \text{A78}$$

Where G_{io} is the interfacial conductance and C_{io} is the interfacial capacitance. The interfacial admittance, Y_{io} can therefore be represented by the series combination of G_{io} and C_{io} (fig A.2). Three, specific, simplified cases are presented for G_{io} and C_{io} in order to provide a means of calculating the probable range of parameter values applicable to the experimental work.

(i) $(r_e, r_e; \pi_m, \pi_z; 0, M \gg 1)$

In the above case of equal discharge parameters, the interfacial capacitance, C_{io} can be written as;

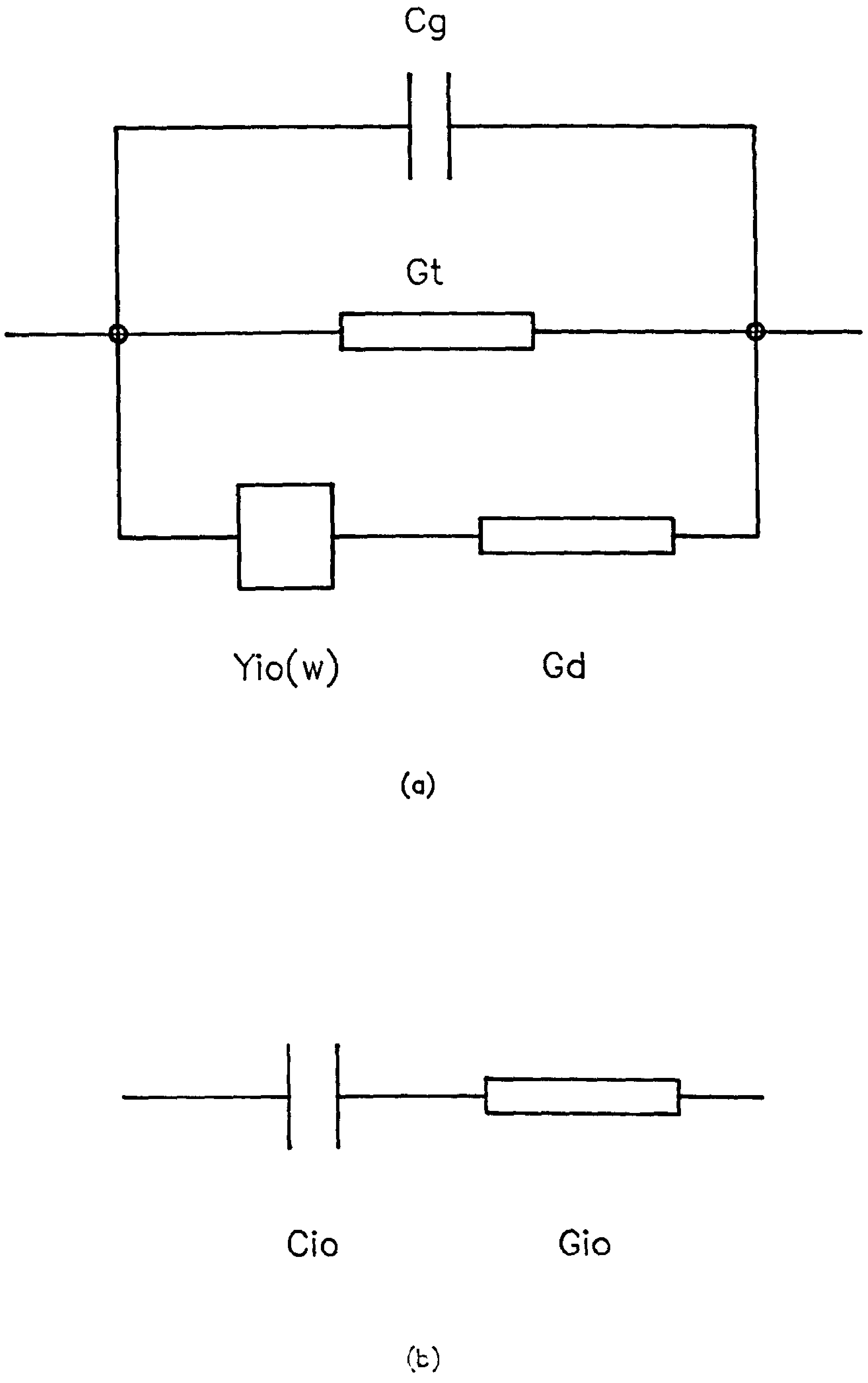

Fig A.2 a) Equivalent circuit representation of the electrode/electrolyte system.

b) The low frequency limiting representation of Yi(w).

$C_{io} = C_g M/(1+r_e/2)^2$ A.79

and the interfacial admittance is given by ;

$G_{io} = G_d\{g_e[(a^{-1})+(ag_e/2M)]\}^{-1}$ A.80

Where $g_e=(1+r_e/2)$ and $a=\delta_p^2/E_p+\delta_n^2/E_n$; $E_p=G_p/G_d$; $E_n=G_n/G_d$ and $G_p=(e/d)(z_p\mu_p p)$; $G_n=(e/d)(z_n\mu_n n)$. As MG_d is an intensive quantity, G_{io} is only fully intensive in the present case when a = 1.

(ii) $(\infty,0;1,1;0,M)$

Where one species discharges and the other is completely blocked at the electrode ;

$C_{io} = (1/12)MC_g(M+3)$ A.81

$\rightarrow M^2C_g/12$ for $M \gg 1$.

$G_{io} \approx G_d[(M^4/45)+(M/2)-1]/[4\{(M^{-1})/4+(M^2/12)\}^2$ A.82

$\rightarrow 4/5$ for $M \gg 1$.

(iii) $(0,0;\pi_m,\pi_z;X,M\{\gg 1\})$

In the case of complete blocking of charge at the electrode ;

$C_{io} = MC_g = \epsilon\epsilon_0/2L$ A.83

$$G_{io} = G_d[a^{-1}+a/2M]^{-1} \qquad A84$$

MC_g is a completely intensive quantity arising from the double layer interface capacitance per unit area of $\epsilon\epsilon_0/L$, localised at each electrode. It is clear from equations A.79 and A.83, that even when both species discharge equally from both electrodes, C_{io}/C_g can be much greater than unity. When one charge is free to discharge and the other is completely blocked, the resulting value of C_{io}/C_g can be 10^5 times greater than in the complete blocking situation (cf equation A.81). This large capacitance occurs only in the differential discharge situation and arises then only if the diffusion length associated with the conduction process becomes comparable to d. It appears in the low frequency limiting saturation region.

Furthermore, it should be noted that C_i and G_i remain very nearly equal to C_{io} and G_{io} for (0,0;1,1;0,M) up to $\Omega \leq 0.1$. However, for most other cases, C_i and G_i remain equal to their low-frequency-limiting values only for considerably smaller Ω. In the frequency range for which C_i and G_i are constant, the low-frequency-limiting forms of the equivalent circuit of fig A.2 are sufficient to describe all the frequency response of the system of interest. Therefore, for the (0,0;1,1;0,M) case, nearly everything of interest occurs in this $C_i \approx C_{io}$, $G_i \approx G_{io}$ range. For this situation, $G_t = 0$, $G_E = G_d$, $C_{io} = MC_g$ and for $M \gg 1$, $G_{io} \gg G_d$, which leads to a very simple equivalent circuit involving a single time constant, simple Debye dispersion. It should also be noted that under certain conditions, regions of approximate w^{-k} response are predicted, where $0 \geq k \geq 1.5$. Such situations include $(r_p,\infty;1,1;0,M)$, $(\infty,r_n;1,1;0,M)$.

A.3.2 Charge Transfer Conductance

$Y_i(w)$ is electrically in parallel with the charge transfer conductance, G_t. G_t is a measure of the ease with which charge can pass to the electrode from ions at the interface and vice versa, and is a function of the electrode reaction rate constants (r_p, r_n);

$$Y_{T0} = G_t \equiv G_d[\epsilon_n r_n + \epsilon_p r_p + (r_n r_p/2)]/\{2[1+r_n/2][1+r_p/2]\} \quad \text{A85}$$

Note that the charge transfer conductance, G_t is zero for the case of complete blocking. Furthermore, since $Y_{T0} = G_t \leq 1$ and $Re(Y_{T\infty}) = 1$, there is a direct, frequency independent conducting charge transfer path between electrodes for all frequencies when r_n and r_p are not both zero.

A.3.3 Electrolyte Conductance

The charge transfer conductance and interfacial admittance are charged and discharged via the bulk electrolyte which has a solution conductance G_d, defined as ;

$$G_d=(eA/d)[z_p \mu_p p + z_n \mu_n n] \quad \text{A86}$$

Alternatively, the solution conductance can be evaluated from a knowledge of the equivalent conductance of the electrolyte. This technique allows corrections for temperature and the variation in dissociation with molarity to be made easily. The solution conductance is then given by ;

$$G_d=(A/d)\Delta(t,m)m/10 \quad \text{A87}$$

Where G_d, A and d are as defined previously. $\Delta(t,m)$ is the equivalent conductance (Harned and Owen, 1958) at temperature T°C and molarity m. Corrections for temperature are made using the relationship;

$$\Delta(t)=(\Delta 25/1.154)(1+\Delta(T-18)) \quad \text{A88}$$

and corrections for molarity are performed using the equation;

$$\Delta(m)=\Delta_0+Bm^{1/2} \qquad A89$$

where Δ_0 is the equivalent conductance at infinite dilution. For KCl at 25°C, $\Delta_0=148.8$ and $B=-65.5$ therefore;

$$\Delta(m)=148.8-65.5m^{1/2} \qquad A90$$

For KCl, the temperature coefficient $\Delta=0.022$, hence

$$G_d=(Am/11.54d)(148.8-65.5m^{1/2})(1+0.022(T-18)) \qquad A91$$

From this equation, if m is known, G_d can be readily evaluated. However, if only G_d is known, m must be evaluated iteratively. That is, an initial guess is used for m from which a value for G_d is obtained. m is then adjusted until the resulting value of G_d equals the measured value.

A.3.4 Geometric Capacitance

Finally, the geometric capacitance of the cell is given by ;

$$C_g = \epsilon_0\epsilon_r A/d \qquad A92$$

At high frequencies the response of the cell is dominated by G_d and C_g.

	π_m (1)	π_z (1)	$L.(mol)^{1/2}$ $mol=2.10^{-4}$	$M.(mol)^{1/2}$ $mol=0.2$	$\Omega.(mol/f)$ $f=10^6$ Hz	Ω $f=10^{-3}$	Ω Hz
KCl	1.01	1.00	6.10^{-9}	4.10^5	$4.4.10^{-11}$	0.22	$2.2.10^{-13}$
KI	"	"	"	"	"	"	"
NaCl	1.54	"	"	"	$5.7.10^{-11}$	0.29	$2.9.10^{-13}$
$CaCl_2$	1.24	0.5	$3.5.10^{-9}$	6.10^5	$2.5.10^{-11}$	0.13	$1.3.10^{-13}$

Table A.1 Summary of main parameter values required to define experimental conditions. Where π_m is the ratio of ionic mobilities, π_z is the ratio of ionic valencies, L the Debye length and M=d/2L where d is the electrode spacing. Ω is the normalised frequency, f the measurement frequency and mol, the electrolyte molarity.

References

Abraham B M and Ketterson J B, (1984), Langmuir, 1, 461-646.

Agarwal V K, (1975a), Elect Sci Tech, 2, 1, 1-31.

Agarwal V K, (1975b), Elect Sci Tech, 2, 2, 75-107.

Agtarap A, (1967), J Am Chem Soc, 89, 22, 5737-9.

Aizawa M et al, (1977), J Membrane Sci, 2, 125-132.

Aizawa M et al, (1980), Anal Chim Acta, 115, 61-67.

Akiake T et al, (1987), 3rd Int Conf Langmiur Blodgett Films.

Appleqvist R et al, (1985), Anal Chim Acta, 169, 237-247.

Arnold M A and Meyerhoff M E, (1984), Anal Chem, 56, 5, 20R-49R.

Band D M and Kratchovil J, (1974), J Physiol, 239, 10P.

Band D M, (1976), Proc Physiol Soc, 265, 5p-6p.

Bard A J and Faulkner L R, (1980), Electrochemical Methods; Fundamentals and Applications, Wiley.

Bard A J, (1983), J Chem Ed, 60, 4, 302-304.

Barnes W L and Sambles J R, (1986), Thin Solid Films, 143, 237-247.

Barraud A, (1980a), Thin Solid, Films, 68, 91-98.

Barraud A, (1980b), Thin Solid, Films, 68, 7-12.

Barraud A, (1980c), Thin Solid, Films, 68, 99-100.

Barraud A, (1983), Thin Solid, Films, 99, 1-3, 317-21.

Berezin I V et al, (1976), in Methods of Enzymology, (ed Mosbach K), 44, 558-571.

Billmeyer F W, (1984), Textbook of Polymer Science, 3rd Ed, NY Wiley.

Blight L et al, (1965), J Colloid, Sci, 20, 393-399.

Blinov L M et al, (1982), Soviet Phys Solid St, 24, 9, 1523-5.

Blinov L M et al, (1982), Soviet Phys Tech Phys Lett, 9, 640.

Boothroyd B et al, (1985), B Poly J, 17, 4, 360-363.

Boukamp B A, (1984), Solid State Ionics, 11, 339-346.

Brand M J D and Rechnitz G A, (1969), Anal Chem, 41, 10, 1185-1191.

Brand M J D and Rechnitz G A, (1969), Anal Chem, 41, 13, 1788-1793.

Brand M J D and Rechnitz G A, (1970), Anal Chem, 42, 4, 478-483.

Broers A N and Pomerantz M, (1983), Thin Solid Films, 99, 1-3, 323-9.

Brown A P and Anson F C, (1977), Anal Chem, 49, 11, 1589-1595.

Brown A D, (1981), PhD Thesis University of Southampton.

Brown C A et al, (1983), J Phys Chem, 87, 19, 3616-19.

Brown H M et al, (1976), Anal Chim Acta, 85, 261-276.

Brundle C R et al, (1979), J Chem Phys, 70, 11, 5190-6.

Buchwald C E et al, (1938), Proc Nat Acad Sci, 24, 204-208.

Buck R P, (1974), Anal Chem, 46, 5, 28-51R.

Buck R P, (1976), Anal Chem, 48, 5, 23-39R.

Carr N et al, (1987), 3rd Int Conf Langmiur Blodgett Films.

Cass A E G et al, (1984), Anal Chem, 56, 667-671.

Cattrall R W and Freiser H, (1971), Anal Chem, 43, 13, 1905-1906.

Cattrall R W and Tribuzio S, (1974), Anal Chem, 46, 14, 2223-2224.

Chang H C and Jaffe G, (1952), J Chem Phys, 20, 7, 1071-1087.

Cheek G et al, (1983), Anal Chem, 55, 380-381.

Chidsey C E D and Murray R W, (1986), Science, 231, 4733, 25-31.

Collman et al, (1980), J Am Chem Soc, 102, 6027-6036.

CRC Handbook of Chemistry and Physics, (1986), ed R C Weast, 67th edn, (Bpca Raton, FL: CRC).

Delaney P A et al, (1985), Thin Solid Films, 123, 353-360.

Diaz A F et al, (1981), J Electroanal Chem, 129, 115-132.

Dickinson T and Whitfield R, (1977), Electrochim Acta, 22, 385-389.

Ducharme D et al, (1987), 3rd Int Conf Langmiur Blodgett Films.

Ebdon L et al, (1982), Analyst, 107, 288-294.

Esashi M and Matsuo T IEE Proc BME, 25, 184-192.

Flanagan M T and Pantell R H, (1984), Elect Lett, 20, 23, 968-970.

Foulds N C and Lowe C R BioEssays, 3, 3, 129-132.

Franceschetti D R and Macdonald J R, (1978), J Electroanal Chem, 87, 419-422.

Franceschetti D R and Macdonald J R, (1979), J App Phys, 50, 1, 291-302.

Franceschetti D R and Macdonald J R, (1979), J Electroanal Chem, 100, 583-605.

Fujihira M et al, (1985a), Thin Solid Films, 132, 77-82.

Fujihira M et al, (1985b), Thin Solid Films, 132, 221-228.

Fujihira M and Araki T, (1986a), Bull Chem Soc Jpn, 59, 2375-2379.

Fujihira M and Araki T, (1986b), Chem Lett, 921-922.

Fujihira M and Araki T, (1986c), J Electroanal Chem, 205, 329-333.

Fujihira M and Poosittisak S, (1986a), Chem Lett, 251-252.

Fujihira M and Poosittisak S, (1986b), J Electroanal Chem, 199, 481-484.

Fujihira M, (1986), J Chem Soc Chem Comm 11, 823-824.

Fung C D and Larkins G L, (1985), Thin Solid Films, 132, 33-39.

Gaines G L et al, (1978), J Am Chem Soc, 100, 21, 6549-6559.

Glarum S H and Marshall J H, (1985), J Electrochem Soc, 132, 12, 2939-2944.

Guibault G G, (1976), Methods of Enzymology Mosbach K (Ed), 44, 579-619.

Halbert M K, (1985), Anal Chem, 57, 591-595.

Handy R M and Scala L C, (1966), J Electrochem Soc, 113, 109-116.

Harned H S and Owen B B, (1958), The Physical Chemistry of Electrolytic Solutions, 3rd edn, (New York: Reinhold).

Hasmonay H et al, (1980), Thin Solid Films, 68, 21-31.

Heckl W M and Mowhald H, (1987), 3rd Int Conf Langmiur Blodgett Films.

Heckmann K et al, (1983), Thin Solid Films, 99, 1-3, 265-270.

Highfield R R et al, (1983), Thin Solid Films, 99, 1-3, 165-72.

Hille, B, (1984), Ionic Channels of Excitable Membranes, Sinauer Associates, Sunderland, Mass. Hodge P et al, (1985), B Poly J, 17, 4, 368-371.

Holcroft B and Roberts G G, (1987), 3rd Int Conf Langmiur Blodgett Films.

Howarth V A et al, (1987), 3rd Int Conf Langmiur Blodgett Films.

Hubrecht J and Vereeken J, (1985), J Electrochem Soc, 132, 12, 2886-2889.

Huheey, J E, (1978), Inorganic Chemistry :Principles of Structure and Reactivity, 2nd Ed, NY Harper and Row.

Iriyama K et al, (1985), Thin Solid Films, 132, 229-242.

James H, (1972), Anal Chem, 44, 4, 856-857.

Janata J and Huber R J, (1979), Ion-Selective Electrode Review, 1, 31-79.

Janata J, (1975), J Am Chem Soc, 97, 10, 2914-2916.

Janata J, (1987), Sensors and Actuators, 12, 2, 121-8.

Kajzar P et al, (1987), 3rd Int Conf Langmiur Blodgett Films.

Kakimoto M et al, (1987), 3rd Int Conf Langmiur Blodgett Films.

Kemp G and Wenner C E, (1972), Biochem Biophys Acta, 282, 1, 1-7.

Khana U and Srivastava V K , (1972), Thin Solid Films, 12, S25-28.

Kissinger P T and Heineman, (1983), J Chem Ed, 60, 9, 702-706.

Kopp F et al, (1975), Biophys Strust Mech, 1, 75-96.

Kyaer K et al, (1987), 3rd Int Conf Langmiur Blodgett Films.

Lando J B and Fort T, (1977), Proc 3rd Midland Maromolecular Monographs NY Gordon & Breach.

Lane R F and Hubbard A T, (1973), J Phys Chem, 77, ,11, 1401-10.

Langmuir I, (1938), J Am Chem Soc, 60, 1190-1194.

Le Blanc O H and Grubb W T, (1976), Anal Chem, 48, 12, 1658-60.

Ledoux I et al, (1987), 3rd Int Conf Langmiur Blodgett Films.

Lieser G et al, (1980), Thin Solid Films, 68, 77-90.

Losche M et al, (1984), Thin Solid Films, 117, 269.

Lyall I R J and Batchelder D N, (1985), B Poly J, 17, 4, 372-376.

Mabbott G A, (1983), J Chem Soc, 60, 9, 697-702.

Macdonald J R, (1980), An Rep Conf Elect Ins Die Phen Boston MA USA Nat Acad Press 3-49.

Macdonald J R, (1974), J App Phys, 45, 1, 73-81.

Macdonald J R, (1974), J App Phys, 45, 5, 2343-5.

Macdonald J R, (1952), J Chem, Phys, 20, 1107-1111.

Macdonald J R, (1954), J Chem Phys, 22, 11, 1857-1866.

Macdonald J R, (1954), J Chem Phys, 22, 8, 1317-1322.

Macdonald J R, (1955), J Chem Phys, 23, 12, 2308-2309.

Macdonald J R, (1956), J Chem Phys, 25, 2, 364-365.

Macdonald J R, (1956), J Chem Phys, 25, 2, 364-5.

Macdonald J R, (1962), J Chem Phys, 36, 11, 3062-80.

Macdonald J R, (1963), J Chem Phys, 39, 2, 412-422.

Macdonald J R, (1971), J Chem Phys, 54, 5, 2026-50.

Macdonald J R, (1973), J Chem Phys, 58, 11, 4982-5001.

Macdonald J R, (1974), J Chem Phys, 61, 10, 3977-3996.

Macdonald J R, (1978), J chem Phys, 68, 4, 1614-1637.

Macdonald J R, (1980), J Chem Phys, 73, 10, 5272-93.

Macdonald J R, (1981), J Chem Phys, 75, 6, 3155-7.

Macdonald J R, (1971), J Electroanal Chem, 32, 317-328.

Macdonald J R, (1972), J Electroanal Chem, 40, 2, 440-443.

Macdonald J R, (1973), J Electroanal Chem, 47, 1, 182-189.

Macdonald J R, (1974), J Electroanal Chem, 53, 1-55.

Macdonald J R, (1976), J Electroanal Chem, 70, 17-26.

Macdonald J R and Garber J A, (1977), J Electrochem Soc, 124, 7, 1022-1029.

Macdonald J R, (1974), J Phys C, 7, 17, L327-L331.

Macdonald J R, (1977), J Phys C, 10, 9, 1459-1471.

Macdonald J R, (1976), Nato Adv Study Inst. Series C. Math and Phy Sci, (No 6033-648), 25 149-183.

Macdonald J R, (1953), Phys Rev, 92, 1, 4-17.

Macdonald J R, (1962), Physica, 28, 5, 485-92.

Macdonald J R, (1976), Solid State Ionics, 25, 149-183.

Macdonald J R, (1981), Solid State Ionics, 5, 137-40.

Macdonald J R, (1982), Solid State Ionics, 6, 1, 65-77.

Macdonald J R, (1985), Solid State Ionics, 15, 2, 159-61.

Maj-Zurwaska M and Hulanicki A, (1982), Anal Chim Acta, 136, 394-398.

Maloy J T J Chem Ed, (1960), 4, 285-289.

Marshmann C E, (1986), Phys Bull, 37, 296-299.

Martin C R and Freiser H, (1980), Anal Chem, 52, 562-564.

Martin C R and Freiser H, (1980), J Chem Ed, 57, 7, 512-514.

Matsuda A et al, (1977), J App Phys, 48, 2, 771-4.

Matsuda H and Ayabe Y, (1955), Z Elektrochem, 59, 494-503.

McIntyre J F and Leidheiser H, (1986), J Electrochem Soc, 133, 1, 43-48.

Millany H M and Jonscher A K, (1980), Thin Solid Films, 68, 257-273.

Mobius D and Bucher H, (1972), Physical Methods of Chemistry, Part IIIB, Optical, Spectroscopic and Radioactivity Methods. Ed Weissberger and Rossiter. Techiques of Chemistry 1 650-675.

Morizumii T et al, (1987), 3rd Int Conf Langmiur Blodgett Films.

Morrison R T and Boyd R N, (1983), Organic Chemistry, 4th Ed, Allyn and Bacon, Boston.

Murray R W et al, (1987), Anal Chem, 59, 5, 379A-388A.

Neupert-Laves K and DobBler M, (1975), Helv Chim Acta, 58, 2, 432-42.

Nicholson R S and Shain I, (1964), Anal Chem, 36, 4, 706-723.

Nicholson R S, (1965), Anal Chem, 37, 11, 1351-1355.

Nicholson R S, (1966), Anal Chem, 38, 10, 1406.

Nicklow R M et al, (1981), Phys Rev B, 23, 3, 1081-7.

Nishiyama K and Fujihira M, (1987), Chem Lett, 1433-1446.

Nylander C, (1985), J Phys E, 18, 9, 736-750.

Oyama N and Anson F C, (1980), Anal Chem, 52, 1192-1198.

Peng J B et al, (1987), Langmuir, 3, 104-106.

Peterson I R et al, (1983), Thin Solid Films, 109, 4, 371-8.

Peterson I R, (1984), Thin Solid Films, 116, 357-366.

Peterson I R and Russel G J, (1985), B Poly J, 17, 4, 364-367.

Peterson I R and Girling I R, (1985), Sci Prog Oxf, 69, 276, 533-550.

Peterson I R et al, (1987), Thin Solid Films, 150, 83-88.

Pethig R, (1984), IEEE Trans Elect Ins, E119, 5, 453-474.

Pitt C W and Walpita L M, (1976), Electronics Letters, 12, 18, 479-81.

Polymeropoulos E E et al, (1980), Thin Solid Films, 68, 173-190.

Pomerantz M, (1980), Phase Transitions in Surface Films, (New York: Plenum Press).

Porter E F and Wyman J, (1937), J Am Chem Soc, 59, 2, 2746-7.

Porter E F and Wyman J, (1938), J Am Chem Soc, 60, 1, 1083-1094.

Porter E F, (1938), J Am Chem Soc, 60, 2, 2855-2869.

Pugh J and Ryan J T, (1979), IEE Conf Pub 177 Dielectric Mats Measurements and Applications 404-407.

Pye E K and Chance B, (1976), Methods of Enzymology, (Ed Mosbach K), 44, 558-571.

Race H H and Reynolds S I, (1939), J Am Chem Soc, 61, 1, 1425-1436.

Rechnitz G A, (1981), Science, 214, 287-291.

Renneberg R et al, (1982), Anal Chim Acta, 134, 359-364.

Renneberg R et al, (1986), Trends Biochem Sci, 11, 5, 216-220.

Richardson T et al, (1987), 3rd Int Conf Langmiur Blodgett Films.

Ries H E and Swift H J, (1978), J Colloid Int Sci, 64, 1, 111-119.

Roberts G G et al, (1978), J Phys Chem, 11, 10, 2077-85.

Roberts G G, (1980), Thin Solid Films, 68, 223-232.

Roberts G G et al, (1981), Proc IEE Part 1, 128, 6, 197-201.

Roberts G G, (1985), Adv Phys, 34, 4, 475-512.

Roberts G G et al, (1985), Thin Solid Films, 132, 113-123.

Rubinstein I, (1987), 3rd Int Conf Langmiur Blodgett Films.

Rudd E J, (1987), Thin Solid Films, 43, 1-39.

Sarkar M and Lando J B, (1983), Thin Solid Films, 99, 1-3, 271-276.

Sibbald A et al, (1983), Clin Chem, 29, 2, 405-406.

Sibbald A et al, (1984), Clin Chem, 30, 1, 135-137.

Sibbald A, (1983), IEE Proc, 130, I-5, 233-244.

Singh A et al, (1987), 3rd Int Conf Langmiur Blodgett Films.

Sprintschnik G et al, (1977), J Am Chem Soc, 99, 15, 4947-4954.

Stefanova A et al, (1983), Chem Abstr 99 165714t; Electrokhimiya, 19, 1225-1230.

Stelzle M and Sackmann E, (1989), Biochimica Biophysical Acta, 981, 135-142.

Stryer, L, Biochemistry, (1981), W H Freeman and Co, 2nd Ed, NY.

Stuart M, (1986), MSc Thesis, University of Wales.

Sugi M et al, (1979), Mol Cryst Liq Cryst, 50, 183-200.

Swalen J D, (1987), 3rd Int Conf Langmiur Blodgett Films.

Takatsu I, (1987), Sens Act, 11, 309-317.

Tamura H et al, (1982), Anal Chem, 54, 1224-1227.

Taylor D M, (1987), J Phys D: App Phys, 20, 1277-1283.

Taylor D M and Mahboubian-Jones M G B, (1982), Thin Solid Films, 87, 167-179.

Tien H T, (1974), Bilayer Lipid Membranes, (BLM),: Theory and Practice, (New York: Dekker).

Trojanovicz M et al, (1982), Talanta, 29, 113-117.

Uekita M et al, (1987), 3rd Int Conf Langmiur Blodgett Films.

Urry et al, (1971a), Proc Nat Acad Sci, 68, 672-76.

Urry et al, (1971b), Proc Nat Acad Sci, 68, 1907-11.

Van Benschoten J J et al, (1983), J Chem Ed, 60, 9, 772-776.

Van Krevelen D W and Hoftyzer P J, (1976), Properties of Polymers: Their estimation and correlation with chemical structure, 2nd Ed, Elsevier Scientific Pub Co, Amsterdam.

Veale G et al, (1985), Thin Solid Films, 127, 293-303.

Vining W J and Meyer M J, (1985), J Electroanal Chem, 195, 183-187.

Walpita L M and Pitt C W, (1977), Electronics Letters, 13, 7, 210-12.

Wei L Y and Woo B J, (1973), Biol Phys, 1, 50-68.

~~Whitten D G, (1977), J Am Chem Soc, 99, 15, 4947-4954.~~

Winter C S et al, (1984), Proc IEE Part I, 131, 4, 125-4

Yokata et al, (1987), J Electroanal Chem, 216, 289-292.

Zaba B N and Bone S IMBME Bangor UCNW.

Zahl P A et al, (1939), Trans Fara Soc, 35, 1, 308-312.

CORRIGENDA

The following references were inadvertently omitted from the above list.

Carter F.L., (1982), Proceedings of the Molecular Electronic Devices Workshop (Naval Research Lab).

Carter F.L., (1987), Proc SPIE-Int Soc Opt Eng, (Opt Hybrid Comput), 634, 179-94.

Fankuchen I, (1938), Phys Rev, 53, 909.

Srivastava V.K. and Verma A.R., (1962), Proc Phys Soc., 80, 1, 222-5.

Srivastava V.K. and Verma A.R., (1966), Solid State Commun, 4, 8, 367-71.

Publications

Taylor D M and Macdonald A G, (1986), 'Measuring the electrical properties of thin insulating films in contact with electrolyte solutions', IEEE Annual Report, Conf Elect Ins Die Phen, 81-86.

Taylor D M, Macdonald A G and Solway A E, (1987), 'AC Admittance and Electrochemical Studies of thin insulating films on metal electrodes immersed in electrolyte solutions', IEEE Annual Report, Conf Elect Ins Die Phen, 146-151.

Taylor D M and Macdonald A G, (1987), 'AC admittance of the metal/insulator/electrolyte interface', J Phys D: Appl Phys, 20, 1277-1283.

Taylor D M, Macdonald A G and Solway A E, (1987), 'AC Admittance and Electrochemical Studies of thin insulating films on metal electrodes in electrolyte solutions', 3rd Int Conf on LB Films, Gottingen, FRG.